

**A Computational Evaluation
of the Passenger Crash Position
in Civil Aircraft**

by

Raf Haidar
BSc (Hons), CEng MIMechE

**Thesis Submitted to the University of Nottingham
for
the degree of Doctor of Philosophy
October, 1995**

CONTENTS

ACKNOWLEDGEMENTS	1
DECLARATION	2
SUMMARY	3
ABBREVIATIONS	4
BACKGROUND	6
1. LITERATURE REVIEW	9
1.1	The History of Crash Injury Research				9
1.2	The First World War		9
1.3	The Second World War		9
1.4	The Post War Years		10
1.5	Aircraft Safety		12
1.6	Airworthiness		13
1.7	Crashworthiness		14
2. THE DEVELOPMENT OF THE 16G PASSENGER AIRCRAFT SEAT	17
2.1	Dynamic Pulse		17
2.1.1	Pulse Duration		17
2.2	Crash Survivability Limits		18
2.3	Performance Criteria		18
2.4	Transport Category Aircraft		18
2.5	Seat Dynamic Tests		19
2.6	Seat Performance Standards		20
2.7	Head Injury Criteria		21
2.8	Spinal Injury		21
2.9	Femur Loading		22
3. IMPACT BIOMECHANICS		23
3.1	Injury Mechanisms		24
3.2	Impact Tolerance		25
3.2.1	Biomechanical Response		25
3.3	Factors Affecting Impact Tolerance		26
3.3.1	Physical Factors		26
3.3.2	Biological Factors		27
3.4	Secondary Impact		27
3.5	Accident Investigations		28

4.	EXPERIMENTAL MODELS IN IMPACT RESEARCH	..	29
4.1	Biological Models	29
4.1.1	The Volunteer	29
4.1.2	The Animal	30
4.1.3	The Cadaver	30
4.1.4	The Accident Victim	31
4.2	Mechanical Models	31
4.2.1	Anthropomorphic Test Dummies	31
4.3	Mathematical Models	35
4.4	Lumped Parameter Models	35
4.5	Distributed Parameter Models	35
4.6	Lumped and Distributed Parameter Models	36
4.7	Development of Lumped and Distributed Models	36
4.8	MADYMO	38
4.9	The MADYMO Crash Victim Simulation Program	38
4.10	MADYMO Model Development	39
4.11	Vehicle Data	39
4.12	Test Results	40
4.13	Component Test Description	40
4.13.1	Knee Bolster Force Deflection Characteristics	40
4.13.2	Seat Cushion Force Deflection Characteristics	40
4.13.3	Seatback Force Deflection Characteristics	41
4.13.4	Seat Friction Coefficient	41
4.13.5	The Floor Force Deflection Characteristics	41
4.13.6	The Belt Force Relative Elongation Characteristics	41
5.	HUMAN INJURY TOLERANCE TO IMPACT	42
5.1	Injury Criteria	43
5.1.1	Head Injury	43
5.2	Concussion	43
5.2.1	Rotational Acceleration	44
5.2.2	Translational Acceleration	44
5.3	Injury Criteria and Tolerance Level	44
5.3.1	Severity Index	44
5.3.2	Head Injury Criteria (HIC)	45
5.4	The Spine	46
5.5	Neck Injury	46
5.6	The Lumbar Spine	47
5.7	The Thorax	48
5.7.1	Thoracic Injuries	48
5.7.2	Thoracic Injury Criteria	49
5.7.3	Chest Deflection	49
5.7.4	Chest Accelerations	50
5.8	The Lower Extremities	50
5.8.1	Femoral Injury Tolerance	50
5.8.2	Tibial Injury Tolerance	54

5.8.3	Hip Joint Pelvis Tolerance	57
5.8.4	Ankle Joint Injury Tolerance	57
5.9	Human Tolerance To Lap Belt Impact Loading	58
6.	BRACE FOR IMPACT POSITIONS	61
6.1	Secondary Impacts	61
6.1.1	Civil Aeromedical Institute (CAMI) Tests	61
6.2	Forward Facing Passengers with Lap Belt Restraint	63
6.3	Rear Facing Passengers with Lap Belt Restraints	64
6.4	Forward Facing Passengers with Lap and Shoulder Harnesses	64
7.	SUMMARY OF RESEARCH OBJECTIVES	65
8.	SIMULATION OF THE KEGWORTH AIR ACCIDENT	66
8.1	The Accident	66
8.2	The Injuries	67
8.2.1	Head Injuries	68
8.2.2	Upper Limb Injuries	68
8.2.3	Neck and Spinal Injuries	68
8.2.4	Chest Injuries	69
8.2.5	Abdominal Injuries	69
8.2.6	Spinal Injuries	69
8.2.7	Pelvic and Lower Limb Injuries	69
8.3	Computer Simulations	70
8.3.1	KRASH Computer Simulation	70
8.3.2	MADYMO Computer Simulation	71
8.4	Data Acquisition	71
8.4.1	Seat Description	72
8.4.2	Seat Profile Measurements	72
8.4.3	Moment of Inertia of the Seat and Seatback	72
8.4.4	Seat Base and Seatback Stiffness Characteristics	72
8.4.5	Seat Front Bar Load Deflection Characteristics	73
8.4.6	Aircraft Floor Stiffness	73
8.5	Model Development	74
8.6	Parametric Configurations	76
8.6.1	Lap Belt Design	77
8.6.2	Folding Seatback Breakover Stiffness	77
8.6.3	Seat Pitch	77
8.6.4	Fixed Seatback Failure Stiffness	78
8.6.5	Seatback Local Stiffness	78
8.6.6	Seat Front Cushion Angle	78
8.6.7	Seat Base Stiffness	78
8.6.8	Lower Leg Position	78
8.6.9	Knee and Lower Leg (to Seat) Contact Stiffness	79
8.6.10	Knee Panel Position	79

8.7	Results	79
8.7.1	Brace Position Sensitivity Study			79
8.7.2	Upright Position Sensitivity Study			81
8.8	Discussion	84
8.8.1	Aircraft Environment	84
8.8.2	Modelling Limitations	85
8.9	Analysis	86
8.9.1	Brace Position Correlation	86
8.9.2	Facial Lacerations	86
8.9.3	Bruising Across Iliac Crest and Upper Thighs					86
8.9.4	Bruising of Right Knee		87
8.10	General	87
8.10.1	Brace Position Sensitivity Studies			87
8.10.2	Upright Position Models	88
8.10.3	Upright Position Sensitivity Studies			89
8.11	Comparison of the Brace and Upright Positions	..				90
8.12	Conclusions	91
8.13	Recommendations	92

9.	UPRIGHT SEATED OCCUPANTS IN ALTERNATIVE TYPES OF AIRCRAFT IMPACTS	101
9.1	Introduction	101
9.2	Occupant Percentile Configurations with Variations In Crash Pulses	101
9.3	Data Acquisition	102
9.3.1	Kegworth Pulse	102
9.3.2	NACA Pulse (Pulse 3)	102
9.3.3	14G Regulatory Pulse (Test 1 Pulse)	103
9.4	Model Development	103
9.5	Percentile Configurations	104
9.6	Results	104
9.7	Discussion	105
9.7.1	Kegworth Pulse	105
9.7.2	50th Percentile Male Seated in Both Seats	106
9.7.3	95th Percentile Male Seated in Both Seats	107
9.7.4	5th Percentile Female in Both Seats	107
9.7.5	95th Percentile Male in Rear Seat, 50th Percentile Male in Front Seat	107
9.7.6	5th Percentile Female in Rear Seat, 50th Percentile Male in Front Seat	108
9.7.7	5th Percentile Female in Both Seats, Lower Legs Vertical	108
9.7.8	NACA Pulse (Pulse 3)	108
9.7.9	14G Regulatory Pulse (Test 1 Pulse)	109
9.8	Conclusions	110
9.9	Recommendations	110

10. SIMULATION OF FORWARD FACING AND REARWARD FACING OCCUPANTS	113
10.1 Introduction	113
10.2 Development of A 3D Mathematical Model	114
10.2.1 Seat Profile And Dimensions	115
10.2.2 Seat Base, Seat Back And Arm Rest Stiffnesses	115
10.2.3 Seat Structure Deformation Characteristics ..	115
10.2.4 Mass And Inertia Of The Seat And Seat Back	115
10.2.5 Seat Belts	116
10.2.6 Crash Pulse	116
10.3 Model Development	116
10.4 Results	117
10.5 Discussion	118
10.5.1 Forward Facing Lap Belted Occupants ..	118
10.5.2 Forward Facing Three Point Belted Occupants	120
10.5.3 Rearward Facing Lap Belted Occupants ..	121
10.6 Conclusions	123
10.7 Recommendations	124
 11. BRACE POSITION CORRELATION WITH IMPACT TESTING AND PARAMETRIC STUDY	 127
11.1 Introduction	127
11.2 Objectives	127
11.3 Sled Test Facility	128
11.4 Dynamic Testing	128
11.4.1 Test Configuration	129
11.5 The Test Device	130
11.6 Test Data Acquisition	130
11.7 Signal Conditioning Instrumentation	131
11.7.1 Dash 16 Acquisition Board	132
11.7.2 Datalab Transient Recorder	132
11.7.3 DT-2821 Acquisition Board (Portax) ..	132
11.7.4 Track Computer And Software	132
11.7.5 Calibration	133
11.7.6 Dummy And Instrumentation	133
11.8 Test Procedure	133
11.9 Data Manipulation	134
11.9.1 Recording Channels 1-32	134
11.10 Sled Test Results	135
11.11 Conclusions	135
11.12 Mathematical Model Data Acquisition	135
11.12.1 Seat Stiffness	135
11.12.2 Lap Restraint Stiffness	136
11.13 Model Development	136
11.14 Parametric Assessment	136
11.14.1 Floor Friction	136

	11.14.2	Seat Pitch	137
	11.14.3	Occupant Lower Leg Angle	137
11.15	Additional Configurations	137
	11.15.1	Standard Bulkhead	137
	11.15.2	Nomex Bulkhead	137
	11.15.3	FAA 16G Crash Pulse	137
	11.15.4	Three Point Belt Restraint	138
	11.15.5	Rearward Facing Seat	138
11.16	Correlation	138
	11.16.1	Seats	139
	11.16.2	Belt Stiffness	139
	11.16.3	Seat Cushion Stiffness	139
	11.16.4	Seat Back Stiffness	140
	11.16.5	Front Seat Luggage Bar	140
	11.16.6	Femoral Separation	140
	11.16.7	High Speed Video Recording	140
11.17	Results	141
	11.17.1	Floor Friction	141
	11.17.2	Seat Pitch	143
	11.17.3	Lower Leg Angle	146
	11.17.4	General	149
11.18	Conclusions	153
	11.18.1	Changes In Floor Friction	153
	11.18.2	Changes In Seat Pitch	153
	11.18.3	Changes In Tibia Angle	155
	11.18.4	Changes In Configurations	156
11.19	Recommendations	158

12.	THE DEVELOPMENT OF A SPINE MODEL FOR THE EVALUATION OF THE BRACE CRASH POSITION	160
12.1	Introduction	160
12.2	Historical Review Of Spine Models	161
12.3	Modelling	162
	12.3.1 WSU Model	162
	12.3.2 Modelling Assumptions	163
12.4	Equations Of Motion	163
12.5	Geometrical Definition Of The Spine	167
	12.5.1 Mass And Moment Of Inertia Of Vertebral Body Segments	167
	12.5.2 Model Physical Constants	167
12.6	Model Validation	168
	12.6.1 Analysis Of The WSU Model	169
	12.6.2 Model Limitations	169
12.7	MADYMO Dataset For Spine Modelling	170
12.8	Results	171
	12.8.1 Base Configuration - Brace Position, Legs Forward, Arms Up	171

	12.8.2	Brace Position - Legs Forward, Arms Up	..	172			
	12.8.3	Brace Position - Legs Back, Arms Down	..	172			
	12.8.4	Brace Position - Legs Forward, Arms Down	..	172			
	12.8.5	Comparison Of The Brace Position With Legs Back And Legs Forward, With Arms Up	..	173			
	12.8.6	Comparison Of The Brace Position With Legs Back And Legs Forward, With Arms Down	..	173			
	12.8.7	Comparison Of The Brace Position With The Arms Up Versus Arms Down With The Lower Legs Positioned Rearward Of The Vertical	..	174			
	12.9	Conclusions	175			
	12.10	Recommendations	176			
CONCLUSIONS	178
RECOMMENDATIONS	186
REFERENCES	190
TABLES	204
FIGURES	228
APPENDIX 1	394
APPENDIX 2	395
APPENDIX 3	397
APPENDIX 4	411
APPENDIX 5	415
APPENDIX 6	420
APPENDIX 7	424
APPENDIX 8	426

LIST OF TABLES

Table 1	FMVSS 208 And AS 8049 Injury Criteria	33
Table 2	Abbreviated Injury Scale Classification	42
Table 3	Spinal Bending Moment Injury Thresholds	48
Table 4	Spinal Load Injury Thresholds	48
Table 5	Recommended Sternal Deflection Limits	49
Table 6	Peak Static Femoral Bending Moment (Weber) Lateral Femoral Bending Moment and Torsional Femoral Moment (Messerer)	51
Table 7	Peak Static Axial Compressive Femoral Load (Messerer)	51
Table 8	Peak Static Bending Moment and Fracture Loads for Wet Femurs (Yamada)	52
Table 9	Peak Dynamic Torsional Femoral Moment (Martens) ..	53
Table 10	Peak Static Tibial Bending Moment (Weber), Lateral Tibial Bending Moment and Torsional Tibial Moment (Messerer)	55
Table 11	Peak Static Axial Compressive Tibial Load (Messerer)	55
Table 12	Peak Static Bending Moment and Fracture Loads for Wet Tibias (Yamada)	56
Table 13	Peak Dynamic Torsional Tibial Moment (Martens) ..	56
Table 14	Frangible Leg Bone Design Criteria (St. Laurent) ..	57
Table 15	Brace Position Sensitivity Study	205
Table 16	Upright Position Sensitivity Study	206
Table 17	Comparison of the Brace and Upright Positions ..	207
Table 18	Occupant Percentile Configurations	208
Table 19	Comparison of the Forward Facing Lap Belted, Three Point Belted and Rearward Facing Occupants ..	209
Table 20	Test Device Measurement Variables	210
Table 21	Description of the Recording Channels	211
Table 22	Instrumentation	212
Table 23	Recording Channels	213
Table 24	Sled test Results	214
Table 25	Comparison of the Test Results and Computer Predictions	215
Table 26	Floor Friction Parametric Study	216
Table 27	Seat Pitch Parametric Study	217
Table 28	Tibia Angle from Vertical	218
Table 29	Aircraft Interiors Alternative Test Configurations ..	219
Table 30	Ankle Joints Bending Moments	220
Table 31	Description of Loads and Bending Moments in Spine Model	166
Table 32	Dimensions of Vertebral Bodies	221

Table 33	Orientations of Vertebral Bodies with Respect to Local Co-ordinate System	222
Table 34	Spine Model Physical Characteristics	223
Table 35	External Body Segments to Spine	224
Table 36	Mass and Moment of Inertia of Body Segments	225
Table 37	Geometrical Definitions of Body Segments	226
Table 38	Spinal Column Peak Results	227

LIST OF FIGURES

Figure 1	Seat Dynamic Test Specifications (Aerospace Standard 8049)	20
Figure 2	G-OBME Impact Sequence	66
Figure 2a	Seating Layout Aboard G-OBME	66
Figure 2b	Distribution of Survivors and Fatalities Aboard G-OBME	67
Figure 2c	Calculated Crash Pulse of Aircraft G-OBME	67
Figure 3	Injuries In Patients Surviving The M1 Aircraft Crash	68
Figure 4	Brace Position Simulation - Rear Occupant Legs Back	229
Figure 5	Brace Position Legs Back Simulation - 550ms to 950ms Sequential Plot	230
Figure 6	Brace Position Legs Back Simulation - 1000ms to 1400ms Sequential Plot	231
Figure 7	Brace Position - HIC, Head and Thorax Acceleration versus Belt Stiffness	232
Figure 8	Brace Position - Pelvis, Femur Axial and Vertical Loads versus Belt Stiffness	232
Figure 9	Brace Position - Lap Belt Load versus Belt Stiffness	233
Figure 10	Brace Position - HIC, Head and Thorax Accelerations versus Seatback Breakover Stiffness	233
Figure 11	Brace Position - Pelvis, Femur Axial and Vertical Loads versus Seatback Breakover Stiffness	234
Figure 12	Brace Position - Lap Belt Load versus Seatback Breakover Stiffness	234
Figure 13	Brace Position - HIC, Head and Thorax Accelerations versus Seat Pitch	235
Figure 14	Brace Position - Pelvis, Femur Axial and Vertical Loads versus Seat Pitch	235
Figure 15	Brace Position - Lap Belt Load versus Seat Pitch	236
Figure 16	Brace Position - HIC, Head and Thorax Accelerations versus Nonbreakover Seatback Stiffness	236
Figure 17	Brace Position - Pelvis, Femur Axial and Vertical Loads versus Nonbreakover Seatback Stiffness	237
Figure 18	Brace Position - Lap Belt Load versus Nonbreakover Seatback Stiffness	237
Figure 19	Brace Position - HIC, Head and Thorax Accelerations versus Front Seat Cushion Angle	238
Figure 20	Brace Position - Pelvis, Femur Axial and Vertical Loads versus Front Seat Cushion Angle	238
Figure 21	Brace Position - Lap Belt Load versus Seat Front Cushion Angle	239
Figure 22	Brace Position - HIC, Head and Thorax Accelerations versus Seat Base Stiffness	239
Figure 23	Brace Position - Pelvis, Femur Axial and Vertical Loads versus Seat Base Stiffness	240

Figure 24	Brace Position - Lap Belt Load versus Seat Base Stiffness	240
Figure 25	Brace Position Simulation - Rear Occupant Legs Forward	241
Figure 26	Brace Position Legs Forward Simulation - 550ms to 950ms Sequential Plot	242
Figure 27	Brace Position Legs Forward Simulation - 1000ms to 1400ms Sequential Plot	243
Figure 28	Upright Position Simulation	244
Figure 29	Upright Position Simulation - 550ms to 950ms Sequential Plot	245
Figure 30	Upright Position Simulation - 1000ms to 1400ms Sequential Plot	246
Figure 31	Upright Position - HIC, Head and Thorax Accelerations versus Belt Stiffness	247
Figure 32	Upright Position - Pelvis, Femur Axial and Vertical Loads versus Belt Stiffness	247
Figure 33	Upright Position - Tibial and Foot Contact Loads versus Belt Stiffness	248
Figure 34	Upright Position - Lap Belt Load Versus Belt Stiffness	248
Figure 35	Upright Position - HIC, Head and Thorax Accelerations versus Seatback Breakover Stiffness	249
Figure 36	Upright Position - Pelvis, Femur Axial and Vertical Loads versus Seatback Breakover Stiffness	249
Figure 37	Upright Position - Tibial and Foot Contact Loads versus Seatback Breakover Stiffness	250
Figure 38	Upright Position - Lap Belt Load versus Seatback Breakover Stiffness	250
Figure 39	Upright Position - HIC, Head and Thorax Accelerations versus Seat Pitch	251
Figure 40	Upright Position - Pelvis, Femur Axial and Vertical Loads versus Seat Pitch	251
Figure 41	Upright Position - Tibia and Foot Contact Loads versus Seat Pitch	252
Figure 42	Upright Position - Lap Belt Load versus Seat Pitch	252
Figure 43	Upright Position - HIC, Head and Thorax Accelerations versus Nonbreakover Seatback Stiffness.. .. .	253
Figure 44	Upright Position - Pelvis, Femur Axial and Vertical Loads versus Nonbreakover Seatback Stiffness	253
Figure 45	Upright Position - Tibia and Foot Contact loads versus Nonbreakover Seatback Stiffness	254
Figure 46	Upright Position - Lap Belt Load versus Nonbreakover Seatback Stiffness	254
Figure 47	Upright Position - HIC, Head and Thorax Accelerations versus Seat Front Cushion Angle	255

Figure 48	Upright Position - Pelvis, Femur Axial and Vertical Loads versus Seat Front Cushion Angle ..	255
Figure 49	Upright Position - Tibia and Foot Contact Loads versus Seat Front Cushion Angle	256
Figure 50	Upright Position - Lap Belt Load versus Seat Front Cushion Angle	256
Figure 51	Upright Position - HIC, Head and Thorax Acceleration versus Seat Base Stiffness	257
Figure 52	Upright Position - Pelvis, Femur Axial and Vertical Loads versus Seat Base Stiffness	257
Figure 53	Upright Position - Tibia and Foot Contact Loads versus Seat Base Stiffness	258
Figure 54	Upright Position - Lap Belt Load versus Seat Base Stiffness	258
Figure 55	Upright Position - HIC, Head and Thorax Acceleration versus Knee Bolster Stiffness	259
Figure 56	Upright Position - Pelvis, Femur Axial and Vertical Loads versus Knee Bolster Stiffness	259
Figure 57	Upright Position - Tibia and Foot Contact Loads versus Knee Bolster Stiffness	260
Figure 58	Upright Position - Lap Belt Load versus Knee Bolster Stiffness	260
Figure 59	Upright Position - HIC, Head and Thorax Accelerations versus Knee Bolster Location	261
Figure 60	Upright Position - Pelvis, Femur Axial and Vertical Loads versus Knee Bolster Location	261
Figure 61	Upright Position - Tibia and Foot Contact Loads versus Knee Bolster Location	262
Figure 62	Upright Position - Lap Belt Load versus Knee Bolster Location	262
Figure 63	Comparison of the Brace and Upright Positions - HIC, Head and Thorax Accelerations versus Posture ..	263
Figure 64	Comparison of the Brace and Upright Positions - Pelvis, Femur Axial and Vertical Loads versus Posture	263
Figure 65	Comparison of the Brace and Upright Positions - Tibia and Foot Contact Loads versus Posture ..	264
Figure 66	Comparison of the Brace and Upright Positions - Lap Belt Load versus Posture	264
Figure 67	50th Percentile Male Occupants Both Seats - Kegworth Pulse	265
Figure 68	50th Percentile Male Occupants Both Seats - Kegworth Pulse 600ms to 1000ms Sequential Plot ..	266
Figure 69	95th Percentile Male Occupants Both Seats - Kegworth Pulse	267

Figure 70	95th Percentile Male Occupants Both Seats - Kegworth Pulse 600ms to 1000ms Sequential Plot ..	268
Figure 71	5th Percentile Female Occupants Both Seats - Kegworth Pulse	269
Figure 72	5th Percentile Female Occupants Both Seats - Kegworth Pulse 600ms to 1000ms Sequential Plot ..	270
Figure 73	95th Percentile Rear Occupant, 50th Percentile Front Occupant - Kegworth Pulse	271
Figure 74	95th Percentile Rear Occupant, 50th Percentile Front Occupant - Kegworth Pulse 600ms to 1000ms Sequential Plot ..	272
Figure 75	5th Percentile Rear Occupant, 50th Percentile Front Occupant - Kegworth Pulse	273
Figure 76	5th Percentile Rear Occupant, 50th Percentile Front Occupant - Kegworth Pulse 600ms to 1000ms Sequential Plot ..	274
Figure 77	5th Percentile Female Occupants - Lower Legs Vertical - Kegworth Pulse	275
Figure 78	5th Percentile Female Occupants - Lower Legs Vertical - Kegworth Pulse 600ms to 1000ms Sequential Plot ..	276
Figure 79	Upright Occupants, Kegworth Pulse - HIC, Head and Thorax Accelerations versus Percentile Configurations	277
Figure 80	Upright Occupants, Kegworth Pulse - Lumbar Spine and Belt Loads versus Percentile Configurations ..	277
Figure 81	Upright Occupants, Kegworth Pulse - Femur Axial and Vertical Loads versus Percentile Configurations ..	278
Figure 82	Upright Occupants, Kegworth Pulse - Femur Bending Moment versus Percentile Configurations	278
Figure 83	Upright Occupants, Kegworth Pulse - Tibia to Seat, Heel to Floor, Foot to Seat Contact Loads versus Percentile Configurations	279
Figure 84	50th Percentile Male Occupants Both Seats - NACA Pulse	280
Figure 85	50th Percentile Male Occupants Both Seats - NACA Pulse 80ms to 240ms Sequential Plot	281
Figure 86	95th Percentile Male Occupants Both Seats - NACA Pulse	282
Figure 87	95th Percentile Male Occupants Both Seats - NACA Pulse 80ms to 240ms Sequential Plot	283
Figure 88	5th Percentile Female Occupants Both Seats - NACA Pulse	284
Figure 89	5th Percentile Female Occupants Both Seats - NACA Pulse 80ms to 240ms Sequential Plot	285
Figure 90	95th Percentile Rear Occupant, 50th Percentile Front Occupant - NACA Pulse	286
Figure 91	95th Percentile Rear Occupant, 50th Percentile Front Occupant - NACA Pulse 150ms to 230ms Sequential Plot	287
Figure 92	5th Percentile Rear Occupant, 50th Percentile Front Occupant - NACA Pulse	288

Figure 93	5th Percentile Rear Occupant, 50th Percentile Front Occupant - NACA Pulse 80ms to 240ms Sequential Plot	289
Figure 94	Upright Occupants, NACA Pulse - HIC, Head and Thorax Accelerations versus Percentile Configurations..	290
Figure 95	Upright Occupants, NACA Pulse - Lumbar Spine and Belt Loads versus Percentile Configurations ..	290
Figure 96	Upright Occupants, NACA Pulse - Femur Axial and Vertical Loads versus Percentile Configurations ..	291
Figure 97	Upright Occupants, NACA Pulse - Femur Bending Moment versus Percentile Configurations ..	291
Figure 98	Upright Occupants, NACA Pulse - Tibia to Seat, Heel to Floor, Foot to Seat Contact Loads versus Percentile Configurations	292
Figure 99	50th Percentile Male Occupants Both Seats - 14G Test Pulse	293
Figure 100	50th Percentile Male Occupants Both Seats - 14G Test Pulse 160ms to 240ms Sequential Plot ..	294
Figure 101	95th Percentile Male Occupants Both Seats - 14G Test Pulse	295
Figure 102	95th Percentile Male Occupants Both Seats - 14G Test Pulse 160ms to 240ms Sequential Plot ..	296
Figure 103	5th Percentile Female Occupants Both Seats - 14G Test Pulse	297
Figure 104	5th Percentile Female Occupants Both Seats - 14G Test Pulse 160ms to 240ms Sequential Plot ..	298
Figure 105	95th Percentile Rear Occupant, 50th Percentile Front Occupant - 14G Test Pulse	299
Figure 106	95th Percentile Rear Occupant, 50th Percentile Front Occupant - 14G Test Pulse 160ms to 240ms Sequential Plot	300
Figure 107	5th Percentile Rear Occupant, 50th Percentile Front Occupant - 14G Test Pulse	301
Figure 108	5th Percentile Rear Occupant, 50th Percentile Front Occupant - 14G Test Pulse 160ms to 240ms Sequential Plot	302
Figure 109	Upright Occupants, 14G Test Pulse - HIC, Head and Thorax Accelerations versus Percentile Configurations	303
Figure 110	Upright Occupants, 14G Test Pulse - Lumbar Spine and Belt Loads versus Percentile Configurations ..	303
Figure 111	Upright Occupants, 14G Test Pulse - Femur Axial and Vertical Loads versus Percentile Configurations ..	304
Figure 112	Upright Occupants, 14G Test Pulse - Femur Bending Moment versus Percentile Configurations ..	304
Figure 113	Upright Occupants, 14G Test Pulse - Tibia to Seat, Heel to Floor, Foot to Seat Contact Loads versus Percentile Configurations	305
Figure 114	Forward Facing Lap Belted Occupants - at 0ms, using NACA Pulse	306
Figure 115	Forward Facing Lap Belted Occupants - at 120ms using NACA Pulse	307

Figure 116	Forward Facing Lap Belted Occupants - at 165ms, using NACA Pulse	308
Figure 117	Forward Facing Three Point Belted Occupants - at 0ms, using NACA Pulse	309
Figure 118	Forward Facing Three Point Belted Occupants - at 220ms, using NACA Pulse	310
Figure 119	Forward Facing Three Point Belted Occupants - at 340ms, using NACA Pulse	311
Figure 120	Rearward Facing Lap Belted Occupant - at 0ms, using NACA Pulse	312
Figure 121	Rearward Facing Lap Belted Occupant - at 225ms, using NACA Pulse	313
Figure 122	Rearward Facing Lap Belted Occupant - at 345ms, using NACA Pulse	314
Figure 123	Seating Configurations with NACA Pulse - HIC, Head and Thorax Accelerations versus Various Restraints ..	315
Figure 124	Seating Configurations with NACA Pulse - Lumbar Spine Resultant and Longitudinal Loads versus Various Restraints	315
Figure 125	Seating Configurations with NACA Pulse - Left Femur Axial, Vertical Load and Bending Moment versus Various Restraints	316
Figure 126	Seating Configurations with NACA Pulse - Right Femur Axial, Vertical Load and Bending Moment versus Various Restraints	316
Figure 127	Seating Configurations with NACA Pulse - Left and Right Foot to Floor Contact Loads versus Various Restraints	317
Figure 128	Seating Configurations with NACA Pulse - Lap Belt Load versus Various Restraints	317
Figure 129	Seating Configurations with NACA Pulse - Front Left and Right Seat Attachment Loads versus Various Restraints	318
Figure 130	Seating Configurations with NACA Pulse - Rear Left and Right Seat Attachment Loads versus Various Restraints	318
Figure 131	Comparison Of The Sled Pulse Against The FAA 16G Pulse	127
Figure 132	Decelerator Track	128
Figure 133	Arrestor Gear	128
Figure 134	Conventions of Translational Accelerations	129
Figure 135	Decelerator Track Data Acquisition System	131
Figure 136	Braced Legs Back Configuration, 32" Seat Pitch ..	133
Figure 137	Sled Yawed 10° To The Right	133
Figure 138a	Sled Test 3672, 0 To 30ms	135
Figure 138b	Sled Test 3672, 40 To 70ms	135
Figure 138c	Sled Test 3672, 80 To 110ms	135
Figure 138d	Sled Test 3672, 120 To 150ms	135

Figure 139a	Sled Test 3673, 0 To 30ms	135
Figure 139b	Sled Test 3673, 40 To 70ms	135
Figure 139c	Sled Test 3673, 80 To 110ms	135
Figure 139d	Sled Test 3673, 120 To 150ms	135
Figure 140	Rear Dummy Lower Legs Inclined 11.5° Rearward Of The Vertical	136
Figure 141	Seat Offset	139
Figure 142	Post Impact, Left Leg Slide	140
Figure 143	Brace Position Correlation Study, Baseline Configuration	319
Figure 144	Brace Position Correlation Study, 80ms To 240ms Sequential Plot	320
Figure 145	Brace Position, Foot To Floor Friction 0.55	321
Figure 146	Brace Position, Foot To Floor Friction 0.70	322
Figure 147	Brace Position Parametric Study - HIC and Head Resultant Accelerations versus Floor Friction Coefficient	323
Figure 148	Brace Position Parametric Study - Thorax Resultant Accelerations versus Floor Friction Coefficient	323
Figure 149	Brace Position Parametric Study - Pelvis Resultant Accelerations versus Floor Friction Coefficient	324
Figure 150	Brace Position Parametric Study - Lap Belt Load versus Floor Friction Coefficient	324
Figure 151	Brace Position Parametric Study - Left and Right Femur Shear Loads versus Floor Friction Coefficient	325
Figure 152	Brace Position Parametric Study - Left and Right Femur Axial Loads versus Floor Friction Coefficient	325
Figure 153	Brace Position Parametric Study - Left and Right Femur Bending Moments versus Floor Friction Coefficient	326
Figure 154	Brace Position Parametric Study - Left and Right Tibia Shear Loads versus Floor Friction Coefficient	326
Figure 155	Brace Position Parametric Study - Left and Right Tibia Lateral Loads versus Floor Friction Coefficient	327
Figure 156	Brace Position Parametric Study - Left and Right Tibia Vertical Loads versus Floor Friction Coefficient..	327
Figure 157	Brace Position Parametric Study - Lumbar Spine Vertical Loads versus Floor Friction Coefficient	328
Figure 158	Brace Position Parametric Study - 27 Inch Seat Pitch At 0ms	329
Figure 159	Brace Position Parametric Study - 27 Inch Seat Pitch At 80ms To 240ms	330
Figure 160	Brace Position Parametric Study - 30 Inch Seat Pitch At 0ms	331
Figure 161	Brace Position Parametric Study - 30 Inch Seat Pitch At 80ms To 240ms	332
Figure 162	Brace Position Parametric Study - 34 Inch Seat Pitch At 0ms	333

Figure 163	Brace Position Parametric Study - 34 Inch Seat Pitch At 80ms To 240ms	334
Figure 164	Brace Position Parametric Study - 36 Inch Seat Pitch At 0ms	335
Figure 165	Brace Position Parametric Study - 36 Inch Seat Pitch At 80ms To 240ms	336
Figure 166	Brace Position Parametric Study - HIC and Head Resultant Accelerations versus Seat Pitch	337
Figure 167	Brace Position Parametric Study - Thorax Resultant Accelerations versus Seat Pitch	337
Figure 168	Brace Position Parametric Study - Pelvis Resultant Accelerations versus Seat Pitch	338
Figure 169	Brace Position Parametric Study - Lap Belt Load versus Seat Pitch	338
Figure 170	Brace Position Parametric Study - Left and Right Femur Shear Loads versus Seat Pitch	339
Figure 171	Brace Position Parametric Study - Left and Right Femur Axial Loads versus Seat Pitch	339
Figure 172	Brace Position Parametric Study - Left and Right Femur Bending Moments versus Seat Pitch	340
Figure 173	Brace Position Parametric Study - Left and Right Tibia Shear Loads versus Seat Pitch	340
Figure 174	Brace Position Parametric Study - Left and Right Tibia Lateral Loads versus Seat Pitch	341
Figure 175	Brace Position Parametric Study - Left and Right Tibia Vertical Loads versus Seat Pitch	341
Figure 176	Brace Position Parametric Study - Lumbar Spine Vertical Loads versus Seat Pitch	342
Figure 177	Brace Position Parametric Study - Leg Angle 6.5° Rearward of the Vertical At 0ms	343
Figure 178	Brace Position Parametric Study - Leg Angle 6.5° Rearward of the Vertical At 80ms To 240ms	344
Figure 179	Brace Position Parametric Study - Leg Angle 1.5° Rearward of the Vertical At 0ms	345
Figure 180	Brace Position Parametric Study - Leg Angle 1.5° Rearward of the Vertical At 80ms To 240ms	346
Figure 181	Brace Position Parametric Study - Leg Angle 3.5° Forward of the Vertical At 0ms	347
Figure 182	Brace Position Parametric Study - Leg Angle 3.5° Forward of the Vertical At 80ms To 240ms	348
Figure 183	Brace Position Parametric Study - Leg Angle 8.5° Forward of the Vertical At 0ms	349
Figure 184	Brace Position Parametric Study - Leg Angle 8.5° Forward of the Vertical At 80ms To 240ms	350
Figure 185	Brace Position Parametric Study - HIC and Head Resultant Accelerations versus Tibia Angle	351
Figure 186	Brace Position Parametric Study - Thorax Resultant Accelerations versus Tibia Angle	351

Figure 187	Brace Position Parametric Study - Pelvis Resultant Accelerations versus Tibia Angle	352
Figure 188	Brace Position Parametric Study - Lap Belt Loads versus Tibia Angle	352
Figure 189	Brace Position Parametric Study - Left and Right Femur Shear Loads versus Tibia Angle ..	353
Figure 190	Brace Position Parametric Study - Left and Right Femur Axial Loads versus Tibia Angle ..	353
Figure 191	Brace Position Parametric Study - Left and Right Femur Bending Moments versus Tibia Angle ..	354
Figure 192	Brace Position Parametric Study - Left and Right Tibia Shear Loads versus Tibia Angle ..	354
Figure 193	Brace Position Parametric Study - Left and Right Tibia Lateral Loads versus Tibia Angle ..	355
Figure 194	Brace Position Parametric Study - Left and Right Tibia Vertical Loads versus Tibia Angle ..	355
Figure 195	Brace Position Parametric Study - Lumbar Spine Vertical Loads versus Tibia Angle ..	356
Figure 196	Brace Position Parametric Study - Bulkhead Simulation At 0ms	357
Figure 197	Brace Position Parametric Study - Bulkhead Simulation At 40ms To 200ms	358
Figure 198	Brace Position Parametric Study - Nomex Bulkhead Simulation At 0ms	359
Figure 199	Brace Position Parametric Study - Nomex Bulkhead Simulation At 80ms To 240ms ..	360
Figure 200	Brace Position Parametric Study - 16G FAA Test Pulse At 0ms	361
Figure 201	Brace Position Parametric Study - 16G FAA Test Pulse At 60ms To 220ms	362
Figure 202	Three Point Belt Occupant Simulation At 0ms ..	363
Figure 203	Three Point Belt Occupant Simulation At 80ms To 240ms	364
Figure 204	Rear Facing Seat Simulation At 0ms	365
Figure 205	Rear Facing Seat Simulation At 80ms To 240ms ..	366
Figure 206	Brace Position Parametric Study - HIC and Head Resultant Accelerations versus Alternative Configurations	367
Figure 207	Brace Position Parametric Study - Thorax Resultant Accelerations versus Alternative Configurations ..	367
Figure 208	Brace Position Parametric Study - Pelvis Resultant Accelerations versus Alternative Configurations ..	368
Figure 209	Brace Position Parametric Study - Lap Belt Loads versus Alternative Configurations	368
Figure 210	Brace Position Parametric Study - Left and Right Femur Shear Loads versus Alternative Configurations ..	369
Figure 211	Brace Position Parametric Study - Left and Right Femur Axial Loads versus Alternative Configurations ..	369

Figure 212	Brace Position Parametric Study - Left and Right Femur Bending Moments versus Alternative Configurations	370
Figure 213	Brace Position Parametric Study - Left and Right Tibia Bending Moments versus Alternative Configurations	370
Figure 214	Brace Position Parametric Study - Left and Right Tibia Lateral Loads versus Alternative Configurations..	371
Figure 215	Brace Position Parametric Study - Left and Right Tibia Vertical Loads versus Alternative Configurations ..	371
Figure 216	Brace Position Parametric Study - Lumbar Spine Vertical Loads versus Alternative Configurations ..	372
Figure 217	Wayne State University Spine Model At 0ms	373
Figure 218	Configuration of Two Successive Vertebrae	374
Figure 219	Free Body Diagram Of Vertebral Body	375
Figure 220	Spine Model with Full Harness Undergoing Ejection for a Period of 200ms	376
Figure 221	Spine Model with Lap Belt Only Undergoing 16G Test Pulse	377
Figure 222	Dataset for Spine Modelling	378
Figure 223	Spine Model Kinematics with Legs Forward at 140ms..	379
Figure 224	Brace Position - Rear Occupant Legs Back, Arms Up at 0ms	380
Figure 225	Brace Position Simulation - Rear Occupant Legs Back, Arms Up At 100ms To 180ms	381
Figure 226	Brace Position - Rear Occupant Legs Forward, Arms Up At 0ms	382
Figure 227	Brace Position Simulation - Rear Occupant Legs Forward, Arms Up At 100ms to 180ms.. ..	383
Figure 228	Brace Position - Rear Occupant Legs Back, Arms Down At 0ms	384
Figure 229	Brace Position Simulation - Rear Occupant Legs Back, Arms Down At 100ms To 180ms	385
Figure 230	Brace Position - Rear Occupant Legs Forward, Arms Down At 0ms	386
Figure 231	Brace Position Simulation - Rear Occupant Legs Forward, Arms Down At 100ms To 180ms	387
Figure 232	Brace Position - Comparison of Peak Axial Loads in Vertebrae for Legs Back and Legs Forward with the Arms Up	388
Figure 233	Brace Position - Comparison of Peak Shear Loads in Vertebrae for Legs Back and Legs Forward with the Arms Up	388
Figure 234	Brace Position - Comparison of Peak Extension Moments in Vertebrae for Legs Back and Legs Forward with the Arms Up	389

Figure 235	Brace Position - Comparison of Peak Axial Loads in Vertebrae for Legs Back and Legs Forward with the Arms Down	389
Figure 236	Brace Position - Comparison of Peak Shear Loads in Vertebrae for Legs Back and Legs Forward with the Arms Down	390
Figure 237	Brace Position - Comparison of Peak Extension Moments in Vertebrae for Legs Back and Legs Forward with the Arms Down	390
Figure 238	Brace Position - Comparison of Peak Axial Loads in Vertebrae for Arms Down and Arms Up with the Legs Back	391
Figure 239	Brace Position - Comparison of Peak Shear Loads in Vertebrae for Arms Down and Arms Up with the Legs Back	391
Figure 240	Brace Position - Comparison of Peak Extension Moments in Vertebrae for Arms Down and Arms Up with the Legs Back	392
Figure 241	Recommended Brace Position	186

ABSTRACT

The crash of the Boeing 737-400 G-OBME at Kegworth on the 8th January 1989 provided an opportunity to investigate how the passengers were injured during the crash. A computer simulation was subsequently set up to assess the kinematics of the passengers and to establish the likely forces which they would have experienced during the crash.

Two computer models were created using the crash victim simulation program, MADYMO. The models were used to study the brace and upright positions and to establish any correlation with body injuries and forces predicted by the models. A parametric study was, subsequently, undertaken with the objective of improving seat design.

Further studies were undertaken to evaluate the effects of body posture and impact pulses upon 5th percentile female, 50th percentile male and 95th percentile male occupants. The objective of the research was to establish the severity of injuries for various occupant statures when seated in accordance with the dynamic seat requirements of Aerospace Standard 8049. The research was used to establish the loads sustained on the head, thorax, lumbar spine, pelvis and lower limbs.

A three dimensional computer model was created with the objective of studying the effect of lateral acceleration components as specified in Aerospace Standard 8049. Furthermore, the model was used to establish the injuries which might be sustained in other types of aircraft accidents. Using the data of the same aircraft, this was further utilised to investigate different seat orientations and restraint systems.

Finally, a spine model was created which examined the detailed loading of the spine using the 16G dynamic test pulse. This showed that the spine of a lap belted occupant is heavily loaded during the impact. Thus, the computer modelling of the brace for impact position led to the recommendation for a new improved brace position which could reduce the likelihood of lower limb flail. In addition, it has been found not to increase spinal loading.

ACKNOWLEDGEMENTS

This research would not have been completed without the help of the following individuals:-

I am extremely grateful for the help and guidance of Dr Colin J.H. Fox and Professor W. Angus Wallace who acted as my supervisors during the preparation and writing of this thesis.

I am indebted to Mr Peter Brownson (Department of Orthopaedic and Accident Surgery, University Hospital, Nottingham) who helped me to perform the impact testing.

I am also indebted to the NLDB team and particularly Mr John M. Rowles who gathered the injury data from the M1 Kegworth Air Crash.

I am grateful to Dr David Parsons and Mr Nigel Rock (HW Structures Ltd, Royal Leamington Spa) for allowing me to use the company's facilities for undertaking this research and to Mr David Green (HW Structures Ltd, Royal Leamington Spa) for his assistance in carrying out the component testing.

Dr Albert I. King and Dr P C Begeman of Wayne State University, Detroit, Michigan kindly provided me with the ejection seat spine model data.

A special thanks must go to the Institute of Aviation Medicine of the Royal Air Force, Farnborough who allowed Mr Brownson and myself to carry out the necessary impact testing and to Wing Commander David Anton for allowing us to use the facility. I am also indebted to Mr Les Neil and Mr Gavin Hall for their practical help in the setting up of the sled facility and to Surgeon Commander Peter J. Waugh for his assistance with acquisition and processing of the data.

This research was funded by the Civil Aviation Authority and HW Structures Limited.

Last but not least, my deepest and wholehearted thanks must go to the love of my life, Mary, for her continual assistance and support in completing the thesis. And finally, I thank my two lovely boys John and Christopher aged 4 and 2 years, respectively, who have helped me prolong the writing of the thesis.

DECLARATION

I declare that I am responsible for the planning and implementation of the work contained in this manuscript with the following exceptions:-

The static component testing of the seats was carried out by Mr David Green under my supervision.

The impact testing was carried out with the aid of Mr Peter Brownson, Mr Les Neil and Mr Gavin Hall.

The ejection seat spine model data was provided by Dr Albert I. King and Dr P.C. Begeman of Wayne State University, Detroit, Michigan.

All the research was carried whilst I was employed by HW Structures Ltd. of Royal Leamington Spa. The research was carried out on a part-time basis.

SUMMARY

Aim of the Research

The evaluation of the crash position in passenger aircraft using computer simulation.

Method

The computer simulation of the Kegworth Air Crash was undertaken to determine the kinematics and forces sustained by the passengers of the Boeing 737-400. The Kegworth study examined two seating postures which were adopted by the passengers of G-OBME. These were of a brace and an upright position. The work was extended to assess, in more detail, the forces sustained by various body segments. This piece of research was divided into two sections:-

1. Impact Testing
2. Computer Simulation

The impact testing was carried out to correlate the computer model. This was undertaken using the decelerator track facility at the RAF Institute of Aviation Medicine. A braced 50th percentile Hybrid III anthropomorphic dummy was used which was propelled on Weber 4001 seats at an acceleration of 16G. The test was set up in accordance with Aerospace Standard 8049.

A detailed three dimensional computer model was constructed which was identical to the test configuration using two triple row seats located at 32 inch pitch. Two braced 50th percentile Hybrid III dummy datasets were positioned on the two rows of seats and correlated to the sled test. On correlating the model, a detailed parametric study was undertaken which examined additional seating configurations.

The research was extended to address the detailed loading imposed on the spine, since it was discovered that on adopting a brace position the spine may be heavily loaded during impact. A detailed spine model was created. This was incorporated into the existing correlated model to determine the load path within the spinal column.

ABBREVIATIONS

Text

AAIB	Air Accidents Investigation Branch
ACIR	Automobile Crash Injury Research
AvCIR	Aviation Crash Injury Research
AFAMRL	Air Force Aerospace Medical Research Laboratory
AIA	Aerospace Industries Association
Ar	Resultant Acceleration
AS	Aerospace Standard
Ax	Acceleration along x-axis (Horizontal Plane)
Ay	Acceleration Along Y-axis (Lateral Plane)
Az	Acceleration Along Z-axis (Vertical Plane)
ATA	Air Transport Association
ATB	Articulated Total Body program
ATD	Anthropomorphic Test Device
C	Cervical
CAA	Civil Aviation Authority
CAMI	Civil Aeromedical Institute
CAL3D	Calspan Three dimensional Computer Model
CAR	Civil Aviation Regulation
CFR	Code of Federal Regulation
CG	Centre of Gravity
CID	Controlled Impact Demonstration
CRUSH	Crash Reproduction Using Static History
CVS	Crash Victim Simulator
DASH16	DASH 16 Data Acquisition Board
DL	Datalab
DRI	Dynamic Response Index
DSM	Dataset for Spinal Modelling
E	Exponential term
FAA	Federal Aviation Authority
FEA	Finite Element Analysis
FMVSS	Federal Motor Vehicle Safety Standard
FSD	Full Scale Deflection
Fx	Force along x-axis
Fy	Force along Y-axis
Fz	Force along Z-axis
G	Gravitational Acceleration
GASP	General Aviation Safety Panel
G-OBME	Call sign of the Boeing 737-400 which crashed
GM	General Motors
Gx	Gravitational Acceleration along x-axis
Gy	Gravitational Acceleration Along y-axis
Gz	Gravitational Acceleration Along z-axis

HIC	Head Injury Criteria
IAM	Institute of Aviation Medicine
K	Kilobyte
kg	Kilogram
kg/m ²	Kilograms per Metre Squared
kN	Kilonewton
L	Lumbar
m	Metre
mm	Millimetre
ms	Millisecond
m/s	Metre per Second
m/s ²	Metre per Second Squared
mV	Millivolt
MADYMO	Mathematical Dynamic Model
MATD	Motorcycle Anthropomorphic Test Dummy
Mx	Moment about x-axis
My	Moment about y-axis
Mz	Moment about z-axis
MN/m ²	Mega Newtons per Metre Squared
MVMA	Motor Vehicle Manufacturers Association
N	Newton
N/A	Not Available
NAC 200	High Speed Video Camera
NACA	National Advisory Committee for Aeronautics
NAS	North American Specification
NASA	National Aeronautics and Space Administration
NHTSA	National Highway Traffic Safety Administration
NLDB	Nottingham, Leicester, Derby, Belfast Study Group
Nm	Newton metre
Nomex	Honey Comb Material manufactured by Du Pont
NPRM	Notice of Proposed Rule Making
Part 572B	Hybrid II dummy
Part 572E	Hybrid III dummy
PC	Personal Computer
PORTAX	DT2821 Data Acquisition Board
PRAKIMOD	Peugeot Renault Accidents Kinematic Model
RAF	Royal Air Force
s	Second
SI	Severity Index
SOMLA	Seat Model Light Aircraft
SOMTA	Seat Model Transport Aircraft
T	Thoracic
V	Volt
WPAFB	Wright Patterson Air Force Base
WSU	Wayne State University
WSUTC	Wayne State University Tolerance Curve
"	Inch
%ile	Percentile

BACKGROUND

The crash of the Boeing 737-400 G-OBME at Kegworth on the 8th January 1989 provided an opportunity to investigate how the passengers were injured during the crash. A computer simulation was subsequently set up to assess the kinematics of the passengers and to establish the likely forces which they would have experienced during the crash. Prior to the crash, the passengers were instructed to adopt a brace crash position. Whilst some passengers adopted a brace position others did not know what a brace position was and remained upright. Two computer models were created using the crash victim simulation program, MADYMO, of passengers seated in the centre section of the aircraft. The models were used to study the brace and upright positions in detail, and to establish any correlation with body injuries and the kinematics and forces predicted by the models. A parametric study was, subsequently, undertaken with the objective of improving seat design.

Further studies were undertaken to evaluate the effects of body posture and impact pulses upon 5th percentile female, 50th percentile male and 95th percentile male occupants. This was performed with the upright seated position and was a directive of the Civil Aviation Authority. The objective of the research was to establish the worst case injuries for various occupant statures when seated in accordance with the dynamic seat requirements of Aerospace Standard 8049. The research was used to establish the loads sustained on the head, thorax, lumbar spine, pelvis and lower limbs.

A three dimensional computer model was created with the objective of studying the effect of lateral acceleration components as specified in Aerospace Standard 8049. Furthermore, the model was used to establish the injuries which might be sustained in other types of aircraft accidents. Using the data of the same aircraft, this was further utilised to investigate different seat orientations and restraint systems.

The computer modelling of the brace for impact position in the Kegworth Accident resulted in recommendations for a new improved brace position which could reduce the likelihood of lower limb flail and subsequent injury in the event of a crash. Up to this time, a number of brace positions had been advocated by regulatory authorities and operators. This lack of a single and clear instruction to adopt one brace position led to misunderstanding and uncertainty amongst aircraft passengers [127].

In order to ascertain the validity of the recommended brace position for adoption in new briefing cards, the CAA sponsored and supported a major piece of research work to establish the forces which may be imposed on the body when subjected to a 16G aircraft impact. The work was divided into two sections:-

1. Impact Testing
2. Computer Simulation

The impact testing took place at the sled facility of the RAF Institute of Aviation Medicine. The facility was selected by the CAA being a government led establishment. Unfortunately, the facility was somewhat limited in capability being a decelerator track. The problems encountered were as follows:-

1. The decelerator track is propelled by stretched rubber bungees over a distance of 46 m. This makes fine control of the impact pulse somewhat variable. The effect of dragging the data acquisition leads down the track serves to reduce the impact velocity due to frictional resistance in the system. The variability in bungee cord stiffness together with the frictional drag led to the acceptance of a slightly reduced impact velocity when compared to the recommended practice as laid down in Aerospace Standard 8049.
2. Only one single Hybrid III anthropomorphic test dummy was available for testing.
3. The Hybrid III dummy was initially positioned 46m up the track and accelerated with the aircraft seats to the appropriate impact velocity. To correlate the computer model, all measurements were taken at this initial position. However, in accelerating the dummy down the track, it was discovered that the dummy had been repositioned due to the inevitable motion in the system. This was ascertained by lack of correlation between the mathematical model and the impact test. Better correlation was subsequently achieved by taking as many of the measurements as possible, from the high speed video tape.
4. The lack of instrumentation in the data acquisition system meant that it was not possible to measure the loads and accelerations in the cervical spine and the thorax, respectively.
5. It was highlighted, at the commencement of the impact testing, that at least five new seats and webbing should be used for the correlation of the mathematical model. However, this was not forthcoming due to financial constraints. Instead, it proved necessary to use seats from the Kegworth aircraft.

As the impact testing took place, a three dimensional computer model was set up and correlated with the test results. Although, there was considerable variability in the impact test results due to dummy positioning, variation in impact velocity and repetitive testing of seats and webbing, there was a good level of comparison between the computer predictions and two sets of test results, 3672 and 3673. On correlating the model, a detailed parametric study of specific parameters were undertaken.

The research findings were presented to the Air Operators Committee at Gatwick Airport, London. Concern was expressed that in both the impact testing and computer simulation a high level of loading was obtained at the lumbar spine for an occupant adopting the brace position. It was initially suggested that a programme of work should be carried out by cadaver testing to determine the loads sustained by the lumbar spine. Over, the next two months, the possibility of undertaking cadaver testing was explored. This was found to be fraught with difficulty, as the legislation to allow cadaver testing to be carried out in the United Kingdom is so complex as to make such testing almost impossible.

An alternative solution was explored, this was to create a mathematical model of the spine which could be incorporated into the existing correlated MADYMO model. Thus, stiffness and physical constant data of the spine were obtained from Wayne State University and Wright Patterson Air Force Base. This allowed the creation of a spine model which was incorporated in the computer model. The creation of an advanced articulating dataset for spine modelling culminated with determining the loads sustained by the vertebrae during an impact. Thus, the injury potential to the brace crash position was evaluated.

A meeting was, subsequently, held at HW Structures, Royal Leamington Spa. The meeting was held with the Civil Aviation Authority and members of the NLDB team. The results of the computer simulation were discussed and recommendation made for the adoption of the new brace crash position.

A notice to the Air Operators Committee, NTAOCH 8/93, was issued by the Civil Aviation Authority in August 1993. This advised operators to take notice of the research and to amend their passenger safety cards, to reflect the new brace position, by April 1994.

1. LITERATURE REVIEW

1.1 HISTORY OF CRASH INJURY RESEARCH

The history of crash injury research begins in the early days of flying, when aircraft were basic and unsophisticated. They were also unreliable and prone to breakdown almost as soon as they were airborne. Crashes were therefore numerous and were frequently caused by technical failures in the machine.

1.2 THE FIRST WORLD WAR

Impact biomechanics has evolved from observations of natural phenomena. Structures which are hard and concentrate loads tend to maximise trauma. Examples of these are clubs and spears. Conversely, shields and armour absorb and dissipate loads thus protecting vulnerable parts of the anatomy [1].

In 1919, it was noted that, in one aircraft type, half of the injuries sustained in aircraft crashes were caused by the aviator striking his head against a sharp cowl of the aircraft [2]. A simple modification was made which involved cutting eight inches away from the cowl, to allow clearance for the pilot's head. This modification substantially reduced head injuries. The same report referred to the use of a simple shock absorber between the aircraft and the restraint system. The energy absorption obtained by the shock absorbers, decidedly, reduced the extent of injuries to the upper abdomen and ribs. The use of energy absorbers reduced the potential of injury and appeared to improve the chances of survivability.

The beginnings of crash injury research are attributed to Hugh De Haven [2, 3, 4]. Following a mid-air collision in 1917, whilst flying with the Royal Canadian Flying Corps, in which he survived and the pilot died, De Haven attributed his lucky escape to the fact that his cockpit had remained intact and he had been adequately restrained by a safety harness that protected him from secondary impact. De Haven noted that his abdominal injuries were caused as a result of contact against the buckle of his harness. The buckle being hard and acting as a concentrated load was able to maximise the trauma.

Swearingen [5] points out that the human body can tolerate high G forces while striking relatively flat yielding surfaces which can absorb energy, however, it is more fragile than china when impaled against narrow rigid tubes, protruding knobs, sharp edges and angles.

1.3 THE SECOND WORLD WAR

With the advent of the Second World War, it became apparent that there was a shortage of trained pilots. Metal monocoque airframes and aero engines were being developed which enabled aircraft to travel at higher speeds. Pilots, however, could no longer abandon a stricken aircraft manually because of the increase in aerodynamic load and the risk of striking the tail fin of the aircraft.

As a result, ejection seats were developed [3, 7]. With this development, came the first study to examine the biomechanics of impact. Essential to this research was the tolerance of the pilot to the loads imposed by the ejection seat.

Chandler [9] describes techniques which were developed in order to simulate the forces experienced by pilots in ejection. Improved test facilities included acceleration towers, swing seats, acceleration and deceleration tracks and drop towers. These facilities served as a basis for the design of modern impact testing facilities. Investigations made on human volunteers at sub-injurious levels enabled investigators to define forces that could be tolerated without injury, provided the correct seat design and restraint system were used.

1.4 THE POST WAR YEARS

Hugh De Haven was the founder of the Crash Injury Research (CIR) project [10]. In 1945, he published the results of the first systematic analysis of injuries in aircraft accidents. De Haven concluded that:-

- ♦ In accidents where the cabin structure was distorted but remained substantially intact, the majority of serious and fatal injuries were caused by dangerous cabin installations.
- ♦ Crash forces, sufficient to cause partial collapse of the cabin structure, was often survived without serious injury.
- ♦ The head was the first, and often the only, vital part of the body exposed to injury.
- ♦ Fundamental causes of head injury were set up by heavy instruments, solid instrument panels, seat backs and unsafe design of control wheels.
- ♦ The probability of severe injuries of the head, extremities and chest was increased by failure of safety belt assemblies or anchorages.
- ♦ Failure of the 454kg (breaking strain) safety belt occurred in 94 cases out of a total of 260 survivors of these crashes. Only 7 survivors showed evidence of injury to the abdominal viscera; 2 of these injuries were classified as serious.
- ♦ The tolerance of crash forces by the human body had been significantly underestimated.
- ♦ If spin-stall dangers were lessened and safer cabin installations used, fatal or serious injuries should be rare in the types of aircraft studied except in extreme accidents.

Meanwhile, Stapp [11] was investigating human tolerance to impact and wind blast. He concluded that the restraint system had a dramatic effect on tolerance of the human to withstand injury. At this time, Stapp was aware that the Royal Air Force lost nearly as many men in automobile accidents as in aircraft crashes. As a result, he developed a research project using salvaged automobiles. In 1955, interest was expressed by the Society of Automotive Engineers (SAE) with the work of Stapp, and as a result, the Stapp Car Crash Conference was established and continues to meet annually. The Stapp Car Crash Conferences have demonstrated that blunt impact and acceleration injury can be significantly reduced in the automobile environment through the use of crushable vehicle structures which absorb impact energy and restraint systems which allow the occupant to decelerate slowly.

Arno Geertz [8] of the Heinkel Aircraft Company examined the biomechanics of the spinal column following ejection seat testing. He stated that "an acceleration can be of any magnitude from the point of view of skeletal strength, if its duration is correspondingly brief".

Eiband, in 1959, [13] indicated that torso and extremity restraint was the principal variable in establishing limits of tolerance. He noted that survival of impact forces was likely to increase with increased distribution of force to the entire skeleton for all impacts from all directions.

In the mid 1960's extensive investigations were being made into the mechanisms needed to generate injuries and methods by which the forces and accelerations applied to vehicle occupants could be modified. This led to the introduction of vehicle safety restraint legislation [3,14, 15, 16].

In 1967, the Aircraft Crash Survival Design Guide was issued. This included the research conducted on both human tolerance of impact and crashworthiness. As a result of this and the crash injury research at that time, two movements took place which were to greatly influence crash injury reduction.

Firstly, the recommendations from the Crash Injury Research Project applied to the automobile industry. Consequently, the project was divided into Aviation Crash Injury Research (AVCIR) and the Automobile Crash Injury Research (ACIR). The latter received large sums of research funding from the car industry and insurance companies, unlike the AVCIR. This is mirrored today as automobile crash injury research has maintained a higher priority than that in aviation [17].

The second event was the development of the legal concept of strict liability. This meant that the manufacturer could be liable, if a design defect was found after an accident. As a result, small aeroplanes were seriously affected by the new development. By the early 1980's, the production of private aeroplanes had almost stopped in the USA.

In 1982, the General Aviation Safety Panel (GASP) was set up under the auspices of the FAA membership. It was comprised of members from all areas of the aircraft industry. The recommendations of GASP in 1983 suggested improved crashworthiness for small aircraft. The group also provided recommendations on test procedures for small aircraft seats, restraints and interior fittings with defined performance standards for the structure and for crash protection. In August 1988, a final ruling was made which adopted the recommendations of the group. As a result, it became evident that similar action would be necessary for other categories of aircraft.

1.5 AIRCRAFT SAFETY

The International Air Transport Association published a set of figures which showed that, in 1991, eighty million people travelled to near and far off destinations by air, in the West. The demand for such a service has necessitated the need for newer and quicker routes to be developed. Emphasis is placed on speed, range and all weather capability [18].

As a mode of transport, commercial aviation is regarded as a relatively safe method of travelling from one destination to another. This assumption is born out by Wilson [19]. He analysed, for a variety of activities, the risks estimated to increase the chance of death in any year by 0.000001 (one part in one million):

<u>Activity</u>	<u>Cause of Death</u>
Travelling 10 miles by bicycle	Accident
Tavelling 150 miles by car	Accident
Travelling 1000 miles by jet	Accident
Living 150 years within 20 miles of nuclear power plant	Cancer caused by Radiation

The key to increased safety in flying lies in the improvement of the interior design of aircraft in order to enable passengers to travel in a safe environment. It is also important to ensure, as far as possible, that the aircraft are in no way defective. The pilots should be trained well, updated regularly and aware of human factors which make accidents more likely. Finally, passengers should be educated to adopt appropriate positions in crash situations.

Professor Murray Mackay [3] noted that aircraft should be certified in two ways. They should be both airworthy and crashworthy.

1.6 AIRWORTHINESS

Airworthiness implies a certain level of safety. According to the Oxford English Dictionary, "worthy" means 'worth, or fitness for use'. In this case, an aircraft that is airworthy is one fit for use in the way it was designed and built to fly.

Airworthiness is directly proportional to the safety inherent in an aircraft and its equipment, the accuracy of the supporting information and limitations given to the pilot who has the job of managing the flight. Efforts are devoted to the improvement of flying safely, by reducing the chance of an accident occurring. Better navigation facilities are provided, new flying aids are introduced. As Tye [18] points out, it appears that although the accident rate can be improved upon, striking reductions cannot be achieved without unacceptable increases in the cost of aircraft and aircraft operations, out of proportion to the consequent reduction of expenditure on insurance premiums.

Flight International in an editorial in January 1990 stated that "the chances of a scheduled passenger being involved in a fatal accident have nearly halved". Today the safe passenger distance in revenue passenger kilometres between fatal accidents, is 2.5 times what it was in the 1970's. On charter airlines, the safe passenger distance has trebled.

Even though the accident rate appears to be declining, it is likely there will be an increase in the morbidity and mortality associated with each accident as the numbers of passengers carried in the aircraft rises rapidly [20]. Higher density seating arrangements together with high approach speeds and huge fuel loads is likely to alter the number of casualties per accident.

Helen Muir [21] has classified aircraft accidents into:-

- a) Those in which no passengers or crew survive, referred to as fatal or non-survivable.
- b) Those in which all the passengers and crew survive, referred to as non-fatal or survivable.
- c) Those in which some of the passengers and or crew survive, referred to as a fatal survivable or technically survivable.

It was also found that although the accident rate has reduced it would appear that there has been no clear trend of improvement in the percentage of passengers surviving accidents.

Learmont [22] points out that today's average "scheduled flight" passenger would have to make 571,000 flights before boarding one which had a fatal accident. Even on such a flight, the passenger's chance of survival would be 65%. In an average airline accident, only 35% of the passengers and 40% of

the crew die. With the emphasis directed towards safety, it is vital to examine secondary safety or crashworthiness. Crashworthiness embraces areas such as ground impact survival, ditching capability, ground fires and emergency egress and its associated cabin safety provisions.

1.7 CRASHWORTHINESS

Crashworthiness is defined as the relative ability of a particular vehicular design to withstand crash impact forces with minimal structural damage [23]. The effectiveness of the structural design is usually considered relative to the occupant protection from serious or fatal injury in a crash impact. Relative to this objective, an aircraft accident is generally considered to be survivable if the crash forces imposed upon the occupants are within the limits of human tolerance. Crashworthiness design of general aviation aircraft thus includes not only reducing collapse of the cabin to prevent impingement or crushing of vital areas of the seated occupants but also various methods of reducing the impact force on the occupants, including restraint systems, energy absorbing seats and delethalization of any environmental structures which may be contacted.

Brown et al have estimated that on average a general aviation aircraft may be expected, during its life time, to experience 1.5 accidents. Reluctant recognition of this has led to the development of various crashworthiness guides to assist the design engineer in providing improved occupant crash protection. Such design guides must draw primarily upon dynamic experimental crash testing, as well as field investigation of crashworthiness performance in actual accidents. The latter can provide the most realistic assessment of how well the occupants are actually protected during crash impact under all conditions.

Secondary safety concerns the vehicle itself, its impact performance, its ability to absorb energy in an accident and the performance of any restraint system [24]. The aim of which is to reduce the risk and severity of traumatic injury to the vehicle occupants.

Hasbrook [25] compared the injuries sustained in accidents with data relating to the physical pre-crash and post-crash environment of each occupant. He showed that safety in survivable accidents can be achieved through improvements in the structural design of the aircraft seats and interior equipment.

As a consequence of this, engineering design can be improved by investigating the specific causes of injury in accidents. Research can be done to prevent unnecessary deaths and injuries in survivable accidents. However, we must accept the premise that some accidents will occur occasionally in spite of our best efforts to prevent them. Human frailties involved in the design, construction, maintenance and operation of aircraft give rise to unpredictable sequences which sometimes produce accidents of an unforeseen

nature. Hasbrook [25] has made recommendations in conducting crash injury research on aircraft accidents. He believed it is important to examine and evaluate the accident conditions with respect to force, the type and design of the occupants' environment, the degree of damage to the vehicle and the occupants' structural environment and the injuries sustained by each occupant.

By this method, Hasbrook stated that the reasons for survival and lack of injury can be ascertained. Similarly, investigations must examine the pathological data on persons fatally injured as this data gives vital clues to the causes of death. Impact studies would show what kind of injuries are sustained by passengers in aircraft seats and secondly, how to determine their frequency and severity.

Design features must consider the aircraft structures, fuel systems, seat restraints, human tolerance levels and the crash environment [28]. However, the major design requirement is to maintain structural integrity of the cabin, fuselage and acceptable seat loading by ensuring sufficient ability to absorb energy which would reduce the decelerative forces on the occupants and hazardous large masses (i.e. high wing aircraft) and that a protective shell be maintained around the occupied area during the crash. The need to provide for post crash emergency egress through operative exits is also an important requirement of crashworthiness design.

Vehicles are being designed to limit the dynamic forces experienced by the occupants to acceptable levels while maintaining a survivable structural envelope around them [29]. This can be achieved by controlling the dissipation of energy throughout the structure during the crash event [30].

The goal of crashworthiness design is to produce passenger vehicles which protect the occupant from injurious forces and encroaching structure that results from specified crash conditions. Generally, the structure outside a survivable envelope must absorb and dissipate most of the impact energy. De Haven [31] noticed that a big factor in head injuries was simply whether the pilot's head hit the structure that would or would not yield under the blow. In the simplest terms, something had to give, either the structure or the head.

The human body can tolerate and expend a force of 200 times the force of gravity for brief intervals during which the force acts in a transverse relation to the long axis of the body [32]. It is reasonable to assume that structural provisions to reduce impact and dissipate pressure can enhance survival and modify injury within limits in aircraft accidents.

The problem of passenger survival in aircraft accidents relates not only to protection from crash forces of survivable limits. It is largely determined by the capacity of the passenger to recover from exposure to the impact forces so that he is sufficiently oriented to release the lap belt and leave the aircraft as quickly as possible [33].

This is especially significant in water ditchings of land based aircraft and when flash fires limit escape to the first few seconds after impact. It is possible for transport crashes to occur in which the forces are sufficiently low to cause little if any direct injury to passengers but their dazed and disorientated condition would prevent rapid emergency evacuation and they would perish from fire injuries. This consideration led to the evaluation of the backwards versus forwards facing seat position as methods of affording maximum protection to passengers in the event of crashes.

2. THE DEVELOPMENT OF THE 16G PASSENGER AIRCRAFT SEATS

Examination of the earliest regulations on aircraft design [34], Aeronautics Bulletin No.14 in 1928, shows there were no design standards for aircraft crashworthiness. A regulatory standard for safety belts first appeared in Aeronautics Bulletin No.7-A, on 1st July 1929. This was to stipulate a design load for the belts of 850 pounds. This Bulletin was later amended on 1st January 1931 requiring that "seats and chairs in cabin planes shall be firmly secured in place". It was not until Civil Aviation Regulation (CAR) part 03 was introduced on the 15th December 1946, that static load factors were first adopted for aircraft seat design.

The static requirements provided that seats and safety belts should sustain the following load factors assuming a minimum seat occupant weight of 77.18 kg:-

Forward	-9.0 G _x
Sideways	+/-1.5 G _y
Downwards	+4.5 G _z
Upwards	-2.0 G _z

From that time onward, the concept of using static load factors to provide a reasonable level of occupant protection in a minor crash landing was carried forth into the Code of Federal Regulations (CFR) 14, Parts 23, 25, 27, and 29 [35, 36, 37, 38].

2.1 DYNAMIC PULSE

The U.S. Army's crashworthiness military standards [39] defines a triangular impact pulse shape as being typical for all aircraft types. The applicability of that pulse shape to general aviation aircraft was confirmed by the General Aviation Safety Panel (GASP). It was found that a triangular pulse shape could be used as an approximation of the measured pulse shapes.

NASA [40] also developed analytical relationships between the normal and longitudinal impulses and the respective primary velocity changes experienced at impact for full-scale impact tests. The data supported the selection of triangular pulse shapes as being representative of general aviation crash events.

2.1.1 Pulse Duration

The work performed by NASA provided an insight into normal impact pulse durations for a data set representing variable aircraft pitch attitude with constant flight path angle and velocity [41]. Review of that data showed that a pulse duration of 0.10 seconds was representative of a typical general aviation impact event.

2.2 CRASH SURVIVABILITY LIMITS

GASP defined seat performance standards based upon the pulse, impact duration and velocity change data obtained from the NASA general aviation aircraft impact tests [40]. The seat dynamic performance standards were defined with the objective of representing the survivability limits of general aviation aircraft accidents. To ensure that the objective was met GASP compared the seat dynamic performance standards with the results of the NASA general aviation impact tests. The comparison shows that, on the whole, there was good agreement in their results.

2.3 PERFORMANCE CRITERIA

The main part of any test procedure is the definition of some form of pass fail criteria. GASP addressed this by defining performance levels which directly relate selected parameters measured during a dynamic test to an injury criteria which is based upon human injury limits. The proposed performance criteria evaluates the seat protection system's potential for preventing or minimising injury to the occupant. GASP evaluated human impact injury criteria which addressed all areas of the human body such as the head, chest, lower torso and extremities. The objective of the performance criteria was to protect an occupant from debilitating injuries. Such criteria must also be easily and repeatably measured for practical applications.

A study of civil rotorcraft accidents identified the frequency of injuries by body region [41]. This led to the selection of performance criteria for limiting head, chest, and spinal injuries.

2.4 TRANSPORT CATEGORY AIRCRAFT

The Federal Aviation Authority (FAA) and NASA conducted an array of full scale impact tests to provide an understanding of the crash response of transport category aircraft. These tests were made to examine the structural failure mechanisms and impulse at impact. This data was to quantify and empirically define the seat dynamic performance standards. The full scale test programme included airframe section drop tests [43, 44, 45, 46, 47], seat dynamic tests [48], an aircraft drop test, and an aircraft air to ground impact test known as the Controlled Impact Demonstration (CID) [49].

The airframe drop tests were conducted to examine the structural failure modes and to obtain the force deflection characteristics of the lower fuselage. The data obtained was subsequently used in the definition of a structural model of the CID by means of the computer program KRASH.

The program KRASH was developed through sponsorship by the FAA. The program utilises beams, springs, dampers, and mass elements to model the airframe of an aircraft. It was initially developed to model helicopters subjected to multidirectional impact forces and later modified to model light

aircraft structures. The program was further developed and applied in the evaluation of transport category aircraft [50].

2.5 SEAT DYNAMIC TEST SERIES

The initial tests were conducted to evaluate the static and dynamic load distributions on the seats, dynamic amplification factors, the effects of floor deformation and combined loads on structural failures, and the types of failures encountered [51].

A second series of 58 tests were later conducted by a joint Aerospace Industries Association (AIA), Air Transport Association (ATA), and the FAA. These tests investigated the effects of pulse shape and magnitude, seat occupancy variations, floor deformation and multiple seat row interactions [48].

The seat to floor retention loads were measured during the dynamic tests and were compared to the static strength levels of the cabin floor structure. It was also shown that the injury fatality protection afforded by transport category aircraft was generally good provided the limits of the structural integrity of the fuselage shell and cabin floor structure are not exceeded.

The technical database which had been accumulated, supplemented by a definition of human impact injury criteria and dynamic test series of aircraft seats, were analysed to formulate the seat performance standards for transport category aircraft.

In 1983, the FAA published a review of crash injury protection in US transport category aircraft between 1970 and 1978. The study was based upon 327 fatalities and 294 serious injuries to passengers involved in accidents on US carriers where seats could have been a contributing factor. Four areas were highlighted as requiring particular attention in order to increase occupant survivability:-

- Definition of the survivable crash environment.
- Development of an understanding of structural component and whole aircraft response to the crash environment.
- Development of validated analytical modelling and test engineering methods.
- Definition of human factors and injury mechanisms for occupants of transport aircraft.

The report also indicated:- "although injuries and fatalities seem to be decreasing in the more recent survivable crashes, seat performance continues to be a factor in these crashes. Failures ranging from seat pan collapse to complete breakaway of the seat assembly from the floor are reported. Floor or cabin deformation is frequently a cause of seat failure. Flailing injuries,

due either to bending over the restraint system or secondary impact with the aircraft interior appear to be common".

2.6 SEAT PERFORMANCE STANDARDS

The transport category aircraft seat dynamic performance standards were adopted into section 14 Code of Federal Regulations (CFR) part 25, amendment 25-64, which has been effective from the 16th June 1988. They provided for improved static load factors of:-

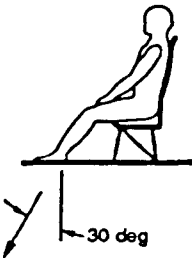
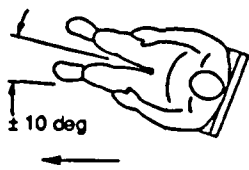
Forward	-9.0 G _x
Rearwards	+1.5 G _x (no previous requirement)
Sideways	+/-3.0 G _y airframe, 4G seats and attachments
Downwards	+6.0 G _z
Upwards	-3.0 G _z

Additionally, Dynamic tests were defined as part of the performance standards as they could demonstrate both the occupant response and the restraint system performance. Dynamic tests provide a more representative evaluation of the occupant to seat and restraint system interaction over static testing. This also yields data for impact injury analysis and provide data to assess the function of any energy absorbing systems.

These tests are conducted with the aid of a 50th percentile (77.18 kilograms) Hybrid II dummy in accordance with 49 CFR part 572 [52]. The anthropomorphic dummy is an accepted industry standard which provides a degree of repeatability.

Two distinct dynamic tests were defined, Figure 1. The first test condition, known as Test 1, provided a combined vertical and longitudinal velocity change. The combined loading vector was oriented at 30 degrees from the vertical, such that the primary velocity change was in a vertical direction. The test condition features occupant vertical loading and assesses the degree of lumbar spine loading and potential injury under a combined vertical and longitudinal loading typically generated by a crash event. The test applies a minimum of 14G deceleration from a minimum velocity of 10.67 m/s.

A second dynamic test, Test 2, was defined with a longitudinal velocity change. This was to provide an assessment of the occupant restraint system, seat structural performance and injury potential to the occupant. The test approximates a horizontal impact with 10 degrees of yaw, applying a minimum of 16G deceleration from a minimum velocity of 13.41 m/s. The effects of cabin floor deformation are also simulated. The parallel floor rails and fittings are misaligned by 10 degrees in pitch and 10 degrees in roll before the application of the dynamic test pulse.

PARAMETERS	TEST 1	TEST 2
ILLUSTRATION SHOWS A FORWARD FACING SEAT Inertial Load Shown by Arrow		Yaw right or Left 
Min Vt, m/s (ft/s)	10.67 (35)	13.41 (44)
Max Tr, sec	0.08	0.09
Min G	14	16
Deform Floor:		
Degree Roll	0	10
Degree Pitch	0	10

**Test Pulse Simulating
Aircraft Floor
Deceleration-Time
History:**

Tr = Rise Time

Vt = Impact Velocity

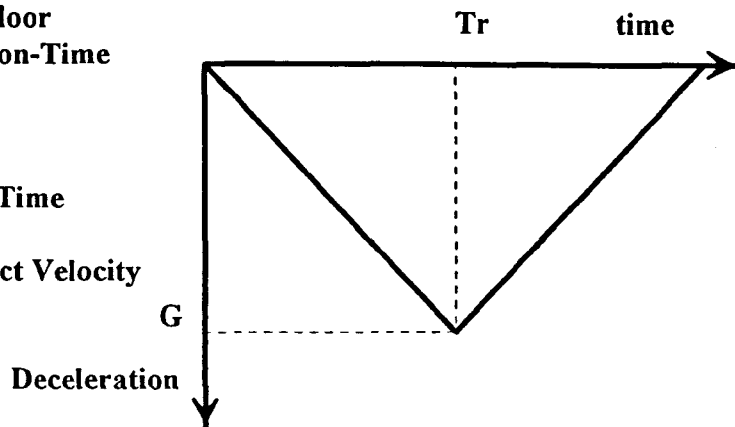


Figure 1. Seat Dynamic Test Specifications (Aerospace Standard 8049).

Both tests require that the seat remains attached to the floor. Aerospace Standard (AS) 8049 stipulates that the longitudinal permanent deflection of the seat structure should not exceed 75mm. The measurement is made from the forward-most hard point of the seat at a height up to and including the armrests. However, there is no limitation on the downward permanent deflection provided it may be demonstrated that the feet or legs of the occupant are not entrapped. The sideward limitation is that permanent deflection should not exceed 40mm towards the aisle at a height below 635mm above the floor and 50mm above this value. The seat base rotational permanent deflection shall not exceed 20 degrees of pitch downwards from a horizontal line and 35 degrees upwards from the same baseline.

Subsequent to the announcement of these rules, the FAA issued a Notice of Proposed Rule Making (NPRM). This stated that as of June 1995, all new aircraft of the current type and within the existing fleet will be installed with the new seats designed to the 16G dynamic requirements.

2.7 HEAD INJURY CRITERIA

Secondary impacts to the head can result in concussion and unconsciousness. The most widely used and accepted measure of potential head injury is the head injury criteria (HIC) which is described in Federal Vehicle Safety Standard (FMVSS) 208.

GASP recommended that the HIC be used when structures or equipment are within the occupant's head strike envelope. The maximum value of the HIC integral was limited to a value of 1000.

2.8 SPINAL INJURY

Spinal injuries frequently take place in aircraft impacts. The Dynamic Response Index (DRI), which is based upon a single lumped mass, damped spring model of the spine has traditionally been used to predict the probability of lumbar spine injury in the evaluation of aircraft ejection seats. However, the differences in function, geometry, dynamic pulse exposure and occupant restraints between ejection seats and those seats found in general aviation aircraft makes the application of the DRI questionable.

A study which was performed at the Civil Aeromedical Institute (CAMI) related the DRI which was measured from accelerations at the seat pan to pelvic load measured in the base of the spine of the Part 572 anthropomorphic dummy [52]. Analysis of the results of that study led GASP to recommend that a 6.672kN pelvic load be used as a performance criteria to assess the probability of spinal injury in evaluating seat dynamic tests.

2.9 FEMUR LOADING

This parameter was adopted for limiting debilitating leg injuries in transport category aircraft. After reviewing the high density seating and emergency evacuation requirements, it was considered appropriate to include a femur injury criteria as part of the performance requirements. A maximum axial compressive load of 10kN, which is consistent with the Federal Motor Vehicle Safety Standard, Part 571.208 [53], was selected as the femoral injury criteria.

3. IMPACT BIOMECHANICS

The study of impact biomechanics requires an approach which encompasses examination of injury mechanisms, tolerance levels and biomechanical responses.

Early studies of biomechanics of impact in Europe were concerned with mechanisms of head injury [26]. In the post war years an enormous growth in car ownership occurred. This led to a parallel increase in traffic casualties. As a result, the 1960's saw a number of epidemiological studies which described this epidemic of traumatic injuries. The search for biomechanical insights and solutions led to several detailed interdisciplinary investigations in which doctors and engineers collaborated in studies of actual collisions.

In Europe, biomechanical research in the early 1970's received a major boost as a result of the introduction of crash performance standards for road vehicles. The concept of performance standards requires knowledge and techniques in four areas:-

1. The concept requires a knowledge of the physical forces, accelerations or displacements and their time histories which relate to various levels of injury severity.
2. Knowledge is required on how tolerance to those applied forces vary throughout the population at risk.
3. Substitutes, either physical or mathematical, are required which have sufficient biofidelity to reproduce experimentally the human response for the conditions for which protection is to be specified.
4. Knowledge of the distributions of the frequencies of the real world of collisions is needed so that appropriate test conditions can be specified to protect chosen segments of the population.

With the rapid growth in air traffic, increasing emphasis has been focused on causes of passenger injuries and deaths in severe, but potentially survivable crashes. The coming of age of the Jumbo jets has changed the concept of disaster planning and those responsible must consider handling hundreds of potential casualties [27]. A major accident is an accident or occurrence which, because of the number of casualties it produces, requires special arrangements to deal with it. Any accident to a large aircraft has the potential to become a disaster. Serious injury according to the International Civil Aviation Organisation (ICAO) requires:-

1. Hospitalisation for more than 48 hours, commencing within seven days of the date the injury was received.

2. Results in a fracture of any bone (except simple fractures of fingers, toes or nose).
3. Involves lacerations which cause severe haemorrhages or nerve, muscle or tendon damage.
4. Involves injury to any internal organ.
5. Involves second or third degree burns or any burns affecting more than 5% of the body surface.

A serious injury may be regarded as an injury normally requiring hospital care [27].

3.1 INJURY MECHANISMS

The mechanism of injury describes the physiological and mechanical changes that result in damage to the anatomical and functional parts of the body. This is fundamental to understanding injury biomechanics as it provides a basis for determining appropriate measures of response and tolerance to impacts in the various parts of the body [54, 55]. The deformation of tissues beyond their recoverable limit is the general injury mechanism associated with blunt impact [56]. This mechanism is measured in terms of strain. There are three types of strain which cause tissue damage and injury. These are tensile, shear and compressive strain.

Tensile strain represents an increase in the length of a line drawn on a body [57]. Shear strain represents a change in the angular relationship of two lines drawn on a body and compressive strain represents a decrease in the length of a line drawn on a body.

In a viscoelastic structure such as biological tissues, the rate of loading and the strain rate are also important factors in the production of injuries. Impact along the axis of the femur causes an increase in its natural curvature [58]. This results in a tensile strain on its anterior surface and a compressive strain on its posterior surface. Fracture will occur when the tensile limit is exceeded.

Shear strain occurs when opposing forces act across a tissue moving in opposite directions [55]. When the limit of resistance is reached, the tissue will then fail. This mechanism is important in the causation of head and visceral injuries. Shear strain also explains injuries due to laceration and bruising.

The rate of loading when applied to a structure is of importance when predicting injury. In a viscoelastic structure, the faster the load is applied the stiffer the material behaves. Failure will occur because the structure cannot deform quickly enough. If loading is slow much of the energy can be

absorbed by deformation without tissue damage. Compact bone as seen in femurs exhibits rate sensitivity during impact. The axial load a femur can withstand increases with impact velocity, however, the bending strain at failure decreases [54, 55, 59].

Fractures can lead to associated injuries involving nearby tissues. These include injury to nearby vasculature (arteries, veins and capillaries) nerves, connective tissue and post traumatic arthritis of joints. Nerves may also be cut or stretched resulting in loss of sensation and movement. The various connective tissues (tendons and ligaments) may be damaged which may affect structure and movement. Bone movement following joint disruption, even without bone fracture, may also injure nearby neuro-vasculature [60]. *Orthopaedic fracture patterns are relevant to the design of occupant protection systems.*

3.2 IMPACT TOLERANCE

In order to design impact protection devices, it is important to know what forces or loads the body can withstand. This is known as the injury threshold and indicates the tolerance of the body to impact. At a measurable level of deformation, magnitude and rate, the tissue will not be able to recover and injury will occur.

Two techniques have been used to investigate the tolerance of the human body or isolated tissues. Firstly, dynamic testing is used to simulate "real world" crash conditions. In addition, impact test facilities are used to predict occupant injury potential by comparing the test results with standard injury criteria. Secondly, static testing is used on isolated tissues or parts of bodies. The loads are applied gradually until failure occurs.

3.2.1 Biomechanical Response

Once a mechanism is described, the biomechanical response during impact must be quantified. Measurements demonstrate how an organ or tissue reacts to deformation or how the inertial resistance of the body or tissue respond to a load or motion. This information is used to analyse the injury criteria and to develop models that behave in a human-like manner under impact conditions.

A variety of different methods of defining tolerance have been used. These are:-

Voluntary tolerance is described as a low level of tolerance which can be withstood voluntarily, without sustaining injury. It is extremely variable and is dependent on the individual pain threshold.

Injury threshold represents a level at which injury just occurs to a given organ or tissue and is usually reached accidentally.

Moderate injury involves impact which results in complete recovery from an injury which is produced without any impairment of function. Injury criteria based on this level are laid down for the design of injury protection systems.

Severe injury occurs as a result of force applied in order to produce injuries which are not fatal or at a level which fatal injuries begin to occur.

Fatal injuries are caused by impact levels in which fatalities occur.

3.3 FACTORS AFFECTING IMPACT TOLERANCE

We should recall that in biomechanics research the living human body can only be used on a voluntary basis and at sub-injurious levels. However, a series of substitutes are available in the form of physical or theoretical models.

Factors influencing tolerance to impact have been reviewed by Snyder [61]. These can be divided into physical and biological factors.

3.3.1 Physical Factors

The orientation of the body has an effect on tolerance and is related to the direction of impact. Head first (-Gz) falls are the least well tolerated [62]. In feet first (+Gz) impacts, severe injuries are seen in the feet, ankles and lower limbs. In seated impacts (+Gz), pelvic and vertebral injuries occur. In side impacts (Gy), the upper extremities, thorax and vertebral column followed by pelvic injuries are most commonly involved. The position of the body in relation to force directly influences the nature and extent of injuries, since structurally, the human body can resist greater forces prior to failure in some directions [61].

a) Magnitude of force

The force magnitude and time relationships are described in terms of the 'G' load and rate of onset.

b) Distribution of Force

The distribution of force at impact cannot be adequately considered independent of other factors. Findings indicate that the distribution of force through the body is intimately connected with magnitude, orientation of the body (direction of force) and the time duration among other factors. It is considered that the greater the area over which the load is applied, the smaller the load per unit area. This principle has been applied to restraint systems which aim to distribute the load over the skeletal framework of the body rather than subjecting soft tissue, such as the abdomen to extensive pressures. Distribution of force is directly related to the transmission and dissipation of energy throughout body tissues.

The greater the area over which a load is applied, the smaller the load per unit area and the greater the survival in free-fall and tolerance to high impact forces [32].

c) Contact Surface

The object contacted in free falls is of great importance as an injury or even survival determinant [61]. The relative elasticity or solidity of structures directly affects the deformation distance and thus, the time duration of impact. It may also affect survival by its contour characteristics. Thus impact with, soft, muddy ground is obviously preferable to jagged rocks.

d) Duration of Impact

Time durations of 0.0004 to 0.0006 seconds, reported in human voluntary deceleration experiments, may preclude serious tissue injury. The duration of time that the force has been applied is recognised as one of the most critical factors in human impact tolerance. The longer an impact acceleration is applied, then the greater will be its effects. An acceleration of 45G can be tolerated in a chest to back (-G_x) direction if applied for a period 0.044 seconds [63]. However, if this acceleration is applied for over a two second period then considerable injury would be sustained.

3.3.2 Biological Factors

The general physical condition of the individual at the time of impact is important as this does have a bearing upon the degree of injuries received, as well as the recovery prognosis. Much of the work, to date, on human tolerance levels has been conducted on young physically fit males. These results are not representative of the population as a whole as they do not include individual variation such as age, sex, physical condition, race, pre-existing pathology and other biological factors.

3.4 SECONDARY IMPACT

Death or severe injury can result from secondary impacts. These impacts cause flailing of the lower limbs, torso, head or failure of the restraint system [5]. Restraint systems and seating design aim to prevent serious secondary impacts. If the force of an abrupt deceleration following an impact exceeds the strength of the retaining devices, the passenger will be hurled like a missile in the corresponding direction sustaining secondary impacts and injuries [25].

3.5 ACCIDENT INVESTIGATIONS

It is impossible to prevent accidents. Without analysis of their causes, their potential for causing death and injury cannot be reduced, if it is not known precisely what injuries are sustained and how they are produced. It is rational, therefore, that accidents should be the subject of routine and comprehensive scientific investigation [64].

Investigation of the series of fatal accidents shows that medical and pathological analysis of the relevant evidence is required if the fullest reconstruction of an accident is to be achieved and all the flight safety implications appreciated.

The main sources of medical evidence are usually the detailed post-mortem reports on the bodies of all deceased passengers. The findings are correlated with the medical histories of the air crew, the laboratory examinations of the specimens taken at post-mortem, the evidence in the victim's clothing and at the scene of the accident. Further and most important, the medical and pathological evidence has to be correlated with, and interpreted in the light of that found by the non-medical investigators.

Detailed examination following an aircraft accident is a practicable proposition. Furthermore, in an aircraft accident more than in any other disaster, such detailed examinations should be an integral part of the investigation of the accident itself.

4. EXPERIMENTAL MODELS IN IMPACT RESEARCH

In impact research, experimental models are used to define injury mechanisms, biomechanical responses and tolerance levels. These models may be classified as biological, mechanical, or mathematical.

4.1 BIOLOGICAL MODELS

4.1.1 The Volunteer

The parameters of human tolerance to experimental application of crash type mechanical force have been determined with respect to onset, magnitude, duration and direction by exposure of volunteer subjects to linear deceleration on a rocket sled [33].

Volunteers are very good models as they are human and the tissues are alive [54]. Strict protocols are in place which limit the acceleration levels which can be placed on volunteers. Pain thresholds vary from individual to individual and for this reason, impact acceleration must start off at low levels gradually increasing until the subject feels pain or discomfort [62]. Therefore, when using the volunteer, the results are limited and may be misleading. Each volunteer can only be exposed to levels of impact up to the individual's pain threshold. This makes reproducibility and repeatability impossible. The volunteer is usually a young fit healthy male. This is not representative of the population as a whole.

In the experimental situation, the volunteer can prepare himself for impact, thus, his muscles are often in a state of contraction or tone. This is not representative of the real world situation where little or no warning is given. The stiffness or muscle tone affects the response of the various occupants [65].

Hidden pathology may be present which will affect the results and is not representative of the average passenger. The strength of an individual's bones depends upon many factors. Bone strength is diminished in the elderly as a result of bone loss. Such effects are more marked in females who experience a period of accelerated bone loss in the immediate post-menopausal period. Some females develop osteoporosis. This is a condition characterised by generalised loss of bone substance. It is associated with a marked reduction in bone strength and may culminate in fracture of the wrist, spine and hip [66].

Experimental work with human subjects has been limited to voluntary tests which have only accidentally exceeded the injury threshold limits. Some individuals are able to tolerate impact forces many times above the accepted levels [61]. This highlights the variability in using human volunteers.

Despite these limitations, the human volunteer can provide useful information on kinematics at low impact levels.

4.1.2 The Animal

The animal is a living model and in contrast to the human volunteer can be subjected to high levels of impacts. However, the animals are anaesthetised and therefore their muscle tone and physiological responses in general are not representative. Muscle relaxation is often part of the anaesthetic process but in addition, muscle relaxants are frequently used to supplement anaesthesia [55, 67]. Also, animals are anatomically different to humans. This alters the response to impact trauma making the findings invalid for humans.

4.1.3 The Cadaver

The cadaver is identical to the living subject except that it is inert. Therefore, it is possible to simulate geometric and material properties of the human or to study the mechanical response of a body segment [55, 63, 68]. However, as it is no longer a functioning biological system, the injury which might occur to soft tissues, hollow and parenchymatous organs can only be speculated upon.

There are problems with cadaveric experiments. The lack of muscle tone with associated flaccidity or rigor mortis affects the kinematic behaviour [63, 67]. The lack of circulating blood in the tissues and organs results in flaccidity. This directly affects the inertial forces and decreases the sensitivity to loads.

Significant reductions in the strength and stiffness properties occurs with advancing age [69]. This alteration in properties occurs as a result of many factors, including degenerative processes, disease effects related to activity status and superimposed disease states. As a high proportion of cadavers will be of advancing age, they are unrepresentative of the general population as a whole.

The effect of the freeze, store and thaw cycle on mechanical properties of 20 anterior cruciate bone-ligament-bone preparations obtained as right-left pairs from 10 rhesus monkeys were made [70]. Statistical comparison of the two groups showed that there was no change in the mechanical properties of the ligaments or their cross sectional areas. This indicates that freezing and thawing of the specimen should not alter its failure characteristics.

Studies on embalmed cadavers have shown that due to the lack of muscle tone and turgidity of organs, their biodynamic properties may be affected [63].

A large part of our existing knowledge on human response to impact acceleration is based on experiments for which the human cadaver was the principal test subject [65]. Research into biological systems is itself a task which intrinsically examines variability [26]. In conclusion, the cadaver is a useful model and has been used extensively in the evaluation of bone tolerance. However, like all other models, it has its limitations.

4.1.4 The Accident Victim

The accident victim is not an experimental model and for this purpose it is a separate entity from biological and mathematical models. It is, however, an important source of data. Reports and studies of accident victims are a valuable source of information in order to investigate injuries and their causes [25, 71].

However, despite obtaining this information, *only a few accidents have been analysed and rarely is any attempt made to correlate the injuries sustained with the causes of the injuries* [4]. Information specifically related to lower limb injuries are seldom reported, yet it is this information that is crucial in determining why the occupant failed to escape following a crash. This is particularly important with regard to fires where rapid escape is required.

Careful analysis of injury in accident victims cannot replace the experimental models because the lack of knowledge of crash parameters means that only rarely are reliable kinematic and dynamic data available to determine relevant tolerance levels. The crash victim is generally assumed to be a linked structure made up of rigid bodies of which the governing equations of motion are the conservation of linear and angular momentum [64].

4.2 MECHANICAL MODELS

Biological surrogates of various types have been used in crash simulation. However, they are difficult to use, do not provide repeatable or reproducible information and are unable to be used once an injury has occurred. Anthropomorphic Test Dummies (ATD's) have a long history of use as surrogates in crash type environments [72]. The environments have included cars, motorcycles, high performance fighter aircraft and commercial aircraft. The needs of the industry have evolved to require high levels of biofidelity, mostly in terms of impact response, repeatability and reproducibility. ATD's are constantly used in assessing the potential for human injury in an impact environment. The dummies are able to simulate the human body with respect to mass, shape, size, stiffness, articulation, energy dissipation and kinematics following an impact [73, 74].

4.2.1 Anthropomorphic Test Dummies (ATD)

The earliest recorded testing involving an anthropometric dummy was conducted by Start and Roth (1944) of Dornier Werke in the development and testing of an ejection seat for the DO335 aircraft. The dummy was a simple wooden form used mainly for ballasting the seat with representative body weights.

In the 1950's, Mathewson and Severy [12] developed the technique of experimental crash testing with instrumented dummies and high speed film analysis.

Crash test dummies have two basic roles in the assessment of vehicle safety. The first is to load the restraint system which requires a simple dummy, while the second is to indicate the type and severity of an injury which a human may sustain in the event of an accident. The latter requires a more complex dummy. In general, complex dummies are designed to be able to detect loads which may cause skeletal fracture, deceleration injury to internal organs and in some cases laceration injuries. Simple dummies, such as head forms, are primarily used to quality assure components in legislative test procedures.

Two main, but different, test devices are currently used to ascertain compliance with the dynamic crash test procedures of Federal Motor Vehicle Safety Standard (FMVSS) 208 in the automotive industry and Aerospace Standard (AS) 8049. They are referred to as the Hybrid II and Hybrid III Anthropomorphic Test Dummies. The description of both dummies are contained in Title 49 of the Code of Federal Regulations, Part 572, Subpart B and E respectively. The Hybrid II dummy, also known as the Part 572 dummy, was developed by General Motors and adopted as a test device by the National Highway Traffic Safety Administration (NHTSA) in 1973.

By 1977, General Motors had gone on to develop the Hybrid III. This dummy was described as more human-like than the Hybrid II, particularly the head, neck and chest regions. The head consists of an aluminium shell covered by vinyl skin. The neck exhibits one piece biomechanical bending and damping response in flexion and extension. The thorax consists of six ribs connected to a welded steel spine. The spine provides for attachment of the neck, clavicles and the lumbar spine. The lumbar spine is a curved polyacrylate elastomer with moulded end plates for mounting. A detailed description of the Hybrid III is found in Foster (1977) [73]. The improved biofidelity of the Hybrid III was most notable in the ability of the dummy to measure chest compression.

Additional transducers may be used to measure pelvic accelerations, cervical spine and tibia loads. The time history results which are obtained, are subsequently used in the estimation of potential injury and disability of the human body. As a result, standard injury limits have evolved which have become injury criteria, Table 1. Such criteria are used in the assessment of injury potential in a repeatable manner, thus safety improvements can be made to occupant protection systems.

CRITERIA	TEST DEVICE	
	HYBRID II	HYBRID III
Head: HIC	<1000	<1000
Chest Acceleration 'G' (3ms Limit)	60	60
Femur Load (kn)	10	10
Chest Compression (mm)	none	75
Lumbar Spine Load (kn) (AS 8049 Only)	6.7	6.7

Table 1. FMVSS 208 and AS 8049 Injury Criteria

The classification of an ATD is dependent on its physical size [74]. The height and weight of the adult male dummy approximates to the median height and weight of the adult male population of the United States. Other adult dummies are available such as the 95th percentile adult male dummy and the 5th percentile female dummy. Child dummies are also available and are classified according to the age of the child.

ATD's are used in impact testing to give an indication of the loads that would be experienced by a human. The efficacy of the ATD for injury prediction is dependent upon the degree to which pertinent physical characteristics are simulated, otherwise known as the biofidelity of the dummy [74]. The ability to measure appropriate mechanical responses. The prediction of injury type and severity based on analyses of the human response.

A deficiency in any of these factors affects the overall result by reducing the effectiveness of the ATD as an injury predictive surrogate. All physical characteristics must be included in the model so that its responses to acceleration and deceleration are representative of a human response to the same conditions. If a model is not instrumented to measure the mechanical response which is related to human injury, injury prediction is made impossible.

Most ATD's are comparable with the total weight and size of the human subject. However, the mass distribution is seldom similar. This is due to the fact that the distribution of flesh organs and body fluids cannot be easily substituted. It must, also be noted that the bone structure of the human is replaced by metallic components in the ATD. This serves to provide adequate durability for repeated impact testing.

Appropriate mechanical responses can be measured. However, the prediction of injury from measured responses in the dummy is impaired by the lack of data available regarding human injury tolerance. The problems with ATD's are:-

1. Most ATD's have been developed for use in the automotive industry and have response characteristics which have been optimised to the horizontal X-axis.
2. There appears to be serious discrepancies in the response of the head and neck.
3. ATD's are particularly limited in the Z-axis behaviour, exhibiting a response that is stiffer than a human subject.
4. Most aircraft accidents have a significant Z-axis component as the principle impact vector.

Crash test dummies are frequently, although not exclusively, used to evaluate secondary safety features both inside and outside of the vehicle [24]. They can be used to determine injury risk or simply to load a surface or a restraint system up to a realistic level in a semi-realistic way. Being a human surrogate, they have to exhibit several human like characteristics, and depending on usage, how well they simulate a human can vary.

Anthropomorphic Test Dummies (ATD's) come in various forms. They can be classified as "frontal impact dummies", "vertical impact dummies" or "side impact dummies".

Both the Hybrid II and Hybrid III dummies are used for aerospace and automotive sled testing. They both represent 50th percentile occupants, in mass and stature. They are primarily frontal impact dummies. In order to convert them into vertical impact measuring devices, an axial load cell is inserted between the pelvis and the lumbar column. This cell allows for the measurement of the axial compressive load in the lumbar spine.

The Hybrid II dummy is more commonly found in the aerospace sector, whereas, the Hybrid III is more widely used for motor vehicle crash testing. Aerospace Standard (AS) 8049 stipulates that a 50th percentile male as defined in 49 CFR Part 572, Subpart B, or an equivalent shall be used to simulate an occupant. For this research, the Part 572E or Hybrid III dummy was used for the impact testing and computer simulation, due to its improved biofidelity.

The biofidelity of ATD's has been criticised as they are unable to simulate physiology and pathology. They are, however, able to simulate acceleration, deformation and kinematic response, which in most cases may be correlated to human impact conditions [73].

4.3 MATHEMATICAL MODELS

Computer simulation in the study of impact biomechanics have evolved over the past three decades. McHenry, in 1963, developed the first mathematical model to be used in the investigation of a vehicle crash. Since then many sophisticated simulators have been developed in the study of occupant kinematics. During the last ten years, many developments have been performed using mathematical models in safety research.

The simulation of crashes is of vital importance in the evaluation and improvement of safety devices and the interior environment surrounding the occupant. The majority of such work is carried out using instrumented dummies or human cadavers. Occasionally, animals or human volunteers may also be used. The increase in use of crash victim simulation in the past decade is attributed to the development of computer hardware and simulation software. Such techniques can contribute significantly in understanding the behaviour of complex dynamic systems during impact.

Mathematical models are valuable tools in the study of trauma. They can be used to predict injury response which cannot be simulated experimentally. There are three types of mathematical models which simulate human subjects:-

4.4 LUMPED PARAMETER MODELS.

These models are made up of masses, springs and dampers which represent the tissue, fluid and bones. These models are frequently used for whole body simulations. Such models are unable to calculate stresses in the tissues. As a result, they cannot predict tissue failure. For this reason, correlation with other tests is imperative if the acceleration and kinematics of the various body segments are to be related to trauma. These models are inexpensive to run and do not require expensive computer hardware. They are extremely advantageous where a large number of parametric changes are to be examined.

For this research, MADYMO, which is a lumped parameter model, was chosen. This decision was made on the basis that the program had been continuously reviewed and updated and had become the industry standard for computational impact biomechanics.

4.5 DISTRIBUTED PARAMETER MODELS.

These types of models are created using finite element modelling (FEM). Structures are divided into small elements such as bricks, tetrahedrons, plates or membrane elements. Each structure may have its own independent material property. The mass is concentrated along the element nodes. By this method, unusual shapes and combined material properties may be analysed. The finite element method utilises many simultaneous equations for the

structural solution. The volume of data and the number of calculations require powerful computers depending upon the size and number of elements which make up the structure. The cost of the solution increases dramatically for dynamic non-linear events, such as crash simulation. This occurs due to the size of the matrices, large displacements and rotations and the number of contact interactions which are solved.

Finite element analysis (FEA) may be used to calculate internal and external stresses and displacements of structures. For this reason, the researcher is able to obtain facts he could not have anticipated, as this information may be impossible to obtain by any other means. These models are excellent for use in trauma studies as they are able to predict tissue and bone fracture, provided that the body part may be modelled.

4.6 LUMPED AND DISTRIBUTED PARAMETER MODELS.

This type of model is a compromise between a fully lumped and a distributed parameter model. This model is based upon the finite element analysis technique. The areas of particular interest to the researcher are discretised using a finite element mesh. Whereas those regions of the structure which are not so important may be modelled using a lumped mass approach. This helps to reduce the run time of the model, particularly, if large parametric studies are required.

Mathematical models also have limitations [75]. These limitations include:

1. Over-sophistication. It is easy to make a model overly complex rather than make justifiable and realistic assumptions. The former will undoubtedly increase the model run time.
2. Validation. In order for a model to have credibility, it must be correlated with experimental test data. However, in some instances, the experimental tests may be expensive and therefore limited. If a model's response comes close to the measured result, then it is considered to be validated.
3. Lack of properties of biological tissues in the model.

4.7 DEVELOPMENT OF LUMPED AND DISTRIBUTED MODELS

The origins of crash victim simulation can be traced back to the development of the MVMA2D occupant simulation program at Cornell Aeronautical Laboratories [76]. Further development of MVMA2D took place in Europe. This was performed by the Peugeot Renault Association. This development was based on the very first version which became known as the Peugeot Renault Accidents Kinematic MODEL (PRAKIMOD) [77].

The development of CAL3D, a three dimensional occupant simulation program, was initiated by the Calspan Corporation in 1970 [78]. The occupant was described by fifteen segments with forty degrees of freedom. A contact model was developed for generating the external forces acting on the occupant. Restraint systems such as belts and airbags were included. CAL3D also became known as the Crash Victim Simulator (CVS) [78].

CAL3D was further developed by NHTSA and the Air Force Aerospace Medical Research Laboratory (AFAMRL) [79, 80]. The AFAMRL CAL3D became known as the Articulated Total Body (ATB) program. The ATB was primarily enhanced to simulate the aerodynamic forces experienced during ejection. Whole body ejection problems were also attempted [81].

In the majority of CVS programs, the contact interactions between the body and surrounding environment is represented by line segments in the two dimensional case and by a plane in three dimensional simulation. The contact forces are generated as a function of the penetration and stiffness of the adjacent contact surfaces. These surfaces may also be represented using Finite Element Analysis (FEA).

The first program developed to model the interaction of the occupant segments with the structure using FEA was the Seat Model Light Aircraft (SOMLA). The program was developed by the Federal Aviation Administration (FAA) to provide an engineering analysis tool in the design of aircraft seats [82, 83]. This was also used in the analysis of light aircraft crashworthiness [84].

SOMLA comprises a three dimensional occupant model which contains a 29 degree of freedom system consisting of 12 rigid bodies. This interacts with a finite element seat model which uses linear (FEA) techniques. The seat pan may be discretized using membrane elements and the supporting structure by beam elements. Limitations in the program have resulted in the element formulation, material representation and solution procedures.

The MADYMO (MAThematical DYnamic MOdel) occupant simulation program consists of a two dimensional and a three dimensional version. The formulation of the two packages are similar and were completed in 1975 at TNO, Netherlands. Since 1975, the simulation program has undergone considerable refinement and optimisation at TNO. The first reference to the package was made in the literature by Wismans, Maltha, et al in 1979 [85] where the model responses were compared with sled tests using a child dummy and child cadavers.

Gross motion simulators are a group of mathematical programs formulated to describe a vehicle occupant in planar or three dimensional motion during impact using the lumped parameter approach. The occupant is represented by a set of rigid bodies linked by various types of joints in an open loop system

known as a tree structure. The equations of motion which govern such rigid bodies are derived using Lagrangian and Newtonian mechanics.

The shapes of the rigid bodies are described by ellipses in the MVMA2D, by ellipses or hyperellipses in the MADYMO2D version and by ellipsoids in the CAL3D and MADYMO3D. The CAL3D and MADYMO3D also utilise hyperellipsoids. The relative rotation between individual elements are resisted by non-linear torsional springs, viscous dampers and/or Coulomb friction.

4.8 MADYMO

MADYMO is a world wide accepted engineering analysis program, developed by the TNO Crash-Safety Research Centre, for the simulation of systems undergoing large displacements. The program has been designed for the study of the complex dynamic response of the human body and its surrounding environment under extreme impact conditions.

The MADYMO occupant simulation program consists of two and three dimensional versions. The current code is version 5.0. MADYMO is a non-linear computer program which utilised the lumped parameter modelling technique until August 1994, when a new finite element module was introduced into the program. This latest development allows the researcher to make use of new material models. However, the lumped parameter technique is still being used extensively due to the rapid run times of the simulations and the number of parametric studies which can be quickly undertaken.

In relation to the work carried out in this thesis, the lumped parameter modelling techniques have been used, because at the time of the research being undertaken, the finite element structural algorithm did not exist in MADYMO.

4.9 THE MADYMO CRASH VICTIM SIMULATION PROGRAM

The analytical formulation of the program is described using the equations of motion for multiple tree structures composed of rigid bodies. These are derived using Lagrangian methods. The memory requirements are dependent upon the number of elements in the tree structure and the number of contacts which are made. The fourth and fifth order Runge-Kutta Merson solutions are used for solving the equations of motion. MADYMO contains a set of force models which are capable of modelling restraint systems, for example, belts, airbags and contacts with the surrounding environment. User defined subroutines may be added to the program for special modelling purposes [86].

In order to create an input data file, the user defines the number of systems to be included in the model. These systems may include a dummy dataset, a deformable steering column, an airbag and knee bolsters. For crash dummies, standard datasets are available. For each system the number of bodies and their configuration for each branch in the tree structure is defined.

An input data file is subsequently developed which includes the configuration of the tree structure, the mass distribution and the stiffness characteristics of contact surfaces and joints. Acceleration field models may be applied which calculate the forces at the centres of gravity of the bodies. An acceleration field may be applied to the whole system of bodies or to a single body within an individual system. Planes and ellipsoids may be attached to the bodies which represent their geometrical shapes. The former are also used to define the contact surfaces with other bodies. The contact surfaces may, for example, describe the interaction of the occupant with the vehicle interior. The contact forces which are produced are a function of the penetration of the contact surfaces. In addition, damping and friction may be applied.

Three types of massless spring-damper elements exist. The Kelvin element is a uniaxial element which simulates a spring in parallel with a damper. The Maxwell element is uniaxial which simulates a spring and damper in series. Non-linear spring characteristics and velocity dependent damping may be applied. The point restraint can be considered as a combination of three spring damper elements each parallel to one of the axes of an orthogonal co-ordinate system.

The belt model accounts for belt slack or pretension and rupture of segments. The stiffness characteristics may be applied for each belt segment and slip of belt material from one segment to another may be applied. Sliprings, retractors and pretensioners may also be defined.

The output control parameters of the data file define the output required. A number of output parameters are available such as accelerations, forces, torques, kinematic data and injury level calculation, for example, femur and tibia loads and the Head Injury Criterion (HIC).

4.10 MADYMO MODEL DEVELOPMENT

In order to develop a computer model in MADYMO a variety of information is required. This may appertain to a crash or sled test. For the development of the aircraft seat models, it was necessary to obtain the following information:-

4.11 VEHICLE DATA

1. Package drawings to show the interior geometry of the aircraft showing seat location, pitch and surface geometry as well as the dummy initial position.
2. Knee bar force deflection characteristics.
3. Seat cushion force deflection characteristics.
4. Seat back force deflection characteristics.
5. Moment rotation characteristics of seat back.
6. Seat cushion friction characteristics.

7. Floor stiffness characteristics.
8. Belt force-relative elongation characteristics.
9. Length and material of the belt buckle.
10. The location of the "effective" belt attachment points on the dummy or occupant.
11. Total length of the lap belt for the initial occupant or dummy seated position. This information is required to determine the additional belt length in MADYMO.
12. Initial slack in the belt system.
13. The friction coefficient of the belt slip over different dummy segments.
14. Crash or sled pulse, preferably at the location of the seated occupant.

4.12 TEST RESULTS.

1. High speed film of the test.
2. Measured dummy accelerations as a function of time. For example, head, chest and pelvis.
3. Other dummy measurements, such as femur, tibia and belt loads.
4. Relative displacements in the experiment as a function of time, such as the dummy head, hip and knee relative to the vehicle.
5. Injury criteria, such as the Head Injury Criteria and chest 3ms criterion.

4.13 COMPONENT TEST DESCRIPTION

The majority of the component tests are made to obtain the force deflection or moment rotation characteristics. It is preferable to obtain both the loading and unloading phase which provides the means to model the hysteresis effect.

4.13.1 Knee Bolster Force Deflection Characteristics.

A knee shaped hemisphere is pushed into the knee bolster by means of a hydraulic cylinder with a force gauge and potentiometer. The hydraulic cylinder is positioned such that it is perpendicular to the knee bolster. The force deflection characteristic is obtained for the most severe condition encountered during the crash test.

4.13.2 Seat Cushion Force Deflection Characteristics.

The purpose of this test is to determine the seat cushion vertical displacement as a function of the load on the seat cushion. This load should be applied over an area which closely resembles the dummy contact area with the seat cushion. This may be a pelvic form or a body block. Alternatively, a 50th percentile hybrid II or hybrid III dummy may be used instead of the body block. In this case weights have to be added to the dummy lap whilst measuring the vertical displacement. It is important, however, to remove the

lower legs of the dummy in order not to allow support to be taken up through contact with the lower legs to the floor.

4.13.3 Seat Back Force Deflection Characteristics.

An upper torso body block or the upper body of a dummy may be used to determine the cushion stiffness characteristic using the same procedure as for the seat cushion described above. However, for the rear part of the seat back, where head contact takes place, a head form is used to determine the local stiffness characteristics.

4.13.4 Seat Friction Coefficient.

This may be determined by pulling a known mass or body block along the seat cushion and measuring the force required to move this object. It is essential that the clothing worn by the occupant is replicated in the experiment.

4.13.5 The Floor Force Deflection Characteristics.

This may be determined using the foot of a dummy. The load is applied via an instrumented hydraulic ram to obtain the force deflection characteristics.

4.13.6 The Belt Force Relative Elongation Characteristic.

This is usually obtained from the manufacturer of the belt material. The data must be supplied to MADYMO as a force against percentage elongation characteristic.

5. HUMAN INJURY TOLERANCE TO IMPACT

The field of injury biomechanics deals with the effect on the human body of mechanical loads, in particular, impact loads. Due to the mechanical loads, the body will experience mechanical and physiological changes. This is otherwise termed as the biomechanical response. Injury will take place if the biomechanical response is of such a magnitude as to cause the biological system to deform beyond its recoverable limit. The result is damage to the anatomical structure and alteration in normal function. The mechanism involved is called "the injury mechanism", the severity of the resulting injury is described as "the injury severity". An injury criterion is a physical parameter or a function of parameters which correlate the injury severity of the body region under consideration.

Many schemes have been proposed for ranking and quantifying injuries. Anatomical scales describe the injury in terms of its anatomical location, the type of injury sustained and its relative severity. These scales rate the injuries rather than the consequence of injuries. The most widely used anatomical scale is the Abbreviated Injury Scale (AIS). Although this scale was devised for the assessment of motor vehicle accidents, its use has widened to include the assessment of burns and penetrating injuries. The AIS classifies the injuries accordingly:-

Abbreviated Injury Scale (AIS)	Description of Injury
0	No Injury
1	Minor
2	Moderate
3	Serious
4	Severe
5	Critical
6	Maximum Injury (Fatal)
9	Unknown

Table 2. Abbreviated Injury Scale Classification

The AIS is known as the threat to life ranking. The numerical values have no significance other than to designate order.

A biomechanical tolerance is the magnitude of a biomechanical response of the human body due to an impact which causes a certain defined level of injury, often described by an AIS level. It is important to note that the tolerance is not the same for each individual in the population. The tolerance, in general, is related to a percentage of the population to be protected.

5.1 INJURY CRITERIA

Injury criteria describe the trauma limits of individual human body segments. These are more generally applicable to a variety of impact injury protection systems. To provide data for protection against serious injury or death, biological surrogates are used instead of human subjects in tests. Correlation of data between the biological surrogates and living humans is difficult. Moreover, for evaluating the performance of a protection system, an anthropomorphic test device (ATD) may be used instead of a biological surrogate. The ATD is a rudimentary representation of the human body. Impact injury criteria should, therefore, be expressed in parameters which can be measured by an ATD.

The evaluation of the performance of impact injury protection systems are made by measurements through testing. These impact injury criteria will, therefore, be discussed with specific emphasis on the head, spine, thorax and lower extremities; these being the most pertinent to this research. Historically, measurements of acceleration have been used as impact injury criteria. These measurements have been made through the availability of accelerometers rather than the significance of acceleration as a factor in injury.

5.1.1 Head Injury

Several head injury mechanisms have been postulated which are related to acceleration induced injuries through direct impact with the skull or face. Excessive acceleration can cause brain injury through a variety of effects, none of which are completely understood. Relative motion of the brain and skull can induce a wide range of debilitating effects; the periphery of the brain may be contused, internal brain matter can be sheared by relative motion between its parts, and the brain stem can be distorted by extrusion through the opening at the base of the skull. Finally, excessive tensile stresses can occur independent of any large brain displacement. This usually takes place opposite the impact site and can disrupt a variety of brain functions depending upon its location. Little is known about the effects of multiple or long duration impacts.

5.2 CONCUSSION

In 1966, the Committee of the Congress of Neurological Surgeons defined brain concussion as: " A clinical syndrome characterised by immediate transient impairment of neural function such as alteration of consciousness, disturbances of vision, equilibrium, etc., due to mechanical forces." Concussion is usually a fully reversible injury. It has been widely studied for a number of reasons:

1. It is by far the most prevalent brain injury.

2. Concussion is usually the first functional impairment of the brain to occur as the severity of the head impact increases.
3. It accompanies 80% of all bending skull fractures (however the vast majority of concussions occur without skull fracture).
4. It is reproducible in experiments with animals whereas other brain injuries are not.

Three different aspects of gross skull motion have been suggested as being correlated with concussion:-

- Rotational acceleration.
- Translational acceleration.
- Flexion-extension of the upper cervical cord during motion of the head-neck junction.

Only the first two phenomena have been assessed quantitatively and are discussed below:-

5.2.1 Rotational Acceleration

In most recent years most of the research into the effects of rotational acceleration have been conducted on animal brains, in vivo or in isolation. The establishment of injury criteria and tolerance levels have been attempted [87]. This has been based upon results obtained from several types of monkeys, they have employed scaling laws to apply to tolerance levels of the human.

5.2.2 Translational Acceleration

The Wayne State University Tolerance Curve (WSUTC) is said to provide a dividing line which represents the onset of concussion [88]. The linear acceleration of the skull in the anterior-posterior (a-p) was measured against the duration of the applied impact pulse. This was derived from experiments of embalmed cadavers striking unyielding surfaces on the forehead for durations of 1 to 6 milliseconds.

5.3 INJURY CRITERIA AND TOLERANCE LEVELS

The two principal criteria of brain injury are the Severity Index (SI) and the Head Injury Criteria (HIC). Numerous additional indices of brain injury have been proposed [89].

5.3.1 Severity Index

The WSU Tolerance Curve is difficult to apply to complex acceleration time histories because of the uncertainties in determining the effective acceleration and time. To overcome this problem, Gadd [90, 91] devised a weighted impulse criterion for establishing a Severity Index (SI):-

$$SI = \int_0^T a^n dt$$

Where:-

- a = acceleration in G's.
- n = weighted factor, 2.5 for head impacts.
- T = pulse duration.
- t = time in seconds.

The weighted factor of 2.5 is primarily based on the slope of the straight line approximation of the WSU Tolerance Curve plotted on log-log paper between 2.5 and 50ms. A review of the mathematical derivation of the Severity Index by Versace [92] details the relationship between the WSUTC and SI.

Gadd proposed a tolerance value of 1000 as the threshold of concussion for frontal impact [90]. This tolerance value was mandated in early versions of Federal Motor Vehicle Safety Standard (FMVSS) 208; however, it specified that the SI was to be calculated using the resultant acceleration measured at the centre of gravity (CG) of the head instead of the uniaxial acceleration measured on the occiput in the direction of the blow as was used by Gadd.

For distributed or non-contact injuries to the head, an SI value of 1500 would be a more appropriate concussion tolerance level [93]. Gadd cited the fact that Stapp experienced an acceleration pulse which equated to a biaxial head exposure estimated to have reached a Severity Index of 1500. This occurred in a rocket sled run in which 45G was measured on the seat. There was no brain injury in this exposure although retinal haemorrhages occurred.

5.3.2 Head Injury Criterion (HIC)

The relationship between the WSUTC and SI was examined [92]. In response to this, a new parameter, the Head Injury Criterion (HIC) was defined by NHTSA as:-

$$HIC = \left[(t_2 - t_1) \left\{ \frac{1}{t_2 - t_1} \int_{t_1}^{t_2} a(t) dt \right\}^{2.5} \right]_{\max}$$

Where t_1 and t_2 are the initial and final times (expressed in seconds) of the interval during which HIC attains a maximum value and $a(t)$ is the resultant acceleration (expressed in G) measured at the head CG. The HIC replaced the SI in later versions of FMVSS 208 with a HIC value of 1000 being specified as the concussion tolerance level.

Statistical analysis of direct head impacts using cadaver tests have been used to define a relationship of HIC and injury level for the meaningful interpretation of HIC. A HIC level of 1000 produced a 16% incidence of life threatening brain injury in the adult population, this is equivalent to an AIS 4 [74]. A number of criticisms have been attributed to HIC, these include:-

- HIC is not suitable for scaling injury potential.
- No correlation exists between HIC and head injury severity.
- Matching of the criterion to the WSUTC is erroneous.
- The criterion only applies to translational accelerations.

Despite these drawbacks, HIC is still the most accepted method of assessing head injury and a value of 1000 is the injury threshold.

5.4 THE SPINE

The primary mechanism of injury to the cervical spine involve damage to the bony elements, with subsequent disruption of the spinal cord being the most serious result. The mechanisms involve dislocations of one vertebral body upon another, fracture of vertebral bodies with associated displacement of bone fragments into the spinal canal, and rupture of intervertebral discs with protrusion into the spinal canal. An additional injury mechanism is ligamentous stretching of the spinal cord and or disruption of the cord by associated bony element motions.

Although these mechanisms have been identified in a qualitative manner, the actual loads, moments, displacements, and motions of the cervical spine that lead to injury are not well documented. A further complication is that rather low load levels have been found experimentally to produce serious damage when the spine in an asymmetrical attitude, that is, with the head rotated and flexed on impact [94].

5.5 NECK INJURY

In automobile collisions, neck injuries can occur through bending from head inertial loading, when the torso is violently accelerated or decelerated. The neck skeleton consists of seven cervical vertebrae. These vertebrae are generally referred to by number in order from top to bottom as C-1 to C-7. No two vertebrae are the same, however, C-3 to C-7 are quite similar to one another. Adjacent vertebral bodies are separated by fibrous connective tissue called intervertebral discs. Vertebral articulations are stabilised by fibrous tissues called ligaments. These ligaments also limit the degree of rotation between the vertebrae.

The muscles which are to the rear of the neck are bigger than those found to the front. In addition, the former are located further from the head-neck pivot known as the occipital condyles. Consequently, larger moments can be

developed for resisting flexion than extension. Also, a lower resultant muscle force is required to produce the same magnitude of resisting bending moment in flexion than would be required in extension.

Tests have been conducted on volunteers and human cadavers to determine the neck's reaction on the head under dynamic loading [95, 96, 97]. It was found that the resultant bending moment was an excellent indicator of neck strength. Based on the cadaver data, tolerance levels, for the 50th percentile adult male, were suggested at the occipital condyles.

For flexion, a resultant bending moment of 190Nm was proposed as the lower boundary for an injury tolerance level. This bending moment did not produce a discernible ligamentous damage to a human cadaver.

For extension, a resultant bending moment of 57Nm was suggested. This level was associated with ligamentous damage to a human cadaver. However, it should be noted that the human cadavers were relatively old. Also, there may have been a degeneration of the strength of the ligamentous tissue compared with living tissue. Based upon these results, the neck appears to be at least three times stronger in resisting flexion than extension.

Extrapolation of the above threshold limits to the base of the neck (C7/T1) were made [94], based upon work carried out by Wismans and Spenny in which they found that the bending moment at the base was approximately twice that at the top of the cervical spine. The results of this analysis has yielded 380Nm for flexion and 114Nm for extension.

5.6 THE LUMBAR SPINE

The structure of the lumbar spine is generally similar to that of the lower cervical spine in the context of vertical compressive loading (but not shear and rotational loading). The lumbar spine is, however, larger. Yamada [98] gives the effective cross sectional area of the cervical vertebrae as 305mm^2 and of the lumbar vertebrae as 1055mm^2 . These areas would give a relative linear dimension ratio of 1.87 for the lumbar vertebrae as compared with the cervical vertebrae. Yamada also indicates that the compressive failure stress of the lumbar vertebrae is half that of the cervical vertebrae. Using this approximation, Melvin deduced that for flexion, the resultant bending moment at L5/S1, is 1235Nm. Similarly, for extension the bending moment is 370Nm. Thus, the injury threshold limits for spinal bending moments are summarised as follows:-

Bending Moment Direction	Top (C1)	C7/T1	Base (L5/S1)
Flexion, Nm	190	380	1235
Extension, Nm	57	114	370
Lateral	Between the above	Between the above	Between the above

Table 3. Spinal Bending Moment Injury Thresholds (Melvin).

Similarly, the injury threshold loads for the spine were also determined using this technique. These are shown in Table 4:-

Loading	Cervical Spine	Lumbar Spine
Tension, kN	3.3	12.7
Shear, kN	3.1	10.7
Compression, kN	4	7.0

Table 4. Spinal Load Injury Thresholds (Melvin).

5.7 THE THORAX

The thorax is a ribbed shell which contains the following important organs:- heart, lungs, trachea, oesophagus and major blood vessels. The rib cage is a semi-rigid structure which provides protection to the internal organs and facilitates the mechanics of respiration. The lower part of the rib cage also encloses and protects the liver, spleen, stomach and small bowel.

5.7.1 Thoracic Injuries

Thoracic injury mechanism include ribcage skeletal fractures, contusions of the heart and lungs, tearing and rupture of the vascular and pulmonary systems and disruption of the heart muscles. Many of these injuries are thought to occur due to excessive deformations of the thorax when directly loaded. Severe deformations during frontal impact may result in trapping and crushing of the thoracic organs between the chest wall and the spine. Severe inertial forces on the organs are thought to produce stresses and deformations in the tissues of the organs, resulting in injury. At high accelerations, such injuries may occur with little rib cage deflection.

5.7.2 Thoracic Injury Criteria

Several parameters have been suggested for monitoring the effect of a blow to the thorax based on thoracic acceleration, force, deflection or a combination of these. Rib fractures are a commonly employed means of determining thoracic injury tolerance using cadavers. However, with cadavers, corrections may be required to account for lack of muscle tone and lung inflation compared with the living subjects. Data obtained from animals must be scaled to account for size and shape differences of their rib cage as compared with the human. Injury interpretation is further complicated by differences between the human thoracic organs and those found in animals.

The majority of experimental chest impacts have been undertaken with simple impactors or belt restraint systems. Little data is available on lateral chest impacts and oblique impacts.

5.7.3 Chest Deflection

Researchers have generally concluded that chest deflection shows good correlation with chest injury produced by blunt frontal impacts. Neathery et al. [99] have analysed test results based on 24 cadavers which had been subjected to frontal thoracic impacts using a simple impactor. Neathery related their chest traumas to their chest deflection and ages at death. Based on an injury level of severe and non-life threatening, and an average driving age of 45 years old, Neathery recommended the following sternal deflections:-

Occupant Size	Sternal Deflection Likely to Produce Severe Injury (mm)
5th Percentile Female	60
50th Percentile Male	75
95th Percentile Male	90

Table 5. Sternal Deflection Limits Likely To Produce Severe Injury.

The above severe injury thresholds are also consistent with Melvin's observation which was made for the 50th percentile occupant [100]. Melvin et al. proposed a chest deflection of 44mm if rib cage fracture was to be avoided. He also concluded that a chest deflection of 64 to 76mm would correspond to the same injury level as discovered by Neathery.

The main disadvantage with the chest deflection criterion is the difficulty of carrying out the measurements on the subjects concerned. A further

complication is that a single deflection measurement is not generally representative of the whole thorax deformation behaviour.

5.7.4 Chest Acceleration

The practical difficulties of the deflection criterion have led to the conclusion that acceleration measurements offer a better alternative. Stapp [101] reports on numerous tests where volunteers were subjected to decelerative restraint conditions. For a series of rocket propelled sled tests where the volunteers were restrained using air force harnesses, a drastic drop in blood pressure was noted after the tests where the peak sled deceleration ranged from 26-38G with deceleration rates of 896-1373G/s. However, the subjects were not instrumented with chest accelerometers.

An instrumented stunt man experienced chest accelerations of 46G while impacting a thick foam mattress with his back after falling from a height of 17.4m [102]. Chest accelerations of a performer who regularly dived into a shallow pool from a height of 10.5m onto the water with his stomach [103] were measured. The results, of thoracic spine and sternal accelerations, of 25G and 224G, respectively, were obtained from a height of 4.6m. The authors extrapolated these measured results to 68G and 380G, respectively, for the weights normally used in his performances.

FMVSS 208 currently specifies as acceptable any acceleration pulse which "shall not exceed 60G except for intervals whose cumulative duration is not more than 3ms".

5.8 THE LOWER EXTREMITIES

The elements of the lower extremity consist of the pelvis, femur, tibia, smaller fibula, and the ankle and foot bones. In addition, there is the patella (or kneecap) which cover the knee joints. The fibula is excluded from the discussion as it is not a significant load carrier.

5.8.1 Femoral Injury Tolerance

Early studies of the static strength of the femur were conducted by Weber in 1859 and Messerer in 1880 and have been summarised by Melvin and Evans [104]. Weber performed three point bending tests with the force applied in 245N increments midway between the supports and transverse to the longitudinal axis of the bone. The distance between the supports was 183mm in all cases. Data was obtained from four males and five females. The maximum load to fracture is summarised below:-

Subjects	Peak Static Femoral Bending Moment (Nm)	Peak Static Lateral Femoral Bending Moment (Nm)	Peak Static Torsional Femoral Moment (Nm)
Male	233	310	175
Female	182	180	136

Table 6. Peak Static Femoral Bending Moment (Weber), Lateral Bending Moment and Torsional Femoral Moment (Messerer).

Messerer's femoral bending experiments were performed with a hydraulic testing machine having a load measurement resolution of 10 to 50N. Three point bending tests were conducted with the support span of two-thirds the length of the femoral shaft, that is, 317mm in length. Loads were applied at the midspan. Bones from six males (ages 24 to 78 years) and six females (ages 20 to 82 years) were assessed. For lateral (left to right) loading, the average maximum bending moments at fracture are presented in Table 6.

Messerer also conducted static torsion tests on the femur. Bones from four males (ages 27 to 56 years) and seven females (ages 19 to 81 years) were evaluated. The average torsional moments are shown in Table 6.

He also noted that the upper and lower thirds of the femur were of lower torsional strength than the middle third. All the bones fractured with a spiral pattern at an angle of 45 degrees.

Static axial compression of the femur was conducted by Messerer with the ends of the bones padded with felt to prevent local failure at the point of force application. The average axial compressive failure force for shaft fractures was:-

Subjects	Peak Static Axial Compressive Femoral Load (kN)
Male	7.72
Female	7.11

Table 7. Peak Static Axial Compressive Femoral Load (Messerer).

A more recent study of the static bending strength of the femur was conducted by Motoshima in 1960 and summarised by Yamada [98]. Three point bending

tests were performed on the femurs of 35 subjects. The ends of the specimens were encastred in plaster or concrete with the force applied at midspan in the anterior-posterior direction using a 20mm diameter cylindrical loading head. The average breaking loads and bending moments are summarised below for five age groups:-

Age Groups (Years)	Peak Static Bending Moment (Nm)	Peak Static Load (kN)
20-39	234	2.72
40-49	213	2.47
50-59	203	2.35
60-69	201	2.33
70-89	184	2.14
Average	211	2.45

Table 8. Peak Static Bending Moment and Fracture Loads for Wet Femurs (Yamada).

Yamada indicates that the female femur has five-sixths of the bending strength of the male femur.

There have been a number of studies of the dynamic fracture tolerance of the femur, primarily due to research performed in the automobile industry. While acceptable criteria for predicting fracture have remained elusive, there appears to be universal agreement that the dynamic load carrying capacity of the femur exceeds that under static loading. The load carrying capacity of the femur under dynamic conditions was evaluated by Mather [105] using 32 pairs of human femurs. For each pair, one was loaded statically while the other was loaded dynamically with a velocity of 9.8m/s. Although the data was not able to compare the static and dynamic fracture forces an energy comparison was possible. The mean value of dynamic energy was 1.7 times that of the static energy.

The dynamic torsional loading of the femur was also studied in connection with skiing accidents [106]. Femurs were obtained from 65 autopsy individuals ranging from 27 to 92 years old. The ends of the bones were embedded in gripping blocks and torsionally loaded to failure in less than 100ms. The mean value of the peak torsional moment for males was:-

Subjects	Peak Dynamic Torsional Femoral Moment (Nm)
Male	204
Female	131

Table 9. Peak Dynamic Torsional Femoral Moment (Martens).

Comparing the above data with results of Messerer's static torsional tests shows that for males, the peak dynamic torsional moment is 17% greater than its static counterpart. However, for females the mean peak dynamic torsional results are lower than the static data by 4%. It is suggested that the differences are most likely due to the smaller sample size of Messerer, that is, 7 versus 13 and the size of bones in certain subjects [104].

The first study of femoral impact tolerance was conducted as part of the automotive crash safety research [107]. Ten unrestrained seated, embalmed male cadavers were tested on a sled facility. The knee target areas were covered with 37mm of padding. The results of the research indicated that for a moderately padded surface, an axial compressive force of 6.2kN is a reasonably conservative value for the overall injury threshold level of the patella-femur-pelvis complex. Further tests on two additional cadavers were reported by the authors. Loads of 6.5, 7.6, 8.7, 8.8kN were sustained without fracture. It was suggested that loads of 8.7kN without fracture were not unreasonable.

Knees of 26 fresh cadavers were impacted using impactor tests [108]. There were 15 male and 11 females cadavers. The data indicates that the males ranged in age from 46 to 90 years old, had a body mass of 39.6 to 88.5kg and a height of 1.63 to 1.80m. The females ranged in age from 45 to 89 years old, 21.9 to 65.9kg and 1.50 to 1.66m. The impactor velocities varied from 3.8 to 23.2m/s using unpadded to padded impactor faces. These tests were also applied with variations in applied force, pulse amplitude and duration.

For the seven "rigid surface" impacts for two males and one female cadavers, femoral condyle fractures occurred in two tests. The peak forces associated with these tests were 18.0kN for a female and 19.6kN for a male. There were no femoral fractures in another five tests, where the peak force ranged from 16.2 to 22.7kN on four legs of male cadavers. For 28 lightly padded impacts to nine male and six female cadavers, femoral condylar and supracondylar fractures occurred in five tests, one undefined fracture occurred in a sixth test. Three of these were associated with males and had peak forces ranging from 13.6 to 28.5kN. A further three were associated with females whose fracture forces ranged from 13.3 to 19.6kN. For thick padded impacts, one female age 55 years sustained a femoral shaft fracture at 19.7kN. A 72 year old male cadaver sustained peak forces of 15.7 and 13.7kN without fractures.

A series of six unembalmed cadaver sled tests were performed with the objective of achieving longer impact durations with both femurs being loaded simultaneously [109]. Peak femoral fracture forces ranging from 10.2 to 23.0kN were sustained.

There have been several attempts to define a femoral injury criteria, using the available experimental data, that would enable a femoral fracture or no fracture to be predicted, based on an applied time history. Such a criterion would be useful in analysing crash test data from anthropomorphic test devices with femoral load cells. However, no test device has reproduced the human biomechanical response characteristics of the knee-femur-pelvis region. A Femur Injury Criterion (FIC) was developed [110] which calculates the axial compressive force, F , to produce fracture as a function of the primary load pulse duration, T :-

$$F(\text{kN}) = 23.14 - 0.71T \text{ (ms)}, T < 20\text{ms.}$$

$$F(\text{kN}) = 8.90, T \geq 20\text{ms.}$$

A method is discussed for implementing this criterion for analysing complex wave shapes. Lowne [111] has analysed the data and concluded that the following criterion is appropriate for avoiding unacceptably high femoral compressive loads:-

- 12kN may not be exceeded.
- 10kN may not be exceeded except for durations of less than 3ms.
- 7kN may not be exceeded except for durations of less than 10ms.

The femur limit currently specified in FMVSS 208 and Aerospace Standard (AS) 8049 is a compressive load for each femur of 10kN [112]. Previous FMVSS 208 specifications were 6.23kN and 7.55kN.

Tolerance limits to combined loading, for example simultaneous torsion and axial compression, do not appear to have been addressed to date.

5.8.2 Tibial Injury Tolerance

Early studies of the strength of the tibia were conducted by Weber (1859) and Messerer (1880) following the same procedures which are analogous to their work of femoral impact tolerance. Melvin and Evans [104] also reported this work. For the three point bending tests of the tibia, the distance between the supports was 216mm. The average peak bending moments are summarised as follows:-

Subjects	Peak Static Tibial Bending Moment (Nm)	Peak Static Lateral Tibial Bending Moment (Nm)	Peak Static Torsional Tibial Moment (Nm)
Male	165	207	89
Female	125	124	56

Table 10. Injury Threshold Peak Static Tibial Bending Moment (Weber), Lateral Bending Moment and Torsional Moment (Messerer).

Messerer's lateral three point bending tests on the tibiae utilised an average length between supports of 247mm. This led to an average maximum bending moments, Table 10.

The static torsion tests on the tibia led to an average torsional moment at fracture is presented in Table 10.

Messerer's static axial compression tests of the tibia resulted in average tibial shaft fracture forces of:-

Subjects	Peak Static Axial Compressive Tibial Load (kN)
Male	10.36
Female	7.49

Table 11. Injury Threshold Peak Static Axial Compressive Tibial Load (Messerer).

Yamada [105] has also reported the tibial bending strength tests which were conducted by Motoshima in 1960. The testing technique paralleled that which was described earlier for his tests on the femurs. Three point bending tests were undertaken using a span length of 287mm. The results are summarised as follows:-

Age Groups (Years)	Peak Static Bending Moment (Nm)	Peak Static Load (kN)
20-39	208	2.9
40-49	180	2.52
50-59	174	2.43
60-69	171	2.39
70-89	164	2.29
Average	184	2.60

Table 12. Injury Threshold Peak Static Bending Moment and Fracture Loads for Wet Tibias (Yamada).

As stated for the femurs, Yamada states that the female tibia has five-sixths the bending strength of the male tibia. He also states that the breaking load is not significantly different between the anteroposterior and lateromedial direction.

Similarly, as with the evaluation of the femurs described earlier, Martens et al. [106] has reported on the torsional strength of the tibia. The specimen were loaded to failure in less than 100ms. The mean peak torsional moment were summarised as follows:-

Subjects	Peak Dynamic Torsional Tibial Moment (Nm)
Male	111
Female	71.4

Table 13. Injury Threshold Peak Dynamic Torsional Tibial Moment (Martens).

Comparing these results to those of the static tests by Messerer indicates that under dynamic loading conditions, the torsional strength is increased by a factor of 1.25 for males and 1.28 for females.

Extensive human cadaver testing has been conducted in connection with pedestrian impact protection. Impact loads were applied to cadaver lower legs [112]. 209 tests were carried out using a twin pendulum catapult. Loads were

applied through circular cylindrical impactors having their longitudinal axis perpendicular to that of the tibia. The applied force was calculated from the acceleration of the impacting mass. Impact locations ranged from the centre of the patella down to the shaft of the tibia. Impact speeds ranged from 4 to 8m/s. A wide spread in cadaver tolerance is said to have been obtained due to the fact that some fractures took place at 4m/s and a force of 1.0kN, and yet some legs survived a force of 5.8kN at 7.1m/s without fracture. With a 145mm diameter impactor, a 50% frequency of fracture occurred at an impact speed of 7.1m/s with a force of 4.3kN. On the other hand with a 216mm diameter impactor, the 50% level was 6.3m/s and 3.3kN.

Recent research which has been undertaken on the design of frangible leg bone structures for the development of a Motorcyclist Anthropomorphic Test Device (MATD) has utilised the following fracture criteria [72]:-

Description	Femur	Tibia
Dynamic Bending Moment (Nm)	328	294
Dynamic Torsion Moment (Nm)	192	136
Axial Compressive Load, kN	10.5 (Dynamic)	10.0 (Static)

Table 14. Frangible Leg Bone Design Injury Thresold Criteria (St-Laurent).

5.8.3 Hip Joint Pelvis Tolerance

One mechanism of injury at the hip joint and surrounding pelvic region is that loads across the hip joint as a result of femoral axial compression are of sufficient magnitude to cause hip dislocations and fractures of the pelvic bones.

The testing of 12 embalmed male cadavers produced femoral compressive forces ranging from 1.93 to 17.1kN [113]. Pelvic fractures were obtained following seven tests. Fractures were associated with forces ranging from 6.23 to 17.1kN. However, there were eighteen loadings in the range of 6.23 to 12.2kN where fracture did not take place.

5.8.4 Ankle Joint Injury Tolerance

The left and right ankles of a human cadaver were loaded in increasing increments in an Instron materials testing machine with a cross head speed of 4.2m/s [114]. In each case the lower leg was excised from the cadaver at the mid-shaft of the tibia. The upper ends of the remaining tibia and fibula were embedded into a steel cup for attachment to the testing machine. Shoes were

placed on the feet. Axial force was applied through the cup and downward through the ankle to the shoe, which rested on the platen of the machine.

The force was applied incrementally, with X-ray films taken at each increment. In the right leg audible "popping" was noted at a force of approximately 5.5kN with a 38mm cross head travel. A similar test was conducted on the left leg. The "popping" was noted at a force level of 3.3kN with a 25mm cross head travel. Subsequent examinations showed that fracture of the calcaneum had occurred.

5.9 HUMAN TOLERANCE TO LAP BELT IMPACT LOADING

There are a number of configurations of seat belts which are in use in both the automotive and aerospace industries. These include the lap belt, the three point belt (or a combination of lap and diagonal) and a combination of double lap and double shoulder harness. The term lap belt refers to a single belt across the anterior aspect of the pelvic structure. The term seat belt refers to a combination of lap and torso restraint. There are numerous variations of this type, such as five point belts, double vertical belts without a lap belt and lap and shoulder belts with inertia reels or retractors.

In a 1951 Comet air crash numerous abdominal, thoracic and aortic ruptures were found which were attributed to the snubbing action of the lap belt due to the forced flexion of the torso [115].

In a 1952 study [116], among individuals involved in serious aircraft accidents wearing lap belts, 23 cases of intra-abdominal injuries which could be attributed to the belt, along with 32 cases of contusions along the belt line were found.

Most of the early seat belt developments were directly in response to aviation and aerospace requirements [117]. The lap belt was first offered in the United States as a safety device in late 1955 by Ford and Chrysler.

A considerable number of research and accident investigations have demonstrated the usefulness of the seat belt in reducing injury. The reduction in injury is attributed to the prevention of ejection, which was reported to be the leading cause of both injury and death in accidents. Seat belts were shown to reduce the severity of injury and fatality.

Tourin and Garrett concluded that seat belts "could save at least 5000 lives a year and reduce injuries by one third" [118]. This conclusion has been supported by similar findings relating to the advantage gained by wearing seat belts.

Herbert concluded that standard lap belts reduce the level of injury by 35% and three point belts by 80% . Huelke and Gikas predicted in their study of

fatal accidents that "of 48 ejectees, 38, or 80 percent, would have survived if they had been wearing only the lap seat belt." [119].

Campbell and Kihlberg in 1963 reported on a matched pair study of 232 lap belted occupants half wearing belts and the other half without belts. They found that whilst belts can reduce fatalities, no substantial benefits were shown beyond reducing occupant ejection. They stated that the addition of an upper torso restraint would further increase occupant protection.

Garrett and Braunstein investigated reports of 944 injured occupants wearing seat belts. Of 150 serious lower torso injuries 26 could have been attributed to the belt [120]. They found seven intra-abdominal injuries, seven pelvic fractures, twelve lumbar spine injuries, forty-seven lumbar muscle strains and seventy-seven contusions and soreness over the iliac crests. They also stated that compression fractures to the lumbar vertebrae may occur as the individual jack-knifes over the lap belt.

Kaufer and Smith [121] also reported tension injuries of the lumbar spine in ten subjects.

Howland et al. [122] reported on the transverse fracture of the lumbar spine. It was concluded that the high placement of the seat belt allowed the lap belt to act as a fulcrum, literally "splitting apart" the vertebral body "similar to breaking a stick over one's knee".

Synder et al. [117] carried out five decelerations tests on baboons from 22 to 30G using the three point belt restraint system. No trauma was found with this restraint system, other than minor external belt contusions in forward facing impacts. Synder stated that "this system appeared to offer much better protection than the lap belt only."

Studies on human tolerance to lap belt crash forces were undertaken by Hasbrook, who was subjected to measured seat deceleration of 7G and "probable" chest acceleration of 14G. This resulted in bruising and lower abdominal complaints [123]. Lewis and Stapp [124] carried out 15 to 20G tests on human subjects. These tests resulted in complaints of abdominal pain. They concluded that decelerative forces exceeding 10G at 300G per second rate of onset, for 0.002 second duration would result in minimal contusion over the hip region due to lap belt impingement. At 13G, with the same time duration and rate of onset, in addition to contusions, strain of abdominal muscles could be expected with accompanying soreness.

Lap belt forces of 1518 to 3588lbs (6.7 to 16kN) at 1 to 3ms duration between 15 to 23G were found by Lewis and Stapp with their volunteers tests. Only three of the subjects from a total of 19 received belt bruises, two others were reported to be sore at the lower region of the rib cage, one for 4 days and the other for 2 weeks. However, it must be noted that all the subjects tested were healthy young males.

One run was reported at 26G, the highest human voluntary impact in that series of tests, using a lap belt only, the subject complained of severe epigastric pain persisting for 30 seconds, and pain in the area of the thoracic vertebrae continuing for 48 hours. Seat belt forces were 4290lbs (19kN). The lap belt was 3 inches in width and 16 inches in length. Subsequent human tests on the decelerator track did not exceed 15G in a forward facing lap belted configuration. This is generally considered to be the tolerable upper limit for the human volunteer.

6. BRACE FOR IMPACT POSITIONS

In 1988 Chandler reviewed the brace for impact positions [125]. He stated that the goal of the brace for impact position is to pre-position your body against whatever it is most likely to hit during the crash, and thus avoid secondary impacts.

Whilst this goal is simple, the many conditions which can exist in aircraft operations have resulted in misunderstanding and doubts, due to the inconsistent and sometimes inaccurate advice given to passengers in adopting a brace for impact position.

6.1 SECONDARY IMPACTS

The term secondary impact is applied whenever a space is maintained between a body segment and whatever it may contact during the crash. The deceleration level of the body segment can be much higher than that of the deceleration of the impacting aircraft. This may, therefore, induce a high level of injury depending upon the distance travelled by the body segment and the stiffness characteristic of the contact surface. In order to minimise this effect the following may be used:-

- A restraint system may be used. This may be a lap belt or a combination of lap belt and shoulder harness. This would retard the forward motion of the body.
- The interior of the aircraft may be designed using energy absorbing materials.
- Secondary impacts may be avoided by placing the body in contact with the aircraft interior.

It was this last point which formed the basis for recommending a brace for impact position.

6.1.1 Civil Aeromedical Institute (CAMI) tests

In 1966, Swearingen evaluated eight different seat designs by impacting a dummy head against various locations on the seat backs. He estimated that, of 34 tests at a head impact velocity of 30 feet per second, 30% would have been fatal, 97% would have rendered the passenger unconscious, 80% would have resulted in facial fractures. Only 3% would have produced no injuries or unconsciousness [126]. Whilst the conclusions of Swearingen were focused on the design of seats, they also apply to the adoption of a suitable brace position.

The first tests to be conducted at CAMI for the evaluation of the brace position were conducted by J D Garner in December 1967. This work was conducted in response to questions which were raised by the Society of Automotive Engineers (SAE) S-9 Cabin Safety Committee. The committee

was concerned about the various concerns for protective positions which may be unsafe. Twelve impact tests were completed. These used two rows of passenger seats which were spaced at a pitch of 35 inches. The occupants were represented by 95th percentile anthropomorphic test dummies. Accelerometers were placed in their heads. The dummies were restrained by conventional seat belts.

The tests indicated that the highest head accelerations, of 80G, were recorded when the dummies which were seated upright. The lowest head accelerations, of 8G to 3G were found to occur when the dummies heads were located against the crossed arms which were placed against the seatback in front.

Other tests conducted with the upper torso bent all the way forward and grabbing the ankles would put the head directly against the lower seat back in front. This method would compress the neck and head between the torso and the seat in front, which generated concern about cervical spine injuries.

These tests provided the basis for an early Air Carrier Operations Bulletin pertaining to the brace for impact position (Bulletin No. 69-16). This Bulletin was issued in 1969 and has extensively been revised. This indicated that the "grab ankles" position was least suitable with the 34 to 42 inch seat pitches which were then in use.

One of the limitations recognised by Garner was that the anthropomorphic test dummies then available were poor representations of the human passenger seated in the brace position. Tests were conducted at CAMI in 1981 with much improved dummies compared with those which Garner had used in the 1960's. These were 50th percentile dummies which had considerably been improved in both biofidelity and repeatability. The purpose of the tests was to evaluate the passenger brace position and to analyse secondary impacts with adjacent seats.

The tests assessed the level of injury to the occupant by means of the Head Injury Criterion (HIC). Seven tests were undertaken using three different seat designs. The impact velocities were varied between 48.3 and 51.2 feet per second. The sled decelerations were varied between 6 and 9G and seat pitch between 30 and 34 inches. Fifth percentile female, fiftieth percentile male, and ninety-fifth percentile male dummies were also used.

The highest HIC level measured in the tests was 863, well below the 1000 level which is considered life threatening. This was measured on a 95th percentile dummy which had been initially seated in an upright position. When the dummy was placed in the brace position, the same as that used by Garner in his earlier studies, HIC levels which were approximately one half of those measured with upright seated dummies were experienced. The results of these tests were reflected in a new Air Carrier Operations Bulletin, No. 1-76-23.

Chandler stated that the most appropriate brace position for each occupant in an aircraft will depend on many factors such as the magnitude, direction and sequence of the crash forces, the layout of the interior within the strike envelope of the occupant, the design and configuration of the restraint system, and the size and physical characteristics of the occupant. With so many factors to consider, it is impossible to describe a single brace position which will match every parameter. However, it is possible to note a few general principles which will apply in the selection of a brace for impact position. These are as follows:-

- ♦ Pre-position the body, or body segment against an interior surface in order to reduce the effect of secondary impact. This will also reduce flailing.
- ♦ With the occupant pushed back against the seatback, the seat belt should then be tightened firmly against the occupant. The tighter the seat belt, the better restraint it will provide.
- ♦ The occupant's feet should be placed firmly on the floor.
- ♦ Passengers should not attempt to brace with their legs against the seat in front. This could double the loads acting on the seat in front which may cause it to fail. Seats are not designed to accept these additional loads.
- ♦ The legs should not be wedged under the seat in front because the legs may act as levers which could pry the seats off the floor. This may break the legs or the seat.

6.2 FORWARD FACING PASSENGERS WITH LAP BELT RESTRAINT

Chandler states that the occupant should bend forward over the snug seat belt. The occupant's head should contact the seatback or other part of the aircraft structure. The hands and arms should be placed so that they are between the head and the contact surface, to provide a pad to support the head. If resting against a breakover feature, it may be possible to obtain better support if the seatback is folded forward until it rests against the occupant in front. However, if this is not done, good support may still be provided by the seatback as it folds forward of its own inertia during the crash. The head and arms will slide down the seatback surface. However, these are unlikely to be seriously injured.

Should the seat be located so that the head will not contact any portion of the aircraft interior as the occupant bends forward over the seat belt, the occupant should continue to bend forward and rest the upper torso against the upper legs. The head should be tucked down and not twisted to one side. Twisting of the head will twist the neck. This will reduce the ability of the neck to withstand the impact loads. Flailing of the arms may be reduced in low level crashes if the occupant grasps their ankles or legs.

It is also stated that there may be installations where the interior of the aircraft or the forward facing seat is too far away to provide a secure support for the

head and upper body region but may still be close enough to contact the head during the crash. The head strike envelope of a 95th percentile occupant will extend to between 40 to 42 inches from the intersection point of the seatback and seat cushion. No completely satisfactory solution may be provided for such configurations. Perhaps, the only suggestion is to adopt a brace position with the head well tucked in.

6.3 REAR FACING PASSENGERS WITH LAP BELT RESTRAINTS

Chandler states that passengers in rear facing seats should push themselves back into the seat and tighten their seat belts firmly. They should also sit upright with their heads firmly placed against the headrest. Their lower arms should be placed on the arm rests. This may help to support the upper body and reduce the loads in the spinal column. If the arm rests are not available, the arms should be positioned with the hands on the thighs or clasped in front of the waist. The feet should rest flat on the floor. Clasping of the hands behind the head is not recommended as this may cause stress on the neck due to the mass of the arms and the hands as they react to the impact if the aircraft yaws during the impact.

6.4 FORWARD FACING PASSENGERS WITH LAP AND SHOULDER HARNESES

Chandler states that the forward facing passenger with a lap and shoulder harness should tighten the seat belt in order to eliminate any belt slack after pushing back in the seat so that the torso is firmly against the seatback. The occupant's chin should be placed against the upper torso to minimise secondary impact. The hands should be placed in the lap, however, the wrists and elbows should not be locked. The occupant should not hold on to the restraint system with the hands. This can introduce slack into the system, especially if it is equipped with an automatic locking retractor. Any slack will tend to increase the risk and degree of injury. The feet should be placed flat on the floor slightly in front of the forward edge of the seat, so that if the clearance between the seat and floor is reduced during the crash, the front edge of the seat will not catch the back of the lower legs.

7. SUMMARY OF RESEARCH OBJECTIVES

1. To undertake a computer simulation of the Kegworth air crash, on occupants seated in a Weber aircraft seat, in order to ascertain how certain occupants were injured during the crash.
2. To correlate the contact forces predicted by the computer model with the injuries sustained.
3. To assess the effect of the brace and upright positions adopted on impact.
4. To evaluate the effects of body posture and impact pulses upon 5th percentile female, 50th percentile male and 95th percentile male occupants.
5. To evaluate the loads sustained on the head, thorax, lumbar spine, pelvis and lower limbs.
6. To correlate a three dimensional computer model against impact testing and carry out a detailed parametric study of specific changes to the model.
7. To create a dataset for spine modelling in order to determine the loads sustained by the vertebrae during an impact with the objective of assessing the injury potential of the brace crash position.

8. SIMULATION OF THE KEGWORTH AIR ACCIDENT

8.1 THE ACCIDENT

On 8th January 1989 a Boeing 737-400 codenamed G-OBME was employed in a double shuttle between Heathrow and Belfast. It landed at Heathrow at 18.45 hrs. After completing the first shuttle, it took off for Belfast at 19.52 hrs. During the flight, the crew, having experienced vibration and smoke, shut down the right engine. According to the flight crew, shutting the right engine successfully concluded the problems. However, in the cabin some passengers had seen fire emanating from the left engine.

The crew had advised London Air Traffic Control that they had an emergency aboard the aircraft, which was subsequently diverted to East Midlands Airport. The approach to the airport continued until 20.23 hrs. at a height of 900 feet above ground level when the left engine lost power with high vibration levels. The crew tried to restart the right engine without success. The aircraft subsequently struck the ground at 20.24 hrs. having suffered fan blade failure in the left engine. The crew had mistakenly shut down the wrong engine.

The initial impact with the ground was in a nose-high attitude on level ground just east of the M1 motorway, Figure 2. The aircraft then passed through trees and subsequently suffered a second major impact on the western northbound carriageway of the motorway and with the lower section of the embankment. The second impact took place some 70 metres from the initial ground contact and 10 metres below it [127]. Failure of the fuselage took place as the aircraft came to rest in the wooded area on the embankment.

The wreckage of the aircraft showed two major failure lines in the fuselage, Figure 2a, one was slightly forward of the wing box section and the other rearward of the wing. This had resulted in the nose section becoming detached from the centre section and the tail section rotating over, and to the right of, the mid section. Examination of the engines by the Air Accidents Investigation Branch (AAIB) showed that the left engine had suffered fire damage. The left wing appeared to have contained fuel whereas the right wing had sustained impact damage causing leakage of its fuel contents. This had culminated in a small fire which was rapidly extinguished by the emergency services who had arrived at the scene of the accident. The right engine had shown no evidence of fire damage.

An analysis of the behaviour of the occupants during the accident was made with the objective of increasing survivability in aircraft. The work was performed with the Nottingham, Leicester, Derby, Belfast (NLDB) study group. The analysis consisted of a computer simulation of the motion, acceleration and force histories sustained by the occupants. These were correlated with injury data. The analysis was restricted to those seat positions where the seats were retained in the aircraft. Where catastrophic failure of the

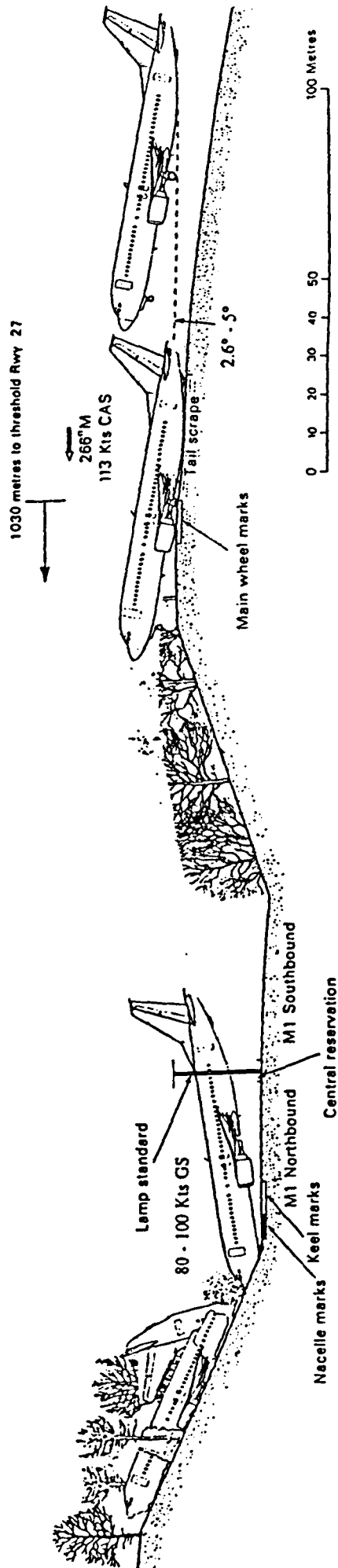


Figure 2. G-OBME Impact Sequence

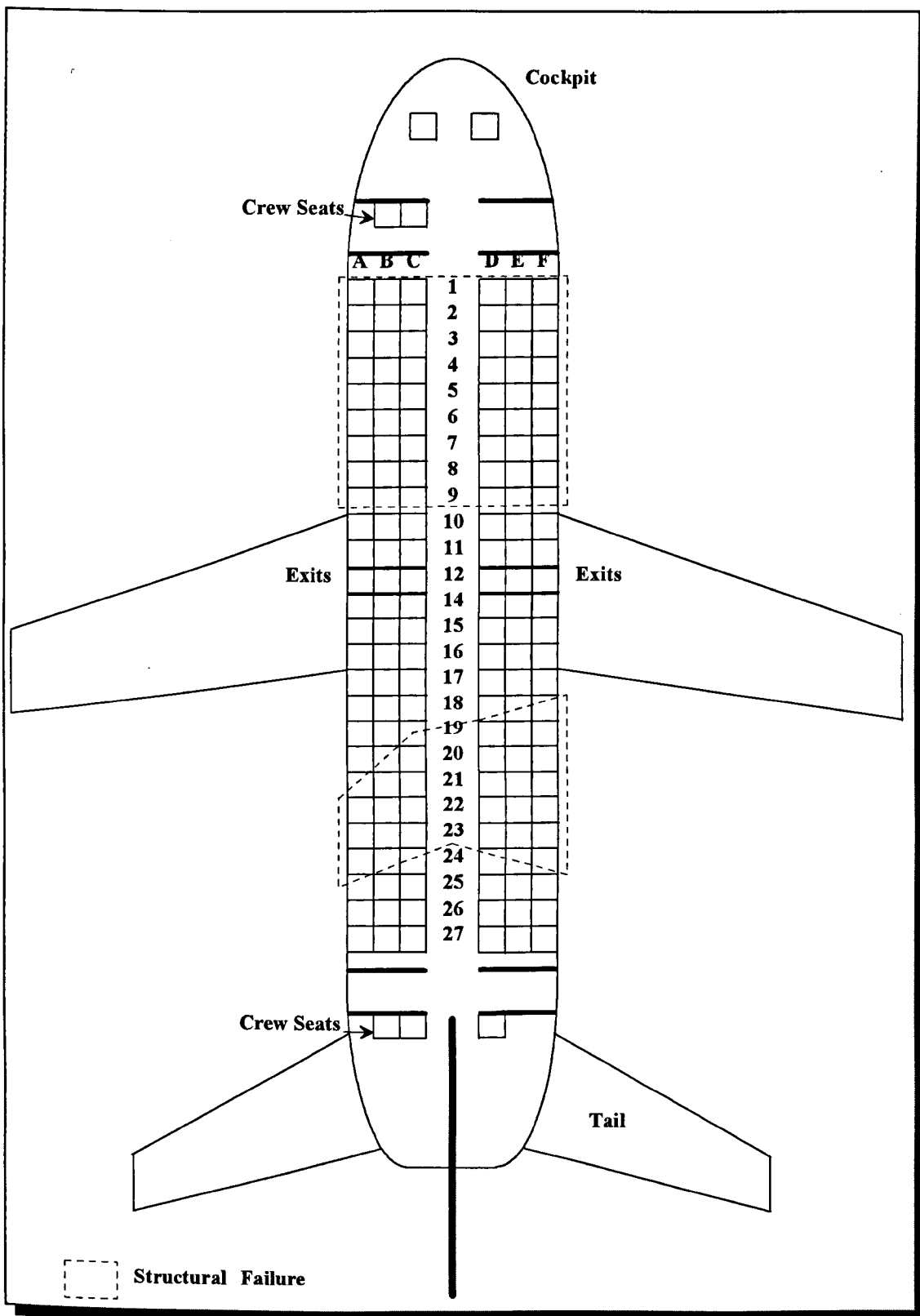


Figure 2a. Seating Layout Aboard G-OBME.

fuselage and floor occurred, there was a loss of survival space and a further understanding of the detailed mechanisms involved could not be fully investigated.

The aircraft sustained an impact estimated to extend for a total period of 2.2 seconds. This commenced with the initial tail skid impact on the east side of the motorway, until the aircraft came to rest in three sections, on the embankment. The tail skid impact is estimated to have had only minor effects on the occupants, from a kinematic perspective.

Some seats were retained in the nose section, mostly those of the crew, and also in the tail section. The latter was exposed to a more complex motion, over a longer distance, as it overrode the central section, coming to rest upside down. The central section was the area of the aircraft best preserved and was chosen for the simulation. The analysis was therefore most applicable between row 10 and row 20, the overwing area.

A survey of structural damage to the aircraft seats and floor was carried out by the NLDB team. The occupant simulation study was set up in the area surrounding seat 15F. The floor was intact and the seats had remained in position. Examination of the seat itself showed deformation of the seat pan and the front support member depressed on the unsupported end. Examination of the nonbreakover seat in front, 14F, showed deformation of the seat back and failure of the seat reclining mechanism.

Immediately prior to the crash the passengers were advised to assume a brace position. Not all of the occupants heeded this advice, and a number remained in an upright position. Accordingly, a model was analysed with the occupant in an upright position. Of the people who assumed a brace position some had their legs in front of them whilst others kept their legs tucked backwards. The model has the occupants legs angled slightly back. Analysis has also been performed with the legs angled slightly forward of the vertical.

8.2 THE INJURIES

There were 126 passengers on board of which 79 survived the accident, Figure 2b. Treatment of the injured was carried out at the Nottingham, Leicester, Derby and Mansfield Hospitals. Varying degrees of injuries occurred, however, the most severe injuries took place between rows 6 to 8 in the region of the forward fuselage break where the floor structure failed. Further serious and fatal injuries occurred at the rear fuselage failure, and in the area where the tail had swung over and into the centre section. Thirty nine passengers died at the scene of the accident, eight more died later in hospital.

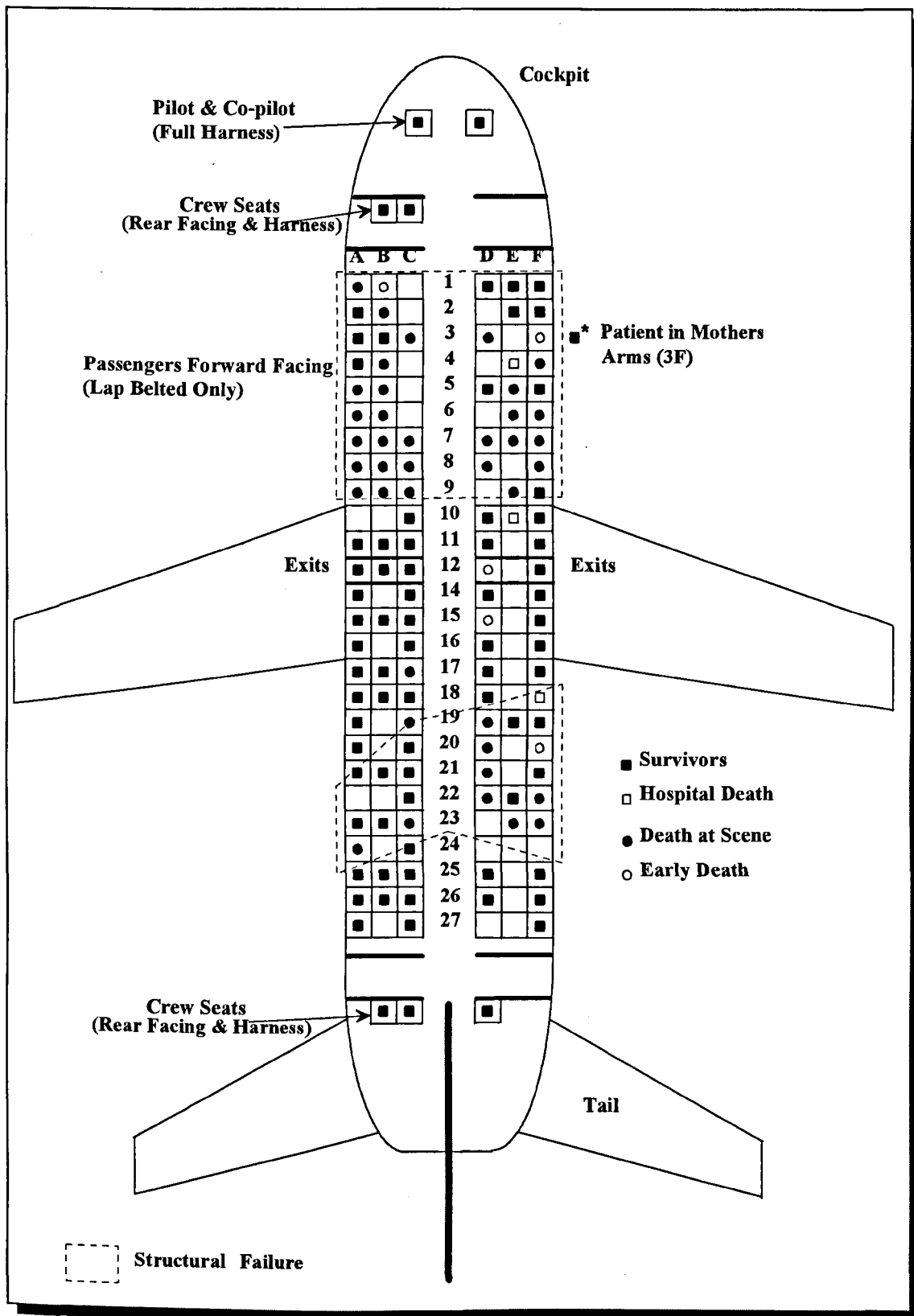


Figure 2b. Distribution of Survivors and Fatalities Aboard G-OBME.

CRASH PULSE OF AIRCRAFT G-OBME AT CENTRE SECTION

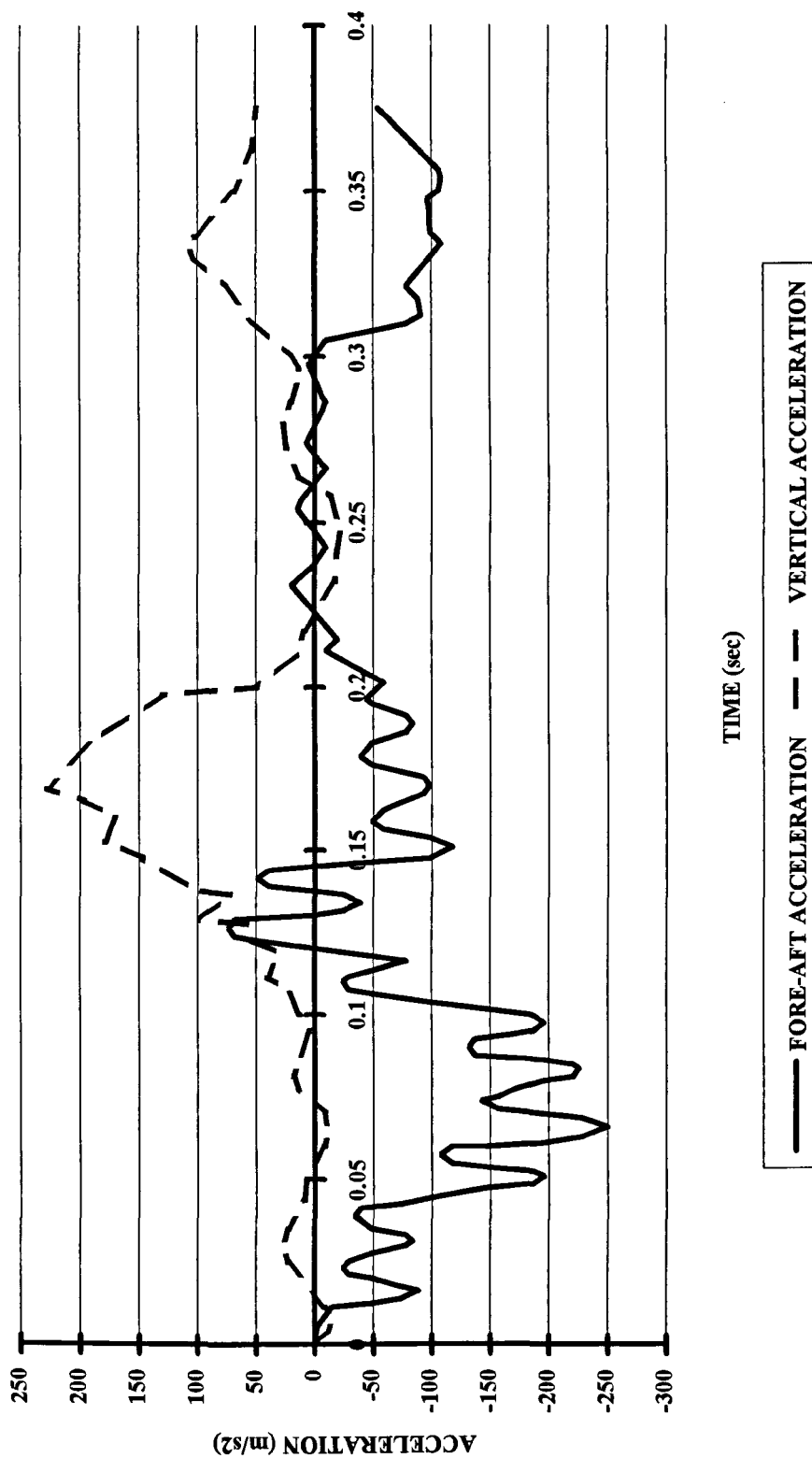


Figure 2c. Calculated Crash Pulse of Aircraft G-OBME

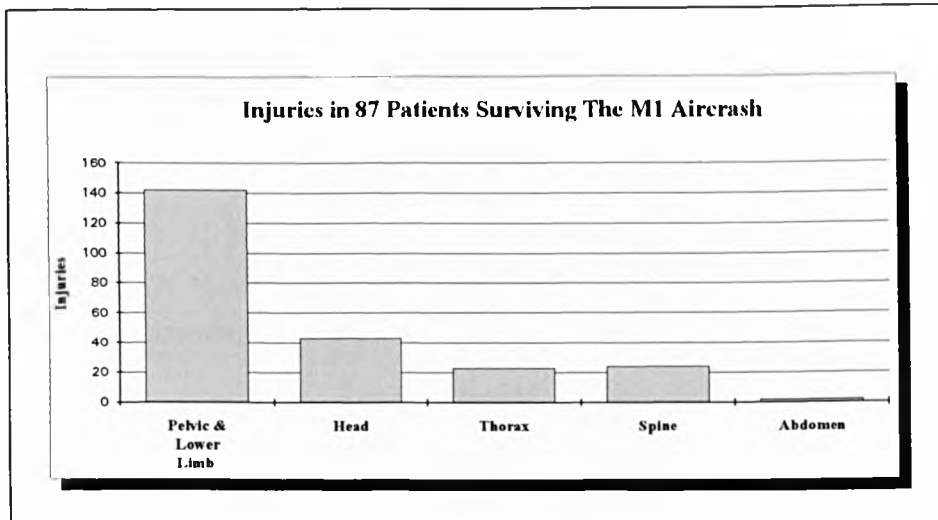


Figure 3. Injuries In Patients Surviving The M1 Aircrash

8.2.1 Head Injuries

All but one of the thirty nine fatalities at the scene of the accident sustained head injuries of varying description. Eighty five per cent of the survivors (77) had evidence of facial or head injuries [128]. Forty five patients had amnesia immediately after the crash. Seven patients had severe head injuries five of whom survived.

The patterns of injuries to the head indicated that 21 patients (24%) had had contact rearward of the vertex. It is suggested that they were struck from behind. Five patients also presented with direct blows to the back of the head. The cause of the injuries may be attributed to falling debris and detachment of the stowage bins at impact.

Facial injuries and unconsciousness were also noted in 43 patients who were treated at hospital.

8.2.2 Upper Limb Injuries

There were 19 non-survivors and 28 survivors who sustained dislocations and fractures of the upper limbs and shoulders.

8.2.3 Neck and Spinal Injuries

The total number of injuries to the neck were 27. These were categorised as 21 in the non-survivors and 6 in the survivors. In addition, there were 6 thoracic fracture dislocations and 12 lumbar fracture dislocations. Spinal injuries were seen in the region of the aircraft which had sustained severe disruption of the fuselage.

8.2.4 Chest Injuries

The majority of the non-survivors were found with major chest injuries (all but one). The degree of injuries in the survivors was found to be severe with major chest trauma [129]. 18 of the 79 survivors had suffered such injuries. It was found that fewer rib fractures were apparent with young patients in comparison with elderly patients who exhibited a higher incidence of rib fracture [138]. A pattern of injury was discovered which showed that the upper part of the lungs had been subjected to a greater loading. The mechanism of injury was thought to be associated with inertial loading of the internal organs, abdomen and lungs against the thoracic apex at the time of the impact.

8.2.5 Abdominal Injuries

There were 36 non-survivors with abdominal injuries compared with only 2 of the survivors who suffered major abdominal injury. 30 patients presented with lower abdominal bruising around the iliac crest. This was associated with the lap belt loading [130].

8.2.6 Spinal Injuries

Spinal injuries were apparent in the area of the aircraft which had sustained fuselage damage. In the survivors, 21 passengers sustained a total of 24 spinal, 6 cervical, 6 thoracic and 12 lumbar fracture dislocations. In the non-survivors, severe spinal injuries were observed. One lumbar fracture was recorded, 6 thoracic and 6 cervical fracture dislocations. The thoracic injuries were generally associated with damage to the aorta and sternal fractures.

8.2.7 Pelvic And Lower Limb Injuries

The number of survivors who sustained pelvic and lower limb injuries were 57. There were 23 pelvic fracture dislocations, these were predominantly in the centre section of the aircraft where the floor and seatbase structures remained largely intact. There were 22 femoral fractures, these occurred throughout the aircraft, however, the centre seats exhibited a higher incidence of femoral fractures, which is thought to be associated with the stiffer front spar. Thus resulting in bending fracture of the femur.

There were 18 knee injuries, these were largely associated with contact with the seat in front. The mechanism of injury is similar to that which is observed in automobile accidents where the knees strike the knee bolster which form part of the instrument panel [131]. Examination of the rearward section of the seat, in line with the knees, showed deformation of the knee panel and the lower region of the seatback.

There were 31 tibial fractures, these injuries were largely observed in the region of the aircraft where severe fuselage disruption had occurred. Some injuries also occurred in the area of the aircraft which had remained intact. These injuries may be attributed to leg flail [5].

There were 26 ankle fractures and 22 foot injuries. The foot fractures which were observed [132] were compound talar fractures. The majority of these injuries were observed in that part of the aircraft which had sustained severe floor deformation. Some injuries may also have occurred as a result of flail and foot entrapment in the section of the aircraft which had remained structurally sound.

The non-survivors sustained a total of 95 pelvic and lower limb injuries. Nine pelvic and 13 femoral fractures, 5 knee injuries, 38 lower leg fractures, 24 ankle fractures and 6 foot injuries. Only 18 surviving and 6 non-surviving passengers had no injury to the pelvis and lower limbs.

8.3 COMPUTER SIMULATIONS

Two independent computer models were set up to investigate the structural and survivability aspects of the accident. The first model was created by Cranfield Impact Centre (CIC) using the computer program KRASH for the structural impact study. The second computer model was created by the author using the crash victim simulation program MADYMO [133] specifically for the occupant survivability study.

8.3.1 KRASH Computer Simulation

As the Flight Data Recorder employed volatile memory buffering, the data for the second and main part of the impact with the ground was not recorded. Therefore, it was necessary to reconstruct the acceleration pulse of the ground impact. This was carried out using the computer program KRASH. KRASH is a hybrid program comprising of a simple library of structural elements which incorporates test derived data for the collapse properties of the structural members. The program was developed by the Federal Aviation Authority (FAA) for the analysis of aircraft impacts. The fuselage of the Boeing 737-400 was modelled in three sections using beam elements [134]. These were the forward, centre, and tail sections and were represented as three lumped masses divided by two break regions to model the collapse mode. The two engines and landing gears were also modelled as lumped masses, thus creating a complete eight mass model of the aircraft. The total mass and moments of inertia of the passengers, luggage and fuel were also added to the lumped masses.

The bending behaviour of the fuselage was achieved using a simple beam element model. Furthermore, contact springs were added to the lumped masses to represent the collapse characteristics of the structure on contact with the ground. The model was then run to derive the crash pulse. Three runs

were performed. Run 1 was conducted for the whole impact sequence. This represented the two ground impacts, on initial touchdown and on striking the western embankment of the M1 motorway. The aircraft was simulated as having a free ballistic trajectory and an estimated coefficient of friction on contact with the ground. However, the trajectory of the second ground impact was initially shown to occur too far up the western embankment.

Run 2 was restarted from the second ground impact with initial horizontal and vertical velocities of 48.9 m/s and 14.4 m/s respectively. On impact with the ground, this produced peak deceleration levels at the centre section of the aircraft of 26.5G horizontally and 23G vertically. These pulses were subsequently filtered using a 60Hz filter which produced a maximum resultant deceleration of 19.5G.

Run 3 was once again restarted from the second ground impact, however, attempts were made to include residual wing lift which approximated to 40% of the aircraft weight. Initial velocities of 37.9 m/s and 11.1 m/s in the horizontal and vertical axes were applied to the model respectively. This gave impact decelerations of 19.5G horizontally and 12.6G vertically. On filtering the signals, this gave a maximum resultant deceleration of 15.5G.

Run 2 and run 3 were then applied to the MADYMO crash victim simulation program. The occupant simulation showed that correlation with body injuries and the kinematics of the occupant could only be obtained with run 2. Therefore, run 2 was subsequently used in the impact study.

8.3.2 MADYMO Computer Simulation

The occupant kinematics were analysed using the crash victim simulation program MADYMO. In order to create the computer model, geometrical data of the seats, aircraft interior environment and component tests were required. The creation of the model is described below:

8.4 DATA ACQUISITION

Drawings supplied by the Air Accidents Investigation Branch (AAIB) were used to define the seat geometry and pitch. A list of drawings used is presented in Appendix 1. In addition, further information was required to establish the interface force-deflection characteristics between the occupant and the interior environment. Measurements were also made to establish the friction and damping. The required information and its source are described below. To develop the crash victim simulation models, a number of tests were conducted. These tests were performed with the aid of a technician under my supervision:-

8.4.1 Seat Description

The seats were made by Weber Aircraft of Burbank, California. The model number was 4001-3. The serial number of the seat, which was tested, was 310. This was of a triple seat construction, Figure A3.13, supported to ground through the mid seat by means of four seat legs. The two front legs were vertical whilst the rear legs were inclined forward at an angle of 45 degrees and attached to the seat base by a triangular structure. The two outer seats were cantilevered by spars running the whole length of the triple row. The spars were made of aluminium alloy. These were attached together by means of perforated aluminium sheet metal, Figure A3.16, with the latter forming the seat base. The seat cushions were made from moulded foam, covered with imitation leather plastic and were attached to the aluminium sheet using Felcro.

For seat 15F, a breakover seatback was attached to the seat base structure through pivots. The seatback was constructed using aluminium alloy tubing, perforated aluminium sheet metal and foam and were similarly covered as the seat cushions. A food tray was attached to the seatback and pivoted through the seatback attachment point by aluminium bars adjacent to the seatback frames.

The seat in front, 14F, was similar in construction to 15F with one exception. As this seat was the exit row seat, it was of the nonbreakover type. Hence it was modelled using the nonbreakover stiffness characteristic of the seatback.

The seat belts were made by AM-SAFE of Phoenix, Arizona. These were attached to the seat base using shackles, Figure A3.16. The belt stiffness characteristics were supplied by AM-SAFE and were of 13% elongation at a load of 10kN.

8.4.2 Seat Profile Measurement.

The seat profile was measured using a Stiefelmeyer electronic profile measuring machine, serial number 30380187. The machine is capable of measurements to a resolution of 0.01mm. This allowed accurate definition of the seat surfaces for construction of the crash victim simulation model.

8.4.3 Moment Of Inertia Of The Seat And Seatback.

The mass moment of inertia of the seatback was determined using the trifilar method. The results are outlined in Appendix 2.

8.4.4 Seat Base And Seatback Stiffness Measurement.

Seat base and seatback cushion stiffnesses were determined using a ballasted dummy, a Salter digital force gauge, model EFG500, serial number 5806 and

a dial test indicator model type 252 made by Mercer. Appendix 3 outlines the force-deflection characteristics derived from test.

The occupant hip rotational point ("H" point) location was obtained using a 50th percentile dummy [135]. The "H" point was determined using the Stiefelmeyer measuring machine. The photographs presented in Appendix 3 show the test set-up.

Knee/lower leg contact stiffness on the seatback was determined. This is presented in a graphical format in Appendix 3.

The foot tray stiffness was determined using the force gauge and dial test indicator. Results of the test are presented in Appendix 3.

The breakover seatback hinge stiffness for a Weber type 424 seat is presented in Appendix 3. This was also determined by test.

The nonbreakover (locked) seatback stiffness for a Weber type 444 seat is presented in Appendix 3.

8.4.5 Seat Front Bar Load Deflection Characteristics.

The seat front bar of row 15 seat F was removed from the wreckage of G-OBME. The objective was to determine the force-deflection characteristics and hence the ultimate tensile strength. The test was carried out using a multi-load range Denison Universal Testing Machine, serial number 28956. A linear voltage displacement transducer was used to record the displacement. The tube was rigidly fixed to a jig, presented in Appendix 3. The photographs show the test in progress.

8.4.6 Aircraft Floor Stiffness

The floor stiffness of the aircraft, at the seat attachment location, was measured in situ using a force gauge, hemispherical loading form and dial test indicator. This gave a result of 175N/mm.

8.4.7 Additional Information Supplied.

The lap restraint was modelled from information supplied by the AAIB, Weber, AM-SAFE, and British Midland Airways at East Midlands Airport. The analysis model accounted for anchorage locations, belt lengths and buckle details. The belt properties are based on information supplied by AM-SAFE. These are presented in Appendix 3.

Seat surface friction was obtained from HW Structures library data using a denim test piece to represent clothing. This gave a friction coefficient of 0.5.

8.5 MODEL DEVELOPMENT

The model was set up using the data acquired and in accordance with the following guidelines, Figure 4:-

- a) Initially the model was built using a single system model, beginning with the occupant of seat 15F. Experience has shown that building the model simply and gradually is the quickest method for understanding the behaviour of the model.
- b) The model was initially set up with the minimum number of interactions, firstly, with the seat base on which the occupant was placed. The dummy database is supplied as a single system comprising of a number of joints attached together using local co-ordinate systems. The dummy dataset was positioned at the 'H' Point. This was subsequently oriented in the seat using the measured posture angles of the torso and limbs.
- c) The model was subsequently run with gravitational acceleration applied to the occupant for a period of 100ms to check that the only force that is active is the seat base contact force and that all other forces were correctly switched off. Using this procedure, the dummy dataset was maintained in equilibrium. The dummy torso should remain static if the seat stiffness and dummy 'H' Point are correctly specified. This was achieved using the product of mass and acceleration and equated to the product of the seat stiffness and penetration.
- d) The contact interactions between the dummy and the interior environment were then introduced gradually. Each interaction was assigned damping, friction and hysteresis.
- e) The front seat was then added to the model with another 50th percentile dataset positioned in it. The front seat was modelled with the seatback fixed. This seat was of the nonbreakover type.
- f) In total, the model comprised of five individual systems, that is, the floor and bulkhead, two seats, and two occupants. Each system was modelled using planes and ellipses with their individual stiffness characteristics.
- g) The aircraft system was represented by two planes each having a stiffness characteristic for the floor and the bulkhead. These stiffnesses were obtained by tests using a head form. The mass of the centre section of the aircraft and the moment of inertia were supplied by CIC. These were positioned at the centre of gravity of the wing box section.

- h) Each seat system was modelled using planes and ellipses. Joints were applied to the seatbacks to represent the breakover characteristics of the rear seatback, and for the front seatback, the nonbreakover characteristics. Each seat base was modelled with planes to represent the surface of the seat. Three planes were used for the top surface of the seat base. Each plane was assigned a stiffness characteristic and a contact interaction with the pelvis and femurs of the occupant.
- i) To represent the front curvature of the seat, a number of smaller planes were used for aesthetic purposes and were not assigned contact interactions with the occupant. The latter was performed as the code had difficulty representing the correct interactions with small planes. The base of the seat comprised of two ellipses and planes. These were used to model the two spars and the aluminium panels respectively beneath the seat cushion.
- j) Each seatback was modelled utilising a number of planes to define the seatback cushions, food tray and the aluminium panels. These were also assigned their respective stiffness characteristics. The seat bases and seatbacks were also tested using a trifilar apparatus to determine their moments of inertia. These were also weighed individually. This data was then used to model the seat system.
- k) On modelling the seat systems, these were subsequently positioned at a pitch of 32 inches apart. Both seats were then fixed to the floor of the aircraft by point restraints. The acceleration pulse, which was determined by CIC, was then applied to the floor of the aircraft (model).

To represent the occupants, a two dimensional dummy database was used. This was supplied by TNO. This comprised of nine joints each linked to an element using local co-ordinate systems. Each element represented one body segment having its own mass and moment of inertia. The joint characteristics were obtained by test and represented the joint characteristics of the Hybrid III dummy. The body segments of the dummy were represented by second order ellipses. These were assigned individual stiffness characteristics. Each segment was then assigned a contact interaction with adjacent surfaces.

The results obtained from the model were focussed on only the rear occupant. These were the resultant head and thorax accelerations, the pelvis, the femur and the tibial contact loads, and the lap belt load. The Head Injury Criteria (HIC) was subsequently calculated from the resultant head acceleration.

Pre and post-processing was achieved using Madprep and Madpost [136]. The occupants were simulated by a Hybrid III dummy dataset. Although other sizes of occupant were available, it was decided to use an average (50th percentile) male dummy dataset which represented the stature of the occupant seated in seat 15F. Further investigation [132] showed that most occupants in

the area of interest could be approximated to 50th percentile, and the work would have the widest generality.

Initially a single occupant, for whom a fairly comprehensive set of data was known, was selected for the study. This was to permit correlation with body injuries to be made since, unlike a controlled test, there were obviously no instrumentation results available. The occupant chosen for the correlation was seated in row 15, seat F directly behind the emergency exit in the centre section. This occupant had assumed a brace position prior to the crash with the lower arms vertically between the head and the facing seatback.

The simulation comprised of two seat rows. The front seat held a second, supplementary, 50th percentile occupant. This was for the purpose of creating the correct response and contact environment for the primary occupant. In front of the second occupant a bulkhead was modelled to provide an additional restraint and reduce the forward translation of the front occupant.

Studies using a sister aircraft (G-OBMF) were used to determine a probable brace position of the occupants, Figure A4.2, supplemented by the anecdotal evidence of survivors.

Most of the seat backs have been designed such that if a small force is applied in the forward direction they will collapse (Weber type 424). This is achieved by incorporating a torque limiting device at the base of the back frame. This breakover facility is to aid in the evacuation of a smoke filled cabin. The configuration of this type of aircraft also contained nonbreakover (i.e. locked upright) seats (type 444). Thus, with row 15 directly behind the emergency exit the seatbacks of the row in front, 14, were of the nonbreakover type.

Inspection of the aircraft after the crash showed that many locked seatbacks had suffered total bending failure, thus the model was set up with an appropriate nonbreakover stiffness characteristic. This stiffness was obtained by test, Appendix 3.

In addition to the breakover stiffness the rear of the seat back carries a service table. This feature defines the local stiffness of the rear of the seat back. The effect of the local stiffness was also examined.

8.6 PARAMETRIC CONFIGURATIONS

A parametric study was performed to study the effects of making changes to the computer model. This study concentrated on making changes to the design of the seats for both brace and upright positions, with the objective of improving aircraft crash survivability.

8.6.1 Lap Belt Design

The design of the belt system is crucial in reducing the forward travel of the occupant and subsequent injuries sustained. From automotive experience, the significant parameters which affect the severity of the injuries are the belt slack, the lap belt angle and the belt stiffness. The amount of slack in the system allows the occupant to travel further forward in the seat before the belt takes effect. Thus, this increases the rate of change in velocity of the body before contact occurs with the seat in front. At Kegworth, it is understood that the crew had instructed the occupants to pull their belts tight prior to impact.

The lap belt angle has considerable effect on the restraint of the pelvis and the risk of submarining. The latter occurs when the pelvis rotates backwards such that the lap belt travels over the iliac crest. The result is to allow the belt to travel through the soft tissue of the abdominal region causing severe disruption of the internal organs. Should the lap belt angle be too low relative to the horizontal, this is likely to induce submarining. At Kegworth this angle was set at 65 degrees to the horizontal and proved to be effective in restraining the occupants. Thus submarining injuries were not apparent [132].

For the parametric study, it was decided to examine the effect of varying the belt stiffness characteristics. The seat belt stiffness specifications had a wide manufacturing tolerance band as compared to automotive applications. The maximum belt elongation was specified as 18% strain at a load of 2500lbs, with an average elongation of 14% strain at a load of 2500lbs. The latter is equivalent to 13% strain at a load of 10kN. Belts of 13% strain at 10kN were used in the baseline models. In addition, the following belt elongations were examined in the parametric study, 8% strain at 10kN, 12% strain at 10kN, and 16% strain at 10kN.

8.6.2 Folding Seatback Breakover Stiffness

The majority of seats in an aircraft have the capability of falling forward under the application of a small force, and G-OBME was no exception. This is for the purpose of aiding evacuation in the event of fire. This equivalent torque has been measured and is given in Appendix 3. Three levels of breakover stiffness have been analysed. Modelling of these parameters was achieved using a cardan joint which was located at the hinge mechanism of the seatback.

8.6.3 Seat Pitch

It was decided to investigate the use of varying seat pitches as this could affect the injuries sustained by the occupant during the crash. It is the responsibility of the operator of the aircraft to decide upon the seat pitch to be employed during flight. It is obvious that this parameter has a direct influence on the cost to the operator. A closer seat spacing is more cost beneficial to the

operator. However, since 1989, the operators have been set a minimum seat pitch of 28 inches by the CAA. For this study, three different seat pitches were investigated, 31 inches (787mm), 32 inches (813mm), and 36 inches (914mm). The majority of seats were spaced at 31 and 32 inches. The seat pitch between rows 14 and 15 were set at 32 inches.

8.6.4 Fixed Seatback Failure Stiffness

The occupant chosen for the correlation work was positioned behind a seat which had been locked in an upright position, that is, it had a nonbreakover seatback. As stated earlier, most of the seats aboard a passenger aircraft are of the breakover type. However, those seats which are adjacent to the exit are designed to have fixed seatbacks. This is for the purpose of not impeding evacuation in the event of an emergency landing. For the parametric study, the torque for seatback failure was doubled and halved.

8.6.5 Seatback Local Stiffness

It was decided to investigate the influence of varying the seatback local stiffness against which the head of the rear occupant contacts in the event of a crash landing. Many seatbacks are designed with stowable food trays which are stiff in construction and may fracture in the event of impact. Their frames are made from solid aluminium bars which may cause injury. As a result, parametric studies of the seatback local stiffness were assessed. The parameters chosen were the doubling and halving of the stiffness characteristics.

8.6.6 Seat Front Cushion Angle

In automotive applications, the risk of inducing submarining may be reduced by inclining the front section of the seat base upwards. It is recommended that this angle be in the region of 12 to 16 degrees. Thus the angle of the seat front cushion was varied to study the effect this may have on the occupant. The measured angle for the baseline model was 7 degrees relative to the horizontal. The alternative angles analysed were 11 and 15 degrees.

8.6.7 Seat Base Stiffness

In automotive impacts, the stiffness of the seat base also affects the risk of inducing submarining. Thus the seat cushion stiffnesses were varied to study whether this phenomenon is likely to occur. The baseline stiffnesses are presented in Appendix 3. For the parametric study, these characteristics were doubled and halved.

8.6.8 Lower Leg Position

In assuming the brace position, some occupants maintained a brace position with their lower legs "tucked" backwards slightly under their seat, whilst

others placed their legs forward of the vertical. Two positions were consequently investigated one with the lower legs 11 degrees rearward of the vertical and the other 11 degrees forward of the vertical. The former is depicted by the baseline model. The luggage bar forms a natural stop for the lower legs against which they were positioned. This formed an angle of 11 degrees rearward of the vertical. In the two dimensional model the luggage bar was excluded, as no contact was shown to occur with it anyway.

8.6.9 Knee and Lower Leg (to Front Seat) Contact Stiffness

In automotive impacts, the knee bolster, which forms part of the instrument panel, plays an important role in reducing the forward travel of the occupant and thus the change in velocity. This parametric study was conducted on the upright occupant, where considerable knee and tibial contact took place. The contact stiffness of the knee panel was doubled and halved to study this effect.

8.6.10 Knee Panel Position

Investigation of the knee panel position was made to assess the differences in injury levels on the upright occupant. The knee panel was moved 50mm forward and rearward of the mean position.

8.7 RESULTS

The results obtained from the analysis are displayed in the tables and figures. A summary of maximum values is presented in Tables 15 to 17. Also presented is the Head Injury Criteria (HIC) which defines acceleration time history in a single digit. Regulations require this figure to be below 1000, which is considered to be a survivability threshold and therefore injury may occur at lower levels. This study considers femur loading to be at the limit of injury threshold at 4000N for bending and 10000N axially.

8.7.1 Brace Position Sensitivity Study

The Baseline model consisted of belts of 13% strain at a load of 10kN, seat stiffness as shown in Appendix 3 and the front seat of type 444 construction (with a nonbreakover seatback). The model was verified by correlation with the recorded injuries of the occupant of 15F and with the structural damage to seats 15F and 14F. Figures 4 to 27 show the occupant kinematics and the sensitivity study associated with the analysis. Table 15 presents the peak injury levels sustained by the rear occupant.

Belt Stiffness

Figures 7 and 9 show the results of the belt stiffness analysis. Decreasing the belt stiffness from 8% strain at 10kN to 16% strain at 10kN increases the Head Injury Criterion (HIC), Figure 7. It is also observed that both the head and thorax accelerations have increased.

Figure 8 shows the load versus percentage elongation. As the percentage elongation is increased the axial femur load is decreased, however, the vertical femur loads are increased. The pelvis load is also reduced.

Folding Seatback Breakover Stiffness

Figures 10 and 12 show the results of the seat breakover stiffness. Increasing the stiffness causes a slight reduction in the head acceleration and consequently the HIC value. The thorax accelerations remained relatively constant, Figure 10.

Figure 11 shows the load versus seatback breakover stiffness. The belt, femur vertical and femur axial loads are largely independent of the breakover stiffness, but pelvis loads are increased with increasing stiffness of breakover.

Seat Pitch

Figures 13 to 15 show the results of the seat pitch analysis. Increasing the seat pitch for the brace position reduces the HIC value, Figure 13. This also reduces the peak head acceleration. The thorax acceleration remains relatively constant.

Figure 14 shows the load versus seat pitch. It is observed that the axial and vertical femur loads are reduced together with the pelvis load. An increase in belt load is also apparent in Figure 15.

Fixed Seatback Failure Stiffness

Figures 16 to 18 show the nonbreakover seatback stiffness. Figure 16 shows the HIC and acceleration results associated with increasing the stiffness of the seats (Type 444). It is apparent the HIC and head and thorax accelerations are reduced.

Figure 17 shows the load versus seatback nonbreakover stiffness. It is apparent that both axial and vertical loads decrease as the nonbreakover seatback stiffness is increased. This decreasing trend is also apparent with the belt loads, Figure 18.

Seat Front Cushion Angle

Figures 19 and 21 show the results of the seat front cushion analysis. Figure 19 shows the HIC and head acceleration. The thorax acceleration decreases as the angle of the seat base front cushion is increased.

Figure 20 shows that the axial femur load decreases as the cushion angle is increased. The vertical femur load and belt load, Figure 21, increase with an increase in the front cushion angle. The pelvis load increases as the angle is increased from 7 to 11 degrees, however, this decreases as the angle is increased from 11 to 15 degrees.

Seat Base Stiffness

Figures 22 and 24 show the results of the seat base stiffness sensitivity study. It is observed in Figure 22 that the HIC and head acceleration increase as the stiffness of the seat base is increased. There is an increasing tendency in thorax acceleration as the seat base stiffness is decreased by a factor of 2.

Figure 23 shows that the axial femur load decreases with an increase in the seat base stiffness, however, the vertical femur load decreases as the stiffness is increased. Both pelvis and belt loads increase with an increase in seat base stiffness, Figures 23 and 24 respectively.

Lower Leg Position

Figures 25 to 27 show the kinematic results of the lower leg positioned 11 degrees forward of the vertical. It is apparent the lower leg rotates forward and the tibia strikes the seat in front. A significant increase in injury level is obtained above the established baseline value, Table 17.

8.7.2 Upright Position Sensitivity Study

The Baseline model consists of belts of 13% strain at a load of 10kN, seat stiffness as shown in Appendix 3 and front seat of type 444 construction (with a nonbreakover seatback). Figures 28 to 62 show the sequential kinematics and the sensitivity results of the upright position baseline analysis. A greater degree of knee and tibia contact occurred, compared with the brace position. Higher rotation of the knee and ankle joints also took place as the feet struck the aircraft floor.

Flailing of the lower legs was observed. Flailing refers to the uncontrolled behaviour of the lower limbs, following an impact. The lower legs are thrown forwards and upwards causing hyperextension of the knee joints. Head and pelvis penetration into adjacent surfaces were more apparent with a HIC value of 974, and pelvis loads in excess of 7kN. These values are on the threshold of serious debilitating injury.

Belt Stiffness

Figures 31 to 34 show the results of the belt stiffness study. Increasing the percentage elongation from 8% strain at 10kN to 16% strain at 10kN increases the forward translation of the occupant. This causes an increase in both HIC and head acceleration, Figure 31. There is a tendency for the thorax acceleration to increase at 7% strain with a subsequent decrease at 16% strain.

Figure 32 shows the load versus belt percentage elongation. The pelvis load increases rapidly with an increase in elongation. The pelvis contacts the seat front bar causing the occupant to rise, thus reducing the axial femur load. The belt load, Figure 34, increases with an increase in belt elongation. Figure 33 demonstrates that the tibia and foot loads increase as the elongation of the belts are increased.

Folding Seatback Local Stiffness

Figures 35 to 38 show the results of increasing the seatback stiffness on which the rear occupant strikes. Figure 35 shows that increasing the stiffness causes the HIC and head acceleration to increase. A slight increase in thorax acceleration is also observed.

Figure 36 shows that a marked increase in pelvis load is observed.

Figure 37 shows that as the stiffness is increased a small increase in the tibia load occurs with a significant increase in foot load.

Seat Pitch

Figures 39 to 42 show the seat pitch sensitivity study. Increasing the seat pitch causes the HIC and head acceleration results to increase. The thorax acceleration reduces slightly.

Figure 40 shows that an increase in seat pitch slightly increases the vertical femur load. It is apparent that the axial femur loads increase at 32 inch pitch and reduce at 36 inch pitch. The belt loads, Figure 42, increase with an increase in seat pitch.

Figure 41 shows the results of the foot and tibia loads. It is observed that a significant increase in foot load is obtained. The tibia contact loads decrease as the seat pitch is increased.

Fixed Seatback Local Stiffness

Figures 43 to 46 show the results of changing the local stiffness of the locked seatback against which the rear occupant strikes. Figure 43 shows that the overall tendency is for an increase in HIC, head and thorax acceleration as the stiffness is increased.

Figure 44 shows that the femur vertical load remains relatively constant. An increase in the axial femur load is observed with subsequent reduction, as the pelvis load increases. The belt load, Figure 46, remains relatively constant.

Figure 45 shows the result of the tibia and foot loads. It is apparent that as the tibia load increases, the foot load decreases.

Seat Front Cushion Angle

Figures 47 to 50 show the result of changing the front seat cushion angle from 7 degrees to 15 degrees. Figure 47 shows that as the angle is increased, the HIC and head accelerations are increased. A small reduction in thorax acceleration is observed.

Figure 48 shows the effect of load against change in angle. It is observed that the femur vertical load reduces slightly. A more marked reduction is obtained in the axial femur load. Both the pelvis and belt loads, Figure 50, also decrease as the angle is increased.

Figure 49 demonstrates that increasing the front seat cushion angle increases the tibia load. The increase in tibia load reduces the foot load.

Seat Base Stiffness

Figures 51 to 54 show the results of changing the seat base stiffness. Doubling the stiffness causes the body to ride higher in the seat, consequently the head contacts the front seatback above the region covered by the food tray. Figure 51 shows that increasing the seat base stiffness increases the HIC, head and chest accelerations at the baseline factor of 1, however, this decreases as it approaches a factor of 2.

Figure 52 demonstrates that increasing the seatbase stiffness reduces the axial, vertical femur loads, however, this increases the pelvis load.

Figure 53 shows the result of the tibia and foot loads, it is observed that as the tibia load increases from a factor of 0.5 to 1.0, the foot load decreases. This is followed by an increase in foot load and a subsequent reduction in tibia load.

Lower Leg Position

No studies were made under this heading for the upright occupant. The principal reason for investigation of the lower leg position was to improve the kinematics in the brace position.

Knee Bolster Contact Stiffness

Figures 55 to 58 demonstrate the results of the knee bolster leg contact stiffness sensitivity study. Figure 55 shows the HIC and thorax acceleration have a tendency to increase as the contact stiffness increases.

Figure 56 shows that the vertical femur load decreases with increasing contact stiffness. The axial femur load increases to a stiffness factor of 1.0 followed by a decrease in the load. The pelvis load decreases to a factor of 1.0 and increases to a factor of 2.0. The tendency of the belt load, Figure 58, is to increase as the knee bolster contact stiffness is increased.

Figure 57 shows the results of the tibia and foot load. Increasing the knee bolster contact stiffness increases the tibia load. Consequently this reduces the foot load.

Knee Panel Position

Figures 59 to 62 show the effect of moving the knee bolster panel position. Figure 59 demonstrates that the head and thorax acceleration increases by positioning the knee bolster panel 50mm forward.

Figure 60 shows the change in load versus relative bolster panel position. Moving the bolster panel forward increases the vertical and axial femur loads. Increasing this parameter causes the pelvis and belt loads, Figure 62, to increase.

Figure 61 demonstrates the load on the foot increases with forward knee bolster panel movement. Consequently, the tibia load decreases, as the load is transferred onto the feet.

8.8 DISCUSSION

The analysis has yielded a large amount of data, which is relevant to the consideration of aircraft survivability. It is necessary, however, to consider the circumstances peculiar to this accident, and the nature of the analysis performed.

8.8.1 Aircraft Environment

The analysis was carried out in the central section of the aircraft between rows 10 and 20 where the structure was best preserved, and the floor and majority of the seats remained intact. The analysis was performed on row 15 seat F, the starboard side of the aircraft and close to the emergency exit. It was apparent that most of the occupied seats, particularly the outboard seats of the triple row, sustained significant front seat bar deformation. In other areas of the aircraft, the seats had broken away from the floor rails. Securing the seats

to the fuselage side at the outer edge of the seat base would increase the probability of seat retention in an impact.

Seat fixing locations should also be considered against the energy absorption of the front bar. In general, for this type of seat design the front bar produces the reaction for a large proportion of the occupant loads. On impact, loading of the bar, from the femurs and pelvis occurs. Consequential bending of the bar meant that the centre and outer seating positions exhibit a somewhat different behaviour - the outer position absorb more energy in bending. Appendix 3, Figure A3.14 shows the angle of the bar under deformation. On balance, seat security is the primary issue, energy absorption devices can be the subject of local design.

During the course of data collection for the study, seat 14F was examined in detail. It was apparent that the seat did not reflect optimum design with a view to protecting the occupant of the seat behind. Protrusions, sharp flange edges and lack of effective knee bolstering were observed. It should be noted, however, that the features of this seat were in line with contemporary industry practice. Many of the injuries in G-OBME were caused by contact between unfriendly adjacent seat surfaces.

There was also evidence to suggest that occupant injury was caused by the loss of retention of cabin fitments, including ceilings and overhead bins. Improvements to the occupant kinematics would not be fully effective unless a thorough review of the security of bins and ceilings was made.

8.8.2 Modelling Limitations

The MADYMO analysis package is a rigid body mechanics computer program. Although datasets are highly developed no soft tissue data was available. The program relies on the engineer's skills to derive appropriate analysis models. Throughout the modelling process certain assumptions have been made.

The analysis neglected the small lateral acceleration component of the crash, hence the use of the 2D package. The cross curvature of the seat was not modelled although rounded edges on seat cushions and softening at the seat edges were accounted for.

Friction and damping factors were based on previous experience, supported by measurements. These were tuned for seat, seat belts and contact surfaces.

The seat stiffnesses were based on static non-linear test results.

The floor was modelled as a flat plane, taking account of carpet penetration.

8.9 ANALYSIS

Although there was contact between the tail skid and the ground on the east side of the motorway, the acceleration levels were small, estimated at 1g. The analyses were therefore run for a period of 1.4 seconds (1400ms), beginning at the instance when the aircraft was in horizontal flight over the motorway. This embraced all the significant events which gave rise to the injury prediction levels.

Two main analyses were examined for braced and upright occupants. This was undertaken, as some occupants adopted the brace position and others, not knowing what the crash brace position was, remained upright. The passengers experienced a double impact most clearly observed in the kinematics. Head and arm contact occurred between the facing seatback in the brace and upright positions. In the case of the 'breakover' seats (Weber type 424) this acceleration was sufficient to release the seat backs before occupant contact. In the case of the emergency exit "nonbreakover" seats (eg. Weber type 444) the impact of the occupant caused structural failure of the seatback frame. The seat back was subsequently only retained by trim, and 'failed' for the remainder of the period.

8.9.1 Brace Position Correlation

The correlation of the body injuries was made with one occupant who sat in row 15 seat F.

The following injuries were recorded for the occupant of seat 15F and to which correlation has been made:

8.9.2 Facial Lacerations

The front of the head of the simulated occupant hits the table of the seat in front causing minor injuries. HIC values of just under 300 have been predicted thus facial lacerations would be expected although it is unlikely that serious head injury would occur.

In the accident the site of head contact was identified by witness marks on the seat back and confirmed the analysis. Additionally the levels of facial injury were also as expected. The occupant of seat 15F did not lose consciousness. This is commensurate with a HIC of circa 300 [137].

8.9.3 Bruising Across Iliac Crest And Upper Thighs

The belt loads predicted by the simulation were in the order of 9kN which was likely to cause bruising around the iliac crest. As the occupant moved up and backward in the rebound, so the belt slipped down his legs causing bruising on the outer thighs.

The seat belt motion described above only offered a partial explanation of the outer thigh bruising. Medical advice from the NLDB team indicated that the injury data were recorded two days after the accident. It was thought that gravitational tracking of blood could also be partly responsible for the bruising observed at these sites.

8.9.4 Bruising of the right knee

From the kinematics, contact can be observed between the knee and the seat in front. It was known that the seat structure deformed significantly on the right hand side of the body which would have caused the body to twist pushing the right knee forward and into the back of the seat in front. This twisting mechanism would probably have allowed the pelvis to move further forward, for the same belt load, than can be predicted with a 2D simulation.

The right knee of the occupant suffered bruising as described above. It was considered that the level of injury was commensurate with a contact force of circa 3000N, and witness marks on the seat back tend to confirm this finding.

8.10 GENERAL

Although correlation was only examined in detail against a specified occupant, there was good reason to believe results could be extrapolated to other occupants of the aircraft on a qualitative basis. The results would generally be applicable to occupants in a braced position in the same seat pitch, who approximated to a 50 percentile male. It would be possible to generate different size datasets for larger or smaller occupants, however it was felt appropriate to use a standard validated dataset. It was encouraging that such good correlation was achieved in view of the variety of sources of data. In particular the correlation represented a tribute to the veracity of the Hybrid III dummy in representing a real human being, in a real accident.

8.10.1 Brace Position Sensitivity Studies

The sensitivity studies, examined, were in all cases referenced to the brace position baseline model, Table 15, that is the lap belted rear occupant.

The rear occupant showed injury levels within the established limits in the case of 8% and 12% belts, with a slight increase of 6% in pelvic and 8% in axial femur loads respectively. Overall the best occupant performance was obtained with belts of 8% strain at 10kN. This has a more stabilising effect on the occupant and does not allow excessive forward movement.

The breakover (foldable) seatback study shows that the overall injury levels are increasing against the established baseline limits, except the head injury criterion where a slight reduction is observed. This indicates that insufficient energy is absorbed by the seatback to reduce the relative velocity of the occupant. It is suggested that a controlled energy absorbing foldable seatback

is required to arrest the occupant's forward movement gradually. This trend has been demonstrated in the non-breakover (locked) seatback, where energy has been absorbed by the failure of the seatback.

Increasing the seat pitch to 36 inches reduces the injury levels. Reducing the seat pitch has an adverse effect on the injury level, particularly the head injury criterion and axial femur load. A higher degree of knee penetration occurs, hence the increase in the axial femur load.

Increasing the non-breakover (locked) seatback stiffness reduces the injury levels, with HIC and thorax accelerations below the established baseline limits. Reducing the nonbreakover stiffness shows an increase in the injury levels. The noticeable increases being in HIC and vertical femur loads.

Increasing the front seat cushion angle reduces the overall injury levels, particularly the HIC, thorax and femur axial loads. It was considered impractical to analyse a reduction in this angle since this leads to greater front bar to pelvis and femur contact.

Increasing the seat base stiffness has an adverse effect on the injury levels. Reducing this stiffness has a favourable effect on the injury levels.

Moving the lower legs forward from the vertical has considerable adverse effects on the injury levels with 91% increase in HIC, 29% increase in thorax acceleration, 38% increase in axial femur load and 51% increase in vertical femur load. This also leads to tibia contact. The findings suggest that the occupant's lower legs should be placed rearward of the vertical in the brace position.

A comprehensive survey of airlines safety instruction has shown a considerable variation in bracing positions. In addition, emphasis is placed on the wearing of life vests. However, instructions on adopting a clearly defined brace position would certainly be more beneficial than the mandatory life vest demonstration. Survivability in aquatic ditching (or fire hazard) will be dependent on the occupant's capacity to disembark. This study has addressed criteria affecting disablement, in addition to the risk of direct fatality. The latter appears a low risk for a belted occupant in a retained seat.

8.10.2 Upright Position Models

As previously stated, many of the occupants in the aircraft did not comply with the advice of the crew to adopt a brace position, and remained seated upright. It was consequently decided to examine the kinematics and injury levels sustained by these occupants.

The simulation of the upright occupants utilises a 50th percentile hybrid III dummy dataset seated in two rows. The front seat holds the second,

supplementary, 50th percentile occupant. This was for the purpose of creating the contact environment for the primary occupant.

Unlike the situation for the braced occupant, where a single, well documented occupant was selected for correlation purposes, an equivalent upright occupant could not be identified for close study. Nonetheless several similar occupants were examined in a more general way.

The injury levels which were obtained from the simulation were found to be consistent with injuries sustained by the survivors. Head injury criteria are consistent with concussion. Contacts representative of pelvic and lower limb injuries were well predicted.

Medical records of the NLDB team [128] show that there was an increased incidence of unconsciousness due to concussion for those passengers who assumed an upright position. A significant number of passengers displayed injuries consistent with the contacts predicted by the analysis.

A comparison of the upright occupant simulation with the brace position showed considerable differences in results. Significantly higher HIC, thorax, femur and pelvis injury levels were obtained. The kinematic plots indicate a higher degree of penetration of the occupant into the facing seatback with increased head, chest and knee contact. Severe rotation of the knee and foot joints are also apparent. These are attributed to the increased relative velocity of the upper body before striking the facing seatback.

The general trend in results of the upright position suggest the injury levels are more severe than those of the brace simulations. The injury levels obtained show that the upright position is not to be recommended.

8.10.3 Upright Position Sensitivity Studies

The sensitivity studies examined were referenced to the upright position baseline model, Table 16.

The rear occupant showed the overall injury levels to be within the established baseline limits for belts of 8% strain at 10kN. The 12% and 16% belts show overall tendencies in excess of the baseline injury levels. Lower limits in femoral loads are observed with belts of 16% strain at 10kN. However, this is offset by an increase in tibia load. A favourable occupant performance is obtained with belts of 8% strain at 10kN load.

The breakover (foldable) seatback local stiffness study shows the injury levels are well in excess of head injury limits. Ranging from increases of 80% for the reduced stiffness to 292% for the increased stiffness. A reduction in femoral loads is observed. As with the brace position, this indicates that insufficient energy is absorbed by the seatback to arrest the occupant satisfactorily with the higher velocities involved.

Increasing the seat pitch increases the overall injury levels. This may be attributed to the increased velocity of the head and upper torso relative to the seatback in front. Reducing the seat pitch reduces the injury levels. This is because earlier contact occurs and the occupant is arrested over a longer distance, thus the applied forces are lower.

Reducing the local stiffness of the nonbreakover seatback reduces the overall injury levels, a slight increase in HIC and foot load is observed. Increasing the stiffness has an adverse effect on the injury levels, showing high HIC and thorax acceleration. This indicates that reducing the table stiffness on the facing seatback would have a beneficial effect for the occupant, and clearly has implications for the introduction of seat back video screens. An energy absorbing material could be used to decelerate the head of the occupant gradually.

Increasing the front seat cushion angle showed little effect on the injury levels and therefore would appear not to be worthwhile. A reduction in axial femur load is obtained. However, this is offset by an increase in tibia and foot load.

Reduction of the seat base stiffness causes higher axial and bending loads compared with established baseline injury levels. Increasing the stiffness has a favourable effect on the overall injury levels, particularly the axial femur loads. However, higher pelvic, tibia and foot loads are also observed. Energy absorbing material at the underside of the seat would have been beneficial in reducing the tibia and foot loads.

Reducing the lower knee bolster contact stiffness has a favourable effect on the occupant injury levels. This suggests that energy absorbing materials would reduce the injury levels. Conversely, increasing the stiffness has an adverse effect on the injury levels, particularly the tibia loads.

Moving the knee panel geometry forward (away from the occupant) has adverse effects on the injury levels. The lower part of the occupant induces a greater relative velocity before contacting arresting surfaces. The contrary can be argued when the knee panel is moved rearward.

8.11 COMPARISON OF THE BRACE AND UPRIGHT POSITIONS

Comparison of the brace against the upright position, Figures 63 to 66, shows that an increase in injury potential for occupants seated in an upright position has been obtained.

Figure 63 indicates that a seated occupant with the legs positioned rearward of the vertical is at a lower risk of sustaining injury to the head and thorax than a braced occupant with the lower legs placed forward of the vertical.

Figure 64 shows that an upright seated occupant is exposed to a greater loading of the pelvis than when braced. The braced legs back position shows a comparatively higher loading of the pelvis than the braced legs forward case. Femoral axial loading is shown to rise for the braced legs forward and upright seated occupants. Comparison of the femoral vertical loading shows a higher degree of loading for a braced occupant with the legs rearward of the vertical.

Figure 65 shows that wherever flail has occurred tibial contact with the seat in front has taken place. Adopting a brace position with the legs rearward of a vertical line drawn through the knee reduces the risk of flail and contact with the seat in front.

The lap belt indicates a slight reduction in loading for an upright seated occupant, Figure 66. This may be explained by the increased axial loading of the femurs with the front seat.

8.12 CONCLUSIONS

The 2D models allowed good correlation to be achieved efficiently. The move to 3D would allow greater detail and accuracy to be gained.

The correlation of the brace position was extremely good considering the multi-variable, non-linear nature of the analysis models and the modelling limitation outlined. The correlation was against one crash, studying other crashes is recommended.

Two main analyses have been conducted. The conclusions drawn, from the studies, which give reductions in injury levels are:-

Brace Position

- (i) Belts of 8% strain at 10kN.
- (ii) The use of energy absorbing foldable seatbacks.
- (iii) Increasing the seat pitch.
- (iv) Increasing the seat front cushion angle.
- (v) Reduction in seat stiffness.
- (vi) Moving the lower legs rearward of the vertical.

Upright Position

- (i) Belts of 8% strain at 10kN.

- (ii) Use of energy absorbing foldable seatback.
- (iii) Reducing the food tray stiffness.
- (iv) Reducing the seat pitch.
- (v) Reducing the knee bolster contact stiffness.

The study has demonstrated that it was possible to correlate the occupant kinematics of the Kegworth Aircrash with sustained injuries. The kinematics showed the mechanism of injury. The simulation was extended into a parametric study to provide recommendations for greater survivability in future accidents.

The major value of this study was to show for the first time, that a definitive estimation of occupant kinematics and the effects on the victim, are possible for an aircrash.

8.13 RECOMMENDATIONS

Brace Position

A braced position, similar to that illustrated in Figure 4, is to be recommended for occupants exposed to aircraft accidents.

The brace position should include an instruction to hold the feet back, that is, under the seat to reduce foot and lower leg injuries.

Upright Position

An upright seated position is not recommended. This increases the injury levels sustained by the occupants.

Seat Design

Multi-row installations of seats could and should be engineered to control the kinematics of the occupant of the seat behind. This would apply to those rows pitched within the flailing range of the occupant.

Aircraft seats should be designed to produce a more friendly environment for the occupants. Flanges, sharp edges, tables, seat back video screens and arm rests should all be designed in the expectation of occupant impact.

Knee bolstering by the introduction of a controlled deformation, padded structure is increasingly an automotive design device. Such design features would reduce injury and should be considered at the rear of aircraft seats.

The seat back "breakover" stiffness is critical to control occupant kinematics and the breakover force seems relatively uncontrolled in the design process. A tight tolerance for this force should be considered.

Aircraft seats utilising a tube across the front of a triple row are in common use and G-OBME was no exception. Cantilevered seat support structures produce radically different stiffnesses between outer and centre positions. Leg injuries would be expected to be more severe in the centre seat. It is recommended that this be investigated.

The tolerance of seat belt webbing stiffness used in G-OBME appeared wider than typical automotive applications. Belt stiffness is critical to occupant kinematics. The use of belts of 8% strain at a load of 10kN is recommended.

General

Regulations should control both femur bending (or normal loading) and axial compressive loading, rather than axial loading alone. Presently only axial compressive loading limits are specified.

Foot contact loads against the floor of the aircraft should be addressed in detail in future work.

The analysis used in this chapter utilised an additional occupant seated in the row in front to simulate the forward contact environment (a twin row analysis). The effect of the occupant seated behind the primary occupant should be assessed (a triple row analysis).

It is recommended that further work be made to examine a variety of crash scenarios to gain a greater understanding of the occupant kinematics.

Work should be conducted to assess the occupant kinematics against regulatory standards with direct correlation with sled testing.

Pages 94 to 100

Intentionally Left Blank

9. UPRIGHT SEATED OCCUPANTS IN ALTERNATIVE TYPES OF AIRCRAFT IMPACTS

9.1 INTRODUCTION

This chapter presents an investigation into the safety of passenger aircraft cabins under impact conditions. The work is directed at assessing the occupant kinematics and injury prediction in multiple row seating. The research focuses on the injuries which may be sustained by upright seated occupants in accordance with the proposed dynamic test regulations.

The study addresses various configurations of upright seated passengers of different statures between 5th female and 95th male percentiles. Assessments of three crash pulses are also made.

9.2 OCCUPANT PERCENTILE CONFIGURATIONS WITH VARIATIONS IN CRASH PULSES

The research examines different occupant percentiles using two dimensional occupant analysis. The study assesses the effects of occupant size on the injuries sustained by aircraft crash victims. The relative severity and characteristics of three different crash pulses were evaluated. The research consisted of sixteen aircraft crash simulations with variations in deceleration pulses and occupant configurations. In all cases the occupants were located on Weber breakover seats identical to those used in the Kegworth study, as described in the previous chapter.

The simulations carried out consisted of two forward facing rows of seated passengers. The occupants were restrained by lap belts. The configurations consisted of combinations of three occupant sizes, the 95th percentile male, the 50th percentile male and the 5th percentile female. Each occupant configuration was analysed using two different crash pulses and a test pulse. The analyses provided the motion, acceleration and force time histories sustained by the occupants.

The first crash pulse was obtained from the Kegworth accident. The second crash pulse was developed from the results of a full scale impact test of a pressurised transport aircraft [139]. The pulse was obtained from aircraft crash tests which were conducted by the National Advisory Committee for Aeronautics (NACA). This pulse, known as "Pulse 3", is characterised by a predominant fore-aft acceleration component compared to the Kegworth pulse which has both vertical and fore-aft accelerations, Appendix 5. The "Test 1" 14G pulse, detailed in Aerospace Standard 8049, has also been utilised.

The objective of the research was to assess the significance of occupant size on the injuries sustained in an aircraft accident. The study also examines the proposed dynamic seat requirements with regard to survivability.

9.3 DATA ACQUISITION

The analysis models of the seats were identical to the model used in the Kegworth study. The data required to build the seat models is detailed in the previous chapter. The crash pulse used in the Kegworth study was also used. The data to define the NACA crash pulse and the 14G test pulse are described below. All three pulses are presented graphically in Appendix 5.

9.3.1 Kegworth Pulse

This pulse was originally calculated for the Kegworth accident investigation by Cranfield Impact Centre. This contained a longitudinal component with a peak acceleration of 15G, a peak vertical component of 23G and a small lateral acceleration whose magnitude was less than 2G. The latter was neglected in this work and thus allowed for the creation of a two dimensional analysis.

9.3.2 NACA Pulse ("Pulse 3")

The "Pulse 3" was developed from results of a full scale impact test of a pressurised transport aircraft.

The Civil Aviation Authority (CAA) expressed a preference that the acceleration time history developed should have a more predominant fore-aft component in comparison to the Kegworth pulse which had a pronounced vertical component.

The test results, chosen from NACA Technical Note 4158, were of a 29 degree impact of a pressurised transport aircraft. The results obtained were from accelerometer station 490. The accelerometer station was located on the aircraft centre line in the wing box region of the aircraft. The total pitch angle of the wing section of the aircraft during the impact was less than that of the Kegworth impact.

The aircraft rotation time history during the impact, was obtained from the sequence of photographs in Figure 3c of the NACA Technical Note 4158, Appendix 5. The fore-aft and vertical acceleration time histories were digitised from the graphs in Figure 3c of the NACA Technical Note. The digitised accelerations were measured in the aircraft axes system. Using the measured rotation time history, they were then transformed into the ground axis system.

A lateral acceleration component was calculated for use in the analysis. The magnitude of this component is the resultant of the fore-aft and vertical components from the test results multiplied by the sine of 10 degrees. The angle of 10 degrees was chosen, as this reflects the set-up of the 16G pulse (Test 2) as detailed in AS 8049. The purpose of Test 2 is to determine the

protection provided in crashes where the predominant impact is in the longitudinal direction, in combination with a lateral component.

A plot of the crash pulse is presented in Appendix 5. This shows the three components of the pulse separately. The lateral component of the crash pulse is oriented to cause the occupants to move towards the aisle of the aircraft during the impact.

The fore-aft and vertical components of Pulse 3 were used in the two dimensional analysis.

9.3.3 14G Regulatory Pulse (Test 1 Pulse)

The "Test 1 Pulse" has been extracted from AS 8049. This pulse determines the protection required when the crash environment is such that a predominant impact load is directed along the spinal column of the occupant, in combination with a forward component.

9.4 MODEL DEVELOPMENT

The occupant kinematics have been analysed using the crash victim simulation program MADYMO version 4.3. Post-processing was performed using the software MADPOST.

The baseline occupant was simulated by a MADYMO version (v) 4.3 50th percentile male Hybrid III dummy dataset. This dataset represents the 50th percentile male Hybrid III manakin. From this dataset, other unverified 5th percentile female and 95th percentile male datasets were developed using anthropometric data [140].

The MADYMO v4.3 50th percentile male Hybrid III dataset differs from the v4.2 50th percentile male Hybrid III dataset used in the Kegworth analysis. The updates to the v4.3 dataset, which are of significance, are the larger chin ellipse and the repositioned pelvis and lower abdomen ellipses. The femur of the v4.3 dataset is slightly longer than the v4.2 dataset and has been modelled to allow the extraction of femur vertical and axial loads and bending moments. It was felt that these changes were not sufficiently significant to prevent meaningful comparison.

In each simulation, the 50th and 95th percentile male occupants were seated in an upright position in accordance with AS 8049, with their lower legs vertical. The 5th percentile female occupant could not be seated in this position due to the small leg dimensions. The lower legs of the 5th percentile female were positioned at 15 degrees forward to the vertical. In one model the lower legs of 5th percentile female were positioned vertically. This resulted in a gap between the seat back and the pelvis, an uncomfortable and potentially unstable seating position.

All the seats used in the analyses are of the breakover type. They are identical to the baseline seats used in the Kegworth analysis. The measurements obtained and level of breakover stiffness are detailed in the previous chapter. The seats were positioned at a pitch of 32 inches. The lap belt restraint system utilises webbing of 13% strain at a load of 10kN.

9.5 PERCENTILE CONFIGURATIONS

Parametric studies were performed using five occupant configurations in the two rows of seats. Each configuration was analysed with three deceleration pulses. An additional analysis was performed using the Kegworth Pulse to determine the effect of positioning the lower legs of a 5th percentile female occupant vertically.

The five occupant configurations are described as follows:-

- ♦ 50th percentile male in both front and rear seats, Figure 67. This model is the baseline configuration.
- ♦ 95th percentile male in front and rear seats, Figure 69.
- ♦ 5th percentile female in front and rear seats, Figure 71. Lower legs inclined 15 degrees from the vertical.
- ♦ 95th percentile male in rear seat, 50th percentile male in front seat, Figure 73.
- ♦ 5th percentile female in rear seat with lower legs inclined 15 degrees from vertical. 50th percentile male in front seat, Figure 75.
- ♦ 5th percentile female in front and rear seats with lower legs vertical, Figure 77.

9.6 RESULTS

The results obtained from the analysis are shown in tabular, graphical and chart form together with appropriate kinematic plots. Table 18 summarises the peak force and acceleration values for each configuration. This table also includes the Head Injury Criteria (HIC) values. The kinematic plots, graphs and bar charts are presented in Figures 67 to 113. The kinematics plots illustrate the initial position of the models and the occupant simulation. The graphical results consist of time histories of accelerations forces and bending moments. The bar charts illustrate the maximum results obtained for each configuration.

The results are only considered for the rear seated occupant. The front row occupant is included in the model in order to create the correct contact

environment. Three groups of results have been obtained for the Kegworth pulse, Pulse 3 and Test 1 pulse.

The Kegworth pulse, Pulse 3 and Test 1 Pulse graphical results and kinematic plots are presented in Figures 67 to 83, 84 to 98 and 99 to 113 respectively. The tabulated results for all the pulses are presented in Table 18. This provides a comparative assessment of the occupant kinematics.

9.7 DISCUSSION

The Kegworth pulse and Pulse 3 are representative of crash pulses which can be considered to be survivable. The Test 1 pulse is idealised, intended to assess a particular aspect of an aircraft impact in isolation.

The injury levels predicted in the analyses were consistent with the characteristics and severity of the deceleration pulses. The resultant injury levels varied significantly depending on the deceleration pulse used. The Kegworth pulse analysed produced the highest injury values, the Pulse 3 analyses were not as high but predicted severe and potentially unsurvivable injuries. The Test 1 pulse analyses produced much lower injury values. This pulse is intended to assess the potential injury to an occupant during an impact which results in a predominantly vertical deceleration. Emphasis is placed upon assessing axial spinal-lumbar loading.

9.7.1 Kegworth Pulse

The kinematics are characterised by leg flailing and forward pitching of the occupant. The early, high fore-aft component of the deceleration pulse causes leg flailing and considerable upper body forward motion to occur. This leg flailing is due to the initial lower leg position in combination with low upwards floor accelerations during the period of high fore-aft deceleration. In the case of the 5th percentile females, where there is no initial foot to floor contact, leg flailing is inevitable.

The most severe injury levels occur at the maximum fore-aft deceleration. This peak occurs at around 620ms and is of the order of 20g. The resulting upper body forward motion causes the head to contact the seat in front, approximately 100ms later in the crash sequence. This contact results in the severe injury levels and also coincides with a large vertical acceleration peak of 23g. Although the vertical peak occurs at the same time as the maximum injury levels, it is the initial fore-aft deceleration which is critical. However, due to the large vertical accelerations applied to the occupant whilst pitched forward, cervical, lumbar spine and pelvic fracture could occur.

There is a combined vertical and fore-aft peak at approximately 900ms which results in high head acceleration, belt load and foot to floor loads. This combined peak causes the occupant to be forced downwards into the seat, resulting in hyperextension of the neck and knee joints.

In all cases the legs are extended when the occupant pitches forward due to the initial fore-aft deceleration. Restraint is provided to the upper body by the upper legs which induce large femoral bending moments. On impact, the heels contact the floor, and the legs provide a resisting moment for the upper body. The head of the rear occupant strikes the front seat back. The subsequent vertical deceleration causes the upper body of the occupant to be forced downwards into the front of the seat cushion resulting in severe hyperextension of the knee.

Survival, in terms of head injury, is heavily dependent upon the occupants posture at the time of impact, as described in the brace position study. In addition, the position of the lower legs in the brace position has a significant effect upon lower limb flailing. HIC values are substantially reduced when the occupant adopts a brace position and the standard seat back is of the nonbreakover type which fails gradually on impact.

For all configurations, the lumbar and belt loads vary in proportion to the size of the occupant as do the femur axial and bending loads. The variation is due to the increased masses and dimensions of the larger occupants compared to the smaller occupants.

The results and occupant kinematics for each occupant configuration are discussed in detail below.

9.7.2 50th Percentile Male Seated in Both Seats

As the dummy datasets had been updated, a comparison was made between the new and old version. The results showed that the behaviour of the dummy datasets were consistent with the predictions made earlier. The rear occupant pitches forward. Head contact takes place against the seat in front at approximately 650ms with the legs extended due to the longitudinal deceleration of the aircraft. The occupant continues to pitch forward with the head remaining in contact and sliding over the seat back surface. At 710ms, maximum head and thorax accelerations occur. The occupant then rebounds from the seat back with the legs remaining extended. At 950ms the head is again thrown forward into the seat causing hyperextension of the cervical spine.

Figure 68 illustrates the occupant kinematics. The predicted HIC value, Figure 79, is beyond the maximum permitted injury level of 1000 for an upright seated occupant and is consistent with the original Kegworth study. This injury level is likely to cause severe injury and possible fatality.

Other predicted values which were found to be excessive, were the seat belt and spinal lumbar loads, Figure 80. The seat belt load was 9.3kN. The high lumbar tensile loads may also cause spinal damage.

9.7.3 95th Percentile Male Seated in Both Seats

This analysis predicted higher values for all the measured injury criteria compared to the 50th percentile male. All the major injury criteria levels were exceeded.

In this configuration, the tibia strikes the front seat during leg flailing, Figure 70. This is due to the increased leg dimensions. Femur axial loads are within the 10kN acceptance level, Figure 81. However the longer leg length in combination with the increased upper body inertia of the large occupant results in severe leg bending moments, Figure 82. The reverse bending of the knee, seen in the kinematics, compromises the representation of the knee joint in the dataset. Severe knee rotation occurs which indicates that leg and knee injuries are likely.

The head contact with the front seat back results in a higher deceleration due to the increased arc of the head trajectory. Neck hyperextension occurs as a result of the vertical acceleration.

9.7.4 5th Percentile Female in Both Seats

Results of the 5th percentile analysis, as for the 50th percentile and 95th percentile male, have injury values well above the survivability thresholds, Figure 79. The peak head accelerations are higher than the previous two configurations. This is due to the reduced head trajectory and subsequent head strike with the front seat back hinge area. The upper torso does not contact the front seat and continues to displace downwards. This causes severe neck hyperextension.

The kinematics plot, Figure 72, illustrates the extensive flailing of the legs, an obvious consequence of the absence of initial foot to floor contact. The heel contact with the floor was due to the upper body being restrained by the legs. The femur bending moments were lower than in the previous two cases due to the shorter leg length. The heels lose contact with the floor prior to the maximum vertical acceleration and only regain contact with the floor later in the crash sequence.

9.7.5 95th Percentile Male in Rear Seat, 50th Percentile Male in Front Seat

These results are virtually identical to those predicted with the earlier configuration of a 95th percentile male present in both seats. There is a minimal reduction in the accelerations and forces, Figures 79 to 83. The results indicate that the injury levels experienced by the rear row 95th percentile male occupant are not especially dependent upon the size of the front seated occupant.

9.7.6 5th Percentile Female in Rear Seat, 50th Percentile Male in Front Seat

The results were found to be largely unaffected by the size of the occupant of the seat in front. There was a small reduction in force and acceleration levels measured on the 5th percentile occupant in the rear row.

9.7.7 5th Percentile Female in Both Seats, Lower Legs Vertical

The effect of positioning the tibiae vertically was to set the body in a slouched position, Figure 77. This initial position did not comply with the seat testing requirements of AS8049. However, the resulting gap between the pelvis and seat back was similar to having excessive belt slack in the restraint system. This is likely to cause the occupant to submarine under the lap belt with significant abdominal injuries.

On subjecting the occupant to the Kegworth pulse, with a slouched position and the lower legs vertically upright, the results showed little change in the behaviour of the 5th percentile female. This is due to the fore-aft deceleration component which causes the occupant to translate forward and the subsequent rotation of the upper torso about the lap belt restraint, Figure 78.

9.7.8 NACA Pulse ("Pulse 3")

Comparison of the NACA pulse results with the Kegworth pulse showed that the magnitude of the predicted accelerations and HIC values are generally 40% lower, Table 18, for all the occupant configurations. Pulse 3 is characterised by a triangular 250ms duration fore-aft deceleration component with a 20g peak and by an irregular but continuous vertical acceleration component which varies between approximately 2g to 8g, Appendix 5. The initial peak of the Kegworth pulse has a comparable maximum value but rises from zero to this value within 50ms and reduces to zero again 50ms later. The vertical peak acceleration component of the Kegworth pulse occurs 100ms after the fore-aft peak.

Pulse 3 results in lower levels of injury values, Figures 94 to 98, as the fore-aft deceleration rises more gradually than the Kegworth pulse. This results in less severe rotation of the upper body with lower relative contact velocity between the head and the front seat back. The fore-aft deceleration component is accompanied by a vertical floor acceleration which eliminates the effect of leg flail for the 50th and 95th percentile occupants. In addition, the foot to floor friction which is generated, helps to further reduce the head to front seat back contact velocity. The abdomen and chest contact with the upper leg provides restraint to the upper body earlier in the crash sequence than would be possible if leg flail occurred.

The HIC values remain well above the maximum acceptable injury threshold, Figure 94. The results of the head accelerations, spine lumbar axial loads and belt loads all indicate excessive injury levels for all configurations, Figure 95.

With the exception of the 5th percentile female configurations, the femur bending loads are excessive, Figure 97. The heels of the 5th percentile female do not contact the aircraft floor as the initial fore-aft deceleration is less severe than the Kegworth pulse. This results in much lower femur bending loads in the 5th percentile female. The 50th and 95th percentile male occupants experience high femoral bending moments. This is due to upper torso and abdominal contact with the femurs. However, it must be emphasised that the contact model of the upper torso to leg is idealised in the two dimensional version of MADYMO. This causes the contact forces to be applied at discrete points. In a test, the contact between the torso and upper legs of the Hybrid III dummy would result in a more consistent load distribution. Some of the contact load may be transferred directly from the chest onto the knees and lower legs. The idealised contact in the model induce somewhat higher bending moments than may be observed in reality.

Generally the lumbar, femur and belt loads vary in proportion to the size of the occupant. This effect is due to the increased masses of the larger occupants. In some cases, earlier contact for the larger occupants ameliorate this effect.

9.7.9 14G Regulatory Pulse (Test 1 Pulse)

The 14G pulse tests the response of the lumbar spine to a predominantly vertical deceleration pulse. Figures 99 to 113 illustrate the comparative values for the five occupant configurations.

The kinematics illustrate the occupant descending into the seat with a combined motion of the head moving into the thoracic region. The fore-aft component of the pulse also causes the occupant to move towards the front of the seat. There appears minimal femoral contact with the front seat knee contact panel for both the 50th percentile male and 95th percentile male occupants. The 5th percentile occupant has no initial foot contact with the floor. However, during the impact, the lower legs contact the floor causing the feet to rebound.

The nature of the contact with the floor may account for the marginally higher lumbar loads experienced by the 5th percentile female compared to the 50th percentile male, Figure 110. The legs of the 50th percentile remain in contact with the floor throughout the simulation thus stabilising the occupant kinematics.

There is little difference between the lumbar tensile loads for all configurations. The 95th percentile occupant experiences marginally higher loads throughout the analysis than the 50th percentile.

9.8 CONCLUSIONS

The studies of configurations of different sized occupants show the effects of seating both small, medium and large occupants. These were defined as 5th percentile female, 50th percentile male and 95th percentile male. Although there was some slight reduction in injury levels for smaller occupants, no substantial change was found. All the injury levels remained beyond the threshold of survivability for head injury, when using the Kegworth acceleration pulse, with the occupants seated upright. The 95th percentile occupant experienced tibia strike on the seat in front, whereas the 5th and 50th did not.

Significant tensile forces in the spine were observed, whereas only compressive loads are controlled by regulations. Once more the importance of bending in the femur has been highlighted. Heel to floor contact loads have been found to be very substantial in a Kegworth type of impact in the order of 5000N. This helps to explain the preponderance of ankle injuries in the accident [132].

This study has shown that the maximum femur axial load of 4.7kN, obtained with the most severe pulse does not approach the regulated injury limit of 10kN. This suggests that this injury criterion is less appropriate to aircraft crash victim simulation than femoral bending, tibial and foot loads. Extra load cells would require incorporation in the femur and tibia of test dummies to measure such forces; it is suggested that an accelerometer could be used to indicate foot loading.

The use of the NACA pulse (pulse 3) has shown a general reduction in injury levels in comparison with the Kegworth pulse. The following overall reductions have been observed, 72% in HIC, 24% in thorax acceleration, 8% in lumbar loads, 68% in axial femur loads, 250% in tibial loads and 22% in heel loads. The following increases have also been observed, 168% in femur vertical loading, 2% in femoral bending moment and 9% in belt loads. It must be noted, however, that the new crash pulse derived from the demonstration test is somewhat less severe than the Kegworth pulse.

The test pulse derived from AS8049, is less severe than both the Kegworth and NACA pulses. The compressive loads in the spine are however, higher due to the predominant vertical vector. Very little difference between sizes of occupant was noted.

9.9 RECOMMENDATIONS

Injury criteria for the lower limbs of test dummies should be revised in AS8049. In particular, the femoral compressive maximum load should

be replaced with a maximum bending requirement, and loads for the tibia and foot specified.

**This Page
Intentionally Left Blank**

10. SIMULATION OF FORWARD FACING AND REARWARD FACING OCCUPANTS

10.1 INTRODUCTION

The controversy surrounding the adoption of rearward facing versus forward facing seats has been a matter of debate for many years. Proponents of forward facing seating indicate that the force on the seat attachments and seat legs are smaller if the decelerating passenger is held at his hips by a seat belt in a forward facing seat than it would be in a rearward facing seat. For the latter seat, the centre of gravity of the occupant is approximately 300mm above the seat belt anchorages. The rearward facing seat, therefore, has higher bending moments in the legs and floor attachments.

Proponents of rearward facing seats point to the smaller load per unit area imposed on the rearward facing passenger who is supporting the decelerative force with the broad area of his back. In addition, rearward seating avoids the flexing of the torso over the seat belt. This occurs in forward facing seating, resulting in head injuries.

Eiband indicated that rearward facing seating would offer the best protection in the event of an aircraft impact [13]. He suggested that the seat should include a lap and torso belt, a winged seat back with full head rest, load bearing arm rests with recessed arm holes and provision to prevent arm and leg flail. For forward facing seating, he suggested that a full body restraint be employed with full height seat back and integral head rest.

Pinkel compared the theoretical performance of forward and rearward facing seats [141]. He assumed that the occupant restraint forces were applied through the seat back attachment points on the forward facing seats and through the seat back for the rearward facing seats. He calculated that the rearward facing seat would have half the design strength of the forward facing seats, if the increase in weight due to the need for a stronger seat back was ignored.

Mason also compared rearward and forward facing seats [142]. He quoted one series of investigations in which 19% of forward facing occupants died compared with 5% of rearward facing occupants. In another study, 11% of passengers in forward facing seats were killed and 84% were uninjured with comparable figures for rearward facing seats of 1% killed and 98% uninjured.

Pinkel analysed the mass associated with forward and rearward facing seating. He indicated that rearward facing seats are heavier than forward facing seats, if the same impact performance is required. Increased floor strength and mass are also required if the increased loads on impact, with rearward facing seats, are to be resisted by the aircraft structure, without catastrophic failure. The FAA investigated the cost implications and found that each 0.454Kg mass increase in an aircraft can cause 56.8 litres of additional fuel burn per annum

[143]. However, it must be stated that the mass penalty may be minimised by concurrent improvements in design and selection of materials. With few exceptions, increased safety must be bought at a cost, but where the results are calculated to be worthwhile, such costs are fully compensated.

There is considerable reluctance on the part of the commercial airlines to adopt rearward facing seats. This is based on the concept that it is an unacceptable configuration on aesthetic grounds. Two sets of data suggest this is not so. A large statistical survey was carried out by the United States Air Force (USAF) Air Transport Command which showed an overwhelming response to the question "Considering Safety, do you favour this idea"? Out of 1024, 959 replied yes, 49 no and 16 did not comment. For the question "Should we reverse all passenger seats"? 896 replied yes, 85 no and 39 no comment. The personnel filling the questionnaire included approximately 15% civilians.

Dudgeon [144] covering 10,000 personnel, did not mention to the passengers any question with respect to safety but merely asked questions about airsickness, comfort, etc. The rear facing configuration was preferred by 65%, found unpleasant by 3% (mostly crew) and the remaining 32% either did not mind which way they faced, or did not reply (2%).

Finally, it is stated that passengers seated in rearward facing seats are at a higher risk of induced injury due to loose objects which may become detached from overhead bins. Such objects are accelerated to the front of the aircraft in the event of a crash. As long as such objects are pillows or blankets, it is unlikely that injury would occur. However, if hard objects break free, then there is an increased chance of passenger injury taking place. A number of researchers believe that forward facing seated occupants are at a reduced risk of injury from such missiles [20].

10.2 DEVELOPMENT OF A 3D MATHEMATICAL MODEL

When aircraft cabin safety is discussed the suggestions most regularly put forward for its improvement are rear facing seats and three point belt systems. Thus these situations were modelled. In both cases an upright occupant position was simulated.

This chapter utilises three dimensional (3D) occupant kinematic simulations in the study of three point belted and rearward facing occupants. The three dimensional computer model consisted of using the NACA pulse, which was developed from the results of a full scale impact test. The pulse is characterised by a predominant fore-aft component, an additional lateral component was introduced in the simulation. The study examined the injury levels and seat structural loading.

The model consisted of analysing three different seating and constraint configurations. The first configuration was of two rows of forward facing

triple seats, with six occupants restrained by lap belts. The second was of a single forward facing triple seat, with three occupants restrained by three point lap and diagonal belts. The final configuration was of a rearward facing triple seat, with a single occupant restrained by a lap belt. The seat models were three dimensional equivalents of the two dimensional seat models used in the Kegworth simulation. The occupants were represented by fiftieth percentile datasets.

The objectives of the research were to evaluate the use of three point belt and rearward facing occupant restraint systems. In addition, the use of three dimensional occupant analysis in aircraft crash victim simulation was to be demonstrated.

The analysis models of the seats were 3D equivalents of the 2D seat models used in the Kegworth (2D) analysis. These were based upon row 15 on the right hand side of the aircraft G-OBME. The data acquired for the 2D analysis was thus directly applicable. More extensive use was made of the data acquired previously in developing the 3D analysis models. The data used for the 3D analysis is described below.

10.2.1 Seat Profile And Dimensions

The seat centre line profiles were identical to those used in the 2D analysis. The data on the seat structure dimensions was obtained from the drawings supplied by the AAIB. This was supplemented by direct measurement of seat parts supplied by the AAIB. These parts were from the wreckage of G-OBME.

10.2.2 Seat Base, Seat Back And Armrest Stiffnesses

The test results from the stiffness measurements, made for the 2D analysis, were used. These tests measured the stiffness on the seat base and seat back cushions at high loading levels. The stiffness arising from the deformation of the aluminium sheets attached to the seat frame and stiffness of armrests were also obtained.

10.2.3 Seat Structure Deformation Characteristics

The seat front spar load deflection characteristics measured for the 2D analysis were used to calculate the non-linear bending properties of the front spar. The strength and deformation characteristics of all other parts of the seat structure were calculated using standard formulae.

10.2.4 Mass And Inertia Of The Seat And Seat Back

The most critical values used in the analysis, the mass and moment of inertia of the seat back, were measured for the 2D analysis. All other seat inertias and masses were estimated.

10.2.5 Seat Belts

All belt data was based on the 2D Kegworth simulation model.

10.2.6 Crash Pulse

The NACA crash pulse was used in the model.

10.3 MODEL DEVELOPMENT

The geometry of the seat was represented by 3D contact surfaces. All the structural members of the seat were modelled as ellipsoids. The seat base and seat back cushions were created using planes, as were the aluminium sheets attached to the seat base and seat back structures. The armrests and the tables mounted in the seat backs were modelled using ellipsoids. The stiffnesses obtained from the acquired data were assigned to the appropriate contact surfaces.

The contact surfaces were attached to rigid elements which were connected by joints with non-linear stiffness properties. The joints are capable of fully representing the non-linear collapse behaviour of a structural member. By including joints at key points in the structure, this allowed the deformation characteristics under the dynamic loading to be simulated. Also, joint loads could be extracted. This allowed seat attachment point loadings to be determined.

The occupants were simulated by MADYMO version 4.3 50th percentile Hybrid III dummy datasets. This dataset represents the 50th percentile Hybrid III dummy. In all the simulations carried out, the occupants were seated in an upright position in accordance with AS 8049, with their lower legs vertical.

Models for three different seating configurations were developed. The configurations were as follows. Six forward facing lap belted occupants in two rows of triple width seats. Three forward facing three point lap and diagonal belted occupants in a single triple width seat. A single lap belted occupant in a rearward facing triple width seat. Figures 114, 117 and 119 show the initial model set-up for the three configurations. The details of the three models are described below.

The seat modelled in the first configuration was of the breakover type. The breakover stiffness was modelled in the seat back joint as an increasing stiffness followed by a reducing rotational resistance. This model had the structural properties of the seat structure represented by non-linear joint stiffness functions. The crash pulse used has a relatively high lateral acceleration component. Six forward facing occupants were restrained by lap belts. The two seats were placed at a pitch of 32 inches. Both seats were of the breakover type as the work was to have the widest generality.

The seat modelled for the second configuration required the seat structure, specifically the seat back, to be strengthened. This model simulates three forward facing occupants restrained by three point lap and diagonal seatbelts. The seat structure was not designed to cope with this type of restraint system. All the joints in the seat structure were made elastic to prevent any collapse occurring. The shoulder belt was configured to pass over the right hand shoulder. The upper end of the shoulder belt was attached to the seat back structure just behind the occupants shoulder.

The seat modelled for the third configuration required strengthening to cope with the additional loading imposed by the rear facing occupant. Both the seat back and the seat legs required strengthening. The single lap belted occupant was placed in the right hand seating position. This seat was essentially the reversed seat model of configuration 2. This results in the seat legs being offset away from the aisle side of the seat centreline, not towards it as in the forward facing seat models.

A 2D model, which was equivalent to the 3D model of six forward facing lap belted occupants in two rows of triple seats, was also developed. The purpose of this model was to allow a correlation study between a 2D and a 3D analysis to be carried out. The former model was identical to the baseline model from the Kegworth study. Since the lateral component of Pulse 3 could not be included in the 2D analysis, this imposed limitations on the correlation study.

10.4 RESULTS

The 3D analysis results are presented in both tabular and graphical form and also as kinematics plots. Table 19 summarises the peak forces and accelerations as well as the Head Injury Criteria (HIC) values. The kinematics plots and the graphical results are presented in Figures 114 to 130. The kinematic plots show the initial set-up of the models, the motion of the occupants at an intermediate point in each simulation and also the position of the occupants at the end of each simulation. The graphical results consist of accelerations, forces and bending moments.

Table 19 summarises the peak forces and accelerations as well as the Head Injury Criteria (HIC) values for the correlation study between the six person 3D model and the 2D model.

The occupant results are considered for only one occupant in each of the simulations. For the first configuration, the two rows of forward facing lap belted occupants, output is only obtained for the right hand occupant in the rear triple seat. For the second simulation, the single row of three lap and diagonal belted occupants, output is obtained for the right hand occupant. The rearward facing seat simulation, the third configuration, only has one occupant present. This is consistent with the 2D Kegworth analysis which set out to correlate the injuries of the occupant of seat 15F, the right hand seat of a triple

row in the aircraft G-OBME. The seat model in the 3D analysis was based upon this particular triple seat row. The 2D analysis results are for the occupant of the rear seat.

10.5 DISCUSSION

The three configurations simulated demonstrate the relative merits of forward facing seats with lap belts, forward facing seats with lap and diagonal three point belts and rearward facing seats with lap belts. The seat and belts are not optimised for the latter two configurations, the detail design of the seat and belt systems are not ideal.

The crash pulse developed for this section, the 'Pulse 3' crash pulse, is based upon an actual aircraft crash pulse obtained from full scale testing. It is not entirely dissimilar to the Kegworth crash pulse, the magnitude and time durations of the accelerations are similar. The Kegworth crash pulse and the Pulse 3 acceleration time history, can reasonably be considered to be of equivalent severity. The Kegworth impact occurred at a larger impact angle than the test impact resulting in a more pronounced vertical acceleration component.

The relative magnitude of the Pulse 3 fore-aft component compared to the lateral component is similar to that of the 16G crash pulse specified for Test 2, in AS8049, Appendix 6. The general motion of the occupants in Test 2 would be similar to the motion of the occupants in this analysis. However, Pulse 3 is significantly more severe, it is longer in duration and larger in magnitude than the Test 2 pulse. The injury predictions in the analysis carried out for this section will, therefore, be more onerous.

10.5.1 Forward Facing Lap Belted Occupants

The behaviour of the occupants in this simulation is consistent with the occupant kinematics predicted in the Kegworth analysis. The rear row occupants pitch forward, head contact is made with the seat backs of the front row of seats and the legs extend due to the fore-aft deceleration. The occupants continue to pitch forward with head contact continuing down the front seat backs. Figures 114 to 116 show the occupant kinematics.

The lateral acceleration component in the crash pulse results in lateral motion of the occupant towards the aisle of the aircraft. This is most pronounced in the motion of the unrestrained upper body. The initial head contact point of the rear occupant with the front seat back, Figure 116, is on the left hand side of the seat back table. Contact with this point instead of the seat back centreline will result in higher head accelerations as the effective stiffness of a seat back table will be higher in the vicinity of the seat back frame. In the simulation, the HIC value of the rear right hand occupant is approximately 1100. This is above the head injury limit of 1000. The stiffness values used for the food tray were measured on the seat back centreline. The lateral

motion of the occupants upper body means that the HIC value predicted is conservative. Much more detailed stiffness test results would be required to increase the accuracy of the prediction.

If the lateral acceleration component was higher, it could cause the rear occupants head to initially strike either on the edge of seat back table, between two seat backs or on an adjacent seat back. The aisle side occupants head may be deflected into the aisle. There is also the added risk of head contact with the rear end of the armrests of the front seat row. The hinge bracket for the armrests is at the rear of the armrests and is extremely stiff. Contact with the armrest in the vicinity of this hinge could result in high head accelerations. The risk would be higher for occupants smaller than the 50th percentile male, as initial head contact may occur in this area due to the reduced arc of the head trajectory.

The legs of the rear row occupants extend forwards in the simulation. Some minor contact occurs with the seat legs of the front seat row. The contact forces are low and unlikely to cause severe injury. Subsequent to the full extension of the legs, and loss of contact with the floor, the upper body is retarded by contact with the upper legs. This contact with the legs, forces the heels back onto the floor. The retardation of the unrestrained upper body results in large foot contact forces with the floor, see Table 19. This causes vertical shear forces in the upper femurs which are relatively low. However the bending moments in the upper femurs are high due to the large distance to the heels along the extended legs. The bending moments predicted are sufficiently high to cause the femur to break.

Normal foot to floor loading can clearly be increased by an upwards acceleration of the floor, and also reduced by a downwards acceleration. A downwards acceleration could cause the feet to lose contact with the floor, and upwards accelerations are clearly more desirable from this viewpoint.

The foot to floor friction coefficient is a significant factor in preventing leg flailing in the upright position. However, there is a potential wide variation in the footwear worn by aircraft occupants. This will result in wide variations in foot to floor friction coefficients.

Posture can be used to maximise the normal loading on the floor as demonstrated in the Kegworth study. The ability to achieve a satisfactory leg angle is dependent upon the occupants upper and lower leg length and the seat base and luggage bar geometry. Occupants with legs shorter than a 50th percentile male are at risk of being unable to achieve a satisfactory lower leg position. Upward floor accelerations are highly beneficial and can compensate for poor leg positioning. The relative timing and magnitude of fore-aft and vertical accelerations can also negate any benefit.

The problem of lumbar spine injury due to an occupant pitching when restrained only by a lap belt is very evident. Figure 124 shows that a very

large tension loading in excess of 11kN occurs in the spine due to the occupant pitching forwards. The risk of lower back injury is high.

The analysis has shown that seat leg loads can be readily calculated. Limited deformation can also be modelled. Catastrophic failure could cause numerical problems with the solution algorithm, but, as the requirement is for a seat to display controlled deformation, this does not impose a limitation. Figures 129 to 130 show the results of the seat attachment loads. These loads can be used to assess the strength requirements of the floor rails.

The worst case loading on the floor rails could be determined by parametric studies of various occupant seating configurations. Although initial floor deformation cannot be directly simulated in MADYMO this does not necessarily affect the loads obtained from the analysis. If the performance of the seat structure and legs is compromised by initial deformation this could be accounted for by building the seat model in the initially deformed condition along with the use of appropriate joint properties to simulate any distorted sections.

Load time histories at key points in the seat structure can be obtained. The final distortion of the seat base and seat back can also be assessed under dynamic occupant loading. This would allow a seat structure to be optimised for both strength and energy absorption.

The analysis has highlighted some interesting findings in respect of the femur loads for the forward facing lap belted occupants. Aircraft seat regulations have been based on FMVSS 208 automotive practice, disregarding the vertical femur loading which is possible in an aircraft accident. It has been shown that a significant increase in femoral bending moment has been obtained.

10.5.2 Forward Facing Three Point Belted Occupants

The simulation consisted of a row of three point belted occupants seated on a triple seat. The seat backs were constrained. The occupant kinematics were more controlled than the lap belted configuration. The resultant forces and accelerations imposed upon the occupant were greatly reduced compared to the forward facing lap belted configuration. The results show no particular concerns.

The shoulder belts were mounted on the seat back and were modelled to include an inertia reel retractor. The short belt length from the seat back to the shoulder increases the risk of the belt slipping off the occupant's shoulder if lateral upper body motion occurs.

The legs extend in this simulation. This does not result in any concerns as the shoulder belt restraint prevents the upper body from contacting the upper legs. The heels are not forced onto the floor and high femur bending loads do not occur. The upper body restraint also prevents large tension loadings on the

spine. Only compressive loads occur and these are approximately half the tension loads of the forward facing lap belted occupants.

The upper body restraint increases the risk of submarining. If the combination of lap and shoulder belts are not properly configured, the occupant's lower torso could move forward more than the upper torso. There is also a larger vertical loading on the seat base. This could result in the lap belt slipping over the iliac crest. The requirement to spool sufficient shoulder belt length to prevent it slipping off the shoulder will be beneficial in pitching the upper torso forward relative to the lower torso. However, this will only be true if the shoulder belt does not readily spool belt into the lap belt section of the lap and diagonal belt system.

Consideration should be given to separate lap belts and shoulder belts. An inertia reel shoulder belt could be fitted to the seat back. The lap belt could be a static belt which can be used in-flight for protection in turbulent conditions. Both belts would be used for takeoff and landing and in emergencies. This analysis has not assessed whether submarining will occur but correct design of the restraint system, seat base structure and seat base cushion will prevent this phenomenon.

The seat attachment point resultant loadings increase significantly, see Table 19. This is predominantly due to very large increases in vertical loading. Figures 129 to 130 show the peak resultant loads of the seat attachment points. Table 19 shows that increased vertical loads are due to the shoulder belt loading high on the seat back. This loading is counteracted by a moment provided by the vertical reactions at the seat legs. The current rear seat leg design is not entirely suitable to sustain this loading. A relatively minor modification to the rear seat leg design would resolve this problem.

The three point belted seat model was strengthened to prevent any structural failure during the simulation. It is possible from this analysis to calculate loads in the seat structure and output belt forces. This would allow an assessment of the seat strength requirements to permit the fitting of seat back mounted shoulder belts.

The installation of three point belt systems in wide bodied passenger aircraft may not be a feasible proposition. However, it should be stated that this is not an impossibility. The installation of such systems would involve structural modifications with resultant cost implications to aircraft manufacturers. Introducing this restraint method into smaller commuter aircraft is more appropriate.

10.5.3 Rearward Facing Lap Belted Occupants

Only one occupant was modelled. The forces and accelerations on the occupant are lower than in the three point belted simulation. The design of the seat back would, however, cause significant injury to the neck. Severe

neck hyperextension occurs as the seat back is not designed with a suitable head restraint.

The restraint of the lower legs imposes a high loading in the ankle area. This is undesirable but could be easily remedied by fitting a heel plate to the luggage restraint bar. The detailed design of the seat back and seat base would also need to be modified to prevent injury being caused to the occupant by high localised contact loads with the seat structure. An example of this would be the transverse spar in the seat back which would result in localised loading on the spinal column. In addition, the seat back should be shaped to provide lateral restraint to the upper torso. The armrest design should be modified to prevent any risk of abdominal injuries and to provide lateral restraint to the occupants lower torso. The latter requirement is applicable to all three configurations.

The occupant kinematics have been predicted for an occupant initially seated in an upright position. However, if an occupant was leaning forward on impact, this would cause higher loadings on the seat back and increase the forces and accelerations imposed upon the occupant. It would cause problems in restraining the head where wraparound seats and head rests are not fitted. If significant lateral motion occurred, the head trajectory could be such that it did not contact the head restraint. The aisle side occupant could potentially end up falling towards the aisle. The fitment of a shoulder belt which initially located the occupant in an upright position would prevent this and would also be beneficial in any accident which resulted in the occupant being accelerated towards the rear of the aircraft, for example, on rebound. If it was necessary to only fit a lap belt, it would be desirable for breakover seat backs to be retained.

A major advantage of rearward facing seats is that seat back video screens could be more safely incorporated into the seat design. In the forward facing configurations, even with shoulder belts fitted, they would present difficulties in meeting accepted injury criteria. There is a much lower chance of head impact with the seat back in the rearward facing configuration. Also it is highly probable that the impact velocity of the head would be lower if contact occurred. These two factors could make the seat back video screen an acceptable design feature. The fitting of seat back video screens also overcomes the problem of restricted cabin vision for a television monitor caused by the higher seat backs required to incorporate adequate head restraints.

The seat structure and the seat legs were strengthened to prevent collapse of the seat structure under the increased loading imposed. The loading in the seat structure could be calculated to allow an assessment of the structural requirements to allow a seat to be fitted in a rearward facing direction. The seat leg design would have to be modified to suit the new direction of loading. As only one occupant was seated in the rearward facing simulation, the seat

attachment point loads cannot be directly compared with the other two simulated configurations.

The introduction of rear facing seats in civil aircraft has, so far, not been widely adopted. Principally, the objections have been passenger preference and comfort, but the issue continues to be controversial. Rear facing seats have been used more widely in military aircraft. The crew of G-OBME who were seated in rear facing seats sustained only minor injuries.

Notwithstanding the controversy surrounding rear facing seats, definitive observations have been made in this study. The analysis of the occupant kinematics shows penetration into the seatback, with neck hyperextension and tibia strike against the seat front bar. Extending the head rest and 'padding' the seat front bar would greatly reduce these phenomena.

Significant improvements in injury levels are obtained with rear facing seats, particularly in HIC, femur and belt load. Whilst reduced belt loading may be an obvious consequence of a rear facing installation, the HIC is also favourable having been reduced significantly. It is likely that much greater improvement may be obtained in a purpose designed rear facing seat. Increased loading on the lower leg may be readily addressed in a well designed rear facing seat.

It has previously been argued that cabin debris would be more injurious to a rear facing occupant, since this will be moving forward through the cabin. There is substantial evidence that debris was responsible for death and injury in G-OBME, despite the use of forward facing seats [128]. Regardless of seating configuration, debris is a major hazard worthy of improvement.

10.6 CONCLUSIONS

An aircraft impact is generally a three dimensional event, although lateral and yaw effects may be comparatively small. Two dimensional modelling often adequately represents the impact. The ability to model in three dimensions is clearly beneficial. This is of most use when there is a significant lateral component which may change the strike zones such that a less friendly surface is contacted.

The extension from 2D into 3D shows an increased capability to model occupant interaction with an aircraft interior during an impact. The limitations imposed by utilising only 2D analysis techniques are overcome. The 3D geometry allows the occupant's motion to be fully determined. Examples of the effects which were modelled in the analysis include, asymmetric deformation of the seats, oblique occupant impacts with complex structures and lateral acceleration and motion of the aircraft.

The comparison of three dimensional with two dimensional simulations is not pure, since the lateral component is, of necessity, neglected in the two dimensional analysis. This limitation notwithstanding, the levels of correlation are generally satisfactory in terms of injury criteria. The increased sophistication provided by three dimensional analysis gives rise to improved modelling of the legs in particular, and their contacts with the chest and seat structure. In addition, 3D modelling is required to represent the requirements of the 16G dynamic test.

It has proved possible to simulate the asymmetric deformation of the seat structure and its interaction with the occupant. It is anticipated that this capability will be an increasing requirement in the future. It may be that improvements in processing power of computers will favourably influence the availability of finite element based analysis, rather than mechanisms based analysis. This would enhance the ability to model occupant kinematics and non-linear structural deformation simultaneously.

The analyses showed that forward facing lap belted occupants are more vulnerable to injury compared to rear facing lap belted occupants. However, in the rear facing analysis, the lateral component combined with the low height of the head rest cause the head and neck to impinge on an area where in reality there may be internal framework of the seat structure. High and full width headrest would improve this situation.

Forward facing occupants restrained by lap and diagonal belts experienced similar upper body forces consistent with similar injury levels to the rear facing occupant. Although the head and neck contacts of the rear facing seat are avoided, lap and diagonal belts for the forward facing occupant result in spinal loads close to the maximum permitted. Additionally, considerable lower leg flailing occurs which require measures to combat injury under the seat in front.

For the NACA pulse, both rear facing seats and forward facing lap and diagonal belted seats, impose higher floor loadings than the forward facing lap belted seats. On average the percentage increase in loads are 52% for the rear facing seat and 33% for the lap and diagonal belted seat. However, it must be stated that with the exception of the lap belted seats, the other seating in question are not purpose designed. In the analysis, both rear facing and lap and diagonal belted seats are rigid.

10.7 RECOMMENDATIONS

Analysis work should be undertaken to establish crashworthiness requirements for aircraft seat rail and floor support structures. A programme of research should be undertaken to assess the most efficient design for impact, while optimising the mass of the floor structure.

Simulation techniques should be encouraged as a method of identifying worst case seating configurations for subsequent certification tests.

Further research is required to establish the potential for injury using the regulatory 16G pulse.

Securing the seats to the fuselage side at the outer edge of the seat base (a single pedestal installation) would represent a cost and mass effective method of improving seat strength. A further study is recommended of the feasibility of such designs.

Three point belts offer major improvements in the reduction of head, femoral and pelvic injuries, due to improved kinematics and load distribution. Such installations should be considered for small commuter type aircraft.

Rear facing seats would reduce the risk of injury significantly. The seat back must be strengthened and increased in height, with shaping of the head rest to prevent lateral displacement of the head. Also, a heel plate to prevent rearward displacement of the feet should be incorporated. The use of a lap belt is still required in the event of occupant rebound.

With the introduction of seat back video screens the potential risk of injury to forward facing passengers is significantly increased. The use of rear facing seats when seat back video screens are installed should be strongly encouraged.

**This Page
Intentionally Left Blank**

11. BRACE POSITION CORRELATION WITH IMPACT TESTING AND PARAMETRIC STUDY

11.1 INTRODUCTION

This chapter undertakes a study of the passenger brace position with the objective of correlating the results of the computer simulation with those from sled testing, using the 16G dynamic test pulse. The study examines the injury mechanisms, accelerations and forces which are imposed on the occupant during impact and assesses the effect of floor friction, seat pitch, lower leg angle and alternative seating configurations on occupant injury.

The computer simulation and sled tests were carried out with economy class Weber seats from the Boeing 737-400 G-OBME which crashed at Kegworth. Two triple-row breakover seats were used with a test dummy placed in differing brace positions in the centre seat of each row. The rear dummy was an instrumented Hybrid III manikin whose output was utilised as the basis for correlation.

The analytical model was correlated against sled tests which were conducted at the Institute of Aviation Medicine (IAM), Farnborough.

The acceleration time history of the sled was determined by the Institute of Aviation Medicine (IAM). This was of similar magnitude to the FAA 16G pulse with a prescribed 10° yaw component, Figure 131.

11.2 OBJECTIVES

The objectives of the work was to correlate a MADYMO 3D simulation model with a sled test. To establish the ability of the computer model to simulate an impact test. To undertake a parametric study by varying a number of parameters:-

1. Floor friction.
2. Tibia angle.
3. Seat pitch.
4. Alternative Seating Configurations.

In correlating the model, particular attention was paid to occupant trajectory, head injury criteria, head, chest and pelvic accelerations, and tibial and femoral loads.

In addition, an analysis of an occupant striking a bulkhead, a forward facing three-point belted occupant and a rearward facing seated occupant were also examined.

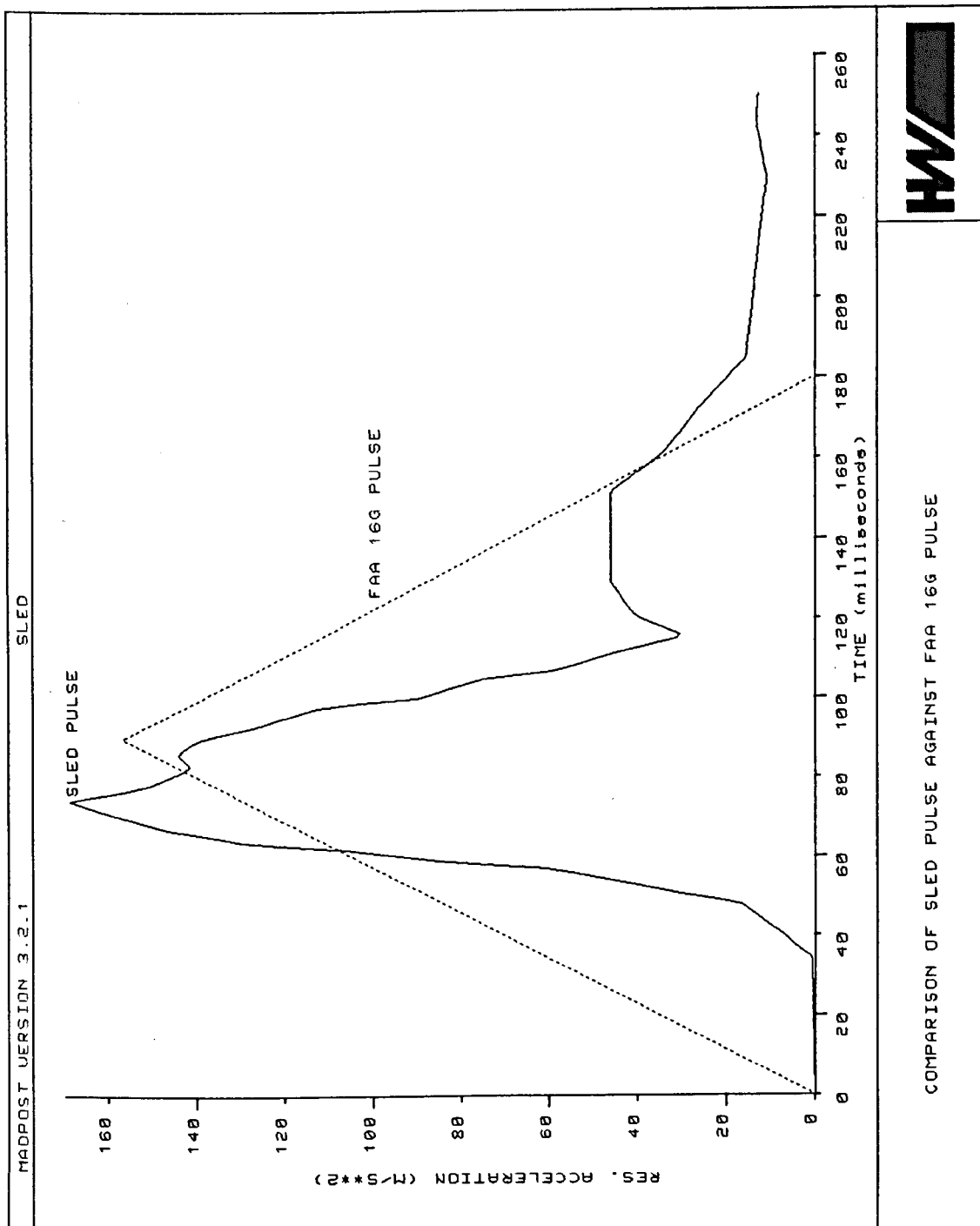


Figure 131. Comparison Of The Sled Pulse Against The FAA 16G Pulse

11.3 SLED TEST FACILITY

The sled test facility, which was used to obtain the data for the correlation study, was a linear decelerator track, Figure 132 and 133. This is described by Giles [145] and Dutton [146].

The facility comprises a wheeled vehicle which runs on a track measuring 46m in length with a mass of 432kg. The vehicle has a capacity of 250kg. The test vehicle is propelled by a number of stretched rubber cords (or bungees). On release, the vehicle accelerates over 26m and is allowed to coast over a further 13m before it is arrested by hydraulic energy dissipators which are adjustable to alter the deceleration profile.

The impact velocity may be altered up to 15m/s. The waveform of the deceleration pulse approximates to a half sine wave curve with a maximum peak deceleration of 50G.

To prime the system the vehicle is hauled back to the release position by a winch located at the release end of the track. Prior to release, the pusher, introduced to propel the test vehicle, is held back against the stretched bungee cords by a 2270kg release unit located in a spring loaded cradle. After release, the pusher and vehicle are decelerated using an arrestor gear.

The main arrestor gear consists of five steel cables 19mm in diameter stretched across the track. They pass around grooved bollards on either side of the track and each end is connected to a piston of 1.22m stroke and 127mm hydraulic cylinder bore.

Hydraulic pressures of up to 17.25MN/m² are induced within the hydraulic cylinders during operation by throttling the hydraulic fluid through orifices and into reservoirs. This causes the decelerative forces to be applied to the vehicle as it impacts and displaces the cables. Each cylinder has two orifices arranged in parallel, a fixed circular one 15.9mm in diameter, and a variable annulus which can be opened to a maximum diameter of 47mm to vary the decelerative force to the vehicle.

11.4 DYNAMIC TESTING

Aerospace Standard (AS) 8049 states that head and femur impacts should be evaluated using multiple row seating configurations. Two triple rows of seats were rigidly mounted through seat tracks to the sled. Floor deformation was not included in the test fixture. This was not included as the seat structural deformation was not being tested in this case.

Induced seat deformation demonstrates whether the seat and restraint system will remain attached to the aircraft structure, in the event that the fuselage and seat are deformed by the impact. The seats were yawed to the right, through the prescribed 10 degree lateral component. The impact pulse which was



Figure 132. Decelerator Track

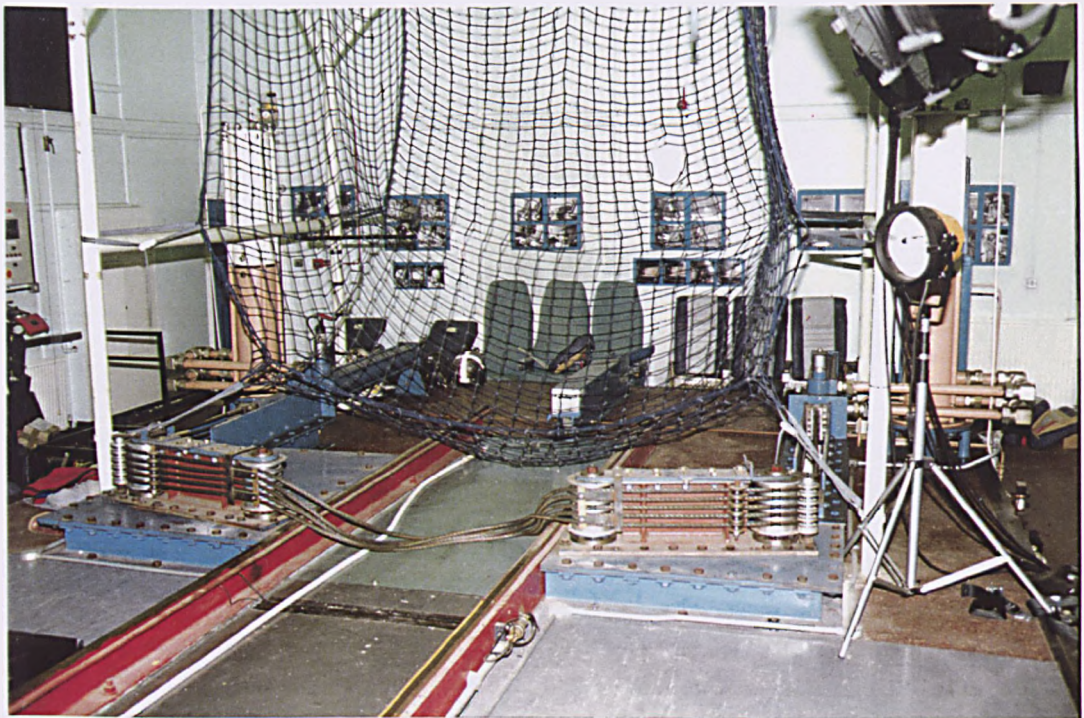


Figure 133. Arrestor Gear

used, approximated to that of the FAA 16G dynamic test pulse (Test 2), which necessitated that the following parameters be achieved:-

Minimum Acceleration = 16G.

Minimum Impact Velocity = 13.41m/s.

Maximum Rise Time = 0.090s.

11.4.1 Test Configuration

A multiple row seating configuration was used to evaluate the head, thorax and femoral injury levels. Each row contained triple seats.

The seats were Weber Aircraft forward facing passenger seats which were manufactured to specification NAS 809 Type 1. The seats were obtained from the Boeing 737-400 G-OBME which crashed at Kegworth. These seats were undamaged or partially damaged. The seats were subjected to non-destructive testing by the Royal Air Force, prior to sled testing, using magnetic particle analysis.

The seats were mounted on the test fixture facing forwards, in a -Gx orientation, Figure 134 shows the translational acceleration convention. The seats were yawed 10° to the right.

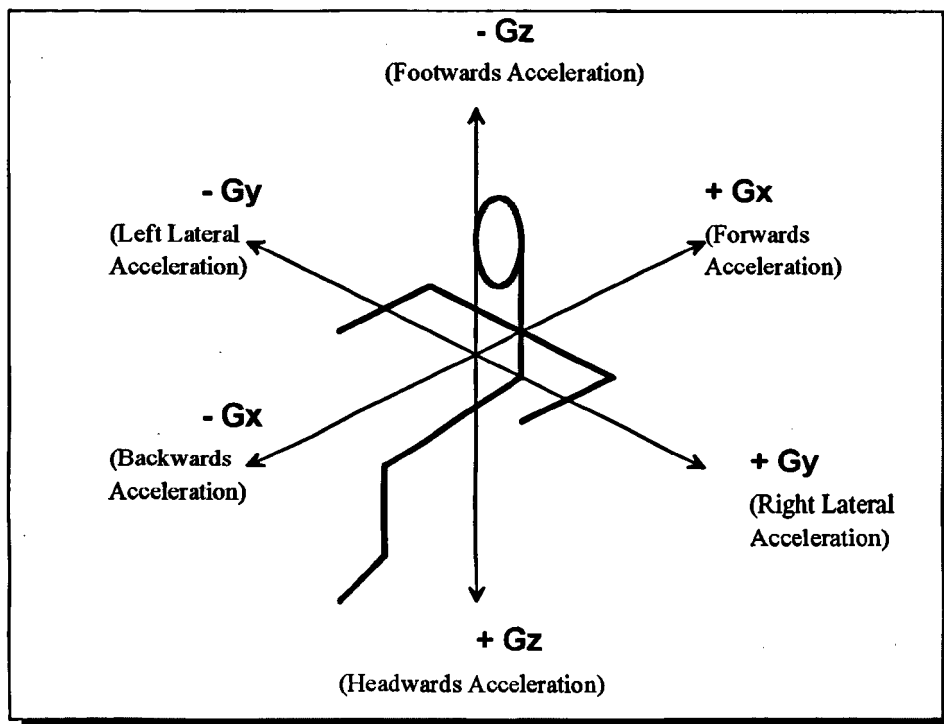


Figure 134. Conventions of Translational Accelerations.

To minimise the risk of seat detachment from the floor tracks, the seat to track interface was reinforced by a metal block [147].

It was decided to place the dummies in the middle of the triple seat rows, as this was the stiffest part of the structure. This was done in order to evaluate the maximum injury levels which would be obtained in this seating configuration. Rowles (1990) showed that passengers seated in the middle of the triple row sustained more femoral bending fractures than those who sat in the aisle or window seats. It was concluded, that more energy absorption had occurred in the cantilevered aisle and window seats in comparison to the middle seat. The latter was vertically supported by the four leg members of the triple row.

The cushions and panelling were removed from the outside seat to facilitate viewing of the occupant kinematics using the NAC 200 video camera.

The two triple rows of seats were subsequently set at a pitch of 32 inches. This represented the commonest seat pitch which was found aboard the Kegworth Aircraft.

The floor of the test fixture was carpeted with the same material as was found aboard G-OBME.

11.5 THE TEST DEVICE

The test device used was a 50th percentile Hybrid III Anthropomorphic Test Device (ATD). AS 8049 stipulates that the dynamic test should be conducted using a Part 572B or Hybrid II ATD or equivalent. In the automobile industry, however, this ATD has been superseded by the Part 572E dummy or Hybrid III. As the Hybrid III is the more advanced test device, this was used for all dynamic testing. The dummy was clothed in form fitting cotton stretch garments with mid-thigh length pants and size 11E shoes weighing 11.6N. The shoes were leather soled. This was chosen as this would represent the worst case condition for foot slide. The coefficient of friction was determined prior to the sled test. This indicated that the coefficient of friction was 0.5.

When fully instrumented the Hybrid III is capable of a number of measurements, Table 20.

11.6 TEST DATA ACQUISITION

Data was obtained from the sled through a system of flying leads. The type of cable used was Filotex Multicore containing 25 wires per cable. Each channel required four wires, thus allowing six channels per cable. The minimum number of cables per test were used as this leads to increased weight and frictional force which has the effect of reducing the sled velocity by as much as 0.5m/s.

The flying leads were attached to the transducers through a panel mounted on the vehicle. This consisted of 30 sockets to facilitate changeover of channels.

In the control room a similar panel was mounted to which the signal conditioning equipment was connected.

11.7 SIGNAL CONDITIONING INSTRUMENTATION

All the transducers, with the exception of the lap belt load cell which required a charge amplifier, necessitated signal conditioning instrumentation to supply power to the bridge and to apply gain to the output of the unbalanced bridge circuit. The instrumentation used included 2100 series strain gauge conditioning amplifiers supplied by Vishay Measurements Group of North Carolina, USA. The amplifiers are capable of producing an excitation up to 12 volts and gain to 2100. The control panel allowed for balancing of both amplifiers and bridge circuits.

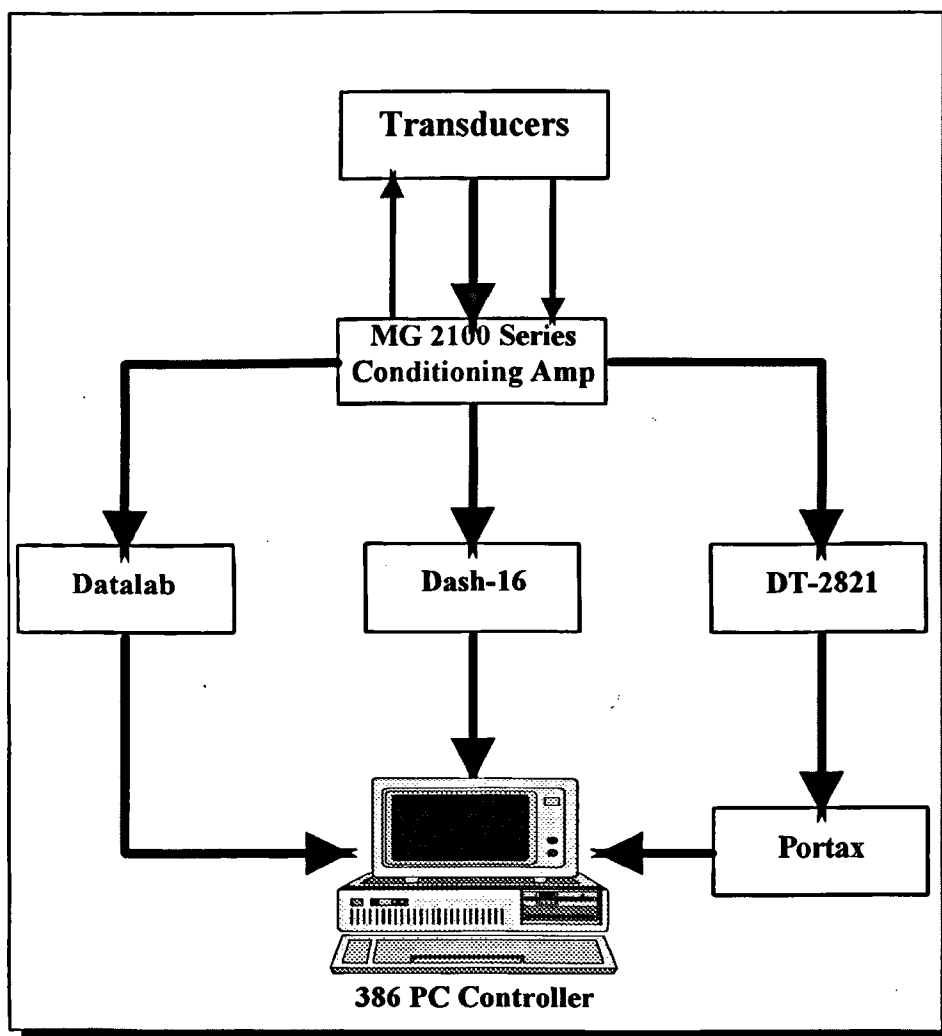


Figure 135. Decelerator Track Data Acquisition System.

The data was obtained in three ways:-

1. Dash 16 Acquisition Board
2. The Datalab Transient Recorder
3. The DT-2821 Acquisition Board (Portax)

The signals derived from the transducers are relayed by the flying leads to the conditioning amplifiers. The amplified signals are acquired through either the Datalab Transient Recorder, the Dash 16 Acquisition Board or the DT-2821 Acquisition Board (Portax) with a common time base. The information is subsequently transferred to the track computer.

11.7.1 Dash 16 Acquisition Board

The Dash 16 is a high speed programmable analogue/digital expansion board for IBM compatible personal computers. The board has 12 bit resolution and is capable of 100,000 conversions per second. It contains an additional port for input from the velocity meter. This acts as the triggering mechanism. This was the central method of obtaining the data and was located inside the track computer.

11.7.2 Datalab Transient Recorder

The Datalab Transient Recorder contains 19 memory modules which are attached together by a master timebase and controller. Each memory module is capable of storing 4096 words, each of 10 bit resolution. When sampling is complete the test data is stored in the memory module. The data is then down loaded to the track computer.

11.7.3 DT-2821 Acquisition Board (Portax)

The DT-2821 Acquisition Board (Portax) is a 16 channel data acquisition card which is located in a PC supplied by Kayser UK. The board is similar in operation to the Dash 16.

11.7.4 Track Computer and Software

The track computer is an IBM compatible PC with the following specifications:-

Type 386 PC
Memory 640K (4096 with expanded memory)
120 Megabyte Hard Disk Drive
ASYST Software

The computer software was designed by Surgeon Commander P J Waugh of the RAF Institute of Aviation Medicine. The scientific programming language was ASYST, produced by Keighley Instruments of Great Britain.

11.7.5 Calibration

The load cells were calibrated by the manufacturer. However, a calibration signal was used which allowed conversion to engineering units. The accelerometers were calibrated on a centrifuge of known radius. Revolutions per minute were recorded on a calibrated tachometer. The calibration signals were therefore obtained by connecting the accelerometer to the datalab whilst centrifuging at a known rate. Calibration was performed at the beginning and end of the experiment to confirm the integrity of the system.

11.7.6 Dummy And Sled Instrumentation

The load cells which were used for the dummy instrumentation were obtained from Robert A Denton, of Michigan, USA which had been calibrated. A triaxial pelvic accelerometer was supplied by Endevco UK Ltd, Melbourn, Royston, Herts. The lap belt force transducer was manufactured by Kistler Instruments Ltd., Whiteoaks, The Grobe, Hartley Wintney, Hants, England.

11.8 TEST PROCEDURE

The test configuration is shown in Figure 136 and 137.

The test fixture was oriented at a yaw angle of 10° to the right.

Each seat was installed in the test fixture and secured to the seat tracks.

An instrumented 50th percentile Hybrid III dummy was placed in the rear centre seat of two triple rows.

The friction in the limb joints was set so that they barely restrained the weight of each limb when extended horizontally.

The ATD was located in the centre of the seat, so as to be symmetrically positioned.

Initially, the back and buttocks of the ATD were located against the seat back without clearance. The dummy was rocked from side to side in order to allow it to settle into the seat.

The knees of the dummy were separated by approximately 100mm.

The ATD was secured with the lap belt. The tension in the belt was set to 70N using a spring balance. This was performed in order to remove any slack



Figure 136. Braced, Legs Back Configuration, 32" Seat Pitch



Figure 137. Sled Yawed 10° To The Right

in the webbing. Although the belt felt firm to the touch, it was not unduly tight.

The ATD was subsequently oriented in the brace position with the head touching the seatback in front. The hands were located on top of the head with the fingers interlocked. The arms were pushed to the side of the head. The lower legs were placed rearward of a vertical line drawn through the knee joints and set to 11.5° and with the feet parallel.

A second uninstrumented 50th percentile (OGLE) dummy was located in the forward triple row in front of the Hybrid III dummy. The dummy was also placed in a brace position.

Prior to testing, the vehicle was winched to the start position and the triggering device was armed.

The sled was then released. The data acquisition system was triggered causing the impact data to be captured.

After each sled test, all components were assessed for possible damage.

11.9 DATA MANIPULATION

The recordings were initially zeroed. This was performed in the following way:-

Each set of data was zeroed by sampling the data between the trigger point and the point of impact. When the data recording equipment is triggered, the sled is in the coast phase. The impact point is then one metre from the triggering point. Therefore at a velocity of 12.7m/s, this represents a time of 78ms.

Using a sampling rate of 5000 samples per second, this represents 400 counts between the trigger point and subsequent impact. Counts of 10-110 were taken and the average obtained. This value was then taken as the zero point. Using this technique helps to minimise the errors induced due to small movements in the initial position of the dummy as it is accelerating down the track. This is a recognised disadvantage of decelerator sleds.

On capturing the data on a computer, it was subsequently manipulated using the ASYST Program. It was at this stage that the calibration data for the load cells and accelerometers were added to convert the results into the correct engineering units.

11.9.1 Recording Channels 1 - 32

The results obtained from the sled tests were recorded using a number of channels. These were designated from 1 to 32, Table 21. Each channel

recorded the time history event of each body segment. The graphs were analysed and the maximum loads and accelerations were recorded. The time (T) at which the peak load occurred was also recorded.

The transducers were allocated a number of channels. These are shown in Table 23.

All impacts were recorded using a NAC 200 high speed video camera which operated at 200 frames per second.

11.10 SLED TEST RESULTS

The results of the sled tests, which were performed to carry out the computer model correlation, are presented in Table 24. Each test run was given a unique test number. Correlation of the computer model was compared with test numbers 3672 and 3673, Figures 138 and 139 respectively.

The sled acceleration was 17.2G with a velocity change of 12.42m/s.

11.11 CONCLUSIONS

The acceleration pulse and velocity were not fully representative of the requirements stated in Aerospace Standard (AS) 8049. This states that the peak acceleration should be 16G with a velocity change of 13.41m/s.

It was not possible to increase the sled velocity without incurring a higher acceleration level. This was due to the limitation of the decelerator track. This is highlighted by test 3670, where a velocity of 13.25m/s was achieved, however, the sled acceleration level was 19.9G.

Due to lack of resources, the seats were acquired from G-OBME which had been subjected to crash conditions. The same seats had to be used for each sled test with the same webbing material. Due to financial constraints, it was not possible to use new seats nor carry out repetitive sled tests to achieve a degree of repeatability.

11.12 MATHEMATICAL MODEL DATA ACQUISITION

The seat profile, mass and inertial properties were based upon the previous model. The stiffness measurements are detailed in Appendix 3.

11.12.1 Seat Stiffness

A new Weber 4001 triple row seat was acquired. The seat cushion stiffnesses were derived from several tests using pelvic, knee and head loading forms, Appendix 3.



Figure 138a. Sled Test 3672, 0 To 30ms

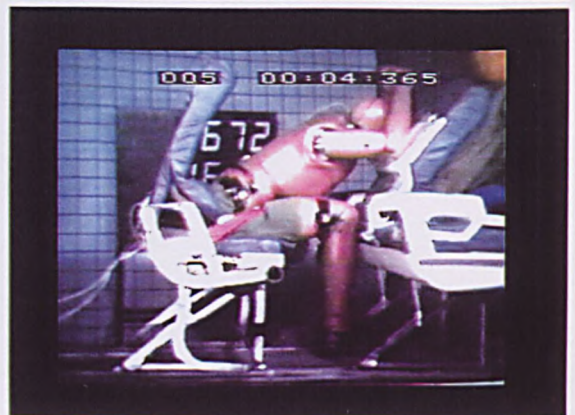


Figure 138b. Sled Test 3672, 40 To 70ms



Figure 138c. Sled Test 3672, 80 To 110ms



Figure 138d. Sled Test 3672, 120 To 150ms

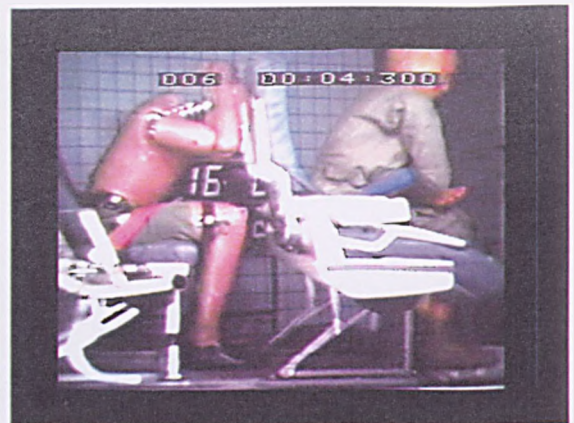


Figure 139a. Sled Test 3673, 0 To 30ms

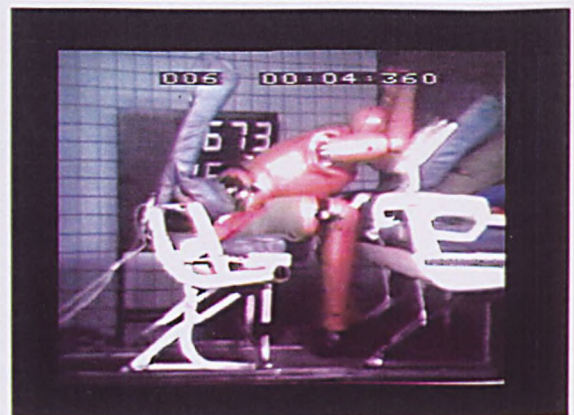
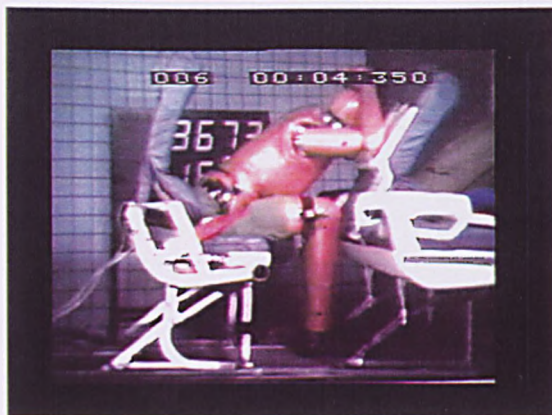
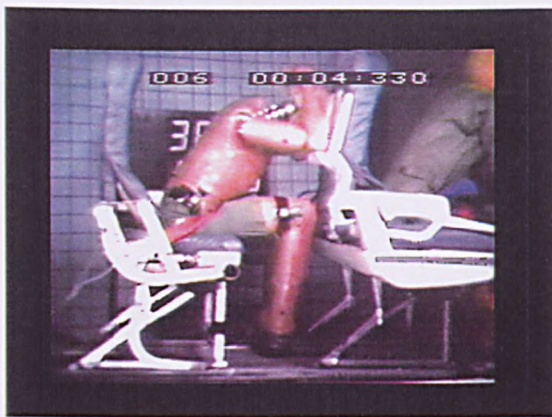


Figure 139b. Sled Test 3673, 40 To 70ms

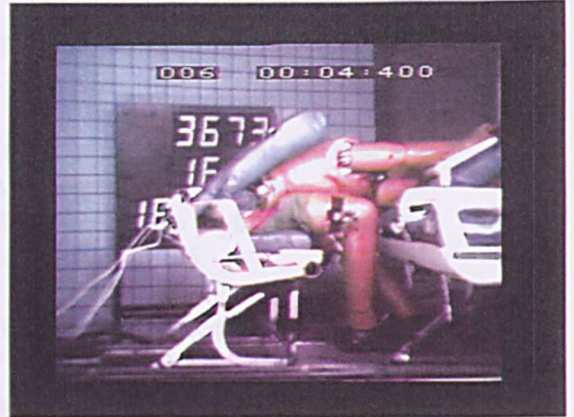
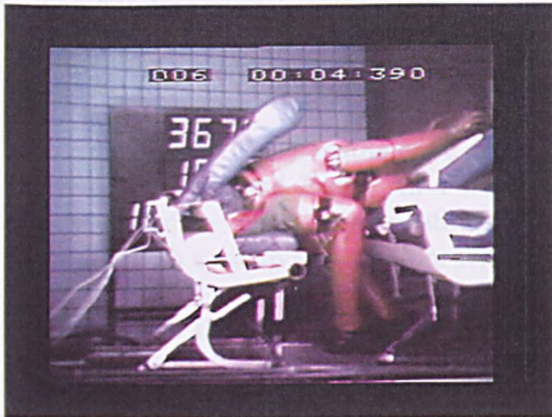
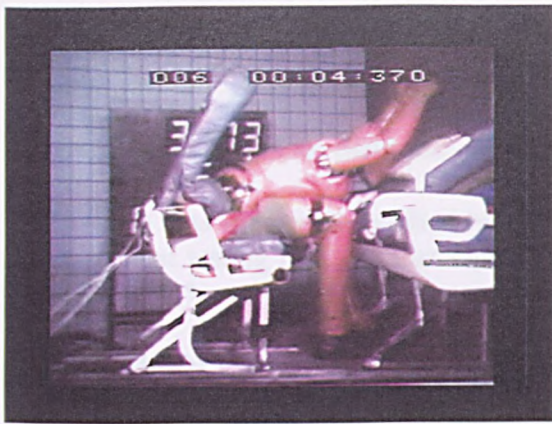


Figure 139c. Sled Test 3673, 80 To 110ms

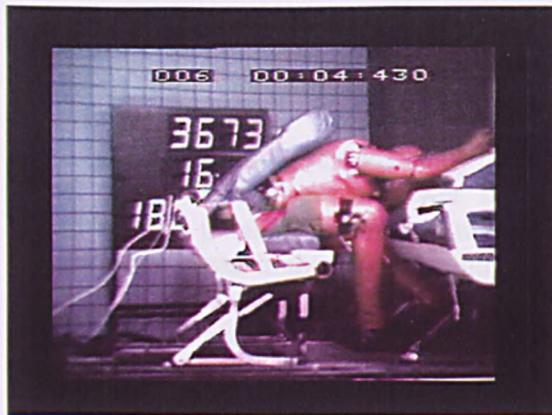
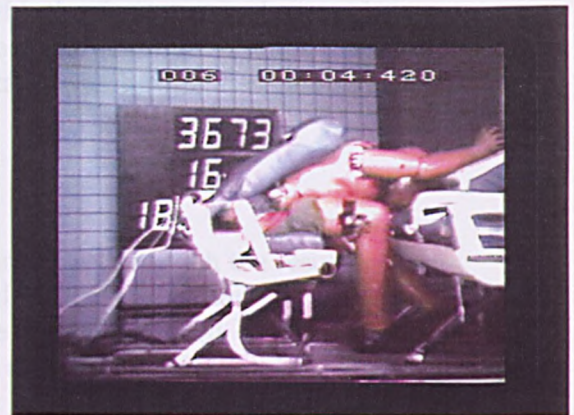
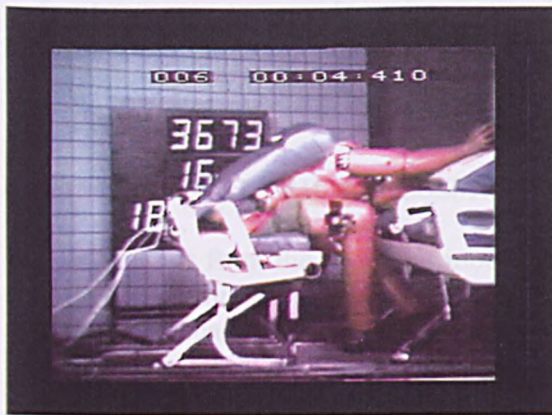


Figure 139d. Sled Test 3673, 120 To 150ms

11.12.2 Lap Restraint Stiffness

This data was originally supplied by the IAM as being 20% strain at 10kN. Subsequent testing revealed that repeated sled testing had caused the belts to stiffen to 11% strain at 10kN, Appendix 7.

11.13 MODEL DEVELOPMENT

The baseline model was developed using MADYMO 3D version 4.3. The new seat cushion stiffness data was incorporated along with the revised lap belt stiffness of 11% strain at 10kN.

The Hybrid III 50 percentile male dummy used in the test in the rear seat was fitted with standard Royal Air Force (RAF) leather-soled shoes. This was represented in the model by utilising a 50th percentile Hybrid III dummy dataset with a relatively low floor friction coefficient of 0.5.

The Hybrid III dummy was placed in the brace position with legs positioned slightly backwards (tibiae placed at 11.5° rearward of the vertical), Figure 140. Accordingly, the dummy datasets were placed in an identical position.

A seat pitch of 32 inches was adopted. The role of the dummy dataset in the front row was to provide an interaction with the front seat and to produce a more realistic contact environment with the rear dummy. In the simulation, only the output from the rear dummy dataset was recorded in line with the impact test.

11.14 PARAMETRIC ASSESSMENT

The findings from the computer model were correlated with the results of the tests carried out at the IAM. The crash pulse generated by the IAM was used to run the baseline model. The baseline model included a floor friction coefficient of 0.5, a 32 inch seat pitch and a braced occupant with a lower leg angle of 11.5° rearward of the vertical. From this baseline, a number of parameters were sequentially investigated.

11.14.1 Floor Friction

It was found in the previous study that the floor friction played an important role in the assessment of lower limb flailing. Thus, it was decided to undertake a parametric analysis to study the effect of floor friction on the occupant's lower limbs. To this end, the floor to foot friction coefficient was varied in increments of 0.05 up to 0.7, from that used in the baseline model. The results were then assessed against the baseline configuration.

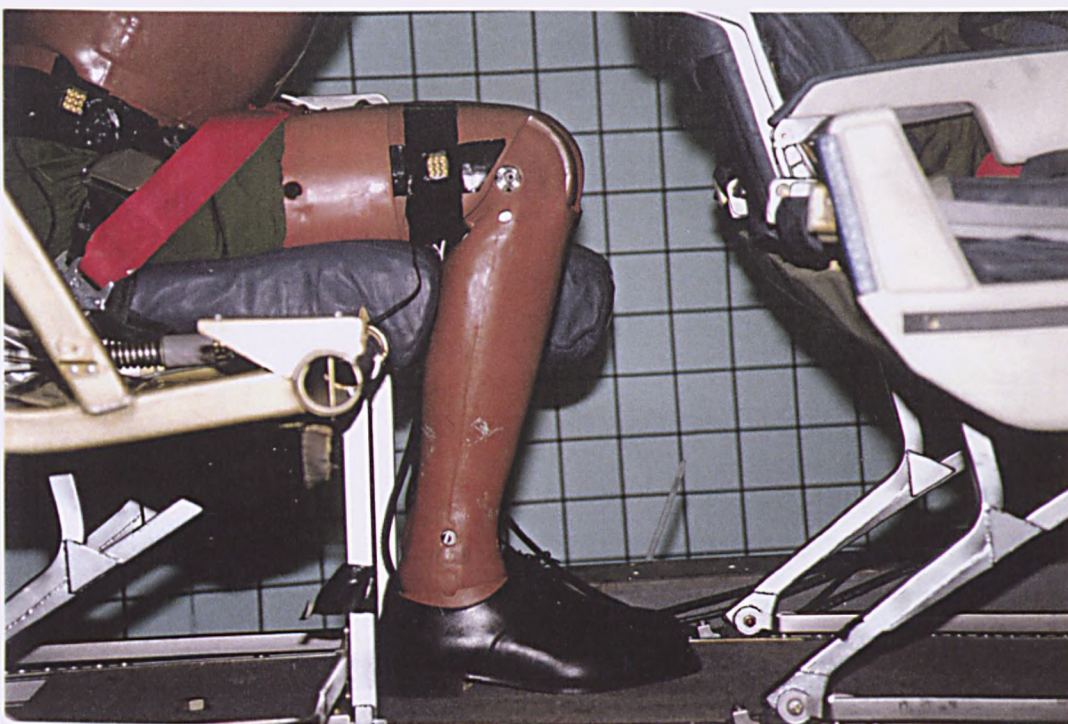


Figure 140. Rear Dummy Lower Legs Inclined 11.5° Rearward Of The Vertical

11.14.2 Seat Pitch

Seat pitch has an important effect on the injuries sustained by the occupant. A parametric study was set up to assess the effect of a variety of seat pitches. The model was used to evaluate seat pitches of 27 inches, 30 inches, 34 inches and 36 inches. The results obtained were subsequently compared with the baseline model.

11.14.3 Occupant Lower Leg Angle

The lower leg angle of the rear occupant was modified in increments of five degrees. A total of four steps were analysed (11.5°, 6.5°, 1.5° rearward and 3.5° and 8.5° forward of the vertical). The different positions were subsequently assessed and compared with the baseline model.

11.15 ADDITIONAL CONFIGURATIONS

Supplementary work was carried out to examine the effect of different interior configurations on the occupant.

11.15.1 Standard Bulkhead

This model was identical to the one used in the previous bulkhead simulation. The contact stiffness was more representative of a typical bulkhead found in current civil aircraft. The results from this model were then compared directly with those from a less stiff "Nomex" bulkhead.

11.15.2 Nomex Bulkhead

This model consisted of a single seat and a 50 percentile male occupant in the baseline braced position. The seat was positioned 35 inches behind a bulkhead (measured from the seat reference point (SRP)). The contact stiffness of the bulkhead was of a non-standard design. Consequently, this simulation represents a less severe environment than that normally found in commercial aircraft.

11.15.3 FAA 16G Crash Pulse

The pulse used in the baseline and parametric study models was the actual acceleration time history recorded by the IAM in their sled test. It is important to note that the required impact velocity and deceleration pulse as laid down by the FAA 16G pulse for transport aeroplanes was not achieved in the test.

In the sled test, an impact velocity of 12.4m/s was attained but the 16G regulation required this to be at least 13.41m/s. Although the minimum requirement of 16G peak deceleration within 0.09 seconds was achieved, the

reduced impact velocity resulted in the sled test producing a less severe pulse from an energy standpoint.

The sled and FAA pulses are compared in Figure 131. The graphical plots show that although the peak deceleration is higher in the sled test, the area under the curve which represents the impact energy is less.

It was, therefore, decided to run the original baseline simulation with the two braced occupants. This was performed with the sled test acceleration time history and the FAA 16G pulse, in order to determine any differences in injury levels.

11.15.4 Three Point Belt Restraint

In the majority of the previous simulations the occupants have been restrained by the conventional lap belt. With a predominantly fore-aft crash pulse, this restraint system does not arrest the upper torso of the occupant.

A model was developed with a three point belted occupant sitting behind a bulkhead and utilising the IAM sled test pulse. The injury levels sustained were then compared with those from the other models.

11.15.5 Rearward Facing Seat

A rearward facing seat configuration was simulated using a single upright lap-belted occupant. The IAM sled test pulse was reversed to simulate the effect of a rearward facing seated occupant under such conditions.

11.16 CORRELATION

The main objectives of this study was to correlate the computer model with the sled test and then to use the correlated model as a benchmark for further assessment of the brace position and in the study of possible alternative interior configurations.

The peak injury values established from the IAM sled test and the final baseline computer model are shown in Table 25, these are compared with two test runs, 3672 and 3673. It is worth noting that there are significant variations between the test results. Figures 138 and 139 show the Hybrid III dummy occupant simulations. Figures 143 and 144 show the occupant kinematics for the computer simulation of the brace position.

There are notable differences between the test and analysis values, specifically in the left femur and left tibia. It is believed that this may be due to errors in the set-up of the seats and the dummy. The following explanations are offered:-

11.16.1 Seats

The twin row seat set-up used for the tests, which had been removed from the Boeing 737-400 G-OBME, contained seats from the rear of the aircraft. The front seat row was from the first row in the aircraft. This installation did not replicate an actual twin row configuration. The seat in front was therefore offset towards the right and was obtained from the left hand side of the aircraft, Figure 141. The seats which were modelled were based on the twin row configuration as used in G-OBME and were identical with seat rows 15 and 16 on the right hand side of the wing box section. This configuration has been consistently used in all research since the accident investigation began. The seats which were tested had been used previously on a complimentary research programme and had been subjected to a number of impact tests.

11.16.2 Belt Stiffness

The manufacturer's data for new unused belts was specified as 20% at a load of 2200lbs. This was initially used in the computer simulation. Due to poor correlation with the sled test results, this was explored further. Subsequent investigation highlighted that the belt on the sled test had been used a number of times on consecutive impact tests before being discarded. This had altered the belt characteristics.

Three samples of new belt webbing were subsequently tested. These showed consistently that the new belts, which were specified by the manufacturer to have a 20% strain characteristic were actually 17%. However, the latter is within the manufacturer's tolerance band. A further parametric assessment was conducted using a wide variety of belt stiffnesses based on the 17% stiffness. This assessment showed that the belt characteristic, which retrospectively could be used to achieve a reasonable correlation, was of 11% strain. The load deflection curves of 11%, 17% and 20% belts are shown in Appendix 7.

11.16.3 Seat Cushion Stiffness

The seat cushions used for the sled tests had been subjected to repeated impacts. It is well known that cushion materials degrade under repetitive loading. The magnitude of the loading under impact conditions accelerates this process and causes the material to initially undergo microscopic and subsequently, macroscopic tearing. Thus, instead of sitting on a resilient cushion the dummy would be seated on a compressed surface. It is worth noting that the cushion stiffnesses, which were used in the computer simulation, were based on new seat cushions. The stiffness had, therefore, to be changed iteratively in the computer model to achieve a degree of correlation with the test. The stiffness of the old cushions were not individually tested because of financial and time constraints.



Figure 141. Seat Offset

11.16.4 Seat Back Stiffness

The breakover stiffness of the seat back in front has a significant effect on the timing of the head acceleration and the magnitude of the Head Injury Criteria (HIC). Under repetitive loading, the seat back breakover mechanism is known to wear. This will undoubtedly change the stiffness of the breakover torque. The use of repetitive impact tests on the seat back not only has an adverse effect on the breakover stiffness but also on the local stiffness. Thus, the food tray is prone to cracking and the aluminium panels are also subject to buckling.

To achieve correlation between the sled test and the computer simulation the stiffness of the seat back had to be increased iteratively in the computer model to allow for the deformation imposed on the seat back through repetitive impact testing.

11.16.5 Front Seat Luggage Bar

It became apparent through the simulation that the feet of the occupant can strike the luggage bar under the seat in front. This was particularly evident when flailing or leg slide took place. Under certain circumstances, foot entrapment under the luggage bar was also observed. On reviewing the high speed video output from the sled tests, it became clear that the luggage bar had not been present in the tests. The loads generated by the foot to luggage bar contacts, particularly if foot entrapment took place, were significant. The entrapment of the feet can cause severe knee hyperextension. The torques generated at the ankle and knee are sufficiently high to cause fracture of the foot, ankle or knee joints. At Kegworth fractures to the foot were seen, these being commonly open talar dislocations and mid-foot fractures. These injuries may have been associated with foot entrapment and contact with the luggage bar.

11.16.6 Femoral Separation

Observation of the high speed video output from the sled tests showed that femoral separation of the Hybrid III took place adjacent to the pelvic region. This, consequently, resulted in a "stepped" femur, thus allowing the pelvis to dig into the seat cushion, Figure 142. This separation could have caused the forward part of the femur to lift and thus may have reduced the degree of forward slide of the right leg. In the computer simulation, this phenomenon was not observed. The distance moved forward by the right leg was slightly more apparent in the computer simulation than in the sled test, although flail did not take place.

11.16.7 High Speed Video Recording

Although all tests were recorded from the right side of the sled using a NAC 200 high speed video camera, no cameras were available to monitor the left

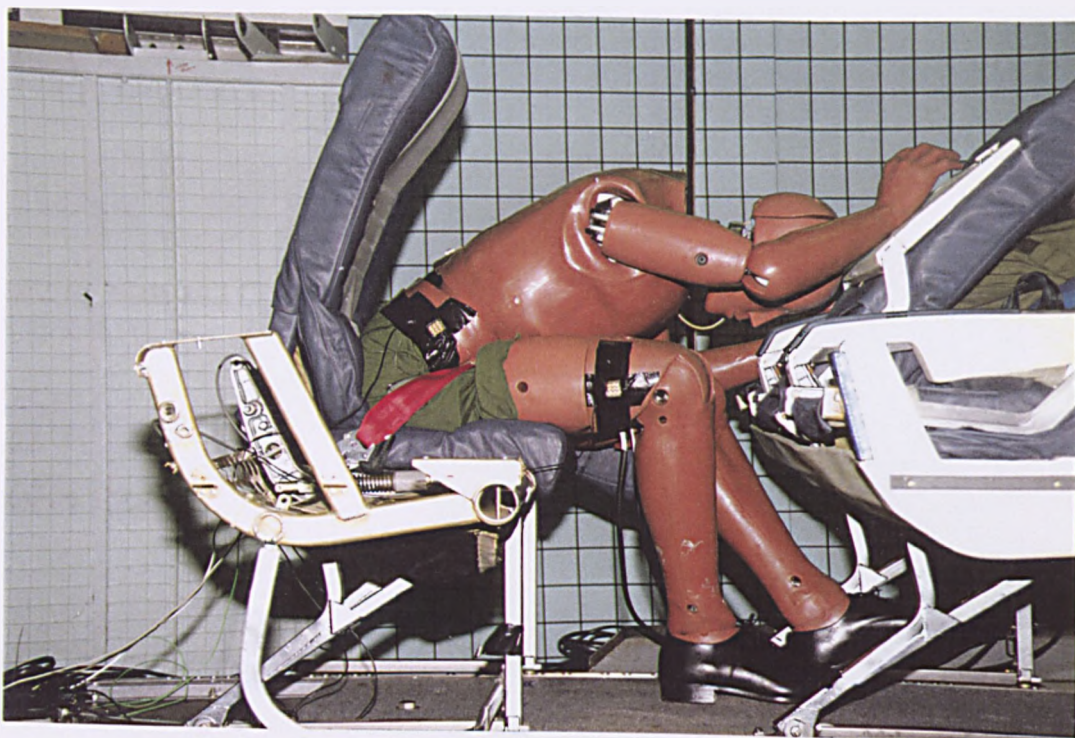


Figure 142. Post Impact, Left Leg Slide

and plan view of the sled. Therefore, it was difficult to fully observe the left femur. In the computer simulation, moderate femoral slide took place, this being as a direct result of the 10° lateral deceleration. The computer simulation showed that the upper torso rotated towards the left which caused the left leg to twist and slide forward.

Left leg slide was reported to occur with the baseline brace position in the un-yawed 16G sled tests which were conducted by Brownson (1993). The test work was performed using the same method described under the section entitled Test Procedure. However, there was one exception. The 10° lateral yaw of the sled, which is stipulated in AS 8049, was not included. Using this test configuration, it was still observed that, left leg slide occurred at 75ms. This occurred when the deceleration was at its maximum. This phenomenon could not be reproduced using the computer model in a straight 16G impact.

11.17 RESULTS

The results of the brace position parametric studies are presented in Tables 26 to 28. Table 26 encompasses the floor friction study, Table 27 the effects of varying the seat pitch, and the tibial angle results are presented in Table 28.

The results from the additional analyses of bulkhead strikes, 16G crash pulse, three point belt and rearward facing seats are summarised in Table 29.

The kinematic plots and trend diagrams are shown in Figures 143 to 216. The kinematics indicate the initial set up position for the occupant, contact zones with the seat in front and a kinematic overview of the occupant behaviour for the crash duration spread over nine frames. The trend diagrams show the effect of different parameter changes on the occupant.

The focus of the results is based on the rear occupant in the twin row configurations. This baseline model is consistent with the earlier analyses.

11.17.1 Floor Friction

The floor friction parametric study comprised the following coefficients of friction 0.55, 0.6, 0.65 and 0.7. The baseline model contained a value of 0.5 which is equivalent to leather soled shoes worn on carpeting, similar to that which was found in aircraft G-OBME. At the other end of the spectrum, a friction coefficient of 0.7 is equivalent to rubber soled shoes applied on the same type of carpeting.

Figures 145 and 146 show the kinematics associated with increasing the friction coefficient from 0.55 to 0.7. It can be observed that the head of the occupant strikes the top region of the food tray. Elbow strike also takes place with this part of the seat back. The head of the occupant remains in contact with the food tray as the seat back breaks over. Head contact is then shown to occur with the lower end of the seat back. No knee or lower leg contact

occurs with the seat in front. However, the kinematics highlight one particular observation, that as the friction coefficient is increased, the degree of foot translation is reduced.

The results of the floor friction coefficient study show very little alteration in injury criteria, Table 26. However, it is shown that on increasing the friction coefficient the likelihood of lower leg flail is reduced.

Figure 147 shows the HIC and head acceleration levels. It is apparent that the results are almost unaffected. A slight increase in both values is shown to occur at 0.7 and is associated with a HIC value of 306 which is well below the injury criteria limit of 1000. This is likely to cause facial bruising but no unconsciousness.

The chest resultant acceleration levels are displayed in Figure 148. The level of accelerations are constant and are well below the standard limit of 588m/s^2 (60G).

The pelvic resultant acceleration and lap belt loading, Figures 149 and 150, respectively show that the trends remain constant.

The femoral shear forces, Figure 151, show a slight upward trend in load for both the left and right femurs. However, the left femur is less heavily loaded than the right. This is associated with the apparent translation of the left femur due to the rotation of the body. The latter takes place due to the 10° lateral acceleration which is imposed on the occupant. The degree of shear loading which is imposed on the femurs is below the average static injury assessment criteria of 2.45kN, as quoted by Yamada, Table 8.

The femoral axial loading, Figure 152, shows a slight upward trend in load on both the left and right femurs. It is also apparent that the left femur has sustained a slightly higher loading than the right, this is associated with the lateral motion which is imposed on the occupant. A maximum load of 1663N has been subjected to the femur, this is well below the maximum permitted injury level of 10kN.

The local horizontal bending moment (My) on both femurs, Figure 153, shows a slight steady increase in bending torque as the floor friction coefficient is increased. It is also observed that the left femur is more heavily loaded than the right. Although a recorded maximum bending moment of 190Nm is observed, this figure is well below the dynamic bending moment of 328Nm, as quoted by St. Laurent, Table 14.

Figure 154 shows the shear force which is imposed on the tibia. This demonstrates a steady upward increase in load which is directly affected by the increase in friction force. A maximum shear load of 489N is shown to occur in the lower section of the tibia close to the ankle joint. This value is

below the static injury assessment criteria of 2.6kN quoted by Yamada, Table 12.

The lateral loads imparted to the lower section of the tibia, Figure 155, are not considered to be significant. These are not likely to cause serious injury, the highest load of 289N is shown to occur with the highest floor friction coefficient of 0.7.

The vertical loads (F_z) through the tibiae show a very slight upward trend, Figure 156. A maximum load of 1861N occurs. This value is well below the dynamic injury limit of 10kN quoted by St. Laurent, Table 14. This load is not likely to cause fracture.

Figure 157 shows that the lumbar axial loading (F_z) is constant. A maximum load of 4904N is shown to occur and is of a tensile nature. The load obtained is below the injury assessment level of 12.7kN quoted by Melvin, Table 4. The loading trend obtained is similar to the pelvic resultant acceleration obtained in Figure 149.

11.17.2 Seat Pitch

The effect of seat pitch was investigated using a total of five parametric runs. This comprised 27 inch, 30 inch, 32 inch (baseline), 34 inch and 36 inch seat pitches. For the 27 and 30 inch pitches, the upper torso of the occupant was rotated anticlockwise because of the reduced seat pitch, as shown in Figures 158 and 160. For the 34 and 36 inch seat pitches, the upper torso was rotated further forwards so that the head contacted the seat back in front, Figures 162 and 164.

Examination of the kinematics of the 27 inch seat pitch, Figures 158 and 159, shows that the head of the occupant strikes the top of the food tray. At 120ms, Figure 159, it can be observed that knee as well as tibial contact have taken place with the seat in front. The lower limb impact with the front seat stops the tibial forward translation.

Observation of the kinematics of the 30 inch pitch, Figures 160 and 161, show that at 120ms, Figure 161, head contact takes place with the top region of the food tray. Arm contact is also shown to occur with the seat back. At 140ms, a tibial glancing contact takes place with the seat in front. At 160ms this forces the tibiae and feet to rotate downward and forward. At 180ms foot entrapment is observed to occur below the front seat luggage bar. The occurrence of foot entrapment in conjunction with the upper torso rotation, at 200ms, forces the knee joints to be severely hyperextended.

Assessment of the kinematics of the 34 inch seat pitch, Figures 162 and 163, show head contact takes place with the middle region of the food tray. This occurs as a direct result of positioning the upper torso closer to the femurs. This is followed by arm contact. It is observed, at 140ms, that the upper

torso contacts the femurs. This, in turn, loads the tibiae and feet which stops the feet from sliding further forwards.

Figures 164 to 165 show the kinematics of the occupant associated with a 36 inch seat pitch. It is apparent, in Figure 164, that the upper torso has been rotated further down towards the femurs. The effect of this, is for the upper torso to contact the femurs earlier in the impact event, thus trapping the lower legs against the floor. This, consequently, stops the lower legs from translating further forwards. The head contact with the seat back occurs towards the lower edge of the food tray. The head continues to travel down the seat back, subsequently impacting against the lower soft region of the seat back.

The head injury criteria (HIC) and head accelerations are presented in Figure 166. The HIC values obtained are dependent upon the head strike zone, that is, whether the head strikes the hard surface of the food tray or the softer part of the seat back. This value is also affected by the position adopted on impact. The semi-braced positions adopted with the 27 and 30 inch seat pitches show an increase in HIC level. The HIC value, at 30 inch pitch, shows a slight increase above the 27 inch pitch. This is due to leg flail and contact with the luggage bar which resulted from the tibial glancing blow against the seat in front.

The optimum HIC value seems to take place with a 32 inch pitch. During the simulation, head strike takes place with the mid section of the food tray. At the 34 inch pitch, the upper torso was rotated further forwards. This allowed the head to strike the lower edge of the food tray causing an increase in HIC. With the 36 inch pitch simulation, the head is observed to strike the lower soft part of the seat back below the food tray. This resulted in a lower HIC value than was seen for the 34 inch pitch. The maximum HIC value of 586 was obtained with the 34 inch seat pitch. This is well below the standard limit of 1000 and would not be expected to cause serious injury.

The thorax resultant accelerations are presented in Figure 167. It is observed the highest acceleration level is obtained with the 34 inch seat pitch. However, the magnitude of the acceleration is 174m/s^2 and is well below the limit of 588m/s^2 (60G). The lowest value occurs with the 30 inch seat pitch.

The pelvis resultant acceleration, Figure 168, shows a downward trend as the seat pitch is increased. The acceleration is highest at 27 inch pitch because of the tibial and femoral strike against the seat in front which occurs at 32, 34 and 36 inch pitches. The reduction in upper torso angles reduces the inertial forces on the upper and lower torso, with a consequent decrease in the pelvic resultant accelerations.

The lap belt loads, Figure 169, are similar in trend to the pelvic resultant accelerations for the 30 to 36 inch seat pitches. It can be observed, however, that at 27 inch pitch a major reduction in lap belt load has occurred. This

decrease is due to load transfer to the tibiae and femurs which is caused by contact with the seat in front.

The femoral shear loads which are presented in Figure 170 show the following results. At 27 inch pitch, the left femur is more heavily loaded than the right, this is due to the lateral loading which is imposed on the occupant on impact with the seat in front. The shear load reduces at 30 inch pitch. The reduction in load is due to the glancing tibial strike. This allows the lower legs to slide forward which reduces the shear loads on the femurs, for the 32 to 36 inch seat pitches, the shear loads on the femurs tend to increase as the femurs are loaded vertically. As the upper torso of the occupant is rotated forwards due to the increase in pitch, the following takes place:-

It is observed that the upper torso strikes the femurs earlier during the impact, this occurs when the lower legs are almost vertical causing an increase in the femoral shear loads. The contact which ensues traps the lower legs against the floor and thus reduces foot slide and subsequent leg flail. The loads obtained in the analysis show that femoral fracture would not be expected to occur by shear failure.

The femoral axial load trend, as represented in Figure 171, shows that a maximum load of 2025N was obtained at a 27 inch seat pitch. The load subjected to the femur is compressive, quite different from the loads observed for the other seat pitches analysed. At 30 inch pitch, the load changes to being tensile. The lower legs are deflected under the seat in front causing the knees to hyperextend. The subsequent contact with the luggage bar causes the left femur load to rise.

At 32, 34 and 36 inch pitches, the axial femoral load is reduced. This reduction is affected by the orientation of the tibia when the upper torso strikes the lower legs. The maximum axial load which is observed is well below the recognised injury threshold of 10kN. It is, therefore, unlikely that femoral fracture will occur under axial loading.

The femoral bending moment (M_y), Figure 172, changes very little with different seat pitches except for the 30 inch seat pitch. At 30 inch pitch, the tibial strike against the seat in front causes foot entrapment below the luggage bar. This causes the bending moment to increase to a value of 484Nm in the left femur and 457Nm in the right femur. These moments are in excess of the maximum dynamic femoral bending moment, Table 14. Thus, it is highly likely that knee ligament damage and femoral fracture will occur.

The tibial shear load, which is presented in Figure 173, shows that at 30 inch pitch the magnitude of the load is greatest. This effect is due to foot contact with the luggage bar. The level of loading is sufficiently high to cause ankle and foot fracture similar to the open talar dislocation and foot fractures which were observed in the Kegworth air crash. It is noteworthy that there is a slight upward trend in shear load at 32, 34 and 36 inch pitches. This trend is due to

the attitude of the tibia at the moment of upper torso contact with the lower limbs.

The lateral loads, to which the tibiae are subjected, Figure 174, are observed to be small in magnitude. The highest load of 283N occurs as a result of striking the seat in front. The magnitude of loading is not sufficient to cause serious injury.

The vertical or axial loadings through the tibiae are presented in Figure 175. At 27 inch pitch, the highest load of 1826N is observed. The load is well below the dynamic injury limit of 10kN, as shown in Table 14. These loads are not expected to cause tibial fracture under axial loading. At 30 inch pitch, there is a reduction in vertical loading. This effect is associated with the tibial glancing strike against the seat in front. Transfer of load has taken place from the vertical to the shear component, Figure 173. At 32, 34 and 36 inch pitches, the vertical loading is almost constant, some variations are observed to occur. These are due to differences in lower leg angles at the point of contact with the upper torso.

The lumbar loading, presented in Figure 176, shows that a maximum load of 5154N occurs following impact, for an occupant in the semi-braced position at a 27 inch seat pitch. All the loads obtained are tensile in nature. At a 30 inch seat pitch, it is observed there is a slight reduction in spinal load. This is attributed to lower leg slide.

11.17.3 Lower Leg Angle

The lower leg parametric study consisted of incrementing the tibial angle forward of the baseline value of 11.5° in steps of five degrees. The individual values investigated were 6.5°, 1.5° rearward of the vertical, 3.5° and 8.5° forward of the vertical. All other parameters were maintained constant at the baseline values.

At an angle of 6.5° rearward of the vertical, with the friction coefficient maintained at the baseline value of 0.5, the results displayed in Figures 177 and 178 show the kinematics associated with the impact event. It is observed that at 120ms, head impact takes place with the seat back in front. At 180ms, foot contact with the luggage bar occurs. The sequential kinematics plot, Figure 178, shows the whole impact event, it is observed that foot entrapment takes place below the luggage bar. This effect causes the knee and ankle joints to hyperextend.

Figures 179 and 180 show the kinematics associated with incrementing the tibia angle to 1.5° rearward of the vertical. It is observed that head and arm contact take place with the front seat back. Foot slide has occurred. The sequential kinematic plot, Figure 180, highlights the contact of the feet with the luggage bar and the subsequent foot entrapment which ensues. It is observed that the right knee and ankle joints have hyperextended, no

hyperextension of the left knee joint has occurred. This is because the left foot has struck the upright seat leg.

The lower leg angles were subsequently positioned at 3.5° forward of the vertical, Figure 181. At 120ms, Figure 182, impact with the front seat back takes place. Head and arm contact occurs. It is also observed that the lower limbs have translated forward. At 180ms, the upper torso is almost horizontal with the head contacting the lower edge of the food tray. The right foot is observed to have slid below the luggage bar, thus causing foot entrapment. At 200ms, the right knee has hyperextended.

Figure 183 shows the tibiae positioned at 8.5° forward of the vertical. The occupant analysis is presented in Figure 184. This impact shows similar results to the previous analysis. At 120ms, head and arm contact occur with the seat in front. The lower legs are observed to translate forward. It is also observed that the lower torso descends into the seat as the belts load the lower torso. This effect causes the heels of the occupant to lift off the floor by a small amount. At 180ms, the right foot contacts the luggage bar. Thereafter, the foot is entrapped below the luggage bar. This causes the right knee to hyperextend.

The changes noted from the tibia angle parametric study are presented in Figures 185 to 195. Figure 185 shows the head injury criteria and head acceleration trends. It is observed that both results increase in value as the leg angles are incremented forwards of the vertical. Although the head injury criteria have increased to a maximum value of 601, this is still below the accepted injury threshold of 1000. Thus, although facial injury is likely, fatal injuries would not be expected.

The resultant thorax accelerations are presented in Figure 186. The highest acceleration levels occur when the tibiae angles are placed at 8.5° forward of the vertical. However, the acceleration level of 194m/s² is well below the maximum accepted injury level of 588m/s² (60G). It is, therefore, unlikely that serious thoracic injury will occur.

The pelvic resultant accelerations, Figure 187, show a slight upward trend in acceleration as the lower legs are incremented forward of the vertical. The lap belt load trends, Figure 188, indicate a slight downward trend in load on positioning the lower legs forward of the vertical. It is believed this occurs due to the lower torso descending into the seat on impact. The downwards movement of the lower torso causes load transference between the seat base and the lap belt, thus reducing the latter.

The shear forces in the femurs are presented in Figure 189. This shows the loads are higher in the right femur, particularly where contact occurs with the luggage bar. This occurrence forces the femur against the front edge of the seat, thus, causing an increase in load. It can be observed from the trend diagram that the highest loads have occurred on placing the tibial angle 6.5°

rearwards of the vertical and 8.5° forward of the vertical. The highest femoral shear load of 3007N was observed to occur in the right femur. This magnitude of loading is above the average static injury limit of 2.45kN quoted by Yamada, Table 8. This is likely to cause femoral fracture

The femoral axial loads, shown in Figure 190, are tensile in nature. There is an upward trend in load as the tibial angle is placed forward of the baseline. It is clear that the highest load has occurred at a tibial angle of 3.5° forward of the vertical. However, the magnitude of the load is 1842N. This is well below the maximum axial femoral injury limit of 10kN. The axial loads sustained by the femurs are not expected to cause femoral fracture.

Observation of the femur bending moments, Figure 191, shows the values are almost constant for both the left and right femurs on positioning the tibial angle at 11.5° rearward of the vertical. At 6.5° rearward of the vertical, the bending moment rises in the right femur. This is associated with foot contact against the luggage bar. At 1.5° rearward of the vertical, severe right foot entrapment takes place below the luggage bar. This results in severe bending moment, of 292Nm, which approaches the fracture limit of 328Nm. The bending moment causes the right knee joint to hyperextend.

In the left femur, a reversal in the bending moment is shown to occur. This is associated with upward rotation of the femur. On placing the tibial angle at 3.5° and 8.5° forward of the vertical, it is observed from the kinematics that foot entrapment takes place. However, on examining the trend diagram, Figure 191, this shows that the bending moments are reducing in magnitude.

The tibial shear loads trend is presented in Figure 192. It is observed the loads are small in magnitude at 11.5° and 6.5° rearward of the vertical. However, at 1.5° rearward of the vertical, the shear load in the right tibia is shown to increase dramatically. The magnitude of the load is 3323N, Table 28. The load is above the average static load limit of 2.6kN quoted by Yamada, Table 12. This is likely to cause tibial fracture and possible damage to the ankle joint. The increase in load is associated with foot entrapment below the front seat luggage bar. This load is observed to reduce in severity as the tibial angle is moved further forwards of the vertical. The level of loading on the left tibia is observed to be less than the right tibia. This effect is due to left foot contact against the upright front seat leg.

The tibial lateral loadings are presented in Figure 193 and Table 28. These show that the loads subjected to the tibiae are not likely to cause any significant injury. The maximum load of 580N is noted to occur when the tibial angle is at 8.5° forward of the vertical.

The vertical loads through the tibiae are presented in Figure 194. The maximum load of 3240N is observed to occur in the right tibia. This is not expected to cause tibial fracture under axial loading. However, the reactive load which is imposed on the ankle joint may well cause dislocation to take

place. The general load trend shows that the loads increase from the baseline position until the tibia angle is almost vertical. A subsequent reduction in load is then noted as the tibia angle is positioned forward of the vertical. However, these loads are of a sufficiently high magnitude to cause injury to the ankles and feet.

The lumbar vertical loads are presented in Figure 195. These show that the loads on the lumbar spine are almost constant in magnitude. The maximum load of 4944N occurs when the tibiae are placed at an angle of 8.5° forward of the vertical. All the loads obtained from the parametric assessment are tensile in nature. The level of loading obtained is tensile and is well below the maximum injury level of 12.7kN as quoted by Melvin, Table 4.

An additional assessment of the bending moments at the ankle joints was made and these are presented in Table 30. The bending moment injury threshold limits are severe in a number of cases. These values indicate that open talar dislocation and foot fracture may occur.

11.17.4 General

Five additional configurations were investigated to address survivability issues. These configurations included the effect of bulkhead strike against a standard bulkhead and a softer "Nomex" bulkhead, a comparison of the baseline pulse with the FAA 16G pulse, and an assessment of three point belted forward facing occupants and rearward facing lap belted occupants.

The effect of striking a standard bulkhead while braced is demonstrated in Figures 196 and 197. This was carried out using the baseline sled pulse. The upper torso angle was maintained at 25° forward of the vertical in order to obtain a direct comparison with the baseline brace position. Figure 197 shows that at 120ms during the impact, head and foot strike take place with the bulkhead. At 140ms, arm contact is shown to occur. It is also observed that severe neck hyperextension has taken place.

The simulation of the "Nomex" bulkhead strike, Figures 198 and 199, is somewhat similar to that of the standard bulkhead. However, the strike which takes place is less severe. This results in neck hyperextension but to a lesser degree, Figure 199.

A further assessment of the brace position was made using the FAA 16G pulse. This showed that the kinematics demonstrated a similar motion to the baseline analysis with one exception, Figures 200 and 201. Between 160ms and 180ms the left foot is observed to slide beneath the front seat. This results in left leg flail.

A three point seat belt analysis was also conducted to evaluate the effect of this type of restraint on an occupant facing a bulkhead, Figure 202, using the baseline sled pulse. Three point belt systems consisting of lap and shoulder

restraints have been in use in the automotive industry for over two decades. Unlike a single lap restraint, the three point belt, in addition to arresting fore-aft pelvis translation, also retards upper torso movement.

The benefits of three point belts when transferred to an aviation environment are obvious if the issues of design, packaging and seat loading are satisfactorily resolved.

The shoulder harness was attached to a retractor which was designed to spool from the top section of the seat back. Figure 203 shows the kinematics associated with the impact. For this analysis, the seat back and seat structure were strengthened to stop failure from occurring. It is quite clear from the kinematics that head strike does not occur with the bulkhead. However, on impact the body is observed to descend into the seat base which allows the femurs to lift. This causes the feet to rotate downwards into ankle plantarflexion on contact with the bulkhead.

An additional configuration was assessed to investigate the effect of being seated in a rearward facing seat. Figure 204 shows the initial occupant position. It should be noted that the head rest has been increased in height and a heel plate has been introduced to stop foot translation under the seat. The seat back and seat structure have been further increased in strength in order not to allow structural failure.

Figure 205 shows the kinematics associated with the rearward facing simulation. It is observed the upper torso moves into the seat back. Foot contact is also apparent against the heel plate. Between 110 and 160ms the upper torso is observed to rebound against the seat back. It is apparent throughout the simulation that no limb flail or major upper torso motion occurs.

The head injury results for these additional studies are presented in Figure 206. It is observed that the HIC value for the baseline simulation is 293. This is not expected to cause loss of consciousness although minor head bruising and skin tearing may occur.

The bulkhead strike analysis against the "Nomex" panel shows an increase in HIC level above the baseline analysis. The HIC value obtained is 739. Although this figure is below the standard injury limit of 1000, it is likely to lead to head bruising with partial loss of consciousness for a proportion of the population.

The highest HIC level of 1937 has been obtained with the standard bulkhead. This value is in excess of the head injury limit of 1000 and is likely to cause fatal injury.

An additional assessment was made with the FAA 16G pulse. A comparison with the baseline pulse shows an increase in HIC level. The value obtained

was 871. It is likely that severe head bruising and a degree of unconsciousness may occur.

The lowest HIC values have been obtained with the three point belted forward facing and the rearward facing lap belted occupants. These values are 46 and 149 respectively. These findings indicate that no facial lacerations or significant head injury are likely to take place.

The thorax resultant acceleration is presented in Figure 207. This shows that the maximum acceleration of 344m/s^2 has been obtained with the standard bulkhead configuration. This value is below the injury limit of 588m/s^2 (60G), as quoted in AS 8049. The lowest thorax acceleration has been obtained with the baseline brace position using the sled pulse.

The pelvic acceleration trends are presented in Figure 208. This shows that the highest acceleration results are observed with the standard bulkhead. This is caused by load generation against the head which is transmitted through the upper torso and subsequently, the pelvis. Although the result from the 16G FAA pulse is lowest, the duration of the acceleration time history is more prolonged than any of the other results.

It is observed from the lap belt load trend diagram, Figure 209, that the maximum belt load has been obtained with the 16G FAA pulse. The value of the load is 7869N. This level of loading is likely to cause tissue damage in the region of the iliac crest. The maximum belt load was obtained with the 16G pulse due to the sustained pelvic acceleration which occurred. It is quite clear that the lap belt load reduces significantly with the three point belt analysis as the loads on the occupant are shared between the shoulder harness and the lap belt. For the rearward facing simulation, the peak lap belt load is 533N. This load is not significant and would not cause any significant injury. The load is generated as the occupant rebounds in the seat.

The femoral shear load results are presented in Figure 210. This shows that a maximum load of 1894N occurs on the right femur. This takes place with the 16G FAA pulse. The lowest loads were observed to occur with the three point belt and rearward facing seated occupants. The magnitude of the loads obtained throughout the analysis indicate that femoral fracture due to shear loading is not likely to occur.

The femoral axial loading, Figure 211, shows that the maximum load of 2024N occurs with the three point belt analysis. The majority of the loads are tensile in nature with the exception of the rearward facing simulation where the load is shown to be compressive. The magnitude of the loads are less than the maximum femoral injury limit of 10kN, quoted in AS 8049. Therefore, it is unlikely that axial femoral fracture will occur.

The femoral bending moment, Figure 212, shows quite clearly that the maximum value has occurred with the FAA 16G pulse. The maximum

bending moment generated of 236Nm occurs on the right femur. This is followed by the baseline simulation which gives a value of 180Nm. The dynamic bending moment injury limit quoted by St. Laurent, Table 14, is 328Nm.

It is observed, however, that there is a reduction in bending moment for the bulkhead strikes, three point belts and rearward facing analyses. This effect is due to the reduced interaction between the upper torso and the femurs on impact. It is interesting to note that significant reductions in bending moments have been obtained with the rearward facing seat. The values obtained are 46Nm and 41Nm for the left and right femurs respectively. This represents on average a reduction of 75% when compared with the baseline brace position.

The shear loads for the tibia are presented in Figure 213. These show that wherever foot contact has taken place against structural members, this has resulted in increased loading.

The simulations carried out using the standard bulkhead recorded loads which were observed to be the highest with loads of circa 6000N being obtained. This value is above the static injury threshold of 2.6kN quoted by Yamada, Table 12. This magnitude of loading is likely to cause fracture to the ankles and feet. It is also observed that with the three point belt the lower tibia shear loads approach a value of 4000N. It is also anticipated that this level of loading will create foot and ankle injury. For the baseline, the FAA 16G crash pulse and the rearward facing configurations, the loads obtained were small in magnitude. These are not likely to cause foot or ankle fracture.

The lateral loads which are subjected to the lower tibia, Figure 214, indicate that no significant injury is likely to occur through this type of loading. The maximum load sustained is 267N on the left tibia and is due to the FAA 16G pulse.

The axial or vertical loading through the tibiae, Figure 215, indicates that a maximum load of 2084N has been obtained with the FAA 16G pulse. The load is below the dynamic injury threshold of 10kN quoted by St. Laurent. For the baseline, bulkhead and three point belt analyses, the loads through the tibiae are almost constant. A significant reduction in load has been obtained with the rearward facing seat. This represents an average reduction of 56% as compared with the baseline analysis.

The lumbar vertical or axial loading, Figure 216, shows that the load is tensile in the baseline, bulkhead and the FAA 16G pulse analysis. For the three point belt and rearwards facing seat, the loads obtained are compressive. It is observed the maximum load of 7483N has been obtained with the FAA 16G pulse. The level of loading obtained is below the injury threshold of 12.7 kN, quoted by Melvin, Table 4.

11.18 CONCLUSIONS

The study to correlate the computer simulation with sled testing has shown a good level of agreement. However, it must be emphasised that accurate and reliable methods of testing are necessary for good correlation to be achieved. The conclusions obtained from the research work on the brace position are as follows:-

11.18.1 Changes in Floor Friction

The effect of increasing the floor friction is to reduce foot slide and ultimately leg flail. It was also observed that small changes have occurred as a result of increasing the floor friction with the following parameters:

- (a) Increases in the head injury criteria and head acceleration results.
- (b) Increases in the femoral shear loads.
- (c) Increases in the femoral axial loads.
- (d) Increases in the femoral bending moments.
- (e) Increases in the tibial shear loads.
- (f) Increases in the tibial axial loads.
- (g) The thorax accelerations, lumbar and lap belt loads remain constant.

It was apparent that the left femur bending moment was more heavily loaded than the right due to the lateral acceleration which was imposed on the occupant. This effect allows the left leg to slide forward of the right, thus increasing the contact forces with the front of the seat base.

11.18.2 Changes in Seat Pitch

The effect of changing seat pitch has produced the following findings:-

- (a) At low seat pitches, an increase in the head injury criteria (HIC) takes place. This is associated with adopting a semi-braced position.

- (b) At higher seat pitches, an increase in the HIC value is observed. This is associated with an increase in the inertial forces on the upper body before striking the seat in front.
- (c) It has been observed the optimum HIC value has occurred with the 32 inch seat pitch.
- (d) At 30 inch pitch, a glancing strike between the tibiae and the front seat takes place. This effect forces the lower legs downwards and forwards. This is followed by foot entrapment below the luggage bar.
- (e) The head resultant accelerations follow the same trends as the head injury criteria.
- (f) The thorax accelerations are all below the injury thresholds. However, the maximum acceleration is induced at a 34 inch pitch.
- (g) The pelvic resultant accelerations show a decreasing trend in results as the seat pitch is increased.
- (h) The lap belt loads show a similar trend to the pelvic acceleration for seat pitches which are between 30 and 36 inches. At 27 inch pitch, a reduction in lap belt load occurs. This is associated with load transfer to the femurs. This effect takes place due to femoral contact with the seat in front.
- (i) The femoral shear forces show a general upward increase in load as the pitch is increased, with the exception of the 30 inch pitch. At 30 inch pitch, the glancing strike of the tibiae against the seat in front cause the femoral shear load to reduce.
- (j) The femoral axial load was found to be highest at 27 inch pitch. These are compressive in nature. The loads gradually decrease from 30 to 36 inch and are tensile.
- (k) The femoral bending moments are constant for the 27, 32, 34 and 36 inch pitches. At 30 inch pitch, a significant increase in the femoral bending moment occurs. This is likely to cause femoral fracture.
- (l) The tibial shear load, in proximity with the ankle joint, has shown a significant increase in load. This is associated with foot entrapment below the luggage bar.
- (m) The tibial lateral loads are small in magnitude. These are not likely to cause major injury in the lateral direction.

- (n) The tibial axial loads increase at 27 inch pitch, decrease at 30 inch pitch, steadily increase to 34 inch pitch and reduce at 36 inch pitch.
- (o) The lumbar loads increase at 27 inch pitch, decrease at 30 inch pitch then gradually rise as the pitch is increased to 36 inches.
- (p) For this particular seat design, a 32 inch seat pitch appears to be the optimum configuration with regard to injury levels.

11.18.3 Changes in Tibia Angle

The effect of adopting a brace position with the tibiae angled forward and rearward of the vertical has the following effects:-

- (a) The head injury criteria and head acceleration increase as the tibiae angles are incremented forward of the baseline position of 11.5 degrees.
- (b) The thorax accelerations show that the highest accelerations occur when the lower legs are incremented forward of the vertical.
- (c) The pelvic resultant accelerations show a slight increase in results as the lower legs are incremented forward of the baseline configuration.
- (d) The lap belt loads show a slight decrease in results as the tibiae are incremented forward of the baseline.
- (e) The femoral shear loads have increased on positioning the tibiae angles forward of the baseline.
- (f) The femoral axial loads show that the highest loads have occurred on incrementing the tibiae forward of the vertical.
- (g) The femoral bending moments increase in magnitude as the tibiae are positioned close to the vertical and reduce as the tibiae are angled forward of the vertical.
- (h) The tibial shear results show there are significant increases in load as the tibial angle is moved forward of the baseline position.
- (i) The tibial lateral loads are low in magnitude. These are not likely to cause significant injury.

- (j) The tibial vertical loads show a significant increase in results as the lower tibiae are placed close to the vertical and subsequently, forward of the vertical.
- (k) The lumbar vertical loads are almost constant in magnitude.

11.18.4 Changes in Configurations

Additional assessments were carried out to compare the effect of bulkhead strike, the FAA 16G pulse, a three point belted forward facing and rear facing lap belted occupants. These have shown the following:-

- (a) The bulkhead strike simulation has produced the highest head injury criteria. This is likely to cause fatal injury.
- (b) The lowest HIC values have been obtained with the three point belt and rearward facing configurations.
- (c) The thorax accelerations show that the lowest value has occurred with the baseline brace position. Whereas, the highest acceleration is shown to occur with the standard bulkhead simulation.
- (d) The highest pelvic acceleration has been obtained with the bulkhead simulation.
- (e) The highest lap belt load has been obtained with the FAA 16G pulse. The lowest belt load was shown to occur with the rearward facing seat.
- (f) The maximum shear load on the femurs have occurred with the FAA 16G pulse. The lowest femoral shear loads were obtained with the three point belt and rearward facing seats.
- (g) The highest femoral axial loads are tensile in nature and occur with the three point belt and bulkhead strike analyses.
- (h) The highest femoral bending moment occurs with the FAA 16G pulse and the lowest value with the rearward facing seat.
- (i) The maximum tibial shear load occurs with the standard bulkhead simulation. This is followed by the three point belted occupant. The lowest loads have been obtained with the baseline, the FAA 16G pulse and rearward facing seating configurations.

- (j) The lateral tibial loads are small in magnitude. These are not likely to cause significant injury. The highest loads occur with the FAA 16G pulse.
- (k) The maximum vertical tibial loads have occurred with the FAA 16G pulse. The lowest loads have been obtained with the rearward facing seats.
- (l) The highest lumbar spine load has occurred with FAA 16G pulse. The lowest load has been obtained with the rearward facing seat.

11.19 RECOMMENDATIONS

It is recommended that the brace position with the lower legs inclined rearward of the vertical should be adopted.

On adopting a brace position, it is recommended that the upper torso be placed close to the femurs wherever possible.

The effect of increasing the foot to floor friction is to reduce foot slide and subsequently lower leg flail. It is recommended that a floor friction coefficient of 0.7 should be aimed for through the use of appropriate carpeting.

The adoption of an upright or a semi-braced position is not recommended. This has been demonstrated to increase the injury level.

It is recommended that with the type of seat investigated in this study, the luggage bar should be redesigned to eliminate leg entrapment and subsequent foot fracture.

The use of seat pitches between 27 and 30 inches results in an increase in the HIC level. This is as a consequence of having to adopt a semi-braced position because of lack of space to crouch down. At higher seat pitches of 34 and 36 inches a higher HIC level was once more observed. For this particular seat design, it is recommended that a 32 inch seat pitch be used as it appears to be the optimum configuration associated with a reduced injury level.

Adopting a brace position with the tibia inclined forward of the vertical is not to be recommended. This leads to an increase in head injury criteria and foot entrapment.

It is recommended that femoral bending moment injury threshold limits be introduced in future regulations. This is a more significant design criteria than the current axial load limit of 10kN.

It is recommended that the dummy dataset be upgraded to include a spine model.

It is recommended that further work be carried out to develop injury criteria for the spine.

It is recommended that three point belt installations be used wherever practicable.

The rearward facing seat position was identified as the position least likely to result in traumatic injury (if facial injury from flying debris is excluded). It is recommended that such installations be adopted.

**This Page
Intentionally Left Blank**

12. THE DEVELOPMENT OF A SPINE MODEL FOR THE EVALUATION OF THE BRACE CRASH POSITION

12.1 INTRODUCTION

In the course of the Kegworth investigation comprehensive medical research was combined for the first time with computer occupant modelling. Extensive knowledge of occupant injury mechanisms was gained, including the effect of initial posture. It was discovered through the computer modelling that the posture of the passenger crash position might have significant effects on the kinematics of the individuals, and thus, on injuries. In particular, there were indications that holding the legs rearward of the vertical produced less leg flail and reduced leg loads. From the computer modelling, there also seemed to be benefits in reducing injury to other body segments.

It was decided to embark upon a programme of testwork using a Hybrid III Anthropomorphic Test Device (ATD). This work was carried out at the Royal Air Force Institute of Aviation Medicine at Farnborough. This work largely confirmed the benefits of a legs back brace position, but there were some reservations regarding the lumbar spine. Brownson (1993) in his assessment of lumbar loading indicated that the shear loads in the lumbar spine were close to the injury limit of 10.7kN, as stated by Melvin [94]. He also showed that the lumbar spine shear loads were higher on adopting a brace position with the legs back as compared with the legs being placed forward of the vertical.

The Hybrid III ATD was developed to assess automotive impacts and is the result of a great deal of research over a number of years. However, the type of kinematic behaviour experienced in a lap belted aircraft seat was not entirely the same as that which it was designed to assess. In particular, the body consists of a set of semi-rigid elements joined by a curved quasi spine, containing a number of load cells. The spine in the Hybrid III ATD does not have individual vertebrae, and insertion of a load cell into the lumbar region stiffens an area representing several vertebrae, into a virtually rigid unit.

The work of Brownson (1993), thus, posed a question over the recommendation of a legs back braced position. This position, which was otherwise deemed to be favourable, could not be recommended if severe spinal injury was to be increased. More detailed knowledge of the spinal loading was deemed necessary to fully explore the implications of the proposed brace position. Two approaches were considered:-

1. Cadaver testing
2. Computer modelling.

Cadaver testing has been extensively used in the development of automotive safety. Whilst it clearly is based on the use of a 'real' human form, it presents many problems. It is expensive, limited in scope and not as representative as

might be supposed. This is largely due to the distribution of bodily fluids, causing elements of the body to interact differently with one another, and lack of muscle tension to produce internal pressure. Conditioning of a cadaver to represent a living human is not readily achieved. It was intended to x-ray the cadaver before and after the test to assess damage. Thus only a "yes/no" damage assessment would be available.

Computer modelling is now a well proven and reliable tool for biomechanical studies in impact, but no suitable model was thought to exist. There was also concern as to the degree of correlation possible from the available data. Conversely, computer analysis is repeatable, is effective in terms of time and cost and can produce extensive numerical data from all parts of the body. Contact loads with the passenger environment can also be determined.

Preliminary enquiries revealed the existence of a Wayne State University (WSU) model of the spine which had been developed for ejection seat analysis [148]. The representation of the spine was in two dimensions. It was, therefore, decided to use the human body data from the WSU model in order to develop a MADYMO two dimensional computer model. This would then be used in the assessment of spinal injury.

12.2 HISTORICAL REVIEW OF SPINE MODELS

In the past two decades, a number of spine models have been developed, both static and dynamic. The former were created to investigate postural problems of the spine, whilst the latter attempted to provide mechanisms of spinal injury during seat to head acceleration. Static models have been created by Schultz and Galante [149] and Panjabi and White [150] and more recently by Belytschko [151]. Dynamic models were developed in the early 1950's and 1960's. The work of Hess and Lombard [152] was the basis of many continuum models whilst those created by Latham [153] and Payne [154] were the original lumped parameter models.

All these models were created to investigate the loads sustained by the spine during pilot ejection. However, these models were subjected to considerable simplification. For example, in the area of continuum models, the spine was represented by a straight elastic or viscoplastic column carrying a noneccentric load. Liu and Murray [155] proposed such a model. Other similar models have been proposed by Terry and Roberts [156], Shirazi [157], Rybicki and Hopper [158]. In all these models, eccentric loading and spinal curvature have not been considered.

Lumped parameter models with similar defects have also been created by Toth [159], Hopkins [160], and Kaleps et al [161]. The model created by Kaleps et al was intended to simulate whole body response and that of the spine was not modelled adequately [148]. This resulted in a lack of bending response.

In 1968, King et al [162] reported on the significance of bending during seat to head acceleration. At the same time, Orne and Liu [163] proposed a distributed parameter model which not only accounted for the effects of eccentric loading but also included the curvature of the spine.

Continuum models which accounted for eccentric loading and curvature of the spine were created by Li et al [164], and Krause and Shirazi [165].

Up until this time, in only one of the fourteen models was an attempt made to compare the results obtained by the model with experimental data.

Prasad et al [166] showed the existence of two load paths along the spine, one through the vertebral body and the other through the lamina, by way of the articular facets. All previous models were inadequate in completely simulating the response of the spinal column.

12.3 MODELLING

The work was divided into two sections, creation of the model and the analysis. It was decided to base all the work on the correlated economy class seating configuration previously described. This would have the widest applicability and would conform with work performed so far. The seat used was the Weber 4001 seat, since this data was available and the seat is one of the most common in use.

12.3.1 WSU Model

A two dimensional discrete parameter model of the spine has been created by Prasad et al [166] which incorporated the two load paths in the spine. The model also considered the natural curvature of the spine and the effects of flexion and eccentric inertial loading. Head and neck kinematics were simulated. Their effects on the thoracic and lumbar spine were also assessed.

The input acceleration pulse to the model could be an arbitrary function of time. The restraint system, which included a harness and seat, had been created to enable the simulation of a fully restrained seated occupant to be undertaken.

The model was originally developed to simulate ejection seated occupants. It was used to assess spinal column loading through two load paths. These were through the main vertebral bodies and discs and through the secondary path of the articular facets. Comprehensive data collection was made in order to validate the model.

The data was obtained from cadaveric tests which included two postures of the spine. The first posture was with the subject seated in an upright or erect position, this being a normal seated posture. The second posture was in a hyperextended mode.

Hyperextension of the spine was accomplished by placing a two inch thick block, four inches high and six inches wide against the seatback so that the centre line was opposite lumbar vertebrae (L1). The shoulders were subsequently pulled back using the shoulder harness so that the spine was hyperextended. Ewing, et al [167] reported that this change in spinal posture from the normal erect sitting position raised the fracture level of the cadaveric spine from 10 to 18G.

The model, which was developed, included the simulation of both spinal postures.

12.3.2 Modelling Assumptions

The model is two dimensional and consists of a head, 24 vertebrae, and a pelvis, Figure 217. Whilst the head has only its own mass, each vertebrae has a respective portion of body mass attributed to it, equivalent to a horizontal slice through the torso. This is the best assumption that can be made, but clearly the mechanism of mass transfer of the neck, torso and abdomen to the spine is complex and variable. The pelvis has the leg mass and inertia attached thereto. The mass of the arms was assumed to be distributed throughout the first five thoracic vertebrae.

Intervertebral connections were made by a system of five linear springs and three linear dampers. The majority of data was based on cadaveric testing of individual elements, although no information was available regarding the physical constants for the articular facets or the upper thoracic vertebrae. It was assumed that deformation occurred at the discs alone.

The intervertebral discs were massless.

The discs were replaced by a system of springs and dampers. One spring and damper for axial forces, one spring and damper for shear forces and another spring and damper for restoring torques due to the relative angular motion between adjacent vertebral bodies.

The facets and laminae were represented as springs connected to the vertebral body by a massless rigid rod.

The rigid bodies were arranged to simulate the curvature of the spinal column as accurately as possible.

12.4 EQUATIONS OF MOTION

Figure 218 shows the representation of two successive rigid links developed by Prasad et al [148]. These have undergone relative translation and rotation due to deformation of the disc. When undeformed, it has been assumed that the axis of any disc is in alignment with the axis of the vertebrae, that is, the

rigid link is below it. The position of the centre of the "i"th rigid link is determined by three generalised co-ordinates, u_i , w_i , θ_i .

The reaction forces and moments developed on the i th rigid body due to deformation of the "i"th and $i + 1$ discs and the laminae are presented in figure 219. The changes in the relative angular orientations and the lengths AC, BC and A1A3 shown in Figure 218, are used to calculate the restoring moments, axial and shear forces on the vertebral body and reaction forces at the articular facets. The moments and forces are presented in the following equations:

$$T7Y_i = XK_i (AC_i - AC_{oi}) + C_i \dot{AC}_i \quad (1)$$

$$T7X_i = XK_{si} (BC_i - BC_{oi}) + C_{si} \dot{BC}_i \quad (2)$$

$$B_i = XKT_i \{(\theta_i - \theta_{oi}) - (\theta_{i-1} - \theta_{oi-1})\} + C_{ti} \dot{(\theta_i - \theta_{oi-1})} \quad (3)$$

Where

- XK_i = Stiffness of the axial spring
- XK_{si} = Stiffness of the shear spring
- C_i = Damping in shear loading
- C_{si} = Damping in shear spring
- XKT_i = Stiffness of restoring torque spring
- C_{ti} = Damping of restoring torque spring

The subscript "o" denotes the state at time zero, and $(\dot{})$ denotes differentiation with respect to time. The forces $T6Y_i$, $T6X_i$ and the moment B_{i+1} are derived by changing the subscript "i" on the right hand side of equations (1) to (3) to $i+1$.

The articular facets have been modelled by two springs, one limiting rotation between the "i"th and $i - 1$ vertebrae in the erect mode is given by:

$$T51 = XK_{hi} \cdot h_i \cdot \sin \{(\theta_{i-1} - \theta_{oi-1}) - (\theta_i - \theta_{oi})\} \quad (4)$$

where

- h_i = Distance of the articular facets from the centre of the vertebral body.
- XK_{hi} = Stiffness of the spring resisting the relative motion.

In the hyperextended posture, due to the forced curvature of the spinal column, it is assumed that the facets have "bottomed out". The lamina act as another beam parallel to the disc. The change in length of A1A2, which is shown in Figure 218, is used as the measure of the axial deformation of this beam. The force developed is given as follows:

$$T51 = XK_{hi} (A_1A_2 - A_1A_{2oi}) \quad (5)$$

The force resisting the sliding motion at the facets between the "i"th and the i-1 vertebra is shown as:

$$FX1 = XKhi (A2A3 - A2A3oi) \quad (6)$$

Since the articular facets overlap, it is difficult to define the point of application of the preceding force. However, it is assumed that the force acts perpendicular to the longitudinal axis of the vertebral body at a point $(di + ACi/2)$ below the centre of the vertebral body, as shown in Figure 219. The reaction of this force on the vertebra immediately below acts at a distance $di - 1$ above the centre of the $i - 1$ vertebra. This assumption is justified since the articular facets on top of the lamina are shorter than those facets which are below the lamina. As demonstrated in Figure 219, the forces on the i th vertebra parallel to the ui and wi axis are as follows:

$$\begin{aligned} \Sigma F_{ui} = & (T6Xi + FX2 - FX1) \cos \theta_i - (T6Yi + T52 - T51) \sin \theta_i \\ & - T7Xi \cos \{ \theta_i - (\theta_{oi} - \theta_{oi-1}) \} + T7Yi \sin \{ \theta_i - (\theta_{oi} - \theta_{oi-1}) \} \end{aligned} \quad (7)$$

$$\begin{aligned} \Sigma F_{wi} = & (T6Yi + T52 - T51) \cos \theta_i + (T6Xi + FX2 - FX1) \sin \theta_i \\ & - T7Yi \cos \{ \theta_i - (\theta_{oi} - \theta_{oi-1}) \} - T7Xi \sin \{ \theta_i - (\theta_{oi} - \theta_{oi-1}) \} \end{aligned} \quad (8)$$

Taking the sum of the moments about the centre of gravity:

$$\begin{aligned} \Sigma M_{Gi} = & T7Yi \cos \{ \theta_{oi} - \theta_{oi-1} \} e_i + B_{i+1} - T6Yi . e_i \\ & - T6Xi . di - T7Yi . \sin \{ \theta_{oi} - \theta_{oi-1} \} di \\ & - T7Xi . \cos \{ \theta_{oi} - \theta_{oi-1} \} di - T7Yi . \sin \{ \theta_{oi} - \theta_{oi-1} \} e_i \\ & - B_i + (T51 - T52)(e_i + h_i) \\ & - FX2 . di - FX1(di + ACi / 2) \end{aligned} \quad (9)$$

There are also additional forces and moments which are to be added to the equations. These loads include the shoulder belt force, lap belt force, seatback reaction, chin to chest contact force and the reaction from the hyperextension block. Details of the auxiliary forces are described by Prasad et al [148].

The equation of motion are quoted as:

$$\Sigma F_{ui} = m_i \{ \ddot{X} + \ddot{u}_i - e_i \ddot{\theta}_i^2 \cos \theta_i - e_i \ddot{\theta}_i \sin \theta_i \} \quad (10)$$

$$\Sigma F_{wi} = m_i \{ \ddot{Y} + \ddot{w}_i + e_i \ddot{\theta}_i \cos \theta_i - e_i \ddot{\theta}_i^2 \sin \theta_i \} \quad (11)$$

$$\Sigma M_{Gi} = I_G \ddot{\theta}_i \quad (12)$$

Where

m_i = Mass supported by the i th body

I_G = Polar moment of inertia about the centre of gravity of the body

DESCRIPTION OF INTERVERTEBRAL LOADS	Designation In FBD
MAX UPPER VERTEBRAL SHEAR LOAD	T6X
MAX UPPER VERTEBRAL AXIAL LOAD	T6Y
MAX LOWER VERTEBRAL SHEAR LOAD	T7X
MAX LOWER VERTEBRAL AXIAL LOAD	T7Y
MAX LOWER FACET LOAD RESISTING ROTATION	T51
MAX UPPER FACET LOAD RESISTING ROTATION	T52
MAX LOWER FACET LOAD RESISTING SLIDING	FX1
MAX UPPER FACET LOAD RESISTING SLIDING	FX2
MAX TOTAL LOAD IN LOCAL X	ΣF_x
MAX TOTAL LOAD IN LOCAL Y	ΣF_y
MAX UPPER BENDING MOMENT	B_{i+1}
MAX LOWER BENDING MOMENT	B_i
MAX TOTAL BENDING MOMENT	ΣB
MIN UPPER VERTEBRAL SHEAR LOAD	T6X
MIN UPPER VERTEBRAL AXIAL LOAD	T6Y
MIN LOWER VERTEBRAL SHEAR LOAD	T7X
MIN LOWER VERTEBRAL AXIAL LOAD	T7Y
MIN LOWER FACET LOAD RESISTING ROTATION	T51
MIN UPPER FACET LOAD RESISTING ROTATION	T52
MIN LOWER FACET LOAD RESISTING SLIDING	FX1
MIN UPPER FACET LOAD RESISTING SLIDING	FX2
MIN TOTAL LOAD IN LOCAL X	ΣF_x
MIN TOTAL LOAD IN LOCAL Y	ΣF_y
MIN UPPER BENDING MOMENT	B_{i+1}
MIN LOWER BENDING MOMENT	B_i
MIN TOTAL BENDING MOMENT	ΣB

Table 31. Description Of Loads And Bending Moments In Spine Model

Equations (10) to (12) are non-linear, second order differential equations. For each body, there are three equations. Since this includes 24 vertebral bodies as well as the pelvis and head. This equates to 78 total equations to be solved. In order to solve these equations simultaneously, the Hammings Predictor Corrector method is used. The accelerations \ddot{X} and \ddot{Y} are input parameters which correspond to the sled acceleration in the x and y-axis.

12.5 GEOMETRICAL DEFINITION OF THE SPINE

In defining the geometry of the spine, the model required the initial conditions of the spine to be created, that is, the co-ordinates of the centre of each vertebral body, the length, the angle the longitudinal axis makes with the vertical, the distance that the articular facets from the centre of the vertebral body and the thickness of the disc which is associated with that vertebra. This was created with the aid of X-ray radiography.

The author, who approximates to a 50th percentile standing height of 1.82m, was X-rayed whilst adopting a brace position. This, together with measurements obtained from Belytschko [168] of a 50th percentile upright seated occupant, helped to establish the locations and orientations of the vertebral bodies and discs, Tables 32 and 33.

12.5.1 Mass And Moment Of Inertia Of Vertebral Body Segments

The spine model requires the distribution of the mass and moment of inertias of the entire torso region. Liu and Wickstrom [169] have estimated the mass distribution of the segmented cadaveric torso. The mass distribution which was used in the model is consistent with their data. The mass and moment of inertia of the different segments were obtained as follows:

At the beginning of their experiment three cadavers were weighed. The torso was then cut at the level of L3 and the two halves were weighed once again to give the total mass above L3. Three additional segments were made of the upper torso. The first consisted of L3 to T8, the second from T8 to C7 and the third from C7 to the head. The three segments were weighed again. Their centres of gravity were obtained by using a loading platform which utilised three load cells at fixed distances from one another. A trifilar pendulum was subsequently used to determine the moment of inertia of the segments. The mass and moments of inertia were subsequently estimated for the various vertebral levels from the experiment.

In the WSU model, the mass of the arms was assumed to be distributed to the first thoracic vertebrae. Similarly, the mass and moment of inertia of the lower limbs were integrated with the pelvis. Figure 217 shows the WSU model.

12.5.2 Model Physical Constants

Each segment in the model has a disc which requires three spring constants. The facets also require two spring constants. Therefore, a total of 130 spring constants are required. All 130 spring constants may be different and should ideally be determined experimentally for each specimen. Little data was available in the literature for the disc spring constants. In the case of the articular facets, no data was available.

King and Vulcan [170] measured the compressive stiffness of the lumbar and lower thoracic vertebrae. Markolf [148] had also measured the axial stiffness of the discs from L4 to T8. He found that the values ranged from 7000lb/in (1226N/mm) in the lumbar region to 19000lb/in (3327N/mm) in the thoracic region. No data was available for the upper thorax. Markolf also reported that the rotational stiffness of the discs were in the region of 700in-lb/rad (79.1Nm/rad) to 24000in-lb/rad (2712Nm/rad).

The rotational stiffness data, which was conducted by Markolf, was obtained at very small deflections. Hence, the rotational stiffnesses were considered to be too low by Prasad [148]. It was, therefore, assumed that the rotational stiffness in the lumbar spine was 6000in-lb/rad (678Nm/rad). In the thoracic region, the rib cage increases the stiffness of the spine. It was, therefore, considered that a rotational stiffness of 12000in-lb/rad (1356Nm/rad) would be more appropriate. In the cervical region, the rotational stiffnesses were obtained from Vulcan [148] and were quoted as 2400in-lb/rad (271.2Nm/rad). The typical physical constants which were used in the model are presented in Table 34.

12.6 MODEL VALIDATION

Experiments were carried out with cadavers to validate the ejection seat model. In both the computer and experimental simulations, the conditions at both ends of the spinal column were specified. An acceleration input was applied to the pelvis while the top of the head was allowed to remain free. In order to correlate the model against the cadaver tests, an intervertebral load cell was developed to provide the magnitude and line of action of the force. The experimental techniques and instrumentation are described by Prasad et al [148].

Three cadavers were subjected to +Gz or seat to head trapezoidal acceleration pulses of 6, 8 and 10G. These were carried out in the erect and hyperextended modes. The rate of onset of the acceleration was approximately 250G/sec. A total of 18 experimental runs, on the three cadavers, were completed.

The results obtained with the model showed that it was able to predict the intervertebral load with reasonable accuracy. As the acceleration levels were low, only one set of constants were used for each cadaver. However, variations among cadavers was permitted, since it is well known that biological differences exist. The values of these differences were not allowed to deviate too far from those which are published in the literature. Little attempt was made to optimise the constants with the experimental data. The model was quite stable in accepting a wide variation in constants.

12.6.1 Analysis of the WSU Model

The data for cadaver 2413 [166] was used to set up the spine model. This data was obtained from Wayne State University. The computer model was provided as a Fortran code. A translator was first written in order to view the spine kinematics and assess the behaviour of the model. The spine model was then run using the cadaver data obtained from WSU. The model was fully restrained using a shoulder harness, with the spine in an erect mode. A 5.5G trapezoidal pulse with a rise time of 35ms was applied in the +Gz direction. The kinematics of the spine are presented in Figure 220.

As stated above, the model was validated against experimental cadaveric ejection seat data and gave good results for occupants oriented in both erect and hyperextended postures. In this simulation, the model produced stable results for a variety of values of constants for a reasonable duration (to 200ms) of input pulse.

12.6.2 Model Limitations

There was an extreme scarcity of data, in so far as the stiffnesses of the facets and the rear region of the vertebra was concerned. Although the model provided for the selection of different spring rates for the facets in compression and tension, the same value was used.

On exposing the model to the very different scenario of a purely lap belted occupant in the passenger aircraft environment, it became unstable. The results of one such analysis are illustrated in Figure 221. A number of concerns were identified. These are listed below:

- The intervertebral spring characteristics were inadequate for representing the behaviour of lap belted occupants when the model experienced the application of a predominantly positive Gx loadcase. This was due to the large deformations thereby produced.
- For such a simulation, the effective stiffness and damping of the thorax and abdomen would need to be included in the model in order to replicate realistic occupant performance. In addition, the neck properties were also re-examined and new tensile stiffnesses were applied. These stiffnesses were obtained from WPAFB [168].
- Contact interactions would need to be included in order to model the contact of the body segments on impact.
- The absence of arm and leg inertial characteristics would affect the occupant kinematics.
- It was therefore decided to use the validated data from the WSU model and integrate it within an existing analytical code. This was carried

out with the aid of user defined joints in the MADYMO code. This code was expected to be capable of resolving the concerns listed above. The objective of the research was to create a more comprehensive dummy dataset utilising an industry standard analysis package.

12.7 MADYMO DATASET FOR SPINAL MODELLING

For the simulation of the brace position, the erect mode was chosen. A new representation of a seated human occupant was created in MADYMO which would be capable of comprehensive data extraction. This was intended to produce the closest possible representation of a living occupant rather than the representation of an ATD. All the data used was derived from validated sources:

- (a) Geometric data of the spine was obtained from X-rays of a 50 percentile male and Wright Patterson Air Force Base (WPAFB), Tables 32 and 33.
- (b) Intervertebral stiffnesses and moments of inertia were obtained from the WSU model input and were applied as user defined joints in MADYMO, Table 34.
- (c) Leg contact stiffnesses were obtained from the Motorcycle Anthropomorphic Test Dummy (MATD) [171]. Inertial characteristics of legs were obtained from the Hybrid III ATD.
- (d) The head representation was from the Hybrid III ATD. This data was converted from the existing 3D model, Tables 32 and 33.
- (e) The neck tensile stiffnesses were obtained from WPAFB [168].
- (f) Thorax stiffness was obtained from WPAFB [168].
- (g) The thorax representation was obtained from the Hybrid III ATD, Tables 35, 36 and 37.
- (h) The abdomen stiffness was obtained from WPAFB [168].
- (i) The abdomen representation was obtained from the Hybrid III ATD, Tables 35, 36 and 37.
- (j) The pelvis representation was obtained from the Hybrid III ATD, Tables 32 and 33.

Thus, the most up-to-date information was used to create a specialist dummy Dataset for Spine Modelling (DSM), Figure 222.

The user defined MADYMO joints were validated through direct comparison of the MADYMO spine simulations with an equivalent WSU run.

It was, however, impossible to validate the completed DSM model as there was no existing equivalent (apart from the living human body which it intends to replicate). However, the pelvic acceleration results were monitored carefully and were found to produce similar values to the Hybrid III model. The DSM kinematics output, was also checked and found to be similar to that of the Hybrid III with the only significant differences being those due to the effects of the increased flexibility of the spine, Figure 223. The kinematics of the model were also compared with a lap belted finite element spine model created by Belytschko [168], Appendix 8. This showed similar kinematics.

The DSM was then considered suitable for assessment of the brace position. It was decided to vary the following parameters against the base brace position, used in the previous studies:

1. Base configuration. Two rows of Weber 4001 seats. Breakover in both rows. 50th percentile male. Legs back 11.5 degrees. Arms raised to the sides of the head. 16G sled pulse in forward direction without the lateral component. "Am Safe" belt webbing without slack.
2. Brace position with legs 11.5 degrees forward and arms raised to the side of the head.
3. Brace position, with legs 11.5 degrees back and arms lowered to the sides of the femurs.
4. Brace position with legs 11.5 degrees forward and arms lowered to the sides of the femurs.

12.8 RESULTS

The peak spinal column results are presented in Table 38. The kinematics of the simulation, together with the graphical comparison of the results are shown in Figures 224 to 240.

12.8.1 Base Configuration - Brace Position, Legs Rearward, Arms Up.

Whilst the kinematics of the base configuration were found to be similar in overall terms, as expected there were significant differences. The Hybrid III ATD used in previous test and analytical investigations is segmented rather than a continuous, flexible entity. Continuous flexion and extension is evident in the spine together with extension and compression in its overall length, Figure 223. This is due to the flexibility in the discs.

The base line configuration for the analysis is shown in Figure 224 with the animation of the impact sequence demonstrated in Figure 225. It is observed

that during the impact sequence foot slide occurs as per the Hybrid III model and the tests conducted at the IAM. The value of foot to floor friction is low, this being set to 0.5, as tested. This value of friction is comparable with leather soled shoes worn on carpeting as found in G-OBME.

Examination of the upper torso trajectory has indicated a similar pattern of events between the Hybrid III model for the first 100ms. However, between 110ms and 180ms, a change in kinematics is observed. This is due to flexibility of the spine as opposed to the rigid body effect which is a feature of the Hybrid III upper torso. The maximum forces which are applied occur between 120 and 140ms. The belt load is at its highest and is in line with the upper torso.

It is observed at this stage that 'snaking' of the spine occurs. At 140ms, elbow contact takes place with the seat back in front, thus allowing the arms to descend downward in a controlled manner. Head contact subsequently takes place with the lower region of the seat back between 160 and 170ms.

Throughout the simulation, it is clear that leg slide takes place. However, flailing of the lower limbs does not occur.

12.8.2 Brace Position - Legs Forward, Arms Up

The brace position with the legs forward and the forearms raised to the side of the head is shown in Figure 226. The kinematics of the impact sequence is demonstrated by Figure 227. For the first 100ms, the body of the occupant translates forward causing initial head contact to occur with the seat back in front. The onset of lower limb flail takes place at 120ms. This causes the tibiae to contact the rear spar. Severe extension of the spine is also apparent at 150ms with elbow contact taking place with the seat back in front. Head contact subsequently occurs with the lowermost region of the seat back.

12.8.3 Brace Position - Legs Back, Arms Down.

The initial position of the brace position with the legs back and arms down is shown in Figure 228. The impact sequence is demonstrated in Figure 229. This shows that initial head contact occurs with the seat back. Hand contact subsequently takes place with the front seat back, at 130ms. This causes the upper torso to retract backwards. Head contact then follows at 170ms with the lower region of the seat back. Throughout the impact sequence, it is apparent that no leg flail has taken place. This is as a result of maintaining the lower leg angle rearward of the vertical prior to impact.

12.8.4 Brace Position - Legs Forward, Arms Down.

One final configuration was assessed, Figure 230, with the legs of the rear occupant positioned forward of the vertical and with the arms placed to the side of the thighs. The impact sequence is demonstrated in Figure 231. Head

contact is once more apparent with front seat back. Leg slide commences at 110ms and results in flail between 140 and 160ms. Hand contact takes place with the lower region of the seat back at 130ms causing the upper torso to flex backwards. Once again, head contact is observed at 170ms with the seat back in front.

12.8.5 Comparison Of The Brace Position With Legs Back And Legs Forward, With Arms Up.

Figures 232 to 234 show the results obtained from the computer model. These show the peak axial loads, shear loads and extension (bending) moments in the spine. These results compare the legs back with the legs forward while maintaining the arms up beside the head. In addition the results are compared against injury thresholds, Table 4. Comparisons of the axial loads, Figure 232, shows that in the lumbar spine loads exceed the injury threshold between L3 and T12.

However, comparison of the legs back versus legs forward results indicate that the legs forward loads are slightly higher in magnitude. This general trend is observed throughout the lumbar, thoracic and cervical spine.

The shear loads are presented in Figure 233. These show that with the legs forward the loads are higher than with the legs back. However, the loads are well below the injury threshold of 10.7kN. The area which shows very high loading is the first cervical vertebrae. The legs forward configuration shows a higher loading trend than with the legs back. However, both the legs forward and legs back positions indicate that injury is likely to occur at C1.

The peak extension (bending) moment, Figure 234, shows that the bending moment in the lumbar spine is higher with the legs positioned forward of the vertical. However, these are not likely to cause injury as the moments are below the injury threshold of 370Nm.

The thoracic region of the spine also shows an increase in bending moment between T7 and T12. The cervical region shows a reduction in moment with the legs forward as compared with the legs back. Damage to the cervical spine is likely with the lower legs positioned rearward of the vertical.

12.8.6 Comparison Of The Brace Position With Legs Back And Legs Forward, With Arms Down.

Figures 235 to 237 show the results of the brace position with the lower legs positioned rearward and forward of the vertical but with the arms positioned to the side of the thighs. The peak axial load, Figure 235, shows an increase in loading with the lower legs placed rearward of the vertical. However, the magnitude of the loads indicate that damage of the lumbar spine is likely to occur for both lower leg positions. An increase in loading pattern is observed in the thoracic and cervical regions of the spine with the lower legs forward of

the vertical. The level of loading imparted to the cervical spine is likely to cause cervical damage.

The peak shear loading trends shown in Figure 236 indicate that there is little difference in results in the lumbar region. The loads are well below the injury threshold of 10.7kN. With the legs placed forward of the vertical, the pattern of loading is observed to rise in the thoracic and cervical regions. At C1, both leg positions indicate that cervical spine fracture will occur.

The peak extension (bending) moment, Figure 237, is shown to be higher with the lower legs placed forward of the vertical. In the lumbar region, the results obtained are well below the injury threshold of 370Nm. However, in the cervical spine, the moments which are generated are a cause for concern. These are likely to cause fracture of the cervical spine.

12.8.7 Comparison Of The Brace Position With The Arms Up Versus Arms Down With The Lower Legs Positioned Rearward Of The Vertical.

Examination of the brace position with the legs back versus legs forward showed that, generally, with the lower legs positioned rearward of the vertical a reduction in injury levels is obtained. It was consequently decided to compare the results of the legs back, with the arms positioned to the sides of the head and the arms placed beside the thighs.

The peak axial loading, Figure 238, indicates a higher level of loading in the lumbar spine with the arms placed to the side of the thighs. This also occurs in the thoracic spine to a lesser degree. In the lumbar region, it is observed that for both the arms up and arms down the loads are above the threshold injury level. It is therefore, likely that spinal injury may be sustained.

The peak shear loading, Figure 239, indicates that the loads in the lumbar spine are slightly higher with the arms down, that is, beside the thighs. The magnitude of the shear loads obtained is well below the injury threshold of 10.7kN. In the thoracic spine, an increased level of loading is observed with the arms up position. This trend is reversed in the cervical spine. It is apparent that an increase in load has been obtained with the arms down. At C1, a severe level of loading has been obtained for both arm positions. This is likely to culminate in neck injury.

The peak extension (bending) moments, Figure 240, indicate there is little difference in results in the lumbar spine between the two arm positions. The thoracic vertebrae between T2 and T7 show an increase in moment with the arms up position. In the cervical spine, the results indicate an increase in bending moment for the arms up case. However, it is likely that hyperextension injuries may be sustained by the neck with both arm positions.

12.9 CONCLUSIONS

Generally spine axial loads, shear loads and bending moments are lower in the legs back position than legs forward.

It has been shown that a lap belted occupant is susceptible to lumbar and cervical spine injury using the 16G dynamic test pulse.

Comparison of the arms up versus arms down positions shows little difference in results. The only significant effect is of reduced lumbar axial loading, with the arms up.

It has been shown that very high loads are developed in the spine during impact. The use of a forward facing, two point lap belt configuration is the fundamental reason for this. This risk of spinal injury is therefore, significant in severe aircraft impact, where this configuration is employed.

12.10 RECOMMENDATIONS

A brace position with the lower legs positioned rearward of the vertical should be adopted prior to impact.

The lower arms should be positioned to the side of the head, with the hands placed on top of one another on the head.

Alternative restraint systems may be beneficial for the reduction of spinal loading. It is, therefore, recommended that research into the effect of alternative restraint systems be instituted.

This Page
Intentionally Left Blank

CONCLUSIONS

1. THE KEGWORTH AIR ACCIDENT

The correlation of the brace position was extremely good considering the multi-variable, non-linear nature of the analysis models and the modelling limitations outlined.

Four main analyses were conducted. The conclusions drawn, from the studies, which give reductions in injury levels are:-

1.1 Brace position

- (i) Belts of 8% strain at 10kN.
- (ii) The use of energy absorbing foldable seatbacks.
- (iii) Increasing the seat pitch.
- (iv) Increasing the seat front cushion angle.
- (v) Reduction in seat stiffness.
- (vi) Moving the lower legs rearward of the vertical.

1.2 Upright Position

- (i) Belts of 8% strain at 10kN.
- (ii) Use of energy absorbing foldable seatback.
- (iii) Reducing the food tray stiffness.
- (iv) Reducing the seat pitch.
- (v) Reducing the knee bolster contact stiffness.

The study demonstrated that it was possible to correlate the occupant kinematics of the Kegworth Aircrash with sustained injuries. The kinematics showed the mechanism of injury. The simulation was extended into a parametric study to provide recommendations for greater survivability in future accidents.

The major value of the study was to show for the first time, that a definitive estimation of occupant kinematics and the effects on the victim are possible in the evaluation of an aircraft crash.

2. UPRIGHT SEATED OCCUPANTS IN ALTERNATIVE TYPES OF AIRCRAFT IMPACTS

The studies of configurations of different sized occupants show the effects of seating both small, medium and large occupants. These were defined as 5th percentile female, 50th percentile male and 95th percentile male. Although there was some slight reduction in injury levels for smaller occupants, no substantial change was found. All the injury levels remained beyond the threshold of survivability for head injury, when using the Kegworth acceleration pulse, with the occupants seated upright. With the lower legs upright, the 95th percentile occupant experienced tibia strike on the seat in front, whereas the 5th and 50th did not.

Significant tensile forces in the spine were observed, whereas only compressive loads are controlled by regulations. Once more the importance of bending in the femur has been highlighted. Heel to floor contact loads have been found to be very substantial in a Kegworth type of impact in the order of 5000N. This helps to explain the preponderance of ankle injuries in the accident [157].

This study has shown that the maximum femur axial load of 4.7kN, obtained with the most severe pulse does not approach the regulated injury limit of 10kN. This suggests that this injury criterion is less appropriate to aircraft crash victim simulation than femoral bending, tibial and foot loads. Extra load cells would require incorporation in the femur and tibia of test dummies to measure such forces; it is suggested that an accelerometer should be used in future to indicate foot loading.

The use of the NACA pulse has shown a general reduction in injury criteria in comparison with the Kegworth pulse. The following overall reductions have been observed, 72% in HIC, 24% in thorax acceleration, 8% in lumbar loads, 68% in axial femur loads, 250% in tibial loads and 22% in heel loads. The following increases have also been observed, 168% in femur vertical loading, 2% in femoral bending moment and 9% in belt loads. It must be noted, however, that the new crash pulse derived from the demonstration test is somewhat less severe than the Kegworth pulse.

The 14G test pulse derived from AS8049, is less severe than both the Kegworth and NACA pulses. The compressive loads in the spine are however, higher due to the predominant vertical load vector. Very little difference between sizes of occupant was noted.

3. SIMULATION OF FORWARD FACING AND REARWARD FACING OCCUPANTS

The analyses showed that forward facing lap belted occupants are more vulnerable to injury compared to rear facing lap belted occupants. However, in the rear facing analysis, the lateral component combined with the low height of the head rest cause the head and neck to impinge on an area where in reality there may be internal framework of the seat structure. High and full width headrest would improve this situation.

Forward facing occupants restrained by lap and diagonal belts experienced similar upper body injury levels compared with the rear facing occupant. Although the head and neck contacts of the rear facing seat are avoided, lap and diagonal belts for the forward facing occupant result in spinal loads close to the maximum permitted. Additionally, considerable lower leg flailing occurs which require measures to combat injury under the seat in front.

For the NACA pulse, both rear facing seats and forward facing lap and diagonal belted seats, impose higher floor loadings than the forward facing lap belted seats. On average, the percentage increase in loads are 52% for the rear facing seat and 33% for the lap and diagonal belted seat. However, it must be stated that with the exception of the lap belted seats, the other seating in question are not purpose designed. In the analysis, both rear facing and lap and diagonal belted seats are rigid.

4. BRACE POSITION CORRELATION WITH IMPACT TESTING AND PARAMETRIC STUDY

The study to correlate the computer simulation with sled testing has shown good agreement. However, it must be emphasised that accurate and reliable methods of testing are necessary for good correlation to be achieved. The conclusions obtained from the research work on the brace position are as follows:-

4.1 Changes in Floor Friction

The effect of increasing the floor friction is to reduce foot slide and ultimately leg flail. It was also observed that small changes have occurred as a result of increasing the floor friction with the following parameters:

- (a) Increases in the head injury criteria and head acceleration results.
- (b) Increases in the femoral shear loads.

- (c) Increases in the femoral axial loads.
- (d) Increases in the femoral bending moments.
- (e) Increases in the tibial shear loads.
- (f) Increases in the tibial axial loads.
- (g) The thorax accelerations, lumbar and lap belt loads remain constant.

It was apparent that the left femur bending moment was more heavily loaded than the right due to the lateral acceleration which was imposed on the occupant. This effect allows the left leg to slide forward of the right, thus increasing the contact forces with the front of the seat base.

4.2 Changes in Seat Pitch

The effect of changing seat pitch has produced the following findings:-

- (a) At low seat pitches, an increase in the head injury criteria (HIC) takes place. This is associated with the need to adopt a semi-braced position instead of a fully braced position because of lack of space.
- (b) At higher seat pitches, an increase in the HIC value is observed. This is associated with an increase in the inertial forces on the upper body before striking the seat in front.
- (c) It has been observed that the optimum HIC value has occurred with the 32 inch seat pitch.
- (d) At 30 inch pitch, a glancing strike between the tibiae and the front seat takes place. This effect forces the lower legs downwards and forwards. This is followed by foot entrapment below the luggage bar.
- (e) The head resultant accelerations follow the same trends as the head injury criteria.
- (f) The thorax accelerations are all below the injury thresholds. However, the maximum acceleration is induced at a 34 inch pitch.

- (g) The pelvic resultant accelerations show a decreasing trend in results as the seat pitch is increased.
- (h) The lap belt loads show a similar trend to the pelvic acceleration for seat pitches which are between 30 and 36 inches. At 27 inch pitch, a reduction in lap belt load occurs. This is associated with load transfer to the femurs. This effect takes place due to femoral contact with the seat in front.
- (i) The femoral shear forces show a general upward increase in load as the pitch is increased, with the exception of the 30 inch pitch. At 30 inch pitch, the glancing strike of the tibiae against the seat in front cause the femoral shear load to reduce.
- (j) The femoral axial load was found to be highest at 27 inch pitch. These are compressive in nature. The loads gradually decrease from 30 to 36 inch and are tensile.
- (k) The femoral bending moments are constant for the 27, 32, 34 and 36 inch pitches. At 30 inch pitch, a significant increase in the femoral bending moment occurs. This is likely to cause femoral fracture.
- (l) The tibial shear load, in proximity to the ankle joint, has shown a significant increase in load. This is associated with foot entrapment below the luggage bar.
- (m) The tibial lateral loads are small in magnitude. These are not likely to cause major injury in the lateral direction.
- (n) The tibial axial loads increase at 27 inch pitch, decrease at 30 inch pitch, steadily increase to 34 inch pitch and reduce at 36 inch pitch.
- (o) The lumbar loads increase at 27 inch pitch, decrease at 30 inch pitch then gradually rise as the pitch is increased to 36 inches.
- (p) For this particular seat design, a 32 inch seat pitch appears to be the optimum configuration with regard to injury levels.

4.3 Changes in Tibia Angle

The effect of adopting a brace position with the tibiae angled forward and rearward of the vertical has the following effects:-

- (a) The head injury criteria and head acceleration increase as the tibiae angles are incremented forward of the baseline position of 11.5 degrees.

- (b) The thorax accelerations show that the highest accelerations occur when the lower legs are incremented forward of the vertical.
- (c) The pelvic resultant accelerations show a slight increase in results as the lower legs are incremented forward of the baseline configuration.
- (d) The lap belt loads show a slight decrease in results as the tibiae are incremented forward of the baseline.
- (e) The femoral shear loads have increased on positioning the tibiae angles forward of the baseline.
- (f) The femoral axial loads show that the highest loads have occurred on incrementing the tibiae forward of the vertical.
- (g) The femoral bending moments increase in magnitude as the tibiae are positioned close to the vertical and reduce as the tibiae are angled forward of the vertical.
- (h) The tibial shear results show there are significant increases in load as the tibial angle is moved forward of the baseline position.
- (i) The tibial lateral loads are low in magnitude. These are not likely to cause significant injury.
- (j) The tibial vertical loads show a significant increase in results as the lower tibiae are placed close to the vertical and subsequently forward of the vertical.
- (k) The lumbar vertical loads are almost constant in magnitude.

4.4 Changes in Configurations

Additional assessments were carried out to compare the effect of bulkhead strike, the FAA 16G pulse, a three point belted forward facing and rear facing lap belted occupants. These have shown the following:-

- (a) The bulkhead strike simulation has produced the highest head injury criteria. This is likely to cause fatal injury.
- (b) The lowest HIC values have been obtained with the three point belt and rearward facing configurations.

- (c) The thorax accelerations show that the lowest value has occurred with the baseline brace position. Whereas, the highest acceleration is shown to occur with the standard bulkhead simulation.
- (d) The highest pelvic acceleration has been obtained with the bulkhead simulation.
- (e) The highest lap belt load has been obtained with the FAA 16G pulse. The lowest belt load was shown to occur with the rearward facing seat.
- (f) The maximum shear load on the femurs have occurred with the FAA 16G pulse. The lowest femoral shear loads were obtained with the three point belt and rearward facing seats.
- (g) The highest femoral axial loads are tensile in nature and occur with the three point belt and bulkhead strike analyses.
- (h) The highest femoral bending moment occurs with the FAA 16G pulse and the lowest value with the rearward facing seat.
- (i) The maximum tibial shear load occurs with the standard bulkhead simulation. This is followed by the three point belted occupant. The lowest loads have been obtained with the baseline, the FAA 16G pulse and rearward facing seating configurations.
- (j) The lateral tibial loads are small in magnitude. These are not likely to cause significant injury. The highest loads occur with the FAA 16G pulse.
- (k) The maximum vertical tibial loads have occurred with the FAA 16G pulse. The lowest loads have been obtained with the rearward facing seats.
- (l) The highest lumbar spine load has occurred with FAA 16G pulse. The lowest load has been obtained with the rearward facing seat.

5. THE EVALUATION OF SPINAL COLUMN INJURIES IN THE BRACE CRASH POSITION

Generally, the spine axial loads, shear loads and bending moments are lower in the legs back position than with the legs forward condition.

It has been shown that a lap belted occupant is susceptible to lumbar and cervical spine injury using the 16G sled test pulse.

Comparison of the arms up versus arms down positions shows little difference in results. The only significant effect is of reduced lumbar axial loading, with the arms up.

It has been shown that very high loads are developed in the spine during impact. The use of a forward facing, two point lap belt configuration is the fundamental reason for this. This risk of spinal injury is therefore significant in severe aircraft impact, where this configuration is employed.

RECOMMENDATIONS

1. THE KEGWORTH AIR ACCIDENT

1.1 Brace Position

A brace position with the lower legs positioned rearward of the vertical, Figure 241, should be adopted for occupants exposed to an aircraft impact.

The brace position should include an instruction to hold the feet back, that is, against the luggage bar to reduce foot and lower limb injuries.

1.2 Upright Position

An upright seated position is not recommended. This increases the injury levels sustained by the occupants.

1.3 Seat Design

Multi-row installations of seats could and should be engineered to control the kinematics of the occupant of the seat behind. This would apply to those rows pitched within the flailing range of the occupant.

Aircraft seats should be designed to produce a more friendly environment for the occupants. Flanges, sharp edges, tables, seat back video screens and arm rests should all be designed in the expectation of occupant impact.

Knee bolstering by the introduction of a controlled deformation, padded structure is increasingly an automotive design device. Such design features would reduce injury and should be considered at the rear of aircraft seats.

The seat back "breakover" stiffness is critical to control occupant kinematics and the breakover force seems relatively uncontrolled in the design process. A tight tolerance for this force should be considered.

Aircraft seats utilising a tube across the front of a triple row are in common use and G-OBME was no exception. Cantilevered seat support structures produce radically different stiffnesses between outer and centre positions. Leg injuries would be expected to be more severe in the centre seat.

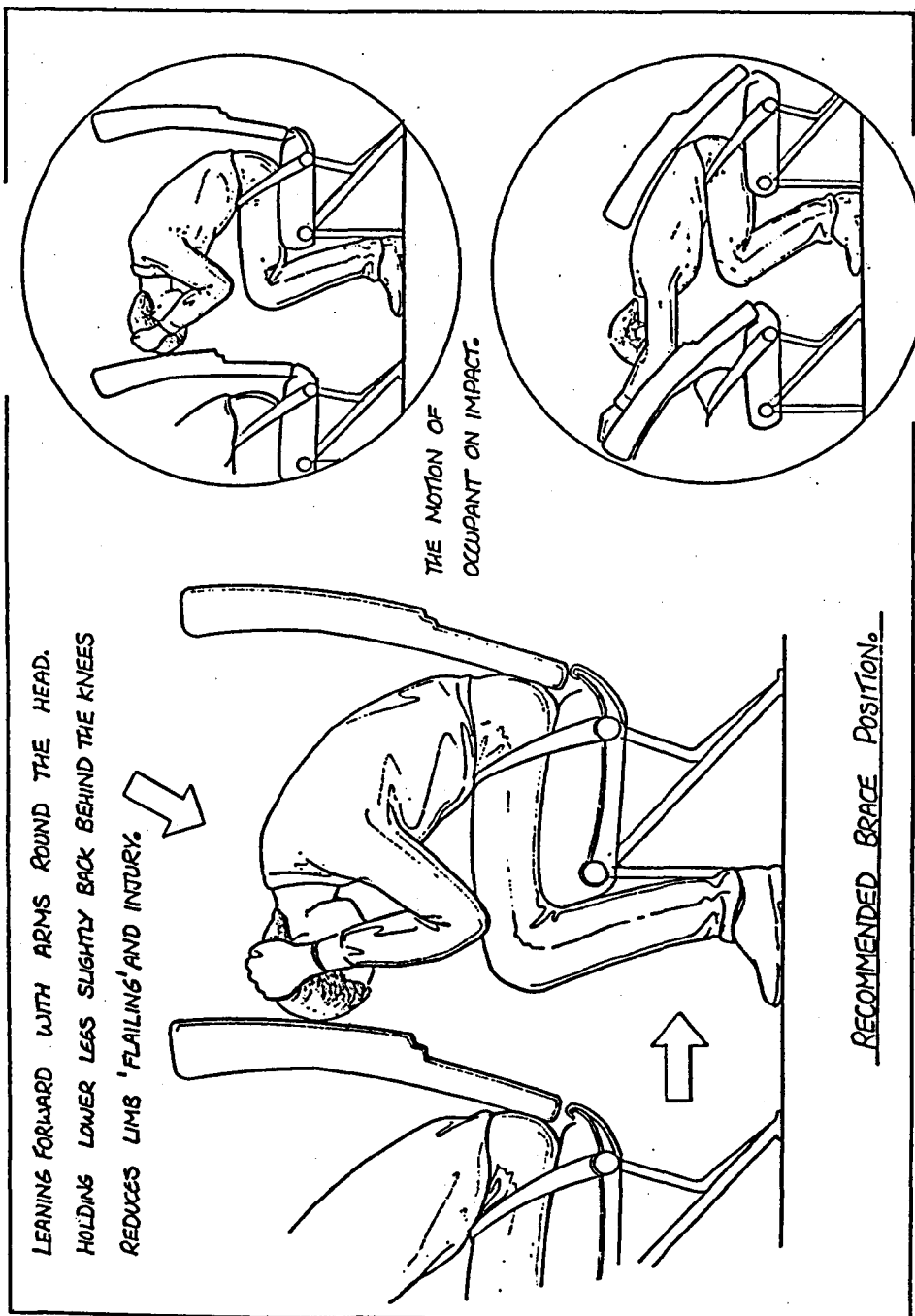


Figure 241. Recommended Brace Position

The tolerance of seat belt webbing stiffness used in G-OBME appeared wider than typical automotive applications. Belt stiffness is critical to occupant kinematics. The use of belts of 8% strain at a load of 10kN is recommended.

The analysis used in this thesis utilised an additional occupant seated in the row in front to simulate the forward contact environment (a twin row analysis). The effect of the occupant seated behind the primary occupant should also be assessed (a triple row analysis) in future studies.

Regulations should control both femur bending (or normal loading) and axial compressive loading, rather than axial loading alone. Presently only axial compressive loading limits are specified which appear from this work to be irrelevant.

2. UPRIGHT SEATED OCCUPANTS IN ALTERNATIVE TYPES OF AIRCRAFT IMPACTS

Injury criteria for the lower limbs of test dummies should be revised in AS8049. In particular, the femoral compressive maximum load should be replaced with a maximum bending requirement, and loads for the tibia and foot specified.

3. SIMULATION OF FORWARD FACING AND REARWARD FACING OCCUPANTS

Analysis work should be undertaken to establish crashworthiness requirements for aircraft seat rail and floor support structures. A programme of research should be undertaken to assess the most efficient design for impact, while optimising the mass of the floor structure.

Simulation techniques should be encouraged as a method of identifying worst case seating configurations for subsequent certification tests.

Securing the seats to the fuselage side at the outer edge of the seat base (a single pedestal installation) would represent a cost and mass effective method of improving seat strength. Further study is recommended of the feasibility of such designs.

Three point belts offer major improvements in the reduction of head, femoral and pelvic injuries, due to improved kinematics and load distribution. Such installations should be considered for small commuter type aircraft. Further research is recommended to examine neck injury.

Rear facing seats reduce the risk of injury significantly. The seat back must be strengthened and increased in height, with shaping of the head rest to prevent lateral displacement of the head. Also, the aircraft floor would need to be strengthened and a heel plate to prevent rearward displacement of the feet should be incorporated. The use of a lap belt is still required in the event of occupant rebound. Preferably, a full harness should be installed which would protect passengers against lateral acceleration components.

4. BRACE POSITION CORRELATION WITH IMPACT TESTING AND PARAMETRIC STUDY

It is recommended that the brace position with the lower legs inclined rearward of the vertical should be adopted.

On adopting a brace position, it is recommended that the upper torso be placed close to the femurs wherever possible.

The effect of increasing the foot to floor friction is to reduce foot slide and subsequently lower leg flail. It is recommended that a floor friction coefficient of 0.7 should be aimed for through the use of appropriate carpeting.

The adoption of an upright or a semi-braced position is not recommended. This has been demonstrated to increase the injury level.

It is recommended that with the type of seat investigated in this study, the luggage bar should be redesigned to eliminate leg entrapment and subsequent foot fracture.

The use of seat pitches between 27 and 30 inches results in an increase in the HIC level. This is as a consequence of having to adopt a semi-braced position because of lack of space to crouch down. At higher seat pitches of 34 and 36 inches a higher HIC level was once more observed. For this particular seat design, it is recommended that a 32 inch seat pitch be used as it appears to be the optimum configuration associated with a reduced injury level.

Adopting a brace position with the tibia inclined forward of the vertical is not to be recommended. This leads to an increase in head injury criteria and foot entrapment.

It is recommended that three point belt installations be used, wherever practicable.

The rearward facing seat position was identified as the position least likely to result in traumatic injury (if facial injury from flying debris is excluded). It is recommended that such installations be adopted in future passenger aircraft.

5. THE EVALUATION OF SPINAL COLUMN INJURIES IN THE BRACE CRASH POSITION

The development of the spine model has shown that a braced lap belted occupant is prone to intervertebral fractures when exposed to a 16G aircraft impact.

The adoption of a brace position with the legs rearward of the vertical, Figure 241, has been shown to be more beneficial to the occupant than with the legs placed forward of the vertical. It is recommended that the braced legs back position be adopted prior to impact.

The lower arms should be positioned to the side of the head, with the hands placed on one another on top of the head.

The use of three point belt and rearward facing seating may be beneficial for the reduction of spinal loading. It is, therefore, recommended that research into the effect of these restraint systems be instituted.

REFERENCES

1. Fung YC. Biomechanics: Mechanical Properties of Living Tissues. Springer-Verlag New York, 1981:
2. Chandler RF. Occupant Crash Protection in Military Air Transport. AGARD-AG-306, August 1990:
3. Mackay M. An Historical Perspective on Impact Biomechanics and some Basic Kinematics. In: The Biomechanics of Impact Trauma ed. Aldman and Chapon 67-80. ICTS Publication, 1984:
4. Snyder RG. Crashworthiness Investigation of General Aviation Accidents. Society of Automotive Engineers, April 1975:
5. Swearingen MS, Hasbrook AH, Snyder RG, McFadden EB. Kinematic Behaviour of the Human Body During Deceleration. Aerospace Medicine, February 1962: 188-197.
6. Brownson P, Wallace WA, Anton DJ. Brace Position Study - Impact Testing. University of Nottingham, 1993:
7. Chandler RF. Data for the Development of Criteria for General Aviation Seat and Restraint System Performance. In: SAE Crash Dynamics of General Aviation Aircraft. SAE Paper No. 85085, April 1985:
8. Geertz A. Limits and Special Problems in the Use of Ejector Seats. D Ing. Dissertation. University of Rostock, 1944:
9. Chandler RF. Design Consideration for Impact Test Facilities. In: AGARD Conference Proceedings No. 88 on Linear Acceleration of Impact Type. AGARD-CP-88-71: Paper B-1.
10. De Haven H. Relationship of Injuries to Structure in Survivable Aircraft Accidents. National Research Council, 1945:
11. Stapp JP. Biodynamics of Deceleration, Impact Blast. In: Aerospace Medicine. Baltimore Williams and Wilkins, 1971:
12. Severy DM, Mathewson JH. Automobile Barrier Impacts. In: National Research Council. Publication 334, Paper No. 91, 1954:
13. Eiband AM. Human Tolerance to Rapidly Applied Accelerations: A Summary of the Literature. Report 5-19-59E. NASA, 1959:
14. Garrett JW, Braunstein PW. The seat Belt Syndrome. Journal of Trauma 1962;2:220-237.

15. Aldman B. Biodynamic Studies on Impact Protection. *Acta Physiologica Scandinavica*;56:Suppl192, 1962:
16. Chandler RF. Dynamic Test Methodology for Aircraft Seat and Restraint Systems. In: SAE General Aviation Aircraft Crash Dynamics. SAE Paper No. 871010, April 1987:
17. Chandler RF. 16G Seat History - Now It Can Be Told. The International Symposium of the Rally of Endeavours to Improve Air Safety, Tokyo, 1992:
18. Tye W. Philosophy of Airworthiness. AGARD Report No.58, 1962:
19. Wilson R. Analyzing the Daily Risks of Life. *Technology Review*, 1979;81(4):40-46.
20. Fryer DI. Aircraft Passenger Seat Design and Crash Survival. Institute of Aviation Medicine Royal Air Force, Farnborough. FRPC 1055, August 1958:
21. Muir HC, Marrison C. Human Factors in Cabin Safety. *Aerospace*, April 1989:18-21.
22. Learmont D. The Arrogant Decade. *Flight International*, 17-23 January 1990:48-50.
23. Lane JC, Brown TC. Probability of Casualties in an Airport Disaster. *Aviation Space Environmental Medicine*, 46(7);1975:958-961.
24. Roberts AK. The Design and Use of Automotive Crash Test Dummies. AGARD-CP-532, Paper No.18, September 1992:
25. Hasbrook AH. Crash Injury Research a Means of Greater Safety in Aircraft Accidents. *Journal of Aviation Medicine*, December 1957:541-552.
26. Aldman B, Mellander H, Mackay M. The Structure of European Research into the Biomechanics of Impact. SAE Paper No. 831610, October 1983:129-136.
27. Star LD, Abelson LC, Goldner AS. Operation S.A.F.E. (Simulated Aircraft Fire and Emergency). *Aerospace Medicine*, 45;1974:888-892.
28. Tennyson RC, Hansen JS. Study of Crash Behaviour of Aircraft Fuselage Structures. In: Jones N, Wierzbicki T. ed. *Structural Crashworthiness*. Butterworths, 1983:219-257.

29. Wittlin G. Aircraft Crash Dynamics: Modelling Verification and Application. In: Jones N, Wierzbicki T. ed. Structural Crashworthiness. Butterworths, 1983:259-282.
30. Hayduk RJ, Fasanella EL. Application of the Non-linear Finite Element Computer Program 'DYCAST' to Aircraft Crash Analysis. In: Jones N, Wierzbicki T. ed. Structural Crashworthiness. Butterworths, 1983:283-307.
31. De Haven H. Beginnings of Crash Injury Research. 13th Stapp Car Crash Conference, Society of Automotive Engineers, 1969:422-428.
32. De Haven H. Mechanical Analysis of Survival in Falls from Heights of Fifty to One Hundred and Fifty Feet. War Medicine, Vol. 2, July 1942:594-596.
33. Lewis ST, Stapp JP. Human Tolerance to Aircraft Seat Belt Restraint. Aviation Medicine, March 1958:187-196.
34. Soltis SJ, Nissley WJ. The Development of Dynamic Standards for Civil Aircraft Seats. Federal Aviation Authority, 1991:
35. Federal Aviation Regulation, Part 23 - Airworthiness Standards: Normal, Utility, Acrobatic and Commuter Category Airplanes. US Government Printing Office, Washington DC, Revised 1st January 1989:
36. Federal Aviation Regulation, Part 25 - Airworthiness Standards: Transport Category Airplanes. US Government Printing Office, Washington DC, Revised 1st January 1989:
37. Federal Aviation Regulation, Part 27 - Airworthiness Standards: Normal Category Rotorcraft. US Government Printing Office, Washington DC, Revised 1st January 1989:
38. Federal Aviation Regulation, Part 29 - Airworthiness Standards: Transport Category Rotorcraft. US Government Printing Office, Washington DC, Revised 1st January 1989:
39. Military Standard, MIL-STD-1290 (AV), Notice 1. Light Fixed and Rotary Wing Aircraft Crashworthiness. Department of Defense, Washington DC, July 1977:
40. Carden HD. Correlation and Assessment of Structural Airplane Crash Data with Flight Parameters at Impact. NASA Technical Paper 2083, NASA Langley Research Centre, Virginia, 1982:

41. Coltman JW. Comments on the GASP Proposed Crashworthiness Certification Criteria. Simula Inc., FAA Docket No. 23494, February 1984:
42. Coltman JW. Analysis of Rotorcraft Crash Dynamics for Development of Improved Crashworthiness Design Criteria. Simula Inc., FAA Contract Report DOT/FAA/CT-85/11, National Technical Information Service, Virginia, June 1985:
43. Hayduk R, Williams S. Vertical Drop Test of a Transport Fuselage Section Located Forward of the Wing. NASA TM 85679, National Technical Information Service, Virginia, August 1983:
44. Williams S, Hayduk R. Vertical Drop Test of a Transport Fuselage Centre Section Including the Wheel Wells. NASA TM 85706, National Technical Information Service, Virginia, August 1983:
45. Pugliese SM. 707 Fuselage Drop Test Report. Report No. 7252-1, Arvin/Calspan Report for FAA, March 1984:
46. Johnson D, Wilson A. Vertical Drop Test of a Transport Airframe Section. FAA Technical Note DOT/FAA/CT-TN 86/34, October 1986:
47. DC-10 Fuselage Drop Test Report. Report No. 7251-2, Arvin/Calspan Report For FAA Technical Centre, New Jersey, September 1984:
48. Webster JL. Results of the AIA/ATA/FAA Dynamic Seat Testing Program. SAE Aerospace Technology Conference and Exposition. SAE Paper No. 881375, October 1988:
49. Johnson D, Garodz L. Crashworthiness Experiment Summary Full Scale Transport Controlled Impact demonstration Program. FAA Report No. DOT/FAA/CT-85/20, FAA Technical Centre, New Jersey, June 1986:
50. Wittlin G, Lackey D. Analytical Modeling of Transport Aircraft Crash Scenarios to Obtain Floor Pulses. Lockheed-California, FAA Report No. DOT/FAA/CT-83/23, NASA CR 166089, April 1983:
51. Chandler RF, Gowdy RV. Loads Measured During Passenger Seat Tests. Report AAC-119-81-8, CAMI, FAA, Oklahoma, January 1983:
52. Code of Federal Regulations, Title 49, Part 572. Anthropomorphic Test Dummies. US Government Printing Office, Washington DC, Revised October 1988:
53. Federal Vehicle Safety Standard (FMVSS) 208, Docket 74-14; Notices 38 and 39, 1985:

54. Viano DC, Stalnaker RL. Mechanisms of Femoral Fracture. *Journal of Biomechanics*, 1980;13:701-715.
55. Viano DC, King AI, Melvin JW, Weber K. Injury Biomechanics Research an Essential Element in the Prevention of Trauma. *Journal of Biomechanics*, 1989;22(5):403-417.
56. Nahum AM, Melvin JW. *The Biomechanics of Trauma*. Appleton-Century-Crofts, 1985:
57. Cochran VB. A primer in Orthopaedic Biomechanics. Churchill Livingstone, 1982. In: Rowles JM ed. NLDB Report on the M1 Aircraft Accident, 1990:
58. Cheng R, Yang K, Levine R, King AI. Dynamic Impact Loading of the Femur under Passive Restrained Conditions. *Proceedings of the 28th Stapp Car Crash Conference*. SAE Paper No. 8416616, 1985:
59. Viano DC. Femoral Impact Response and Fracture. *Proceedings of the 5th International IRCOBI Conference on Biomechanics of Impact*, Birmingham, September 1980:
60. Pike JA. *Automotive Safety - Anatomy, Injury, Testing and Regulations*. Society of Automotive Engineers, Warrendale, 1990:44.
61. Snyder RG. Human Tolerance to Extreme Impacts in Free-Fall. *Aerospace Medicine*, August 1963;34(8):695-709.
62. King AI. Regional Tolerance to Impact Acceleration. *Proceedings of SAE Crash Dynamics of General Aviation Aircraft*. SAE Paper No. 85052, 1985:29-37.
63. Hill IR. *Aerospace Pathology*. MD Dissertation. Clare College, Oxford, March 1984:
64. Stevens PJ. *Fatal Civil Aircraft Accidents - Their Medical and Pathological Investigation*. John Wright and Sons Ltd., 1970:1-10.
65. Begeman PC, King AI, Levine RS, Viano DC. Biodynamic Response of the Musculoskeletal System to Impact Acceleration. *Proceedings of the 24th Stapp Car Crash Conference*. SAE Paper No. 80131, 1980:
66. Kleerekoper M, Feldkamp LA, Goldstein SA. The Effect of Ageing on the Skeleton - Implications for Changes in Tolerance. In: *Biomechanics and Medical Aspects of Lower Limb Injuries*. Warrendale, PA: Society of Automotive Engineers, 1986:91-96.

67. Chapon A. Experimental Models in Biodynamics of Impact. In: Aldman B, Chapon A. Ed. Biomechanics of Impact Trauma. ICTS Publication, 1984:85-90.
68. Kazarian LE, Von Gierke HE. The Validation of Biodynamic Model. AGARD-CP-252-78, 1978. In: Rowles JM, NLDB Report on the M1 Aircraft Accident, 1990:
69. Nyquist GW, King AI. Lower Extremities. In: Melvin JW, Weber K. TRI Report, 1985:
70. Noyes FR, Grood ES. The Strength of the Anterior Cruciate Ligament in Humans and Rhesus Monkeys. Journal of Bone and Joint Surgery, 1976;58-A(8):1074-1082.
71. Fryer DI. The Results of Accidents. In: Giles JA, Ed. A Textbook of Aviation Physiology. Oxford Pergamon Press, 1965:1166-1179.
72. St Laurent A, Szabo T, Shewchenko N, Newman J. Design of a Motorcyclist Anthropometric Test Device. 12th International Technical Conference on Experimental Safety Vehicles. Paper No. 89-6B-0-004, 1989:1-20.
73. Foster JK, Kortge JO, Wolanin MJ. Hybrid III - a Biomechanically Based Crash Test Dummy. Proceedings of 21st Stapp Crash Conference. SAE Paper No. 770938, 1977:975-1014.
74. Mertz HJ. Anthropomorphic Models. In: Nahum AM, Melvin JW, Ed. The Biomechanics of Trauma. Appleton-Century-Crofts, 1985:31-60.
75. Ward CC, Nagendra GK. Mathematical Models, Animals and Human Models. In: Nahum AM, Melvin JW, Ed. The Biomechanics of Trauma. Appleton-Century-Crofts, 1985: 77-100.
76. McHenry RR, Naab KN. Computer Simulation of the Automobile Crash Victim in a Frontal Collision - A Validation Study. Cornell Aeronautical Laboratory, Inc. Report No. YB-2126-V-1R, 1966:
77. Schuller F, Mack P, Brun-Cassan F, Tarriere C. PRAKIMOD: Peugeot/Renault Accidents Kinematics Model - Theory, Validation and Applications. International IRCOBI Conference on the Biomechanics of Impact, Bergisch Gladbach, 14-16 September 1988:
78. Bartz JA. A Three-Dimensional Computer Simulation of a Motor Vehicle Crash Victim, Phase 1 - Development of the Computer Model. Calspan Report No. VJ-2978-V-1, July 1971:

79. Fleck JT, Butler FE. Development of an Improved Computer Model of the Human Body and Extremity Dynamics. Report No. AMRL-TR-75-14, July 1975:
80. Butler FE, Fleck JT. Advanced Restraint System Modelling. Report No. AFAMRL-TR-80-14, May 1980:
81. Frisch GD. Simulation of Occupant-Crew Station Interaction During Impact. In: Ewing et al. Ed. Impact Injury of the Head and Spine. Publisher Charles C. Thomas, Springfield, Illinois:
82. Chandler RF, Laananen DH. Seat/Occupant Crash Dynamic Analysis Verification Test Program. SAE Paper No. 790590, 1979:
83. Bolukbasi AO, Laananen DH. Application of the Non-linear Finite Element Method to Crashworthiness Analysis of Aircraft Seats. AIAA Publication No. 83-0929, 1983:
84. Laananen DH. Validation of SOMLA Occupant Response. In: Crash Dynamics of General Aviation Aircraft. SAE No. SP-622, April 1985:1-12.
85. Wismans J, Maltha J, Melvin JW, Stalnaker RL. Child Restraint Evaluation by Experimental and Mathematical Simulation. Proceedings of the 23rd Stapp Car Crash Conference. SAE Paper No. 791017, 1979:
86. MADYMO Users Manual, Version 5.0. TNO Road-Vehicles Research Institute, July 1992:
87. Hirsch AE, Ommaya AK, Mahone RH. Tolerance of Sub-Human Primate Brain to Cerebral Concussion. Impact Injury and Crash Protection, Charles C. Thomas, Springfield, Illinois, 1970:352-369.
88. Lissner HR, Lebow M, Evans FG. Experimental Studies on the Relation between Acceleration and Intracranial Pressure Changes in Man. Surgery, Gynecology and Obstetrics, 1960;3:329-338.
89. King AI. Survey of the State of the Art of Human Biodynamic Response. In: Saczalski K, Singley GT, Pilkey D, Huston RL. Ed. Aircraft Crashworthiness. University Press of Virginia, 1975:83-120.
90. Gadd CW. Criteria for Injury Potential. Impact Acceleration Press. Publication 977, NAS-NRC, 1962:141-145.
91. Gadd CW. Use of a Weighted-Impulse Criterion for Estimating Injury Hazard. 10th Stapp Car Crash Conference. SAE Paper No. 660793, 1966:

92. Versace J. A Review of the Severity Index. Proceedings of the 15th Car Crash Conference. SAE Paper No. 710881, 17-19 November 1971:
93. Gadd CW. Tolerable Severity Index in Whole-Head, Nonmechanical Impact. Proceedings of the 15th Stapp Car Crash Conference, 17-19 November 1971:
94. Melvin JW, King AI, Alem NM. Advanced Anthropomorphic Test Device (AATD) Development Program. National Highway Traffic Safety Administration, 1985:
95. Mertz HJ, Patrick LM. Strength and Response of the Human Neck. 15th Stapp Car Crash Conference. SAE Paper No. 710855, 17-19 November 1971:
96. Mertz HJ, Patrick LM. Investigation of the Kinematics and Kinetics of Whiplash. 11th Stapp Car Crash Conference. SAE Paper No. 670919, October 1967:
97. Patrick LM, Chou CC. Response of the Human Neck in Flexion, Extension and Lateral Flexion. SAE Vehicle Research Institute, Report No. VRI 7.3, April 1976:
98. Yamada H. Strength of Biological Materials. Baltimore: Williams and Wilkins, 1970:
99. Neathery RF, Kroell CK, Mertz HJ. Prediction of Thoracic Injury from Dummy Responses. 19th Stapp Car Crash Conference. SAE Paper No. 751151, 17-19 November 1975:
100. Melvin JW, Mohan D, Stalnaker RL. Occupant Injury Assessment Criteria. SAE Paper No. 750914, 1975:
101. Stapp JP. Voluntary Human Tolerance Levels. In: Gurjian, Lange, Patrick, Thomas. Ed. Impact Injury and Crash Protection. Published by Charles C. Thomas, 1970:
102. Mertz HJ, Gadd CW. Thoracic Tolerance to Whole-Body Deceleration. 15th Stapp Car Crash Conference. SAE Paper No. 710852, November 1971:
103. Viano DC, Schreck RM, States JD. Dive Impact Tests and Medical Aspects of a 70 Year Old Stunt Diver. 19th Conference of the American Association of Automotive Medicine, 20-25 November 1975:
104. Melvin JW, Evans FG. Extremities: Experimental Aspects. Biomechanics of Trauma Symposium, San Diego, 1983:

105. Mather BS. Observations of the Effects of Static and Impact Loading on the Human Femur. *Journal of Biomechanics*, 1968;1:331-335.
106. Martens M, Van Audekercke R, deMeester P, Mulier JC. The Mechanical Characteristics of the Long Bones of the Lower Extremity in Torsional Loading. *Journal of Biomechanics* 1980;13(8):667-676.
107. Patrick LM, Kroell CK, Mertz HJ. Forces on the Human Body in Simulated Crashes. *Proceedings of the 9th Stapp Car Crash Conference*, 1966:
108. Melvin JW, Stalnaker RL, Alem NM, Benson JB, Mohan D. Impact Response of the Lower Extremities. *Proceedings of the 9th Stapp Car Crash Conference*. SAE Paper No. 751159, 1975:
109. Melvin JW, Nusholtz GS. Tolerance and Response of the Knee-Femur-Pelvis Complex to Axial Impacts - Impact Sled Tests. Final Report No. UM-HSRI-80-27. Highway Safety Research, The Institute of Michigan, Ann Arbor, 1980:
110. Viano DC. Considerations for a Femur Injury Criterion. *Proceedings of 21st Stapp Car Crash Conference*. SAE Paper No. 770925, 1977:
111. Lowne RW. A Revised Upper Leg Injury Criterion. Working Paper No. 42, TRRL, (ISO/TC22/SC12/WG6 No. 109), April 1982:
112. Kramer M, Burrow K, Heger A. Fracture Mechanism of Lower Legs Under Impact Load. *Proceedings of 17th Stapp Car Crash Conference*. SAE Paper No. 730966, 1973:
113. Patrick LM, Mertz HJ, Kroell CK. Cadaver Knee Chest and Head Impact Loads. *Proceedings of 11th Stapp Car Crash Conference*. SAE Paper No. 670913, 1967:
114. Culver CC. Lower leg Axial Force Studies; Exploratory Tests Using Excised Cadaver Leg. Biomedical Science Department, General Motors Research Laboratories, January 1984:
115. Treare D. Post-Mortem Examination on Air Crash Victims. *British Medical Journal*, 1951;2:707-708.
116. DuBois EF. Safety Belts Are Not Dangerous. *British Medical Journal*, 1952 ;2:605.
117. Snyder RG, Crosby WM, Snow CC, Young JW, Hanson P. Seat Belt Injuries in Impact. Federal Aviation Authority, Paper No. AM69-5, March 1969:

118. Tourin B, Garrett J. Safety Belt Effectiveness in Rural California Automotive Accidents. Automotive Crash Research of Cornell University, 1960:
119. Huelke DF, Gikas PW. Ejection - The Leading Cause of Death in Automobile Accidents. Proceedings of 10th Stapp Car Crash Conference, November 1966:156-181.
120. Garrett JW, Braunstein PW. The Seat Belt Syndrome. Journal of Trauma, 1962;2:220-238.
121. Smith WS, Kaufer H. A New Pattern of Spine Injuries Associated with Lap Type Seat Belts. University of Michigan Medical Centre Journal, June 1967, 33;
122. Howland WJ, Curry JL, Buffington CB. Fulcrum Fractures of the Lumbar Spine. Journal of American Medical Association, 1965;193(3):240-241.
123. Hasbrook AH. Design of Passenger "Tie-Down". Some Factors for Consideration in the Crash Survival Guide of Passenger Seats in Transport Aircraft. Report AvCIR 44-9-66. Aviation Crash Injury Research of Cornell University, 1956:
124. Lewis ST, Stapp JP. Human Tolerance of Aircraft Seat Belt Restraint. Journal of Aviation Medicine, 1966;29:187-196.
125. Chandler RF. Brace for Impact Positions. 5th Annual International Aircraft Cabin Safety Symposium, Oakland, California, 1988:279-290.
126. Stapp JP, Lewis ST. Human Factors of Crash Protection in Automobiles. Society of Automotive Engineers, 1957:
127. Air Accidents Investigation Branch. Report on the Accident to Boeing 737-400 G-OBME near Kegworth, Leicestershire on 8 January 1989. Department of Transport, HMSO, Report 4/90, 1990:
128. White DB, Rowles JM, Mumford CJ, Firth JL. Head Injuries in the M1 Boeing 737 Aircrash. British Journal of Neurosurgery, 1990:
129. Morgan WE, Salama FD, Beggs FD, Firman R, Rowles JM. Thoracic Injuries Sustained by Survivors of the M1 Aircrash. European Journal of Cardio-Thoracic Surgery, 1990:
130. Wallace WA, Rowles JM, Haidar R. Computer Simulation of Impact and Correlation with Bodily Injuries. Proceedings of the European Cabin Safety Conference, 1990:

131. Viano DC, Culver CC, Hant RC, Melvin JW, Bender M, Culver RH, Levine RS. Bolster Impacts to the Knee and Tibia of Human Cadavers and an Anthropomorphic Dummy. 22nd Stapp Car Crash Conference. SAE Paper No. 780896, October 1978:
132. Rowles JM. *Impact Biomechanics of the Pelvis and Lower Limbs in Occupants Involved in an Impact Air Accident*. DM Thesis, University of Nottingham, 1993:
133. Madymo Occupant Simulation Program, Version 4.2 (2D). TNO Road Vehicles Research Institute, The Netherlands, 1987:
134. Sadeghi MM, Walton AC, Hashem R. A Computer Simulation of the G-OBME Accident at Kegworth England on January 8th, 1989. Cranfield Impact Centre Ltd., Reported to AAIB, November 1989:
135. "H"- Point. Determined using the Equipment and Procedures Specified in SAE J826, April 1980:
136. Madprep and Madpost, Pre and Post-Processors. HW Structures Ltd., 1989:
137. Perl TR. Deformable Load Sensing Hybrid III Face. SAE Paper No. 892427, October 1987:
138. Locicero J, Mattox KL. Epidemiology of Chest Trauma. Surgical Clinics of North America, 1989:
139. Preston GM. Accelerations in Transport Airplane Crashes. NACA Technical Note 4158, Lewis Flight Propulsion Laboratory, Cleveland, Ohio, February 1958:
140. Anthropometric Data. Published by Alderson Research Laboratories, October 1974:
141. Pinkell II. A Proposed Criterion for the Selection of Forward and Rearward Facing Seats. The American Society of Mechanical Engineers, 1959:
142. Mason JK. Aviation Accident Pathology. London, Butterworths, 1962:
143. Anton DJ. Minimising Impact Injuries to Occupants in a Fixed Wing Aircraft Accidents. BMA Books, In Press:
144. Dudgeon AC. The Case for Backward-Facing Seats. The Aeroplane, 1947;72:131.

145. Giles AF. A Linear Decelerator Track. Proceedings of AGARD Conference No.88 on Linear Acceleration of Impact. AGARD-CP-88-71, Paper B-2.
146. Dutton AD. A Versatile Linear Deceleration Track. RAF Institute of Aviation Medicine, Farnborough. Technical Memo No.360, January 1974:
147. Brownson P. The Brace Position for Passenger Aircraft - A Biomechanical Evaluation. DM Thesis, University Hospital, Nottingham, May 1993:76.
148. Prasad P, King AI. An Experimentally Validated Dynamic Model of the Spine. Transactions of the ASME, Wayne State University, September 1974:
149. Schultz AB, Galante JO. A mathematical Model for the Study of Mechanics of the Human Vertebral Column. Journal of Mechanics, 1970;3:405-416.
150. Panjabi M, White AA. A Mathematical Approach for Three-Dimensional Analysis of the Mechanics of the Spine. Journal of Biomechanics, 1971;4:203-211.
151. Belytschko TB. Analog Studies of Forces in the Human Spine: Computational Techniques. Journal of Biomechanics, 1972;6:361-371.
152. Hess JL, Lombard CF. Theoretical Investigations of Dynamic Response of Man to High Vertical Accelerations. Aviation Medicine, 1958:66-75.
153. Latham F. A Study in Body Ballistics: Seat Ejection. Proceedings of the Royal Society, Series B, 1957;147:121.
154. Payne PR. The Dynamics of Human Restraint Systems, Impact Acceleration Stress. National Academy of Sciences - National Research Council, Publication No.977, Washington DC, 1962:195-257.
155. Liu YI, Murray JD. A Theoretical Study of the Effect of Impulse on the Human Torso. In: Biomechanics, Ed. Fung YC, ASME, 1966:167-186.
156. Terry CT, Roberts VL. A Viscoelastic Model of the Human Spine Subjected to +Gz Accelerations. Journal of Biomechanics, 1968;1(2):161-168.
157. Shirazi M. Response of the Spine in Biodynamic Environments. Symposium on Biodynamic Models and Their Applications, Published by Aerospace Medical Research Laboratory, WPAFB, AMRL-TR-71-29, 1971:843-849.

158. Rybicki EF, Hopper AT. A Dynamic Model of the Spine Using Porous Elastic Material. Symposium on Biodynamic Models and Their Applications, Published by Aerospace Medical Research Laboratory, WPAFB, AMRL-TR-71-29, 1971:851-875.
159. Toth R. Multiple-Degree-of-Freedom, Non-linear Spinal Model. Proceedings of the 19th Annual Conference on Engineering in Medicine and Biology, 1966;8:102.
160. Hopkins GR. Non-linear Lumped Parameter Mathematical Model of Dynamic Response of the Human Body. Symposium on Biodynamic Models and Their Applications, Published by Aerospace Medical Research Laboratory, WPAFB, AMRL-TR-71-29, 1971:649-699.
161. Kaleps I, Von Gierke HE, Weis EB. A Five-Degree-of-Freedom Mathematical Model of the Body. Symposium on Biodynamic Models and Their Applications, Published by Aerospace Medical Research Laboratory, WPAFB, AMRL-TR-71-29, 1971:211-231.
162. King AI, Vulcan AP, Cheng LK. Effects of Bending on the Vertebral Column of the Seated Human During Caudocephalad Acceleration. Proceedings of the 21st Annual Conference on Engineering in Medicine and Biology, 1968;10:32-33.
163. Orne D, Liu YK. A Mathematical Model of the Spinal Response to Impact. Journal of Biomechanics, 1970;4:49-72.
164. Li TF, Advani SH, Lee YC. The Effect of Initial Curvature on the Dynamic Response of the Spine to Axial Accelerations. Symposium on Biodynamic Models and Their Applications, Published by Aerospace Medical Research Laboratory, WPAFB, AMRL-TR-71-29, 1971:553-569.
165. Krause HE, Shirazi M. The Transverse Response of the Lumbar Spine Under Longitudinal Loads. Symposium on Biodynamic Models and Their Applications, Published by Aerospace Medical Research Laboratory, WPAFB, AMRL-TR-71-29, 1971:621-648.
166. Prasad P, King AI, Ewing CL. The Role of Articular Facets During +Gz Acceleration, Journal of Applied Mechanics, ASME, 1974;41(2):321-326.
167. Ewing CL, King AI, Prasad P. Structural Consideration of the Human Vertebral Column under +Gz Impact Acceleration. Journal of Aircraft, 1972;9(1):84-90.
168. Belytschko T, A Model for Analytic Investigation of Three Dimensional Spine-Head Dynamics. WPAFB, April 1976:

169. Liu YK, Wickstrom JK. Estimation of the Inertial Property Distribution of the Human Torso from Segmented Cadaver Data. *Perspectives in Biomechanical Engineering*, Ed. Kennedy RM, University Park Press, Baltimore, 1973:203-213.
170. King AI, Vulcan AP. Elastic Deformation Characteristics of the Spine. *Journal of Biomechanics*, 1971;4:413-429.
171. St. Laurent A, Shewchenko N, Szabo T. Requirements for an ATD for Motorcycle Crash Testing. Dynamic Research Inc., 1989:

TABLES

CONFIGURATION	HIC @ 36ms	Head Accel. (m/s ²)	Thorax Accel. (m/s ²)	Pelvis Load (N)	Femur Axial Load (N)	Femur Vertical Load (N)	Lap Belt Load (N)	Tibial Contact Load (N)	Foot Contact Load (N)
Baseline (13%) Strain	278	534	332	5394	2330	2720	9441	0	0
(8%) Strain @ 10kN	173	490	302	5693	2263	2625	9189	0	0
(12%) Strain @ 10kN	243	481	323	5619	2526	2590	9460	0	0
(16%) Strain @ 10kN	374	582	340	5582	2172	3052	9233	0	0
Breakover Seatback x 0.5	257	543	346	5004	2591	3479	9784	0	0
Breakover Seatback x 1.0	252	532	344	5161	2566	3492	9745	0	0
Breakover Seatback x 2.0	245	523	347	5458	2558	3510	9692	0	0
Pitch 31 Inches	328	552	334	5604	2614	2796	9353	0	0
Pitch 36 Inches	244	454	337	5002	2358	2697	9498	0	0
Nonbreakover Seatback x 0.5	324	557	332	5590	2500	3357	9581	0	0
Nonbreakover Seatback x 2.0	138	415	369	5787	2334	2338	9252	0	0
Front Cushion Angle 11°	250	477	325	5795	1790	2627	9399	0	0
Front Cushion Angle 15°	267	495	289	5375	1585	2775	9397	0	0

TABLE 15. BRACE POSITION SENSITIVITY STUDY

CONFIGURATION	HIC @ 36ms	Head Accel (m/s ²)	Thorax Accel (m/s ²)	Pelvis Load (N)	Femur Axial Load (N)	Femur Vertical Load (N)	Lap Belt Load (N)	Tibial Contact Load (N)	Foot Contact Load (N)
Baseline (13% Strain)	974	798	586	8024	3367	1342	8798	1152	930
(8%) Strain @ 10kN	1100	742	583	6319	2755	1331	8577	965	437
(12%) Strain @ 10kN	1261	848	610	7259	3259	1354	8793	1123	1022
(16%) Strain @ 10kN	1242	894	560	8971	2321	1118	9015	1328	955
Breakover Seatback x 0.5	1758	949	371	7396	2390	1280	8772	1192	0
Breakover Seatback x 1.0	2500	1225	558	7912	2471	1291	8773	1181	1060
Breakover Seatback x 2.0	3821	1980	556	8869	2278	1344	8780	1199	911
Pitch 31 Inches	882	810	533	7658	1725	1204	8481	1398	303
Pitch 36 Inches	1363	1076	471	9218	2444	1396	8822	802	1955
Nonbreakover Seatback x 0.5	1100	700	475	8450	2950	1450	8700	1117	1019
Nonbreakover Seatback x 2.0	1820	1136	685	9161	3244	1328	8779	1200	928
Front Cushion Angle 11°	947	798	549	8008	2866	1315	8712	1294	1113
Front Cushion Angle 15°	1044	834	559	7861	2461	1255	8646	1479	1037
Seat Base Stiffness x 0.5	910	743	471	6763	3866	2113	8894	340	1410
Seat Base Stiffness x 2.0	888	736	523	9458	2087	1204	8853	1332	1309
Knee Contact Stiffness x 0.5	715	657	393	8678	3241	1425	8803	626	1071
Knee Contact Stiffness x 2.0	1039	714	574	8269	2467	1239	8775	1994	692
Bolster Aft 50mm	1039	698	482	6474	2353	1191	8311	1513	0
Bolster Forward 50mm	1085	828	643	8305	3417	1416	8814	205	1068

TABLE 16. UPRIGHT POSITION SENSITIVITY STUDY

POSITION	HIC @ 36ms	Head Acceleration (m/s ²)	Thorax Acceleration (m/s ²)	Pelvis Load (N)	Femur Axial Load (N)	Femur Vertical Load (N)	Lap Belt Load (N)	Tibial Contact Load (N)	Foot Contact Load (N)
Baseline (Braced Legs Back)	278	534	332	5394	2330	2720	9441	0	0
Braced Occupant Legs Forward	531	621	429	4305	3904	1124	9490	918	0
Upright	974	798	586	8024	3367	1342	8798	1152	930

TABLE 17. COMPARISON OF THE BRACE AND UPRIGHT POSITIONS

CONFIGURATION	HIC @ 36ms	Head Accel (m/s ²)	T (ms)	Chest Accel (m/s ²)	T (ms)	Spine Lumbar Load (N)	T (ms)	Femur Axial Load (N)	T (ms)	Femur Vertical Load (N)	T (ms)	Femur Bending Moment (Nm)	T (ms)	Tibia To Seat Load (N)	T (ms)	Heel To Floor Load (N)	T (ms)	Foot To Seat Load (N)	Belt Load (N)	T (ms)
KEGWORTH Pulse																				
50%M/50%M	2521	1144	692	701	705	10850	653	2683	701	1378	702	427	711	0	0	5352	701	633	9252	652
95%M/95%M	2692	1386	698	787	711	14478	654	3526	877	1509	730	561	738	1876	657	4886	878	780	10888	648
5%F/5%F	2231	1543	676	388	714	7456	655	4692	704	1728	667	328	709	0	0	5403	704	140	6181	927
95%M/50%M	2601	1222	699	683	711	14422	656	2197	678	1304	732	508	742	2082	651	4458	732	0	10741	645
5%F/50%M	2407	1563	677	420	715	7524	656	4637	704	1693	667	312	709	0	0	5416	704	206	6157	712
5%FV/5%FV	2206	1497	678	382	715	7352	658	4498	702	1513	666	321	709	0	0	5036	702	0	6194	921
NACA Pulse																				
50%M/50%M	1592	911	175	524	182	9011	164	2810	186	4225	179	453	172	0	0	5763	187	0	10143	184
95%M/95%M	1685	870	184	487	191	13333	202	2297	160	6471	189	704	173	373	193	5293	179	0	12181	188
5%F/5%F	1199	1092	169	477	170	6439	161	1400	192	1542	165	178	179	0	0	2204	139	118	6141	172
95%M/50%M	1510	811	182	472	184	15188	201	2583	162	6334	189	674	206	754	193	5342	174	0	11892	188
5%F/50%M	1240	1190	171	442	169	6361	161	1445	192	1536	165	180	179	0	0	2240	193	278	6760	172
14G TEST Pulse																				
50%/50%M	20	145	90	224	90	2726	80	927	129	336	72	66	222	0	0	1092	108	0	4282	135
95%M/95%M	20	156	92	261	95	3242	87	943	117	843	97	315	97	0	0	1359	115	0	4550	141
5%F/5%F	20	149	86	190	86	3006	73	531	117	371	86	168	84	0	0	584	70	0	2955	132
95%M/50%M	20	156	93	258	94	3243	87	901	117	848	97	330	98	0	0	1293	120	0	4531	140
5%F/50%M	20	151	87	191	87	3008	73	532	117	376	86	168	84	0	0	583	70	0	2954	132

TABLE 18. OCCUPANT PERCENTILE CONFIGURATIONS

SEATING CONFIGURATION	TWO ROWS FORWARD FACING, LAP BELT	ONE ROW FORWARD FACING, 3-POINT	ONE ROW REAR FACING, LAP BELT
NUMBER OF OCCUPANTS	6	3	3
RESULTS PRESENTED FOR:-	REAR ROW RIGHT OCCUPANT	RIGHT OCCUPANT	RIGHT OCCUPANT
HIC (36ms)	1098.9	248.8	108.9
HEAD ACCELERATION (m/s ²)	955.1	374.1	264.4
CHEST ACCELERATION (m/s ²)	403.1	262.6	217.5
SPINAL LUMBAR LOADS			
RESULTANT LOAD (N)	11189	6338	5113
SPINE LONGITUDINAL AXIS (N)	-11129	6287	3214
LEFT FEMUR			
AXIAL LOAD (N)	-2336	-1931	1003
VERTICAL LOAD (N)	1092	1218	381
BENDING MOMENT (Nm)	314.4	107.8	127.9
RIGHT FEMUR			
AXIAL LOAD (N)	-2658	-1997	1097
VERTICAL LOAD (N)	-664	993	459
BENDING MOMENT (Nm)	309.7	88.3	148.2
LEFT TIBIA CONTACT LOADS			
OCCUPANT'S SEAT (N)	0	0	1082
FRONT SEAT ROW (N)	291	n/a	n/a
RIGHT TIBIA CONTACT LOADS			
OCCUPANT'S SEAT (N)	0	0	2436
FRONT SEAT ROW (N)	0	n/a	n/a
LEFT FOOT CONTACT LOADS			
OCCUPANT'S SEAT (N)	0	0	445
FRONT SEAT ROW (N)	280	n/a	n/a
AIRCRAFT FLOOR (N)	1713	1042	1867
RIGHT FOOT CONTACT LOADS			
OCCUPANT'S SEAT (N)	0	0	254
FRONT SEAT ROW (N)	0	n/a	n/a
AIRCRAFT FLOOR (N)	1881	1034	1700
SEAT BELT LOADS			
LAP BELT (N)	8204	6329	9.6
SHOULDER BELT (N)	n/a	5990	n/a
SEAT ATTACHMENT POINT			
FRONT LEFT (N)	38635	53060	60420
FRONT RIGHT (N)	31190	38343	45687
REAR LEFT (N)	31707	40519	49101
REAR RIGHT (N)	39141	49257	78501

Table 19. Comparison of Forward Facing Lap Belted, Three Point Belted and Rearward Facing

Body Segment	Test Device Measurement Variables
HEAD	Linear acceleration in X, Y and Z components Angular accelerations Facial lacerations
NECK	Axial load Shear load Bending moment
THORAX	Linear acceleration in X, Y and Z components Sternum Deflection
SPINE	Axial compressive lumbar load
PELVIS	Linear acceleration in X, Y and Z components Anterior/superior iliac spine load
UPPER EXTREMETIES	Lower arm bending moments
LOWER EXTREMETIES	knee acceleration Femur Load Femur and tibia translation Tibial bending moment Tibial axial load Medial/lateral tibia plateau load Lateral and fore/aft ankle bending moment Shear load

Table 20. Test Device Measurement Variables.

CHANNEL	LOCATION	DESCRIPTION
1	Upr R Tibia Mx	Bending moment in the upper right tibia about the x-axis.
2	Lwr R Tibia Fx	Shear force in the lower right tibia along the x-axis.
3	Upr R Tibia My	Bending moment in the upper right tibia about the y-axis.
4	Lwr R Tibia My	Bending moment in the right lower tibia about the y-axis.
5	Lwr R Tibia Fz	Axial load in the right lower tibia along the z-axis.
6	Upr L Tibia Mx	Bending moment in the left upper tibia about the x-axis.
7	Lwr L Tibia Fx	Shear force in the left lower tibia along the x-axis.
8	Upr L Tibia My	Bending moment in the left upper tibia about the y-axis.
9	Lwr L Tibia My	Bending moment in the left lower tibia about the y-axis.
10	Lwr L Tibia Fz	Axial load in the left lower tibia along the z-axis.
11	R Femur Fx	Shear force in the right femur along the x-axis.
12	R Femur My	Bending moment in the right femur about the y-axis.
13	R Femur Fz	Axial load in the right femur along the z-axis.
14	L Femur Fx	Shear load in the left femur along the x-axis.
15	L Femur My	Bending moment in the femur about the y-axis.
16	L Femur Fz	Axial load in the left femur along the z-axis.
17	Pelvic Gx	Pelvic acceleration along the x-axis.
18	R Femur Mx	Bending moment in the right femur about the x-axis.
19	R Femur Mz	Bending moment in the right femur about the z-axis.
20	Pelvic Gy	Pelvic acceleration along the y-axis.
21	L Femur Mx	Bending moment in the left femur about the x-axis.
22	L Femur Mz	Bending moment in the left femur about the z-axis.
23	Lumbar Fx	Shear load in the lumbar spine along the x-axis.
24	Lumbar My	Bending moment in the lumbar spine about the y-axis.
25	Lumbar Fz	Axial load in the lumbar spine along the z-axis.
26	Vehicle G	Vehicle acceleration.
27	Head Gx	Head acceleration along the x-axis.
28	Head Resultant G	Head resultant acceleration for Head Injury Criteria calculation.
29	Head Gz	Head acceleration along the z-axis.
30	Pelvic Gz	Pelvic acceleration along the z-axis.
31	Lap Belt	Lap belt load in line with the left belt segment.
32	Head Gy	Head acceleration along the y-axis.

Table 21. Description of the Recording Channels

CH	LOCATION	MODE L	SER NO	EXC V	GAIN	FSD SI	UNIT	SENS mV/V
1	Upr R Tibia Mx	1583	411	10	500	395.5	Nm	2.96
2	Lwr R Tibia Fx	1584-A	411	10	500	11125	N	0.97
3	Upr R Tibia My	1583	423	10	500	395.5	Nm	2.96
4	Lwr R Tibia My	1584-A	411	10	500	395.5	Nm	2.9
5	Lwr R Tibia Fz	1584-A	411	10	500	11125	N	0.97
6	Upr L Tibia Mx	1583	415	10	500	395.5	Nm	2.89
7	Lwr L Tibia Fx	1584-A	410	10	500	11125	N	0.97
8	Upr L Tibia My	1583	415	10	500	395.5	Nm	2.89
9	Lwr L Tibia My	1584-A	410	10	500	395.5	Nm	2.96
10	Lwr L Tibia Fz	1584-A	410	10	500	11125	N	0.97
11	R Femur Fx	1914A	220	10	500	13350	N	1.91
12	R Femur My	1914A	220	10	500	339	Nm	1.5
13	R Femur Fz	1914A	220	10	500	22250	N	1.17
14	L Femur Fx	1914A	219	10	500	13350	N	1.92
15	L Femur My	1914A	219	10	500	339	Nm	1.5
16	L Femur Fz	1914A	219	10	500	22250	N	1.19
17	Pelvic Gx	7267A	BJ32	10	500	1500	G	-
18	R Femur Mx	1914A	220	10	500	339	Nm	1.5
19	R Femur Mz	1914A	220	10	500	339	Nm	2.65
20	Pelvic Gy	7267A	BJ32	10	500	1500	G	-
21	L Femur Mx	1914A	219	10	500	339	Nm	1.52
22	L Femur Mz	1914A	219	10	500	339	Nm	2.67
23	Lumbar Fx	1842	99	10	500	13350	N	0.93
24	Lumbar My	1842	99	10	500	565	Nm	1.72
25	Lumbar Fz	1842	99	10	500	13350	N	0.95
26	Vehicle G	PR9367	LO701	4	1200	50	G	0.51
27	Head Gx	7267A	BB61	10	500	1500	G	19.17
29	Head Gz	7267A	BB61	10	500	1500	G	20.66
30	Pelvic Gz	7267A	BJ32	10	500	1500	G	-
31	Lap Belt	300796	-	-	-	-	N	4Pc/N
32	Head Gy	7267A	BB61	10	500	1500	G	22.07

Table 22. Instrumentation

CH	LOCATION	Excitation V	GAIN	Recording
1	Upr R Tibia Mx	10	500	DL
2	Lwr R Tibia Fx	10	500	DL
3	Upr R Tibia My	10	500	DL
4	Lwr R Tibia My	10	500	DL
5	Lwr R Tibia Fz	10	500	DL
6	Upr L Tibia Mx	10	500	DL
7	Lwr L Tibia Fx	10	500	DL
8	Upr L Tibia My	10	500	DL
9	Lwr L Tibia My	10	500	DL
10	Lwr L Tibia Fz	10	500	DL
11	R Femur Fx	10	500	DL
12	R Femur My	10	500	DL
13	R Femur Fz	10	500	DL
14	L Femur Fx	10	500	DL
15	L Femur My	10	500	DL
16	L Femur Fz	10	500	DL
17	Pelvic Gx	10	500	DL
18	R Femur Mx	10	500	DL
19	R Femur Mz	10	500	DL
20	Pelvic Gy	10	500	DASH 16
21	L Femur Mx	10	500	DASH 16
22	L Femur Mz	10	500	DASH 16
23	Lumbar Fx	10	500	DASH 16
24	Lumbar My	10	500	DASH 16
25	Lumbar Fz	10	500	DASH 16
26	Vehicle G	4	1200	DASH 16
27	Head Gx	10	500	DASH 16
28	Head Resultant G			
29	Head Gz	10	500	PORTAX
30	Pelvic Gz	10	500	PORTAX
31	Lap Belt	Piezo	-	PORTAX
32	Head Gy	10	500	PORTAX

Table 23. Recording Channels

CH	LOCATION	UNIT	TEST No 3670	T (ms)	TEST No 3671	T (ms)	TEST No 3672	T (ms)	TEST No 3673	T (ms)
1	Upr R Tibia Mx	Nm	-38	107	-34	107	53	148	-40	112
2	Lwr R Tibia Fx	N	-295	117	-241	117	-266	117	-251	123
3	Upr R Tibia My	Nm	42	112	37	112	39	123	35	123
4	Lwr R Tibia My	Nm	-15	133	-16	133	-12	138	-15	133
5	Lwr R Tibia Fz	N	-1536	123	-1427	128	-1544	123	-1473	128
6	Upr L Tibia Mx	Nm	26	112	29	107	24	112	26	107
7	Lwr L Tibia Fx	N	-114	97	-132	107	258	225	306	225
8	Upr L Tibia My	Nm	25	97	18	92	-22	225	-32	225
9	Lwr L Tibia My	Nm	10	102	11	107	-15	225	-17	225
10	Lwr L Tibia Fz	N	-478	123	-472	116	-357	117	-212	112
11	R Femur Fx	N	-1442	112	-1372	128	-1457	128	-1362	128
12	R Femur My	Nm	-169	123	-164	128	-177	128	-183	128
13	R Femur Fz	N	1248	102	935	97	945	107	929	102
14	L Femur Fx	N	-558	112	-513	112	-502	112	-470	112
15	L Femur My	Nm	-75	123	-69	112	-64	112	-60	112
16	L Femur Fz	N	673	92	888	97	851	102	870	102
17	Pelvic Gx	G	-21.2	102	-16	97	-16.6	102	-17.1	102
18	R Femur Mx	Nm	-39	112	-33	112	-40	128	-37	112
19	R Femur Mz	Nm	-43	138	40	153	64	148	44	148
20	Pelvic Gy	G	-12	107	-8	117	-8	117	-9	112
21	L Femur Mx	Nm	75	123	24	117	27	123	24	120
22	L Femur Mz	Nm	66	117	74	117	59	123	63	117
23	Lumbar Fx	N	9514	117	8599	117	9148	123	8813	123
24	Lumbar My	Nm	498	133	430	138	424	138	401	138
25	Lumbar Fz	N	4945	123	4275	123	5240	128	4812	128
26	Vehicle G	G	19.9	67	16.6	67	17.2	72	17.2	72
27	Head Gx	G	-77	168	-43	164	-55	158	-84	163
29	Head Gz	G	-47	123	-37	123	-39	123	-38	123
30	Pelvic Gz	G	-13	138	-14	139	-12	142	-12	142
31	Lap Belt	N	-8800	112	-8582	123	-9388	128	-8500	123
32	Head Gy	G	-43	163	-25	117	-23	158	-45	168

Table 24. Sled Test Results.

PARAMETER	UNIT	RECORDED RESULTS		
		Test No. 3672	Test No. 3673	Computer Model
Sled Acc. m/s ² , (Vel. m/s)	-	168.7, (12.5)	168.7, (12.4)	168.7, (12.4)
HIC	-	N/A	258	295
Head Acceleration Resultant (Ar)	m/s ²	697	850	674
Ax	m/s ²	-539	-824	-641
Ay	m/s ²	-225	-441	-169
Az	m/s ²	-382	-372	-240
Thorax Acceleration Resultant (Ar) (3ms)	m/s ²	N/A	N/A	174
Ax	m/s ²	N/A	N/A	-71
Ay	m/s ²	N/A	N/A	-27
Az	m/s ²	N/A	N/A	-17
Pelvis Acceleration Resultant (Ar)	m/s ²	216	223	249
Ax	m/s ²	-163	-168	-235
Ay	m/s ²	-79	-87	-81
Az	m/s ²	-117	-117	-101
Lap Belt Load	N	-9388	-8500	-7360
Left Femur Fx	N	502 (shear)	470 (shear)	1362 (shear)
Fz	N	851 (tensile)	870 (tensile)	1629 (tensile)
My	Nm	64	60	180
Right Femur Fx	N	1457 (shear)	1360 (shear)	1419 (shear)
Fz	N	945 (tensile)	929 (tensile)	1591 (tensile)
My	Nm	177	163	178
Left Lower Tibia Fx	N	258 (shear)	306 (shear)	246 (shear)
Fy	N	N/A	N/A	135
Fz	N	357 (compres)	209 (compres)	1633 (compres)
Right Lower Tibia Fx	N	266 (shear)	258 (shear)	276 (shear)
Fy	N	N/A	N/A	198
Fz	N	1544 (compres)	1470 (compres)	1608 (compres)
Lumbar Fz	N	5240 (tensile)	4800 (tensile)	4895 (tensile)

Table 25. Comparison Of Test Results And Computer Predictions

PARAMETER	UNIT	FLOOR FRICTION COEFFICIENT				
		0.5 Baseline	0.55	0.6	0.65	0.7
HIC @ 36ms		295	294	292	295	306
Head Acceleration						
Resultant (Ar)	m/s ²	674	699	702	703	711
Ax	m/s ²	-641	-662	-665	-666	-673
Ay	m/s ²	-169	-175	-174	-173	-176
Az	m/s ²	-240	-240	-240	-240	-239
Thorax Acceleration						
Resultant (Ar) (3ms)	m/s ²	174	173	174	174	174
Ax	m/s ²	-72	-72	-73	-74	-75
Ay	m/s ²	-27	-27	-28	-27	-27
Az	m/s ²	-172	-172	-172	-172	-172
Pelvis Acceleration						
Resultant (Ar)	m/s ²	249	249	248	249	248
Ax	m/s ²	-235	-235	-235	-235	-235
Ay	m/s ²	-81	-71	-73	-75	-76
Az	m/s ²	-101	-101	-103	-101	-104
Lap Belt Load	N	7360	7363	7368	7365	7373
Left Femur						
Fx	N	-1362	-1405	-1429	-1400	-1445
Fz	N	-1629	-1648	-1646	-1663	-1660
My	Nm	180	186	188	187	190
Right Femur						
Fx	N	-1419	-1437	-1452	-1447	-1473
Fz	N	-1591	-1604	-1602	-1613	-1612
My	Nm	178	181	180	181	182
Left Lower Tibia						
Fx	N	246	340	437	449	489
Fy	N	135	64	68	130	289
Fz	N	-1633	-1710	-1775	-1696	-1849
Right Lower Tibia						
Fx	N	276	362	444	438	475
Fy	N	198	166	131	215	239
Fz	N	-1608	-1635	-1665	-1546	-1861
Lumbar Fz	N	-4895	-4898	-4897	-4896	-4904

Table 26. Floor Friction Parametric Study

PARAMETER	UNIT	SEAT PITCH				
		27"	30"	32" Baseline	34"	36"
HIC @ 36ms		384	433	295	586	520
Head Acceleration						
Resultant (Ar)	m/s ²	831	850	674	1092	992
Ax	m/s ²	-780	-809	-641	-1045	-958
Ay	m/s ²	-292	-223	-169	-239	-190
Az	m/s ²	-245	-241	-240	-244	-231
Thorax Acceleration						
Resultant (Ar) (3ms)	m/s ²	170	160	173	174	170
Ax	m/s ²	-118	-79	-72	-70	-68
Ay	m/s ²	-51	-27	-27	-23	-24
Az	m/s ²	-245	-159	-172	-173	-176
Pelvis Acceleration						
Resultant (Ar)	m/s ²	324	273	249	224	206
Ax	m/s ²	-323	-261	-235	-210	-190
Ay	m/s ²	-84	-64	-81	-67	-56
Az	m/s ²	-161	-103	-101	-95	-113
Lap Belt Load	N	6660	7567	7360	7096	6873
Left Femur						
Fx	N	-1310	-1049	-1362	-1440	-1416
Fz	N	2025	-2015	-1629	-1530	-1488
My	Nm	188	484	180	187	182
Right Femur						
Fx	N	-1072	-1047	-1419	-1498	-1430
Fz	N	1844	-1694	-1591	-1476	-1421
My	Nm	174	457	178	186	175
Left Lower Tibia						
Fx	N	-564	-3258	246	375	420
Fy	N	283	-237	135	107	160
Fz	N	-1826	-1484	-1633	-1670	-1605
Right Lower Tibia						
Fx	N	-528	-1645	276	386	425
Fy	N	246	-98	198	170	178
Fz	N	-1749	-1464	-1608	-1679	-1568
Lumbar Fz	N	-5154	-4550	-4895	-5090	-5068

Table 27. Seat Pitch Parametric Study

PARAMETER	UNIT	TIBIA ANGLE FROM VERTICAL				
		-11.5° Baseline	-6.5°	-1.5°	3.5°	8.5°
HIC @ 36ms		295	375	561	598	601
Head Acceleration						
Resultant (Ar)	m/s ²	674	795	1016	1037	1048
Ax	m/s ²	-641	-742	-943	-963	-975
Ay	m/s ²	-169	-190	-228	-233	-246
Az	m/s ²	-240	-236	341	310	324
Thorax Acceleration						
Resultant (Ar) (3ms)	m/s ²	174	172	168	186	198
Ax	m/s ²	-72	-75	-74	-90	-104
Ay	m/s ²	-27	-31	-32	-37	-39
Az	m/s ²	-172	-170	-166	-176	-176
Pelvis Acceleration						
Resultant (Ar)	m/s ²	249	252	253	255	255
Ax	m/s ²	-235	-239	-242	-242	-241
Ay	m/s ²	-81	-74	-71	-68	-65
Az	m/s ²	-101	-105	-133	-133	-129
Lap Belt Load	N	7360	7338	7289	7258	7251
Left Femur						
Fx	N	-1362	1084	1518	1705	1533
Fz	N	-1629	-1602	-1720	-1842	-1593
My	Nm	180	143	-149	-130	-94
Right Femur						
Fx	N	-1419	2626	1615	2399	3007
Fz	N	-1591	-1560	-1627	-1807	-1802
My	Nm	178	220	292	221	150
Left Lower Tibia						
Fx	N	246	-811	-1425	-1202	-1293
Fy	N	135	-143	-151	-192	-199
Fz	N	-1633	-1186	-1607	-1816	-2441
Right Lower Tibia						
Fx	N	276	477	-3323	-2677	-2243
Fy	N	198	-530	-186	-313	-580
Fz	N	-1608	-1857	-3240	-2614	-1688
Lumbar Fz	N	-4895	-4838	-4719	-4796	-4944

Table 28. Tibia Angle From Vertical

PARAMETER	UNIT	CONFIGURATION					
		BASE	NOMEX BULKHEAD	STANDARD BULKHEAD	16G CRASH PULSE	3 POINT BELT	REAR FACING SEAT
HIC @ 36ms		295	739	1937	871	46	149
Head Acceleration							
Resultant (Ar)	m/s ²	674	966	1721	1106	212	511
Ax	m/s ²	-641	-648	-1291	-1028	-148	506
Ay	m/s ²	-169	-250	-611	-352	-23	175
Az	m/s ²	-240	-771	-1388	-296	-202	138
Thorax Acceleration							
Resultant (Ar) (3ms)	m/s ²	173	344	504	253	235	297
Ax	m/s ²	-71	-191	-176	-108	-255	291
Ay	m/s ²	-27	-49	-42	-41	-25	92
Az	m/s ²	-172	-353	-580	-244	-136	94
Pelvis Acceleration							
Resultant (Ar)	m/s ²	249	240	299	213	256	278
Ax	m/s ²	-235	-225	-225	-196	246	-24
Ay	m/s ²	-81	-63	-63	-47	-158	-44
Az	m/s ²	-101	-132	-292	-174	-66	-98
Lap Belt Load	N	7360	7108	7108	7869	4254	533
Left Femur							
Fx	N	-1362	-1278	-1117	-1639	309	265
Fz	N	-1629	-1530	-2034	-1508	-2024	1414
My	Nm	180	145	166	229	164	46
Right Femur							
Fx	N	-1419	-1132	-994	-1894	325	267
Fz	N	-1591	-1489	-2021	-1442	-1952	1321
My	Nm	178	133	159	236	143	41
Left Lower Tibia							
Fx	N	246	2565	5149	346	3915	-582
Fy	N	135	11	42	267	-83	-85
Fz	N	-1633	-1573	-1541	-1859	-1817	-698
Right Lower Tibia							
Fx	N	276	2521	5587	391	3897	-562
Fy	N	198	3	62	226	-84	-94
Fz	N	-1608	-1428	-1462	-2084	-1630	-706
Lumbar Fz	N	-4895	-4648	-4646	-7483	4054	2268

Table 29. Aircraft Interiors Alternative Test Configurations

TIBIA ANGLE (Degrees)	RESULTANT BENDING MOMENT (Nm)	
	Left Hand Ankle	Right Hand Ankle
-11.5	78	70
-5.5	144	181
-1.5	192	217
3.5	191	204
8.5	86	198

Table 30. Ankle Joints Bending Moments.

Body Segment	Vertebral Body Ellipse Dimensions		Degree of Ellipse	Distance of Articular Facet from Centre of Vertebral Body (h _i) (m)
	Major Axis (m)	Minor Axis (m)		
Head	0.10500	0.10500	2	-
Chin	0.03400	0.05000	2	-
C1	0.00992	0.00740	8	0.03000
C2	0.00999	0.00750	8	0.03000
C3	0.01007	0.00756	8	0.03000
C4	0.01008	0.00757	8	0.03300
C5	0.01009	0.00758	8	0.03300
C6	0.01010	0.00758	8	0.04330
C7	0.01074	0.00806	8	0.04200
T1	0.01098	0.00824	8	0.04200
T2	0.01193	0.00895	8	0.04300
T3	0.01233	0.00925	8	0.05000
T4	0.01268	0.00951	8	0.05500
T5	0.01304	0.00979	8	0.05800
T6	0.01326	0.00995	8	0.05000
T7	0.01346	0.01010	8	0.05500
T8	0.01382	0.01037	8	0.05300
T9	0.01431	0.01073	8	0.05000
T10	0.01532	0.01149	8	0.04500
T11	0.01623	0.01217	8	0.04200
T12	0.01712	0.01284	8	0.04700
L1	0.01817	0.01363	8	0.04700
L2	0.01861	0.01396	8	0.05800
L3	0.01834	0.01376	8	0.06300
L4	0.01757	0.01318	8	0.06300
L5	0.01595	0.01196	8	0.05600
Pelvis	0.12500	0.12200	2	-

(Source: WPAFB & WSU)

Table 32. Dimensions of Vertebral Bodies

Body Segment	Description in Madymo Model	Location of Body in Local Coordinate System		Location of Body Centre of Gravity in Local Coordinate System		Orientation in Local Coordinate System
		X (m)	Z (m)	X (m)	Z (m)	θ (Rad)
Head	System 26	1.05E-03	4.42E-02	0.02540	0.00000	-0.06980
C1	System 25	5.86E-07	1.58E-02	0.01270	0.00000	0.00000
C2	System 24	6.38E-07	1.79E-02	0.01270	0.00000	0.00000
C3	System 23	1.01E-03	1.90E-02	0.01270	0.00000	0.00000
C4	System 22	4.98E-04	1.79E-02	0.01270	0.00000	0.00000
C5	System 21	1.01E-06	2.13E-02	0.01270	0.00000	1.23E-02
C6	System 20	-1.35E-06	2.07E-02	0.01270	0.00000	-5.21E-02
C7	System 19	-1.34E-06	2.13E-02	0.01270	0.00000	3.71E-02
T1	System 18	-1.52E-06	2.17E-02	0.00000	0.00000	-2.35E-02
T2	System 17	-8.42E-07	2.07E-02	0.00000	0.00000	-6.45E-02
T3	System 16	-1.91E-08	2.31E-02	0.00000	0.00000	-1.29E-02
T4	System 15	-1.39E-06	2.36E-02	0.00000	0.00000	-4.57E-02
T5	System 14	-1.03E-06	2.33E-02	0.0051	0.00000	-0.18291
T6	System 13	-1.81E-06	2.25E-02	0.01270	0.00000	-8.95E-02
T7	System 12	5.71E-06	2.63E-02	0.01651	0.00000	-4.69E-02
T8	System 11	1.34E-03	2.87E-02	0.01778	0.00000	-0.13805
T9	System 10	-3.48E-07	2.73E-02	0.02286	0.00000	2.54E-02
T10	System 9	2.28E-07	3.10E-02	0.00000	0.00000	-0.15272
T11	System 8	1.62E-06	3.37E-02	0.00000	0.00000	-9.86E-02
T12	System 7	-1.41E-06	3.40E-02	0.00000	0.00000	-7.03E-02
L1	System 6	1.89E-06	3.77E-02	0.00000	0.00000	-6.14E-02
L2	System 5	-1.10E-06	3.53E-02	0.00000	0.00000	-5.35E-02
L3	System 4	-9.79E-07	3.86E-02	0.00000	0.00000	-0.16091
L4	System 3	0.0000	0.03800	0.00000	0.00000	3.19E-02
L5	System 2	-0.0517	0.03920	0.00000	0.00000	-0.10737
Pelvis	System 1	-0.4061	0.55380	0.00000	0.00000	-0.12217

(Source: X-ray, WSU & WPAFB)

Table 33. Orientations of Vertebral Bodies With Respect to Local Coordinate System

Body Seg	Mass (Kg)	Moment of Inertia (Kg m ²)	Disc Linear Stiffness (N/m)	Facet Linear Stiffness (N/m)	Disc Linear Damping (Ns/m)	Disc Rotation. Stiffness Nms/rad	Disc Damping Stiffness Nms/rad
Head	4.57400	0.02510	2950.430	226.000	1110.250	271.200	0.22600
C1	0.22770	0.00015	146.900	226.000	227.6500	271.200	0.11300
C2	0.22770	0.00015	146.900	226.000	227.6500	271.200	0.11300
C3	0.28030	0.00018	180.800	226.000	227.6500	271.200	0.11300
C4	0.43790	0.00028	282.500	226.000	227.6500	271.200	0.11300
C5	0.43700	0.00034	282.500	226.000	455.3070	271.200	0.11300
C6	0.36790	0.00034	237.300	226.000	455.3070	271.200	0.11300
C7	0.36790	0.00045	237.300	226.000	455.3070	271.200	0.11300
T1	1.29300	0.00075	1961.680	226.000	4377.952	1113.000	2.26000
T2	1.29300	0.00210	1961.680	226.000	4377.952	1113.000	2.26000
T3	1.29300	0.00288	1961.680	226.000	4377.952	1113.000	2.26000
T4	1.29300	0.00314	1961.680	226.000	4377.952	1113.000	2.26000
T5	1.29300	0.00384	1961.680	226.000	4377.952	1113.000	2.26000
T6	1.36000	0.00443	877.445	226.000	3502.362	1113.000	2.26000
T7	1.36000	0.00538	877.445	226.000	3502.362	1113.000	2.26000
T8	1.36000	0.00555	877.445	226.000	2626.771	1113.000	2.26000
T9	1.36000	0.00620	877.445	226.000	2626.771	1113.000	2.26000
T10	1.36000	0.00620	877.445	226.000	2626.771	1113.000	2.26000
T11	0.86420	0.00706	904.000	226.000	1751.181	452.000	1.13000
T12	0.86420	0.00177	904.000	226.000	1751.181	452.000	1.13000
L1	0.86420	0.00177	904.000	452.000	1751.181	452.000	1.13000
L2	0.86420	0.00177	904.000	452.000	1751.181	452.000	1.13000
L3	0.86420	0.00177	904.000	452.000	1751.181	452.000	1.13000
L4	2.19000	0.00790	904.000	452.000	1751.181	452.000	1.13000
L5	2.19000	0.00790	904.000	452.000	1751.181	452.000	1.13000
Pelv.	16.96000	0.09090	0.00000	0.00000	0.000000	0.00000	0.00000

(Source: WSU & WPAFB)

Table 34. Spine Model Physical Characteristics.

Body Segment	Description in Madymo Model	Location of Body in Local Coordinate System		Location of Body Centre of Gravity in Local Coordinate System		Orientation in Local Coordinate System
		X (m)	Z (m)	X (m)	Z (m)	θ (Rad)
Abdomen	System 27 (wrt Sys. 4)	-0.0300	-0.08100	-0.0022	0.07720	0.00000
Thorax	System 28 (wrt Sys.14)	0.0982	-0.18770	-0.0031	0.11190	0.26100
Neck	System 30 (wrt Sys.24)	-0.02166	-0.11900	0.000	0.00000	-0.20940
Shoulders	System 29 Element 1	0.02176	0.00272	-.0247	-0.00010	0.61086
Upper Arms	System 29 Element 2	-0.02570	-0.00030	0.0009	-0.13230	0.00000
Lower Arms	System 29 Element 3	0.0000	-0.26460	-.0013	-0.08850	1.65806
Hands	System 29 Element 4	0.0000	-.2512	0.0035	-0.05470	0.00000
Upper Femurs	System 1 Element 2	0.0191	-0.03380	0.2045	-0.00360	-0.04360
Lower Femurs	System 1 Element 3	0.2895	0.00000	-0.085	-.0036	0.0000
Tibias	System 1 Element 4	0.1116	0.00000	-.0011	-0.18940	-0.15710
Feet	System 1 Element 5	0.0000	-.4125	0.0455	-0.05570	0.48000

Table 35. External Body Segments To Spine.

Body Segment	Description in MADYMO Model	Element Orientation θ (Rad)	Mass (Kg)	Inertia (Kg.m²)
Abdomen	System 27 (wrt Sys. 4)	0.00000	Part of Vertebral Body	Part of Vertebral Body
Thorax	System 28 (wrt Sys.14)	0.26100	Part of Vertebral Body	Part of Vertebral Body
Neck	System 30 (wrt Sys.24)	-0.20940	Part of Vertebral Body	Part of Vertebral Body
Shoulders	System 29 Element 1	0.61086	3.06	0.02000
Upper Arms	System 29 Element 2	0.00000	2.12	0.025
Lower Arms	System 29 Element 3	1.65806	2.42	0.03060
Hands	System 29 Element 4	0.00000	1.133	0.02000
Upper Femurs	System 1 Element 2	-0.04360	6.40	0.10870
Lower Femurs	System 1 Element 3	0.00000	6.40	0.10870
Tibias	System 1 Element 4	-0.15710	6.28	0.19580
Feet	System 1 Element 5	0.48000	1.57	0.02000

Table 36. Mass and Moment of Inertia of Body Segments.

Body Segment	Body Ellipse Dimensions		Location of Ellipse Centre		Ellipse Orientation	Degree of Ellipse
	Major Axis (m)	Minor Axis (m)	X-axis (m)	Z-axis (m)	θ (Rad)	
Abdomen (L5)	0.10925	0.03588	0.05325	0.00000	0.00000	6
Abdomen (L4)	0.1095	0.03954	0.04650	0.00000	0.00000	8
Abdomen (L3)	0.1083	0.04127	0.04530	0.00000	0.00000	8
Abdomen (L2)	0.1053	0.04188	0.04730	0.00000	0.00000	8
Abdomen (L1)	0.1000	0.04089	0.05200	0.00000	0.00000	8
Thorax (T5)	0.128	0.156	0.0771	0.03735	0.38397	2
Thorax (T5)	0.132	0.20750	0.04800	1.05E-01	0.38397	2
Thorax (T5)	0.128	0.15600	0.02910	0.15310	0.38397	2
Neck (C1)	0.030	0.00740	0.00000	0.00000	0.00000	8
Neck (C2)	0.031	0.02250	0.00000	0.00000	0.00000	8
Neck (C3)	0.032	0.02268	0.00000	0.00000	0.00000	8
Neck (C4)	0.033	0.02271	0.00000	0.00000	0.00000	8
Neck (C5)	0.034	0.02274	0.00000	0.00000	0.00000	8
Neck (C6)	0.035	0.02274	0.00000	0.00000	0.00000	8
Neck (C7)	0.037	0.02418	0.00000	0.00000	0.00000	8
Shoulders	0.050	0.04000	-0.02710	-0.00260	0.00000	2
Upr Arms	0.048	0.15300	0.00000	-0.11300	0.00000	2
Lwr Arms	0.044	0.14700	0.00000	-0.10000	0.00000	2
Hands	0.048	0.08400	0.00000	-0.06900	0.00000	2
Upr Femur	0.234	0.08300	0.22500	0.00000	0.12217	2
Lwr Femur	0.234	0.08100	-0.06450	0.00000	0.12217	2
Tibias	0.060	0.26000	0.00000	-0.19780	0.00000	2
Feet	0.137	0.04000	0.06310	-0.06740	-0.29671	2

Table 37. Geometrical Definition of Body Segments

DESCRIPTION	BRACE POSITION : LEGS BACK, ARMS DOWN												T12	T11	T10	T9	T8	T7	T6	T5	T4	T3	T2	T1	C7	C6	C5	C4	C3	C2	C1	Head
	Pelvis	L5	L4	L3	L2	L1																										
Axial Load (N)	8260	10200	12200	13600	14200	14300	13500	11700	11000	10000	9070	7760	8440	6760	5810	4300	2800	1110	978	919	1030	718	271	136	441	0						
Shear Load (N)	3380	3690	4810	4250	3940	3760	3910	2770	1580	1610	924	1040	1550	1510	1400	1780	1840	1290	1090	573	457	1060	1520	2090	6270	0						
Bending Moment (Nm)	153	131	90	115	134	116	137	205	208	208	181	176	166	143	132	128	114	79.7	83.5	89.1	84.7	67.4	46.7	45.1	61.1	0						
DESCRIPTION	BRACE POSITION : LEGS BACK, ARMS UP						T12	T11	T10	T9	T8	T7	T6	T5	T4	T3	T2	T1	C7	C6	C5	C4	C3	C2	C1	Head						
	Pelvis	L5	L4	L3	L2	L1																										
Axial Load (N)	7850	9770	11500	12900	13400	13300	12600	11000	10400	9450	8550	7370	8410	6630	5520	3770	2390	1110	1020	890	800	641	299	187	570	0						
Shear Load (N)	3360	3630	4640	4160	3850	3690	3860	2850	1830	1930	1730	1450	1950	2020	1930	1460	1980	1440	1250	790	517	908	1410	2020	6210	0						
Bending Moment (Nm)	154	131	90.1	116	133	116	129	200	209	208	179	192	200	192	174	154	119	68.9	69.2	82.6	83.5	71.8	43.7	53.2	70.5	0						
DESCRIPTION	BRACE POSITION : LEGS FORWARD, ARMS DOWN						T12	T11	T10	T9	T8	T7	T6	T5	T4	T3	T2	T1	C7	C6	C5	C4	C3	C2	C1	Head						
	Pelvis	L5	L4	L3	L2	L1																										
Axial Load (N)	8130	10100	11100	12300	13400	12800	12400	10800	10300	9330	8460	7830	9650	8900	9060	8850	8350	5900	5080	4560	4010	3250	2310	1690	2910	0						
Shear Load (N)	3250	3690	4780	4190	3890	3690	3670	2530	1710	1640	1740	1880	2240	2330	3540	4260	2940	2520	2080	1980	2390	2360	2400	2730	3650	0						
Bending Moment (Nm)	160	133	90.8	121	151	123	148	224	221	214	188	171	143	145	178	202	183	166	169	140	112	104	79.7	66.2	91.5	0						
DESCRIPTION	BRACE POSITION : LEGS FORWARD, ARMS UP						T12	T11	T10	T9	T8	T7	T6	T5	T4	T3	T2	T1	C7	C6	C5	C4	C3	C2	C1	Head						
	Pelvis	L5	L4	L3	L2	L1																										
Axial Load (N)	8210	10000	11600	12800	13500	13000	13000	11500	11200	10400	9490	7970	8220	6830	5450	3530	2460	2330	1830	1530	1570	1450	912	446	742	0						
Shear Load (N)	3640	3670	4920	4290	3910	3850	3880	2790	1430	1790	1380	1520	1620	1370	2450	1460	1820	646	622	963	1410	1650	1810	2110	8360	0						
Bending Moment (Nm)	168	141	97.4	126	156	137	157	239	243	244	221	202	172	181	162	142	146	133	115	90.3	80.9	68.1	30.8	25.5	36.5	0						
Table 38. Spinal Column Peak Results																																

FIGURES

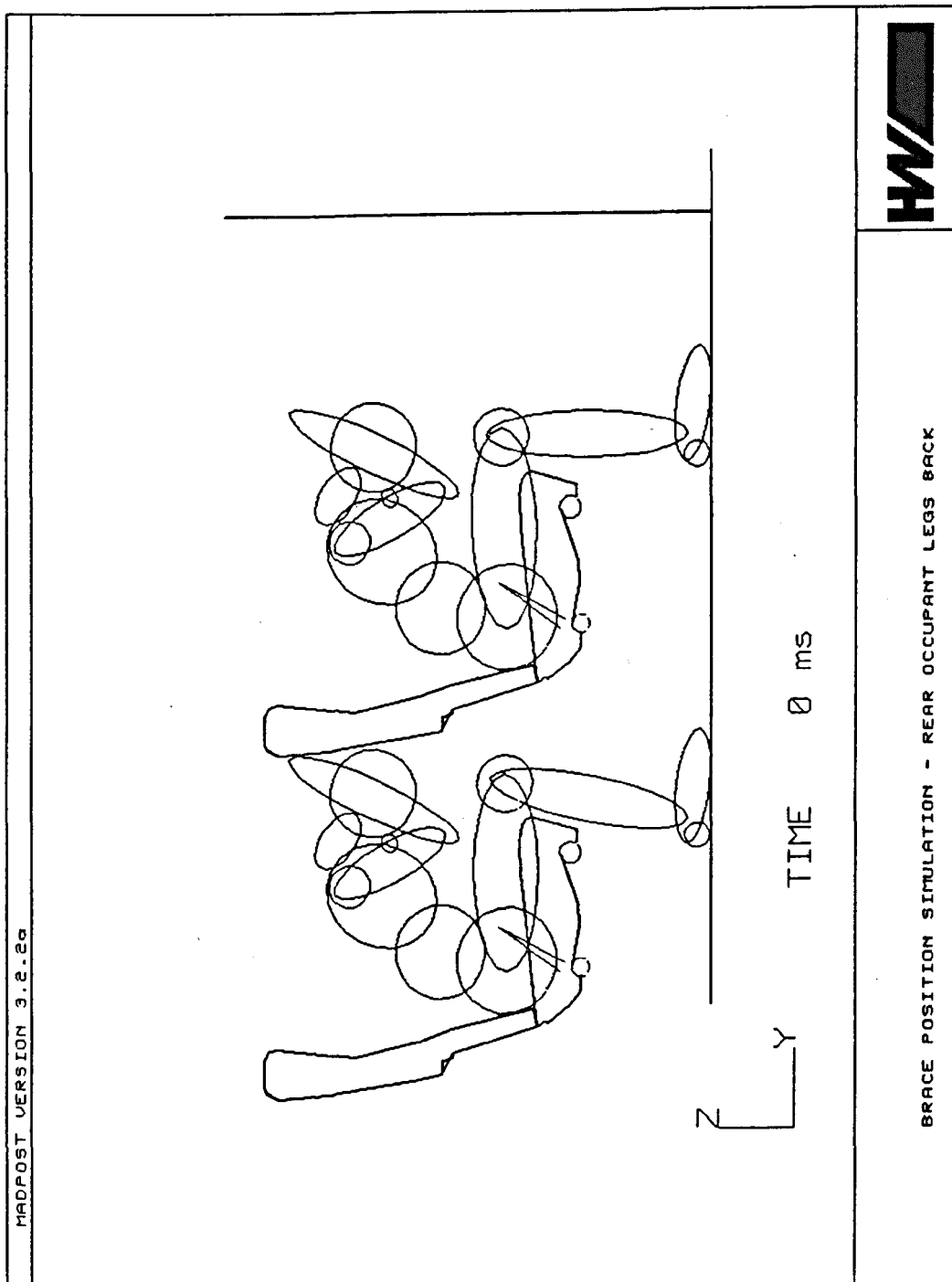


Figure 4. Brace Position Simulation - Rear Occupant Legs Back

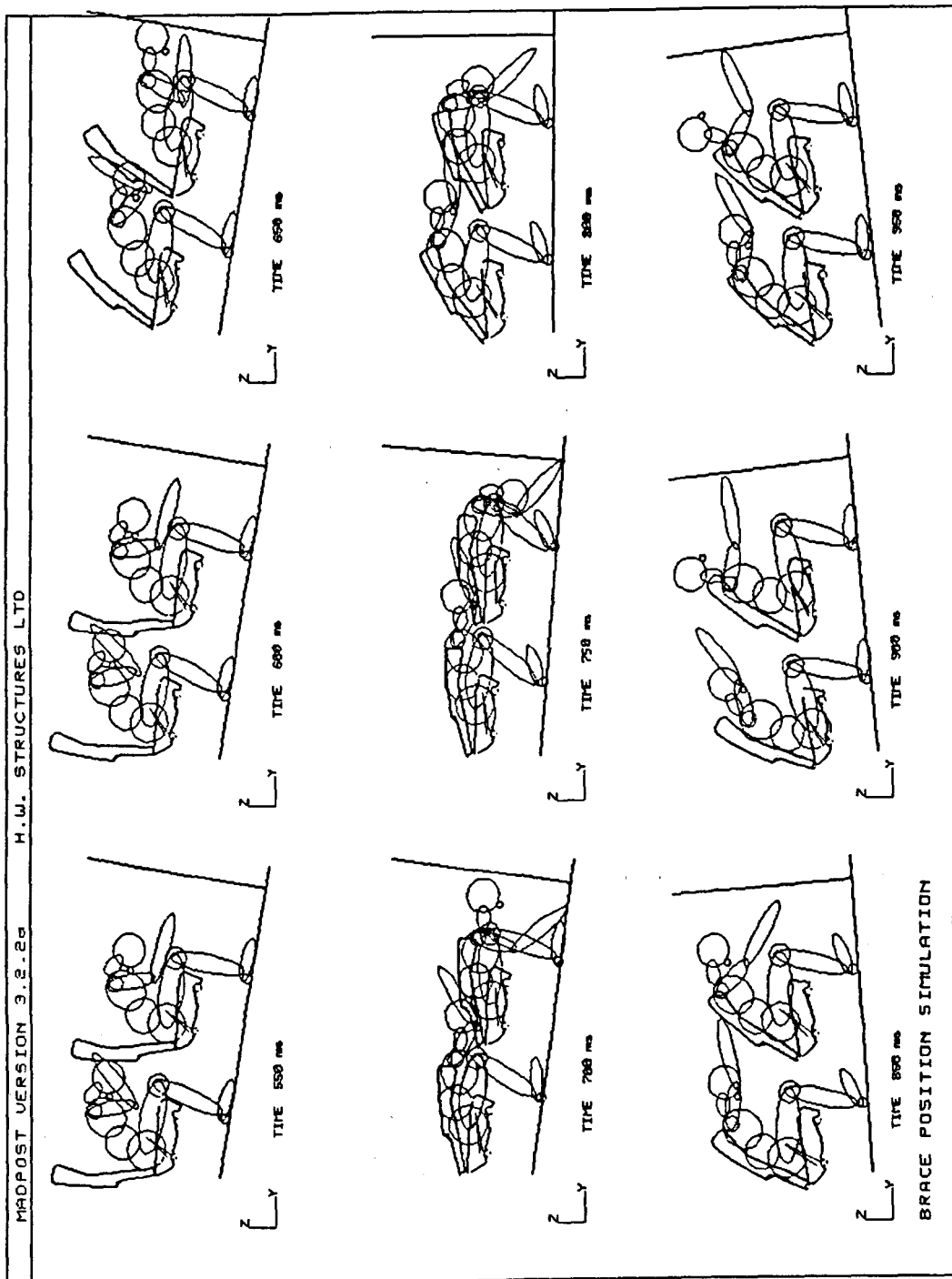


Figure 5. Brace Position Legs Back Simulation - 550ms to 950ms Sequential Plot

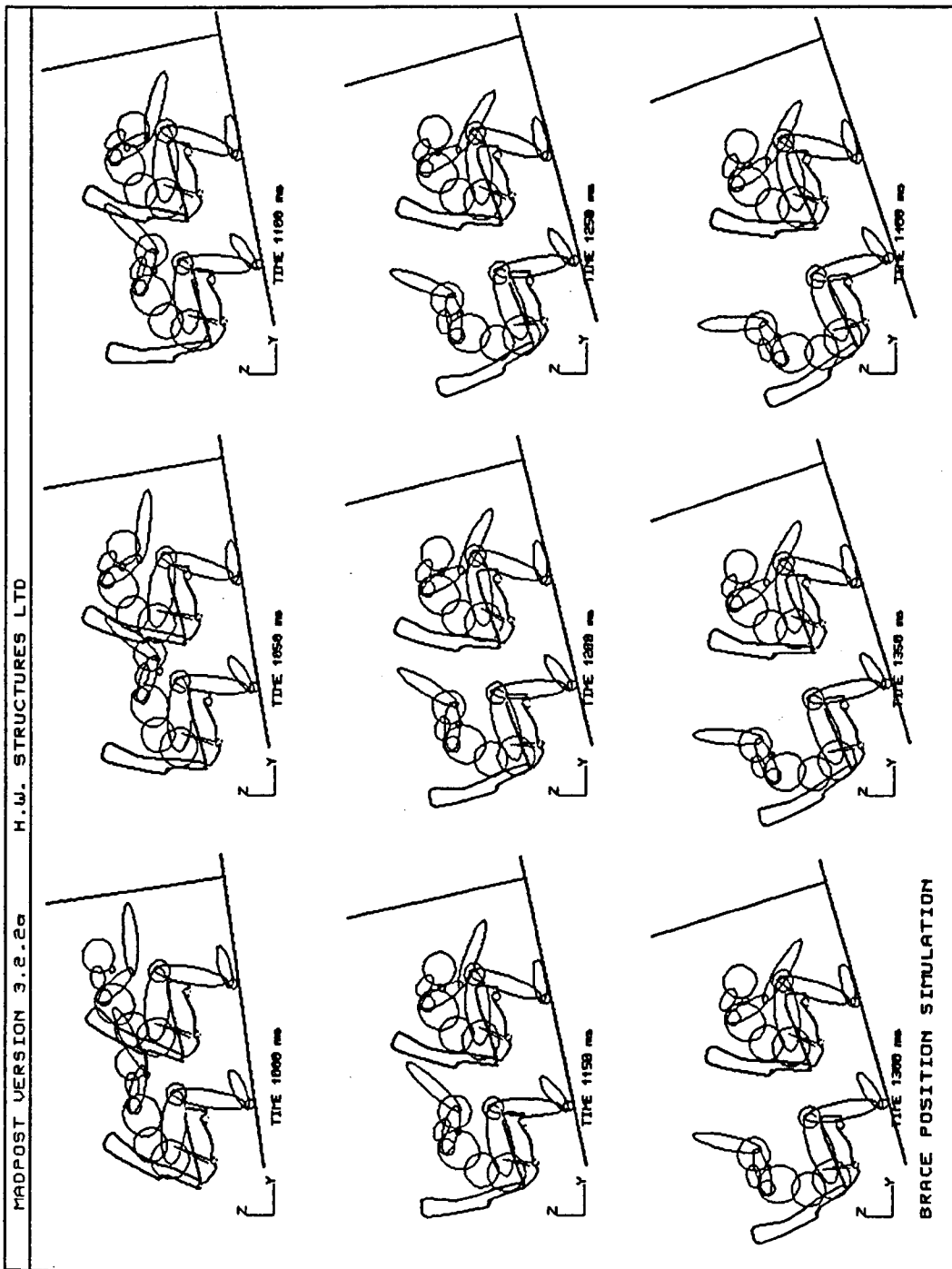


Figure 6. Brace Position Legs Back Simulation - 1000ms to 1400ms Sequential Plot

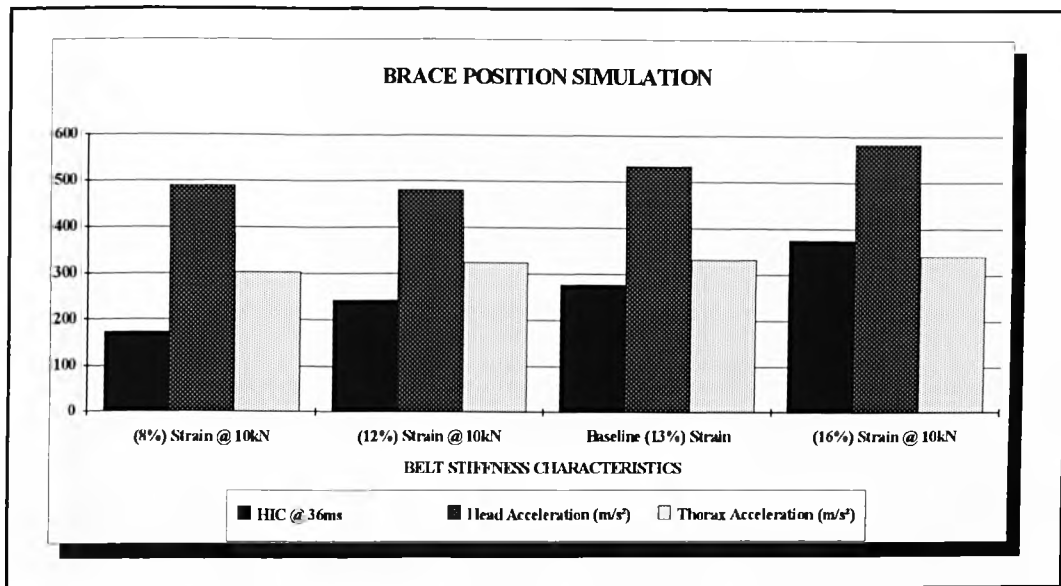


Figure 7. Brace Position - HIC, Head and Thorax Acceleration versus Belt Stiffness

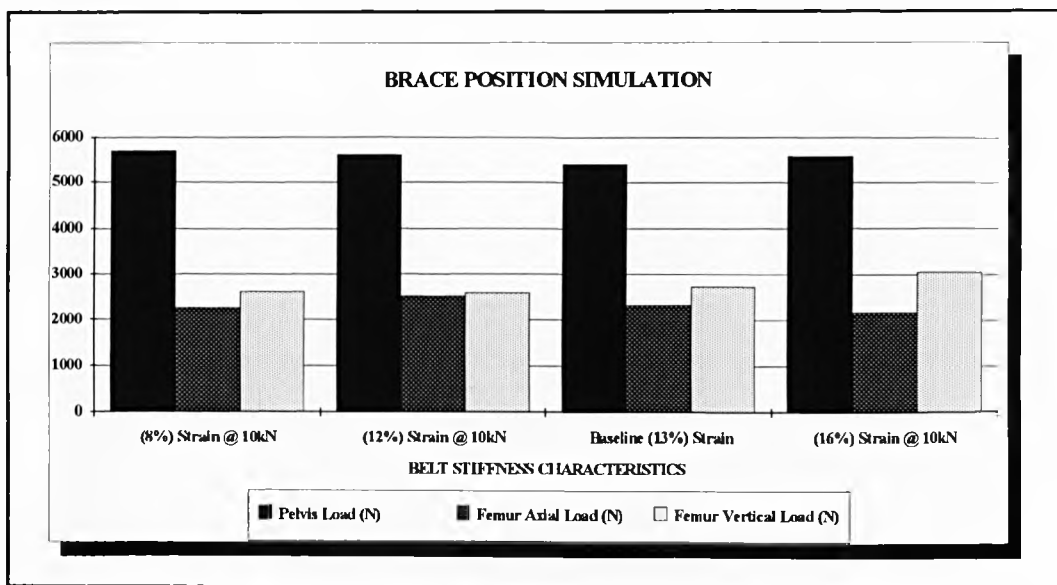


Figure 8. Brace Position - Pelvis, Femur Axial and Vertical Loads versus Belt Stiffness

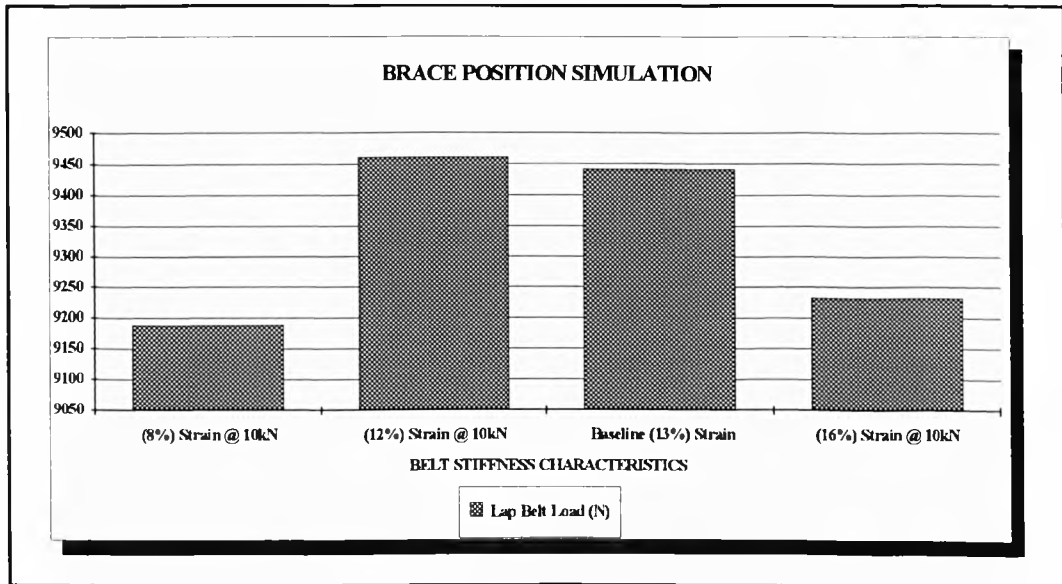


Figure 9. Brace Position - Lap Belt Load versus Belt Stiffness

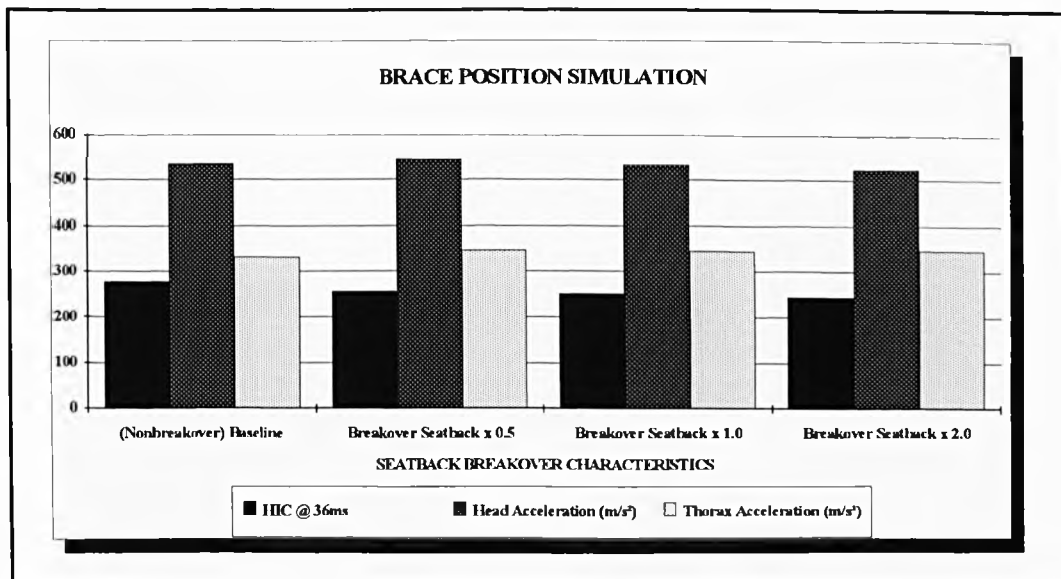


Figure 10. Brace Position - HIC, Head and Thorax Accelerations versus Seatback Breakover Stiffness

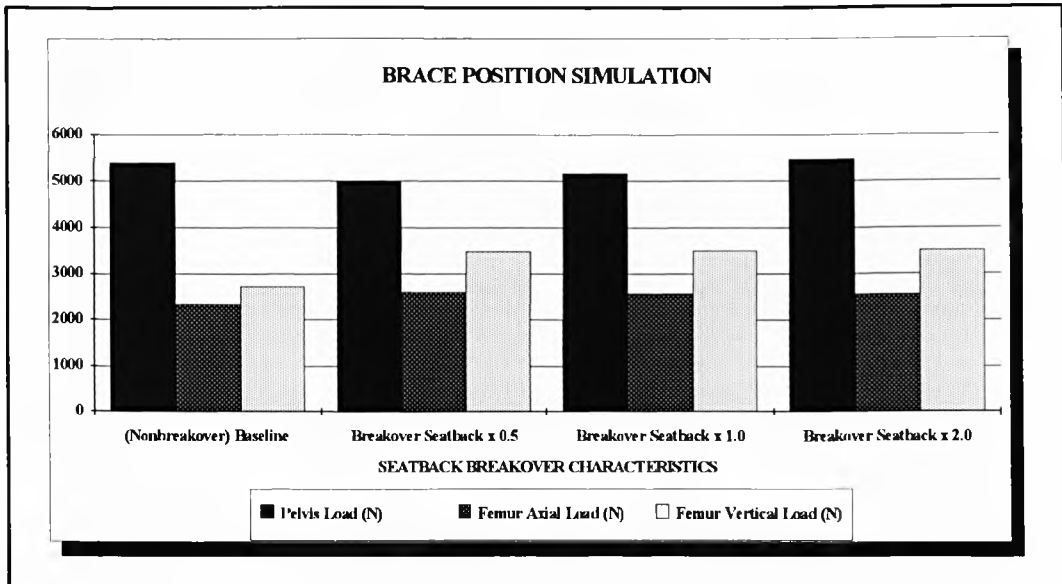


Figure 11. Brace Position - Pelvis, Femur Axial and Vertical Loads Versus Seatback Breakover Stiffness

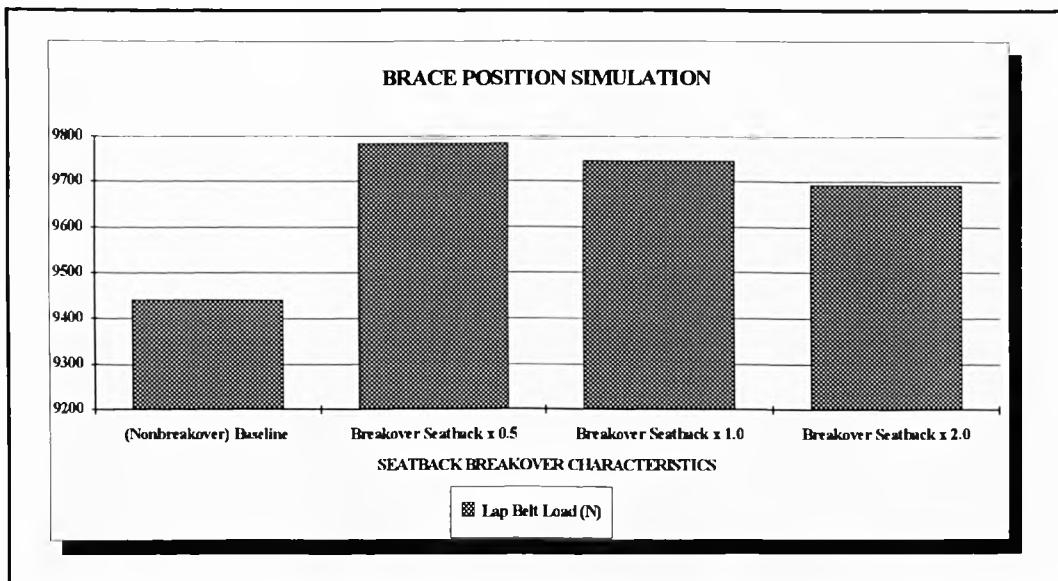


Figure 12. Brace Position - Lap Belt Load versus Seatback Breakover Stiffness

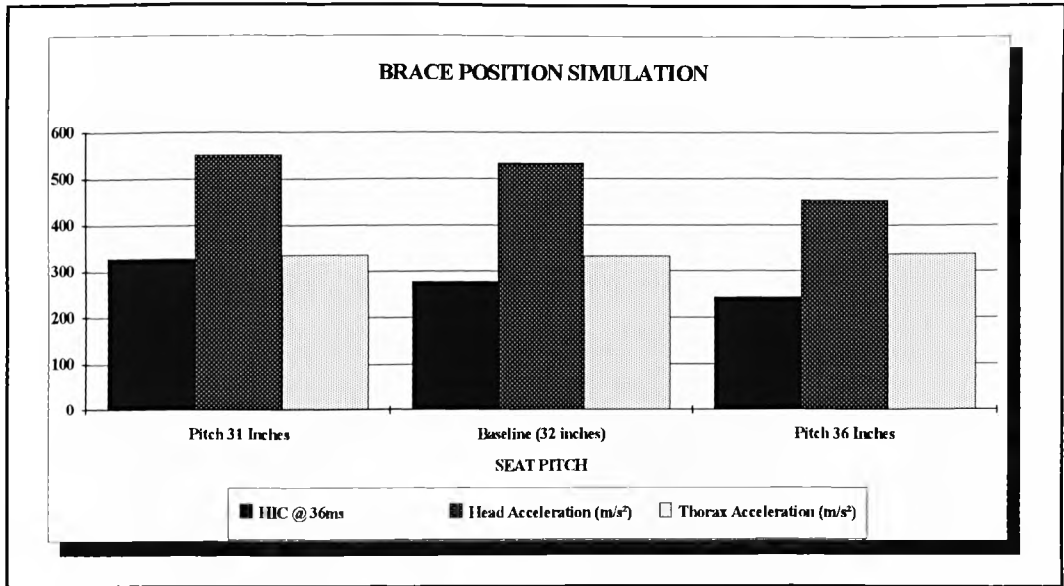


Figure 13. Brace Position - HIC, Head and Thorax Accelerations versus Seat Pitch

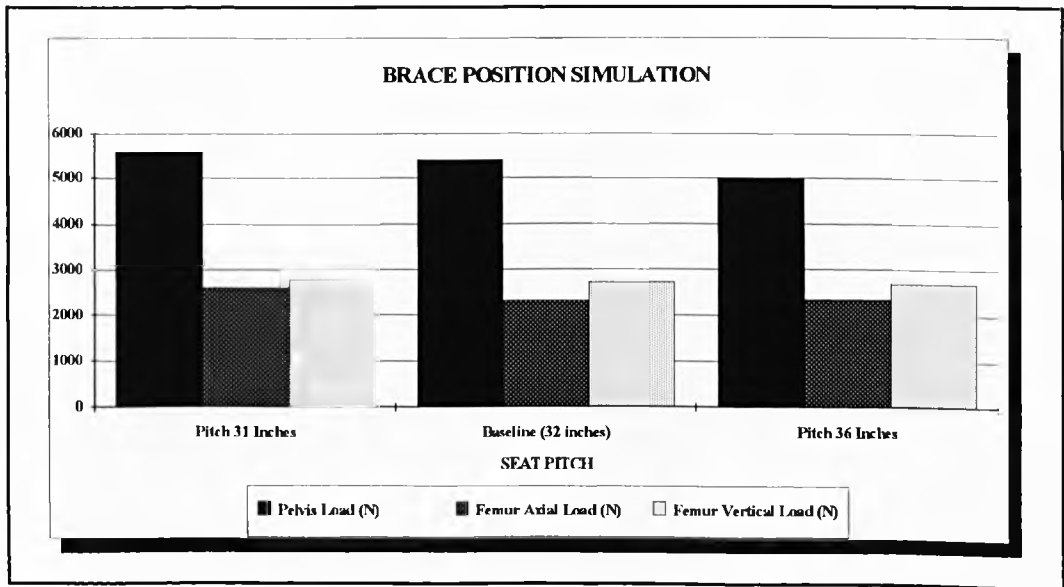


Figure 14. Brace Position - Pelvis, Femur Axial and Vertical Loads versus Seat Pitch

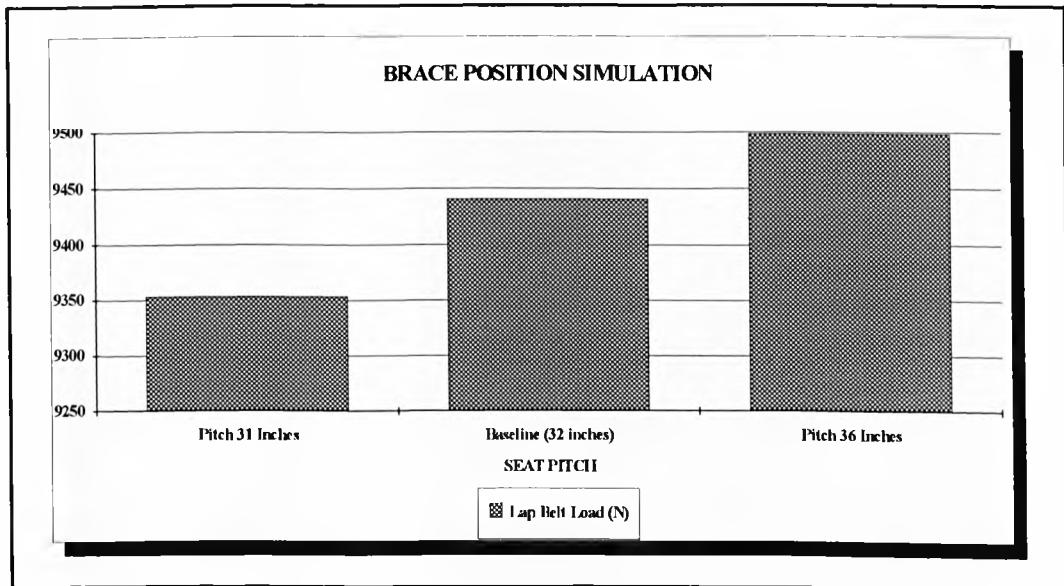


Figure 15. Brace Position - Lap Belt Load versus Seat Pitch

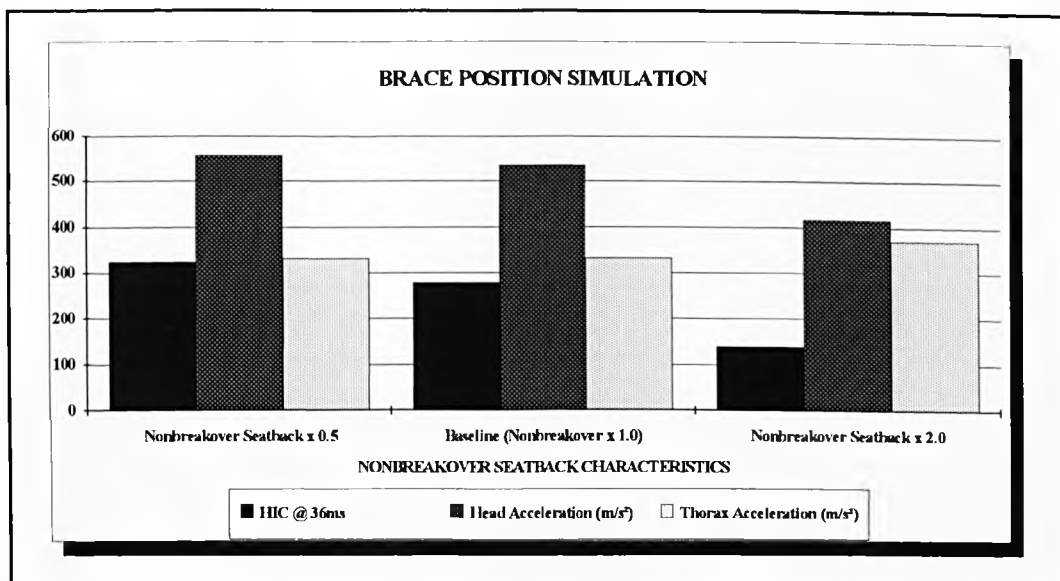


Figure 16. Brace Position - HIC, Head and Thorax Accelerations versus Nonbreakover Seatback Stiffness

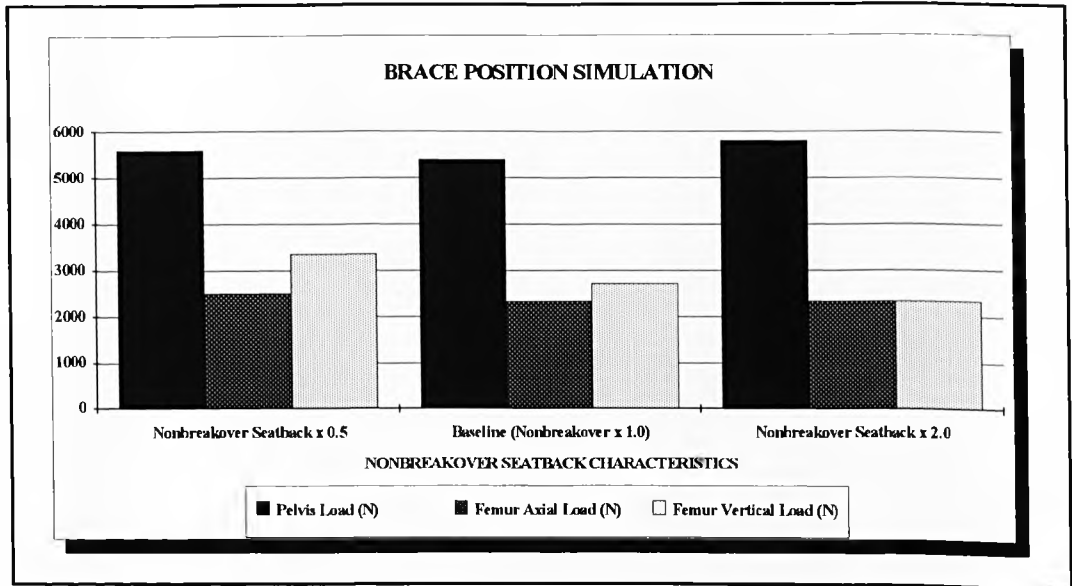


Figure 17. Brace Position - Pelvis, Femur Axial and Vertical Loads versus Nonbreakover Seatback Stiffness

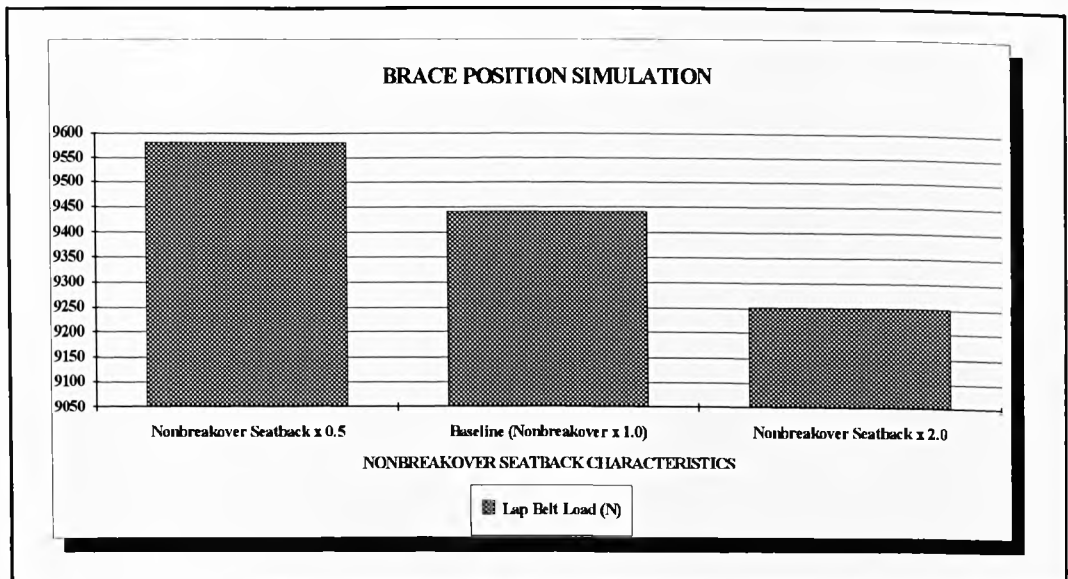


Figure 18. Brace Position - Lap Belt Load versus Nonbreakover Seatback Stiffness

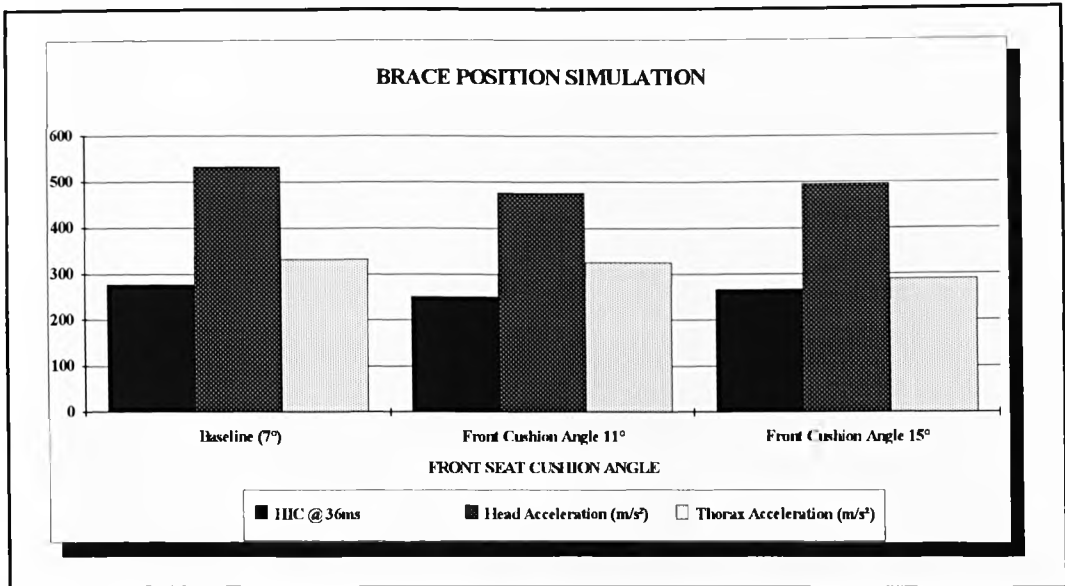


Figure 19. Brace Position - HIC, Head and Thorax Accelerations versus Front Seat Cushion Angle.

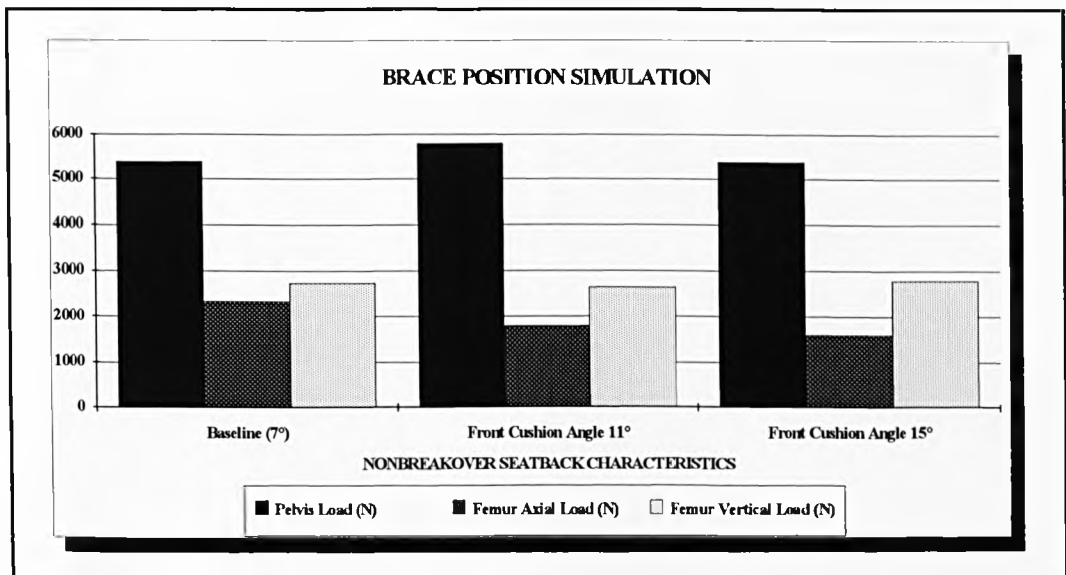


Figure 20. Brace Position - Pelvis, Femur Axial and Vertical Loads versus Front Seat Cushion Angle

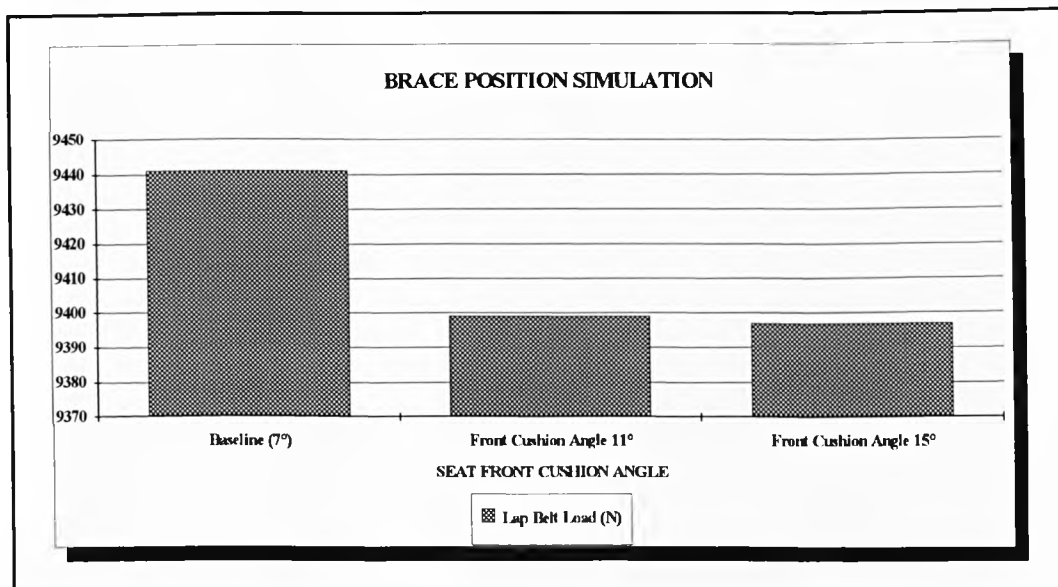


Figure 21. Brace Position - Lap Belt Load versus Seat Front Cushion Angle

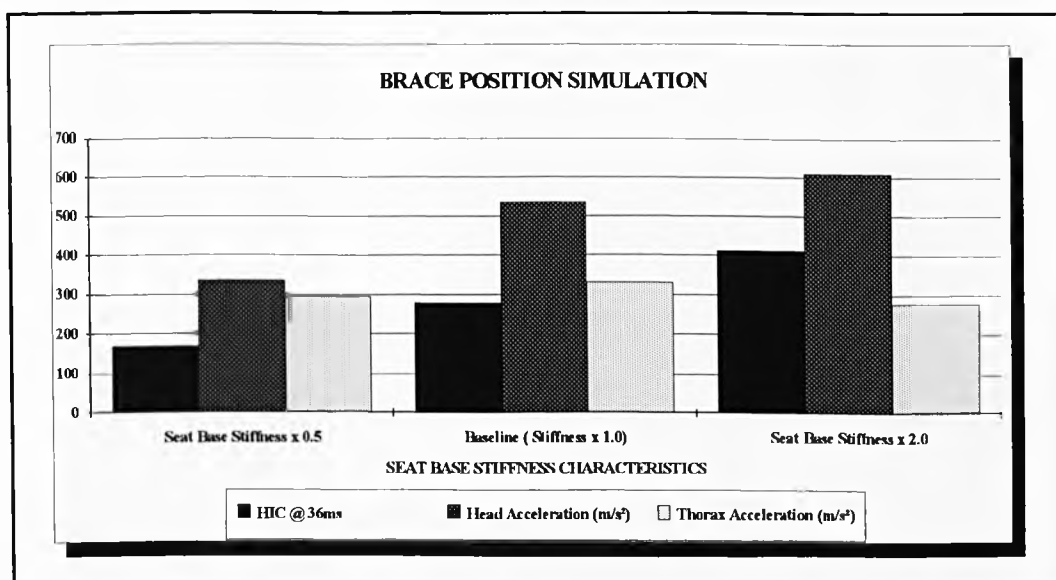


Figure 22. Brace Position - HIC, Head and Thorax Accelerations versus Seat Base Stiffness

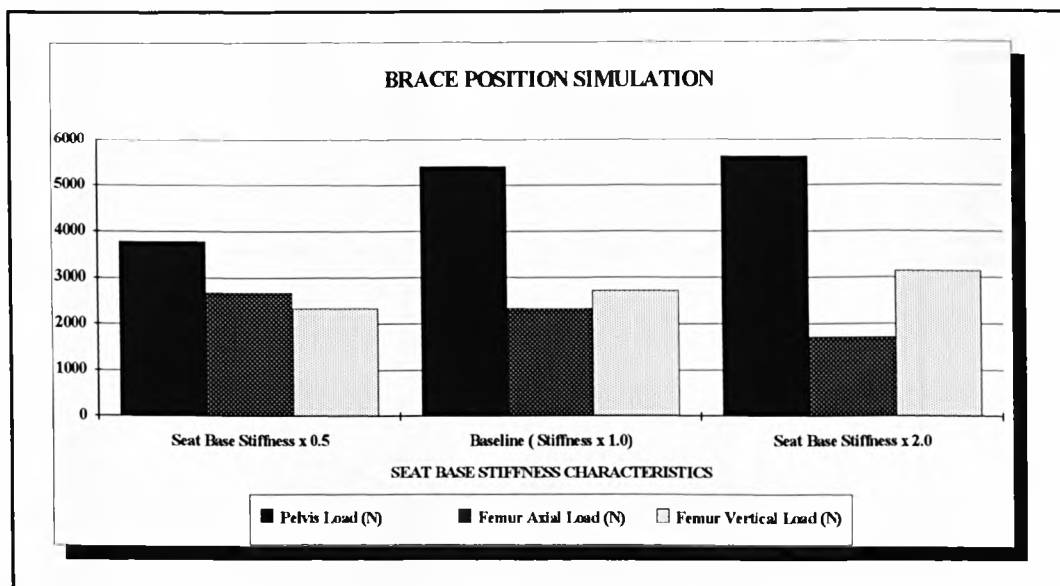


Figure 23. Brace Position - Pelvis, Femur Axial and Vertical Loads versus Seat Base Stiffness

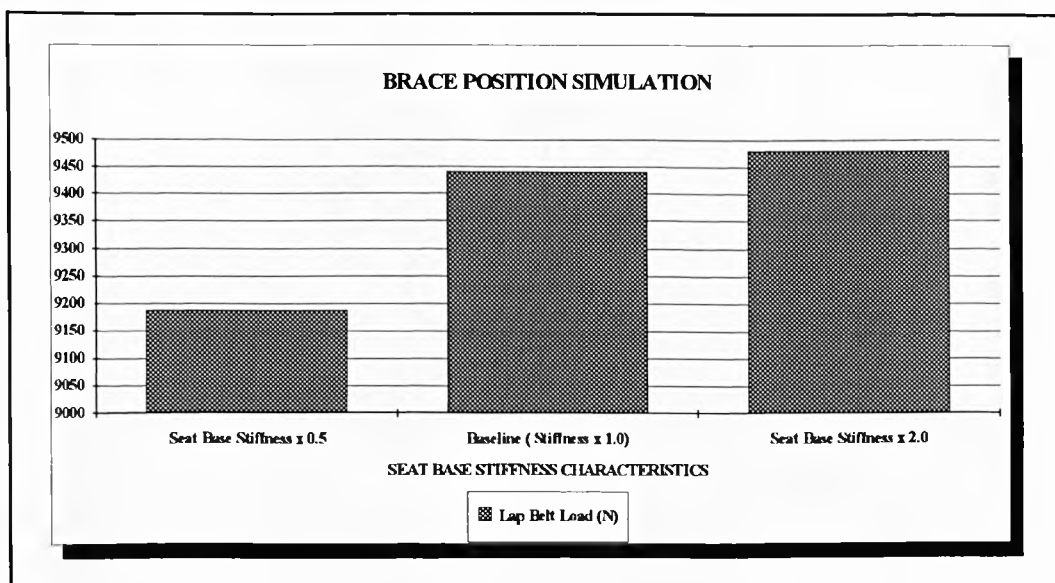


Figure 24. Brace Position - Lap Belt Load versus Seat Base Stiffness

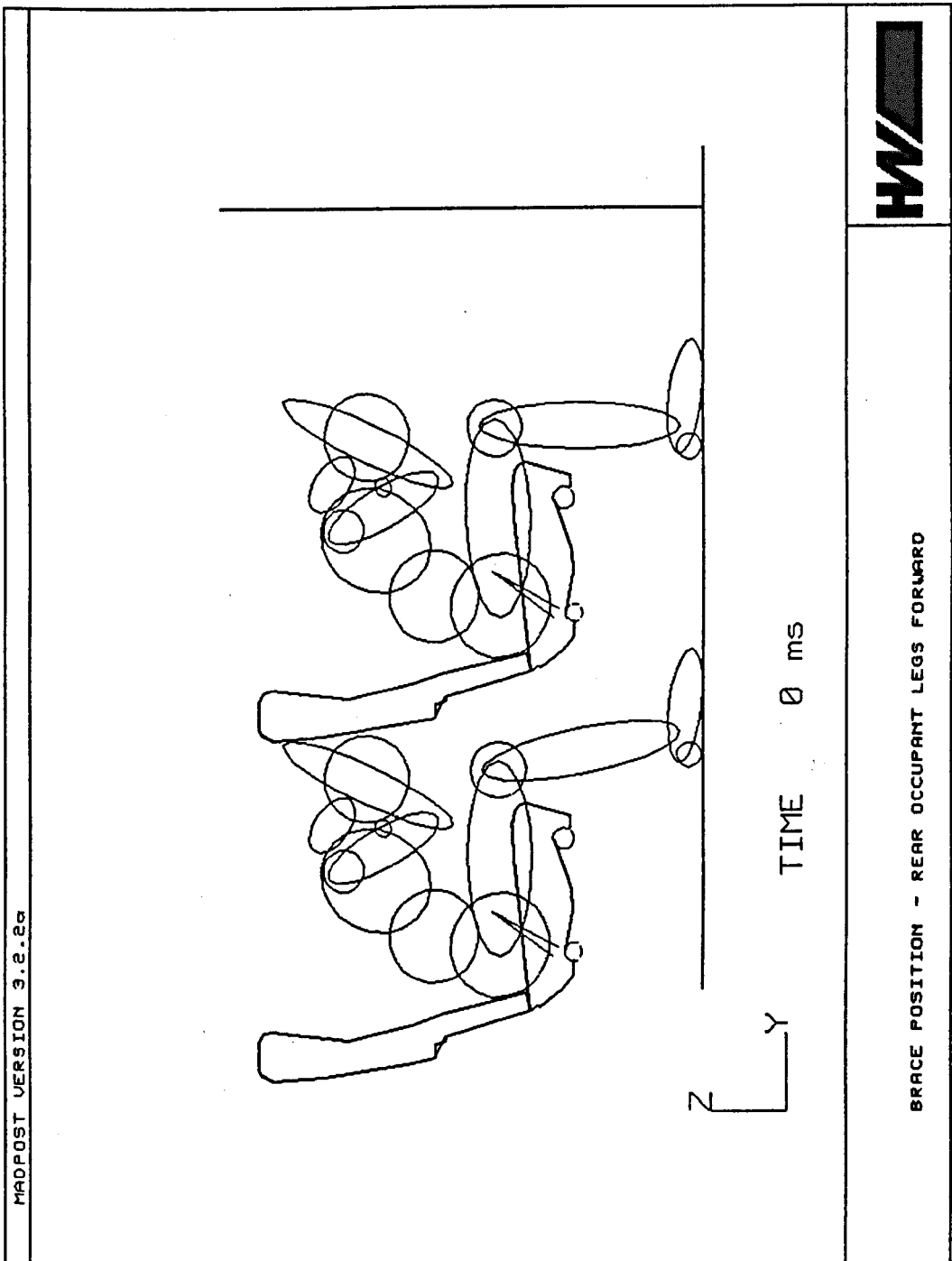


Figure 25. Brace Position Simulation - Rear Occupant Legs Forward

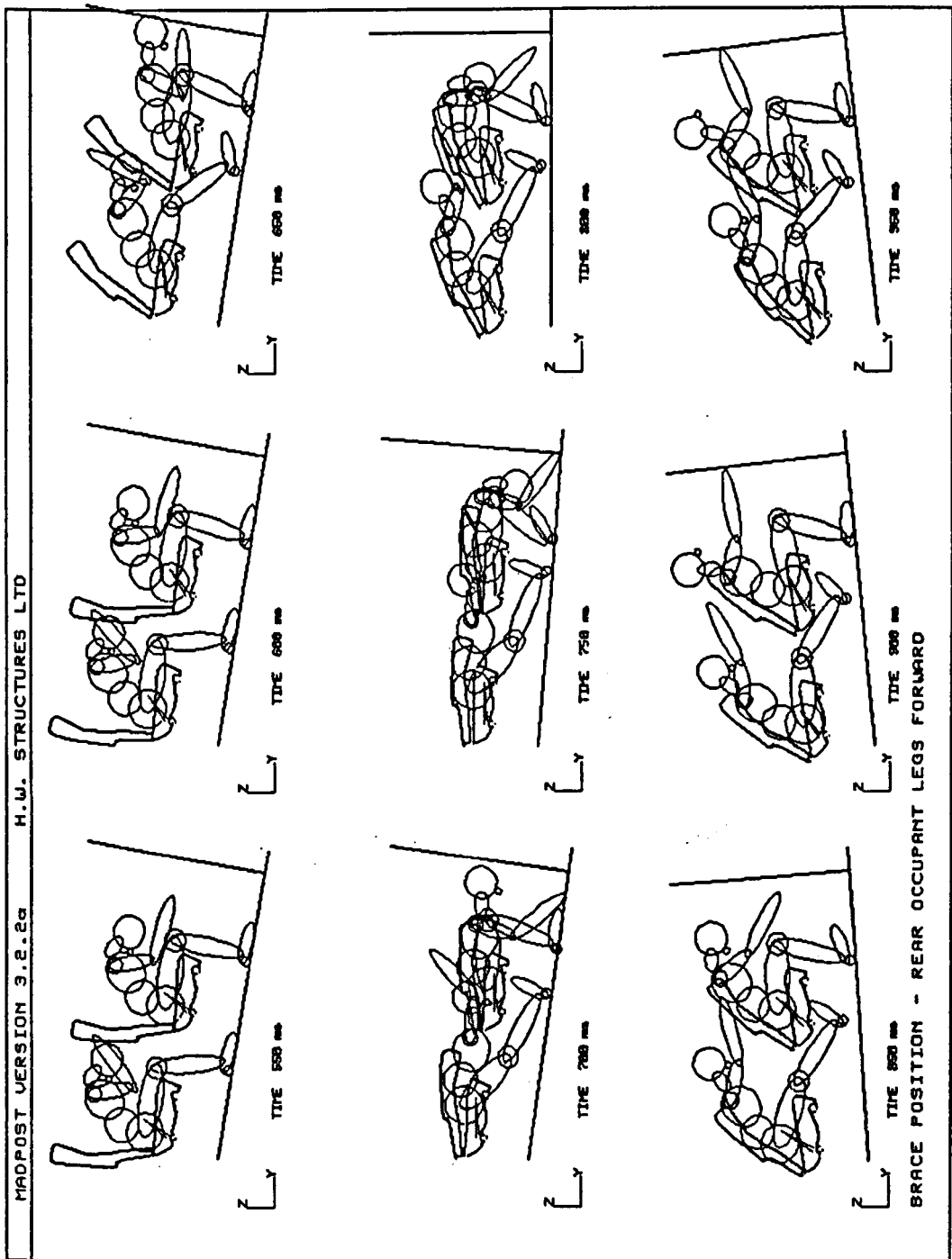


Figure 26. Brace Position Legs Forward Simulation - 550ms to 950ms Sequential Plot

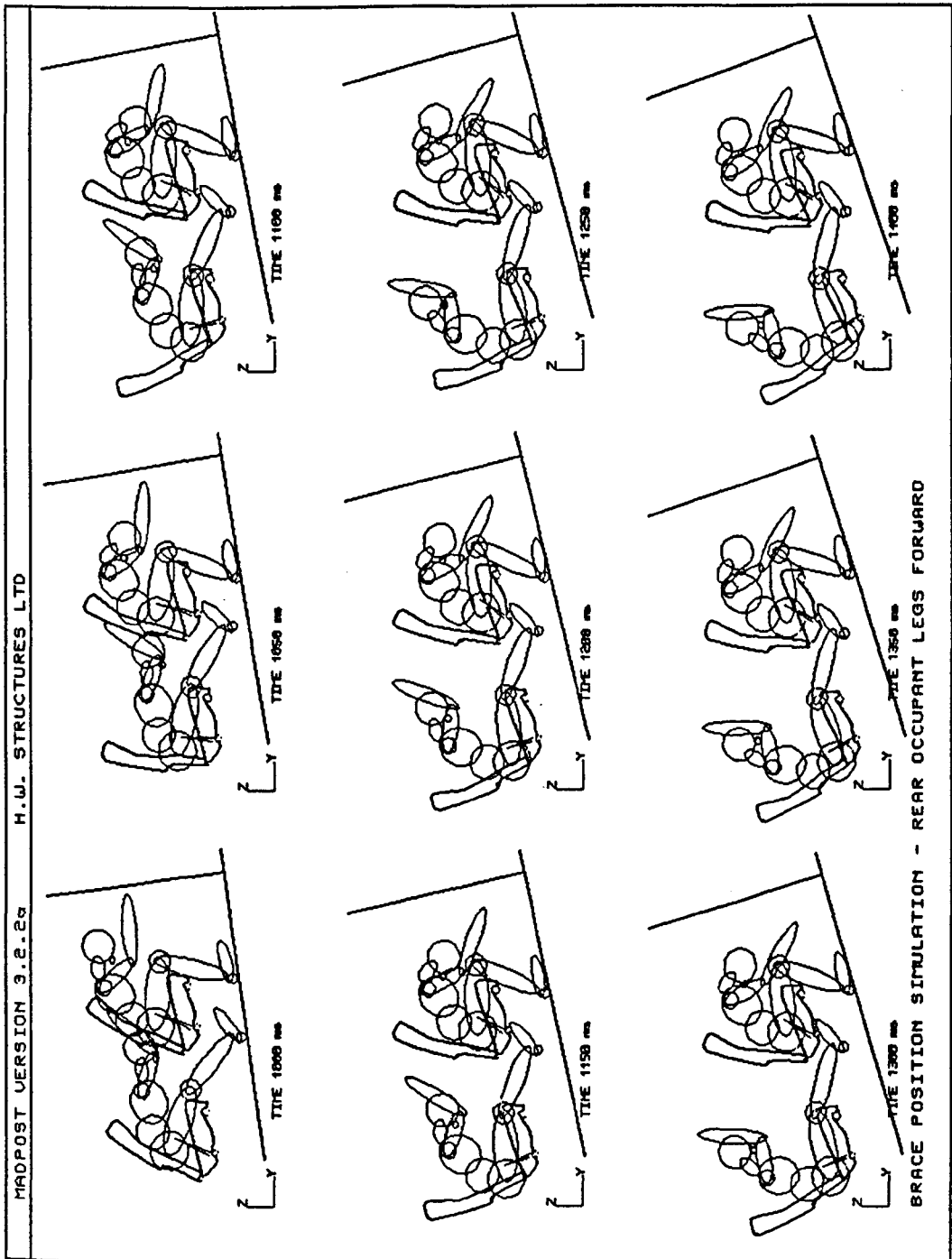


Figure 27. Brace Position Legs Forward Simulation - 1000ms to 1400ms Sequential Plot

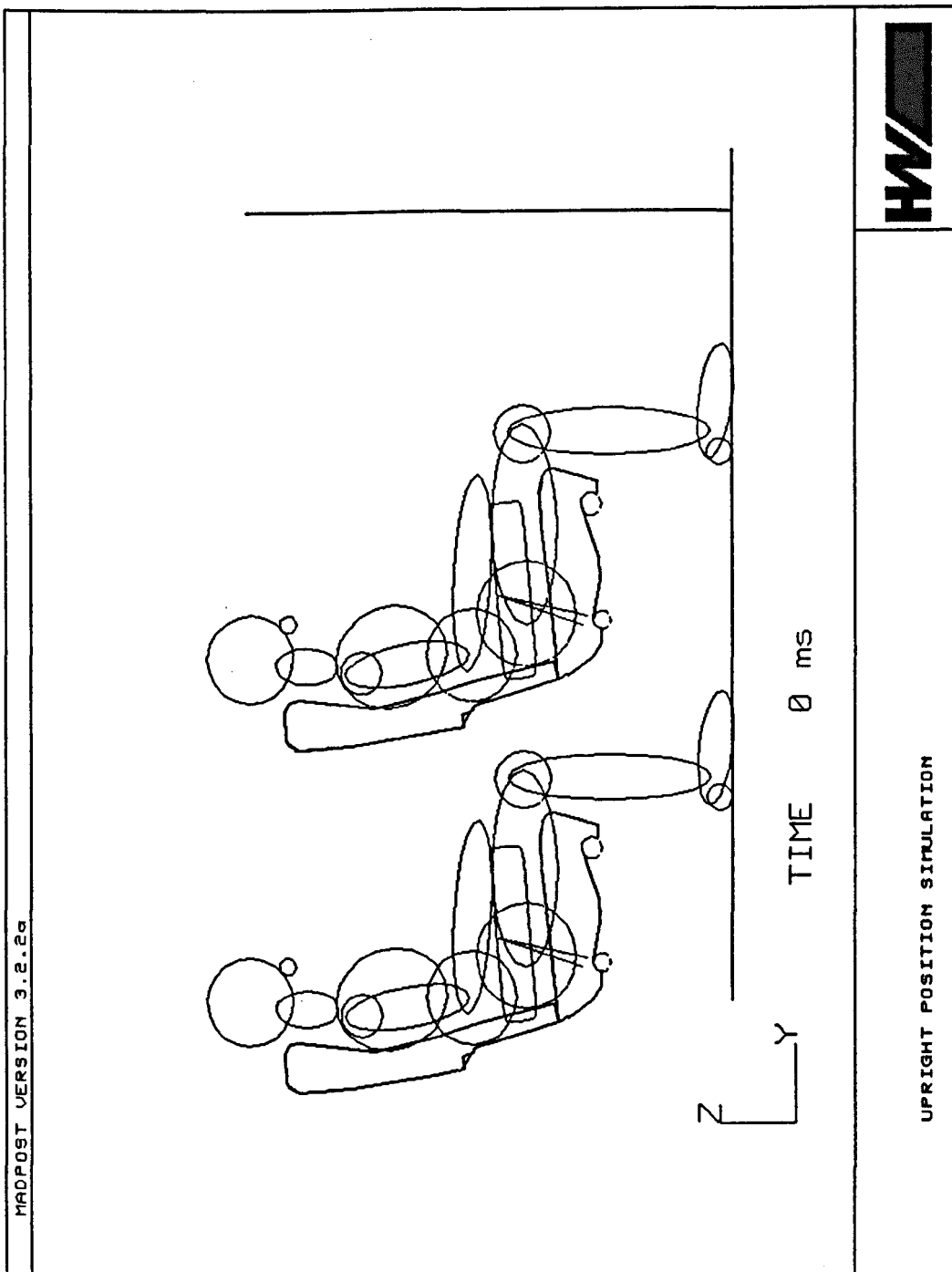


Figure 28. Upright Position Simulation

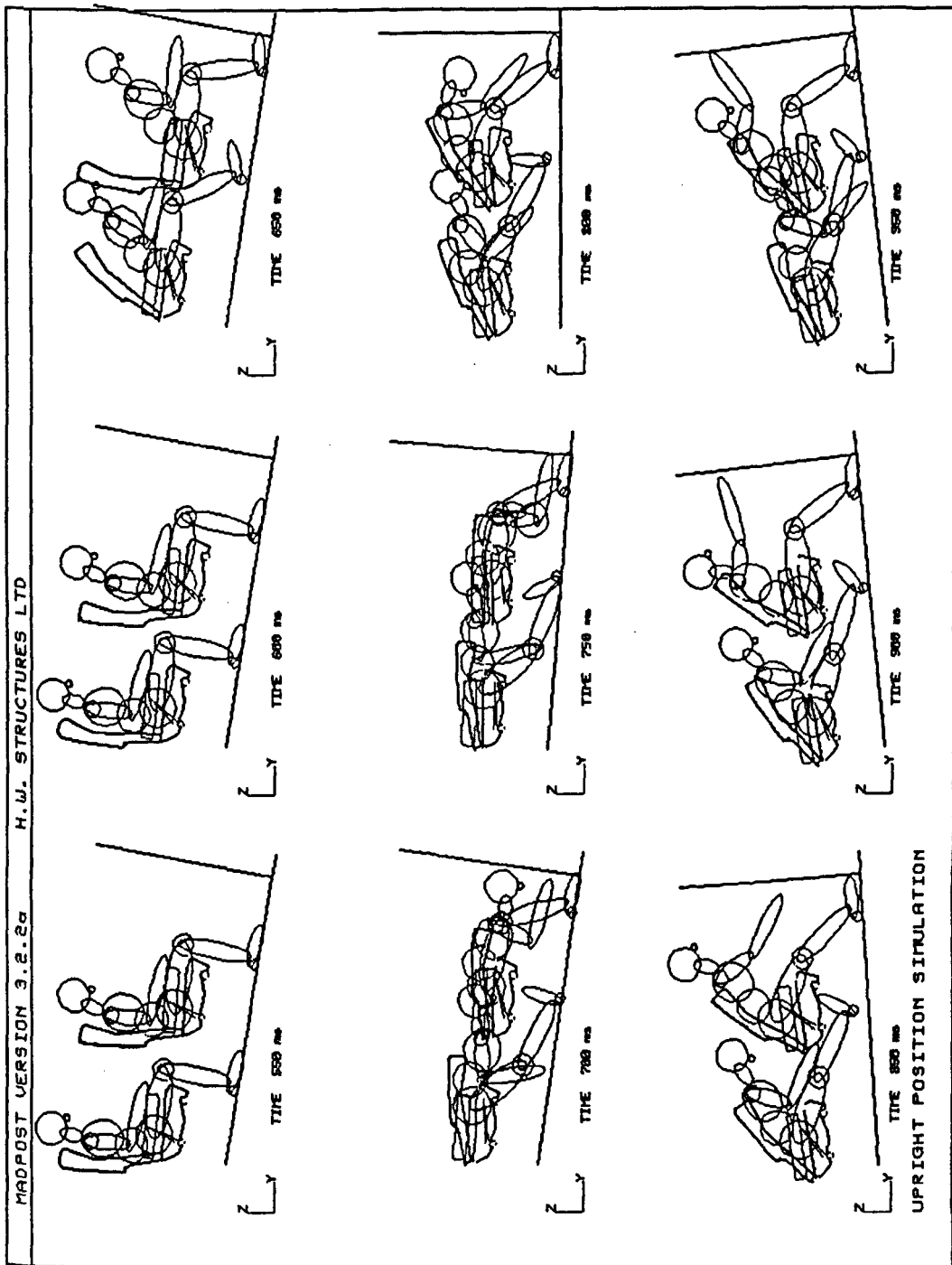


Figure 29. Upright Position Simulation - 550ms to 950ms Sequential Plot

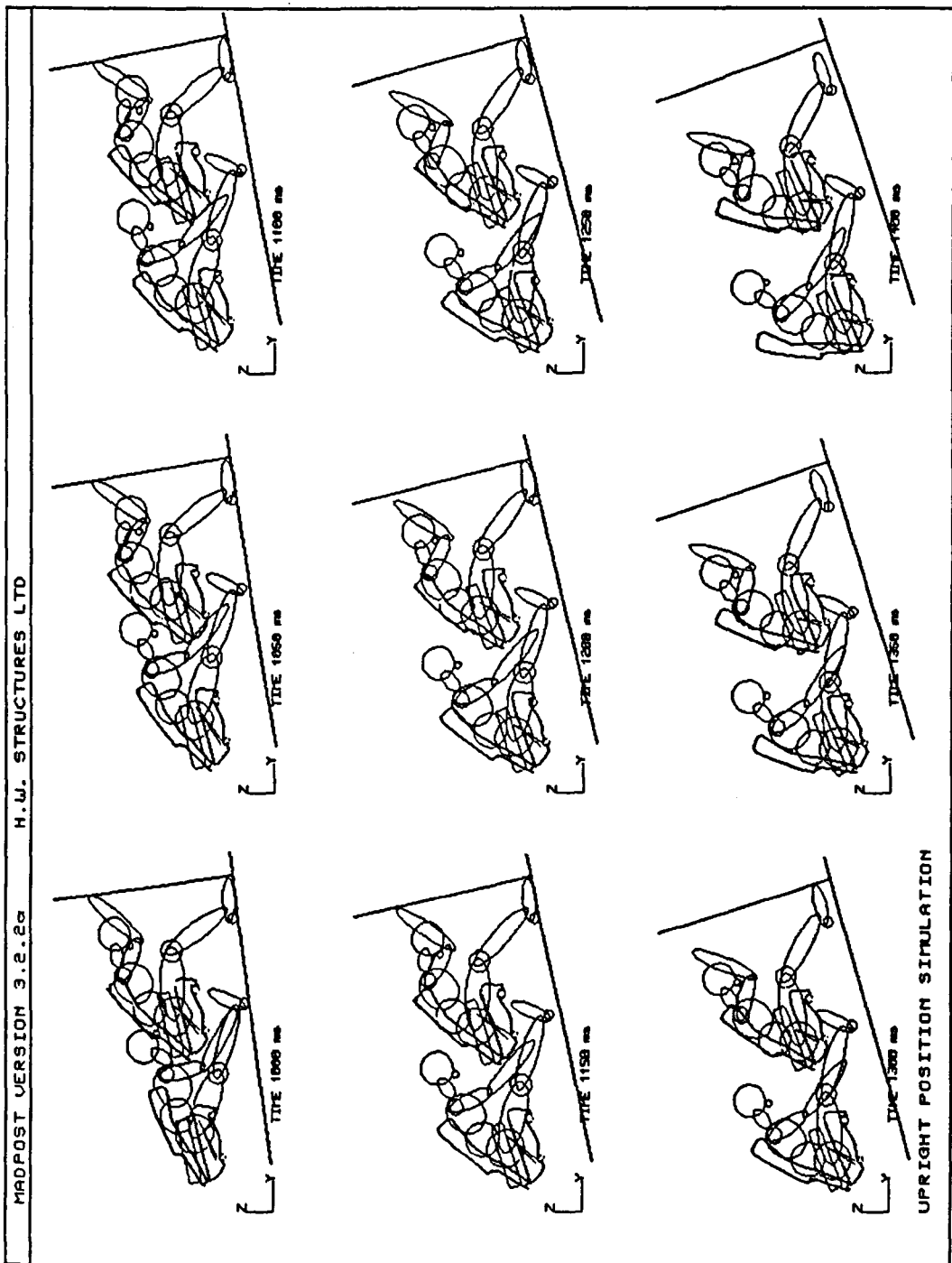


Figure 30. Upright Position Simulation - 1000ms to 1400ms Sequential Plot

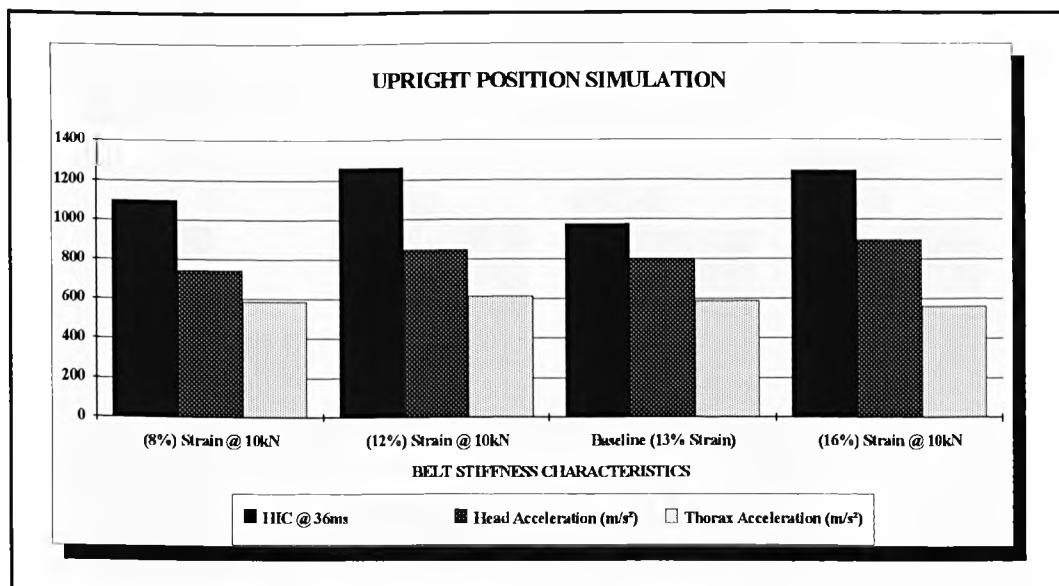


Figure 31. Upright Position - HIC, Head and Thorax Accelerations versus Belt Stiffness

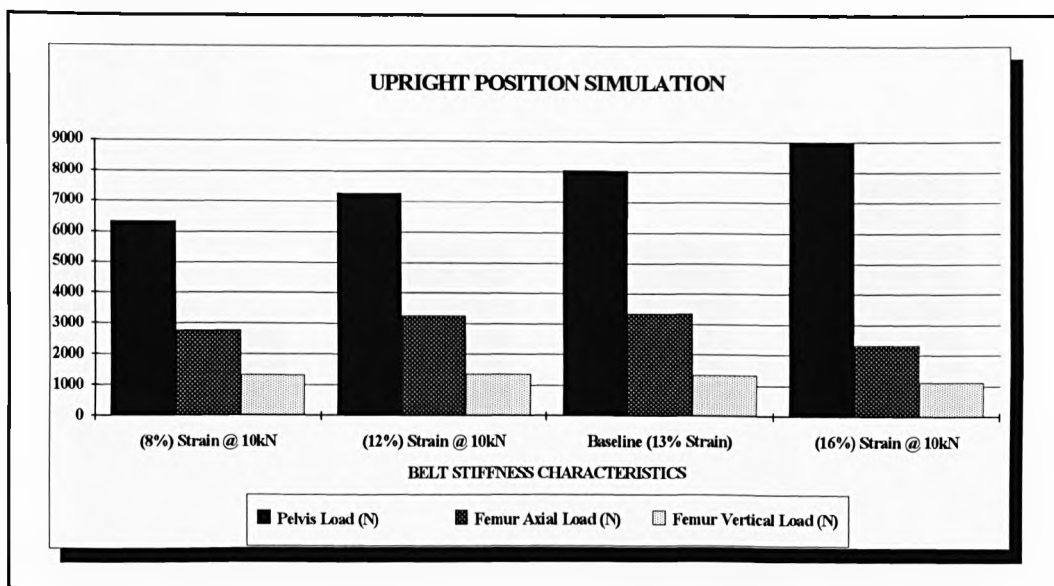


Figure 32. Upright Position - Pelvis, Femur Axial and Vertical Loads versus Belt Stiffness

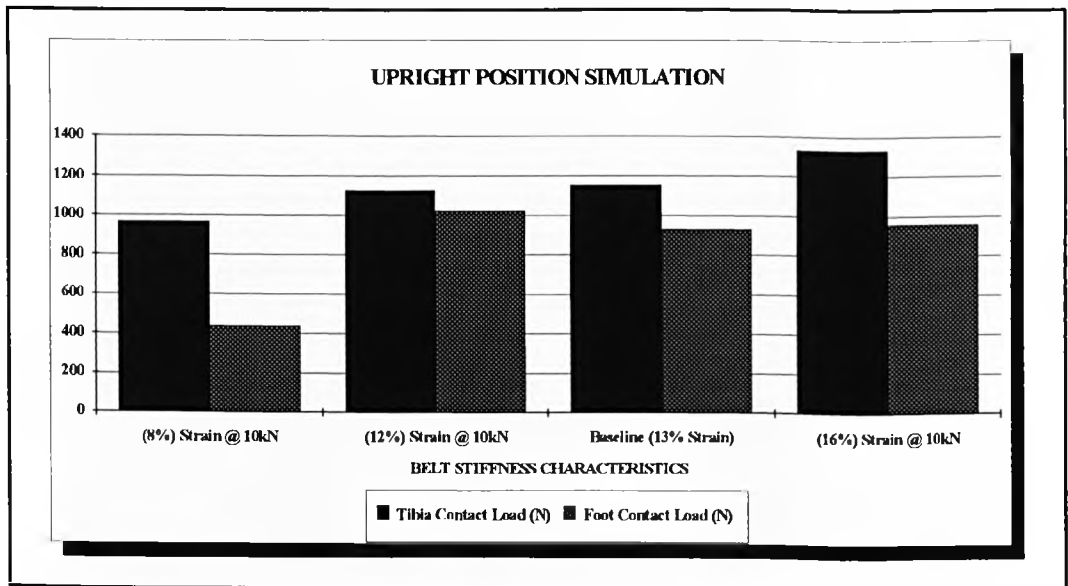


Figure 33. Upright Position - Tibial and Foot Contact Loads versus Belt Stiffness

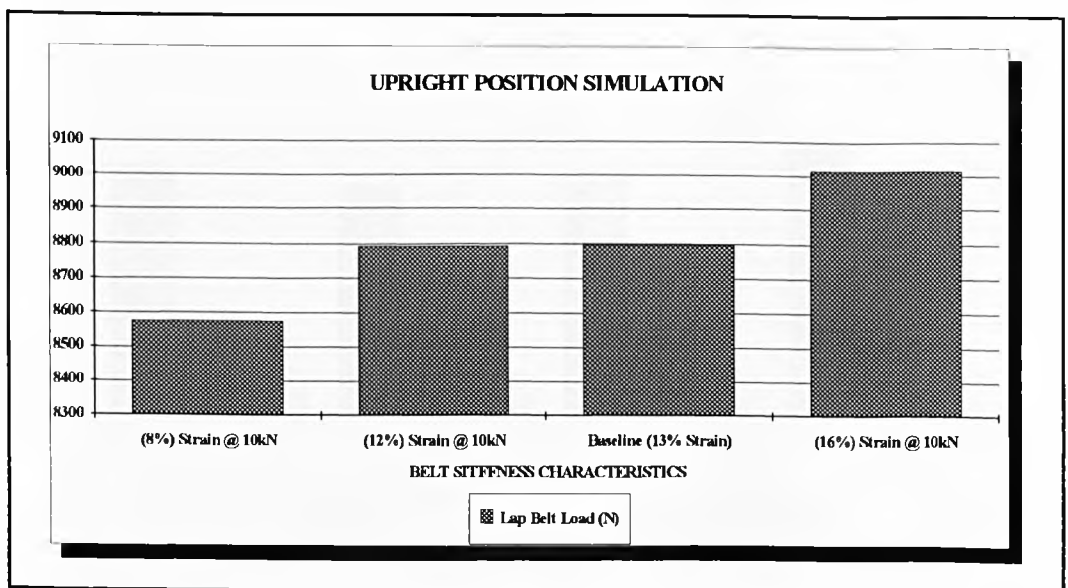


Figure 34. Upright Position - Lap Belt Load Versus Belt Stiffness

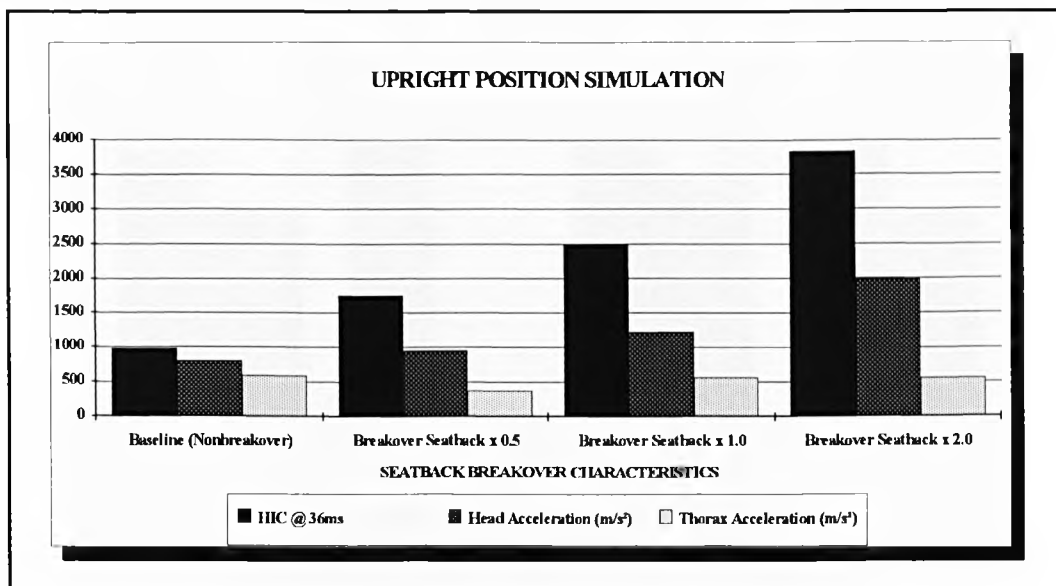


Figure 35. Upright Position - HIC, Head and Thorax Accelerations versus Seatback Breakover Stiffness

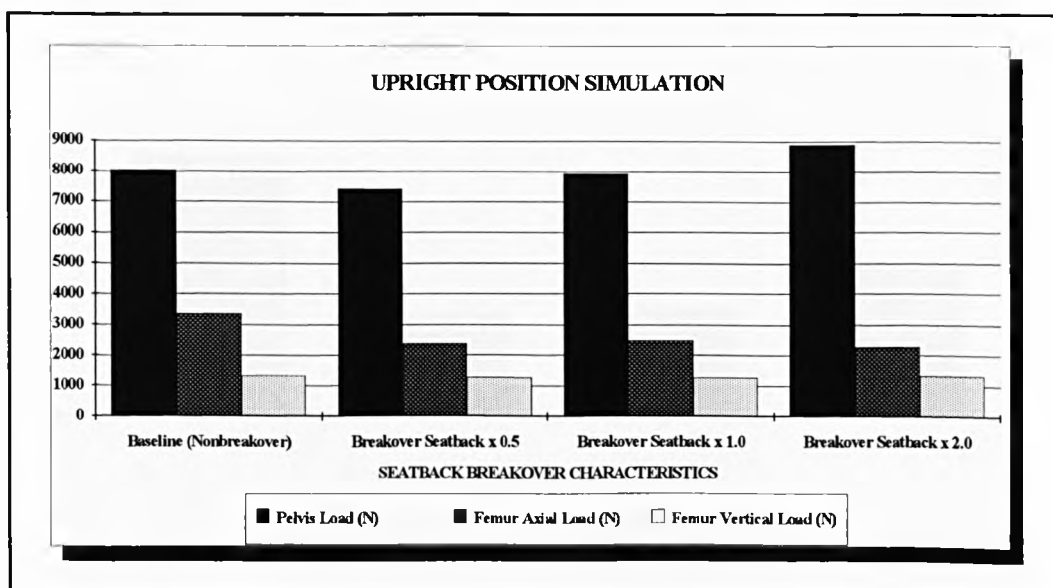


Figure 36. Upright Position - Pelvis, Femur Axial and Vertical Loads versus Seatback Breakover Stiffness

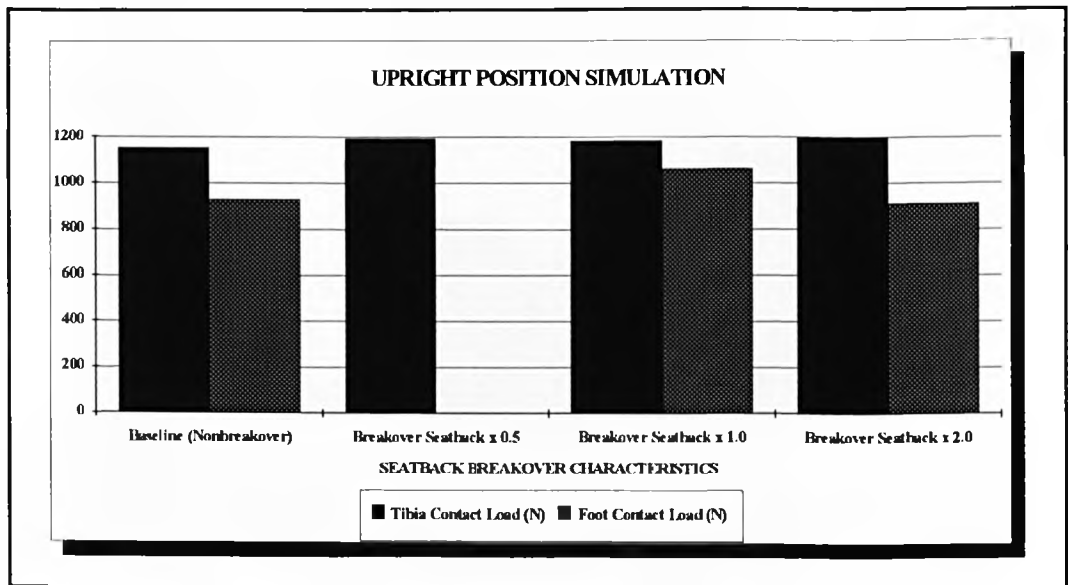


Figure 37. Upright Position - Tibial and Foot Contact Loads versus Seatback Breakover Stiffness

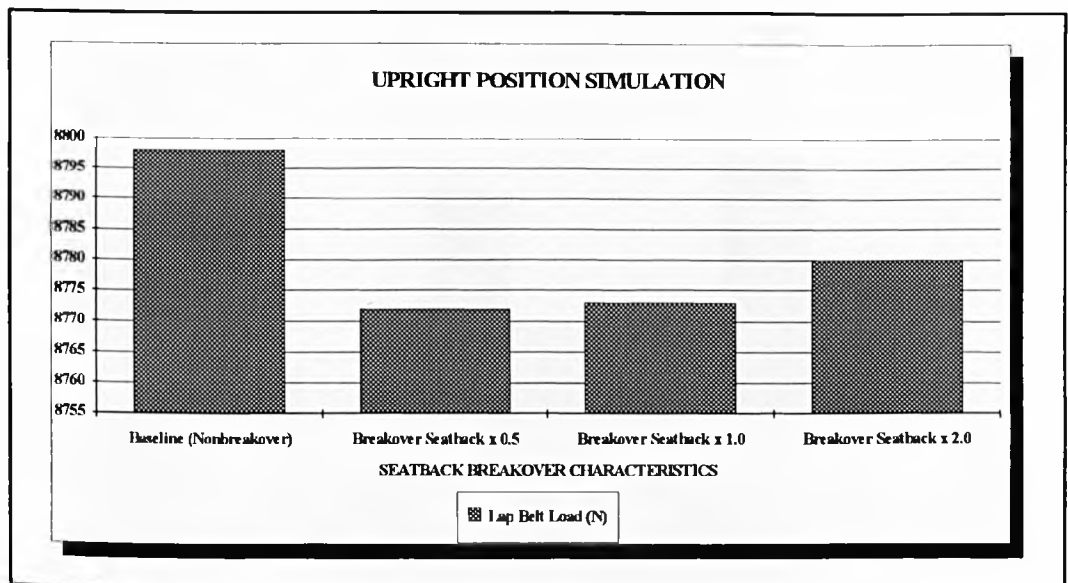


Figure 38. Upright Position - Lap Belt Load versus Seatback Breakover Stiffness

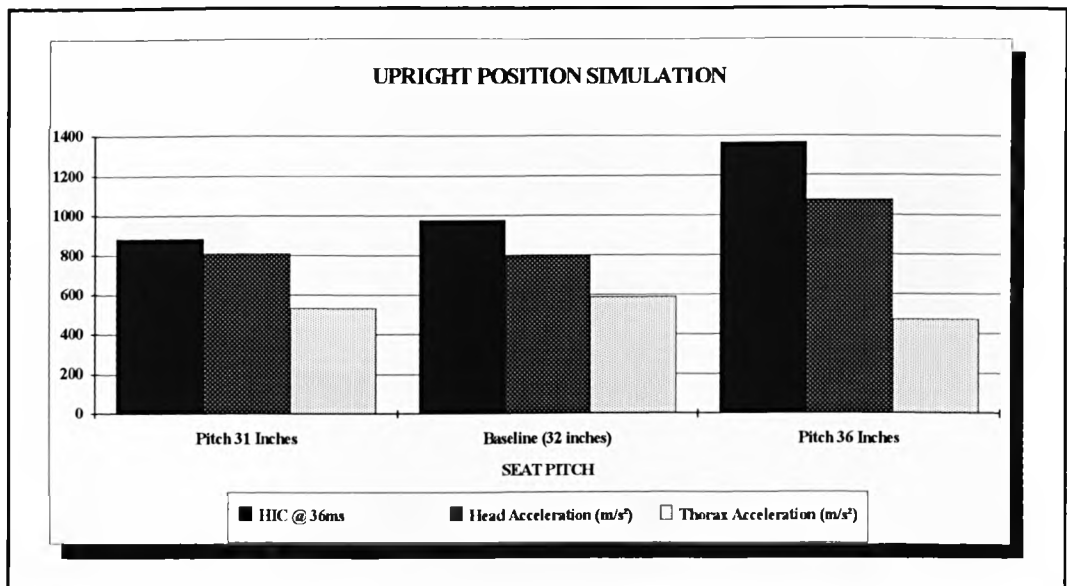


Figure 39. Upright Position - HIC, Head and Thorax Accelerations versus Seat Pitch

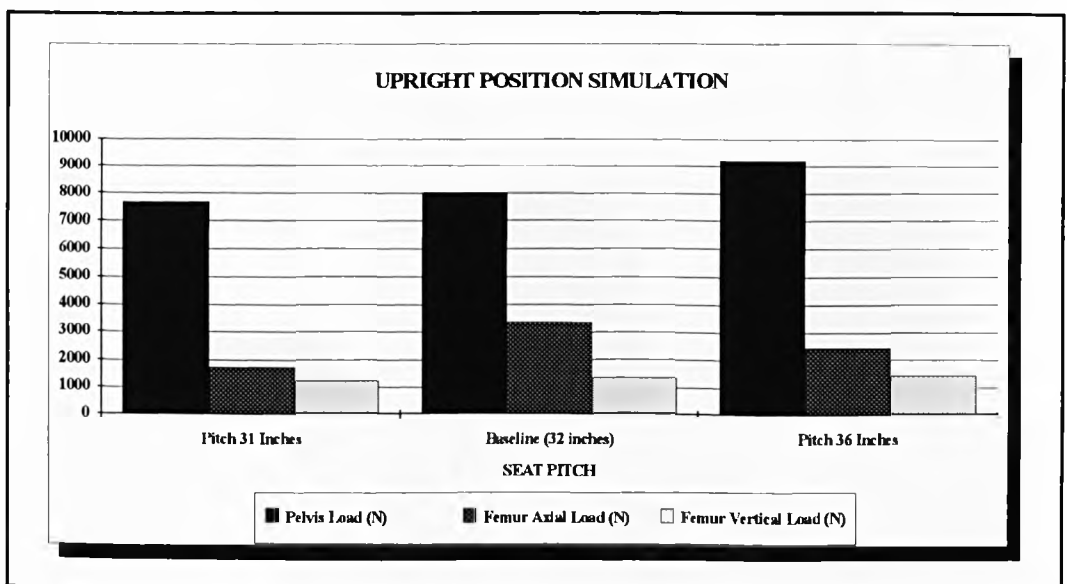


Figure 40. Upright Position - Pelvis, Femur Axial and Vertical Loads versus Seat Pitch

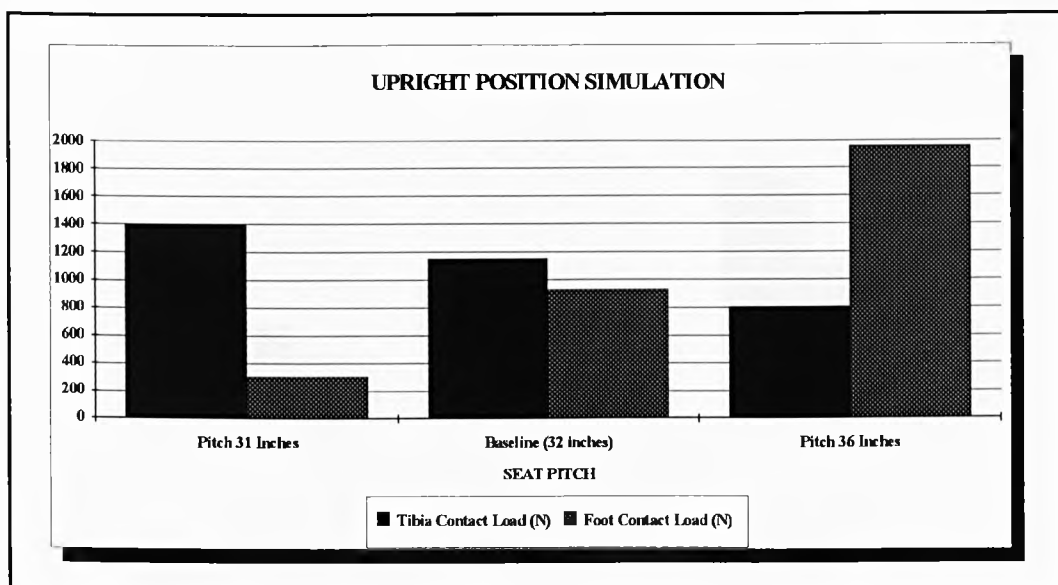


Figure 41. Upright Position - Tibia and Foot Contact Loads versus Seat Pitch

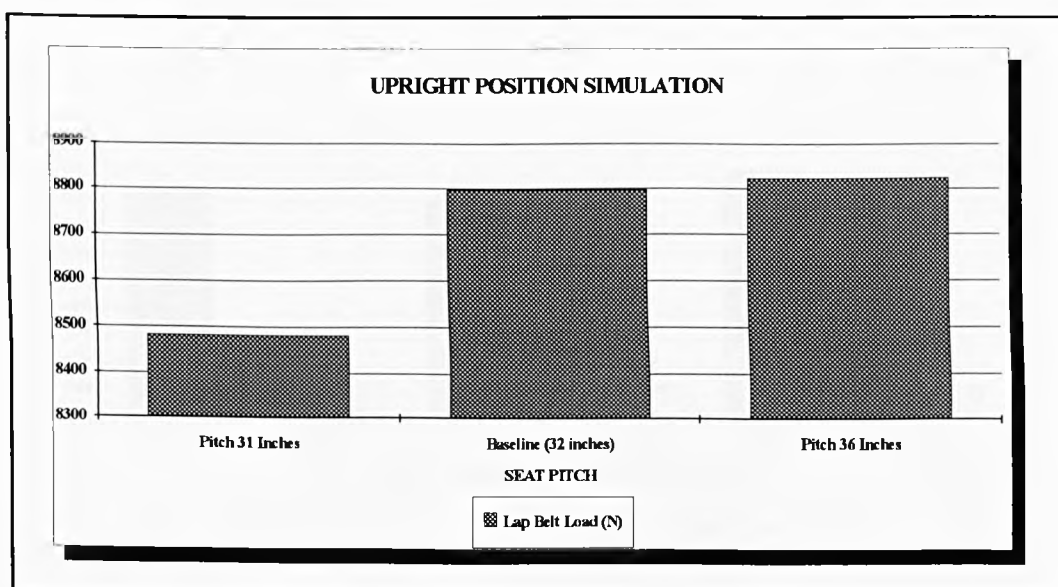


Figure 42. Upright Position - Lap Belt Load versus Seat Pitch

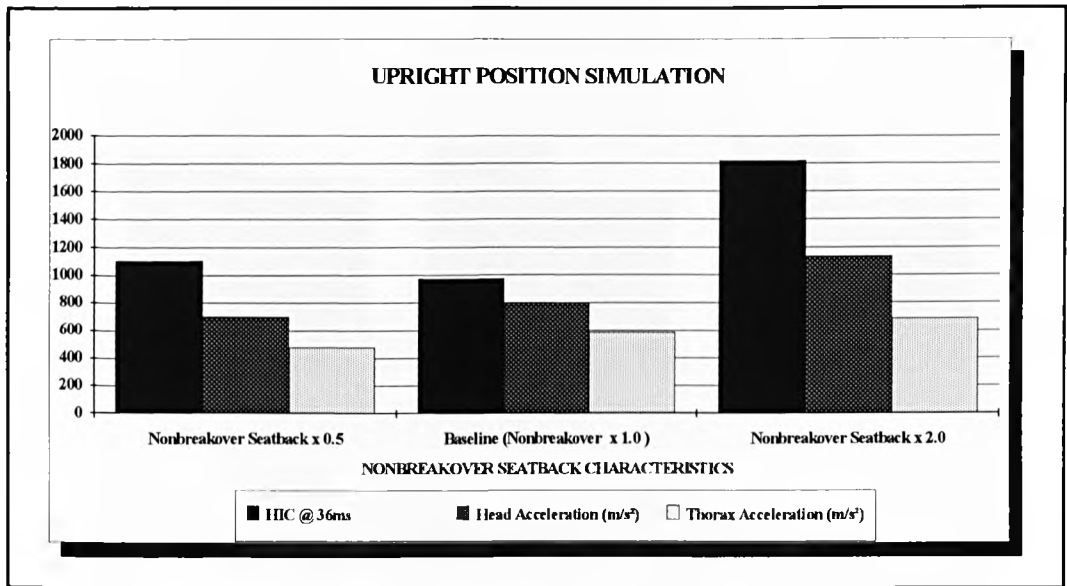


Figure 43. Upright Position - HIC, Head and Thorax Accelerations versus Nonbreakover Seatback Stiffness

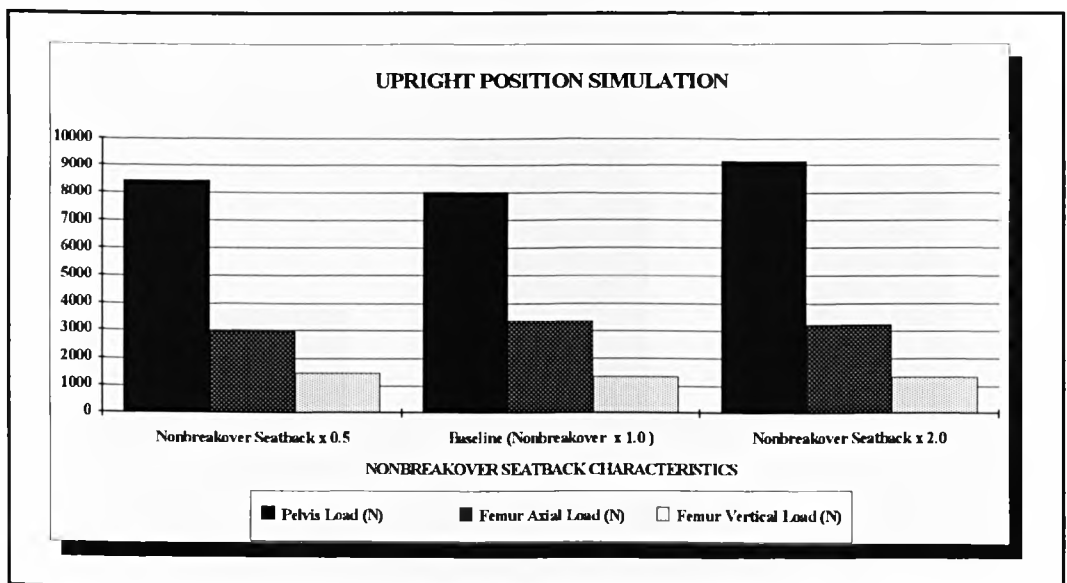


Figure 44. Upright Position - Pelvis, Femur Axial and Vertical Loads versus Nonbreakover Seatback Stiffness

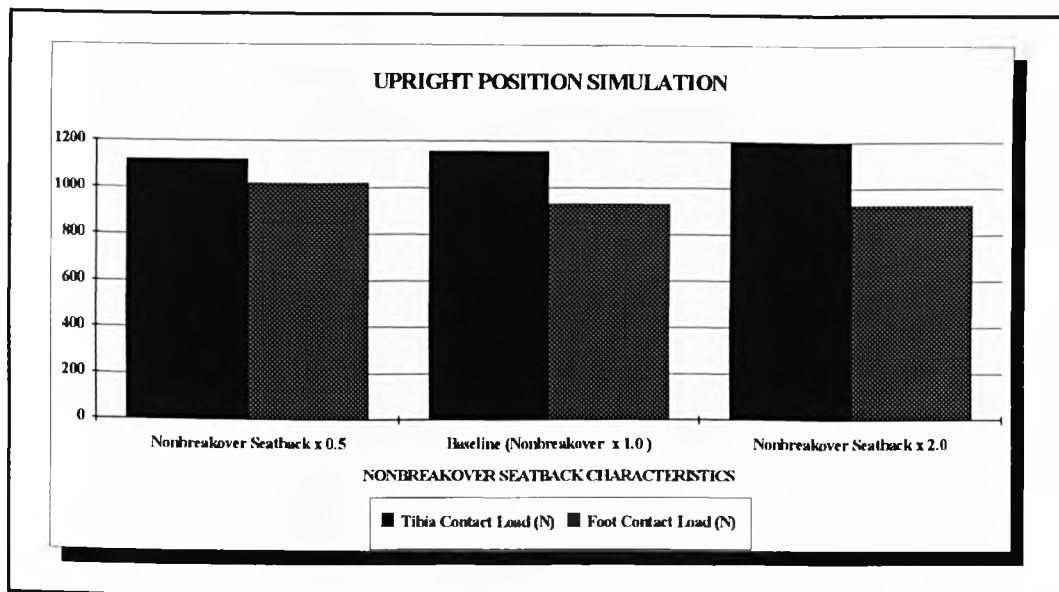


Figure 45. Upright Position - Tibia and Foot Contact loads versus Nonbreakover Seatback Stiffness

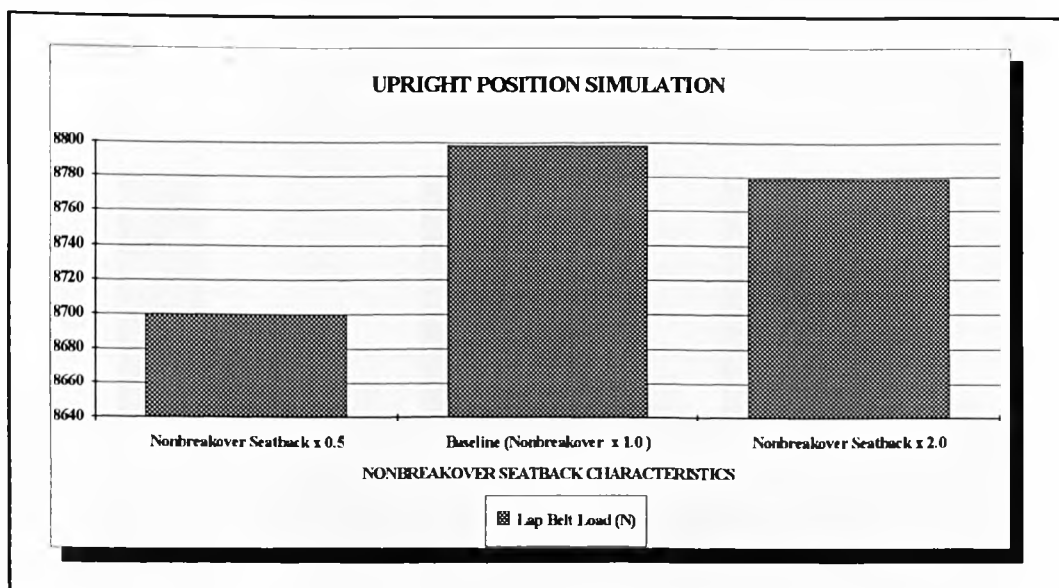


Figure 46. Upright Position - Lap Belt Load versus Nonbreakover Seatback Stiffness

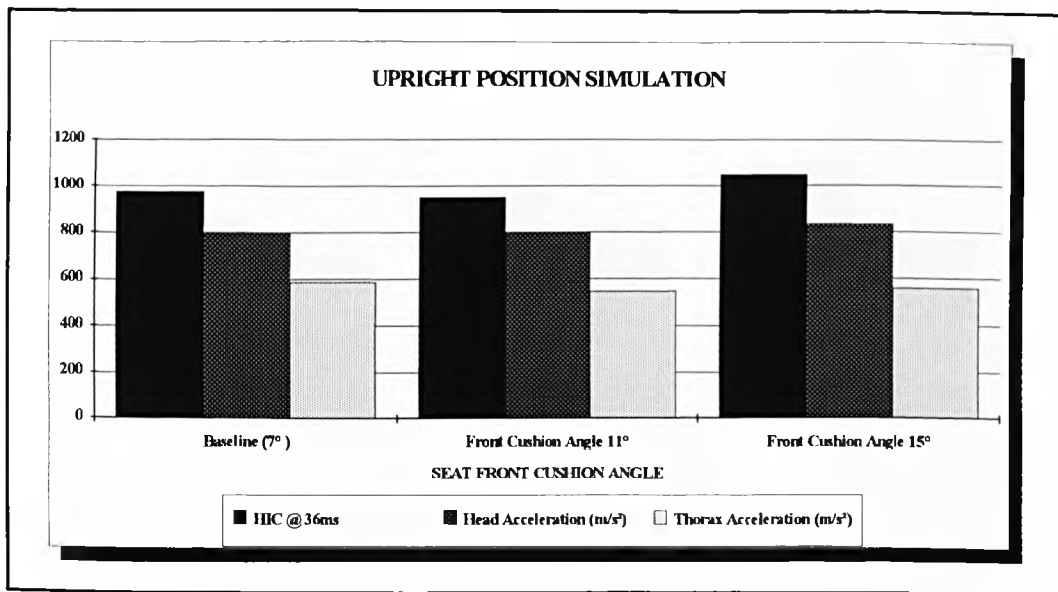


Figure 47. Upright Position - HIC, Head and Thorax Accelerations versus Seat Front Cushion Angle

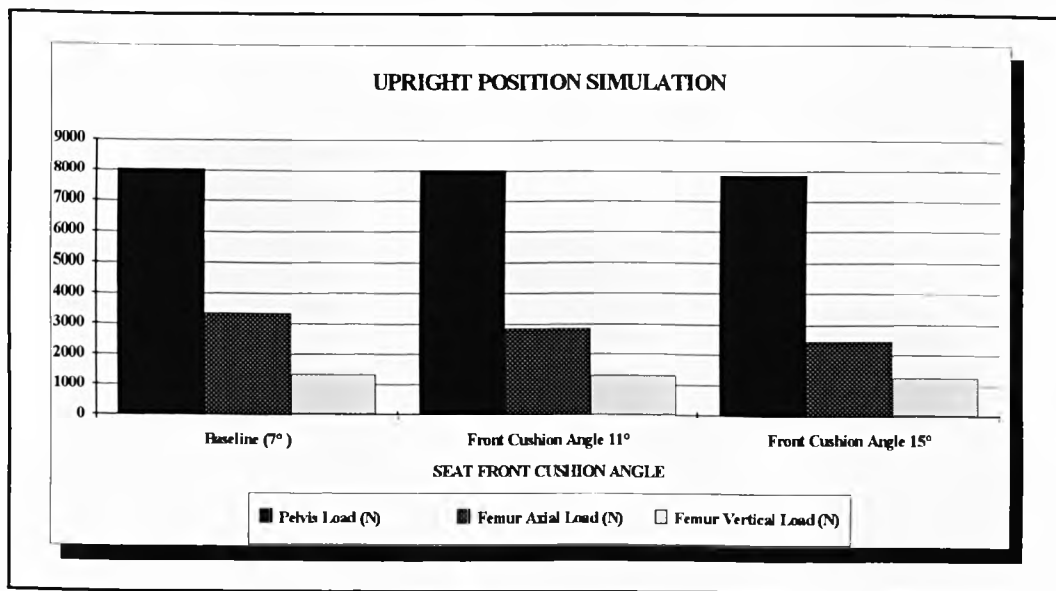


Figure 48. Upright Position - Pelvis, Femur Axial and Vertical Loads versus Seat Front Cushion Angle

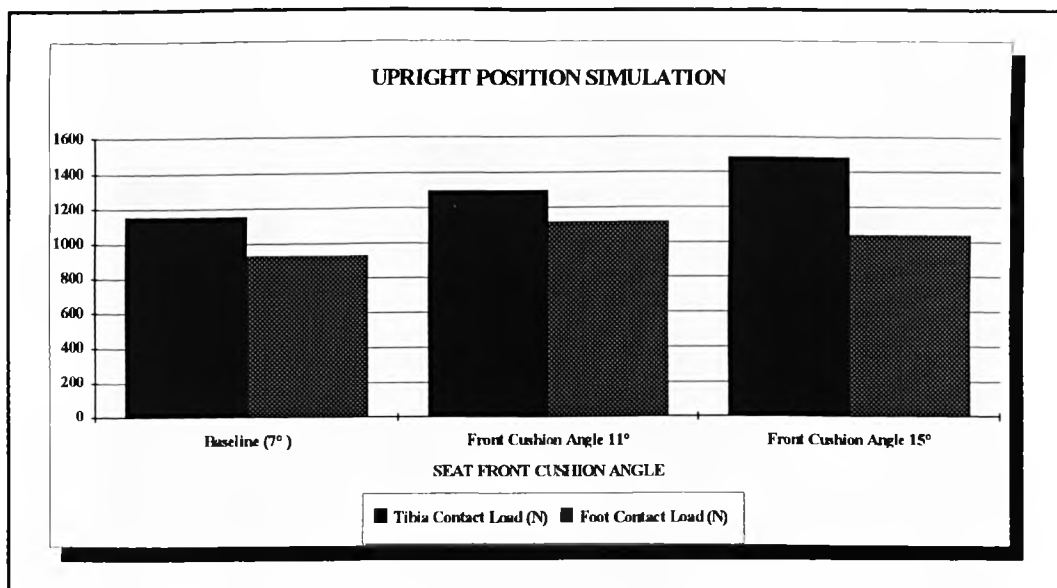


Figure 49. Upright Position - Tibia and Foot Contact Loads versus Seat Front Cushion Angle

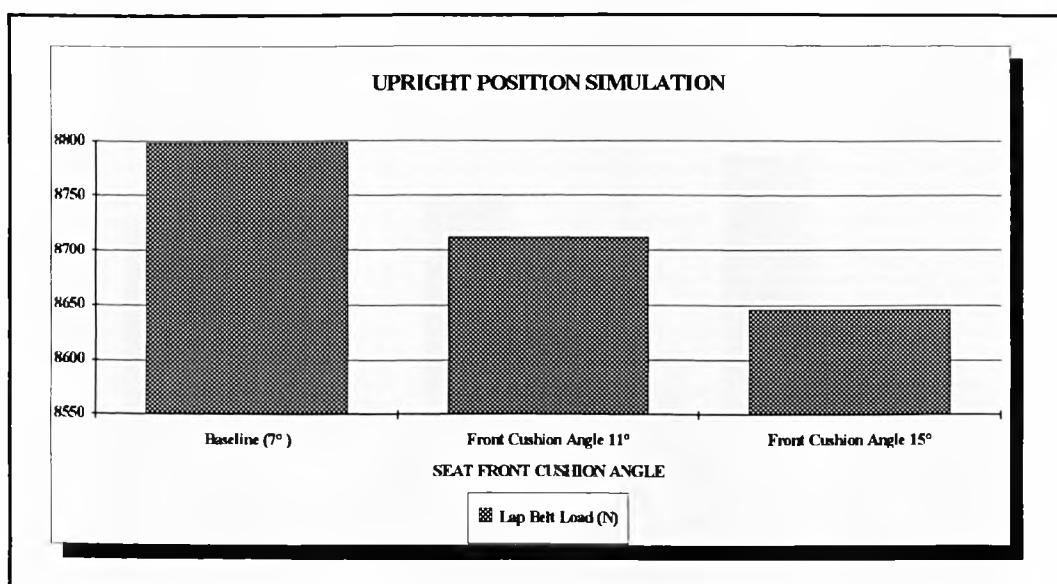


Figure 50. Upright Position - Lap Belt Load versus Seat Front Cushion Angle

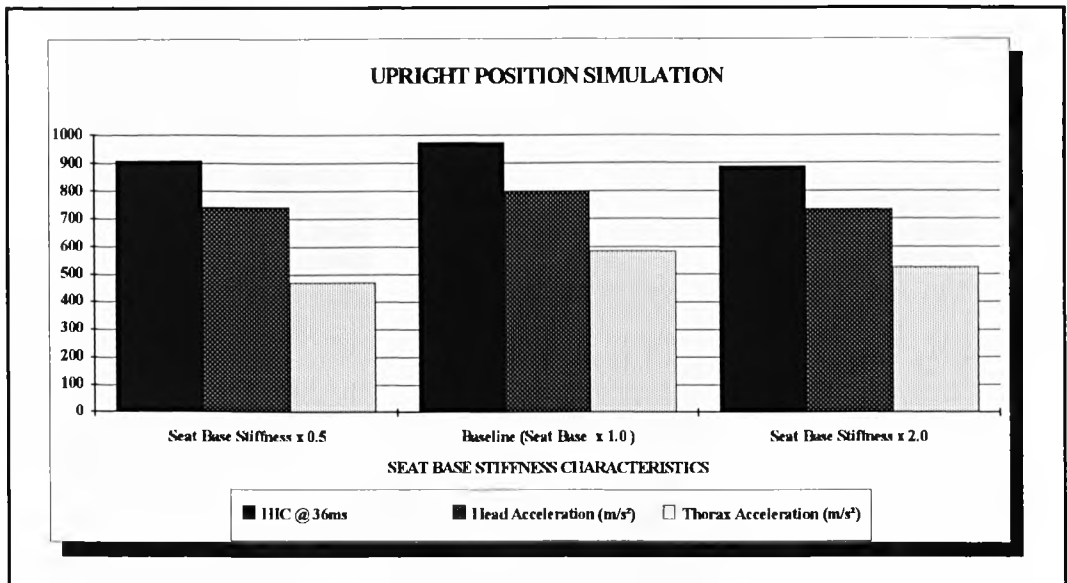


Figure 51. Upright Position - HIC, Head and Thorax Acceleration versus Seat Base Stiffness

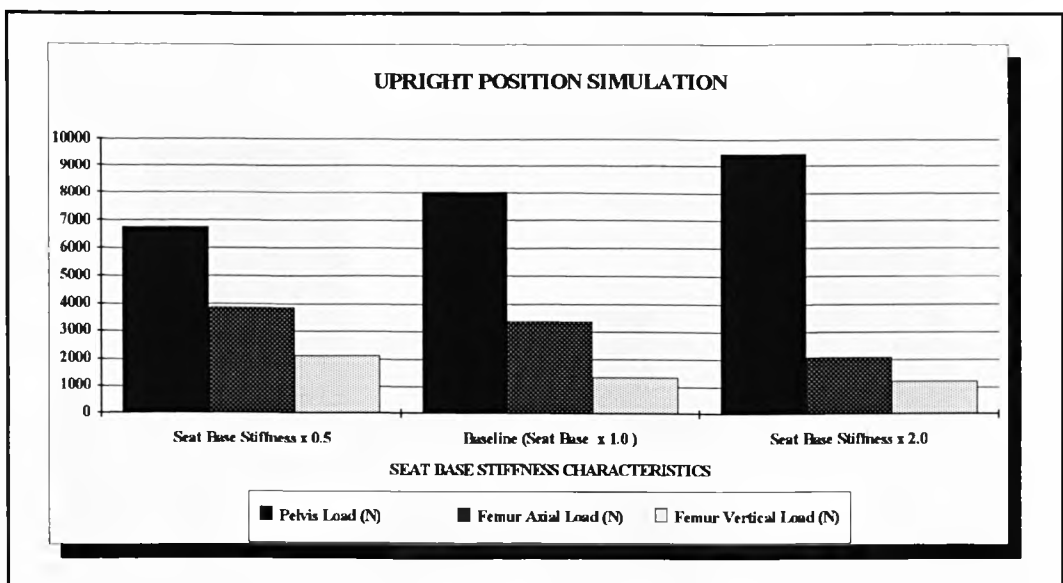


Figure 52. Upright Position - Pelvis, Femur Axial and Vertical Loads versus Seat Base Stiffness

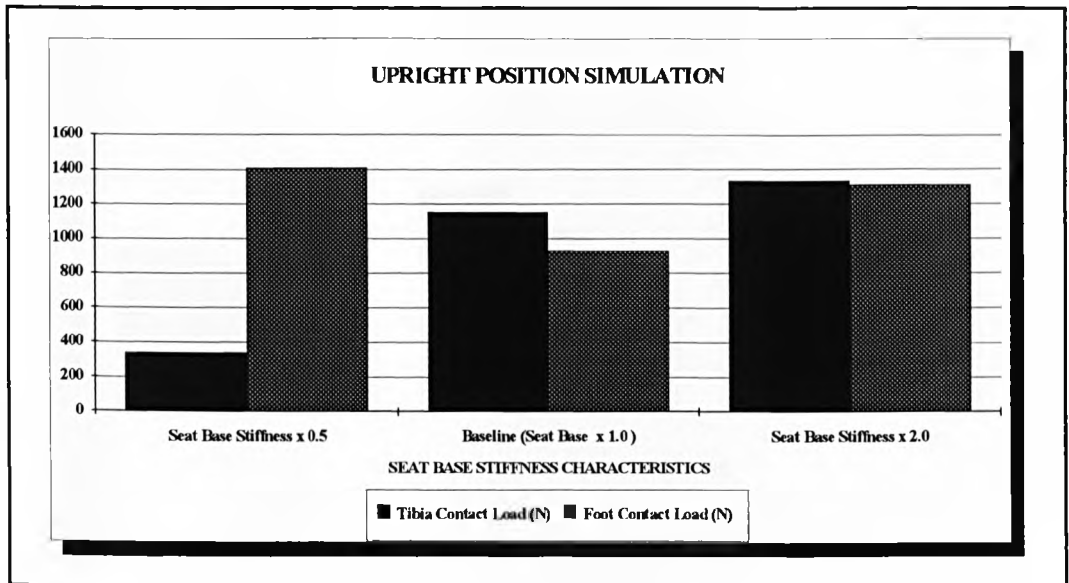


Figure 53. Upright Position - Tibia and Foot Contact Loads versus Seat Base Stiffness

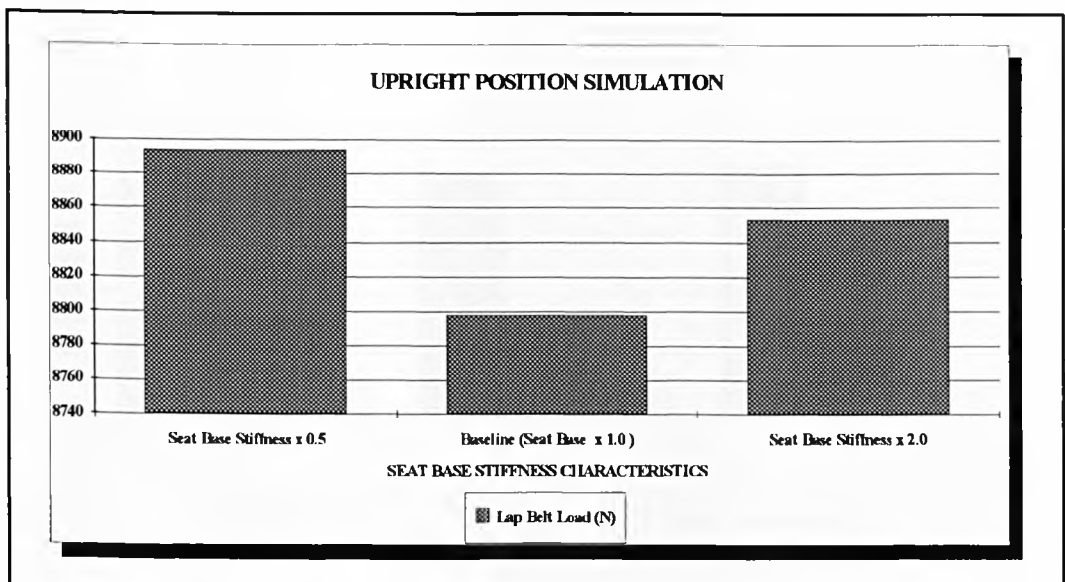


Figure 54. Upright Position - Lap Belt Load versus Seat Base Stiffness

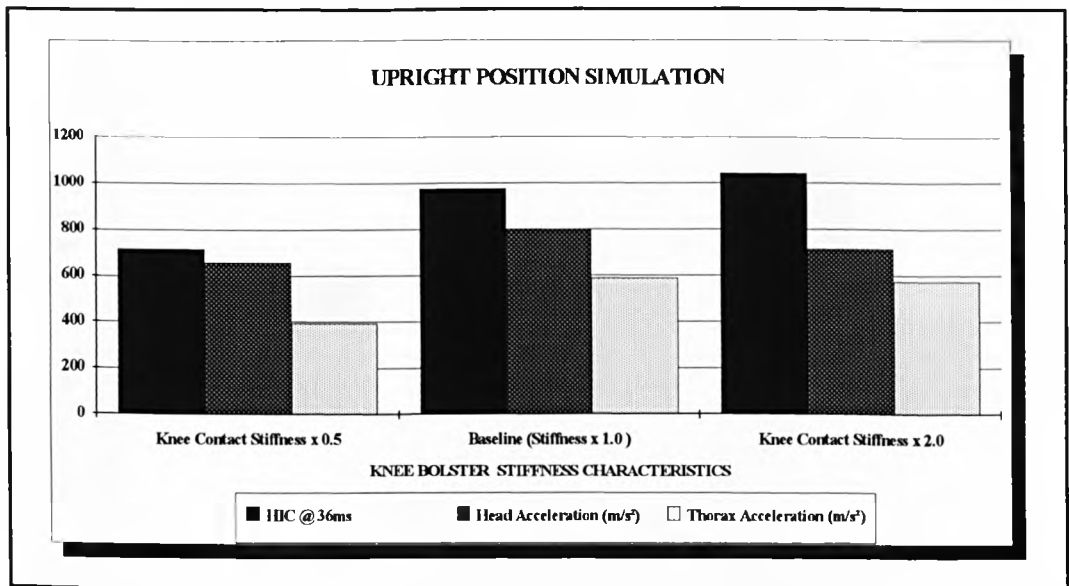


Figure 55. Upright Position - HIC, Head and Thorax Acceleration versus Knee Bolster Stiffness

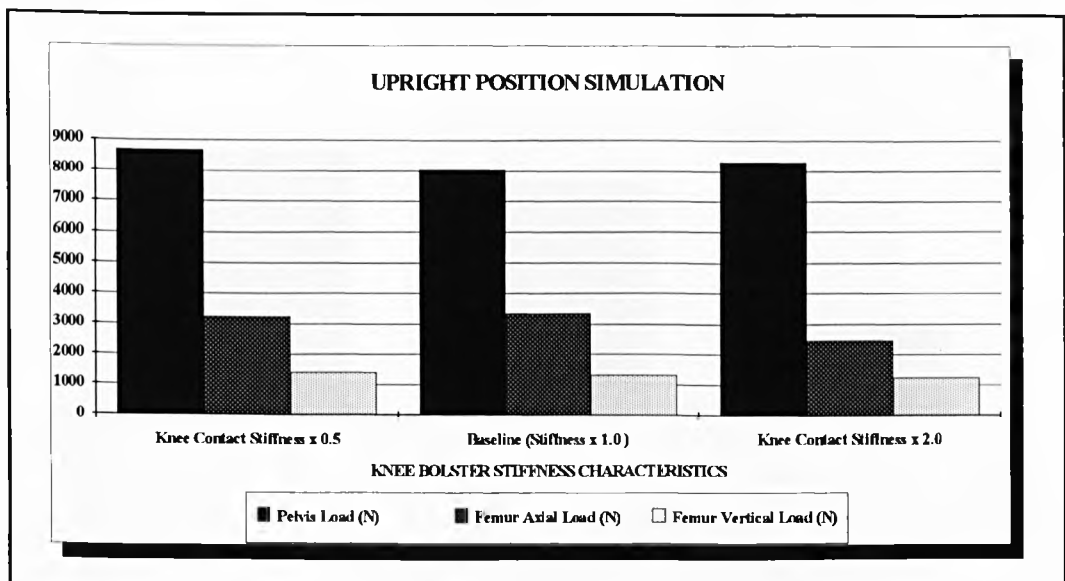


Figure 56. Upright Position - Pelvis, Femur Axial and Vertical Loads versus Knee Bolster Stiffness

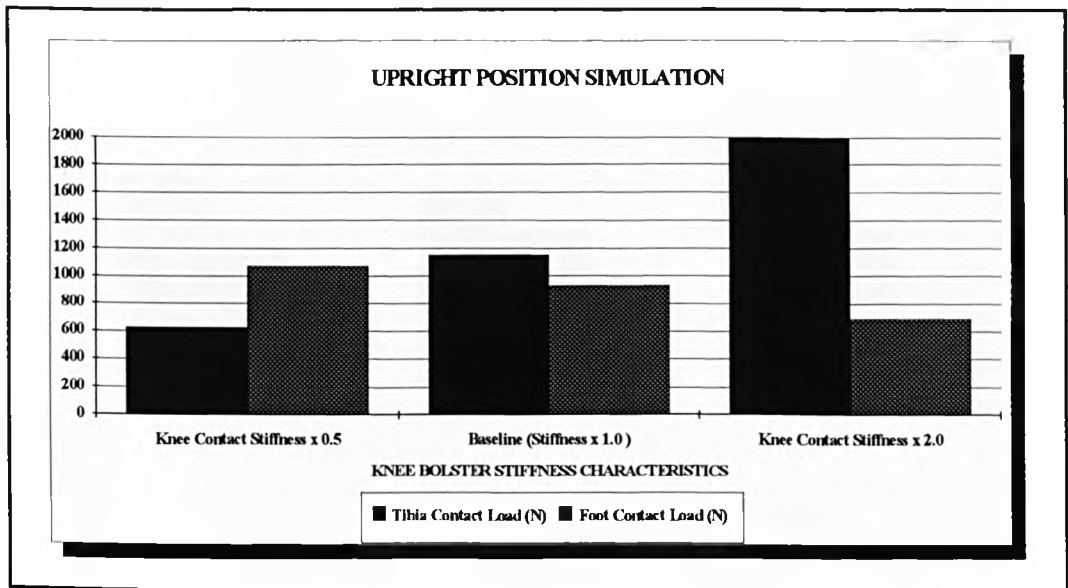


Figure 57. Upright Position - Tibia and Foot Contact Loads versus Knee Bolster Stiffness

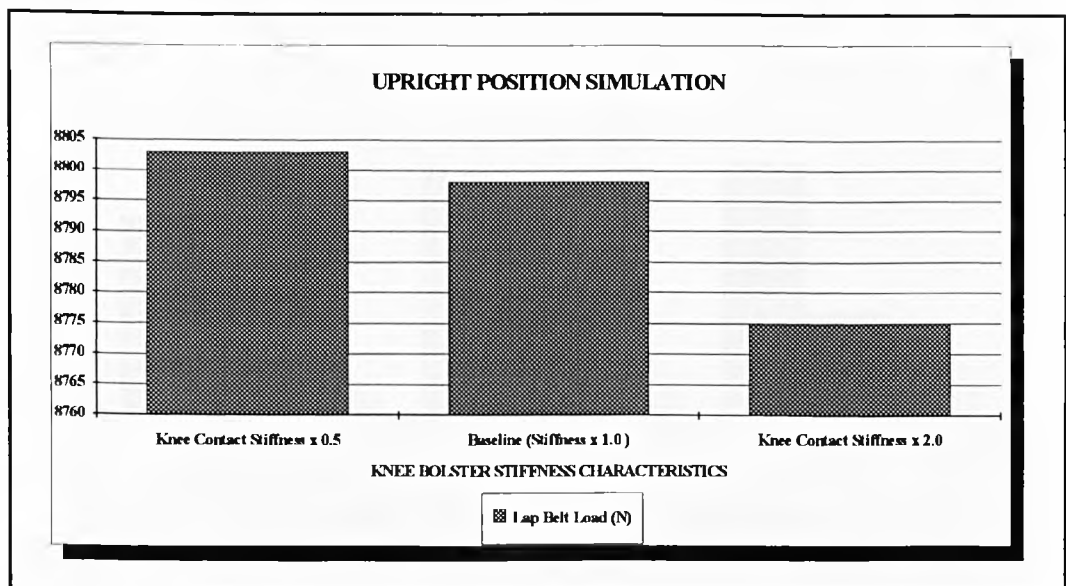


Figure 58. Upright Position - Lap Belt Load versus Knee Bolster Stiffness

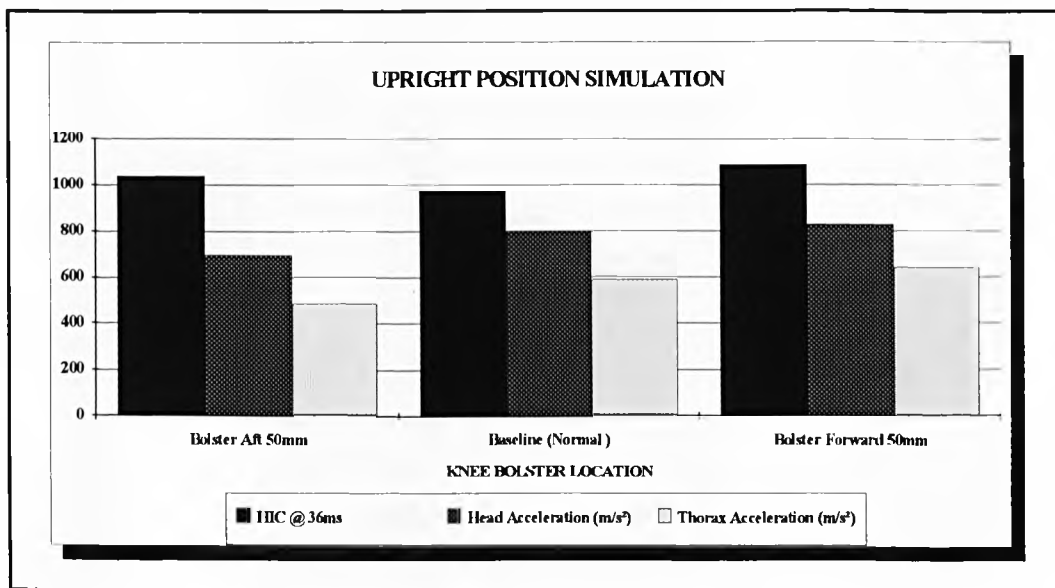


Figure 59. Upright Position - HIC, Head and Thorax Accelerations versus Knee Bolster Location

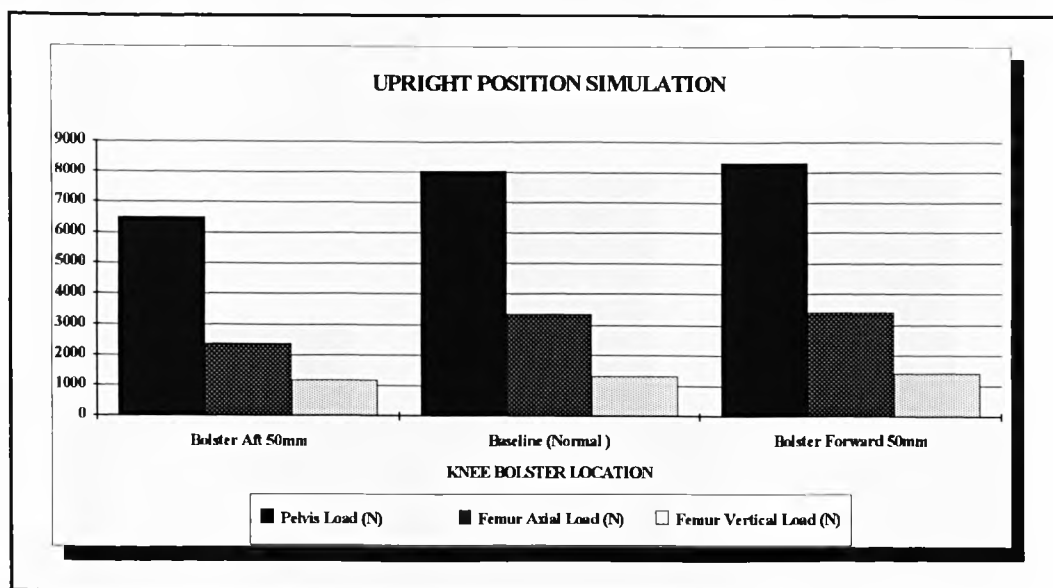


Figure 60. Upright Position - Pelvis, Femur Axial and Vertical Loads versus Knee Bolster Location

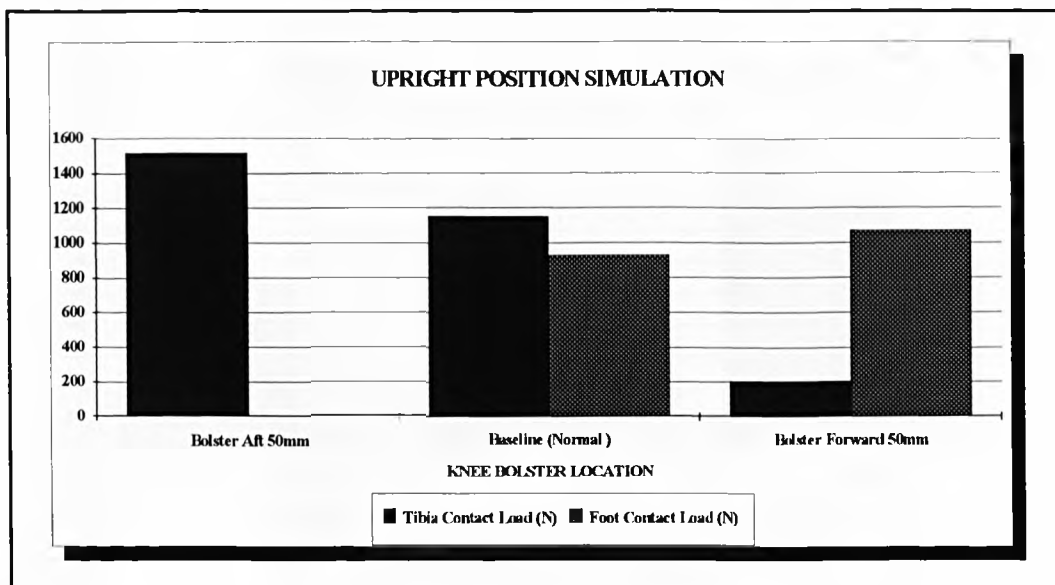


Figure 61. Upright Position - Tibia and Foot Contact Loads versus Knee Bolster Location

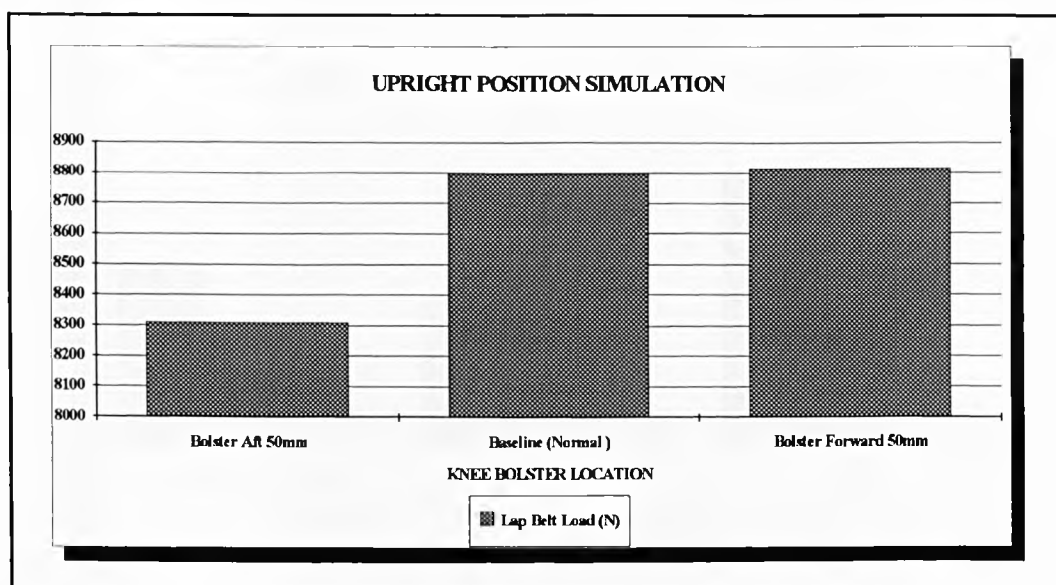


Figure 62. Upright Position - Lap Belt Load versus Knee Bolster Location

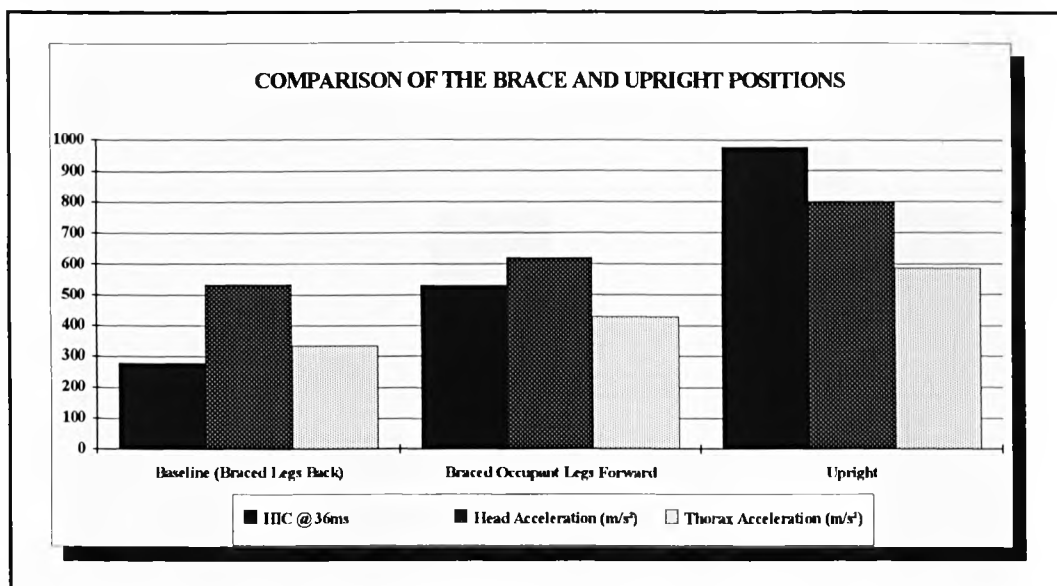


Figure 63. Comparison of the Brace and Upright Positions - HIC, Head and Thorax Accelerations versus Posture

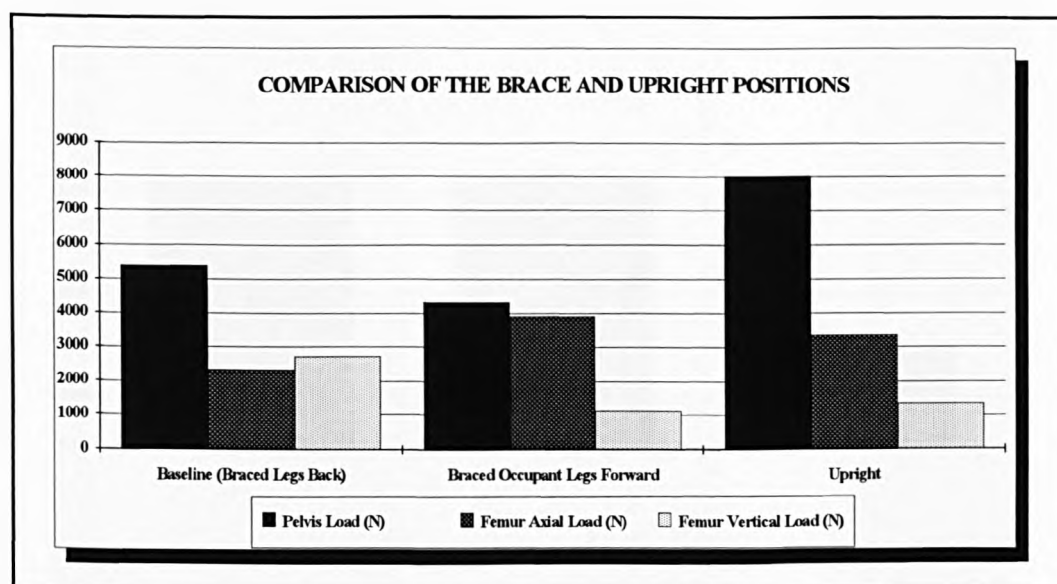


Figure 64. Comparison of the Brace and Upright Positions - Pelvis, Femur Axial and Vertical Loads versus Posture

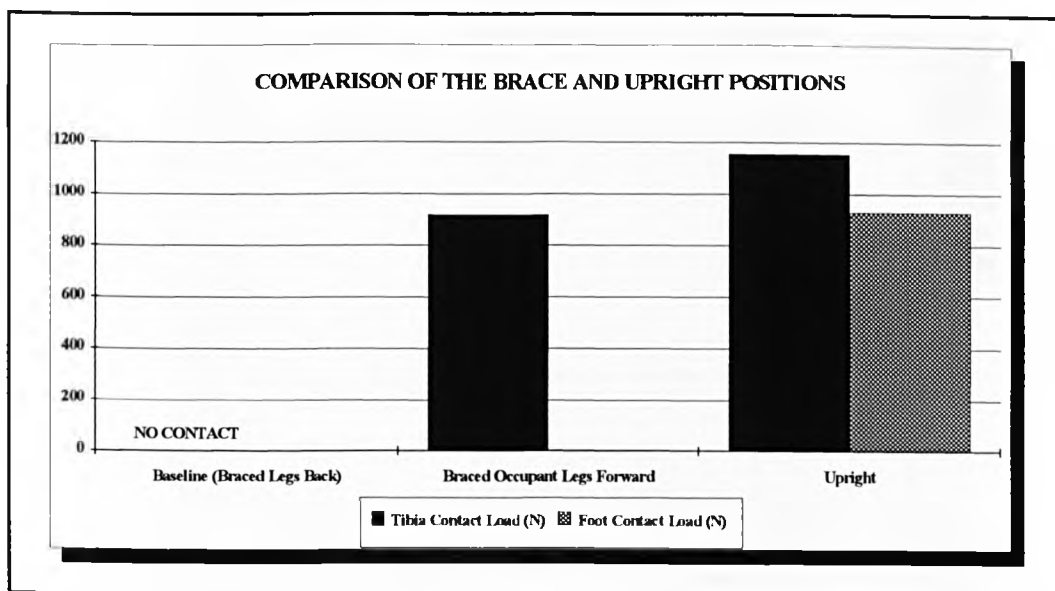


Figure 65. Comparison of the Brace and Upright Positions - Tibia and Foot Contact Loads versus Posture

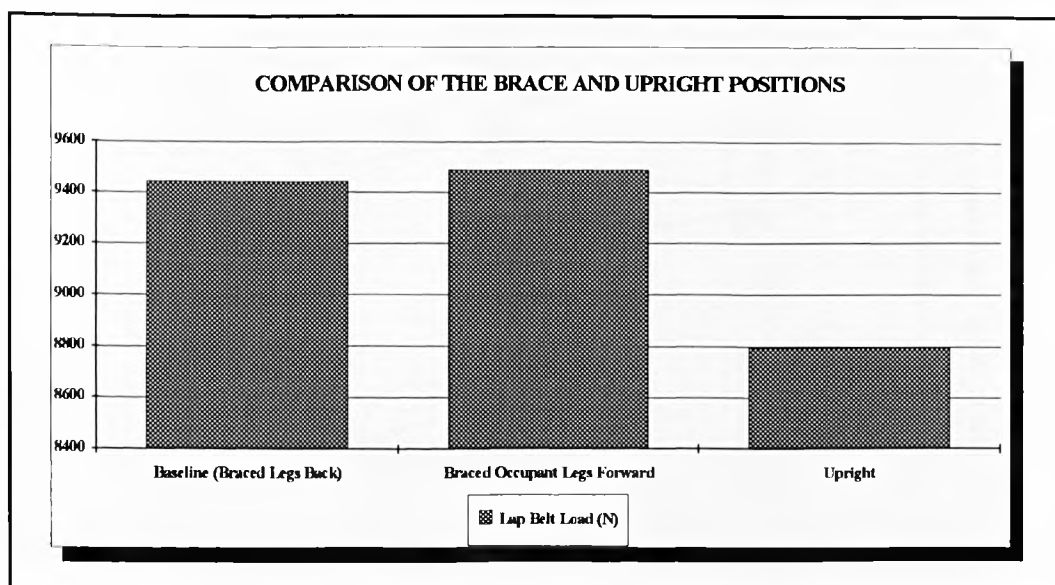


Figure 66. Comparison of the Brace and Upright Positions - Lap Belt Load versus Posture

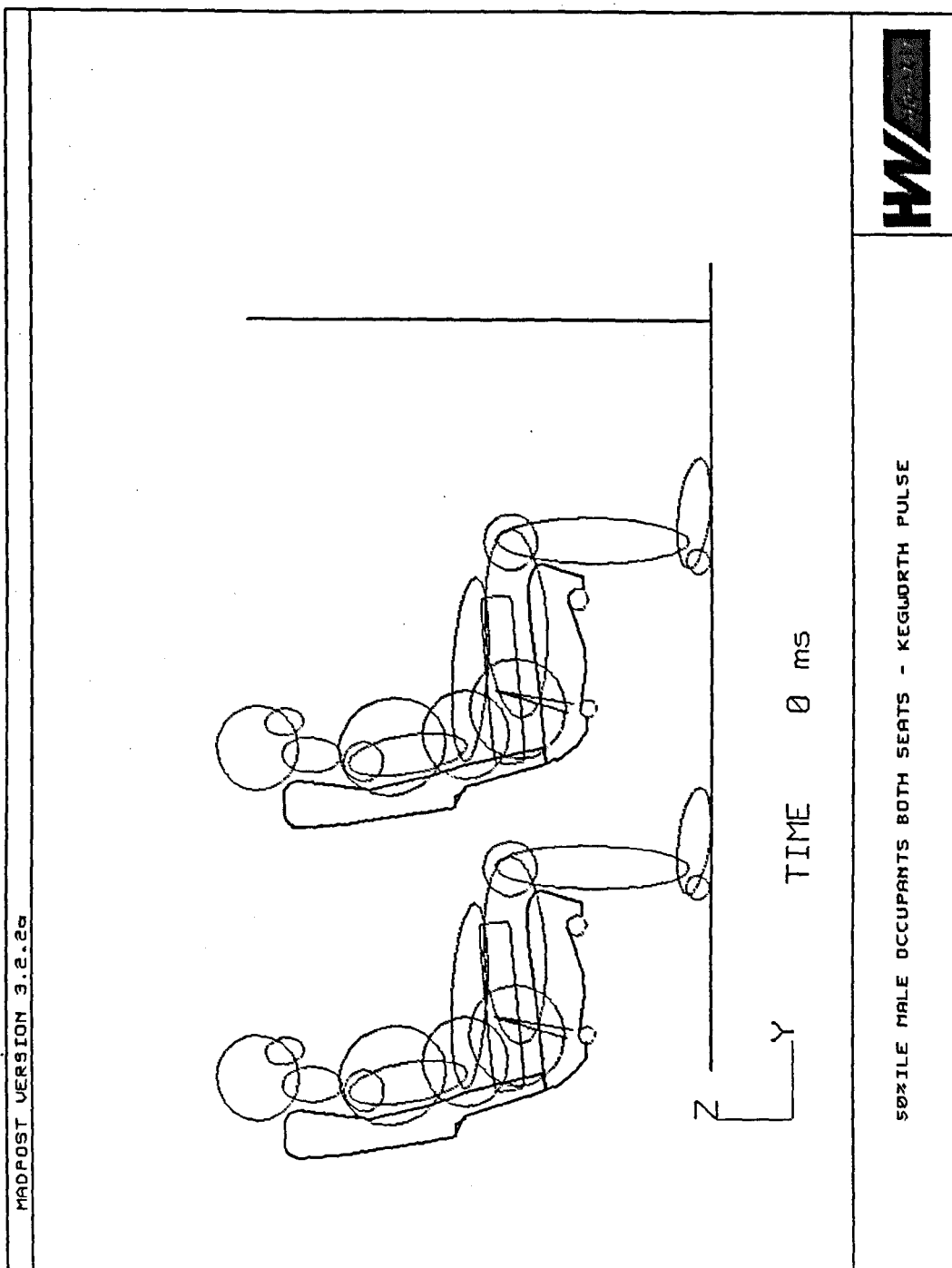


Figure 67. 50th Percentile Male Occupants Both Seats - Kegworth Pulse

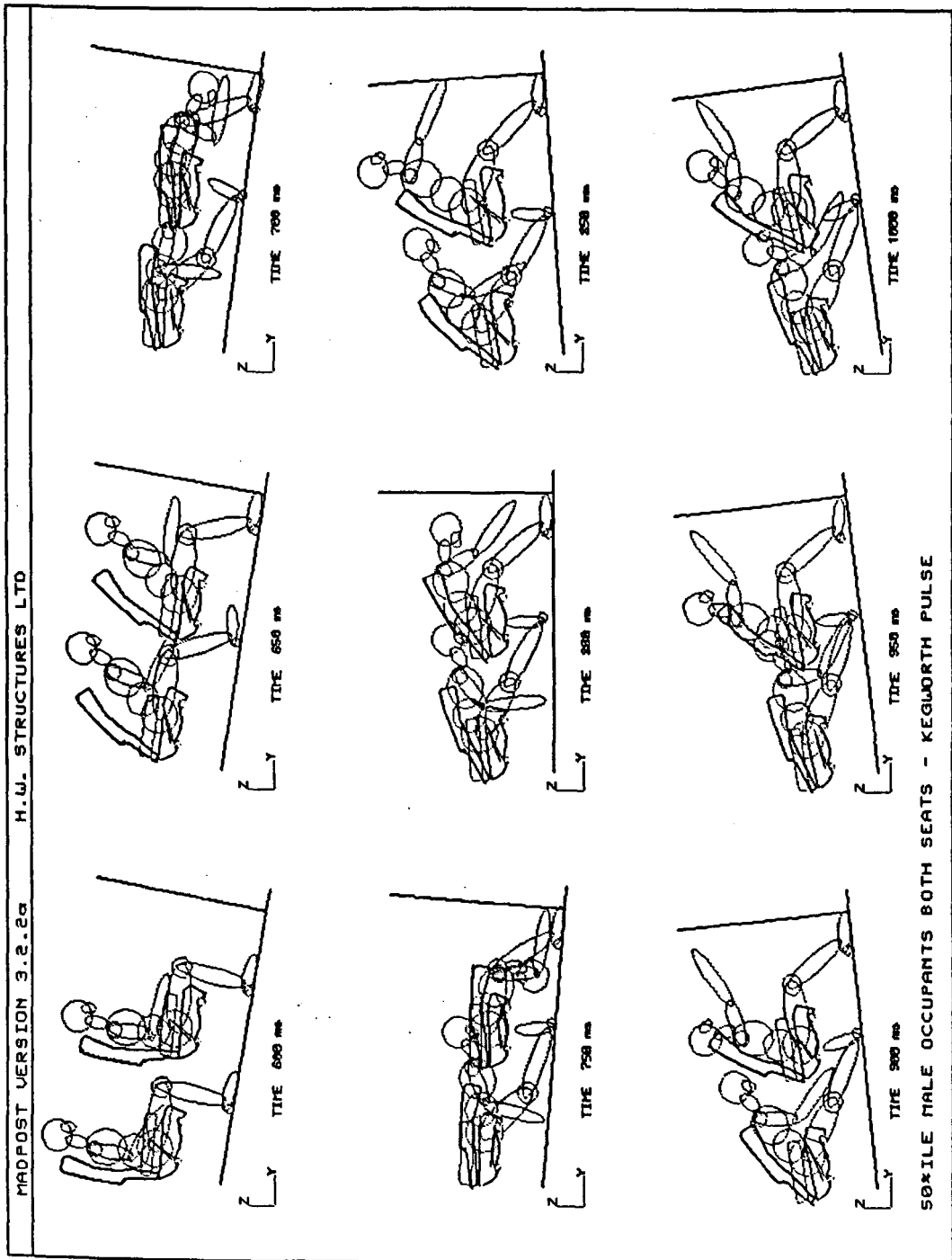


Figure 68. 50th Percentile Male Occupants Both Seats - Kegworth Pulse 600ms to 1000ms Sequential Plot

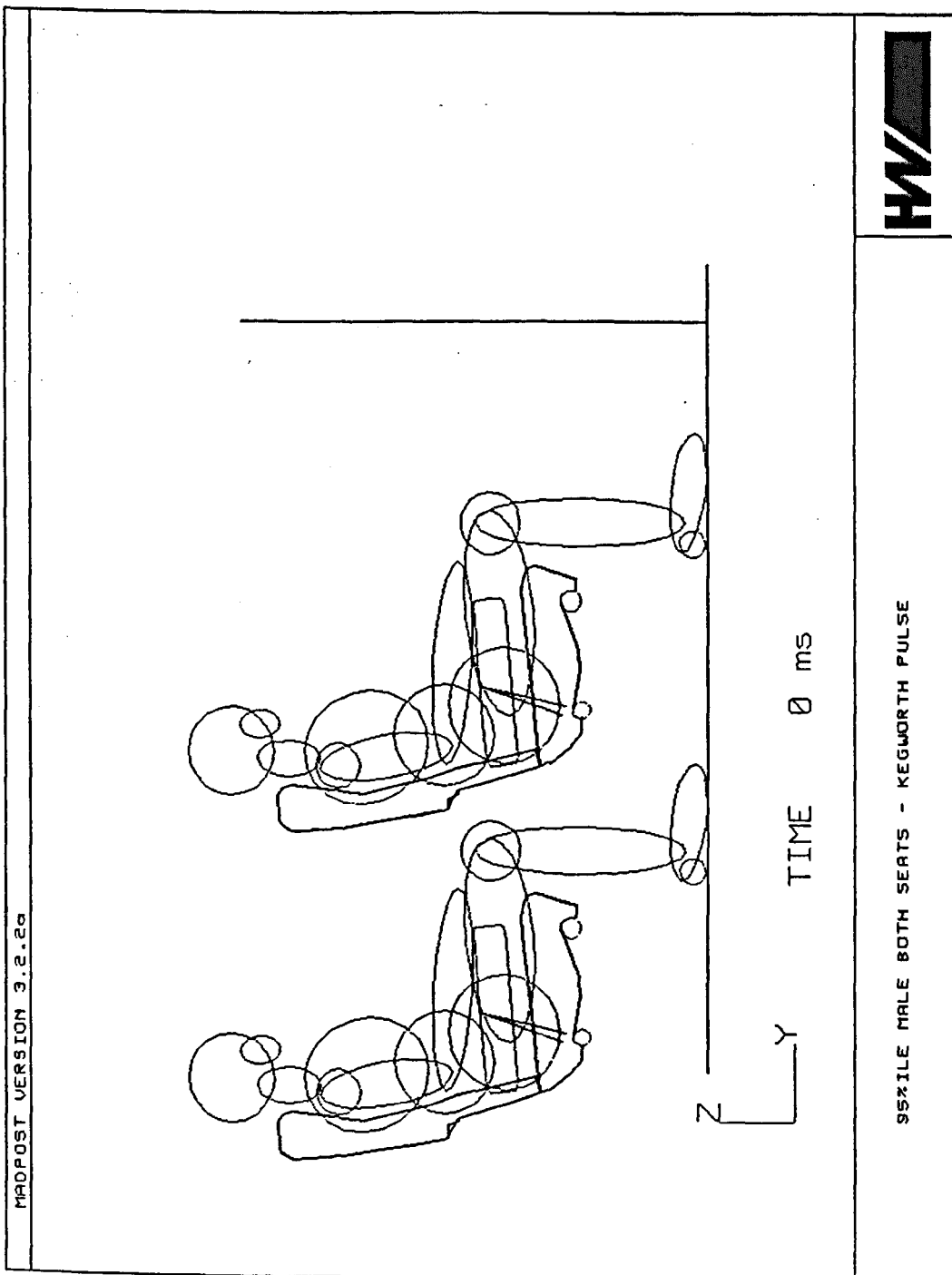


Figure 69. 95th Percentile Male Occupants Both Seats - Kegworth Pulse

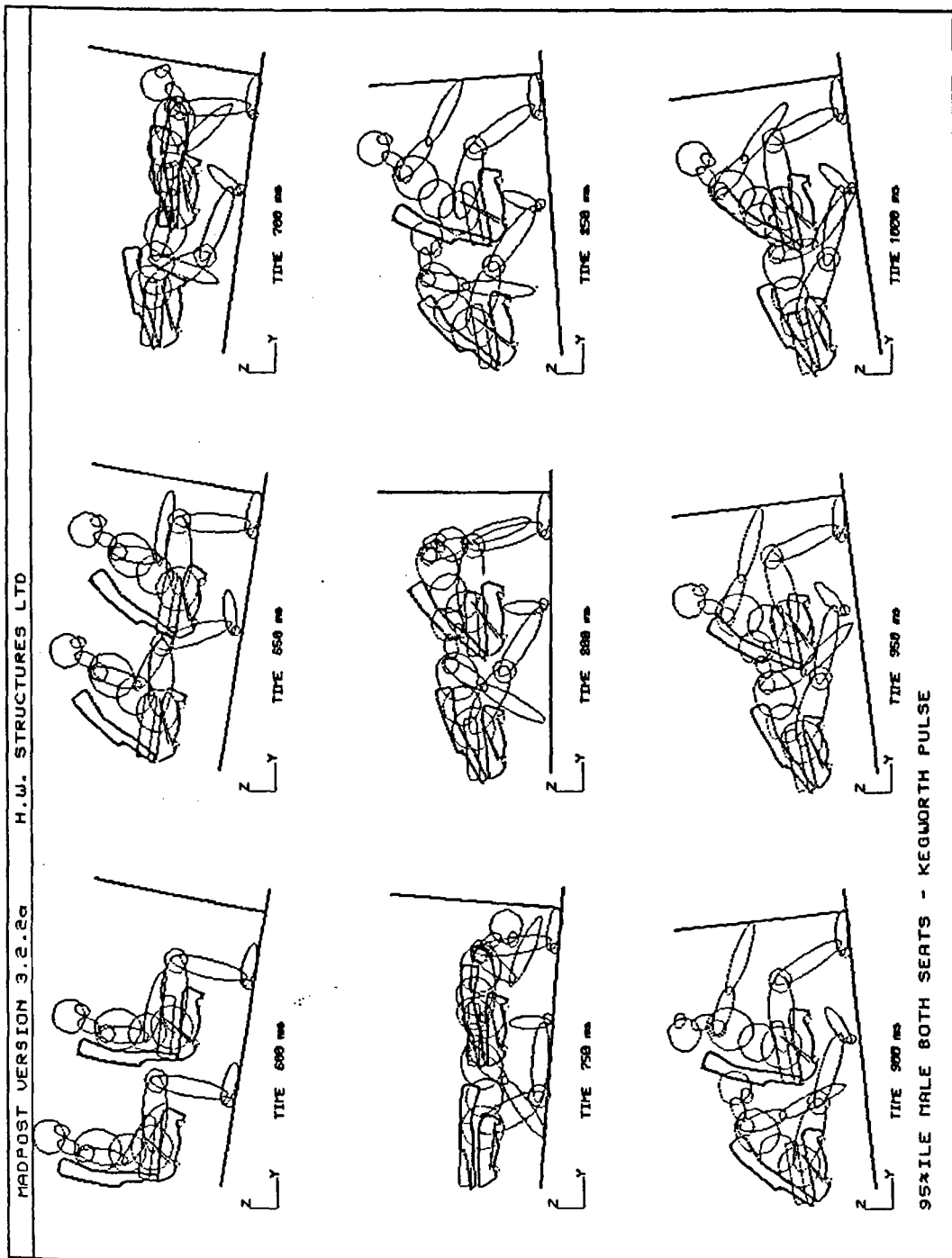


Figure 70. 95th Percentile Male Occupants Both Seats - Kegworth Pulse 600ms to 1000ms Sequential Plot

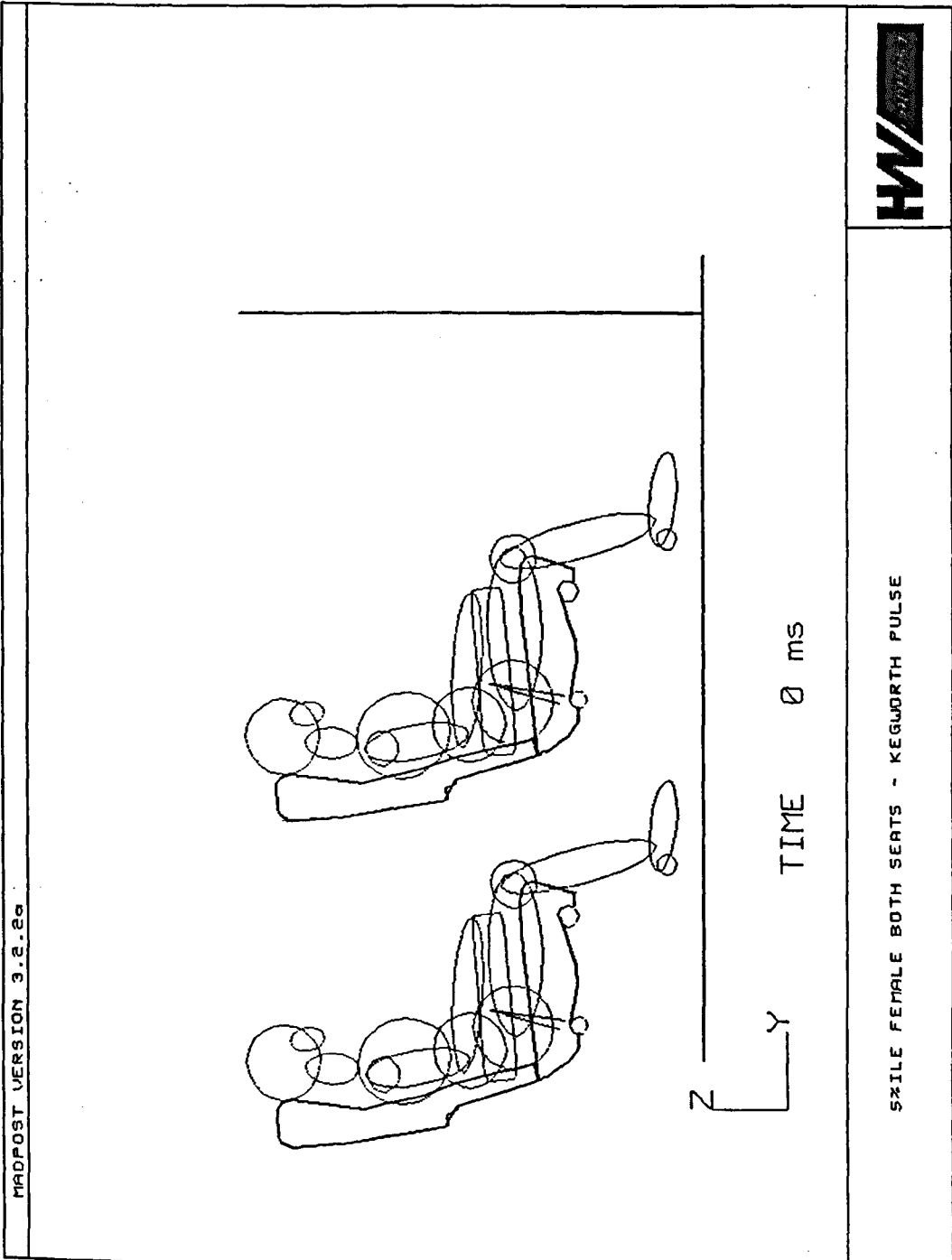


Figure 71. 5th Percentile Female Occupants Both Seats - Kegworth Pulse

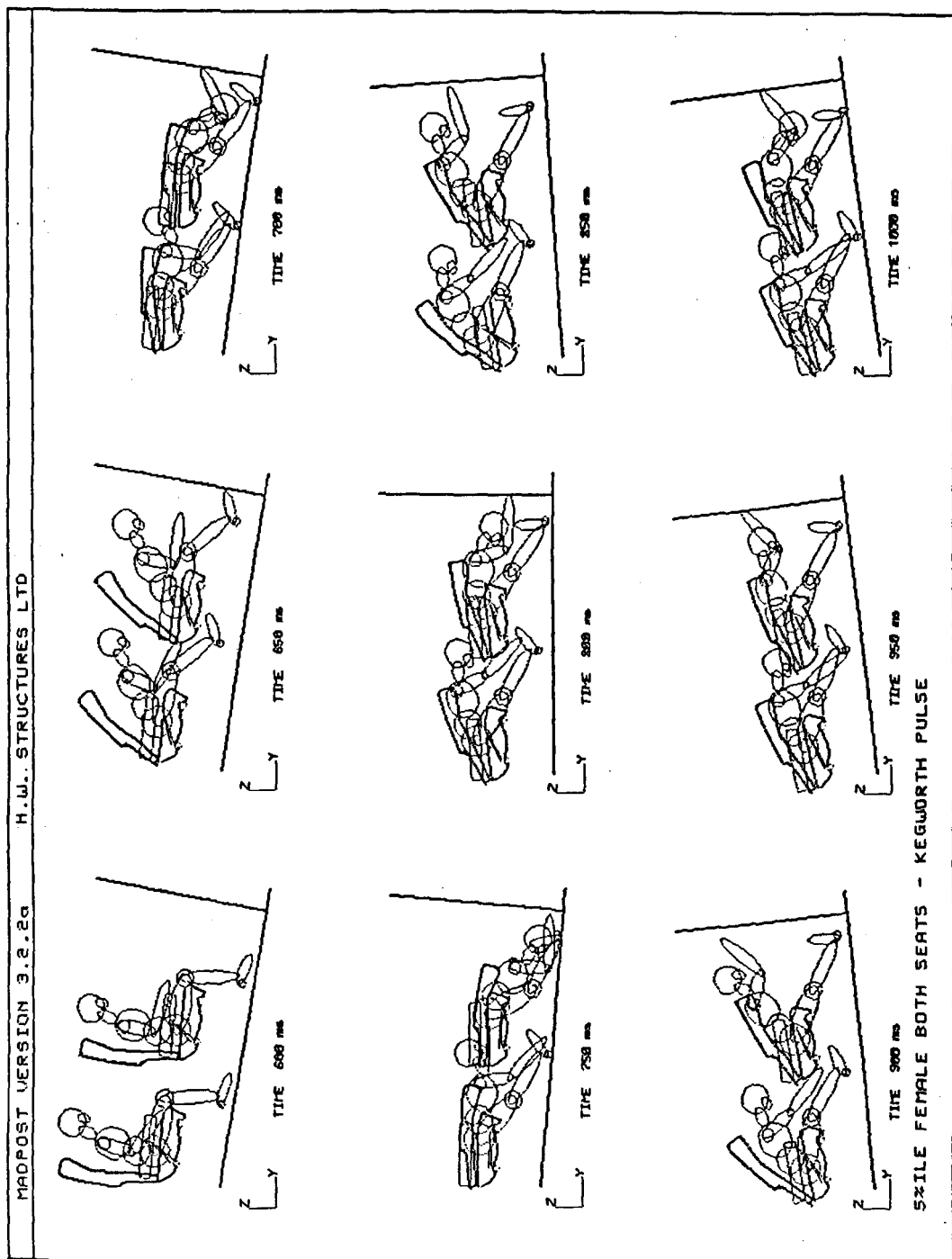


Figure 72. 5th Percentile Female Occupants Both Seats - Kegworth Pulse 600ms to 1000ms Sequential Plot

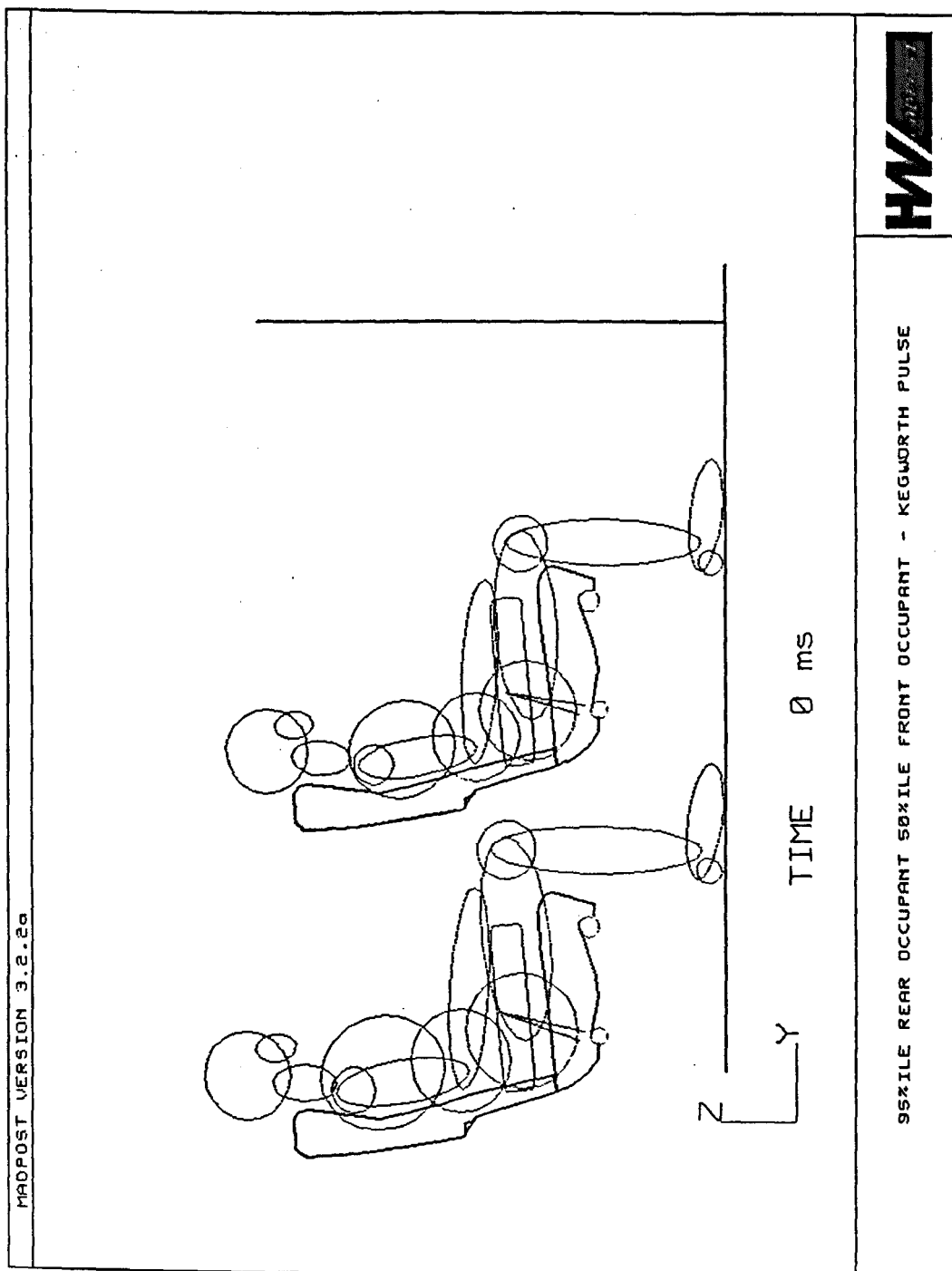


Figure 73. 95th Percentile Rear Occupant, 50th Percentile Front Occupant - Kegworth Pulse

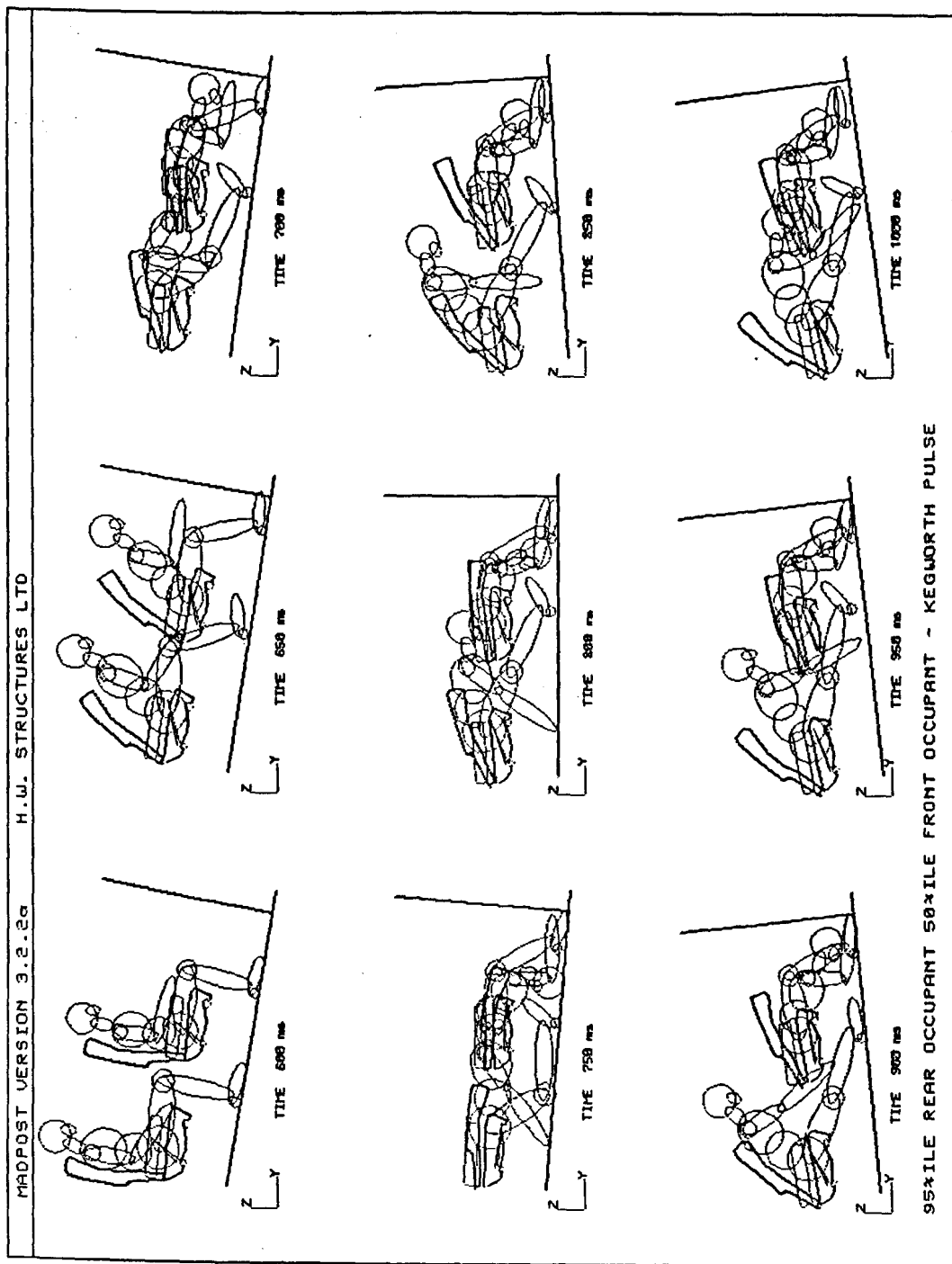


Figure 74. 95th Percentile Rear Occupant, 50th Percentile Front Occupant - Kegworth Pulse 600ms to 1000ms Sequential Plot

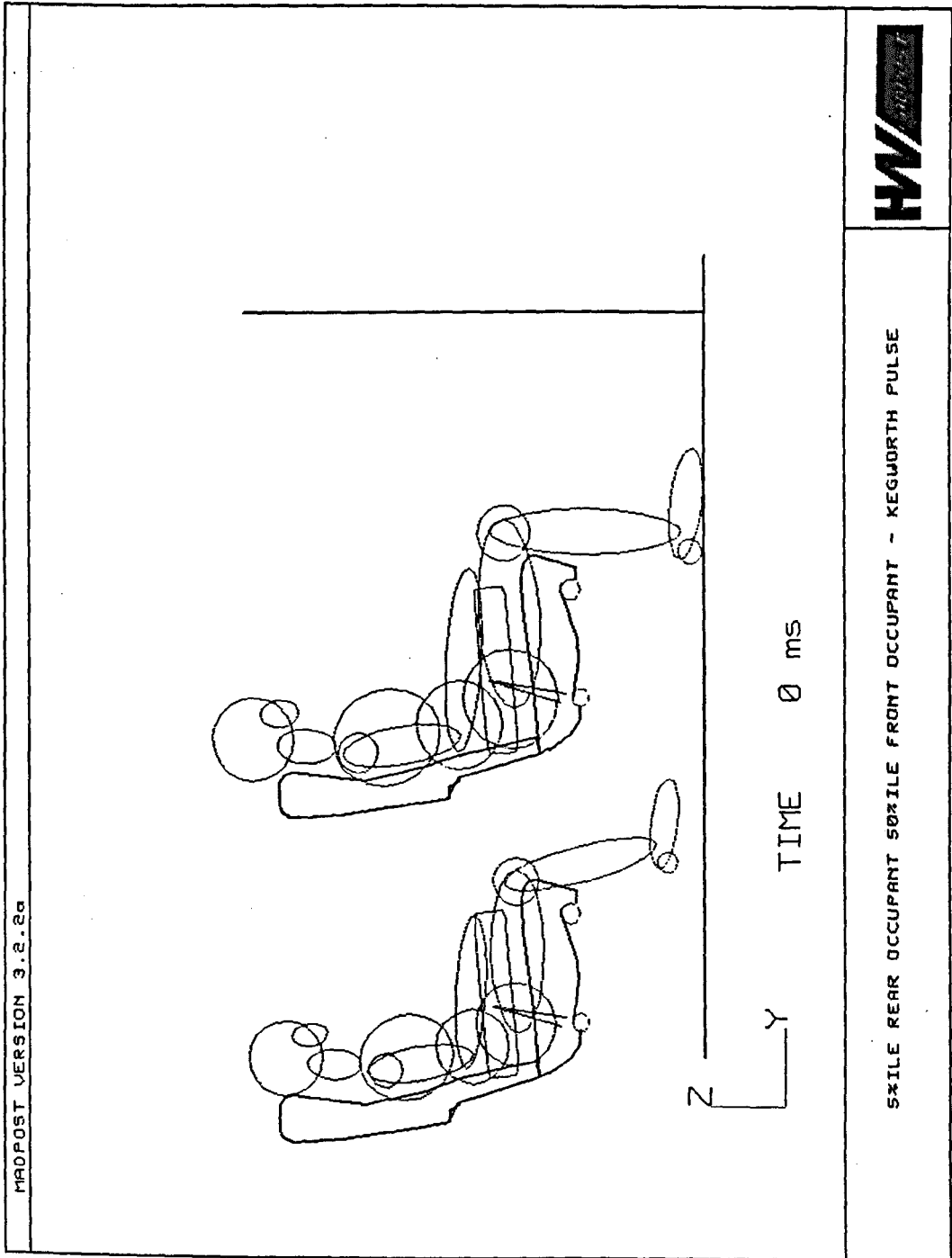


Figure 75. 5th Percentile Rear Occupant, 50th Percentile Front Occupant - Kegworth Pulse

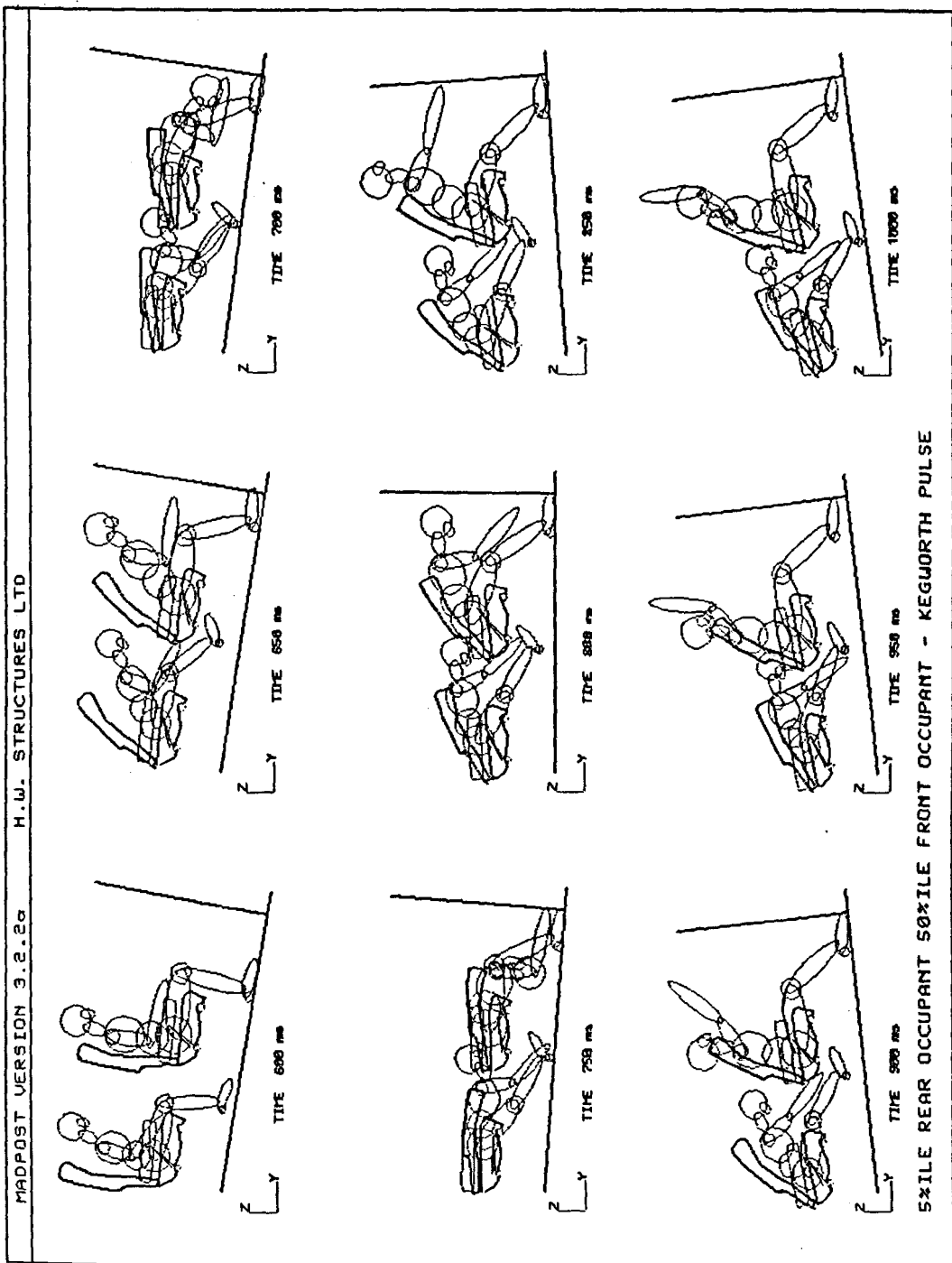


Figure 76. 5th Percentile Rear Occupant, 50th Percentile Front Occupant - Kegworth Pulse 600ms to 1000ms Sequential Plot

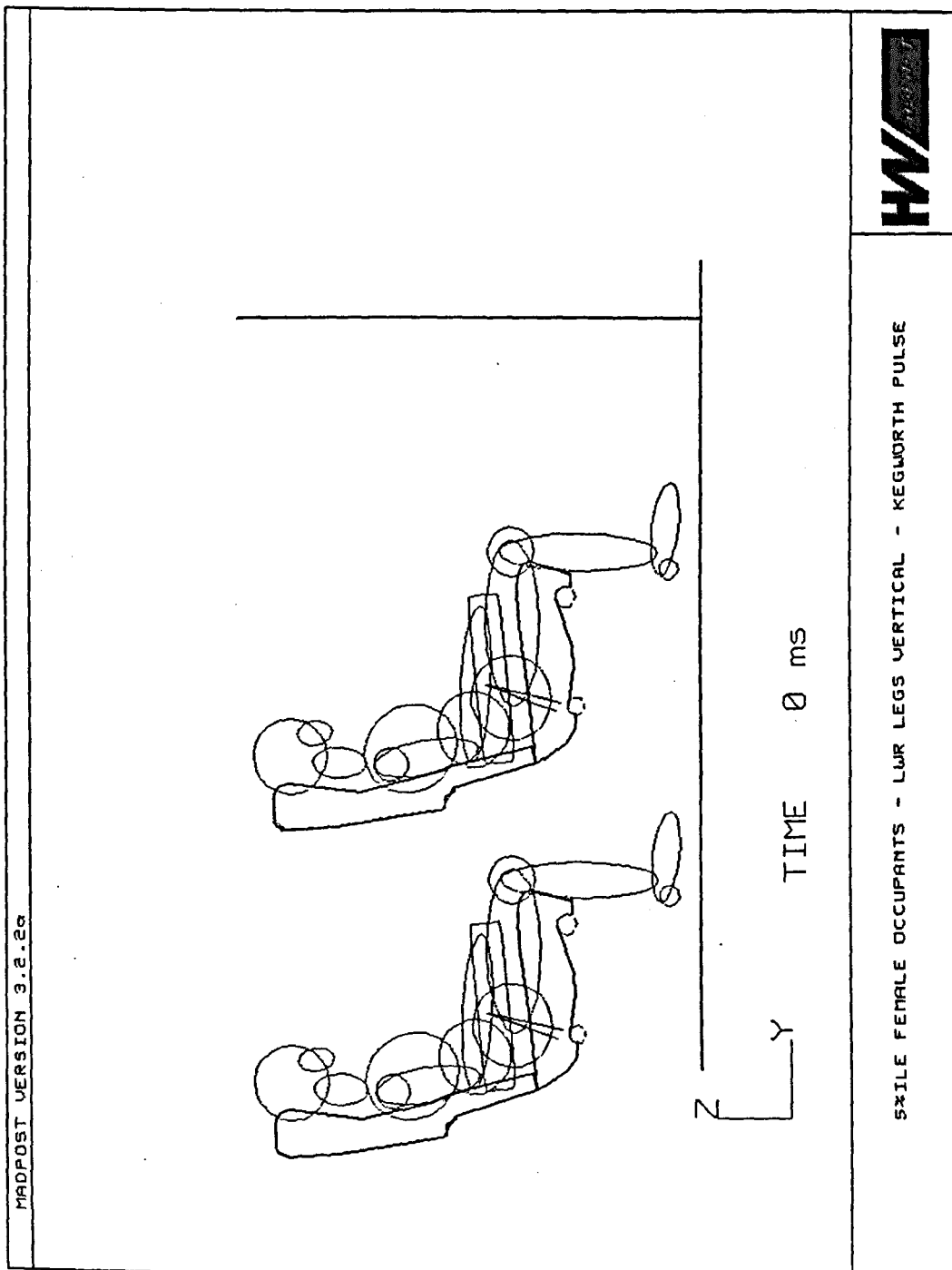


Figure 77. 5th Percentile Female Occupants - Lower Legs Vertical - Kegworth Pulse

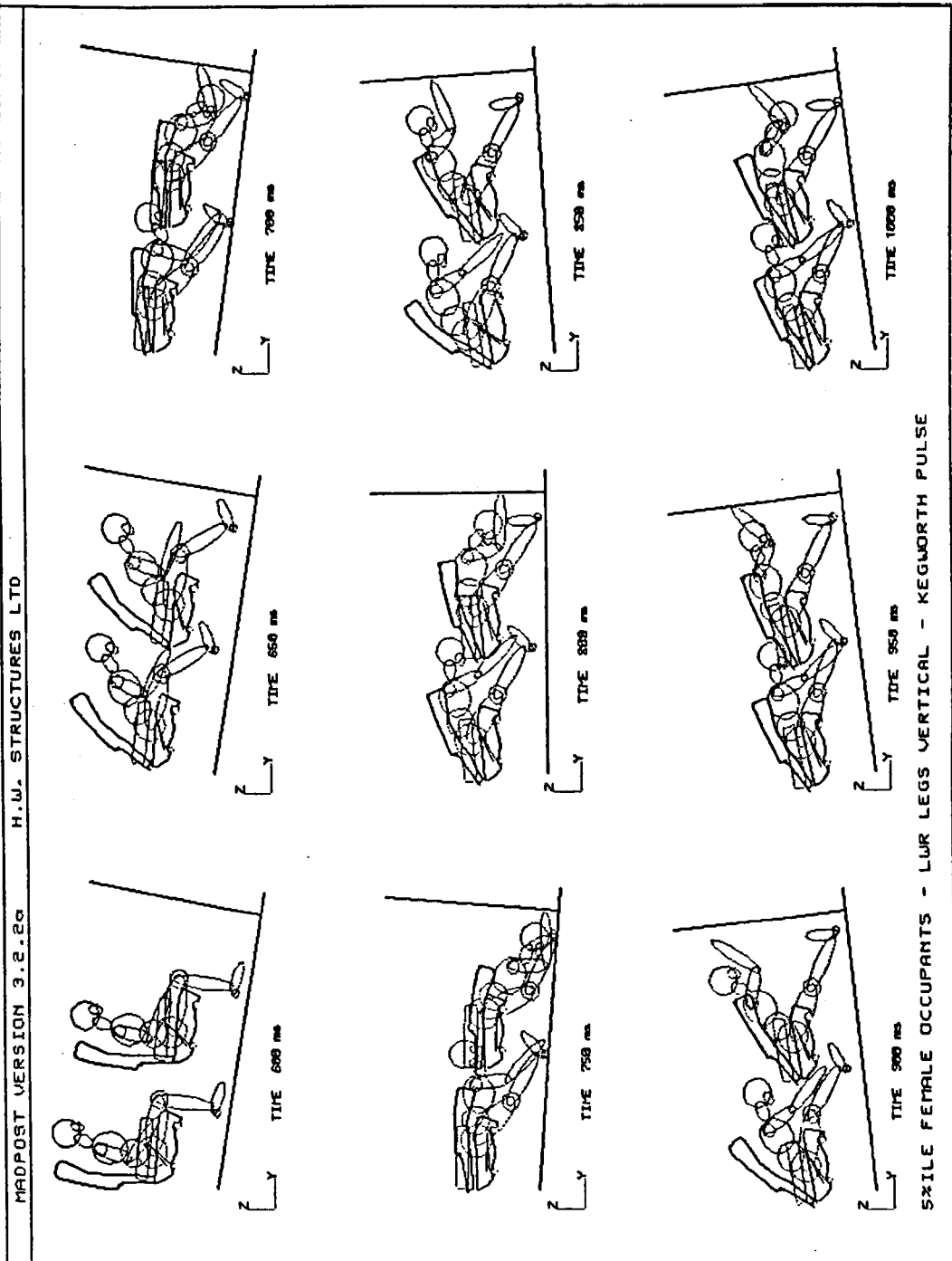


Figure 78. 5th Percentile Female Occupants - Lower Legs Vertical - Kegworth Pulse 600ms to 1000ms Sequential Plot

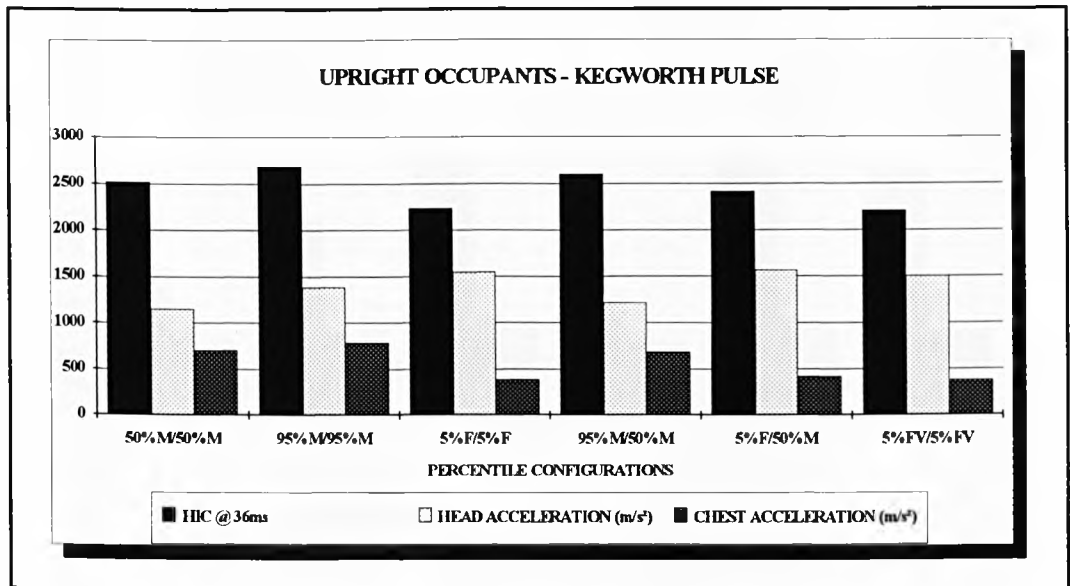


Figure 79. Upright Occupants, Kegworth Pulse - HIC, Head and Thorax Accelerations versus Percentile Configurations

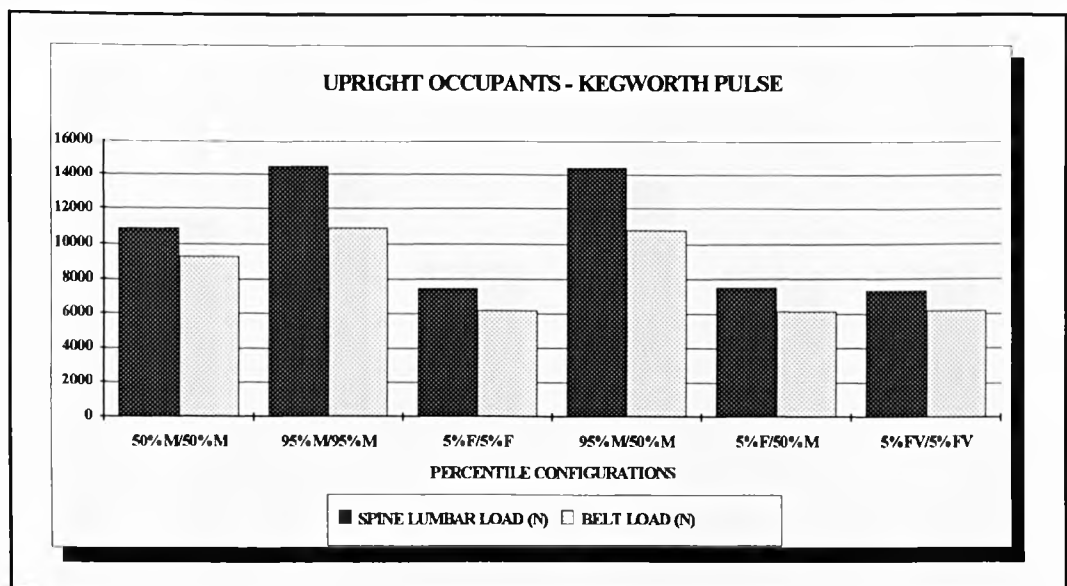


Figure 80. Upright Occupants, Kegworth Pulse - Lumbar Spine and Belt Loads versus Percentile Configurations

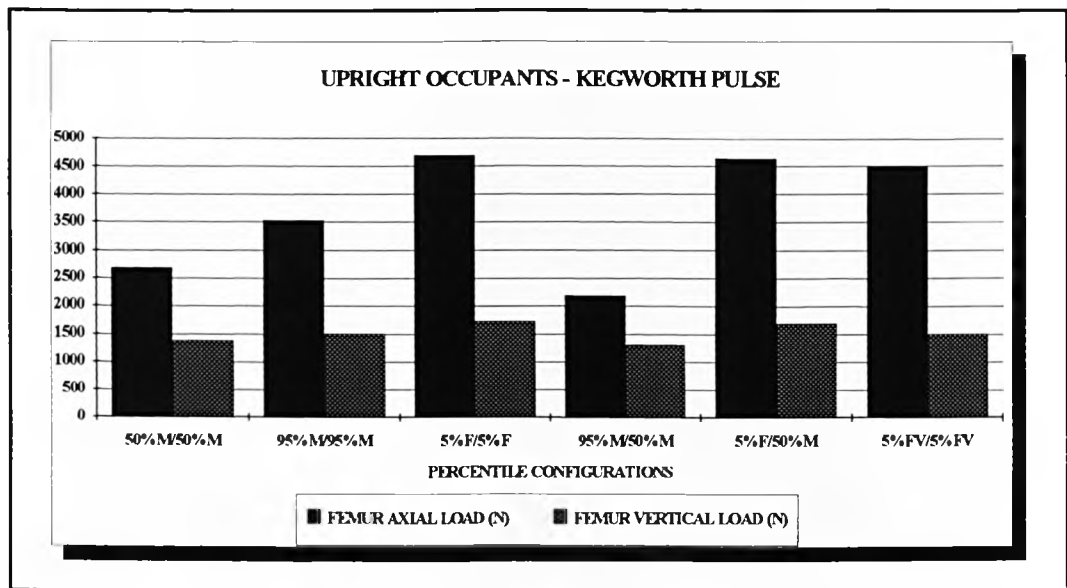


Figure 81. Upright Occupants, Kegworth Pulse - Femur Axial and Vertical Loads versus Percentile Configurations

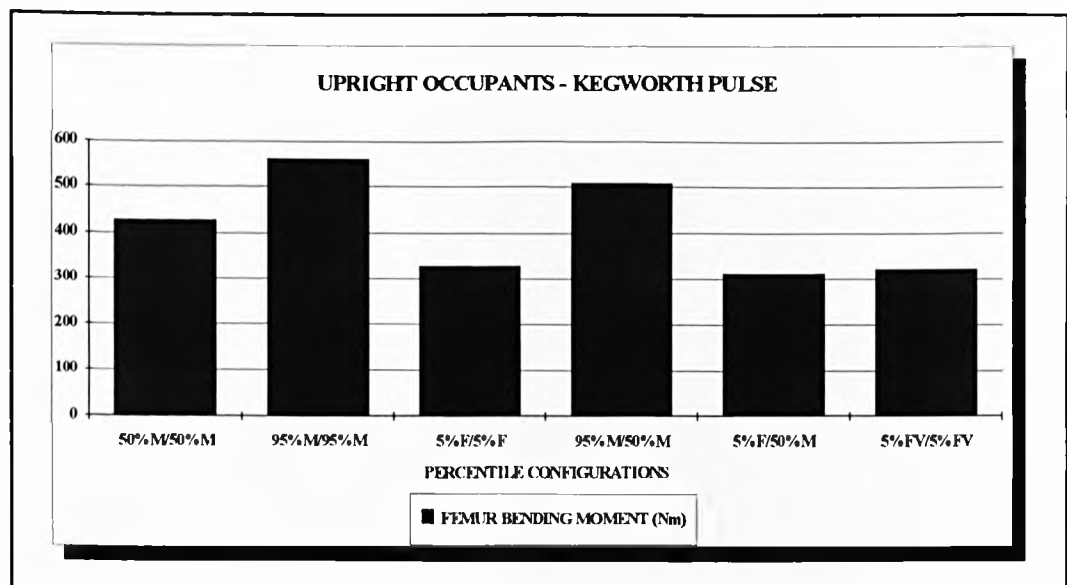


Figure 82. Upright Occupants, Kegworth Pulse - Femur Bending Moment versus Percentile Configurations

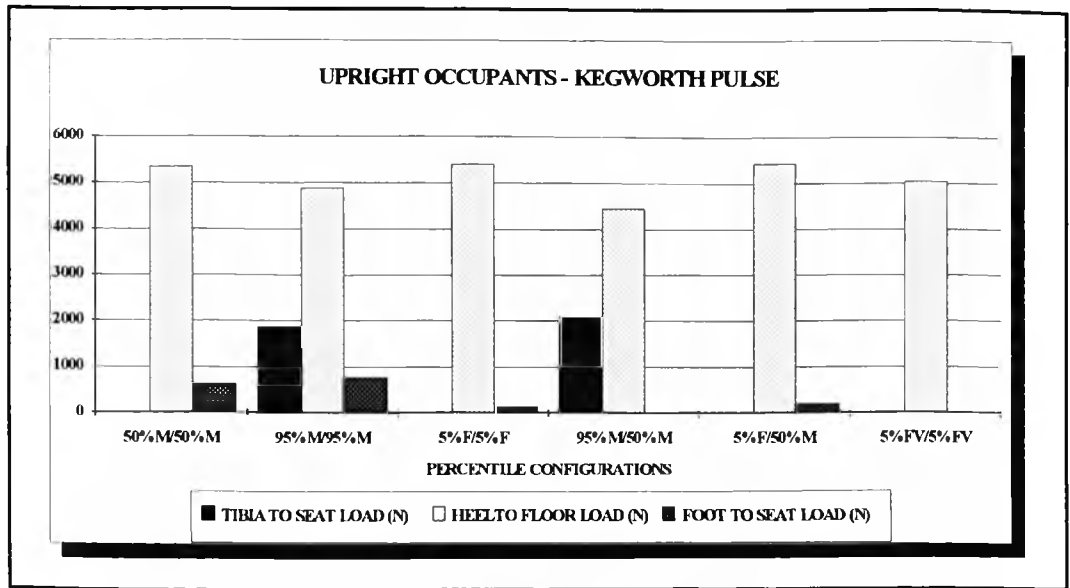


Figure 83. Upright Occupants, Kegworth Pulse - Tibia to Seat, Heel to Floor, Foot to Seat Contact Loads versus Percentile Configurations

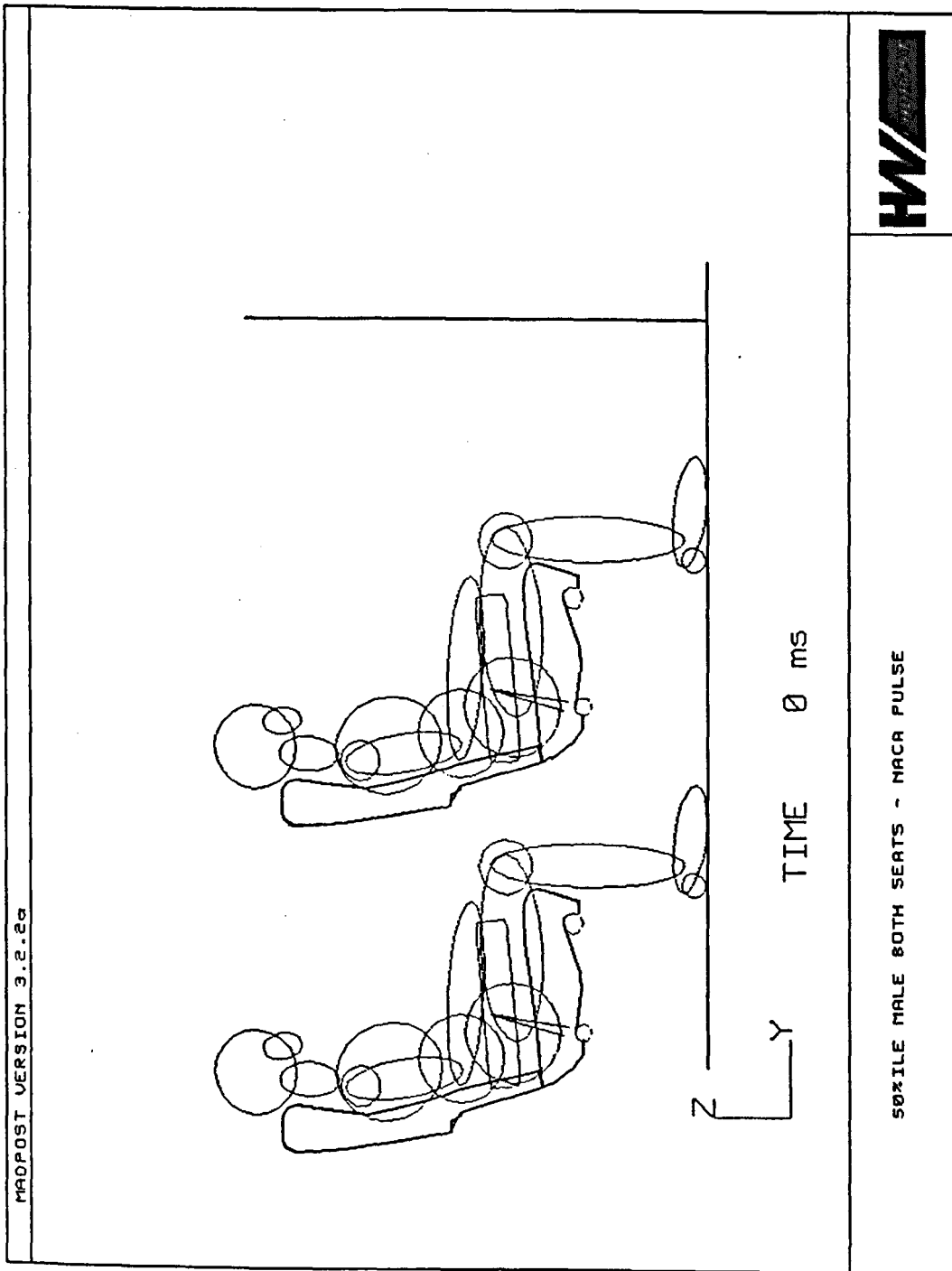


Figure 84. 50th Percentile Male Occupants Both Seats - NACA Pulse

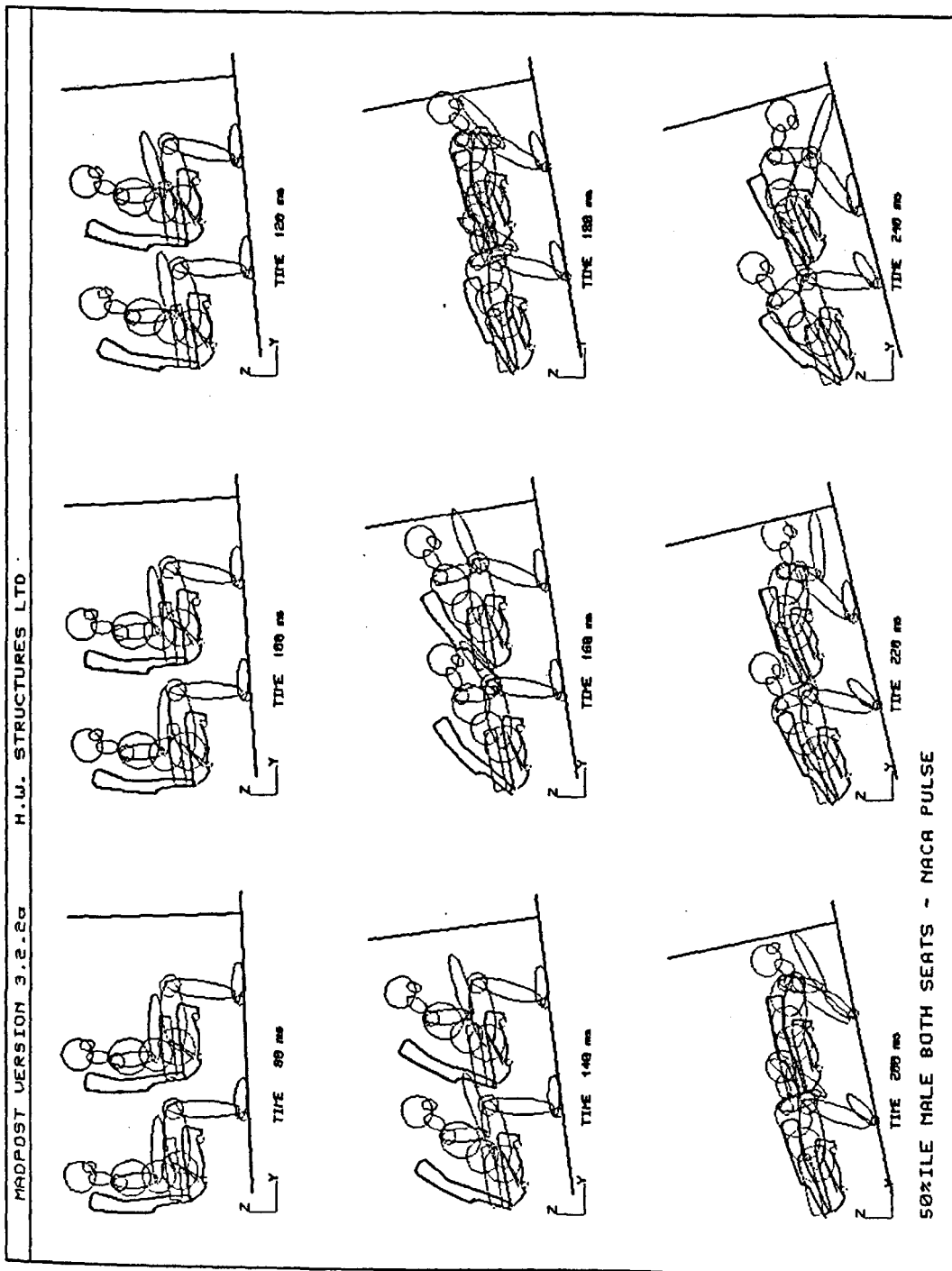


Figure 85. 50th Percentile Male Occupants Both Seats - NACA Pulse 80ms to 240ms Sequential Plot

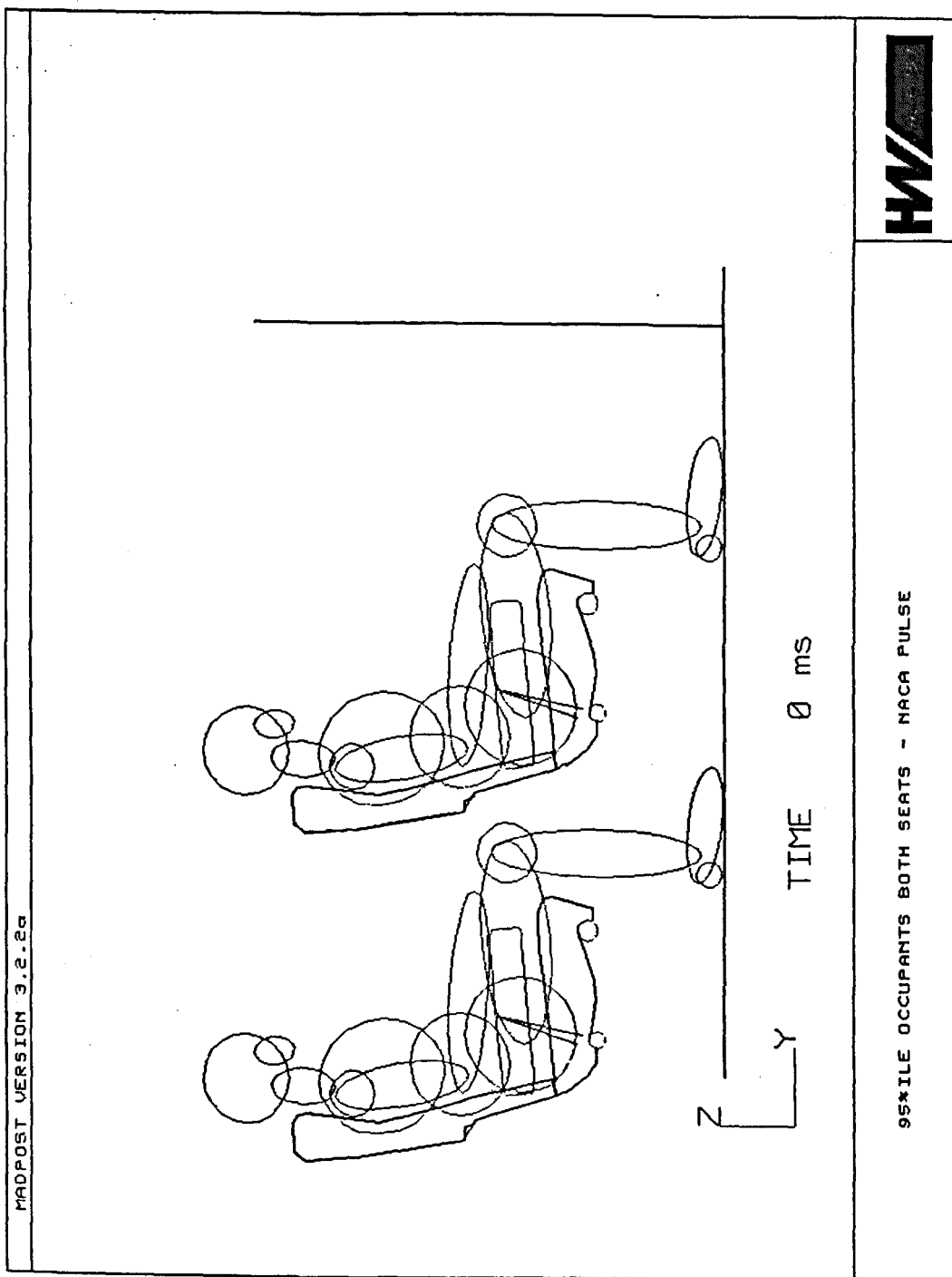


Figure 86. 95th Percentile Male Occupants Both Seats - NACA Pulse

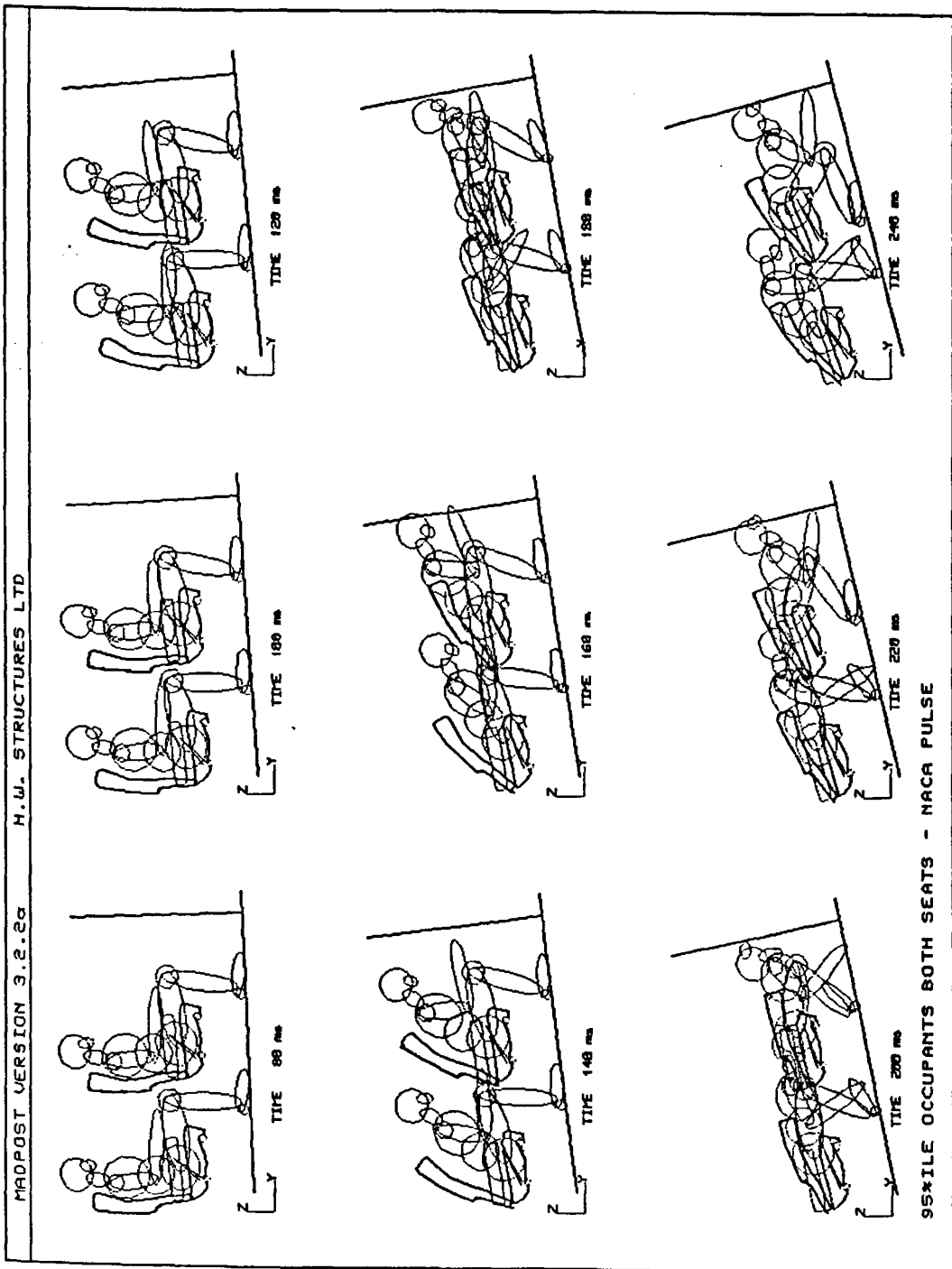


Figure 87. 95th Percentile Male Occupants Both Seats - NACA Pulse 80ms to 240ms Sequential Plot

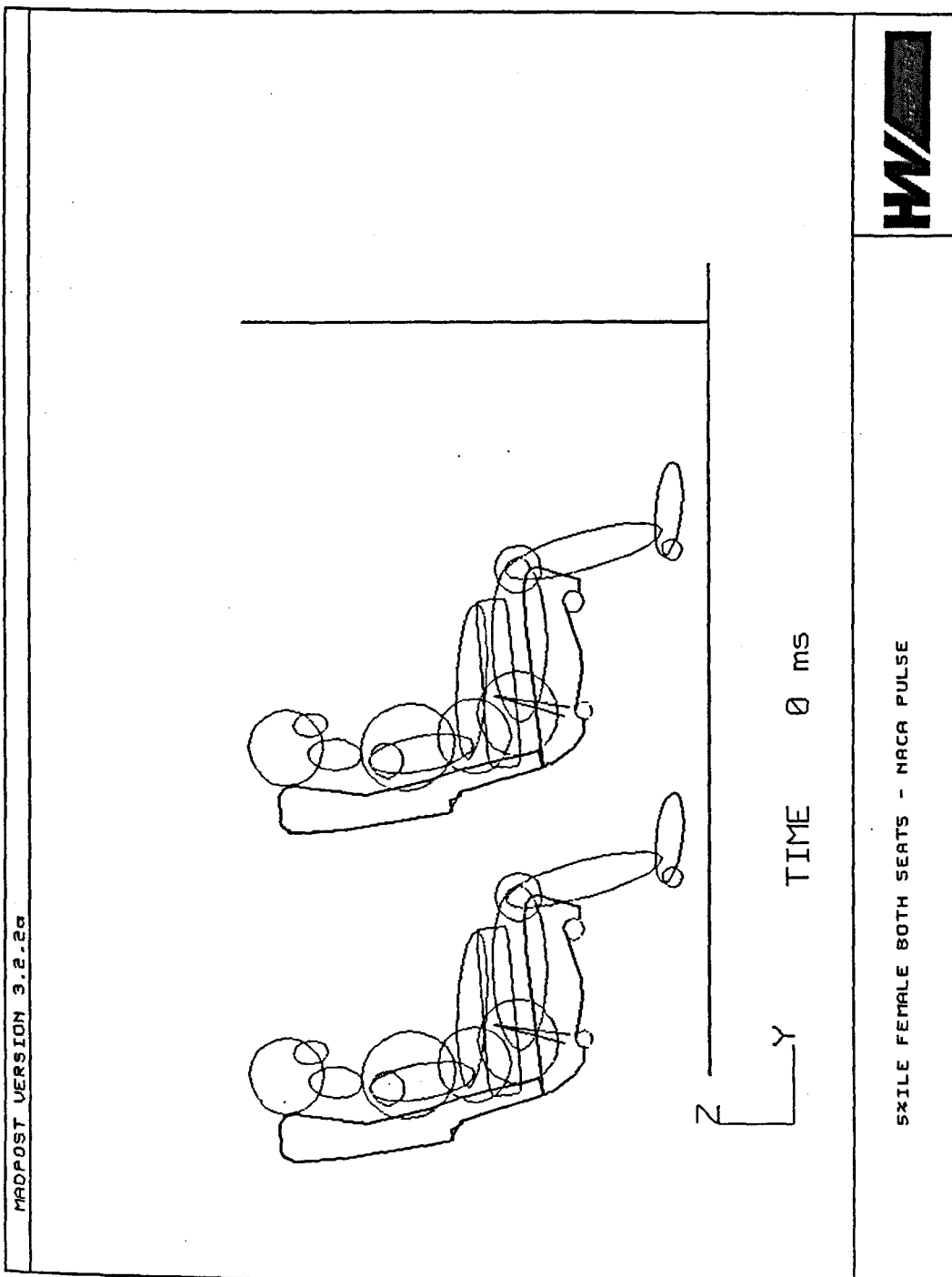


Figure 88. 5th Percentile Female Occupants Both Seats - NACA Pulse

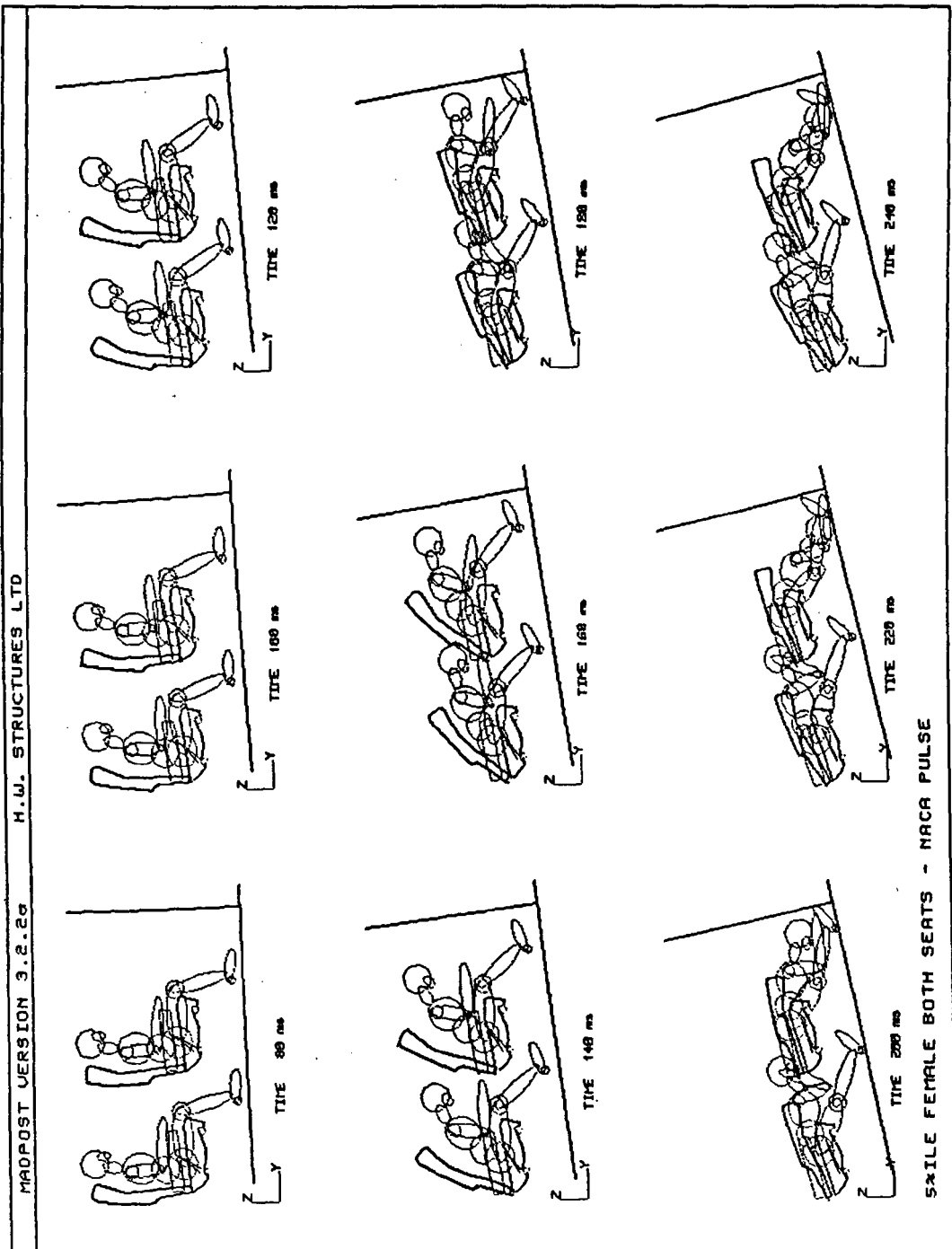


Figure 89. 5th Percentile Female Occupants Both Seats - NACA Pulse 80ms to 240ms Sequential Plot

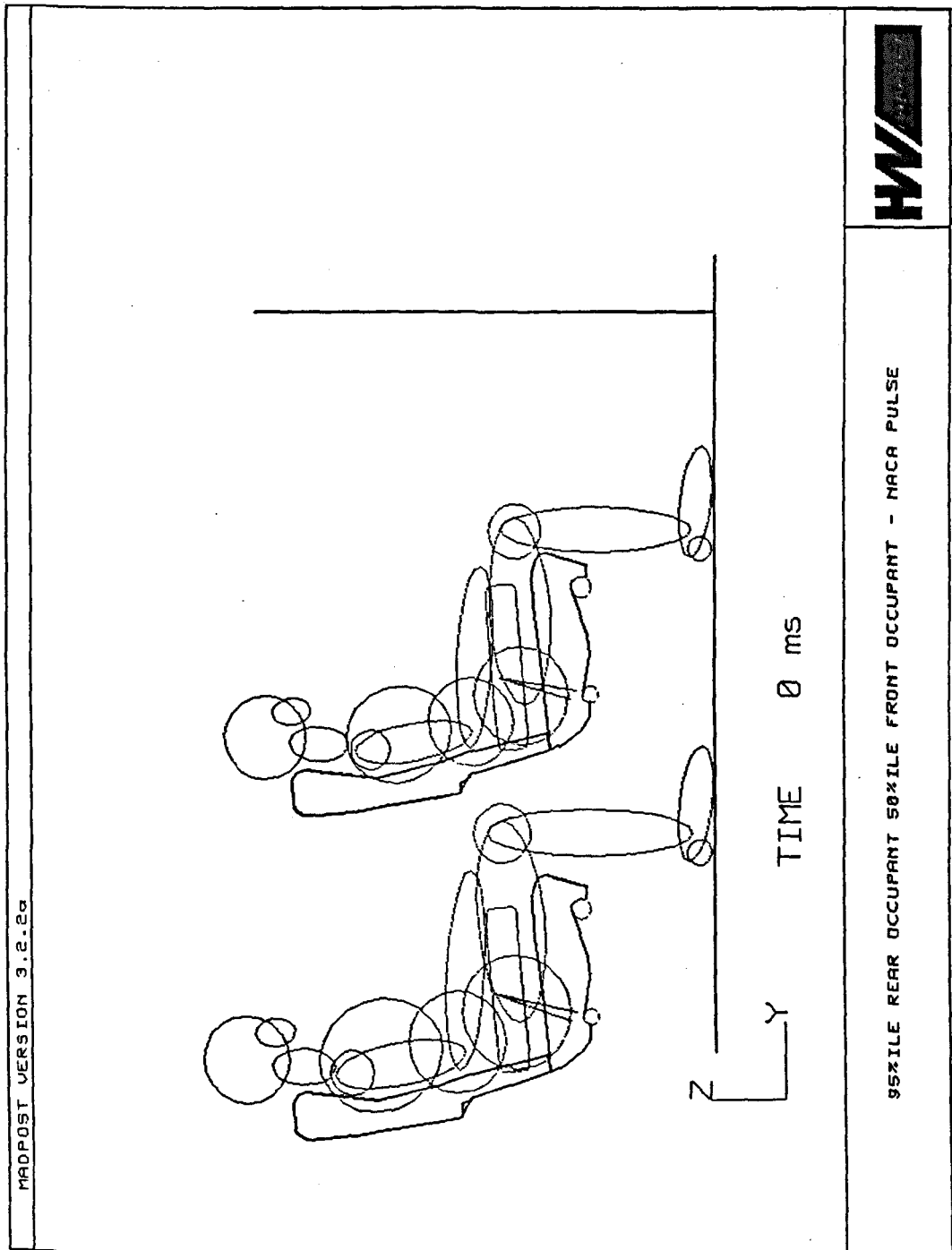


Figure 90. 95th Percentile Rear Occupant, 50th Percentile Front Occupant - NACA Pulse

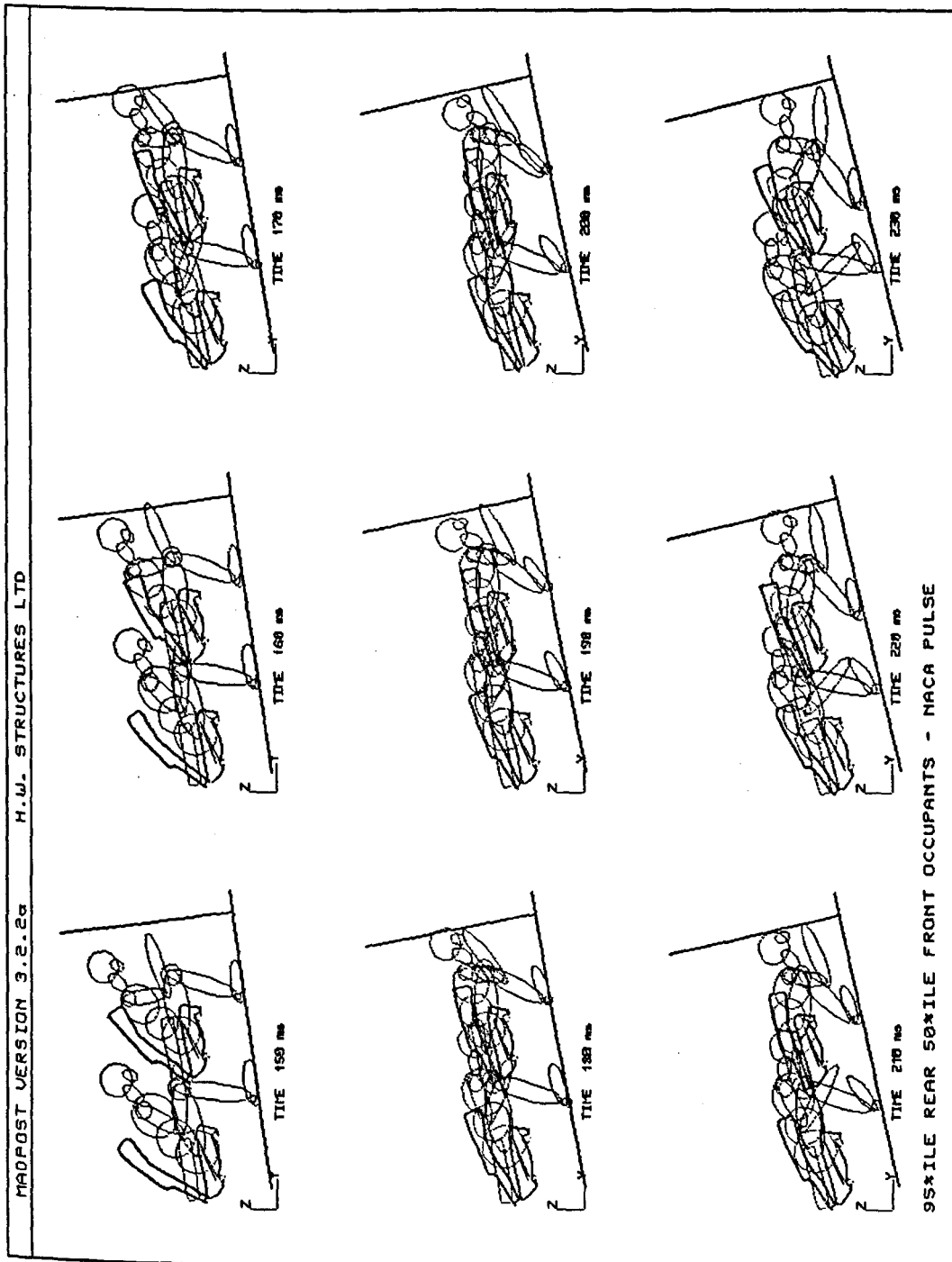


Figure 91. 95th Percentile Rear Occupant, 50th Percentile Front Occupant -
 NACA Pulse 150ms to 230ms Sequential Plot

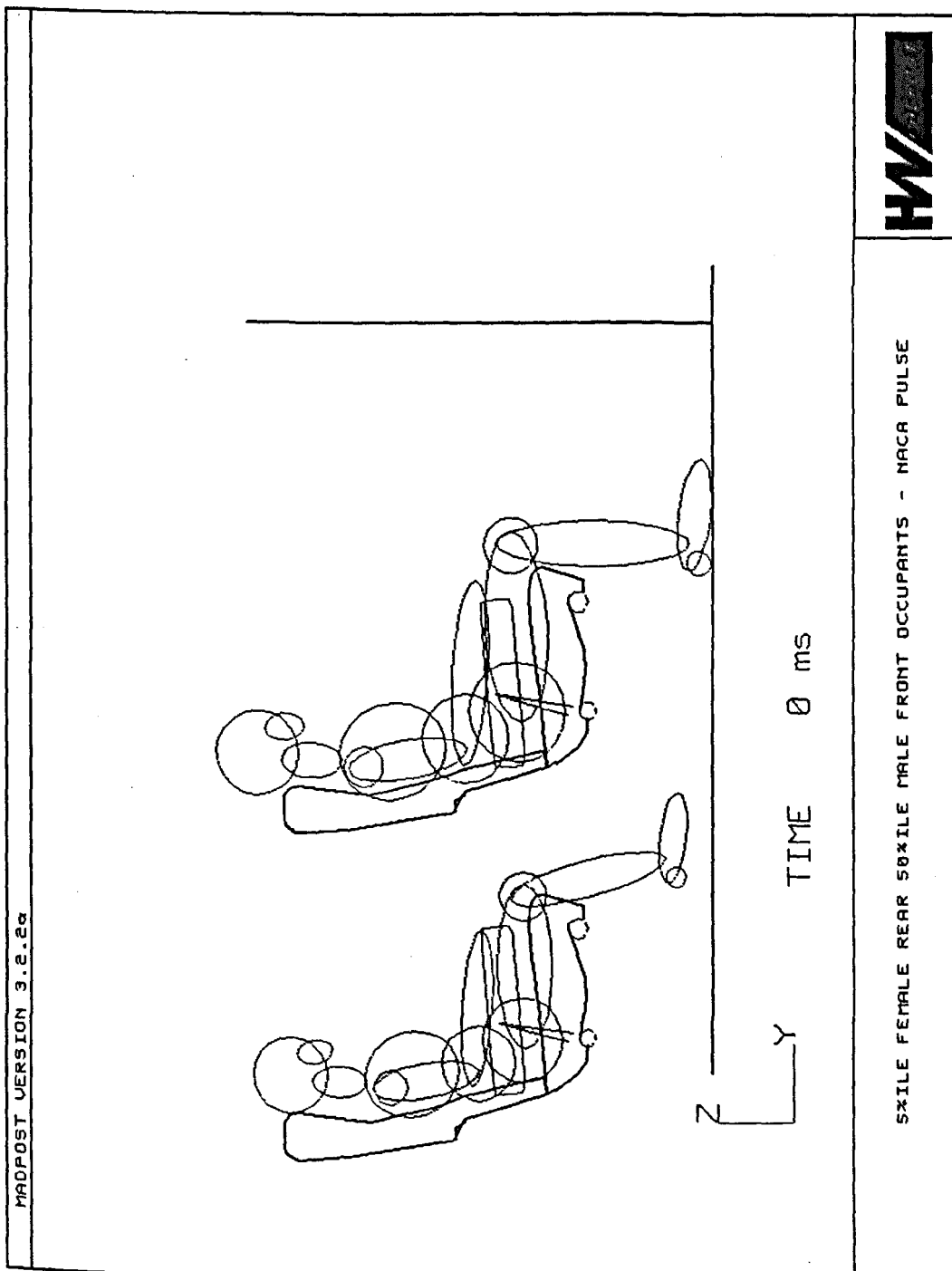


Figure 92. 5th Percentile Rear Occupant, 50th Percentile Front Occupant - NACA Pulse

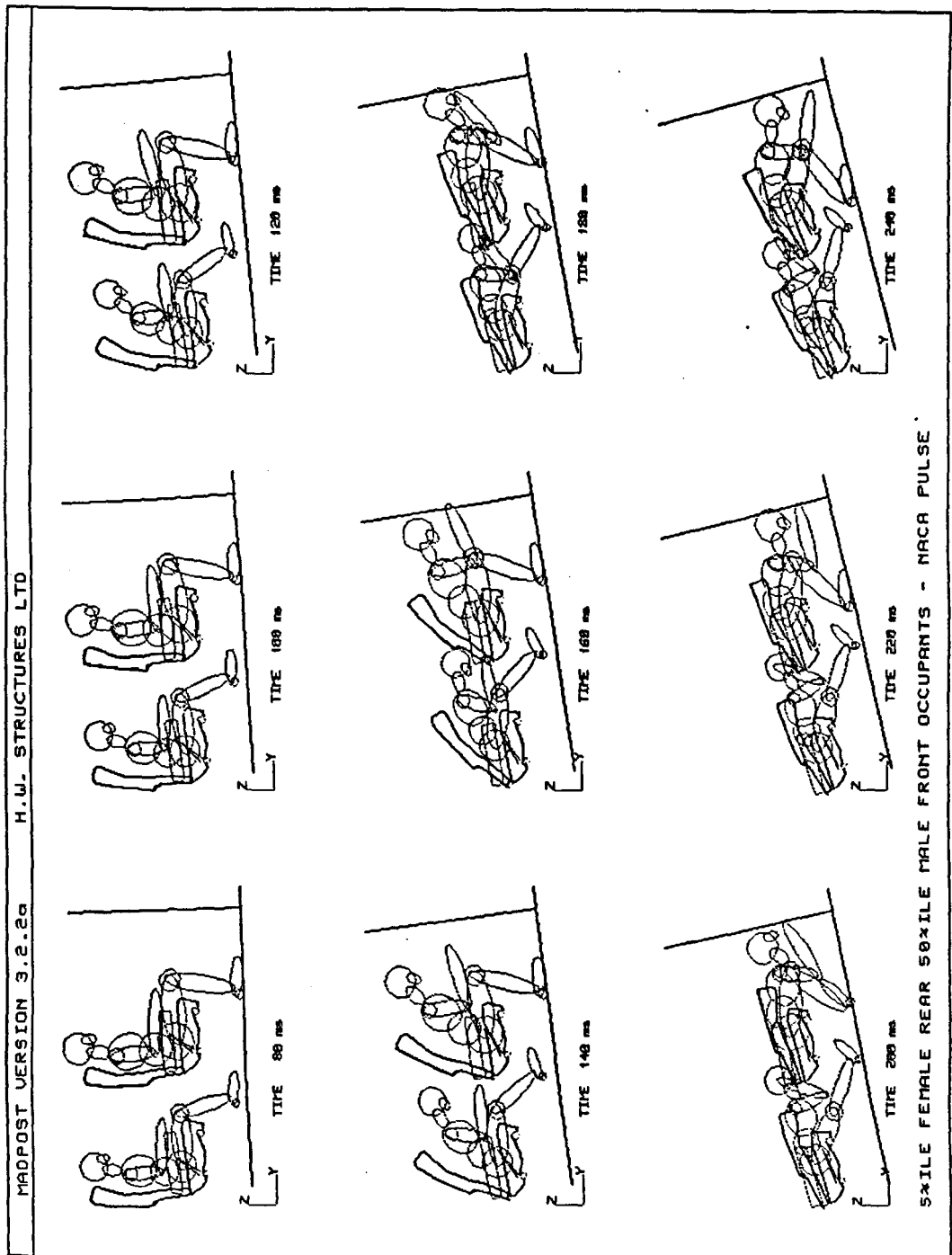


Figure 93. 5th Percentile Rear Occupant, 50th Percentile Front Occupant - NACA Pulse 80ms to 240ms Sequential Plot

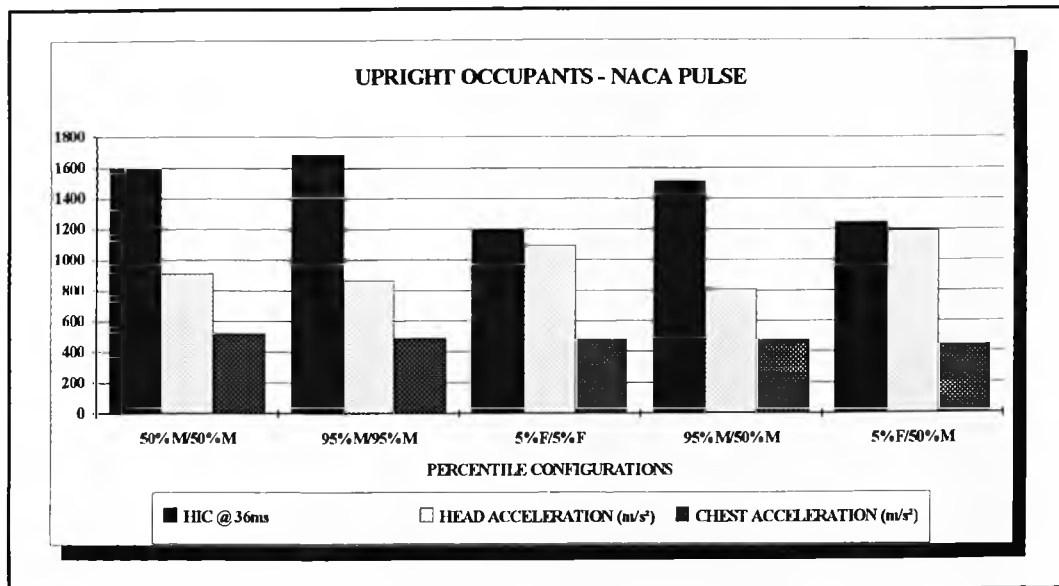


Figure 94. Upright Occupants, NACA Pulse - HIC, Head and Thorax Accelerations versus Percentile Configurations

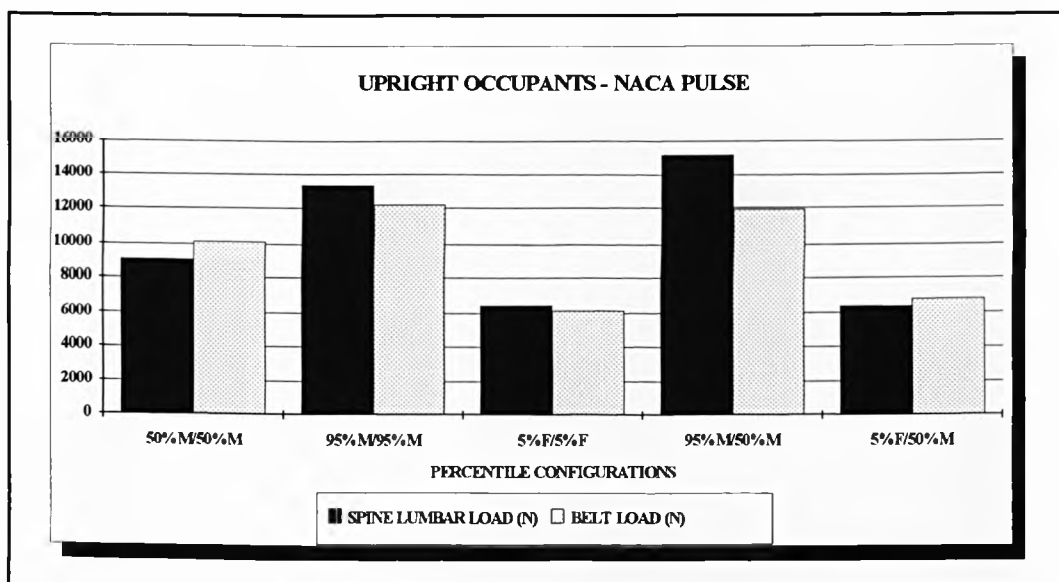


Figure 95. Upright Occupants, NACA Pulse - Lumbar Spine and Belt Loads versus Percentile Configurations

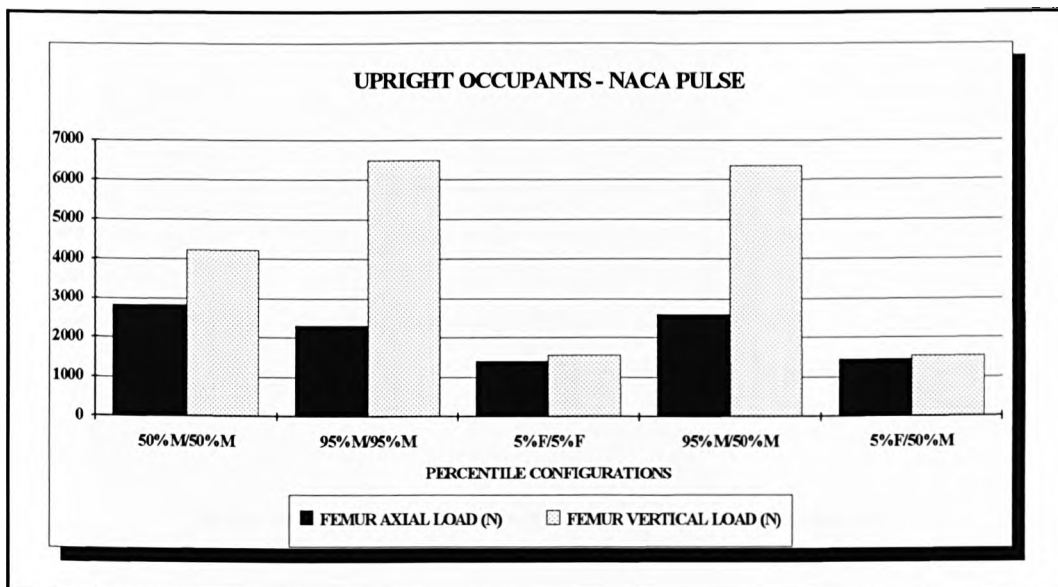


Figure 96. Upright Occupants, NACA Pulse - Femur Axial and Vertical Loads versus Percentile Configurations

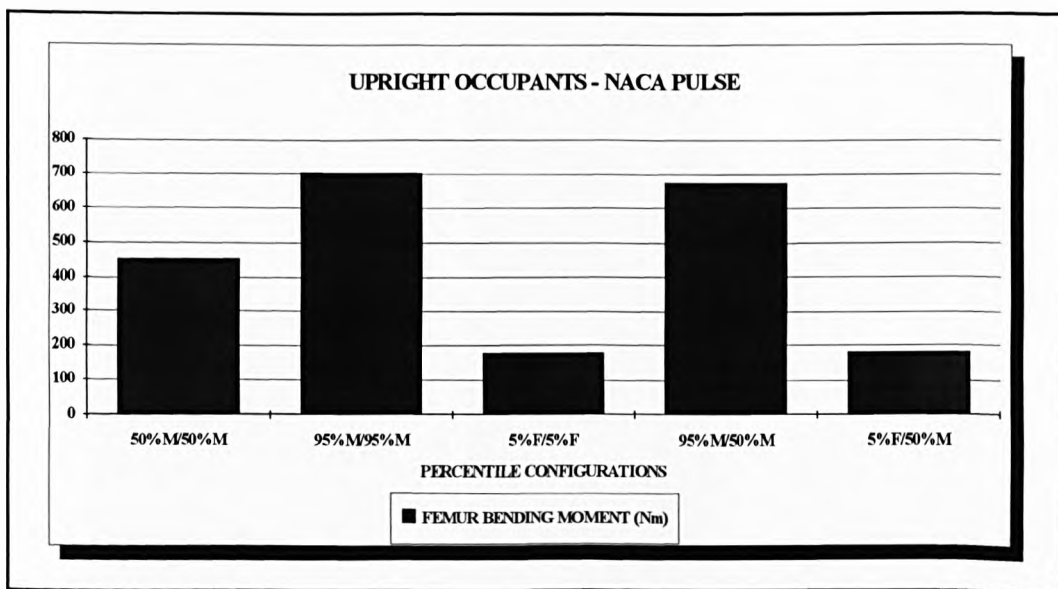


Figure 97. Upright Occupants, NACA Pulse - Femur Bending Moment versus Percentile Configurations

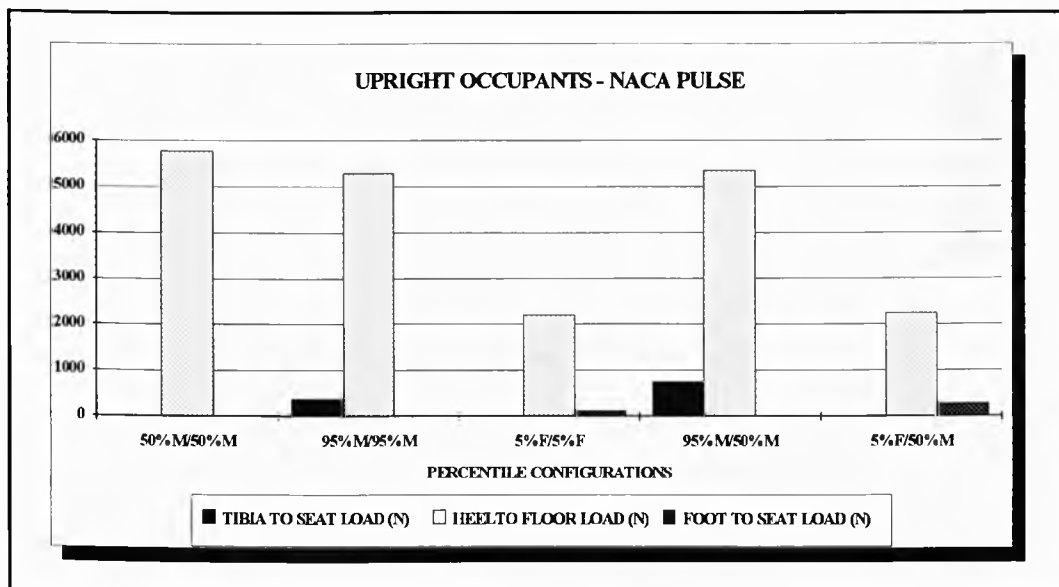


Figure 98. Upright Occupants, NACA Pulse - Tibia to Seat, Heel to Floor, Foot to Seat Contact Loads versus Percentile Configurations

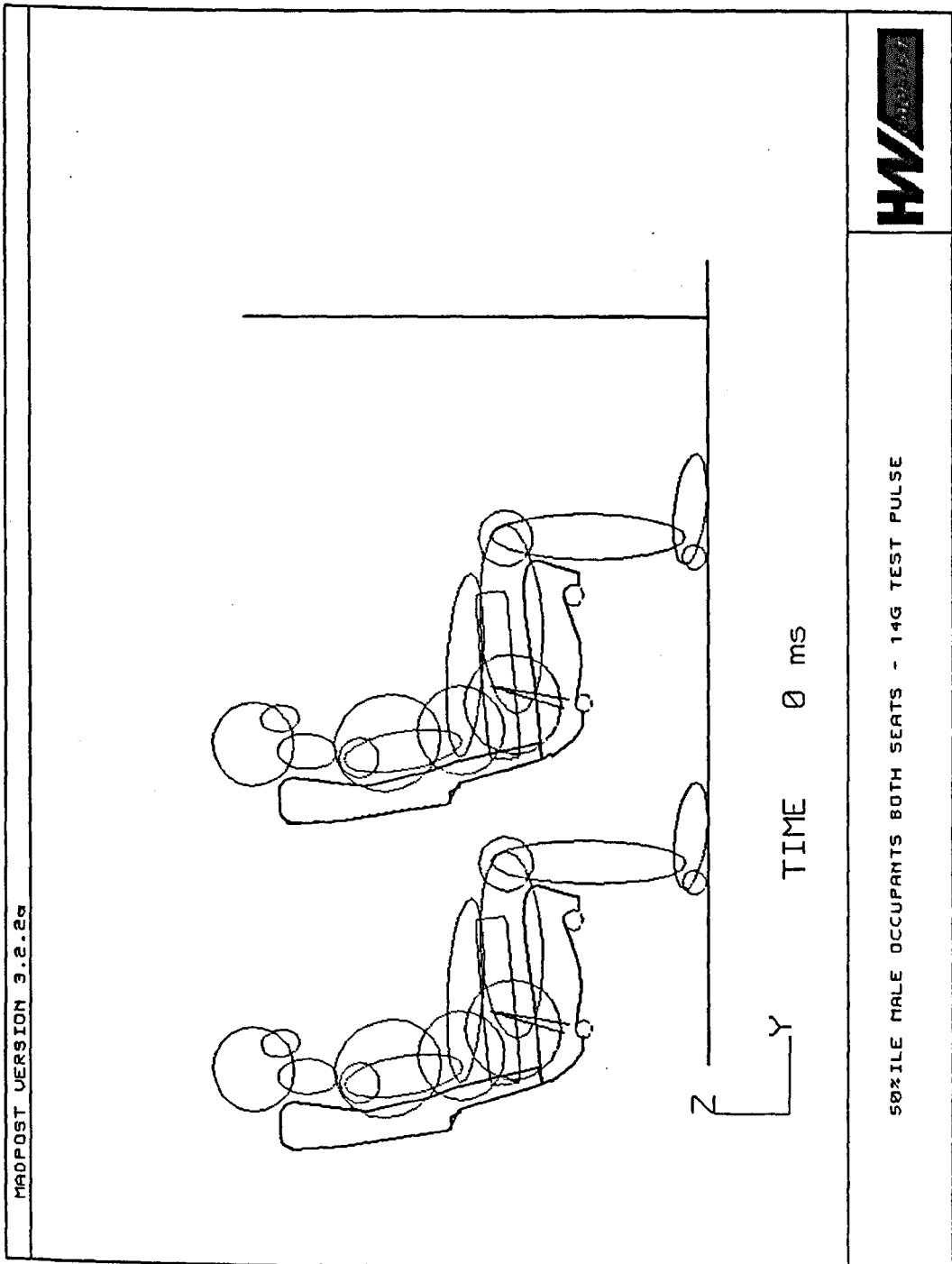


Figure 99. 50th Percentile Male Occupants Both Seats - 14G Test Pulse

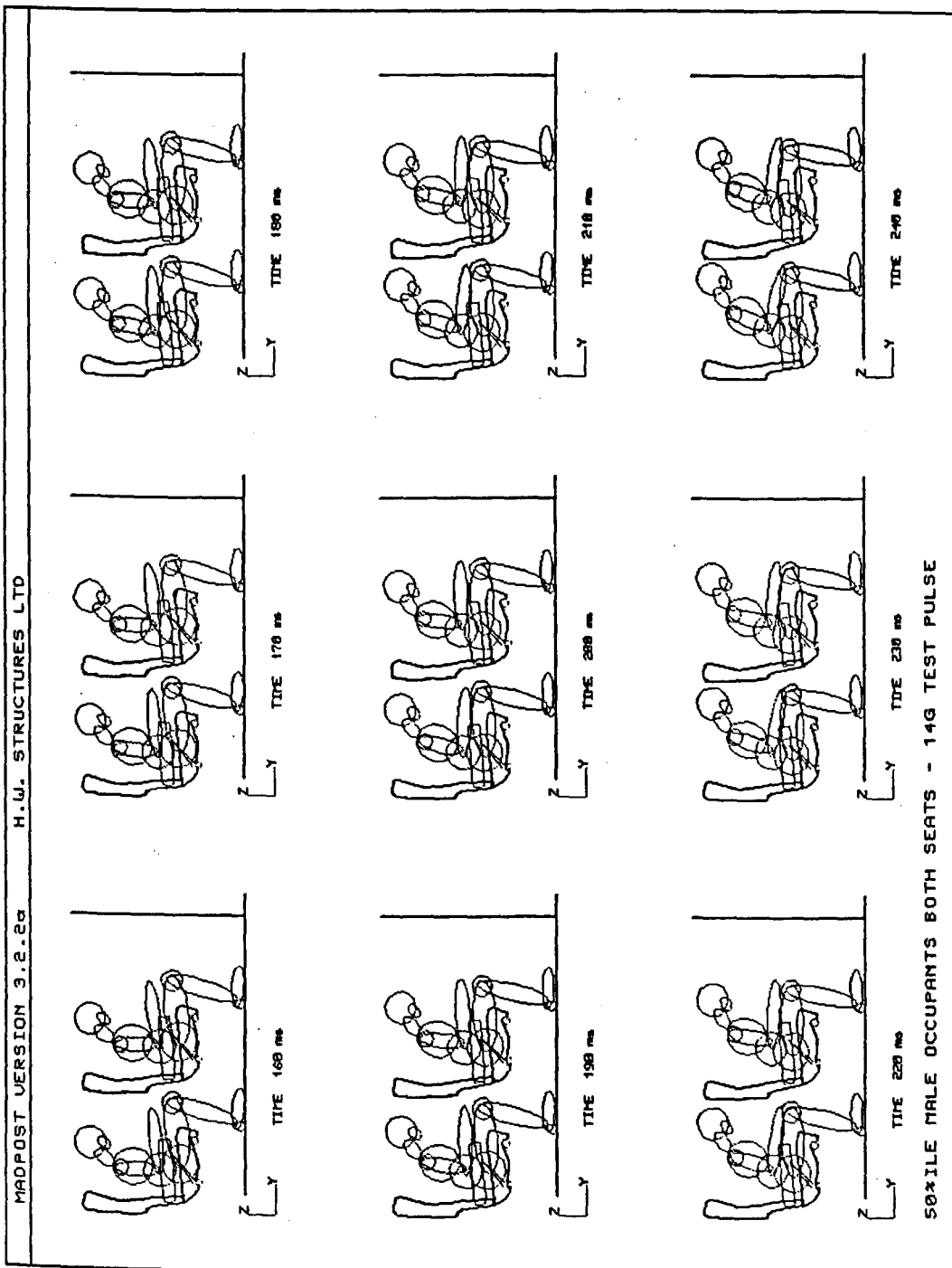


Figure 100. 50th Percentile Male Occupants Both Seats - 14G Test Pulse 160ms to 240ms Sequential Plot

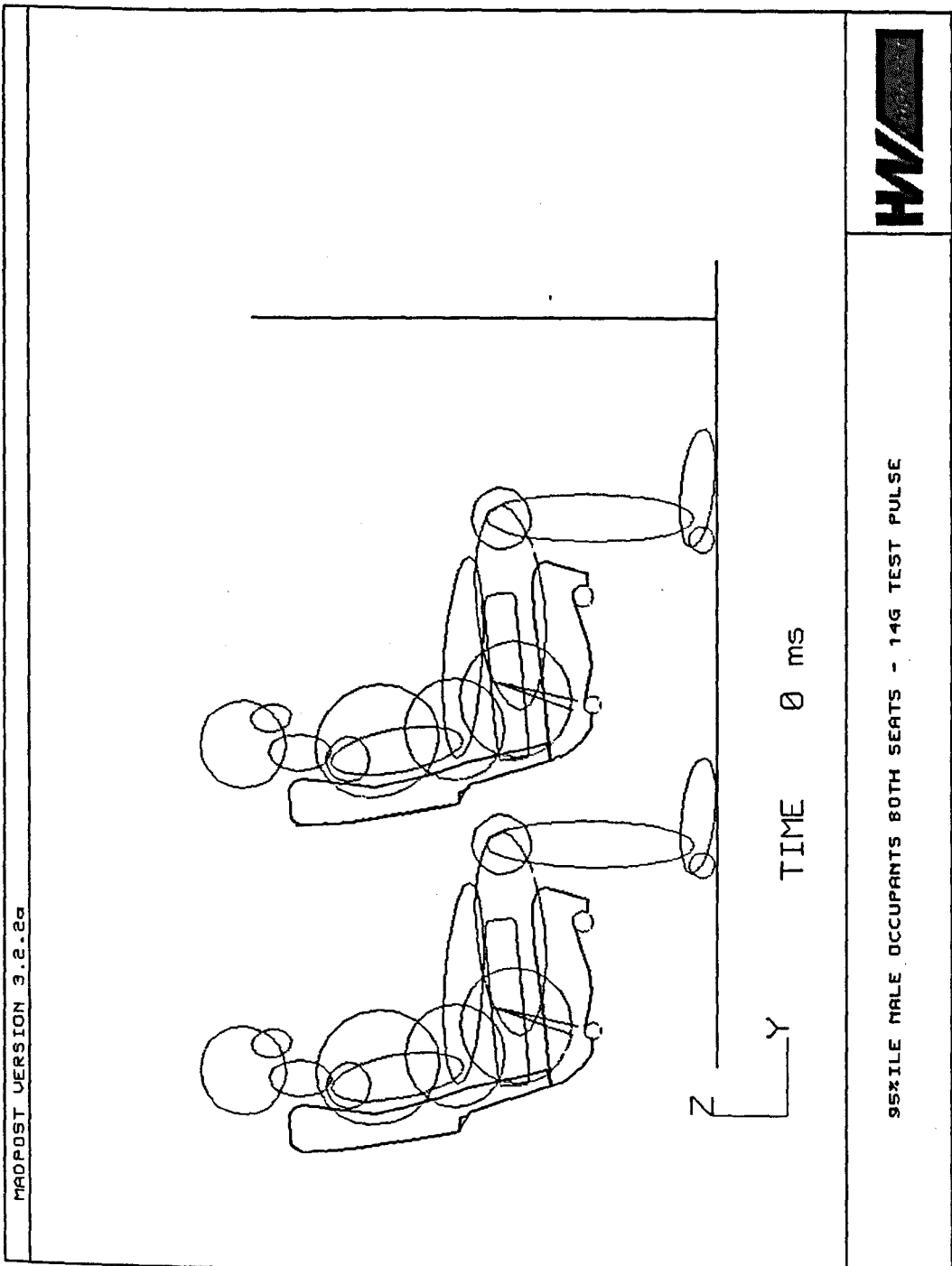


Figure 101. 95th Percentile Male Occupants Both Seats - 14G Test Pulse

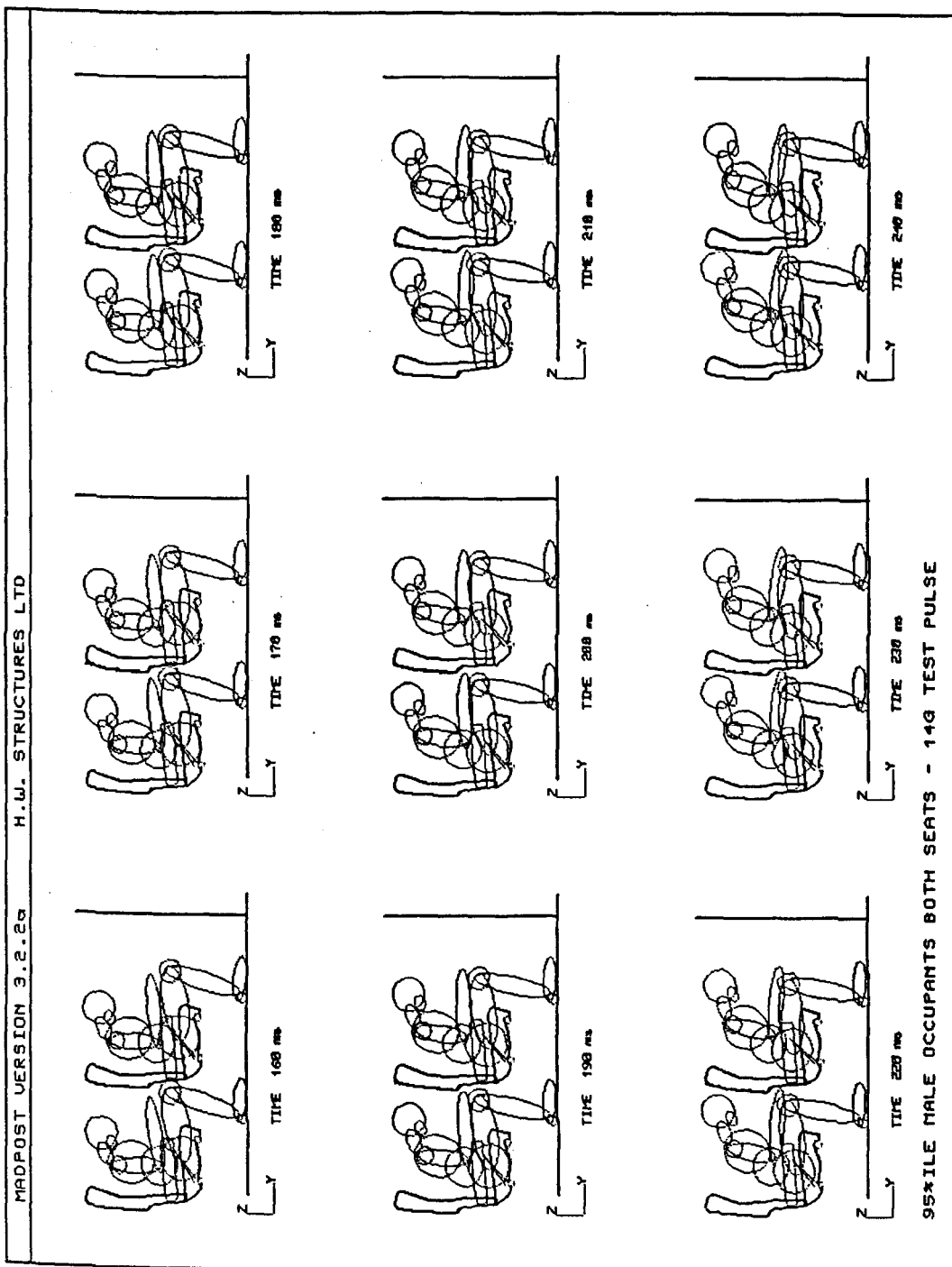


Figure 102. 95th Percentile Male Occupants Both Seats - 14G Test Pulse 160ms to 240ms Sequential Plot

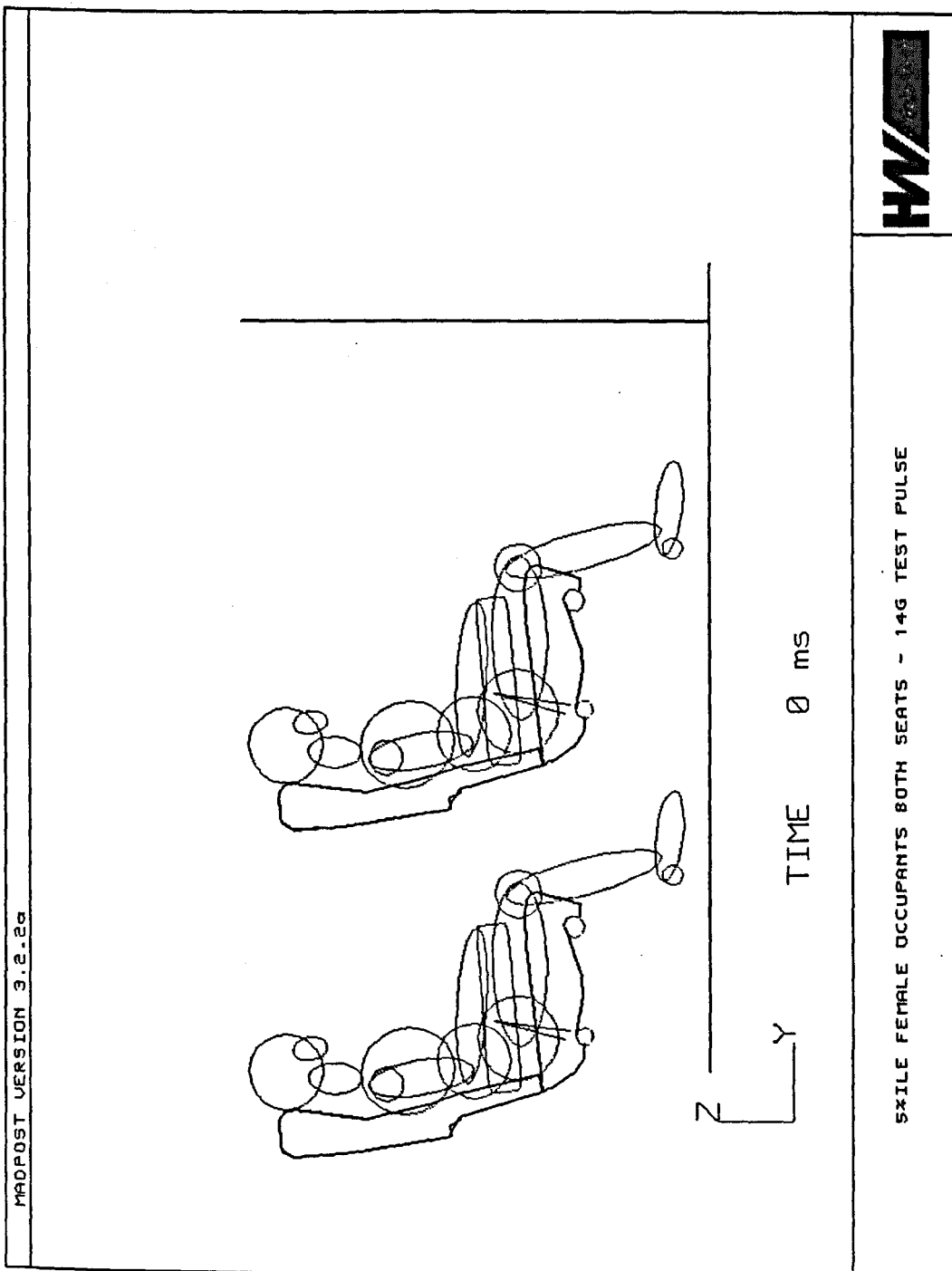


Figure 103. 5th Percentile Female Occupants Both Seats - 14G Test Pulse

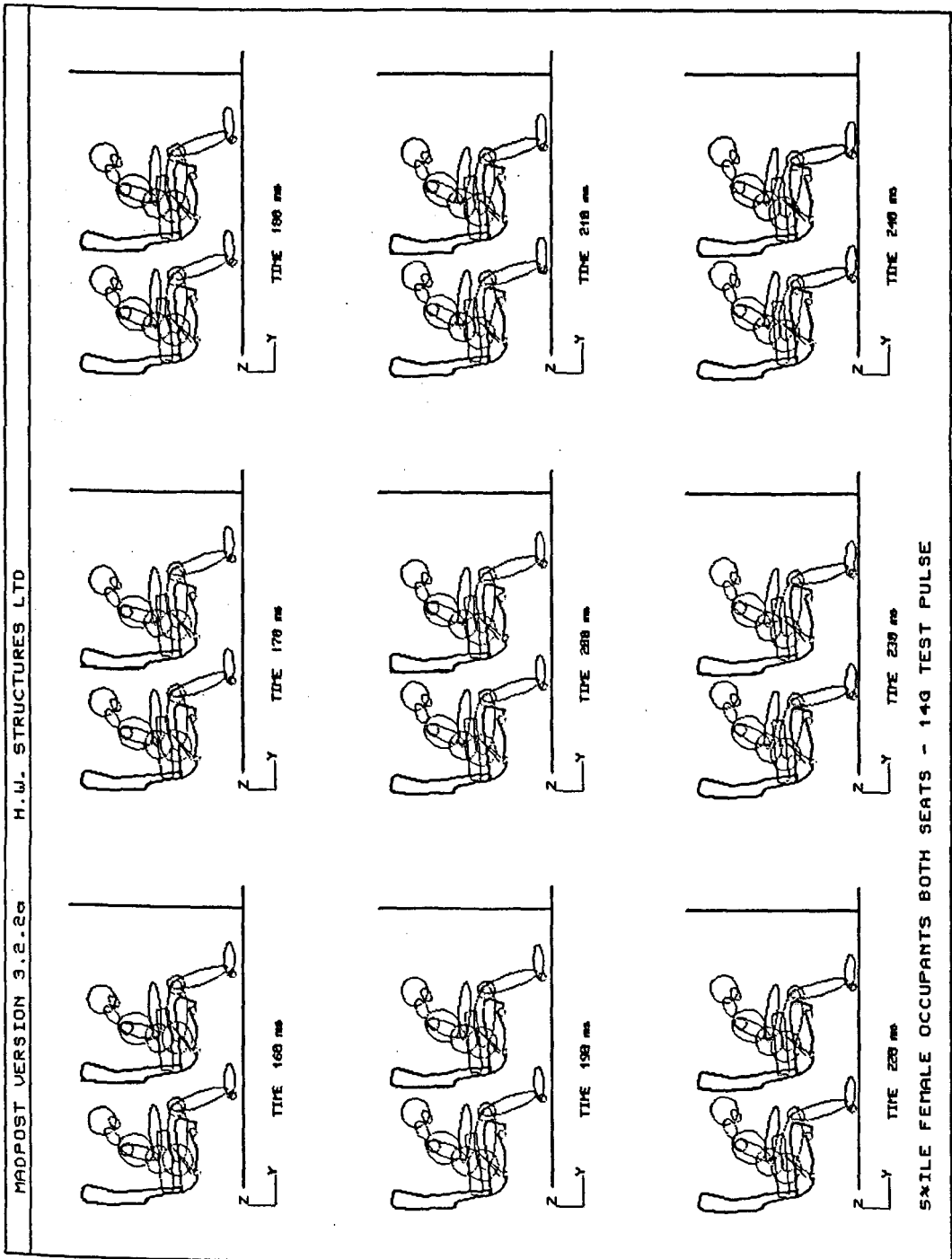


Figure 104. 5th Percentile Female Occupants Both Seats - 14G Test Pulse 160ms to 240ms Sequential Plot

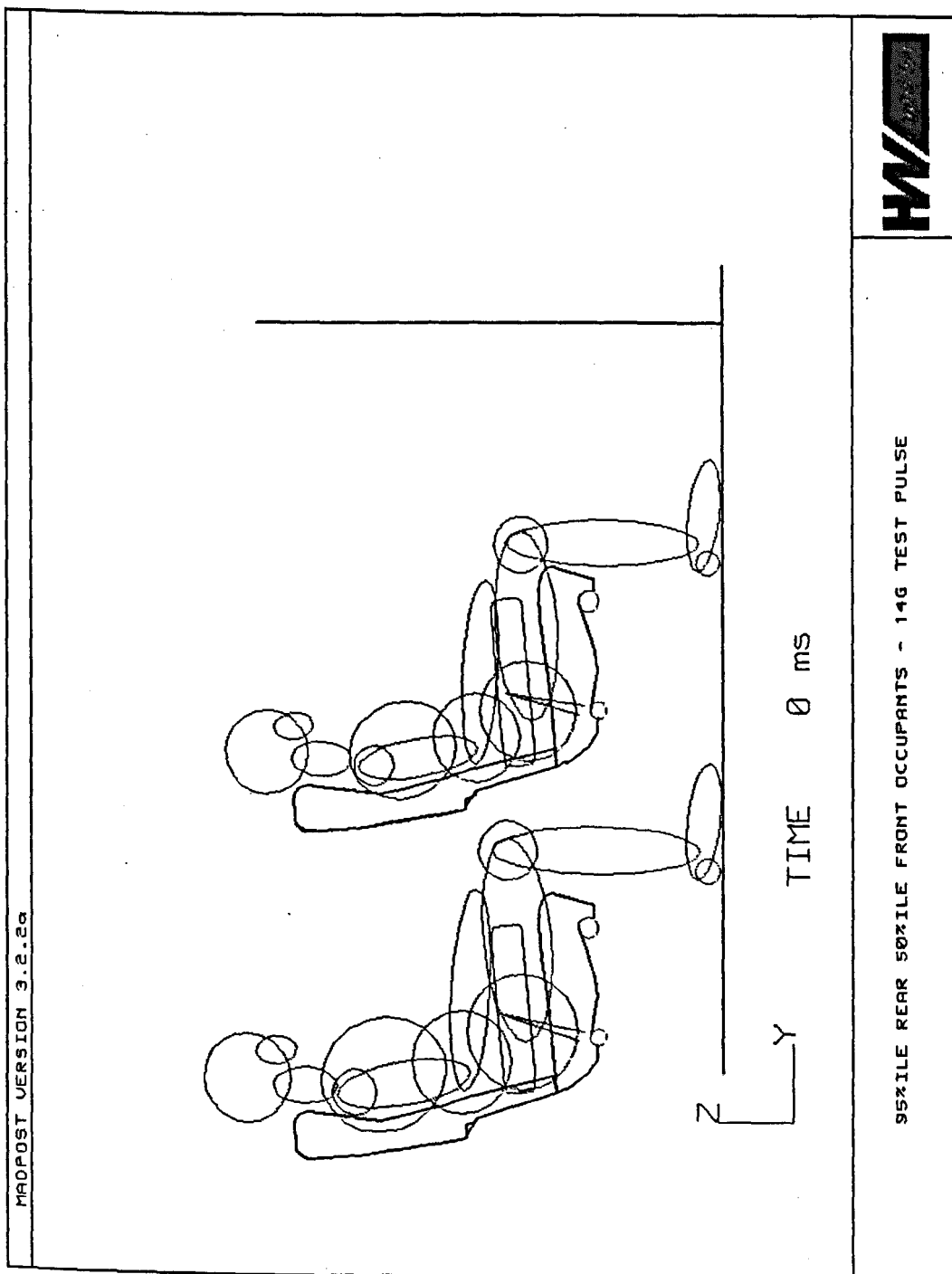


Figure 105. 95th Percentile Rear Occupant, 50th Percentile Front Occupant - 14G Test Pulse

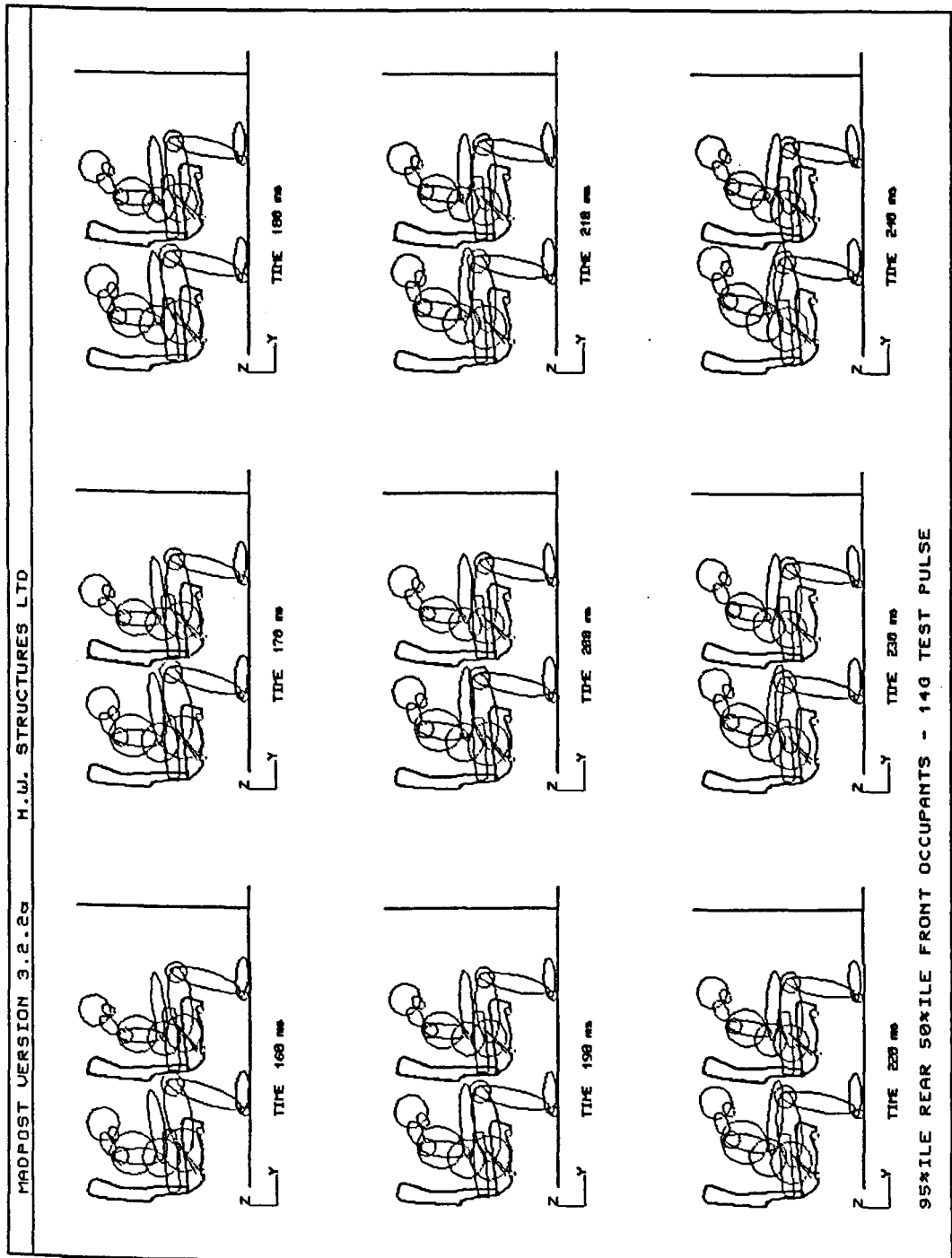


Figure 106. 95th Percentile Rear Occupant, 50th Percentile Front Occupant - 14G Test Pulse 160ms to 240ms Sequential Plot

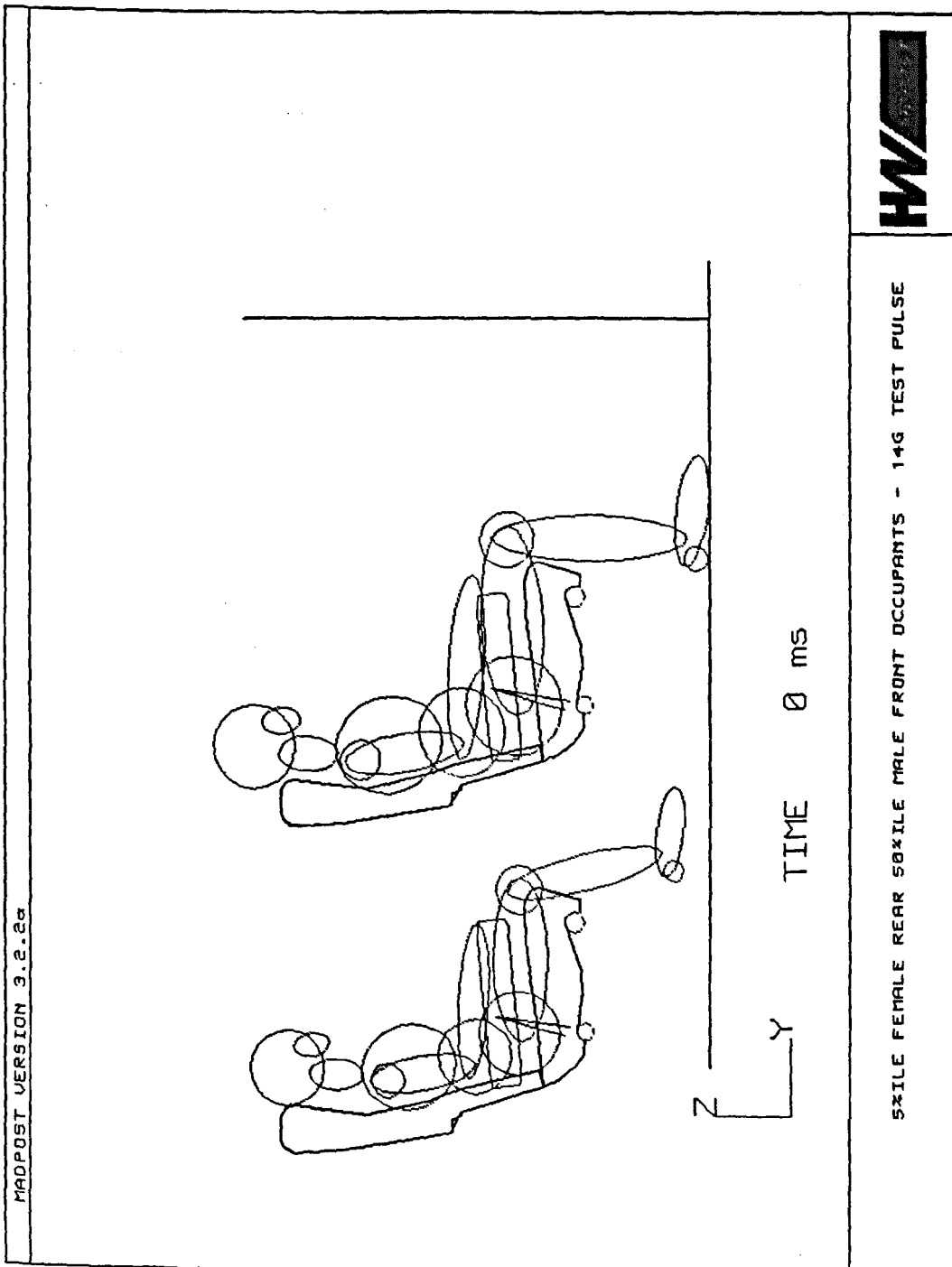


Figure 107. 5th Percentile Rear Occupant, 50th Percentile Front Occupant - 14G Test Pulse

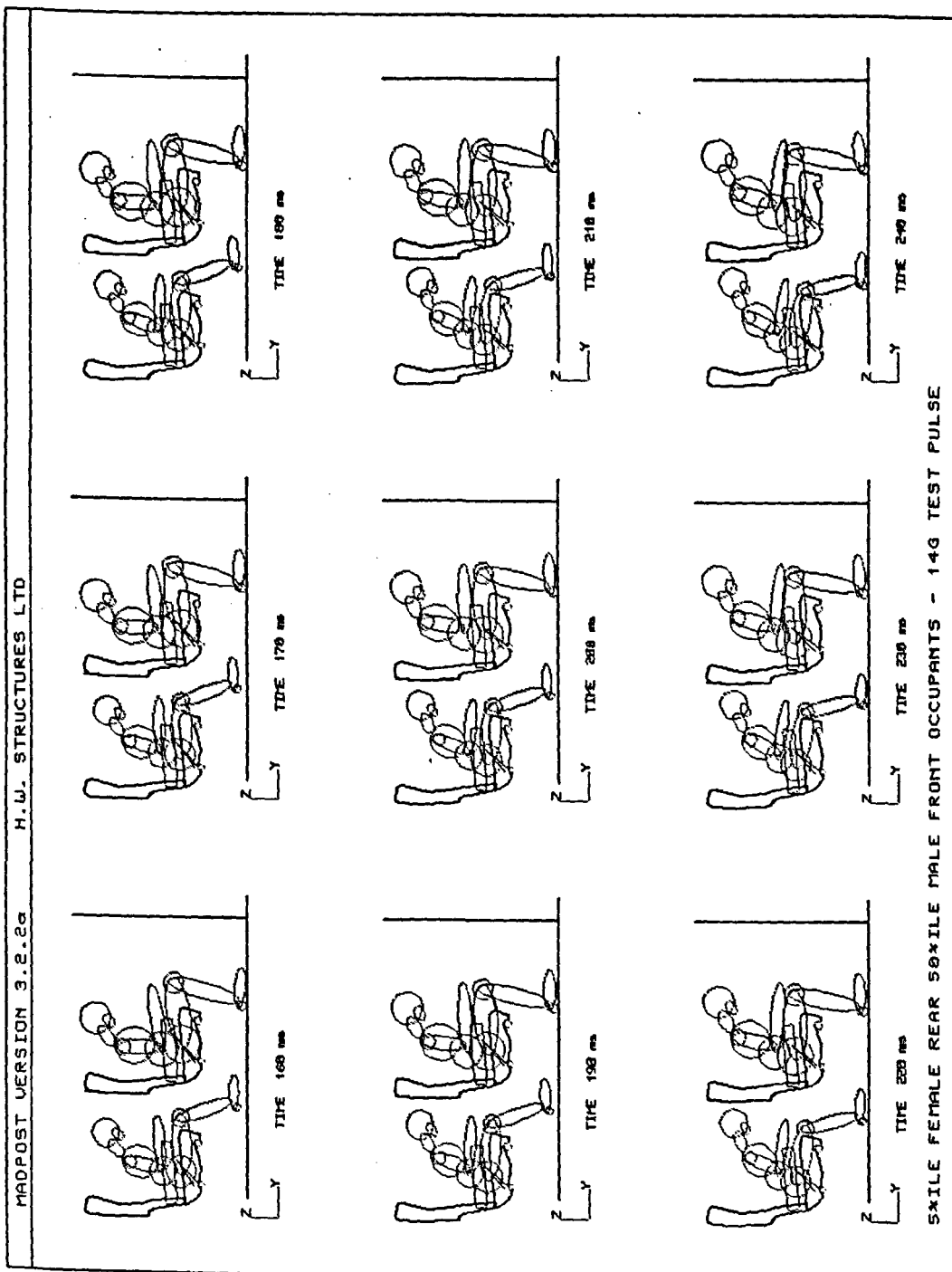


Figure 108. 5th Percentile Rear Occupant, 50th Percentile Front Occupant - 14G Test Pulse 160ms to 240ms Sequential Plot

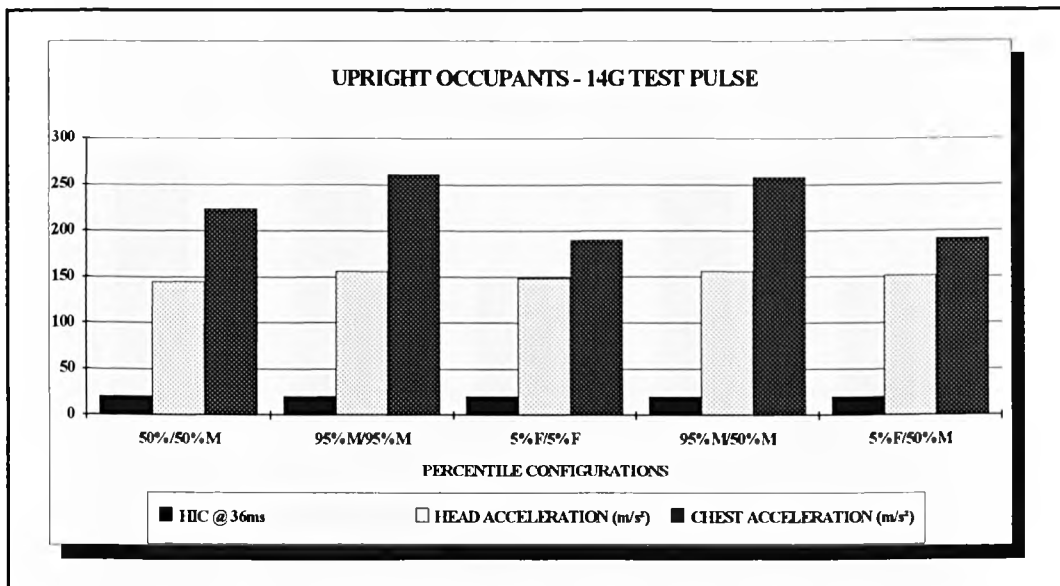


Figure 109. Upright Occupants, 14G Test Pulse - HIC, Head and Thorax Accelerations versus Percentile Configurations

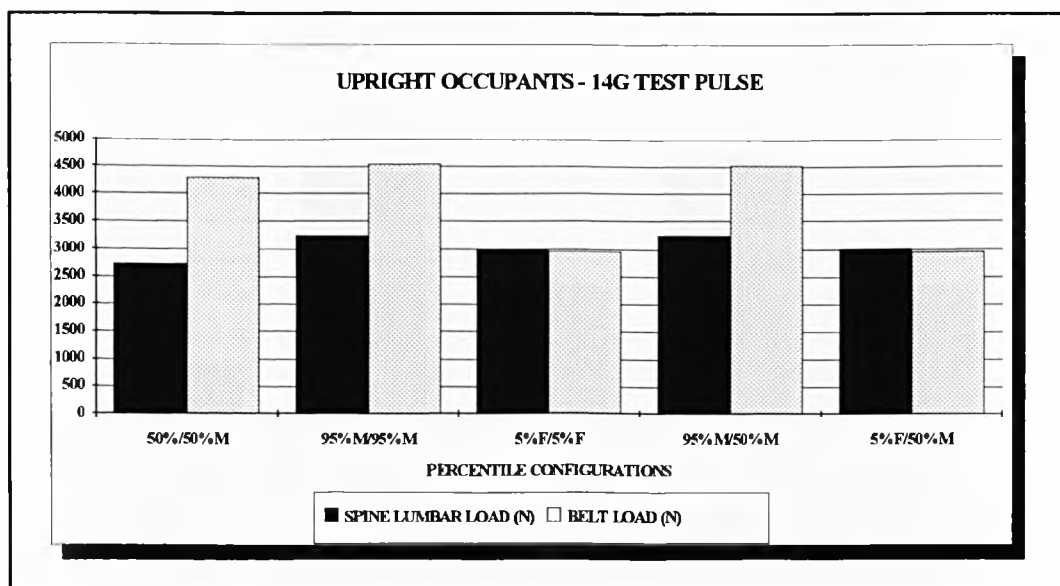


Figure 110. Upright Occupants, 14G Test Pulse - Lumbar Spine and Belt Loads versus Percentile Configurations

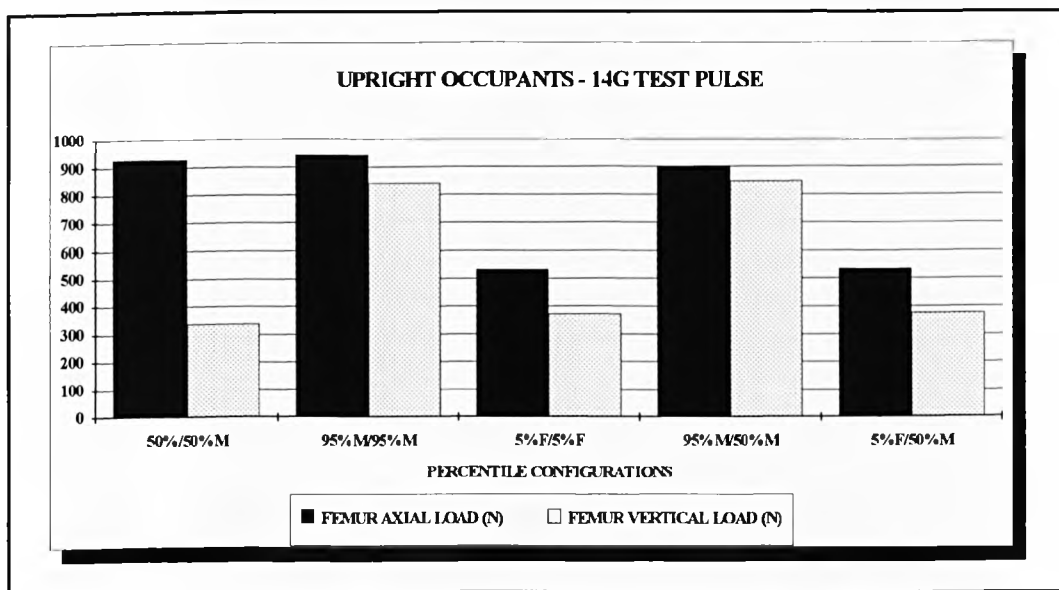


Figure 111. Upright Occupants, 14G Test Pulse - Femur Axial and Vertical Loads versus Percentile Configurations

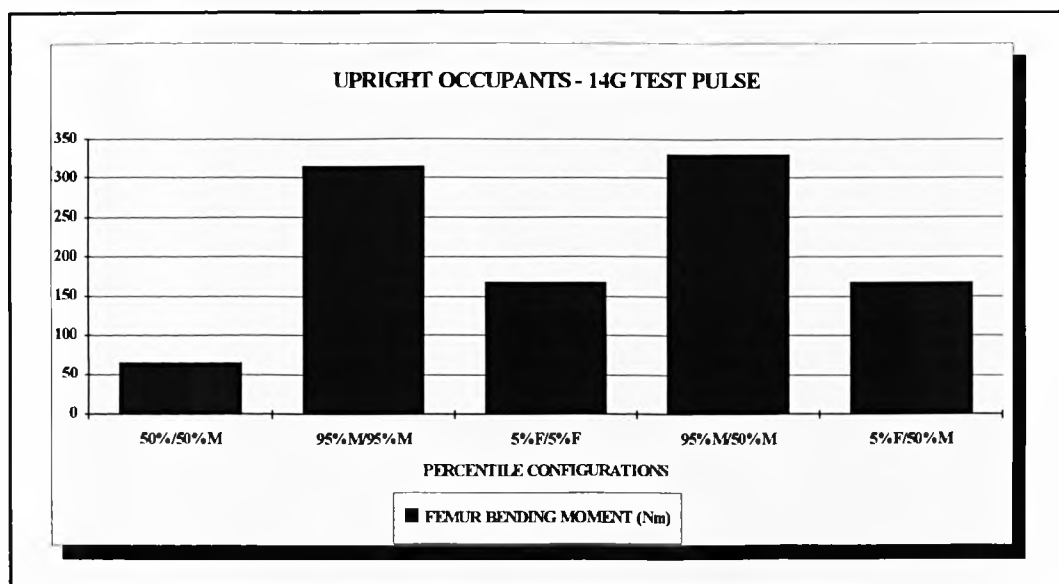


Figure 112. Upright Occupants, 14G Test Pulse - Femur Bending Moment versus Percentile Configurations

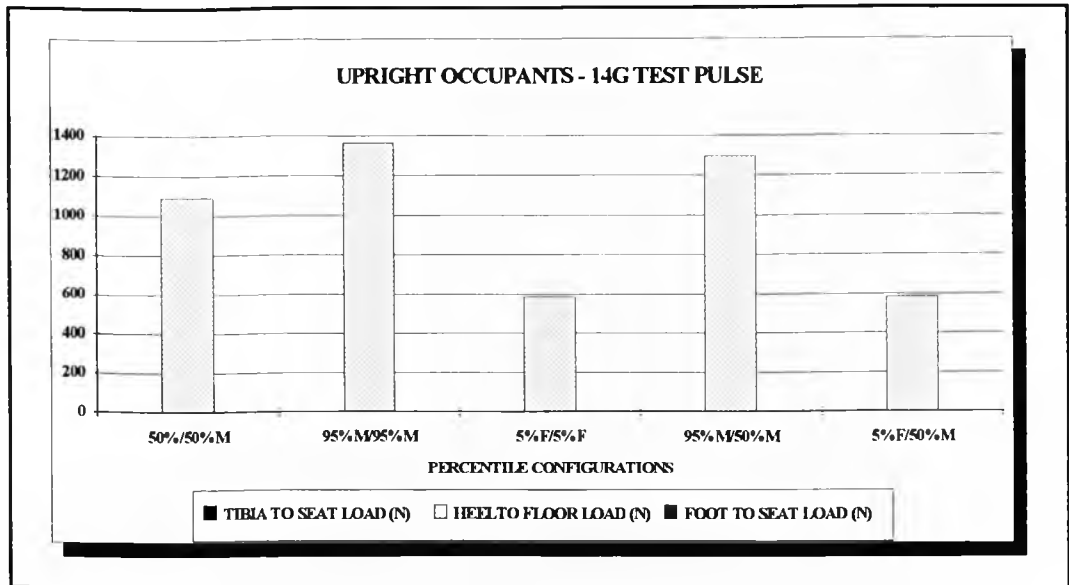


Figure 113. Upright Occupants, 14G Test Pulse - Tibia to Seat, Heel to Floor, Foot to Seat Contact Loads versus Percentile Configurations

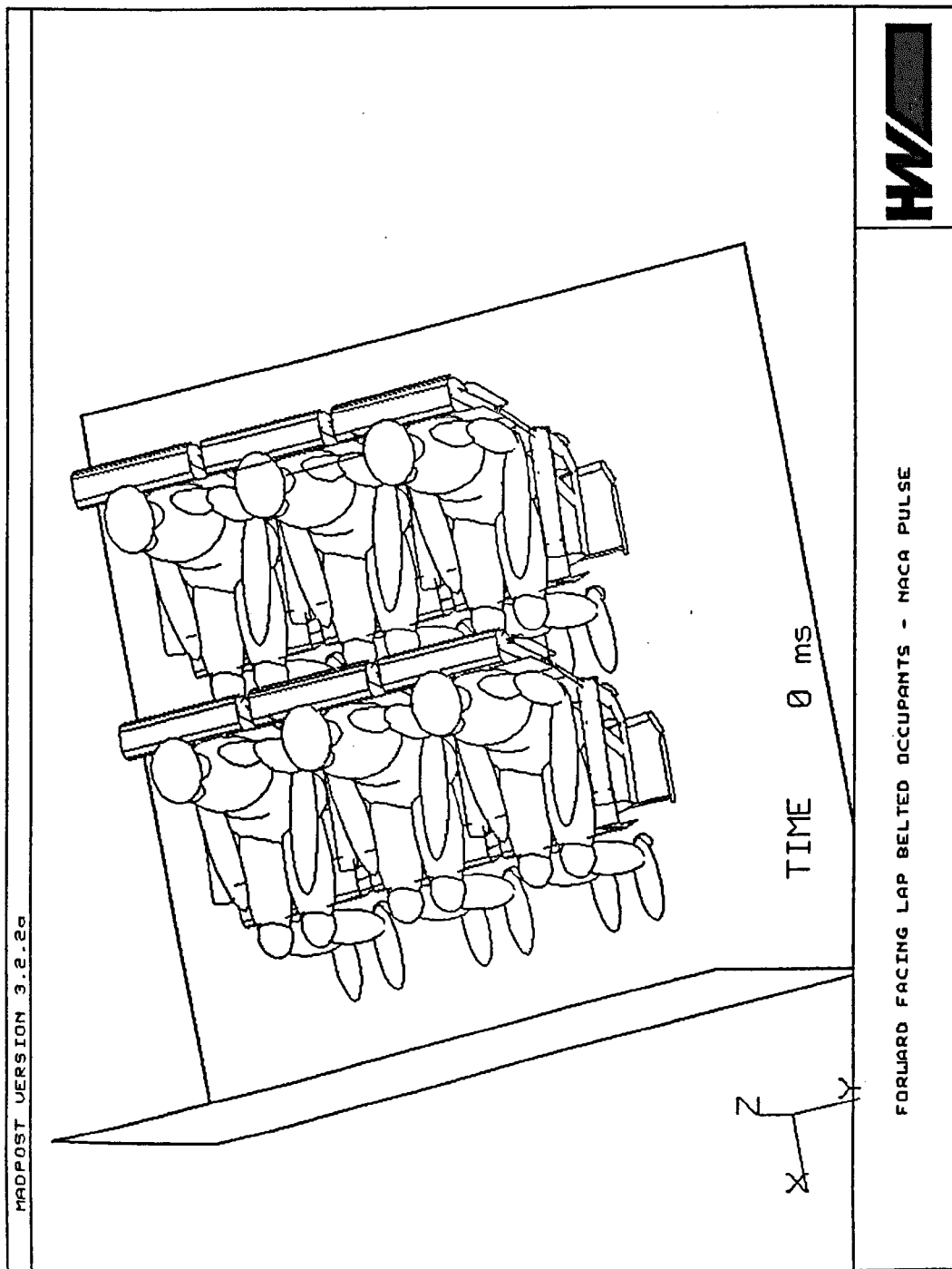


Figure 114. Forward Facing Lap Belted Occupants - at 0ms, using NACA Pulse

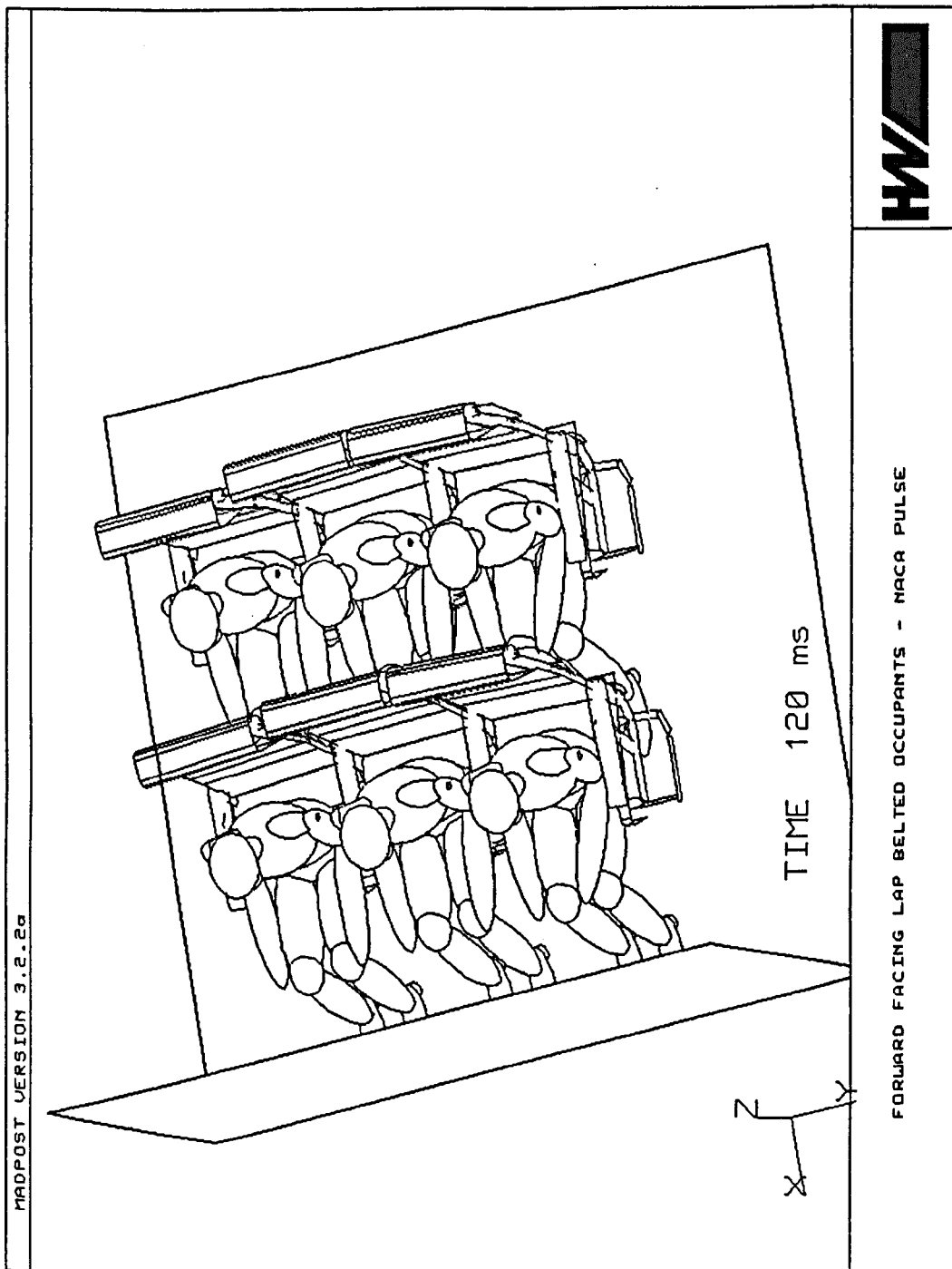


Figure 115. Forward Facing Lap Belted Occupants - at 120ms, using NACA Pulse

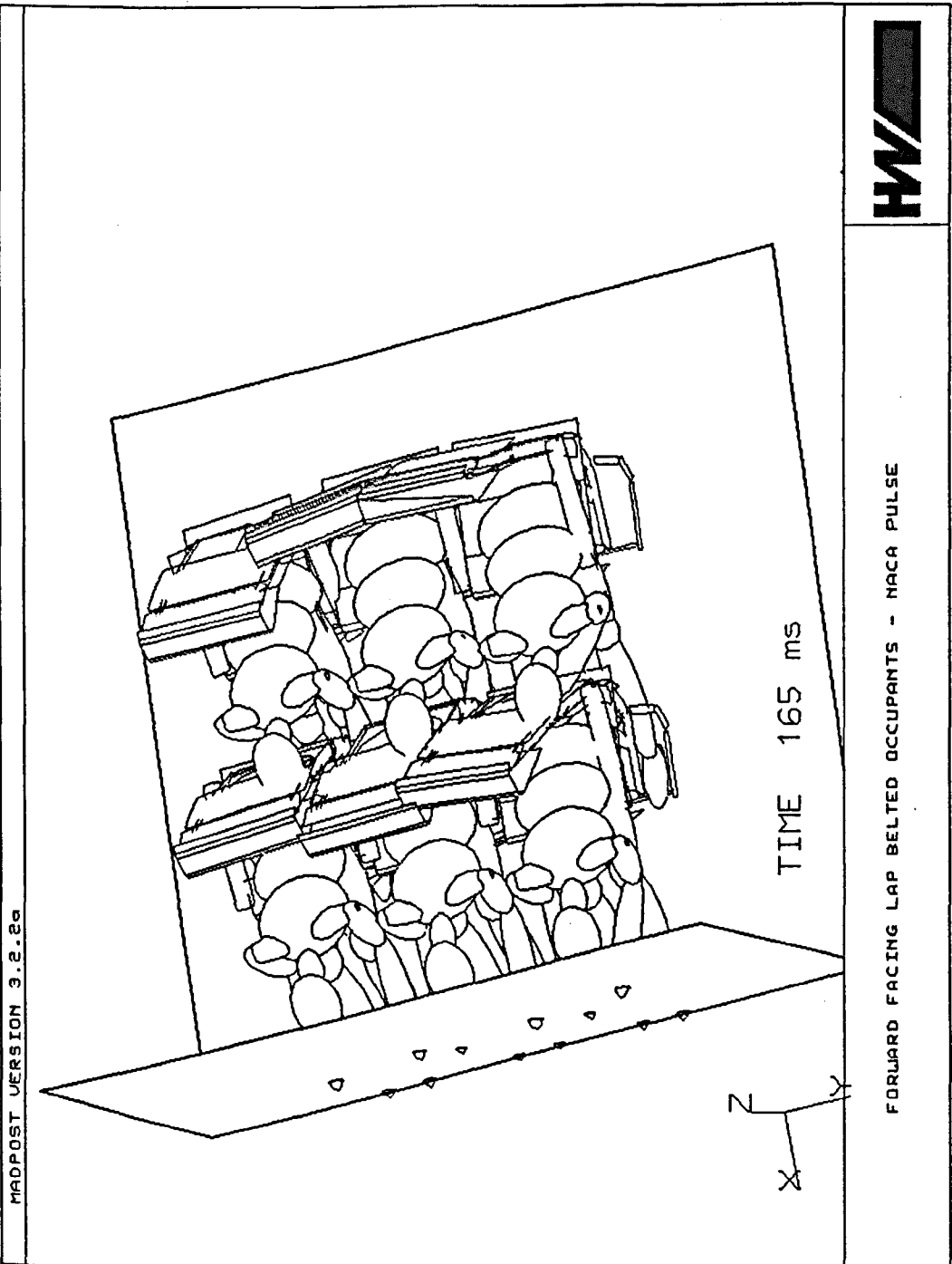
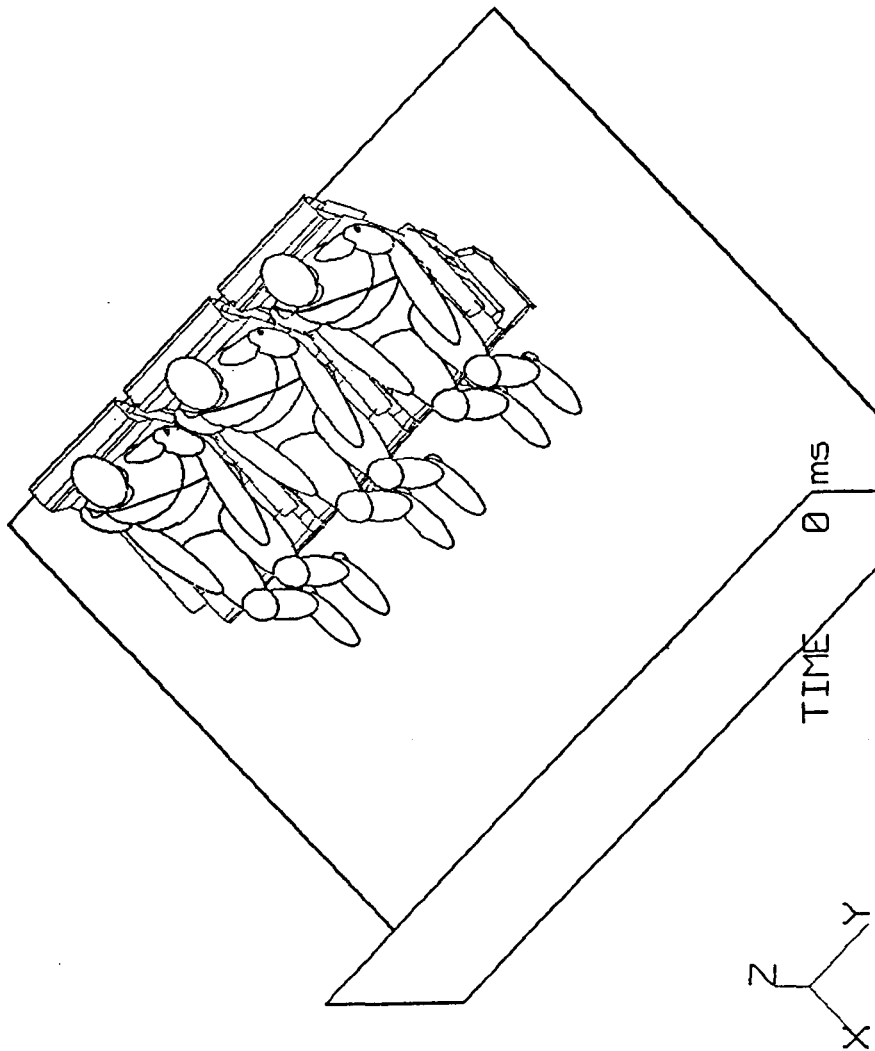


Figure 116. Forward Facing Lap Belted Occupants - at 165ms, using NACA Pulse



FORWARD FACING THREE POINT BELTED OCCUPANTS

Figure 117. Forward Facing Three Point Belted Occupants - at 0ms, using NACA Pulse

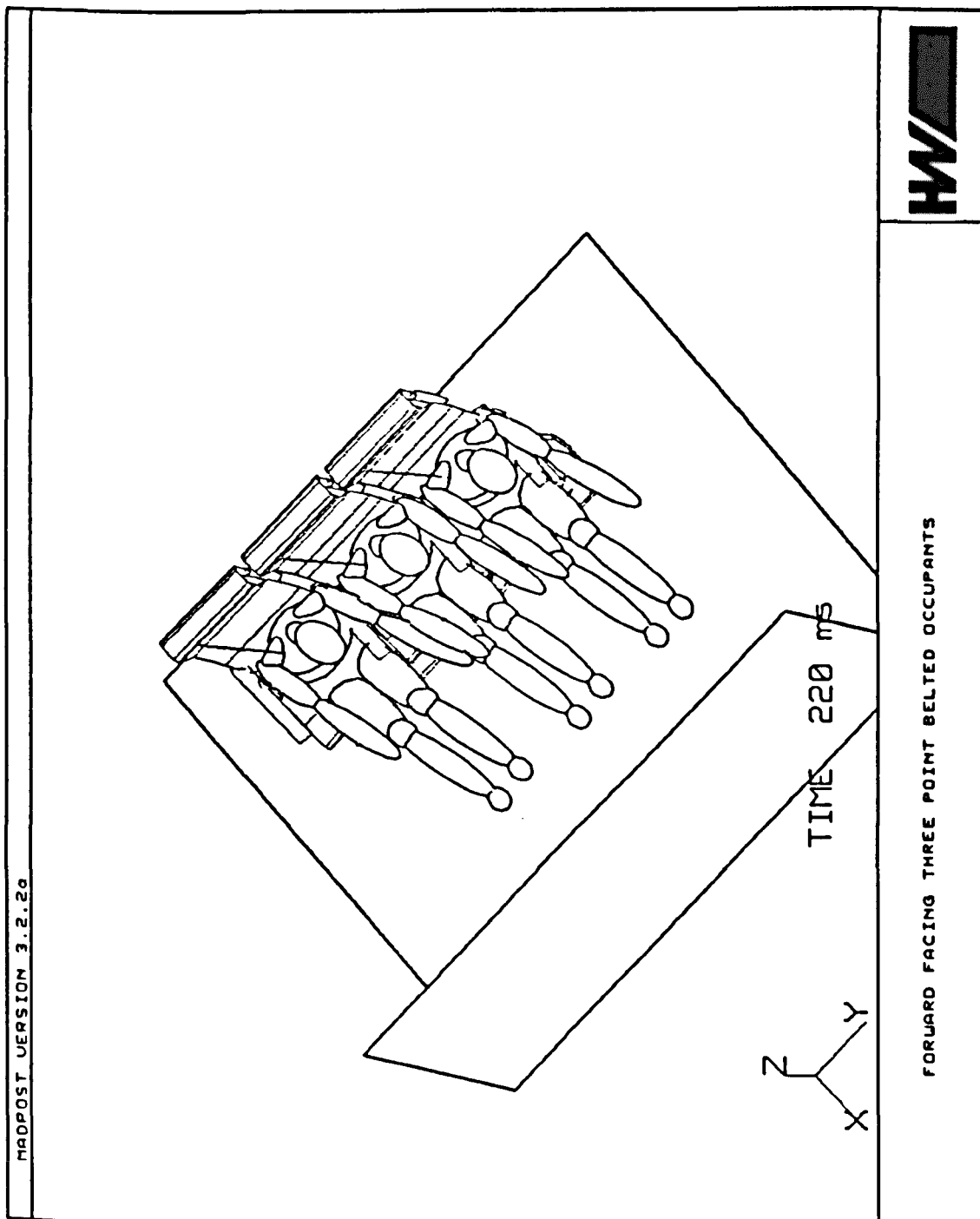


Figure 118. Forward Facing Three Point Belted Occupants - at 220ms, using NACA Pulse

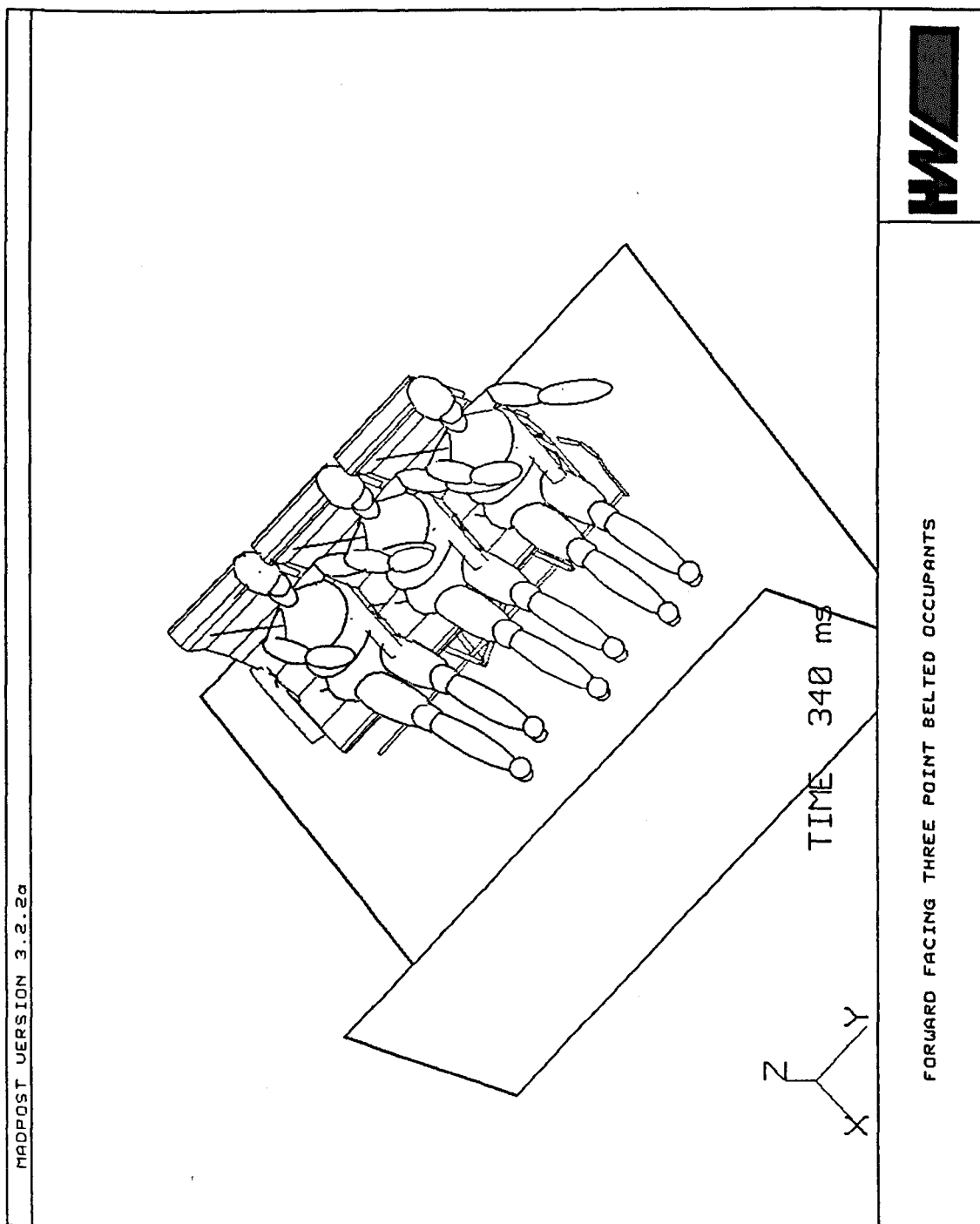


Figure 119. Forward Facing Three Point Belted Occupants - at 340ms, using NACA Pulse

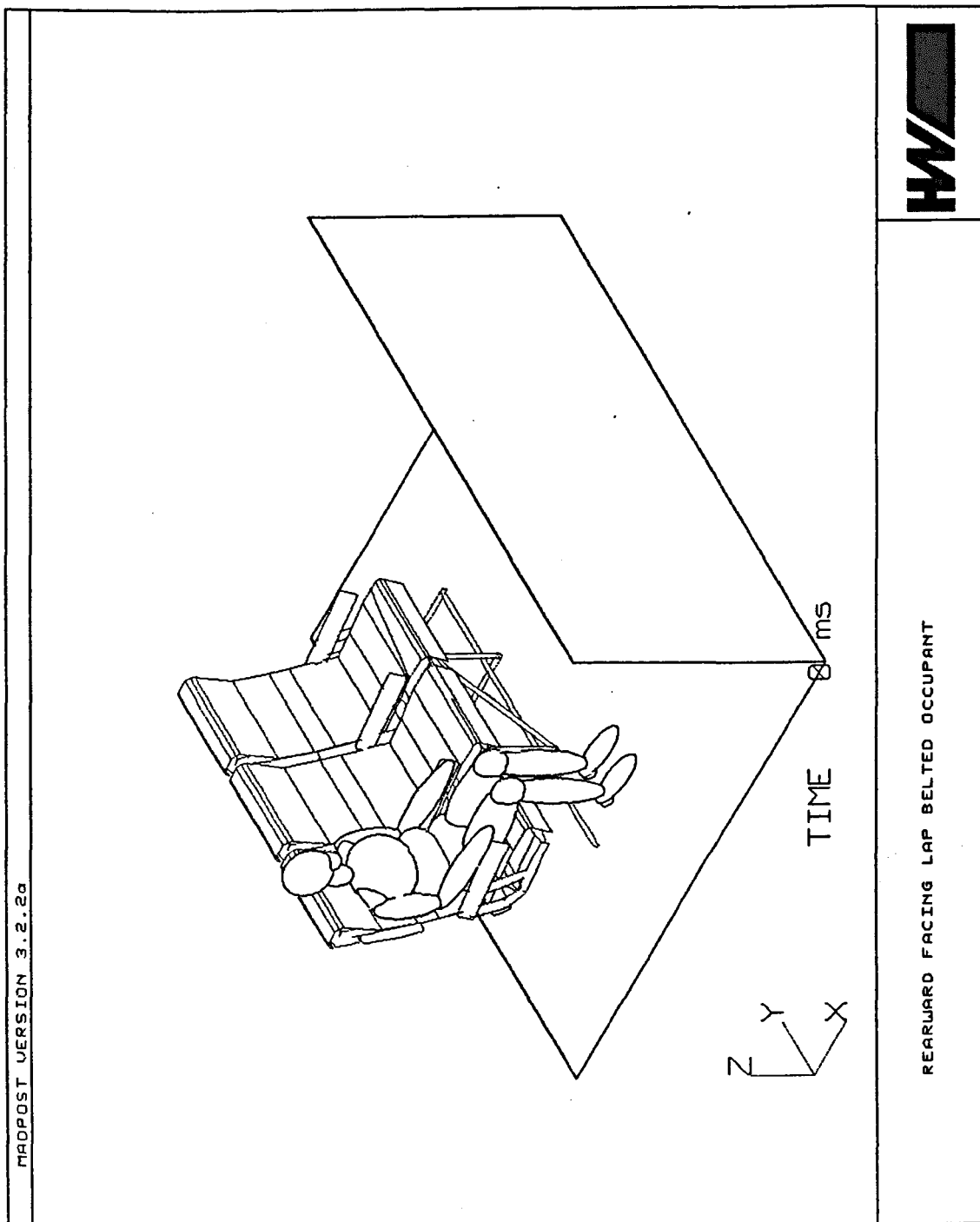


Figure 120. Rearward Facing Lap Belted Occupant - at 0ms, using NACA Pulse

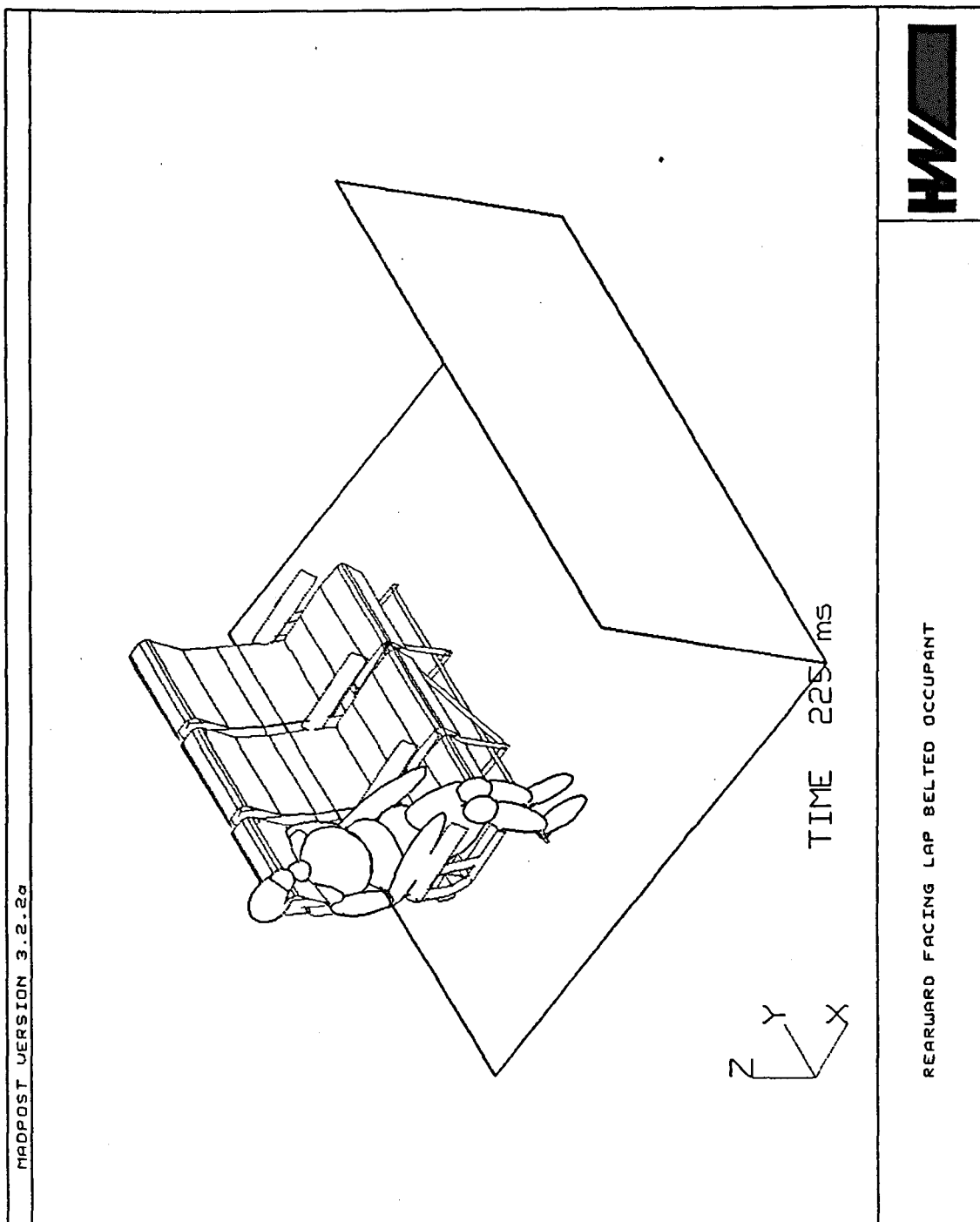


Figure 121. Rearward Facing Lap Belted Occupant - at 225ms, using NACA Pulse

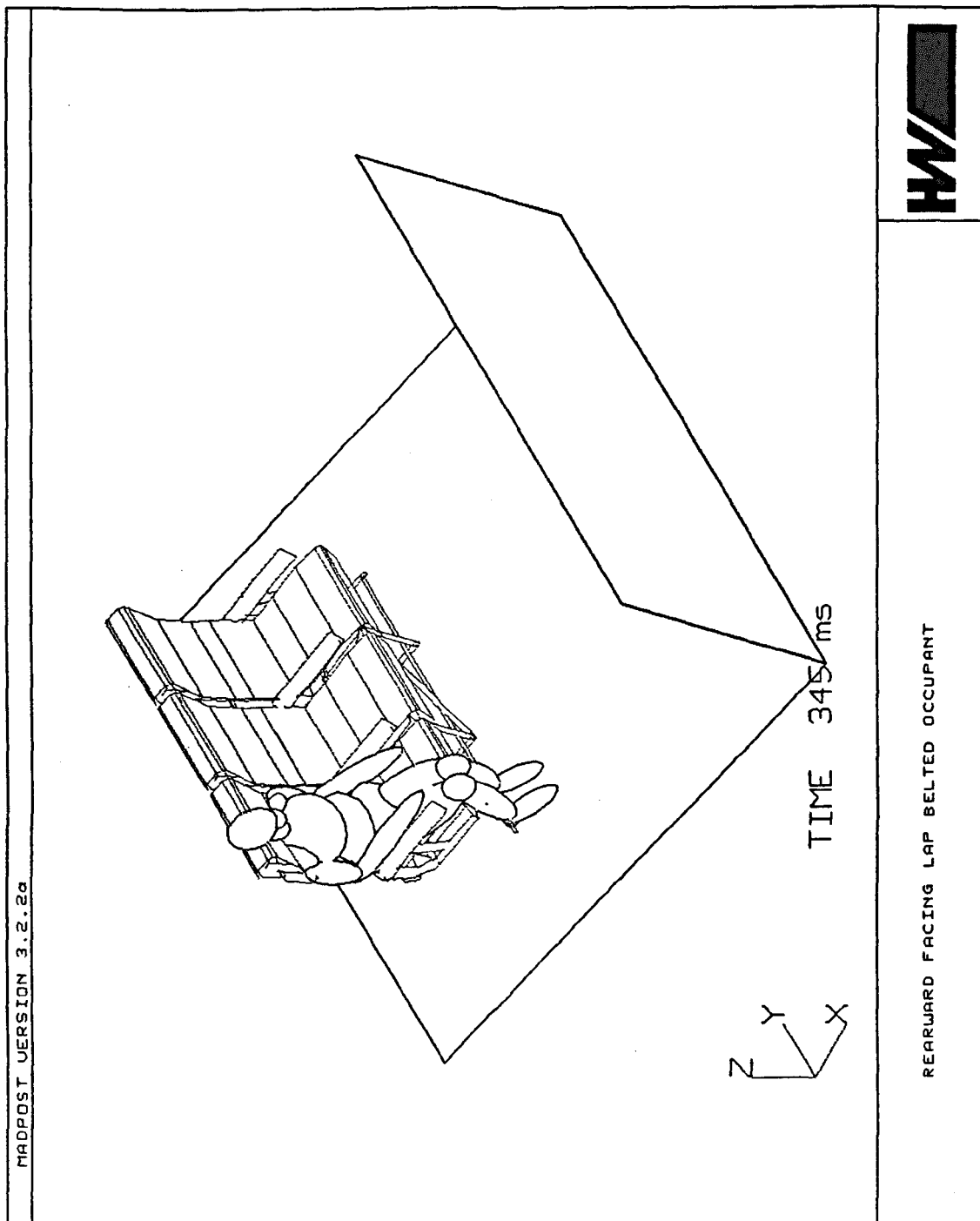


Figure 122. Rearward Facing Lap Belted Occupant - at 345ms, using NACA Pulse

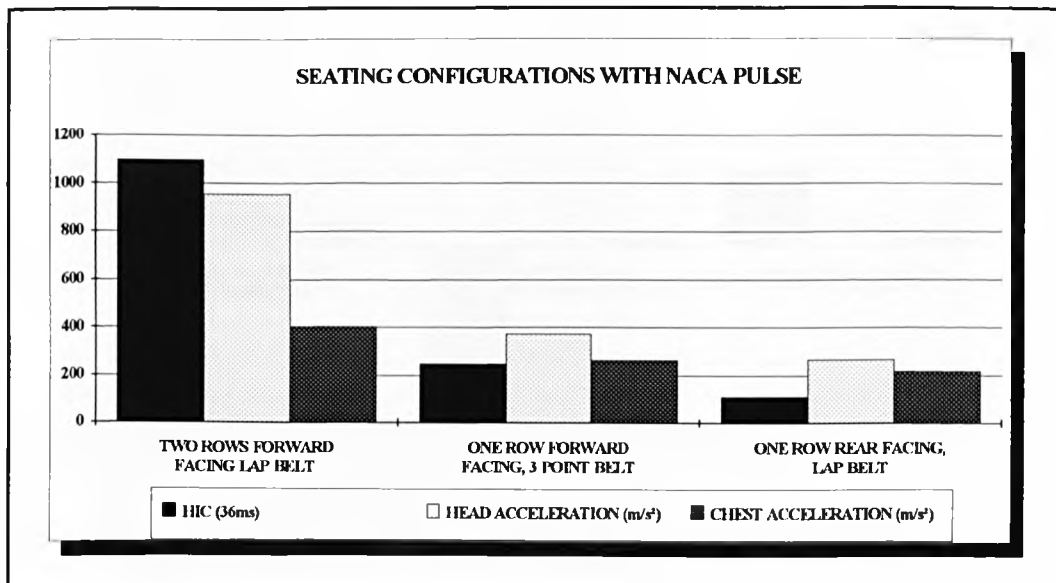


Figure 123. Seating Configurations with NACA Pulse - HIC, Head and Thorax Accelerations versus Various Restraints

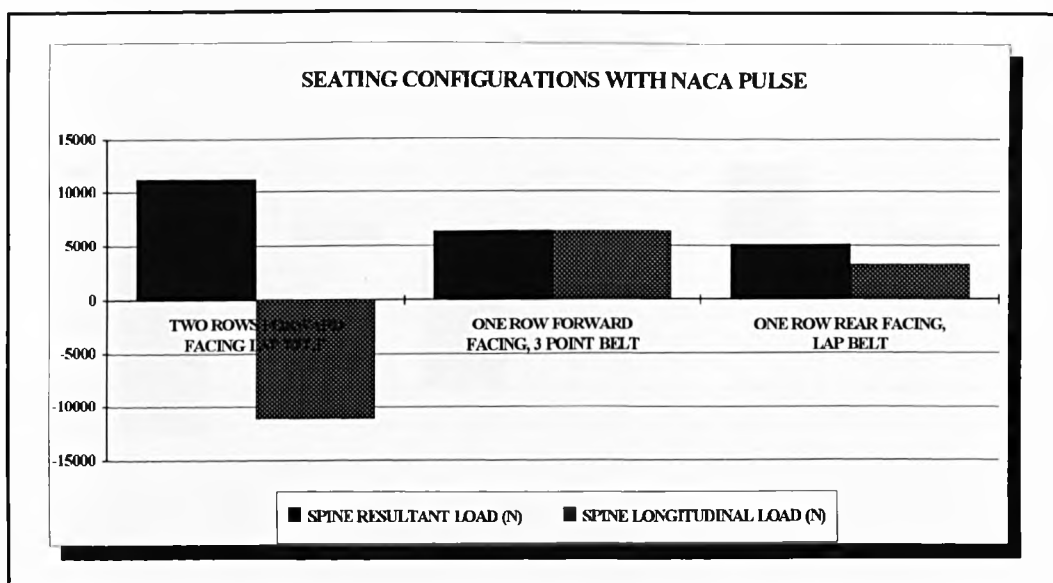


Figure 124. Seating Configurations with NACA Pulse - Lumbar Spine Resultant and Longitudinal Loads versus Various Restraints

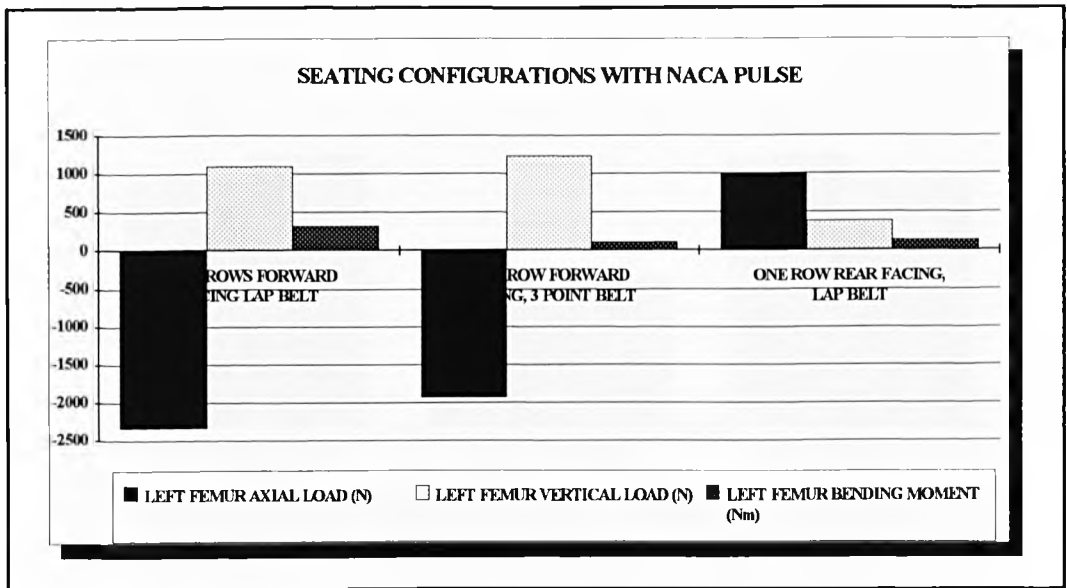


Figure 125. Seating Configurations with NACA Pulse - Left Femur Axial, Vertical Load and Bending Moment versus Various Restraints

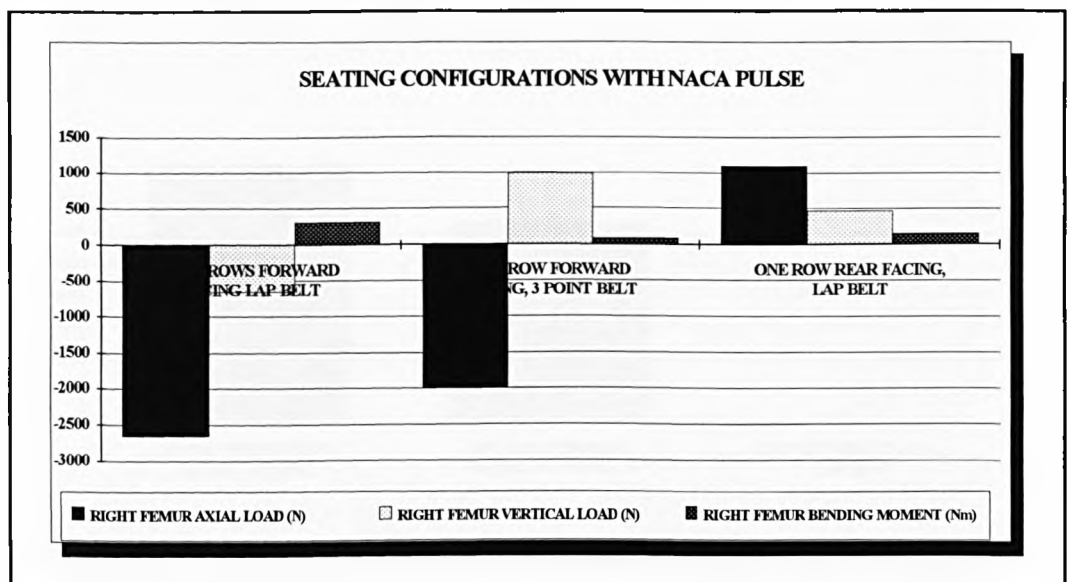


Figure 126. Seating Configurations with NACA Pulse - Right Femur Axial, Vertical Load and Bending Moment versus Various Restraints

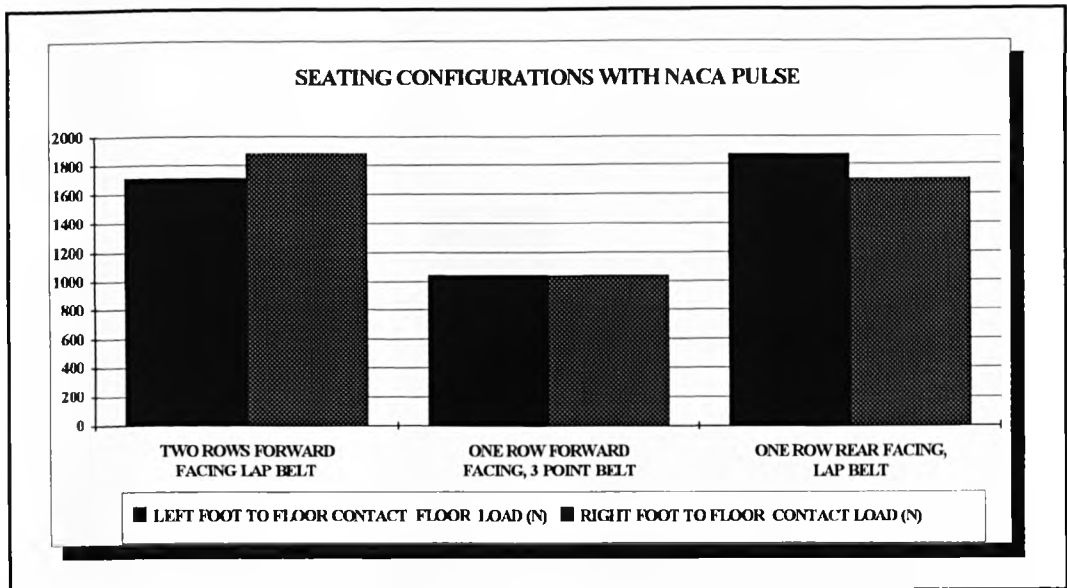


Figure 127. Seating Configurations with NACA Pulse - Left and Right Foot to Floor Contact Loads versus Various Restraints

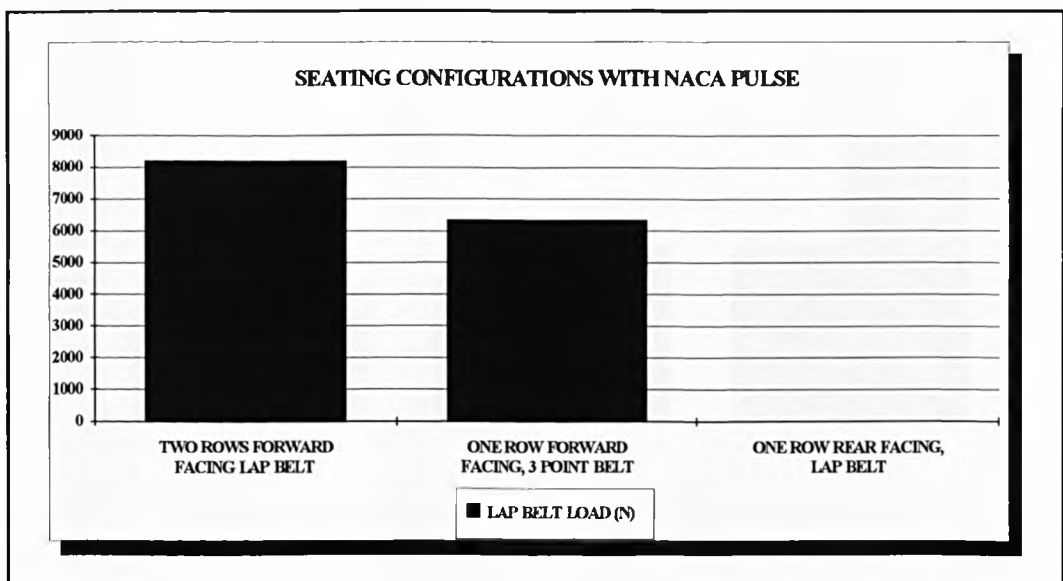


Figure 128. Seating Configurations with NACA Pulse - Lap Belt Load versus Various Restraints

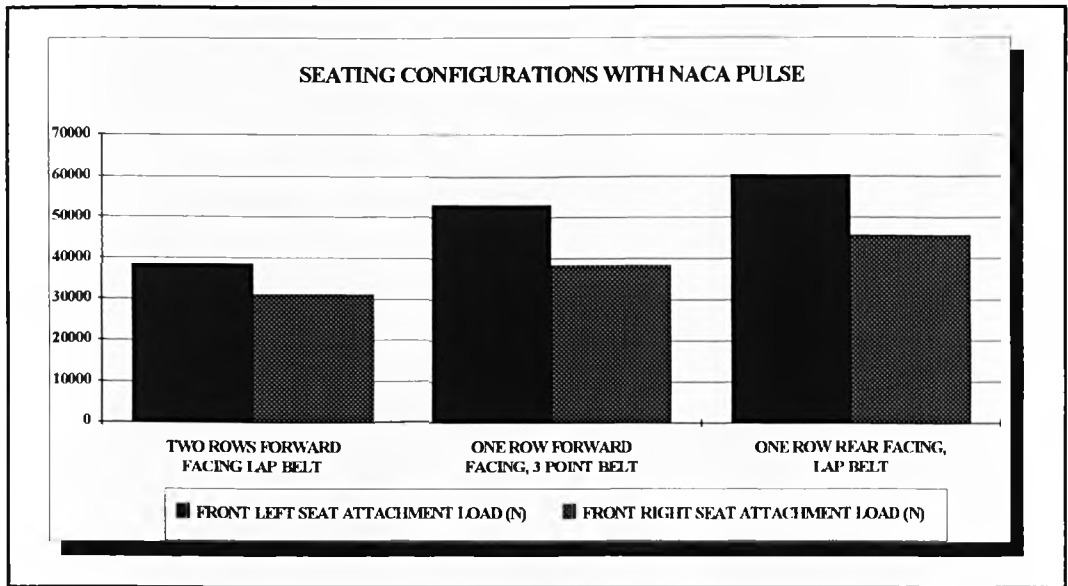


Figure 129. Seating Configurations with NACA Pulse - Front Left and Right Seat Attachment Loads versus Various Restraints

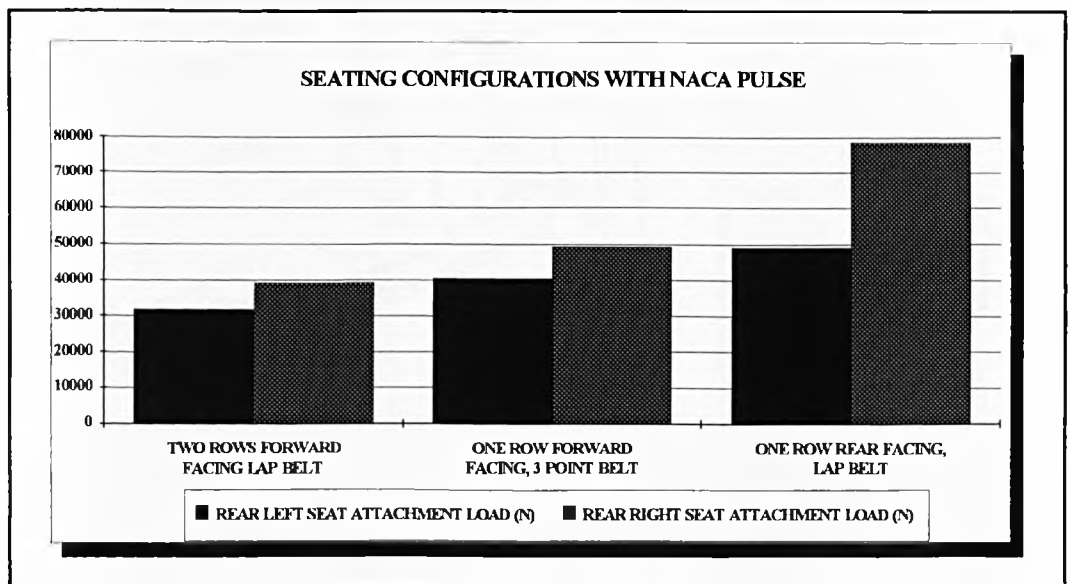


Figure 130. Seating Configurations with NACA Pulse - Rear Left and Right Seat Attachment Loads versus Various Restraints

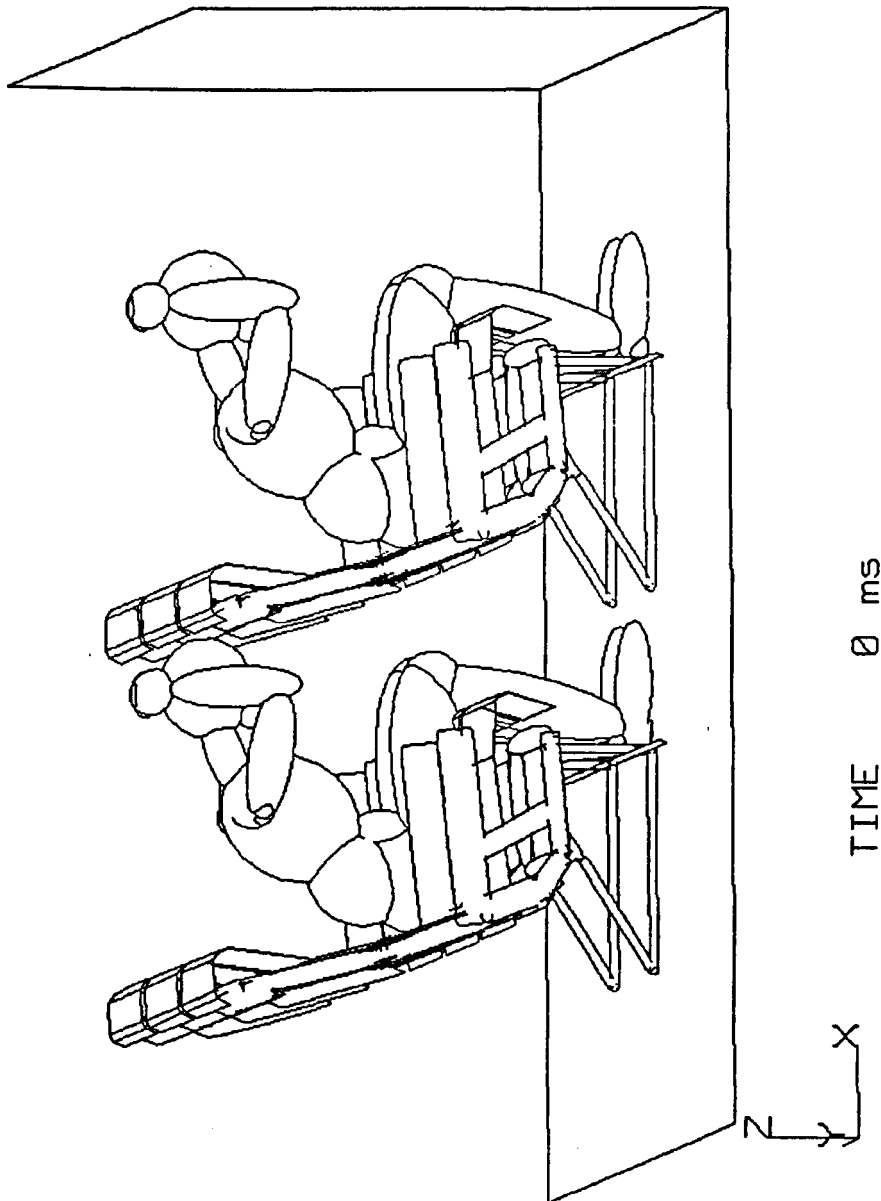


Figure 143. Brace Position Correlation Study, Baseline Configuration

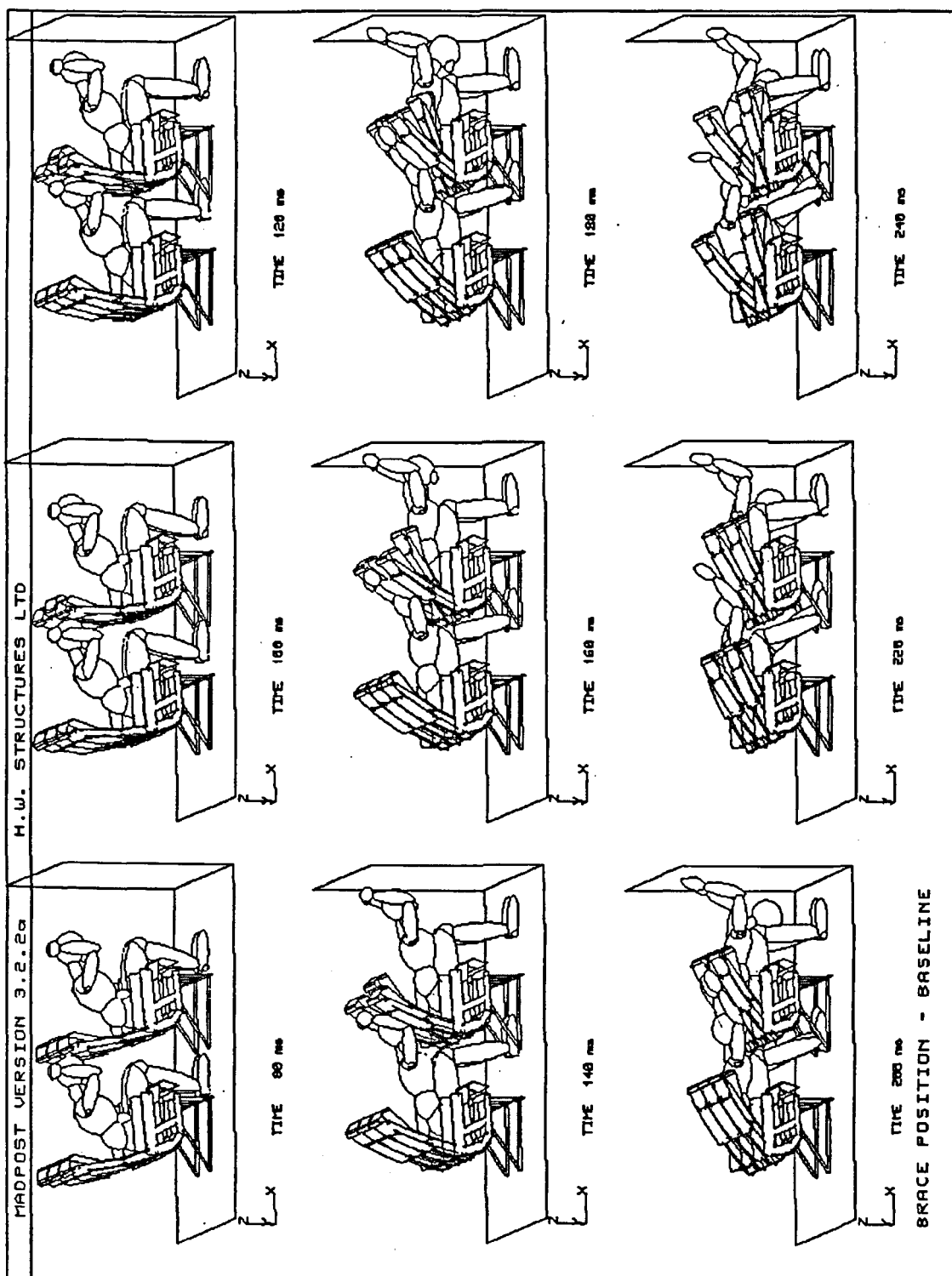


Figure 144. Brace Position Correlation Study, 80ms To 240ms Sequential Plot

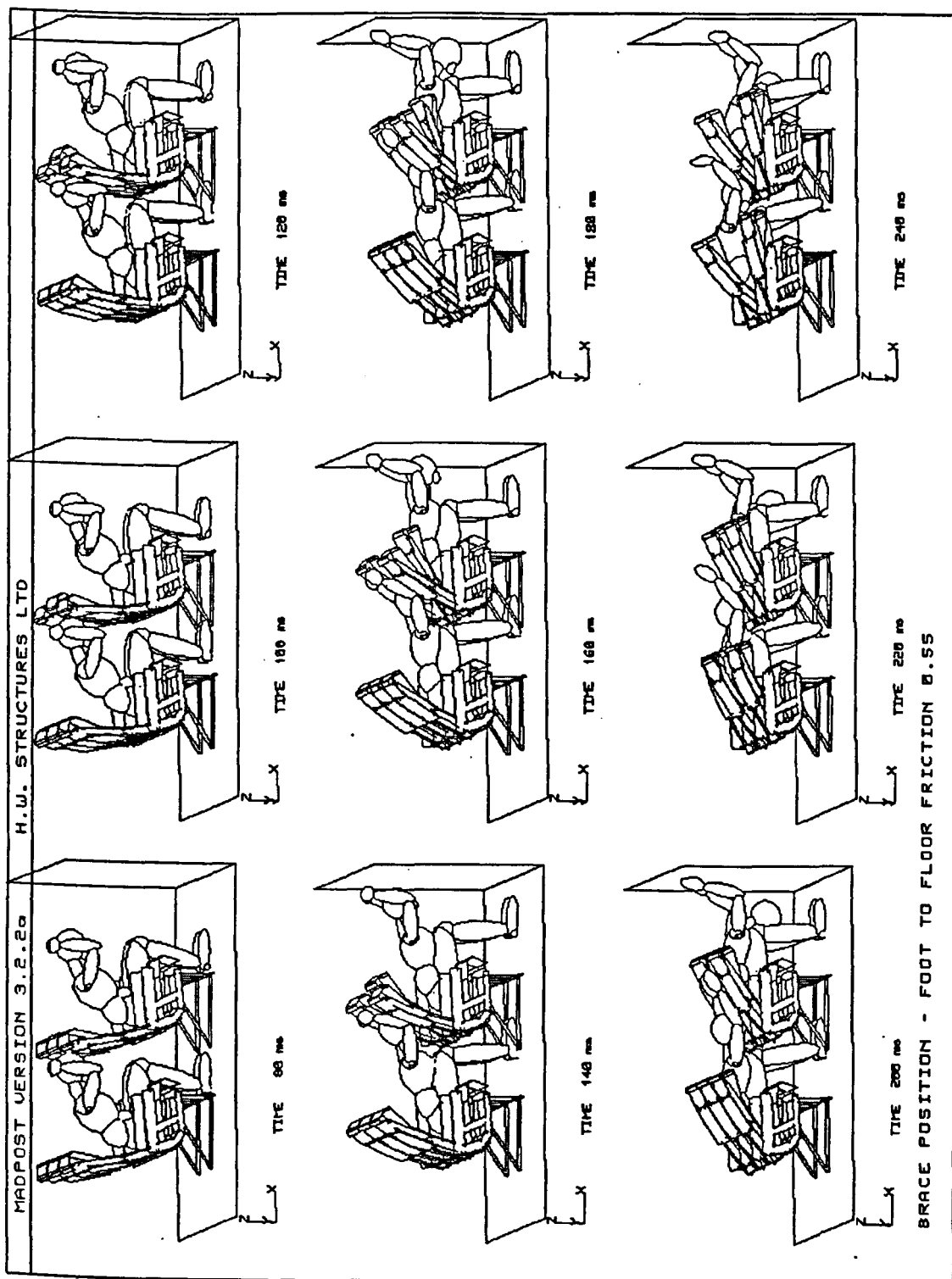


Figure 145. Brace Position, Foot To Floor Friction 0.55

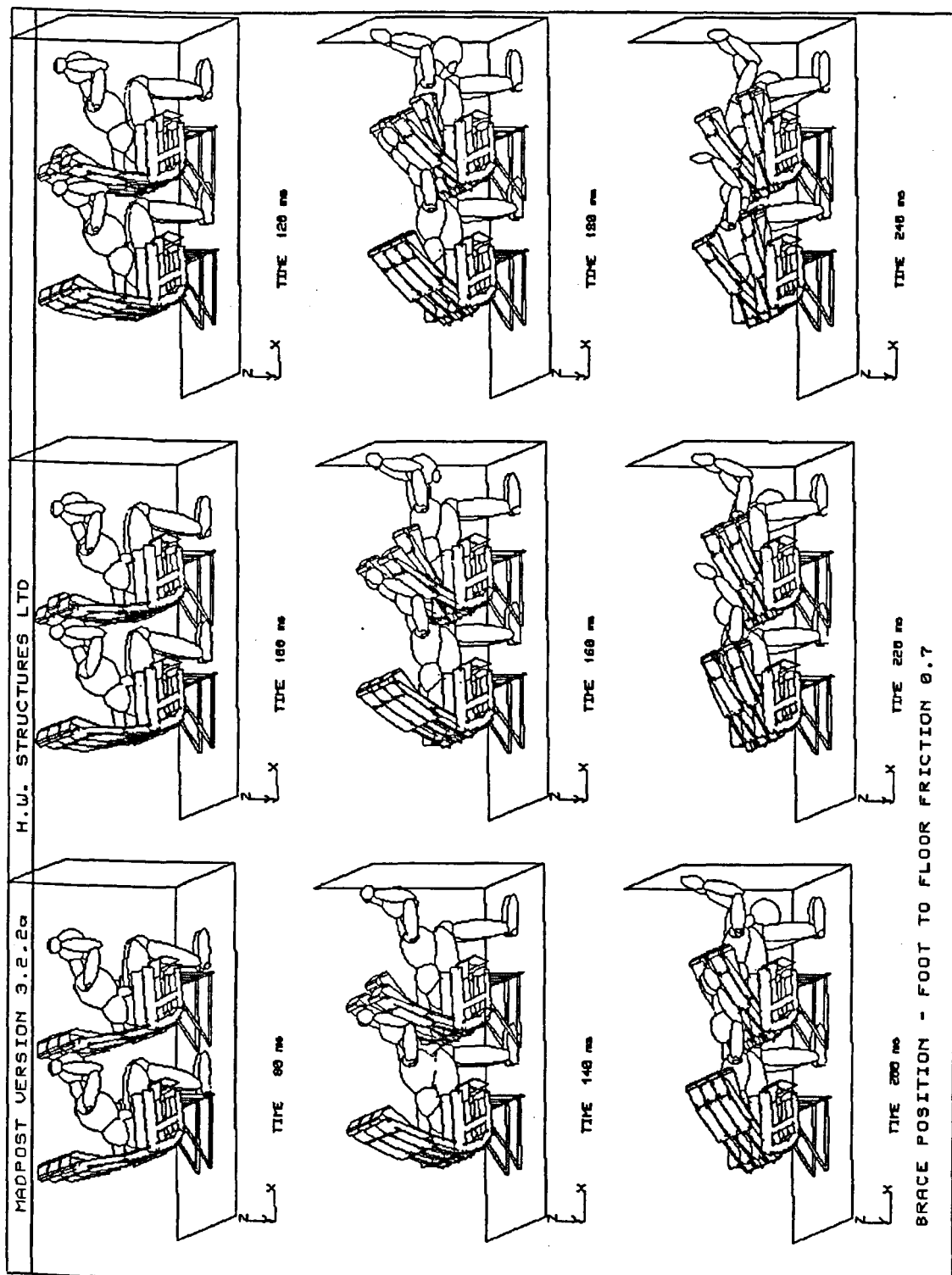


Figure 146. Brace Position, Foot To Floor Friction 0.70

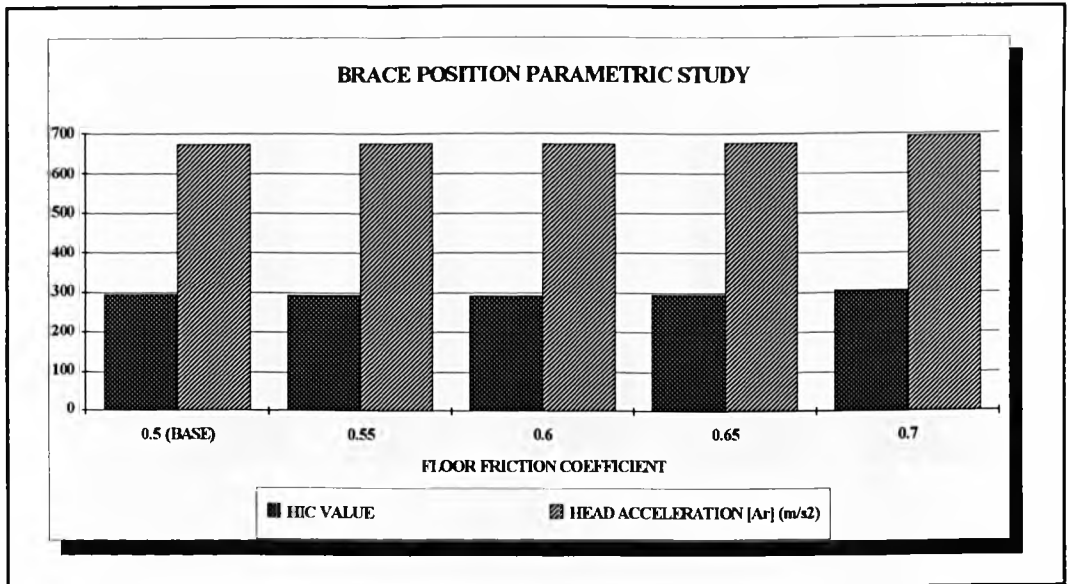


Figure 147. Brace Position Parametric Study - HIC and Head Resultant Accelerations versus Floor Friction Coefficient

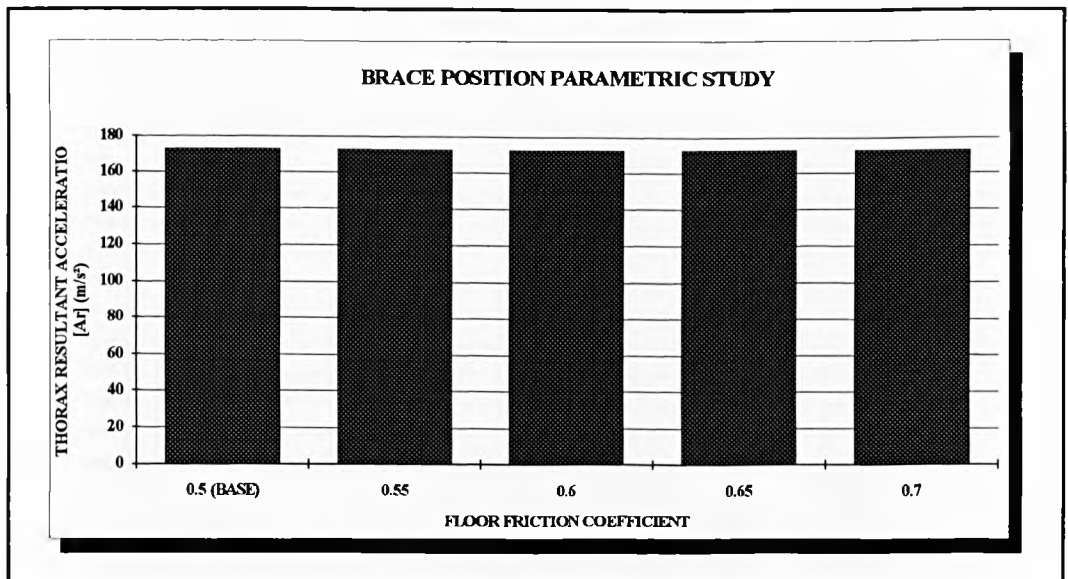


Figure 148. Brace Position Parametric Study - Thorax Resultant Accelerations versus Floor Friction Coefficient

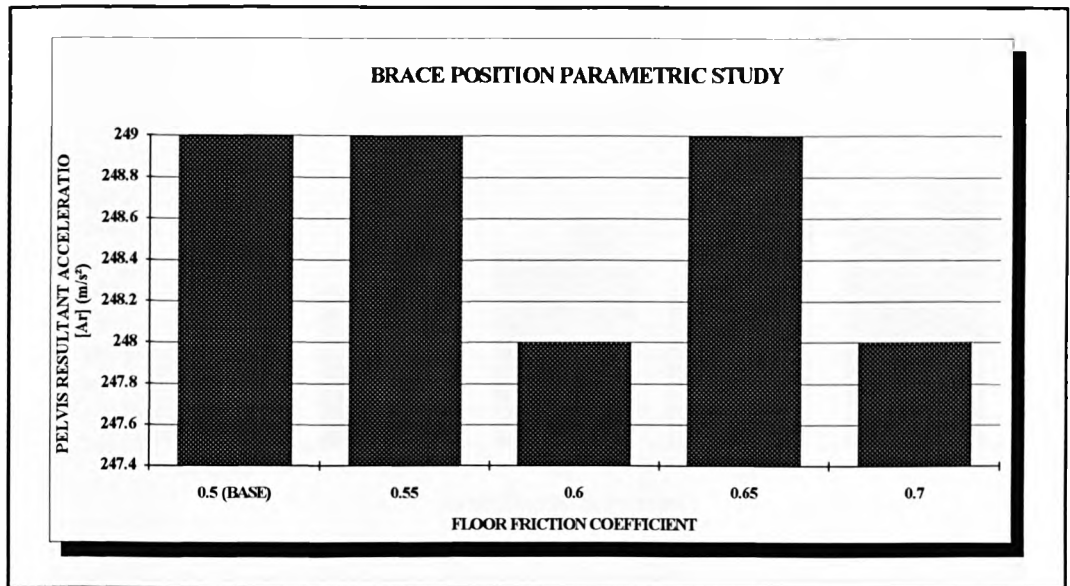


Figure 149. Brace Position Parametric Study - Pelvis Resultant Accelerations versus Floor Friction Coefficient

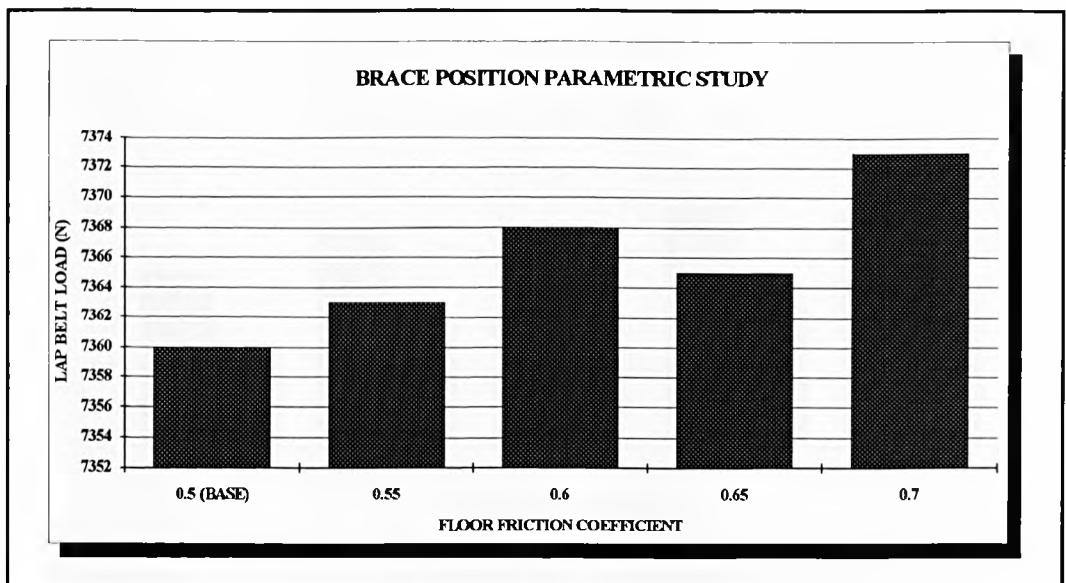


Figure 150. Brace Position Parametric Study - Lap Belt Load versus Floor Friction Coefficient

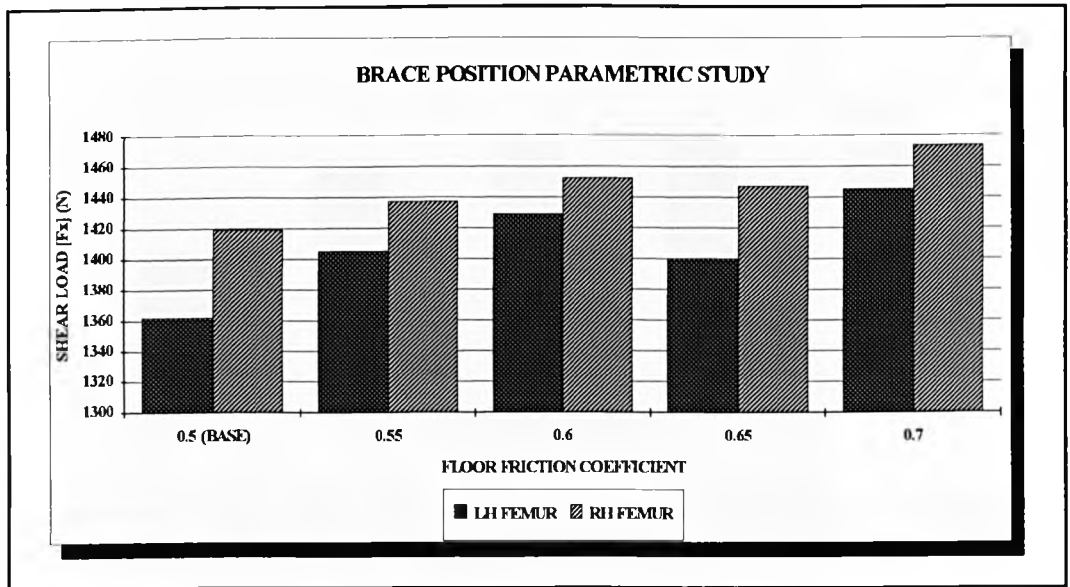


Figure 151. Brace Position Parametric Study - Left and Right Femur Shear Loads versus Floor Friction Coefficient

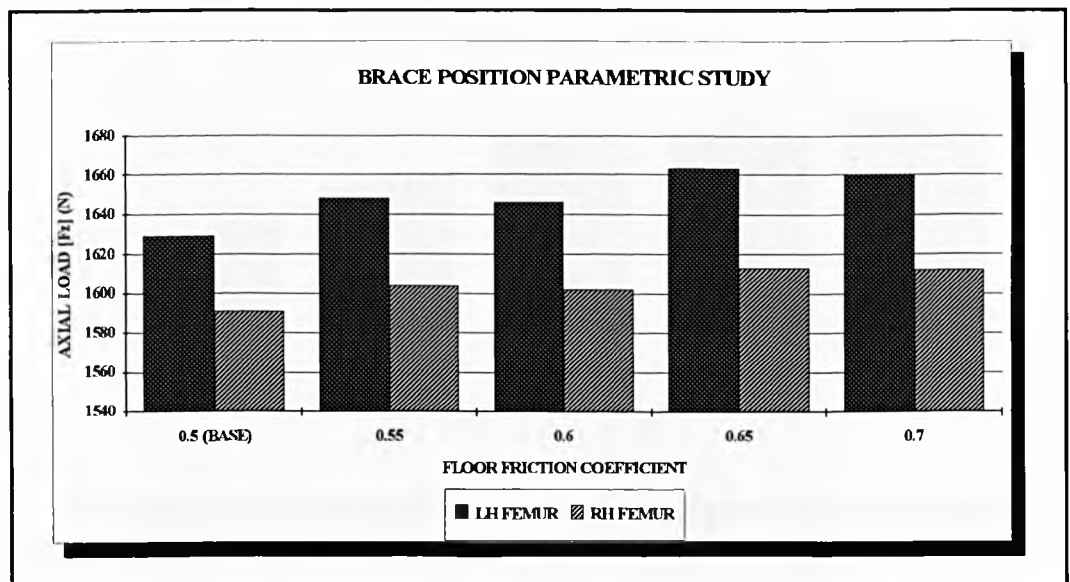


Figure 152. Brace Position Parametric Study - Left and Right Femur Axial Loads versus Floor Friction Coefficient

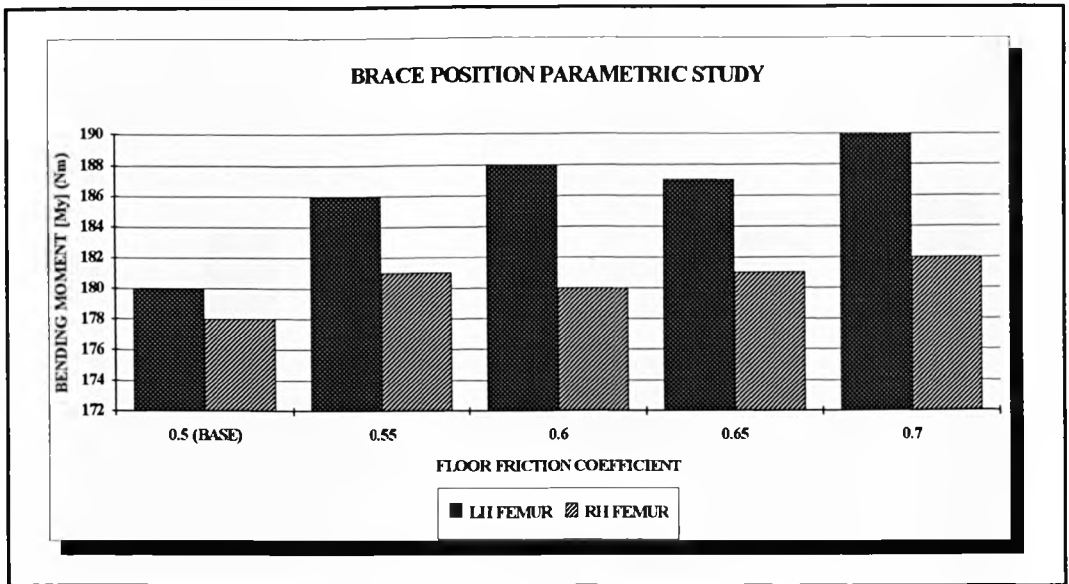


Figure 153. Brace Position Parametric Study - Left and Right Femur Bending Moments versus Floor Friction Coefficient

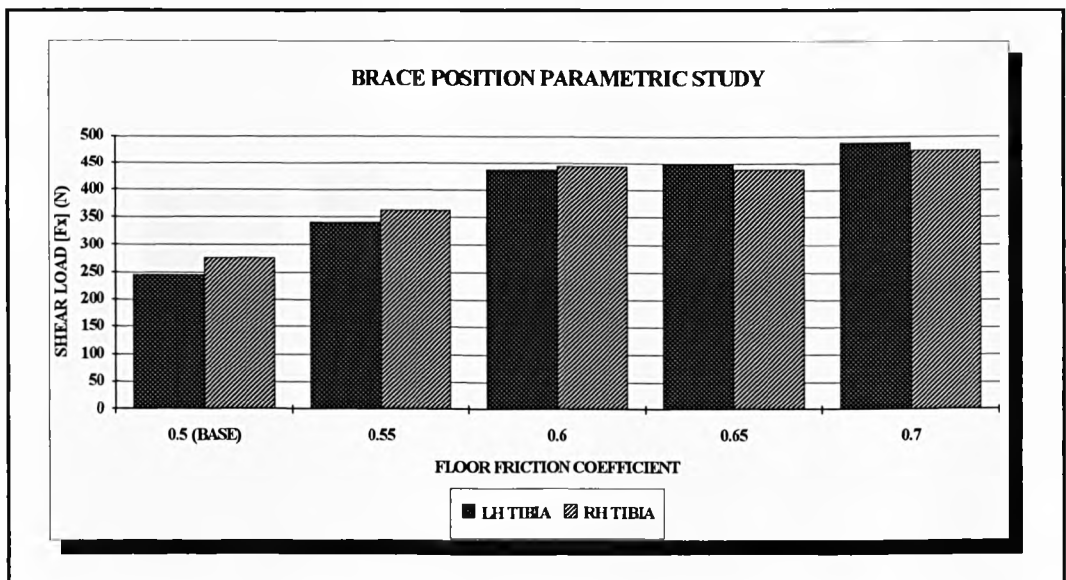


Figure 154. Brace Position Parametric Study - Left and Right Tibia Shear Loads versus Floor Friction Coefficient

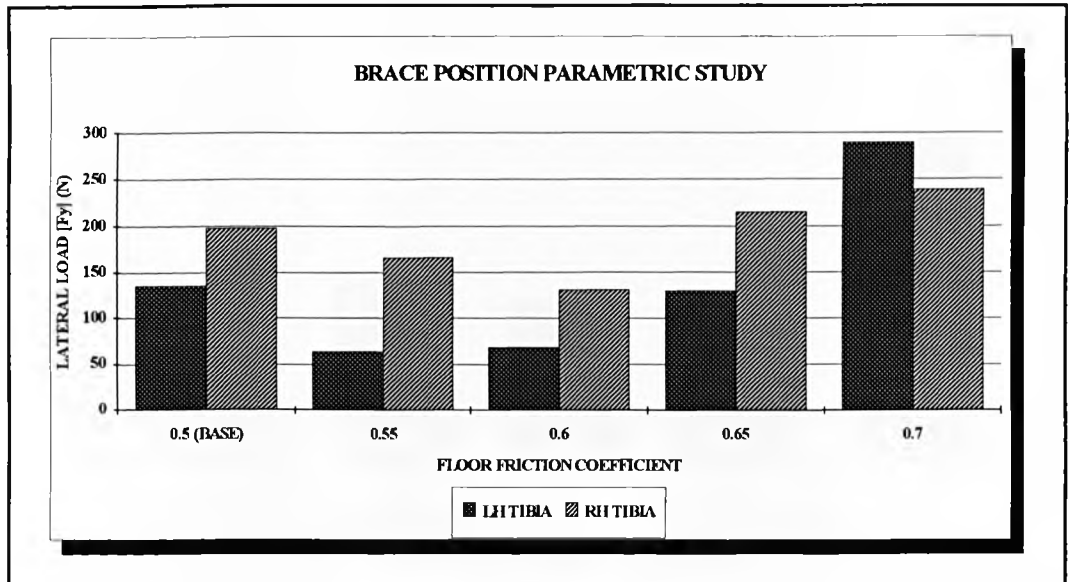


Figure 155. Brace Position Parametric Study - Left and Right Tibia Lateral Loads versus Floor Friction Coefficient

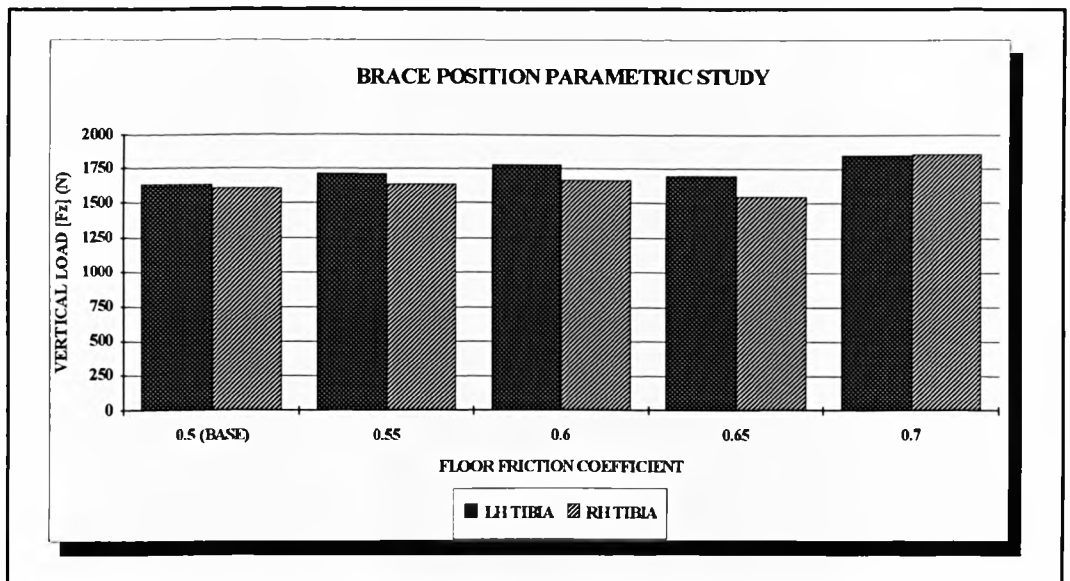


Figure 156. Brace Position Parametric Study - Left and Right Tibia Vertical Loads versus Floor Friction Coefficient

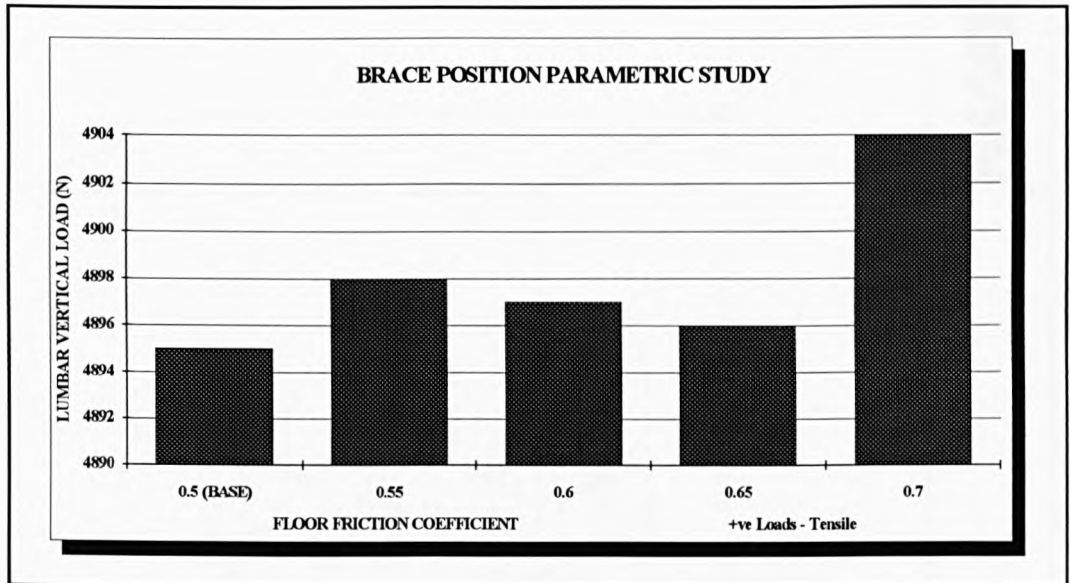


Figure 157. Brace Position Parametric Study - Lumbar Spine Vertical Loads versus Floor Friction Coefficient

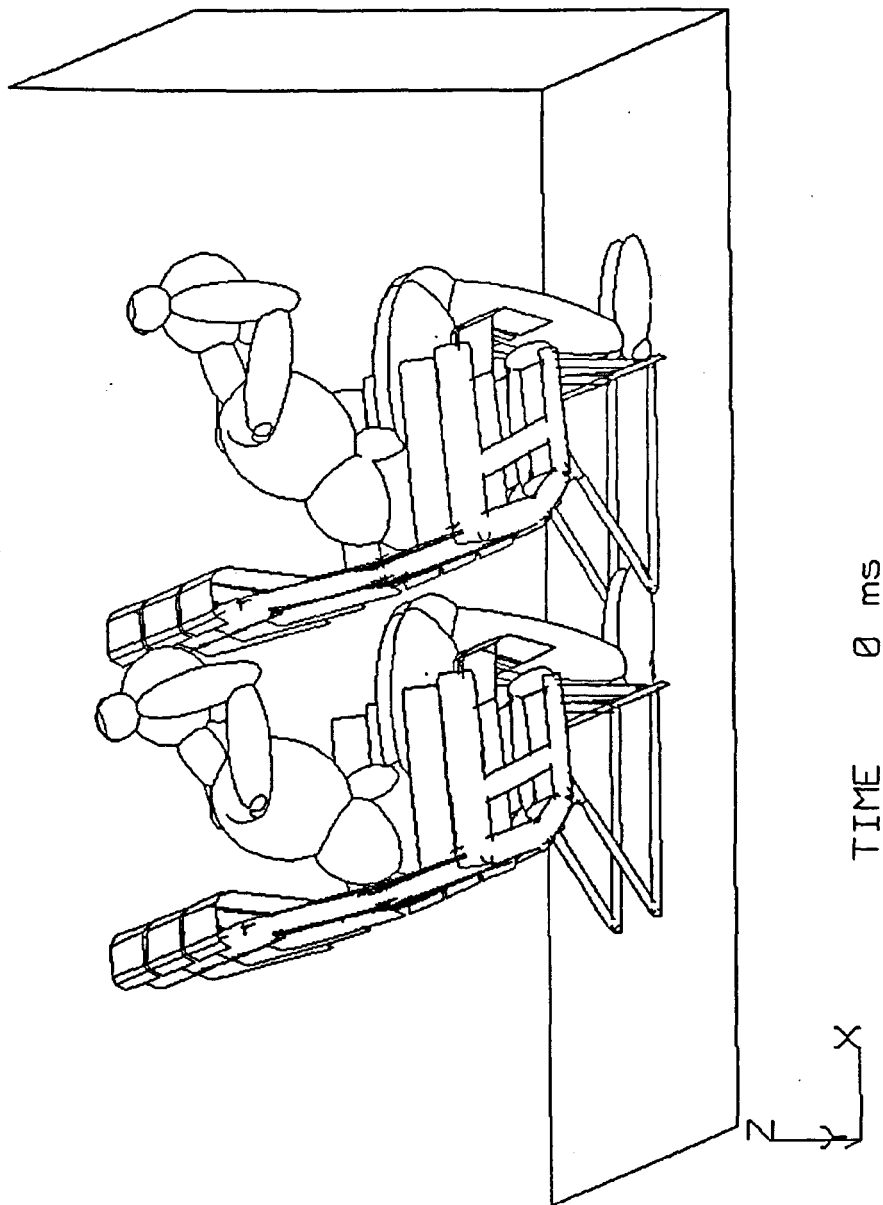


Figure 158. Brace Position Parametric Study - 27 Inch Seat Pitch At 0ms

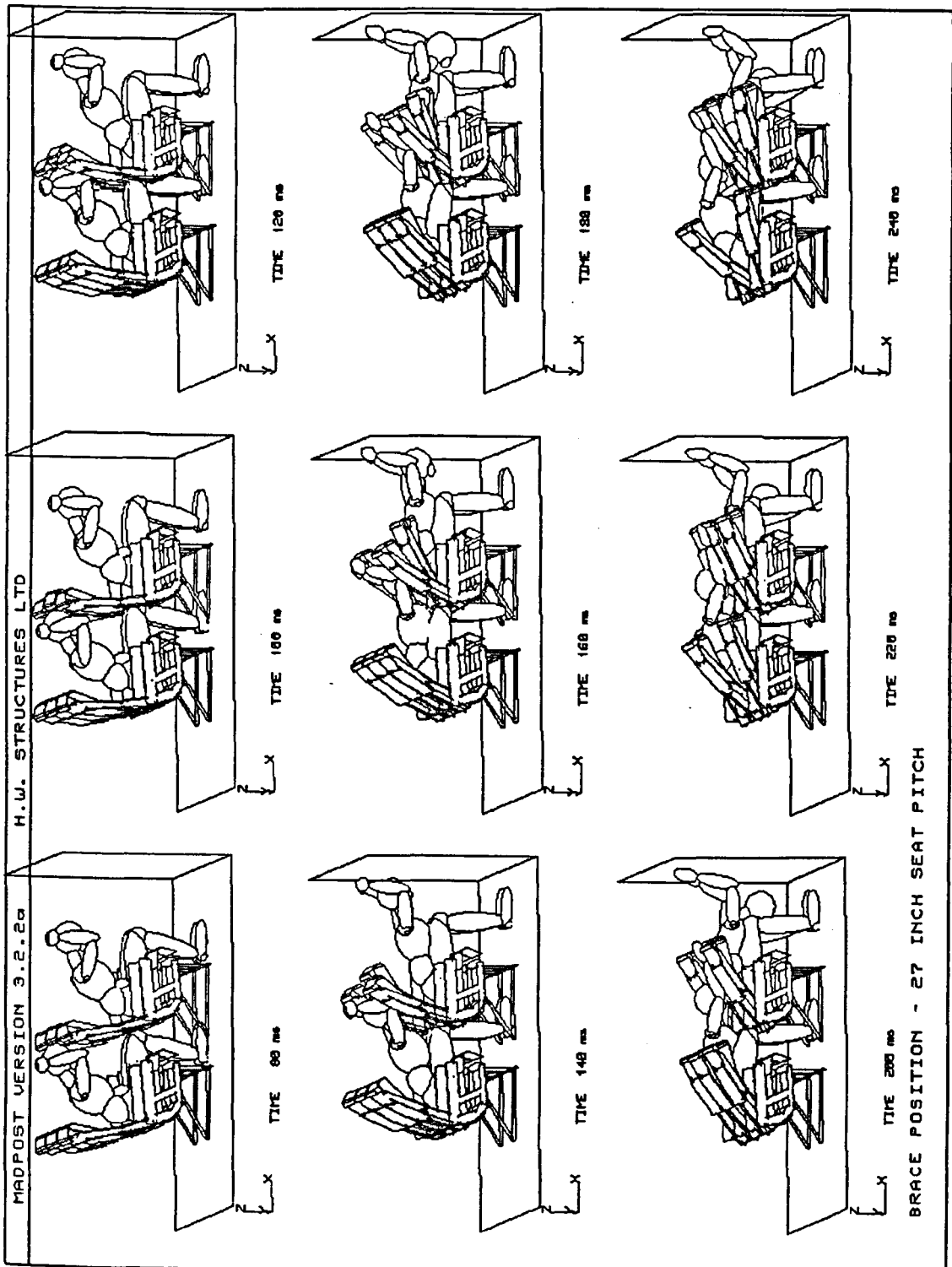


Figure 159. Brace Position Parametric Study - 27 Inch Seat Pitch At 80ms To 240ms

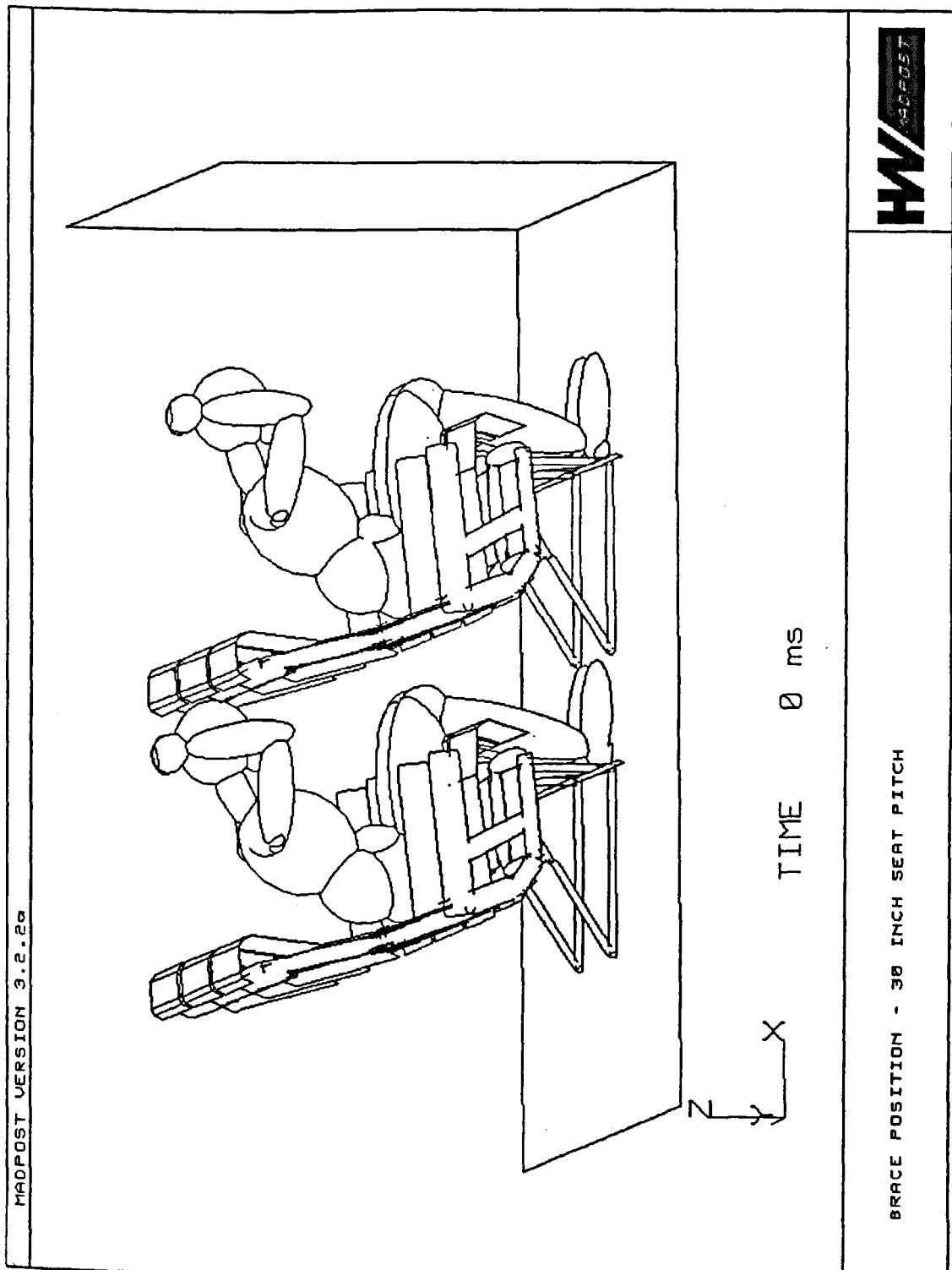


Figure 160. Brace Position Parametric Study - 30 Inch Seat Pitch At 0ms

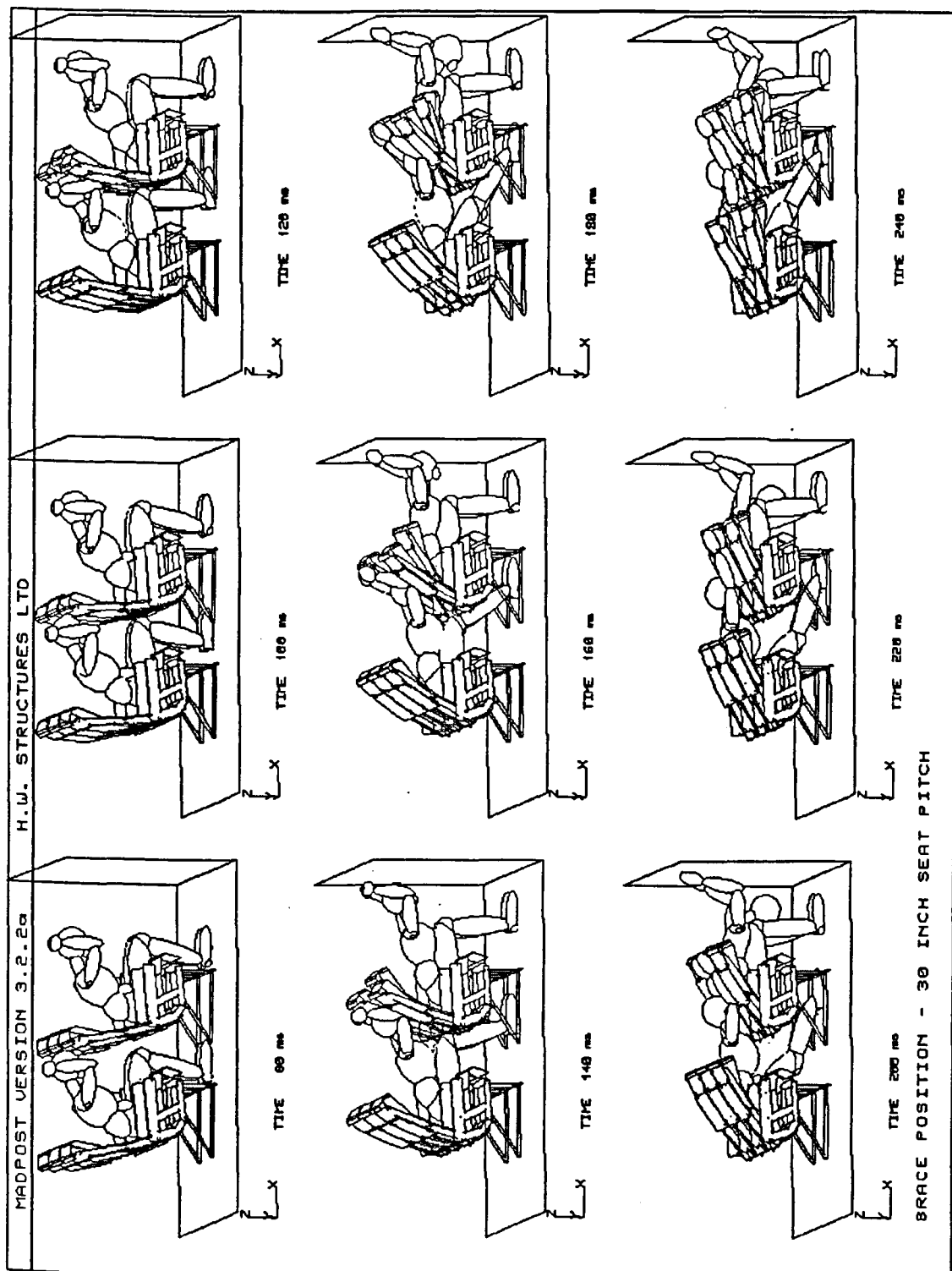


Figure 161. Brace Position Parametric Study - 30 Inch Seat Pitch At 80ms To 240ms

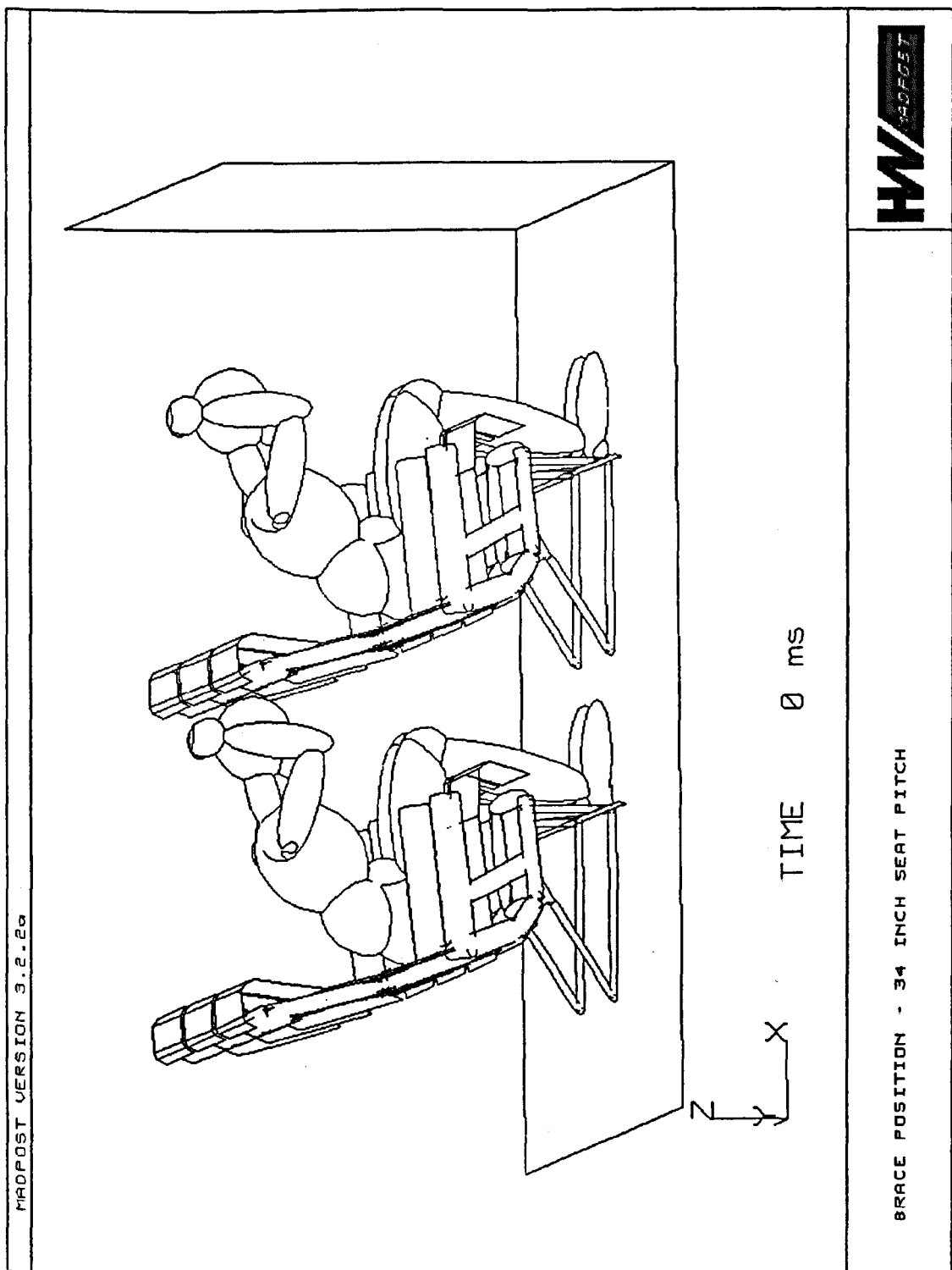


Figure 162. Brace Position Parametric Study - 34 Inch Seat Pitch At 0ms

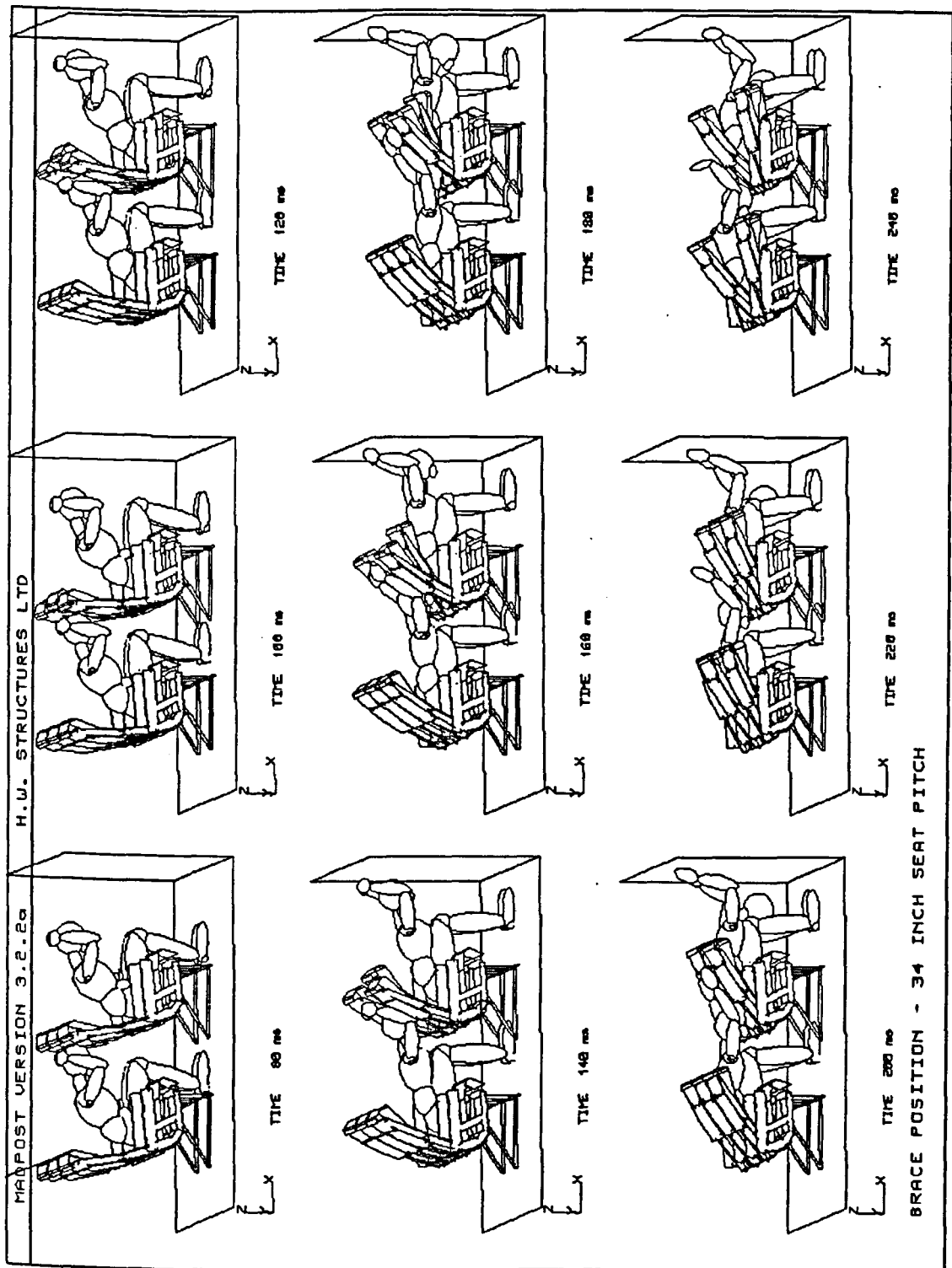


Figure 163. Brace Position Parametric Study - 34 Inch Seat Pitch At 80ms To 240ms

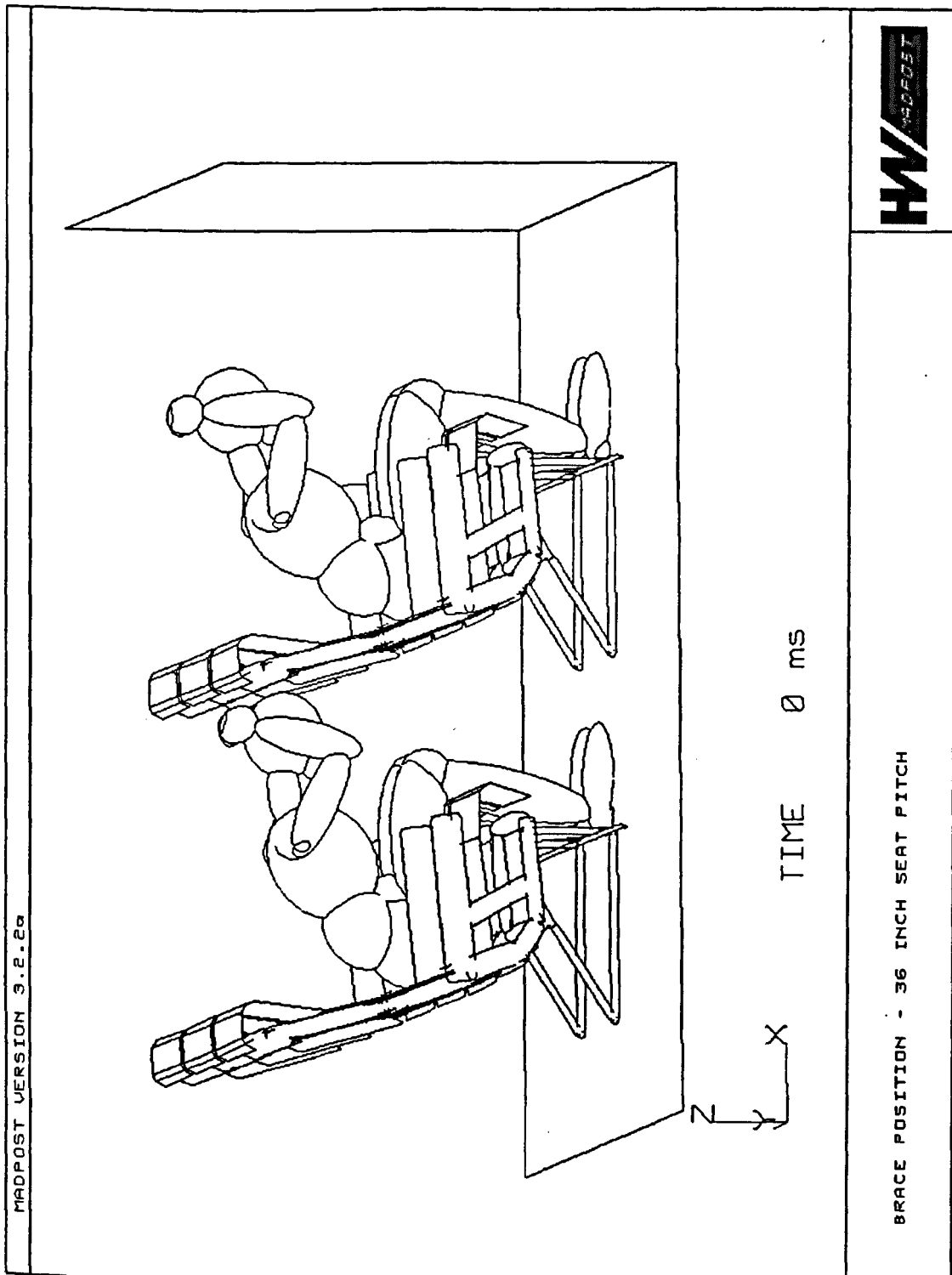


Figure 164. Brace Position Parametric Study - 36 Inch Seat Pitch At 0ms

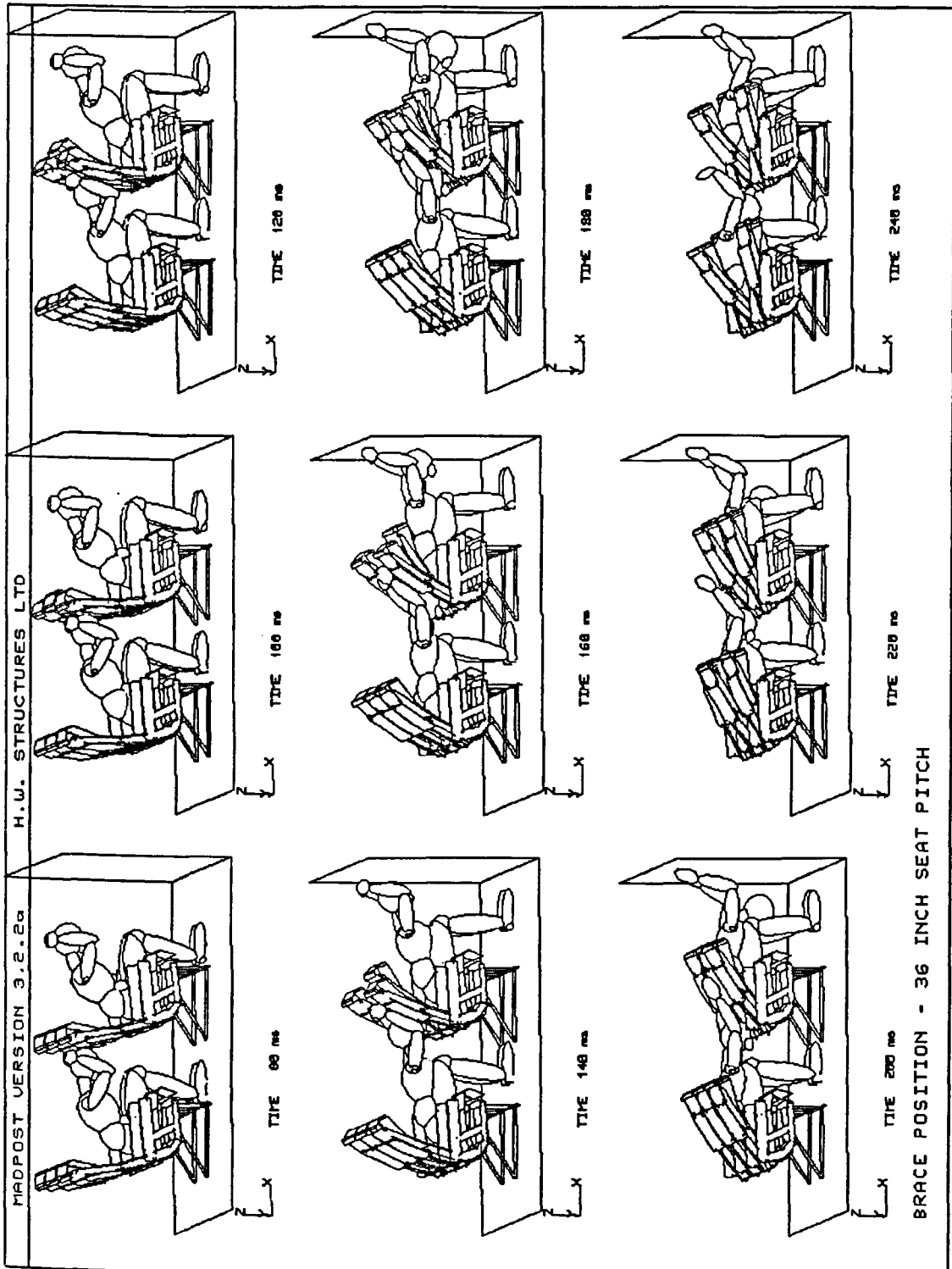


Figure 165. Brace Position Parametric Study - 36 Inch Seat Pitch At 80ms To 240ms

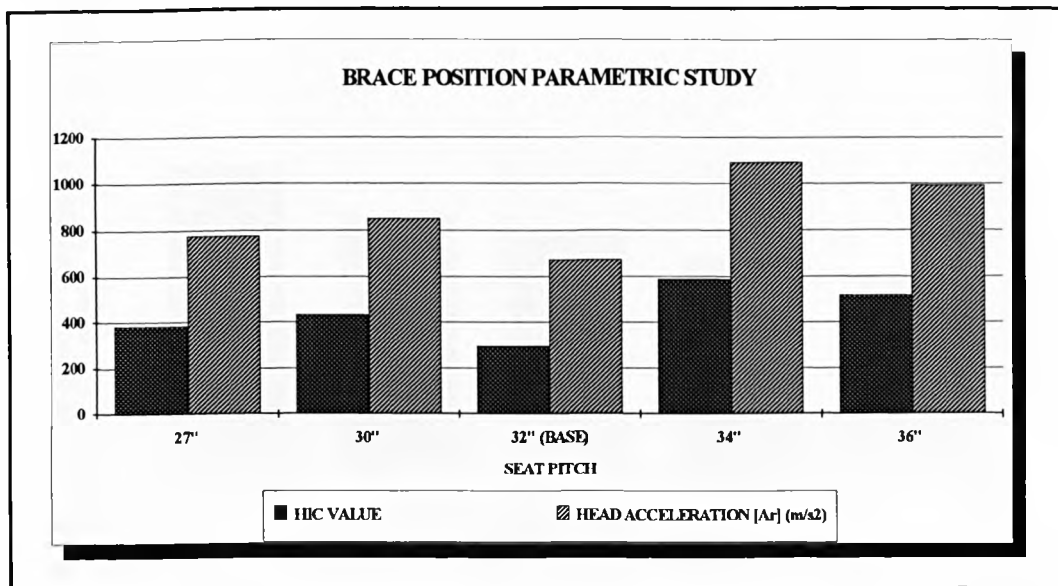


Figure 166. Brace Position Parametric Study - HIC and Head Resultant Accelerations versus Seat Pitch

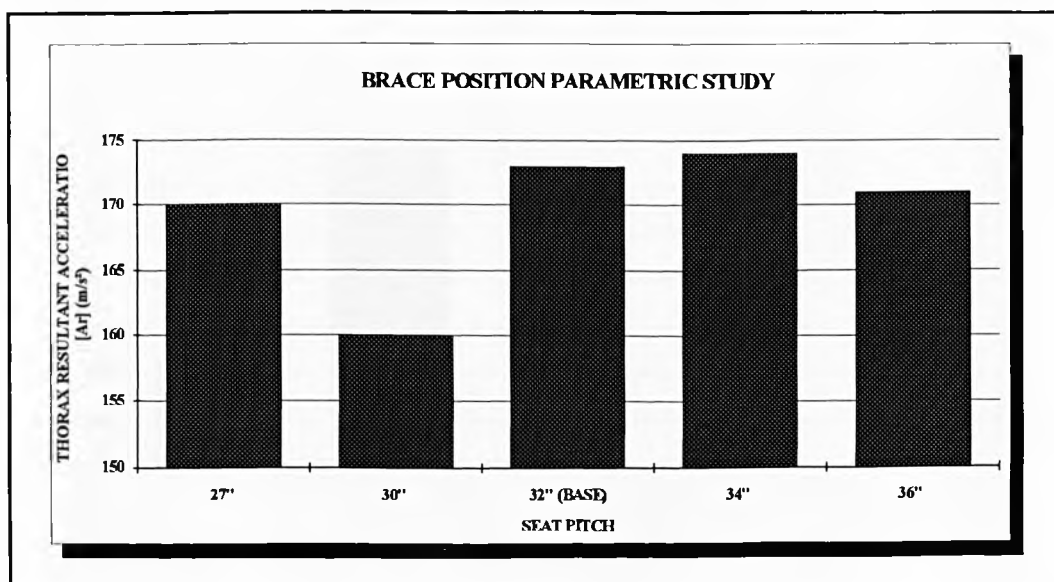


Figure 167. Brace Position Parametric Study - Thorax Resultant Accelerations versus Seat Pitch

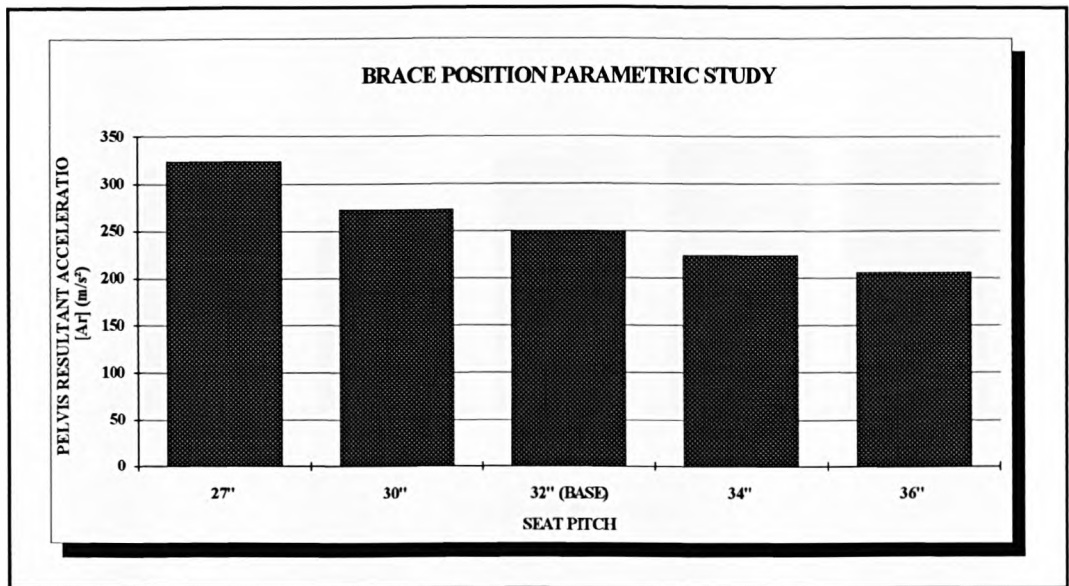


Figure 168. Brace Position Parametric Study - Pelvis Resultant Accelerations versus Seat Pitch

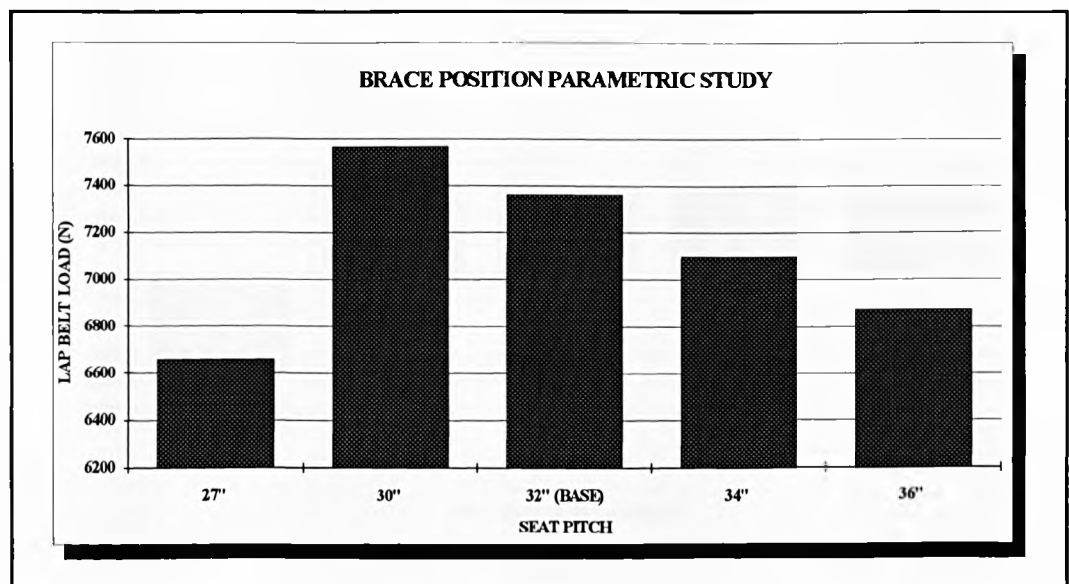


Figure 169. Brace Position Parametric Study - Lap Belt Load versus Seat Pitch

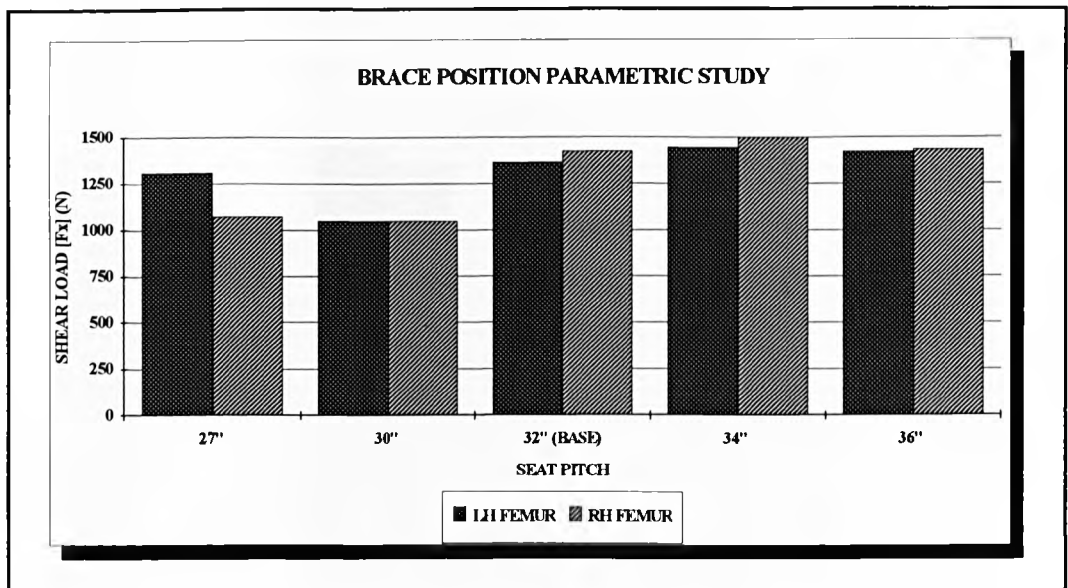


Figure 170. Brace Position Parametric Study - Left and Right Femur Shear Loads versus Seat Pitch

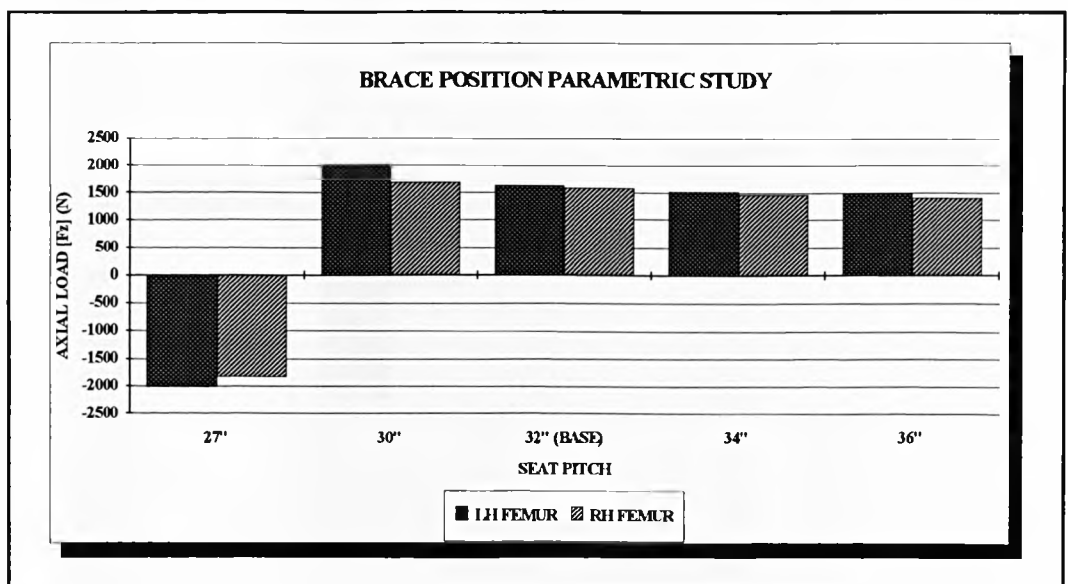


Figure 171. Brace Position Parametric Study - Left and Right Femur Axial Loads versus Seat Pitch

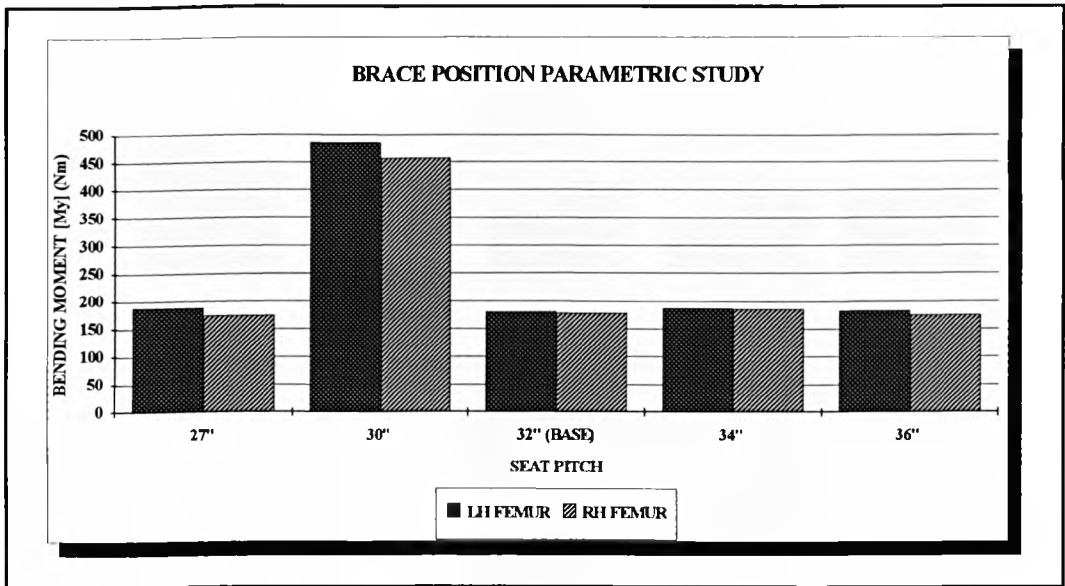


Figure 172. Brace Position Parametric Study - Left and Right Femur Bending Moments versus Seat Pitch

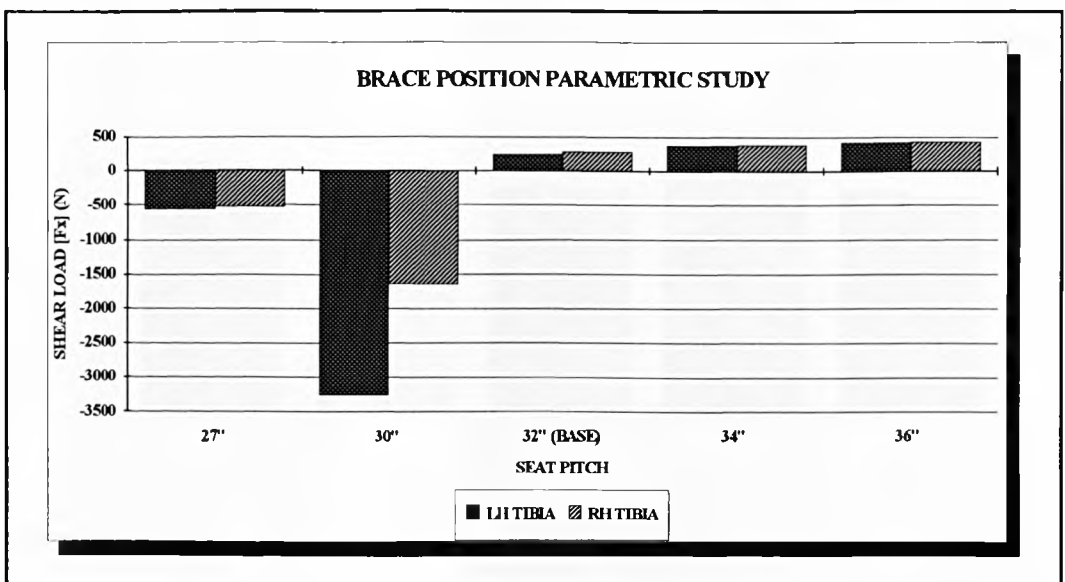


Figure 173. Brace Position Parametric Study - Left and Right Tibia Shear Loads versus Seat Pitch

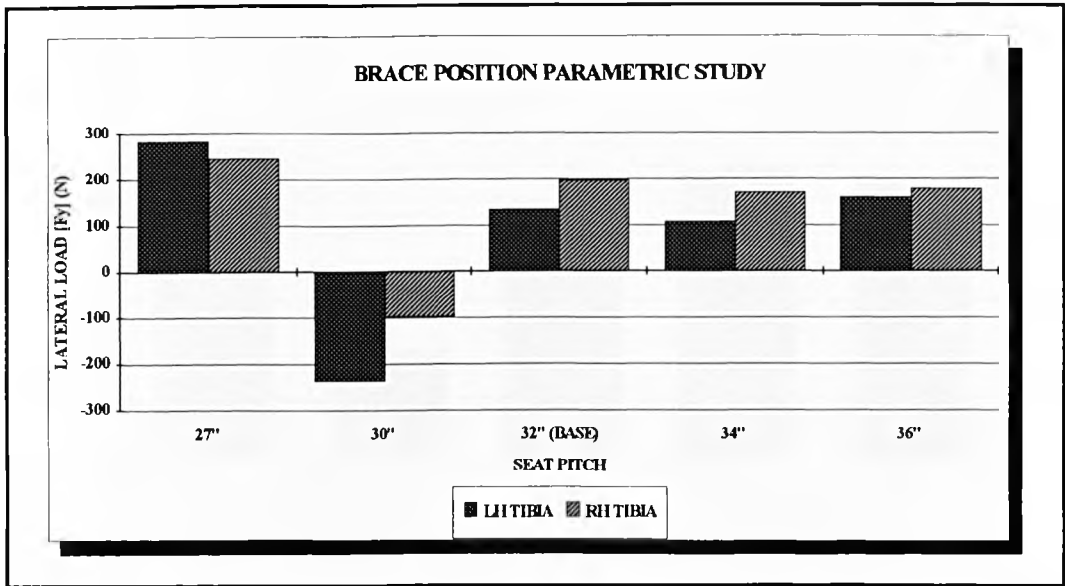


Figure 174. Brace Position Parametric Study - Left and Right Tibia Lateral Loads versus Seat Pitch

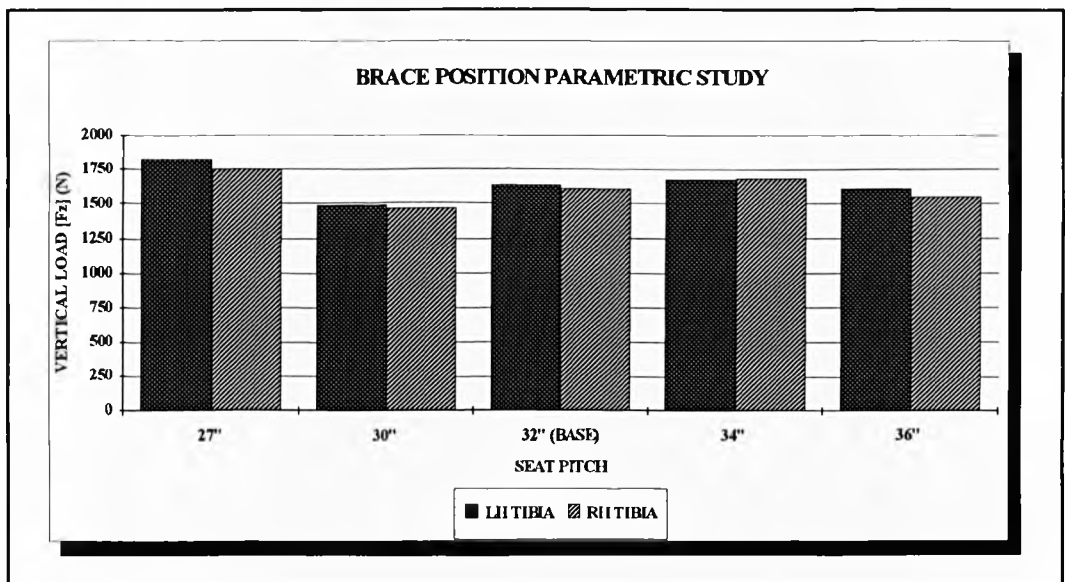


Figure 175. Brace Position Parametric Study - Left and Right Tibia Vertical Loads versus Seat Pitch

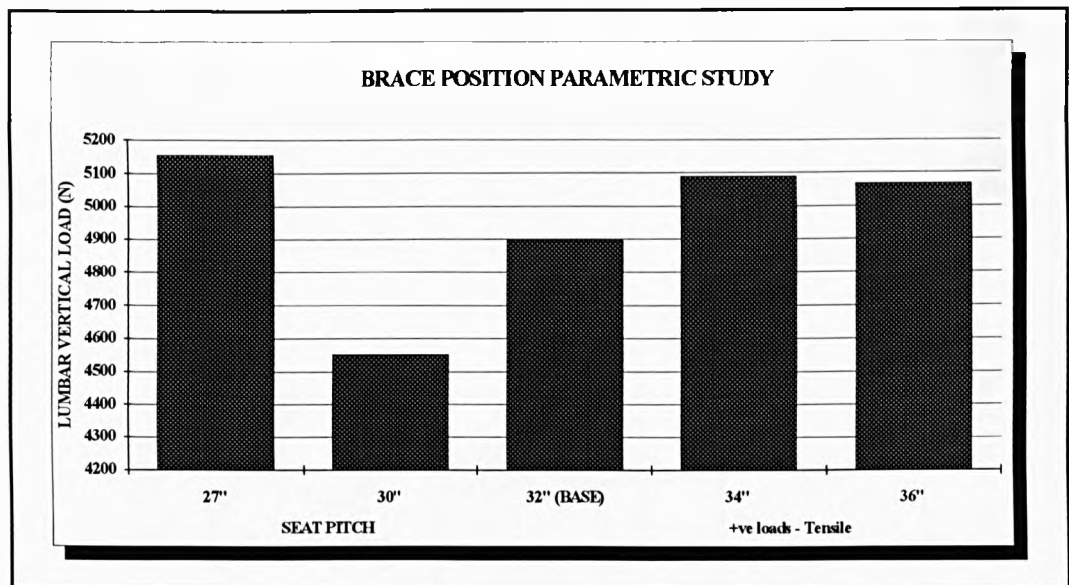


Figure 176. Brace Position Parametric Study - Lumbar Spine Vertical Loads versus Seat Pitch

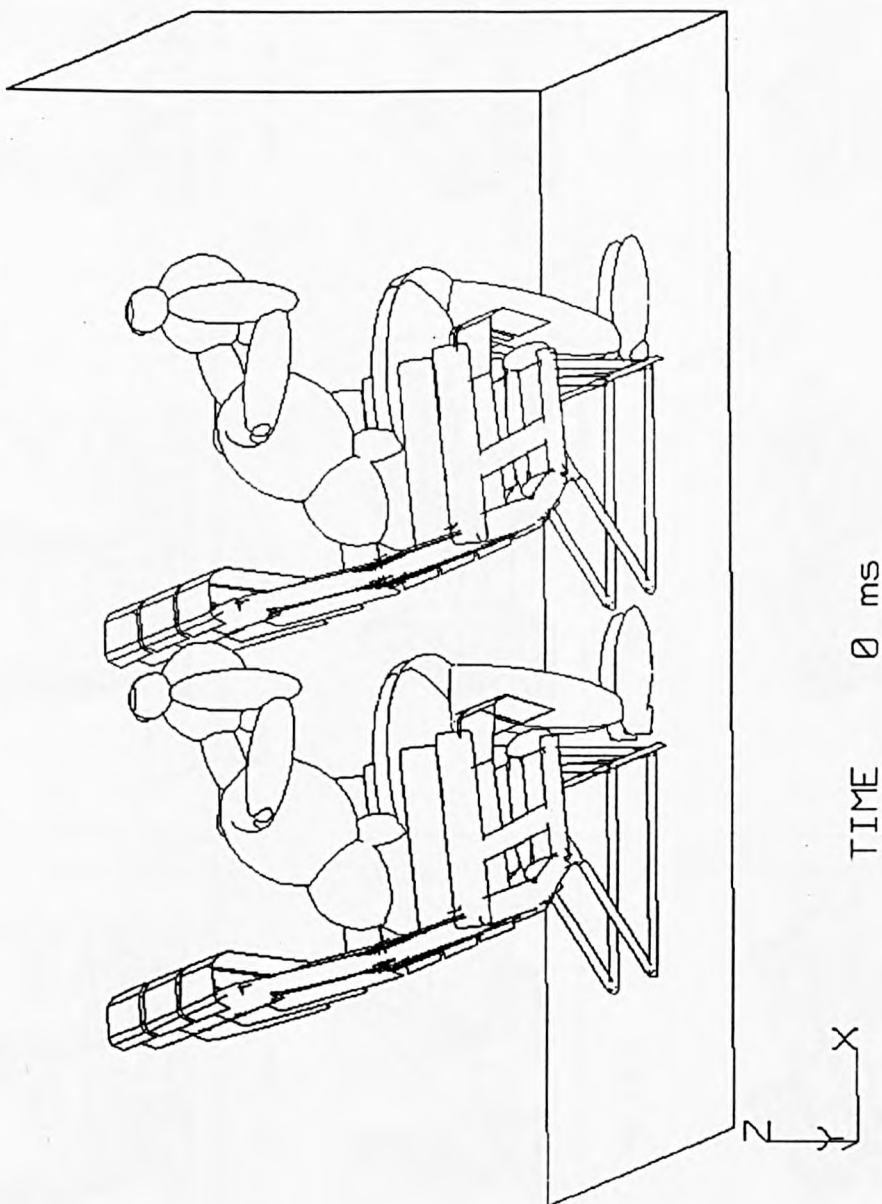


Figure 177. Brace Position Parametric Study - Leg Angle 6.5° Rearward of the Vertical At 0ms

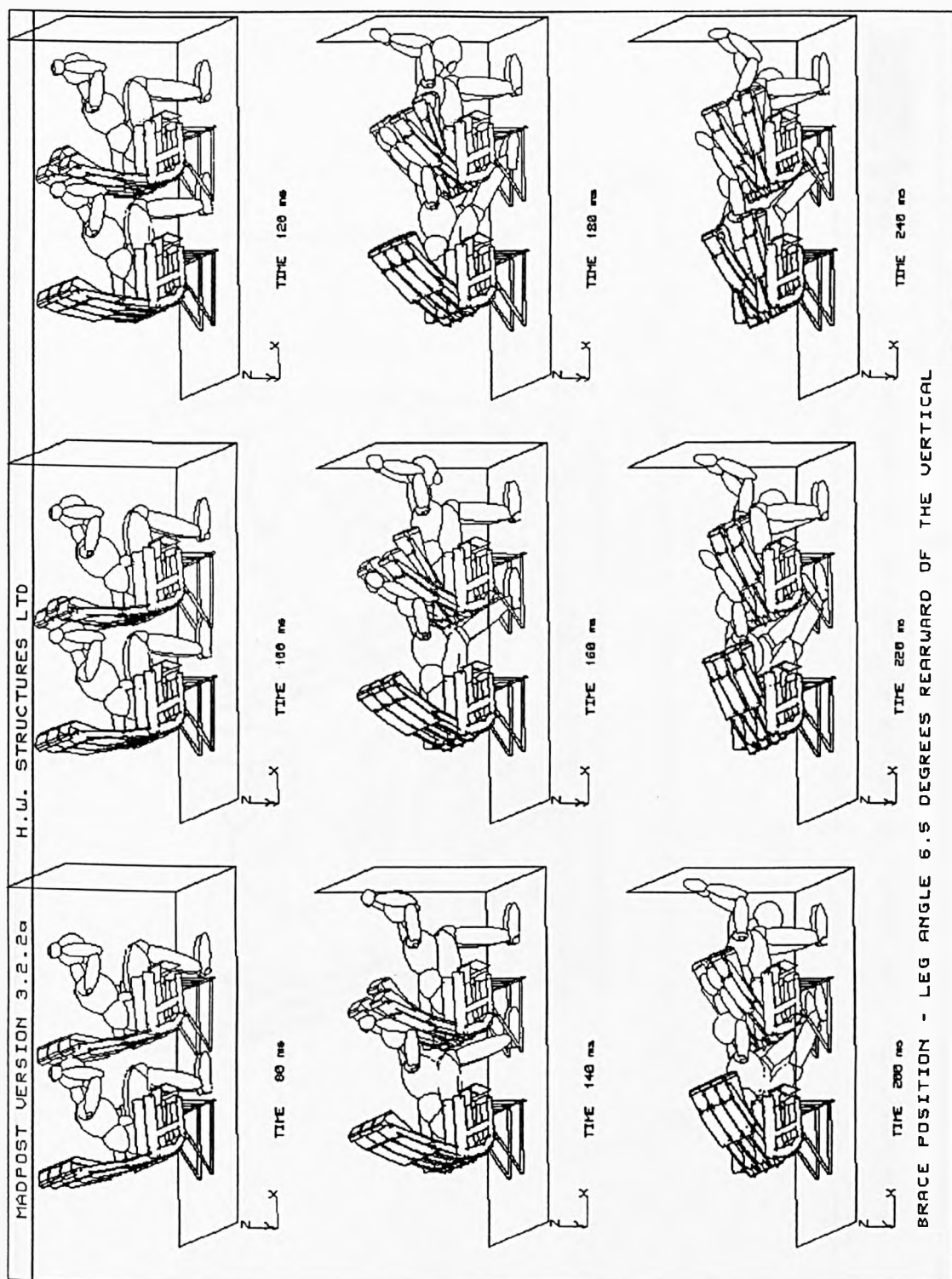


Figure 178. Brace Position Parametric Study - Leg Angle 6.5° Rearward of the Vertical At 80ms To 240ms

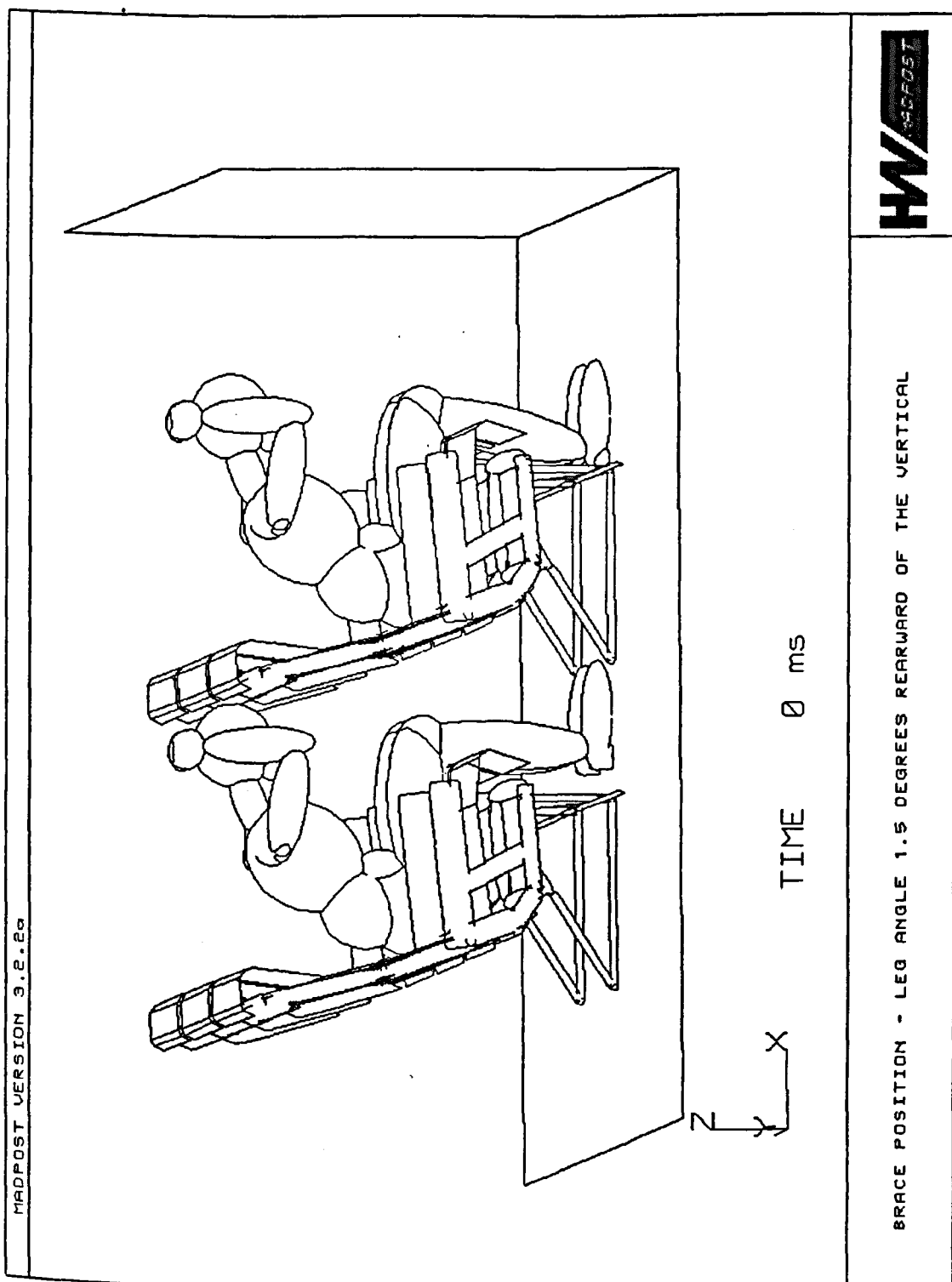


Figure 179. Brace Position Parametric Study - Leg Angle 1.5° Rearward of the Vertical At 0ms

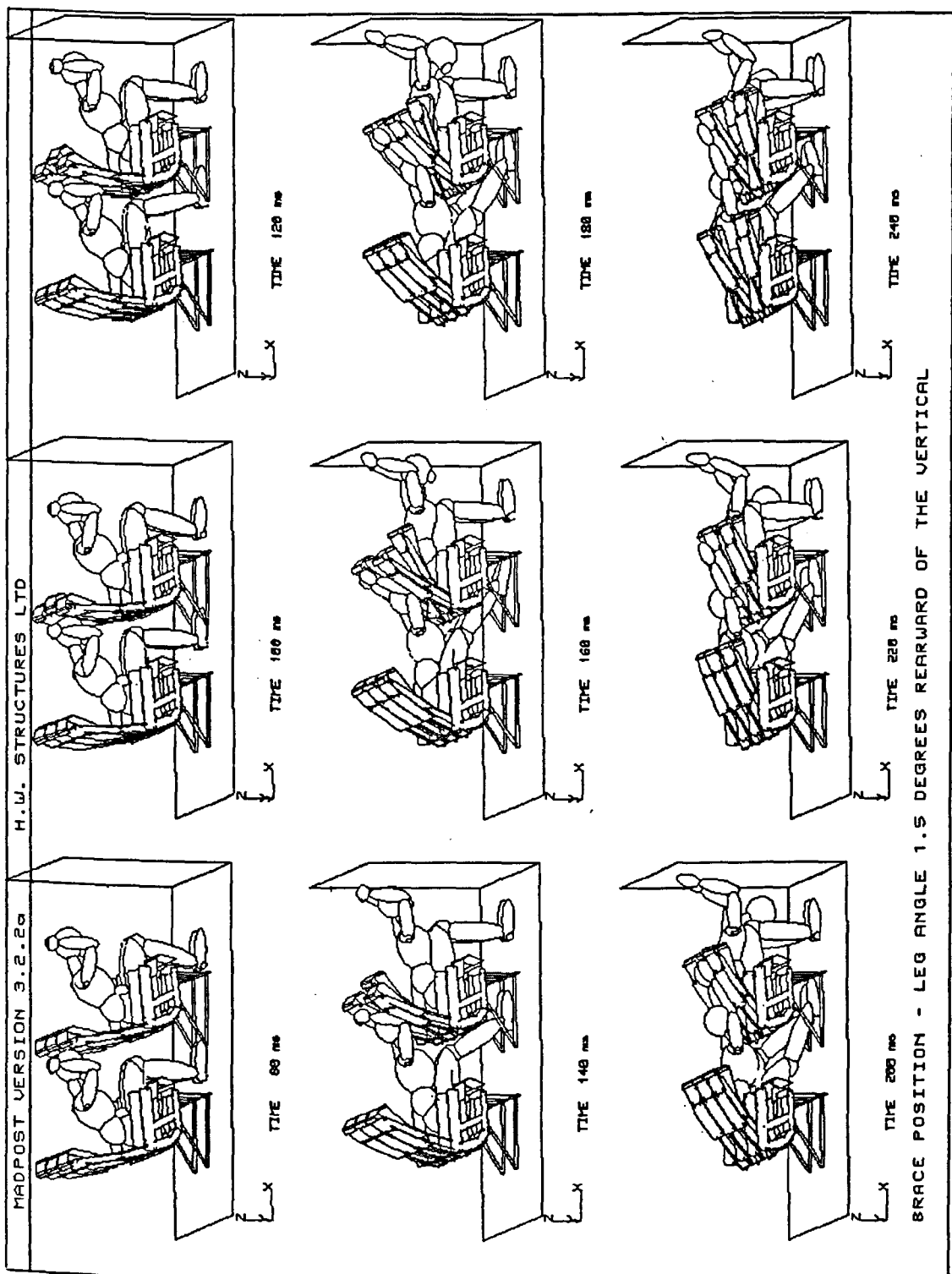


Figure 180. Brace Position Parametric Study - Leg Angle 1.5° Rearward of the Vertical At 80ms To 240ms

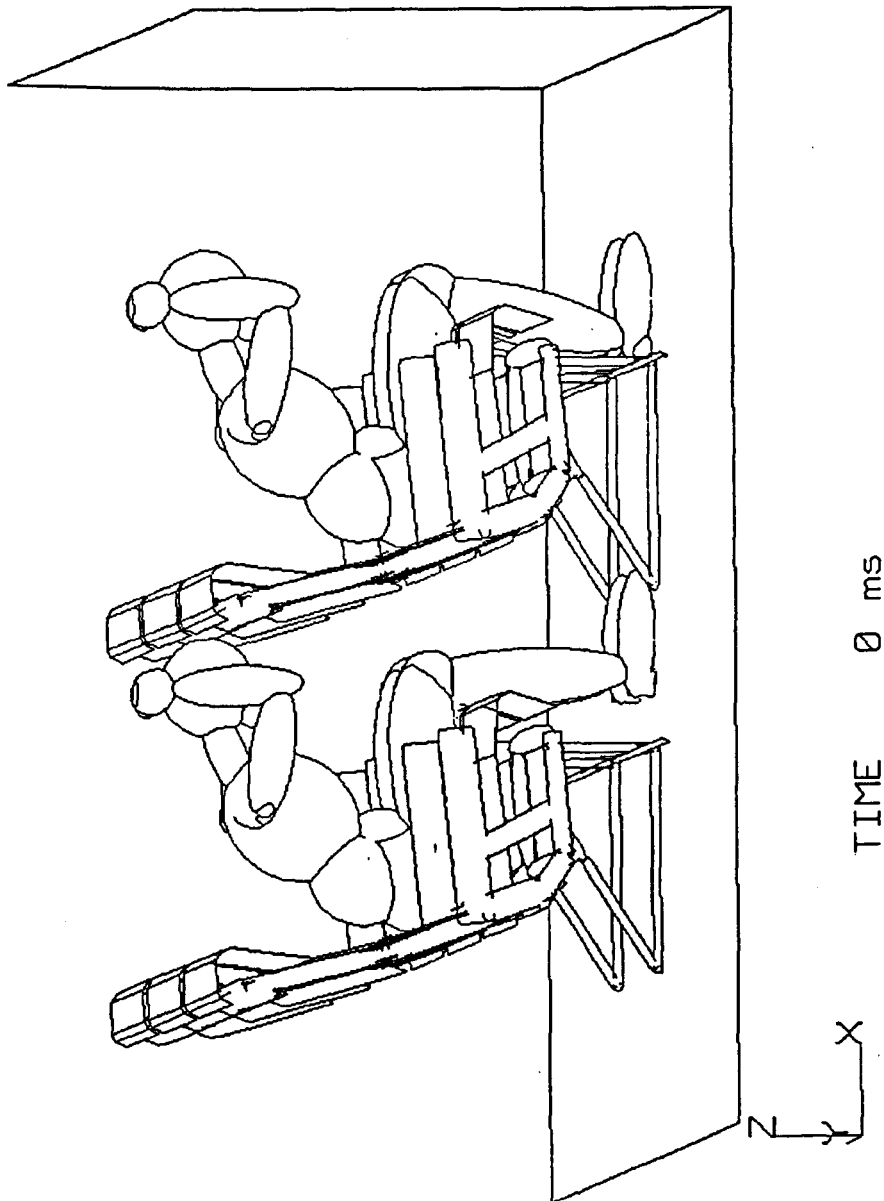


Figure 181. Brace Position Parametric Study - Leg Angle 3.5° Forward of the Vertical At 0ms

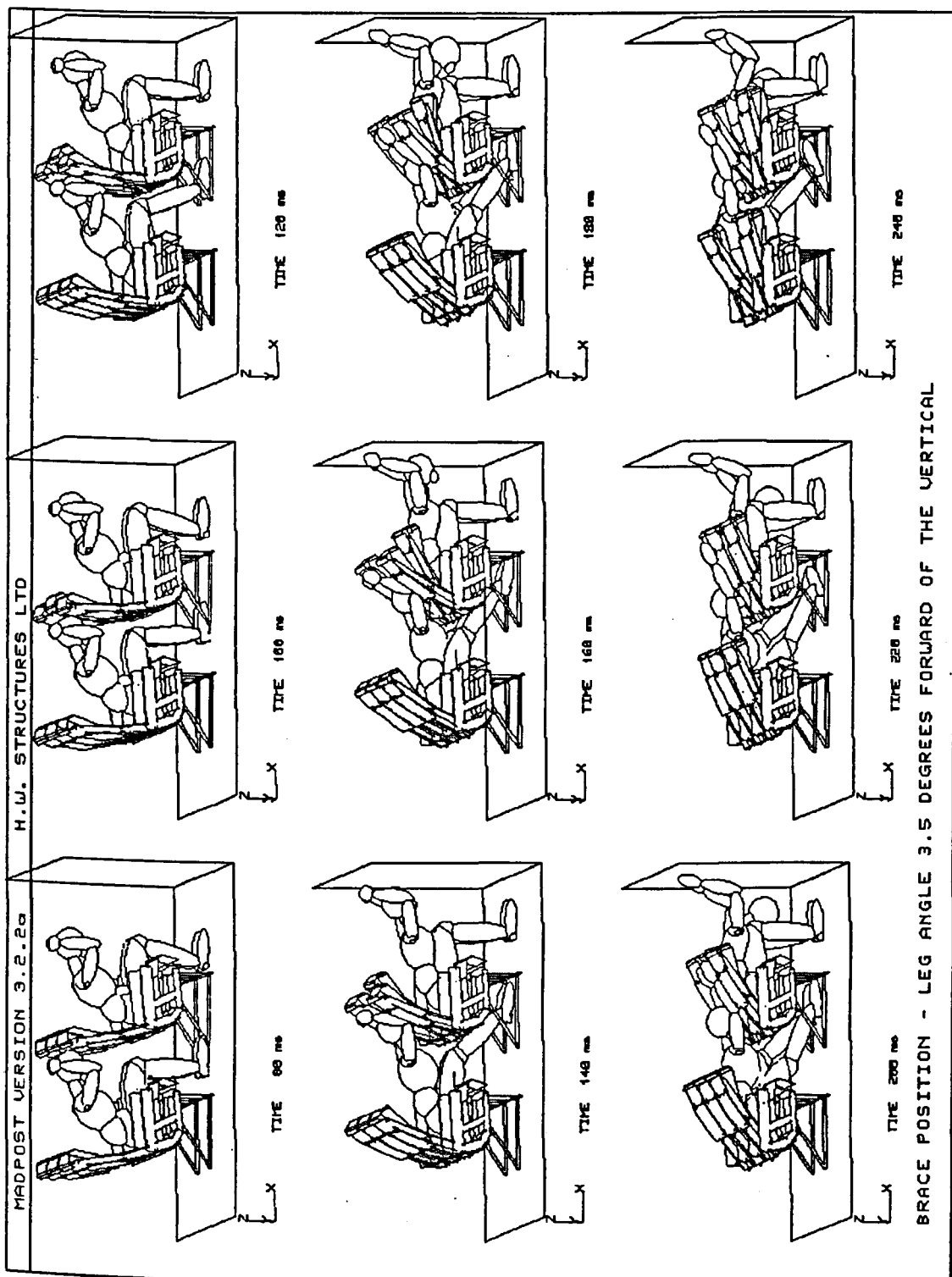


Figure 182. Brace Position Parametric Study - Leg Angle 3.5° Forward of the Vertical At 80ms To 240ms

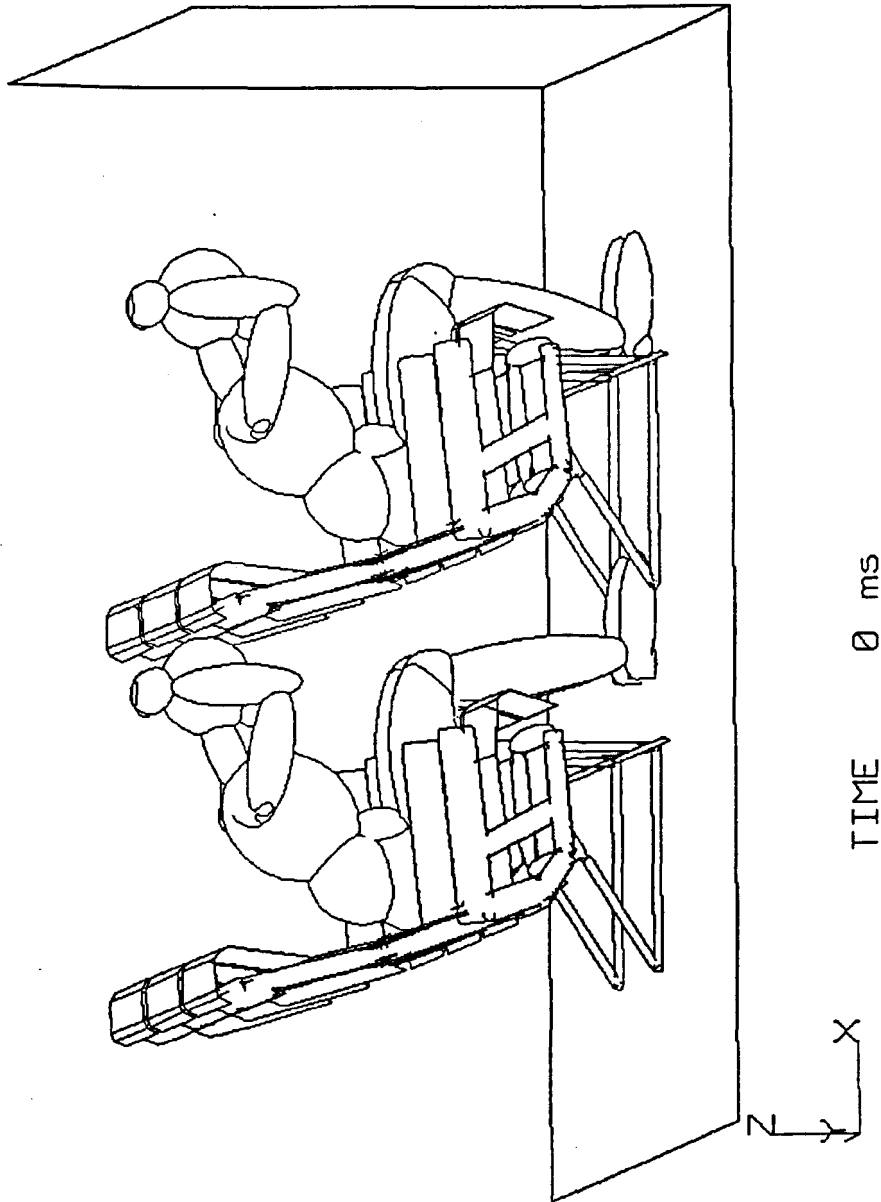


Figure 183. Brace Position Parametric Study - Leg Angle 8.5° Forward of the Vertical At 0ms

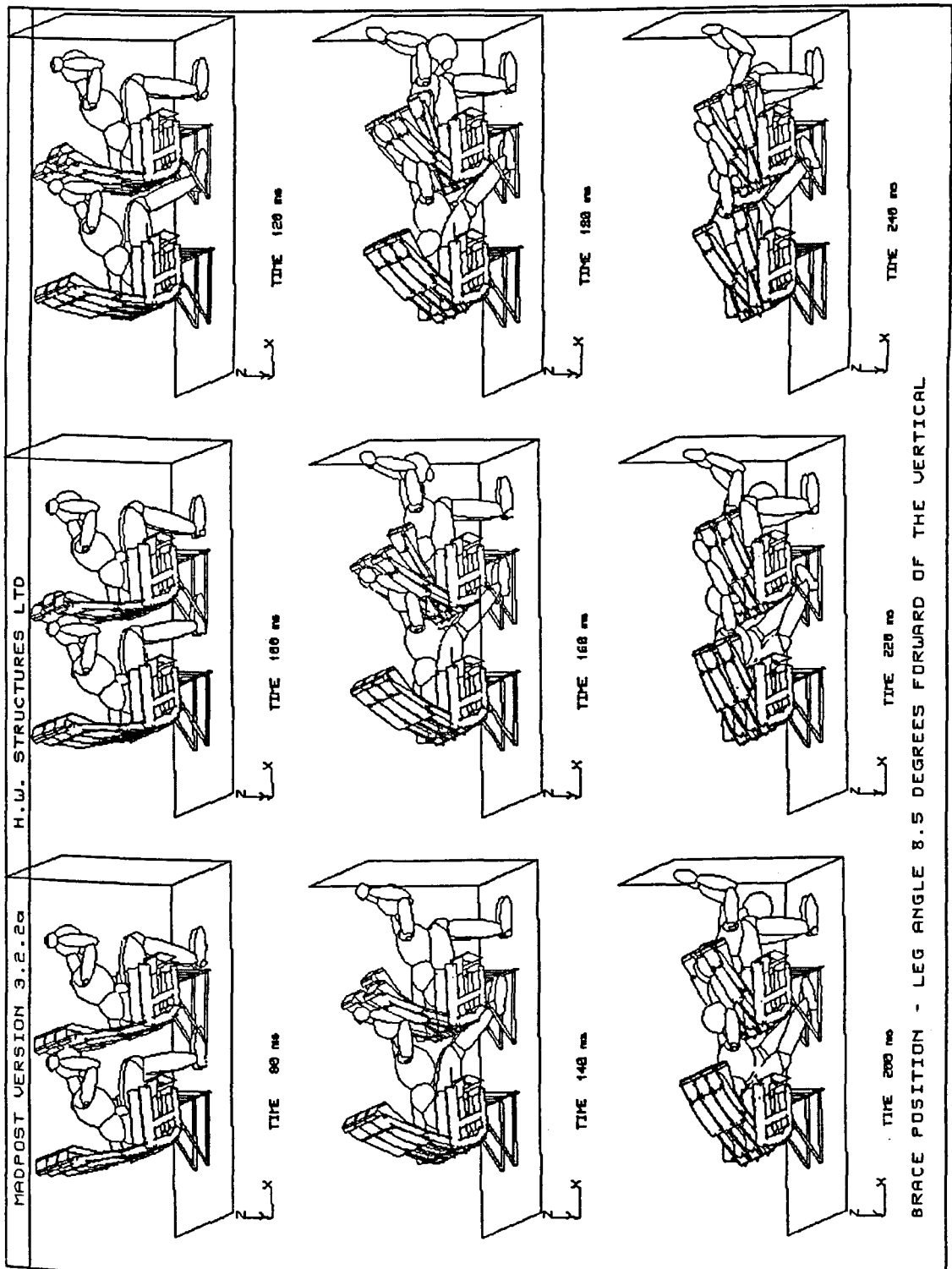


Figure 184. Brace Position Parametric Study - Leg Angle 8.5° Forward of the Vertical At 80ms To 240ms

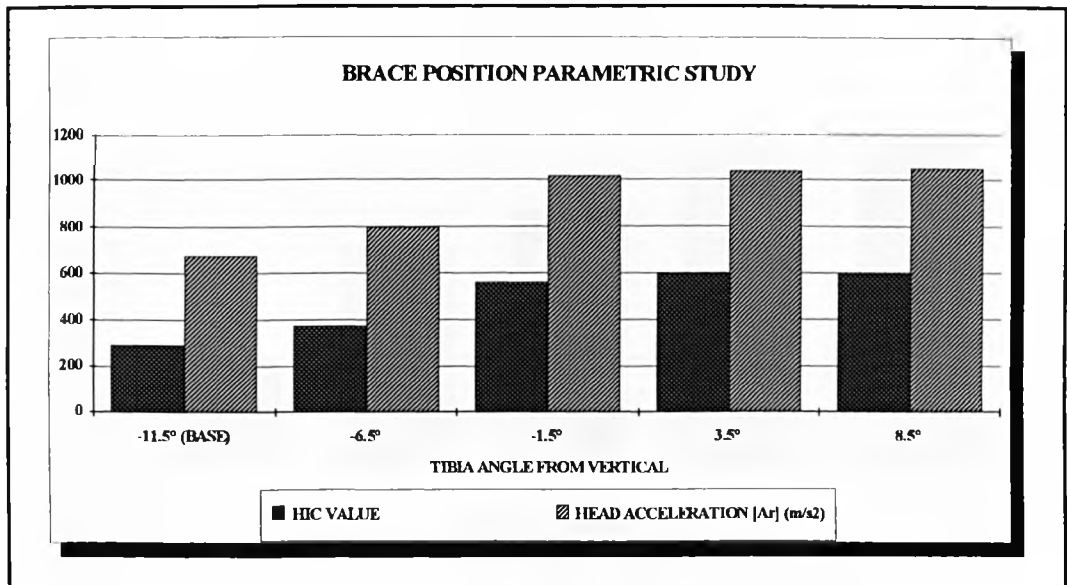


Figure 185. Brace Position Parametric Study - HIC and Head Resultant Accelerations versus Tibia Angle

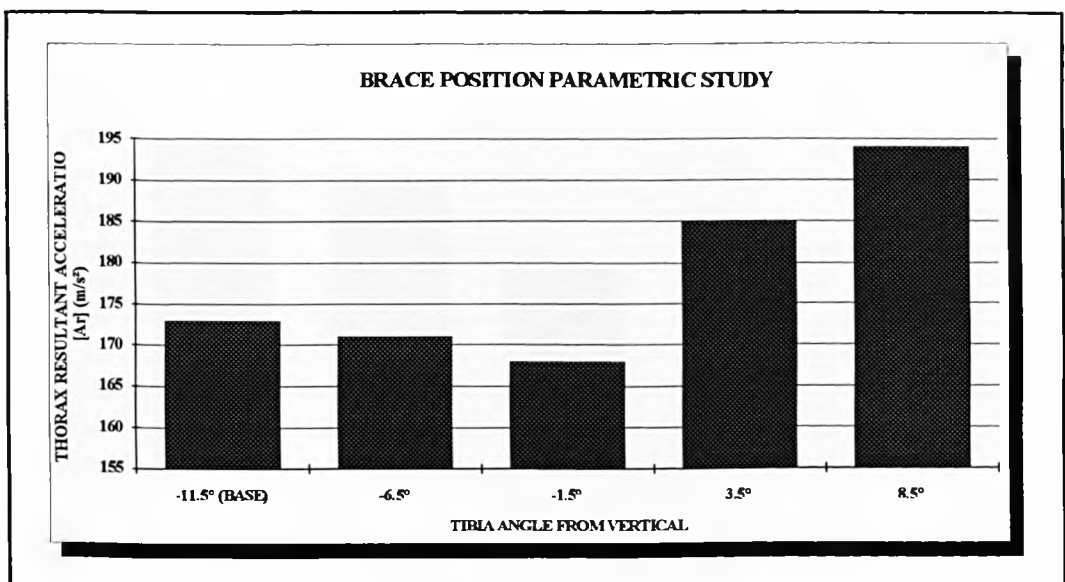


Figure 186. Brace Position Parametric Study - Thorax Resultant Accelerations versus Tibia Angle

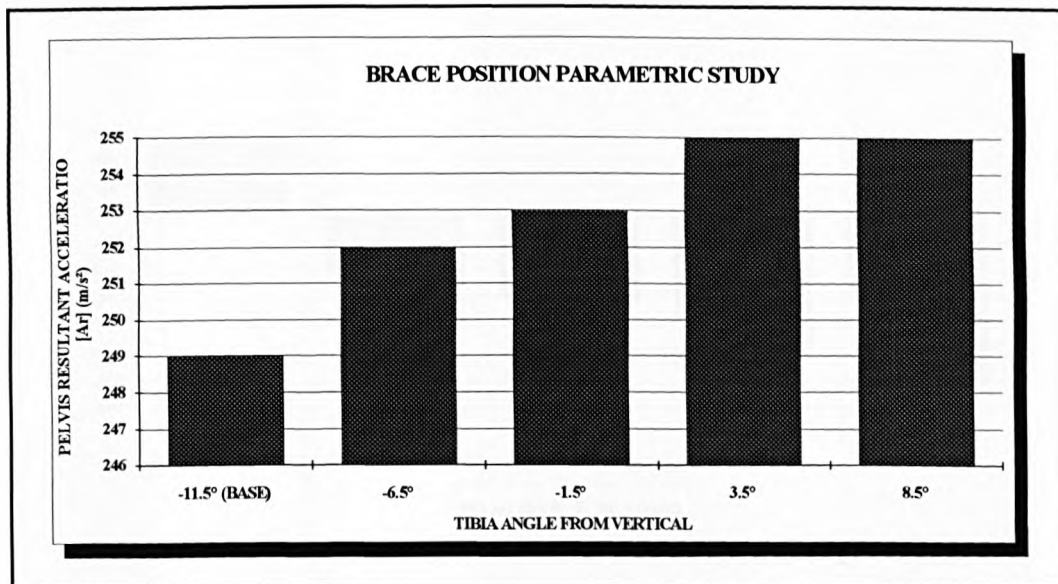


Figure 187. Brace Position Parametric Study - Pelvis Resultant Accelerations versus Tibia Angle

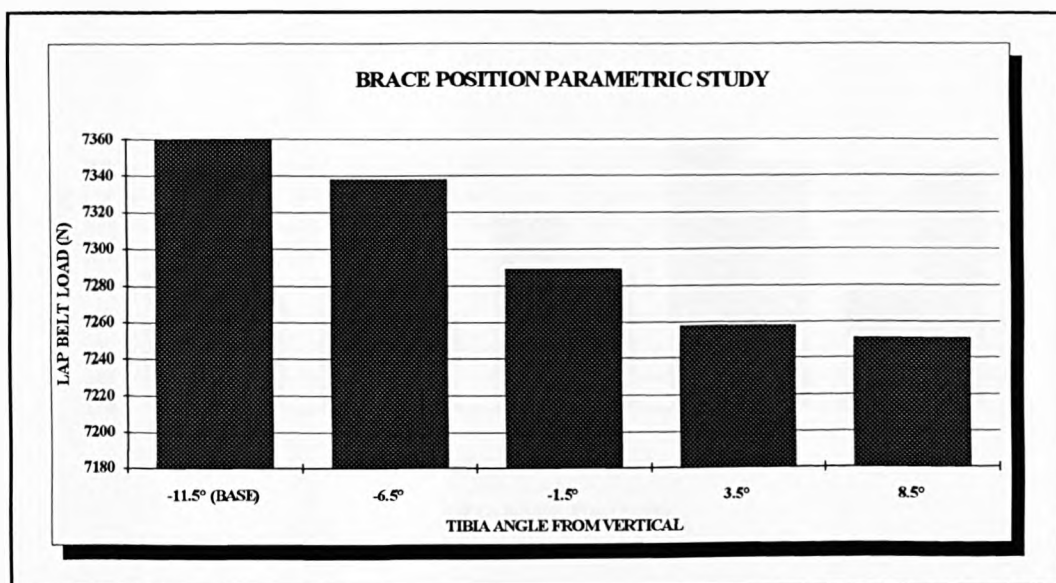


Figure 188. Brace Position Parametric Study - Lap Belt Loads versus Tibia Angle

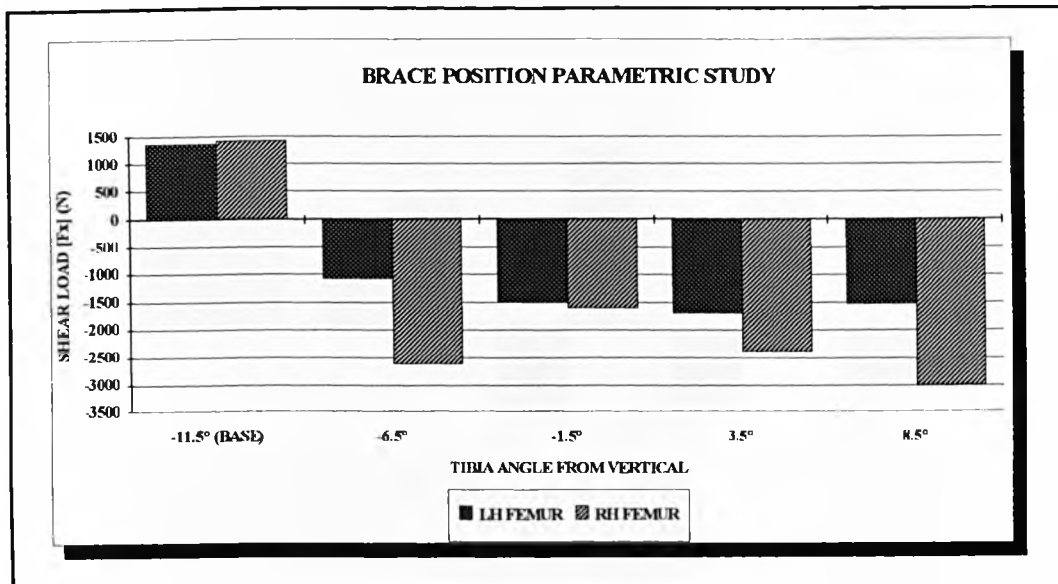


Figure 189. Brace Position Parametric Study - Left and Right Femur Shear Loads versus Tibia Angle

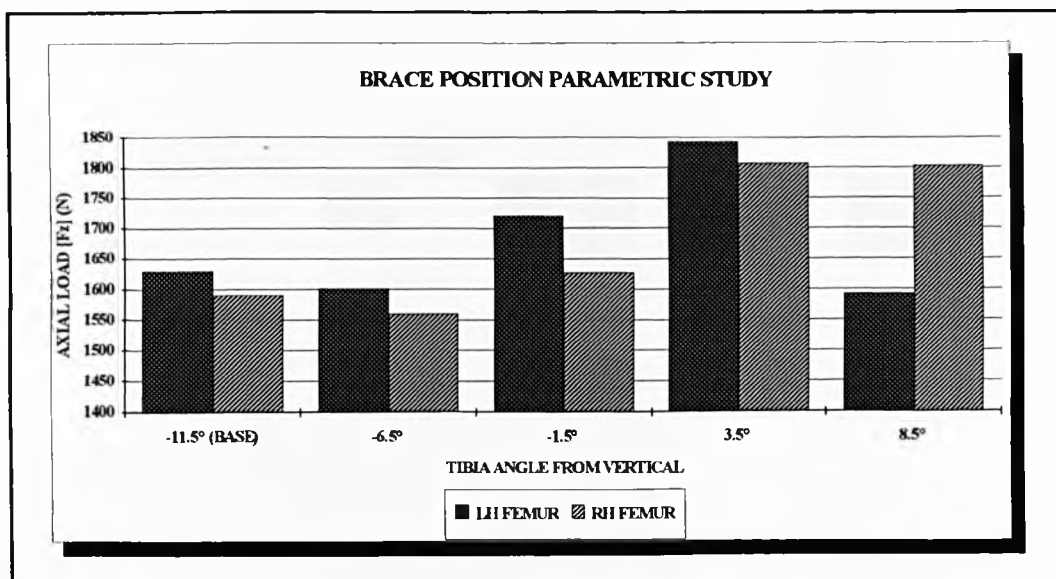


Figure 190. Brace Position Parametric Study - Left and Right Femur Axial Loads versus Tibia Angle

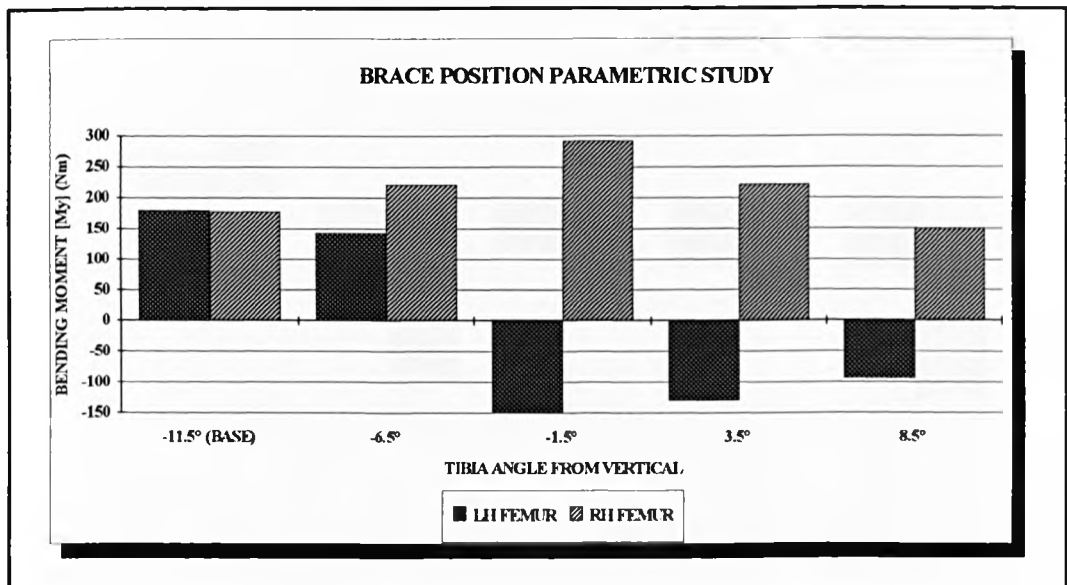


Figure 191. Brace Position Parametric Study - Left and Right Femur Bending Moments versus Tibia Angle

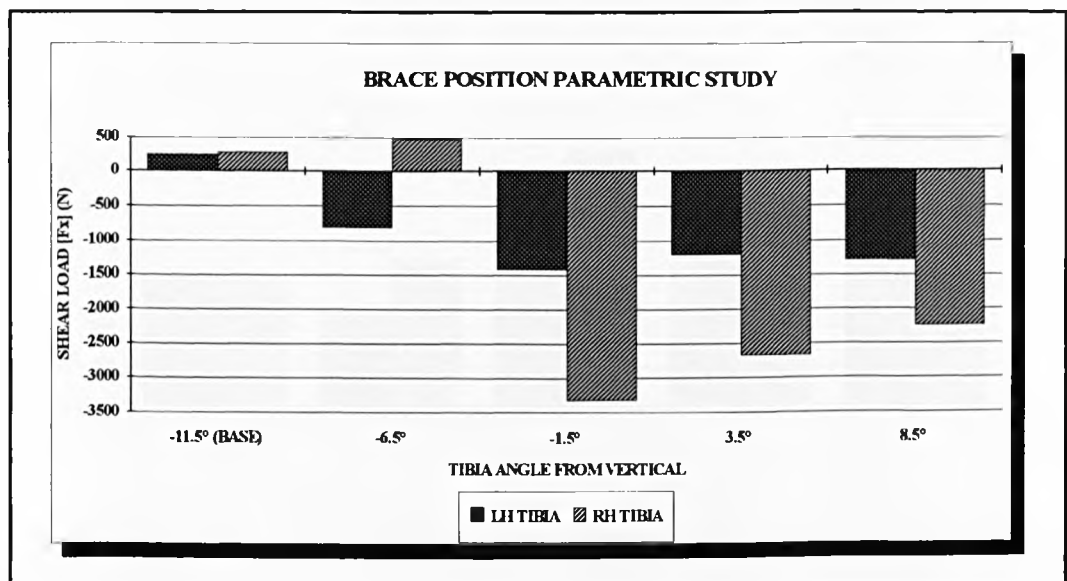


Figure 192. Brace Position Parametric Study - Left and Right Tibia Shear Loads versus Tibia Angle

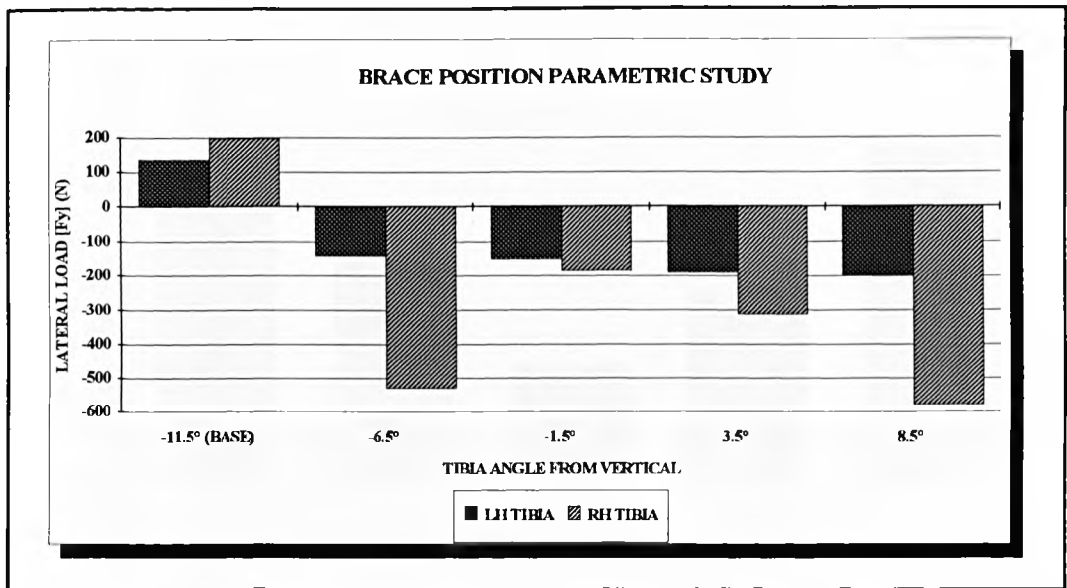


Figure 193. Brace Position Parametric Study - Left and Right Tibia Lateral Loads versus Tibia Angle

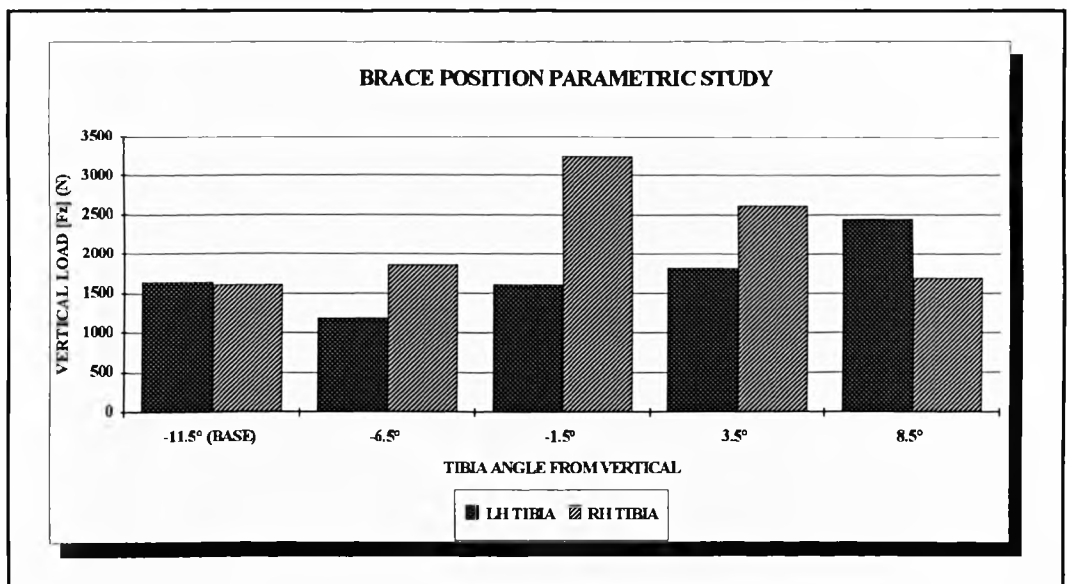


Figure 194. Brace Position Parametric Study - Left and Right Tibia Vertical Loads versus Tibia Angle

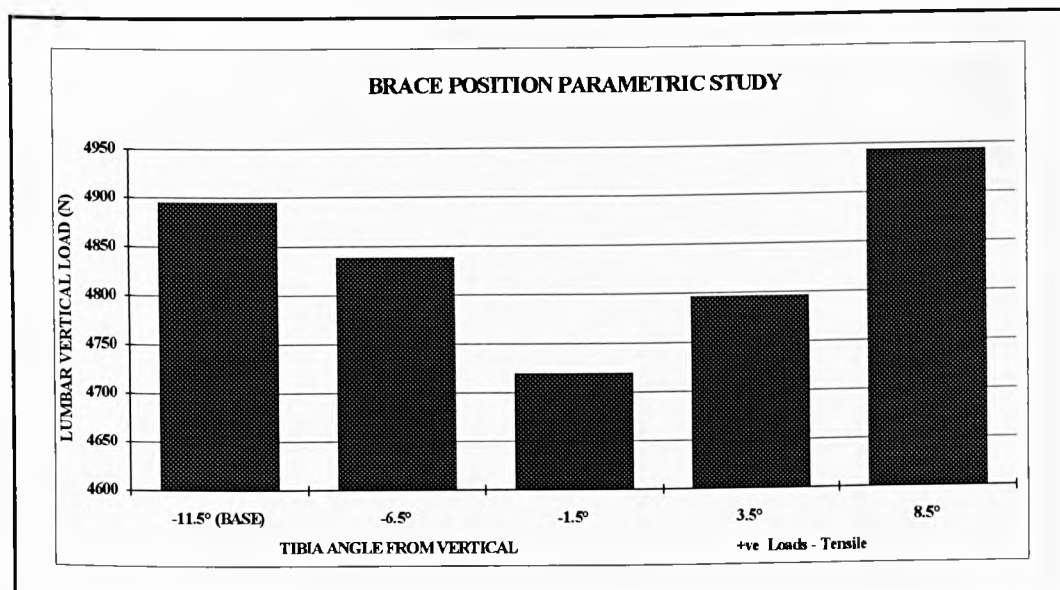


Figure 195. Brace Position Parametric Study - Lumbar Spine Vertical Loads versus Tibia Angle

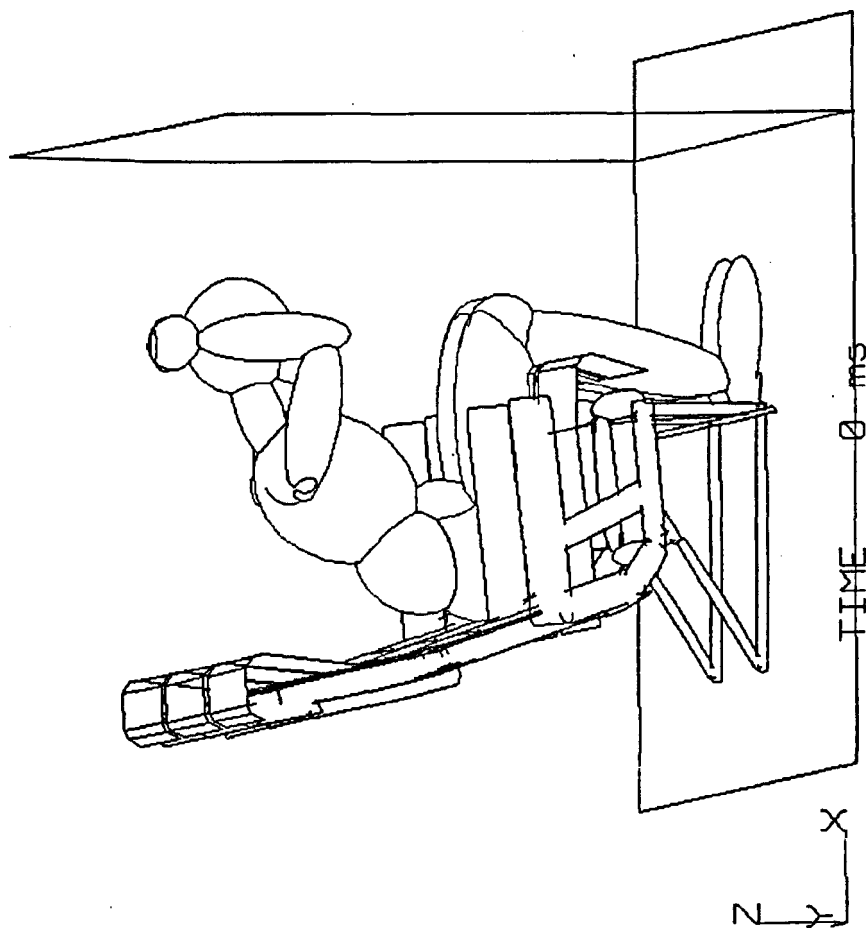


Figure 196. Brace Position Parametric Study - Bulkhead Simulation At 0ms

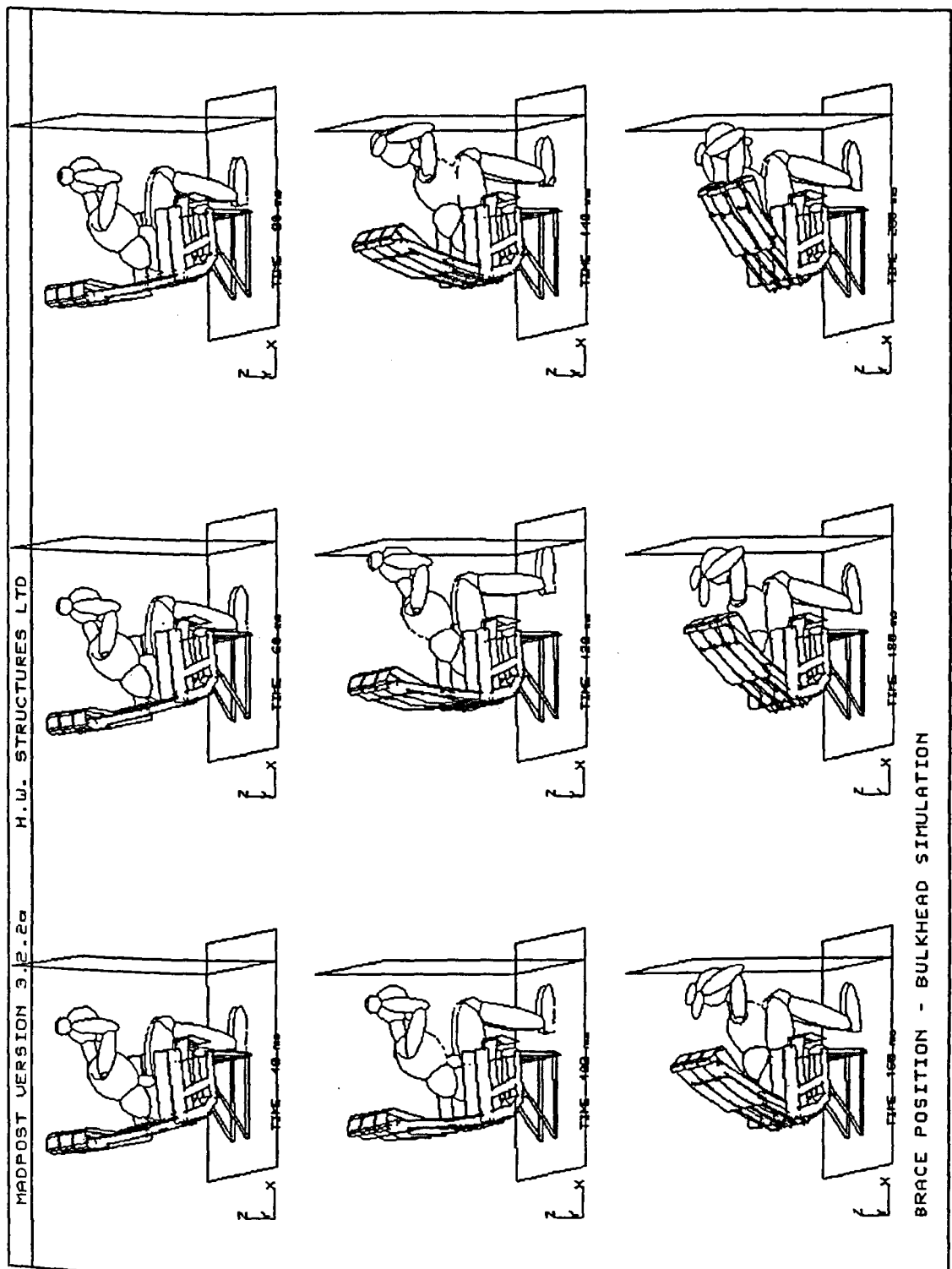


Figure 197. Brace Position Parametric Study - Bulkhead Simulation At 40ms To 200ms

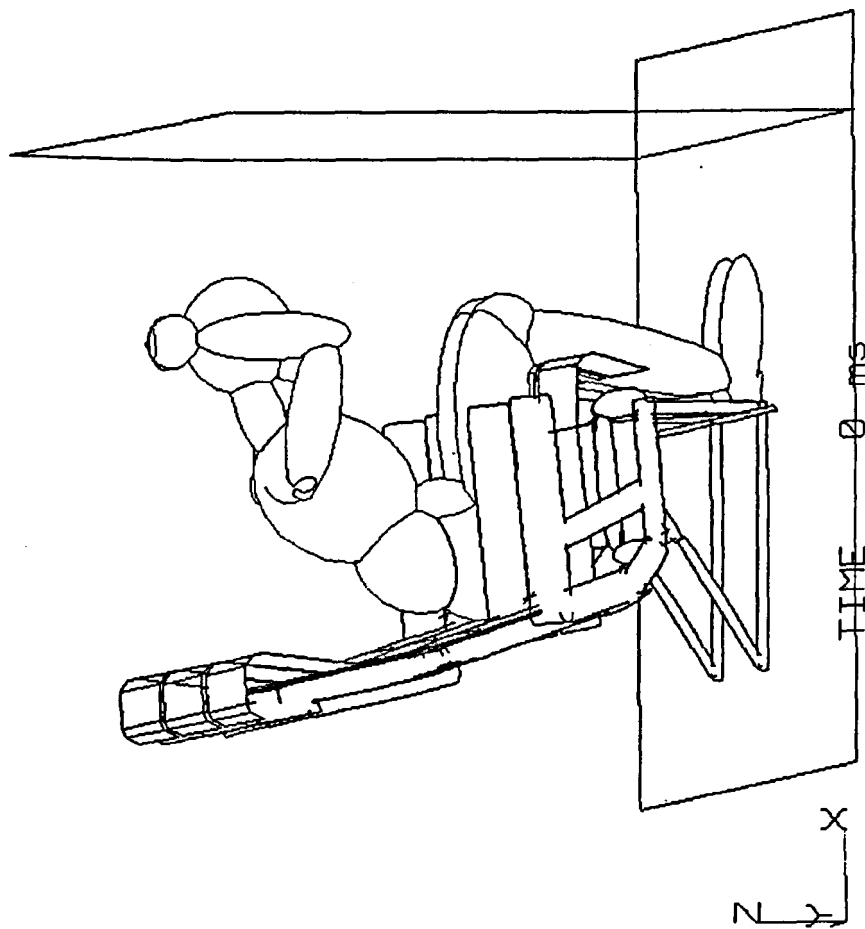


Figure 198. Brace Position Parametric Study - Nomex Bulkhead Simulation At 0ms

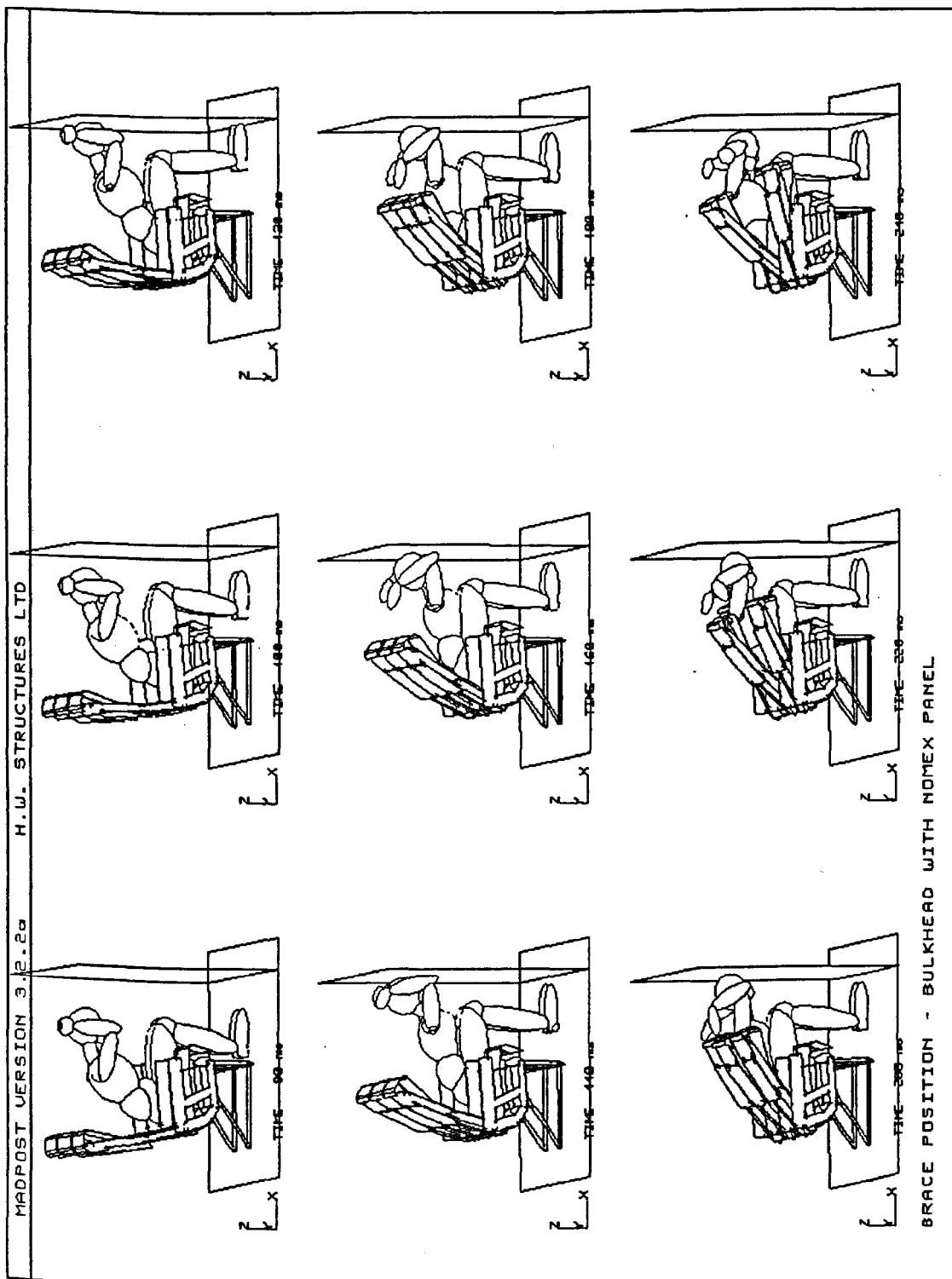


Figure 199. Brace Position Parametric Study - Nomex Bulkhead Simulation At 80ms To 240ms

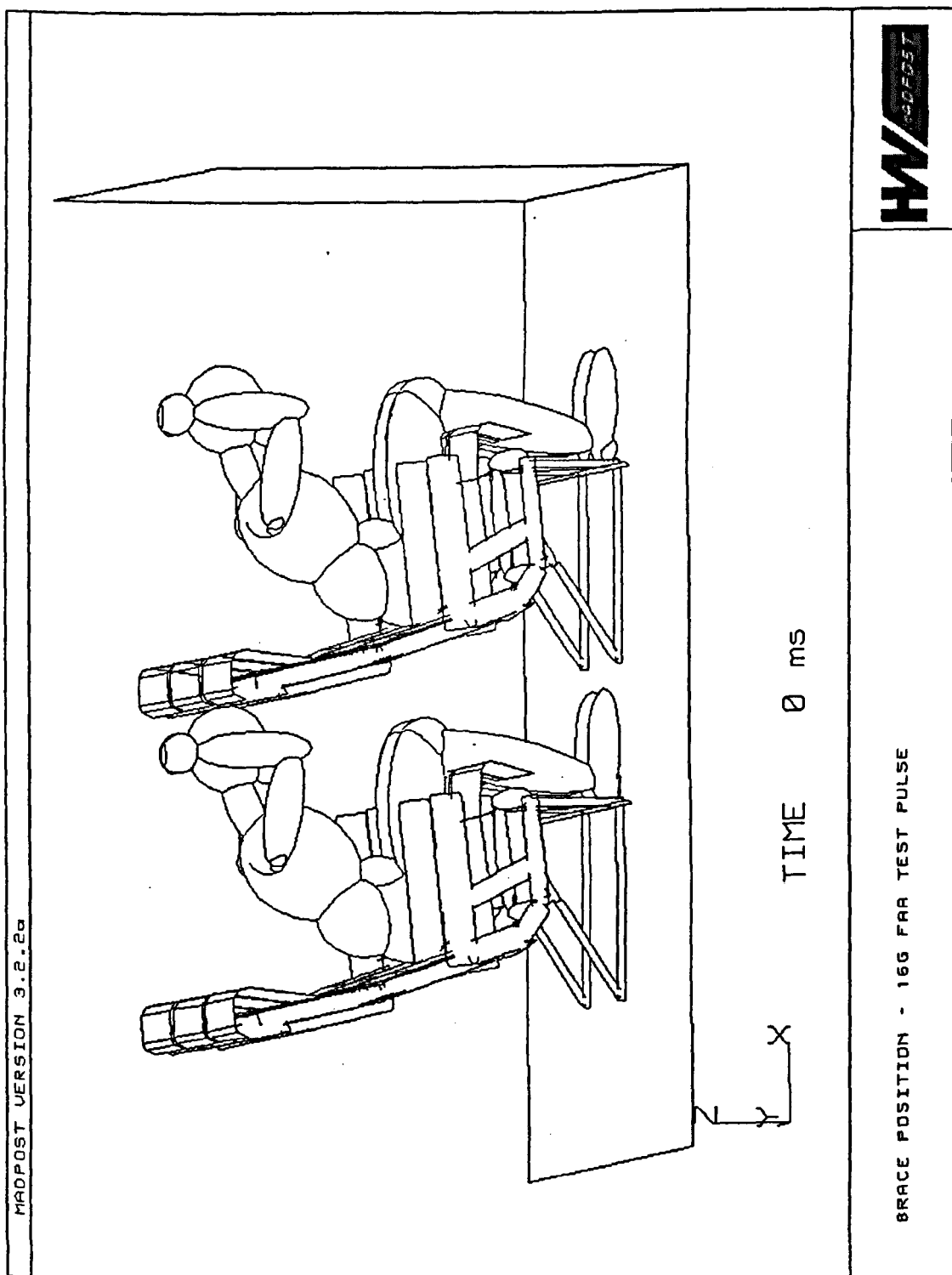


Figure 200. Brace Position Parametric Study - 16G FAA Test Pulse At 0ms

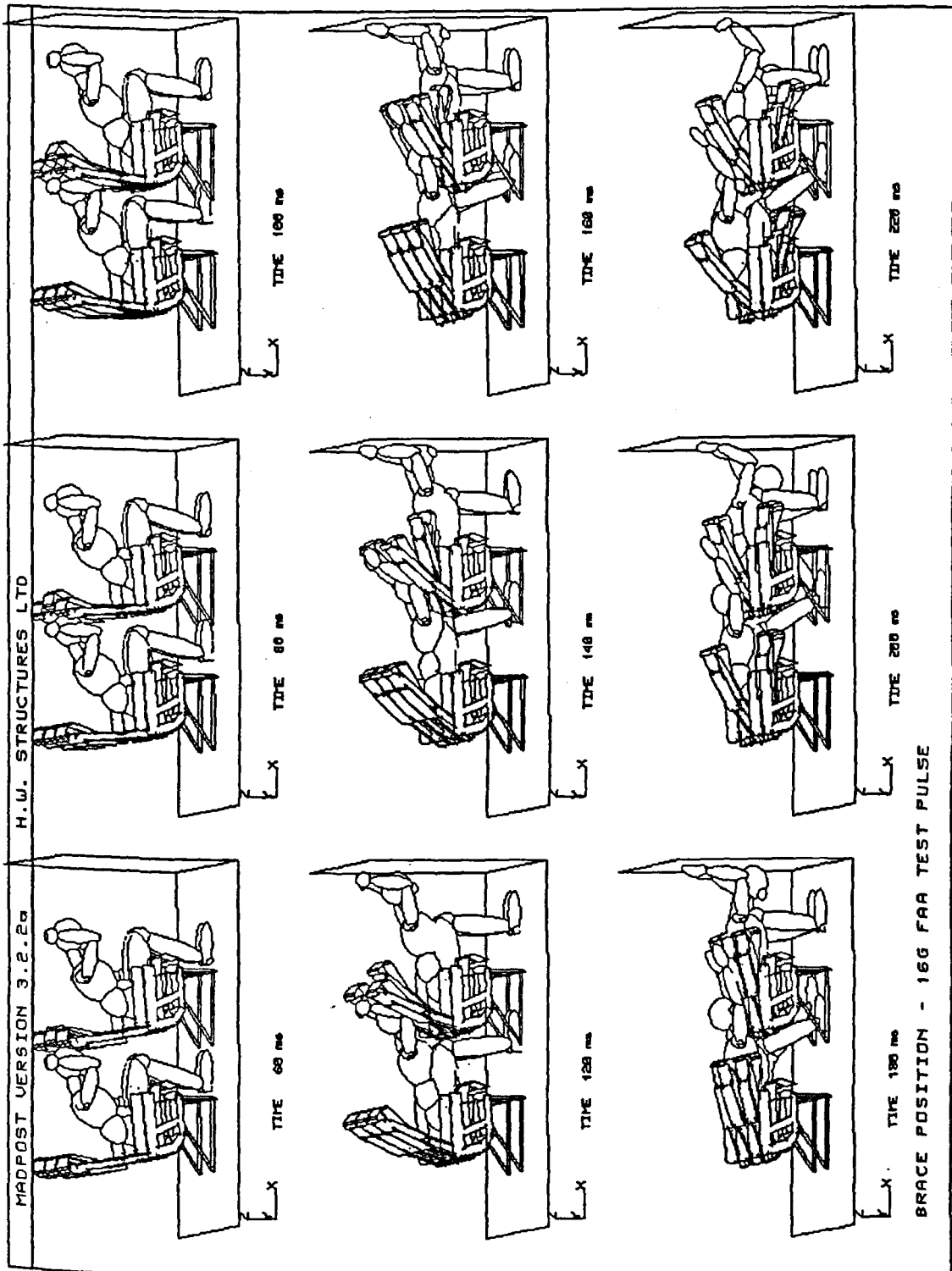


Figure 201. Brace Position Parametric Study - 16G FAA Test Pulse At 60ms To 220ms

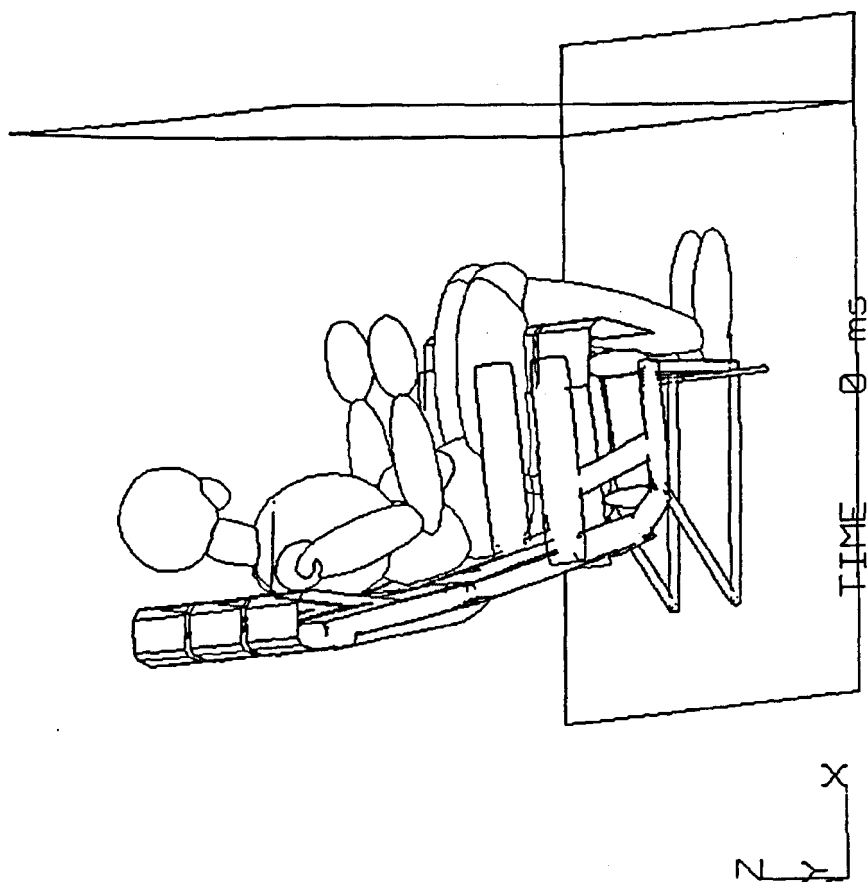


Figure 202. Three Point Belt Occupant Simulation At 0ms

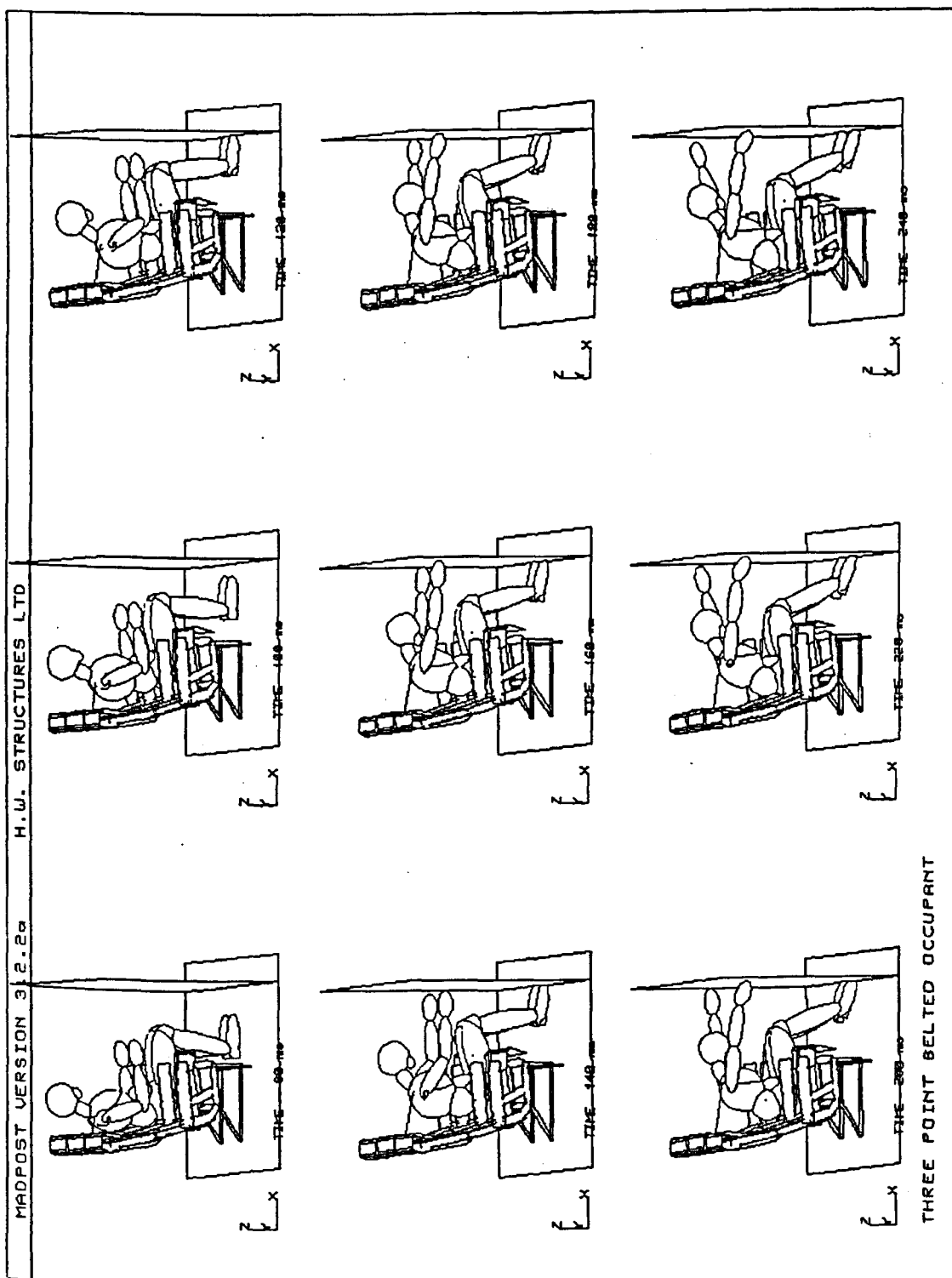
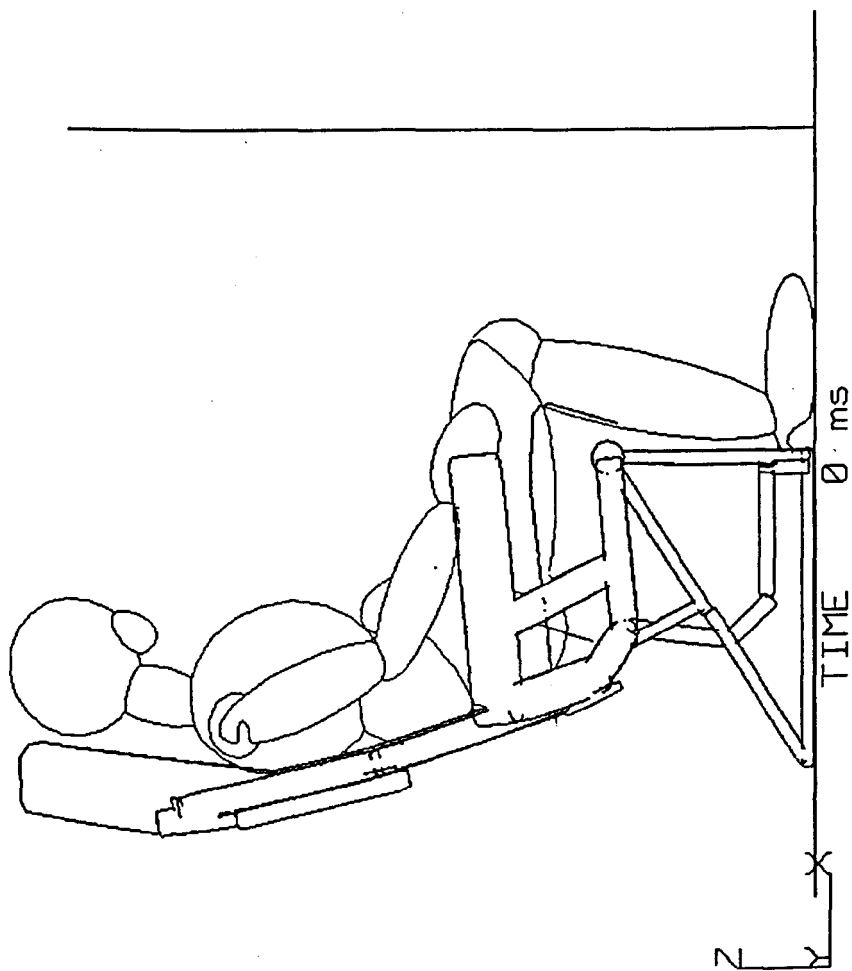
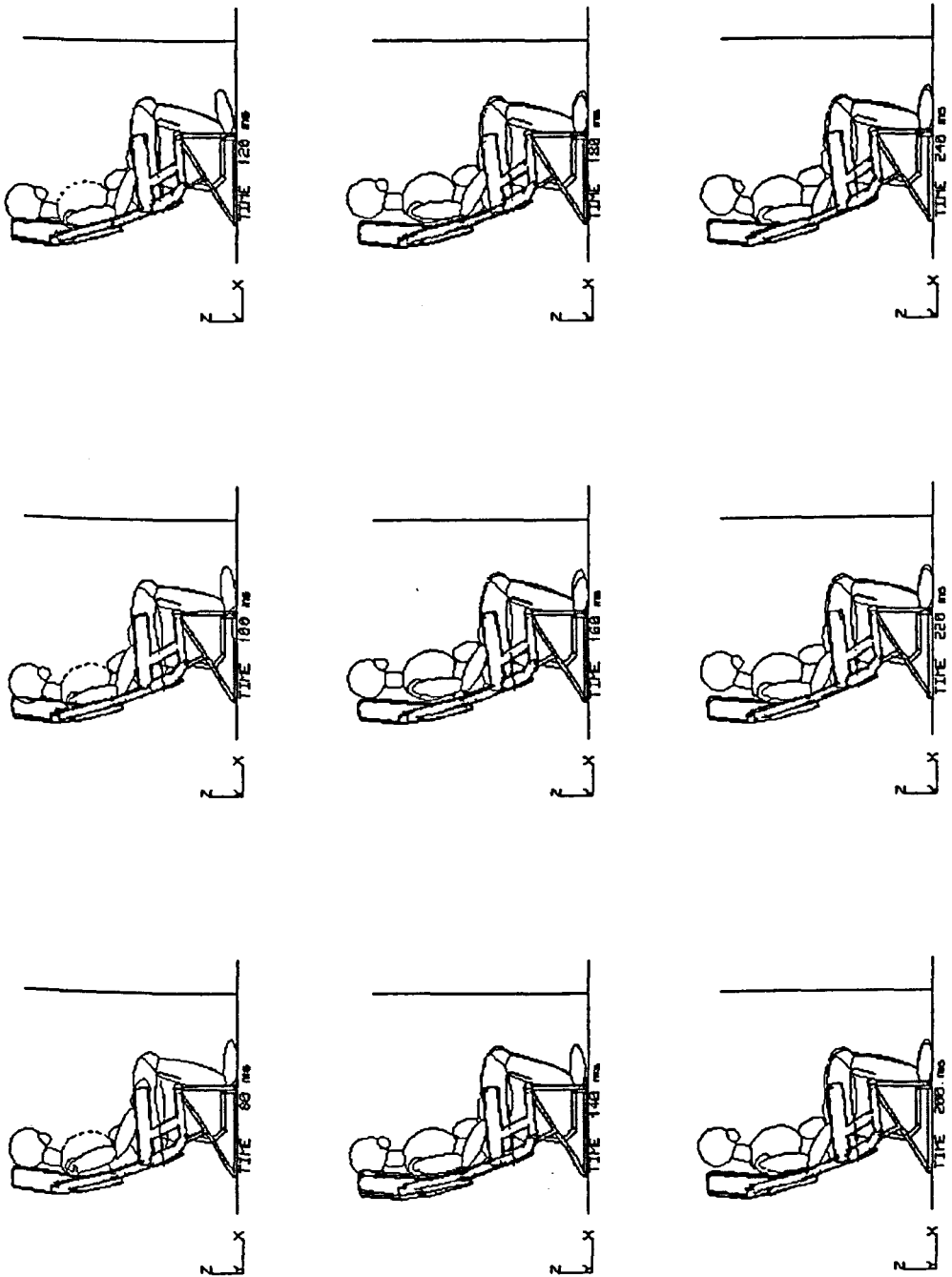


Figure 203. Three Point Belt Occupant Simulation At 80ms To 240ms

**Figure 204. Rear Facing Seat Simulation At 0ms**



REAR FACING SEAT SIMULATION

Figure 205. Rear Facing Seat Simulation At 80ms To 240ms

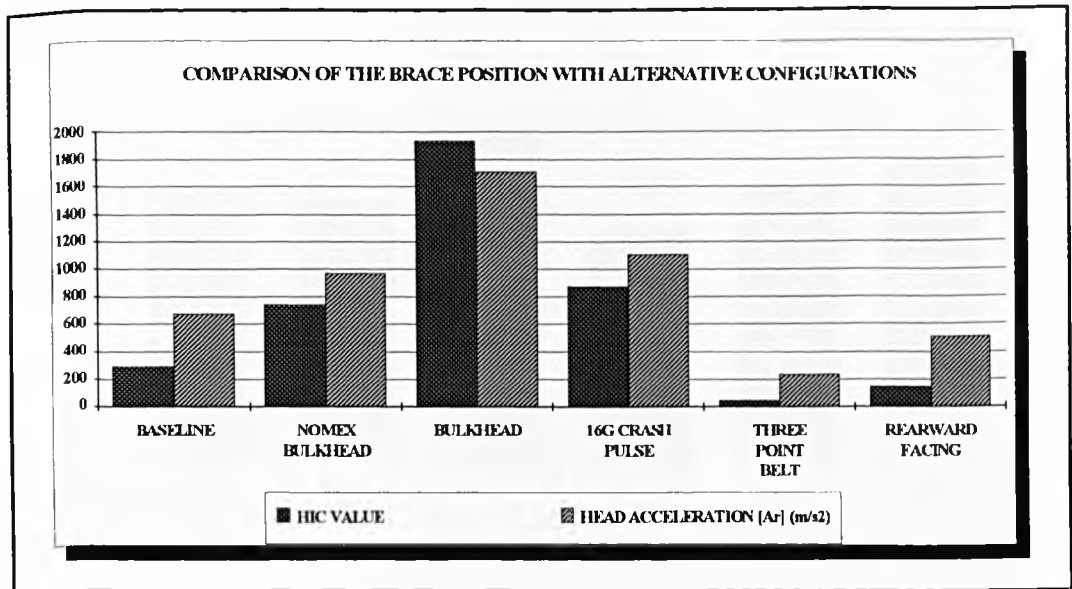


Figure 206. Brace Position Parametric Study - HIC and Head Resultant Accelerations versus Alternative Configurations

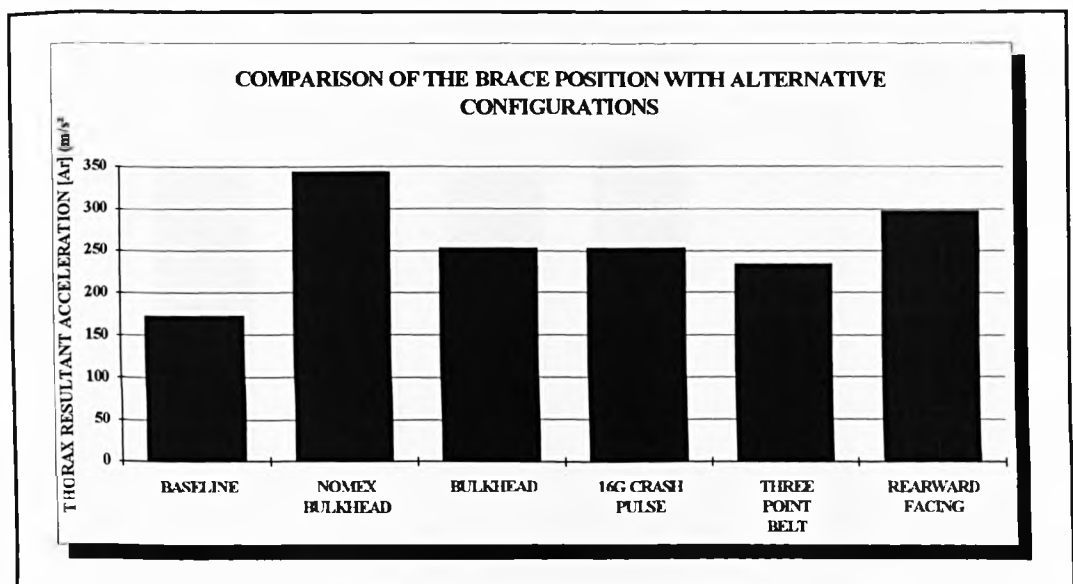


Figure 207. Brace Position Parametric Study - Thorax Resultant Accelerations versus Alternative Configurations

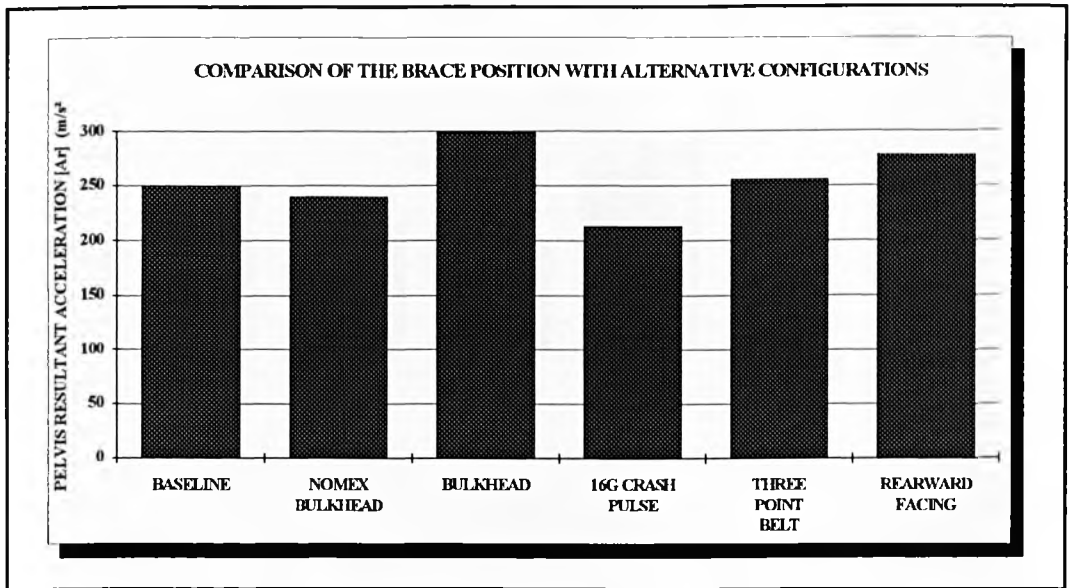


Figure 208. Brace Position Parametric Study - Pelvis Resultant Accelerations versus Alternative Configurations

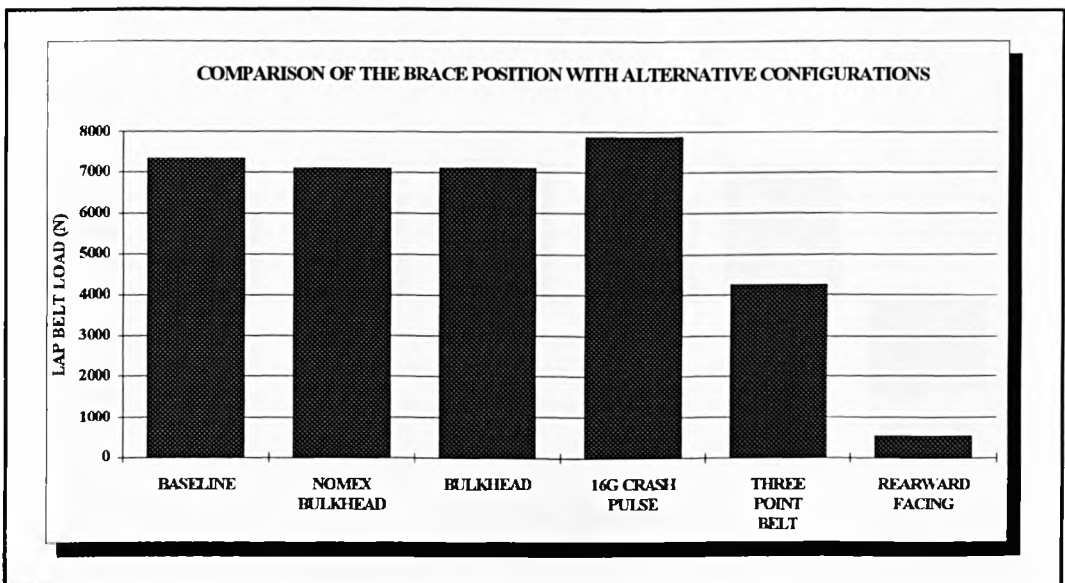


Figure 209. Brace Position Parametric Study - Lap Belt Loads versus Alternative Configurations

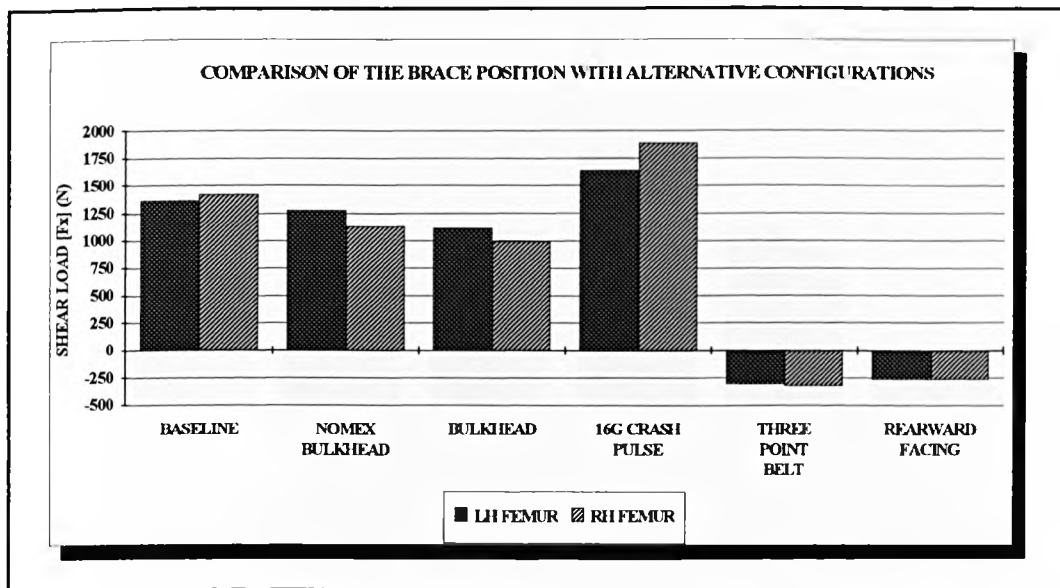


Figure 210. Brace Position Parametric Study - Left and Right Femur Shear Loads versus Alternative Configurations

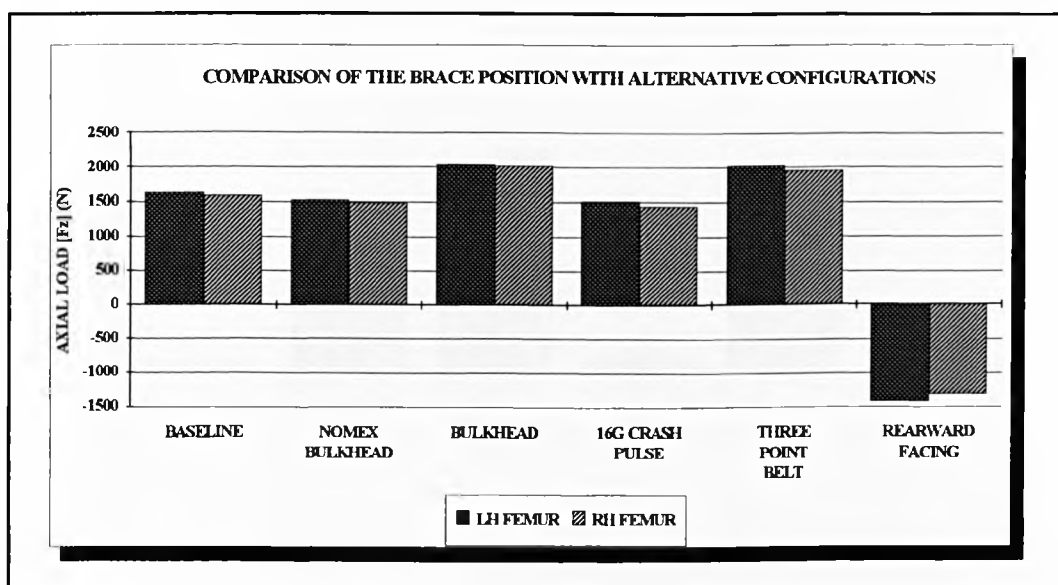


Figure 211. Brace Position Parametric Study - Left and Right Femur Axial Loads versus Alternative Configurations

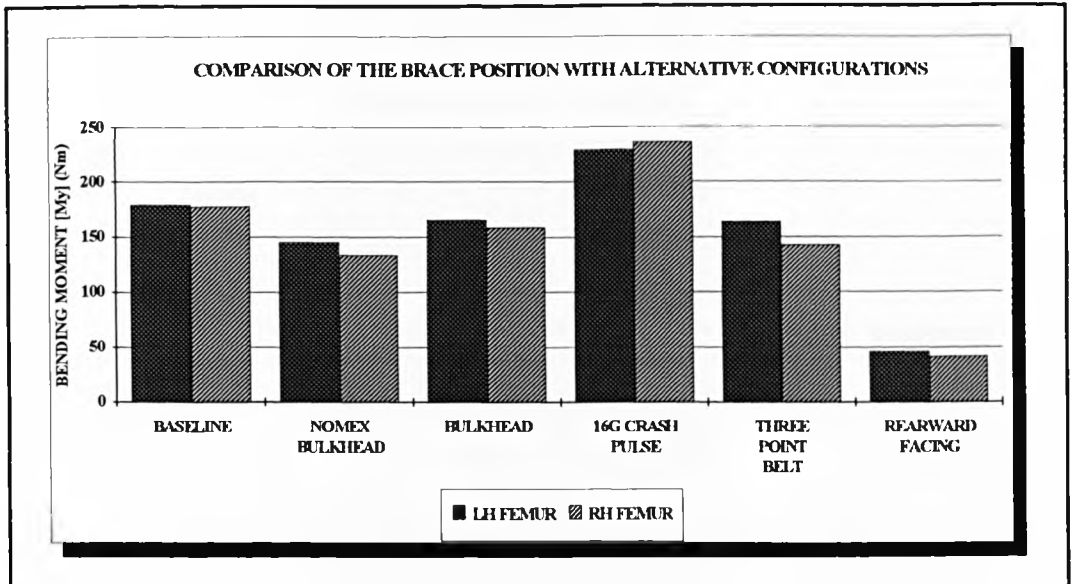


Figure 212. Brace Position Parametric Study - Left and Right Femur Bending Moments versus Alternative Configurations

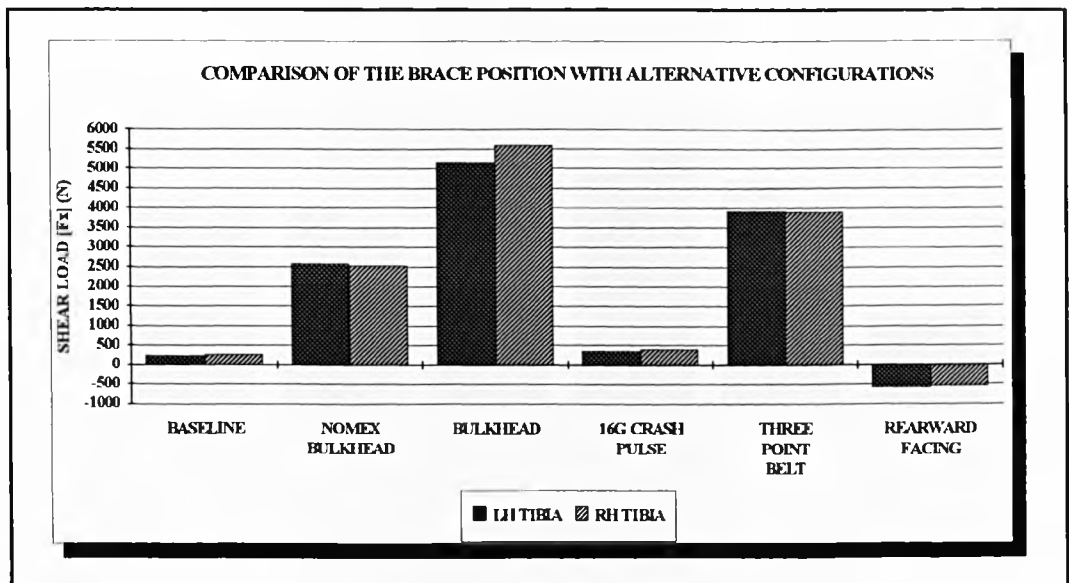


Figure 213. Brace Position Parametric Study - Left and Right Tibia Bending Moments versus Alternative Configurations

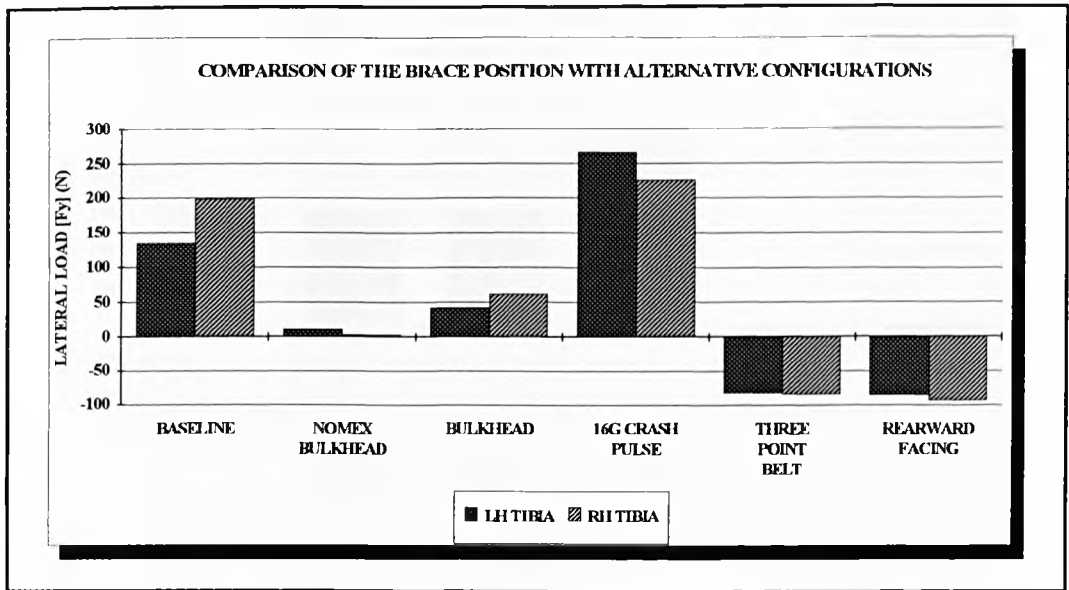


Figure 214. Brace Position Parametric Study - Left and Right Tibia Lateral Loads versus Alternative Configurations

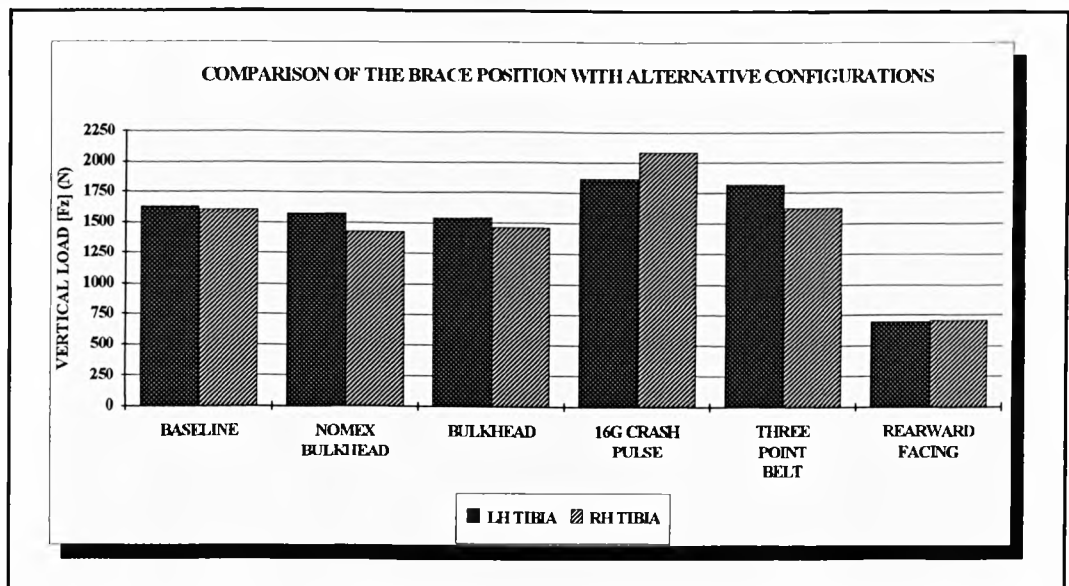


Figure 215. Brace Position Parametric Study - Left and Right Tibia Vertical Loads versus Alternative Configurations

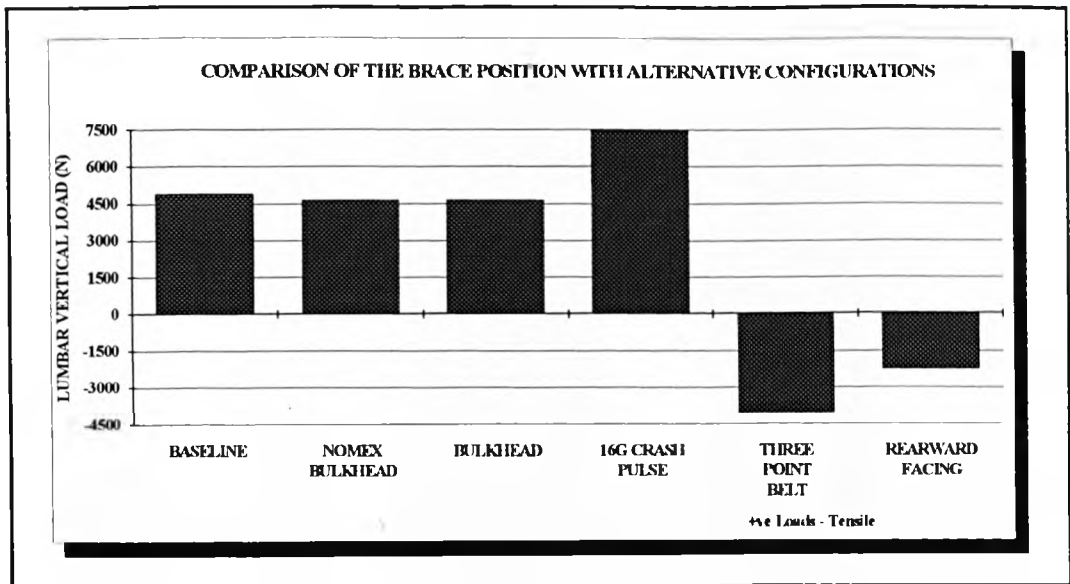


Figure 216. Brace Position Parametric Study - Lumbar Spine Vertical Loads versus Alternative Configurations

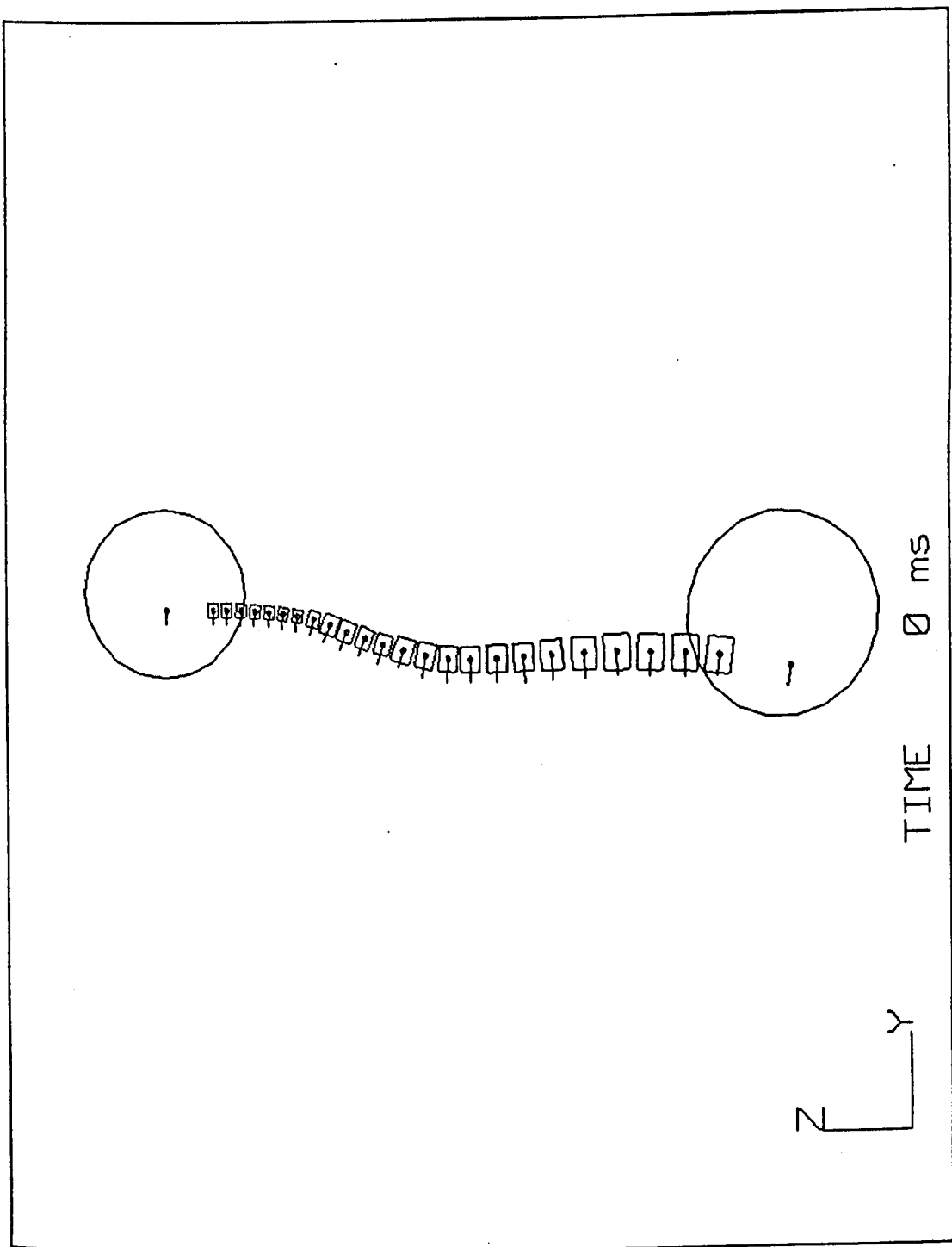


Figure 217. Wayne State University Model At 0ms.

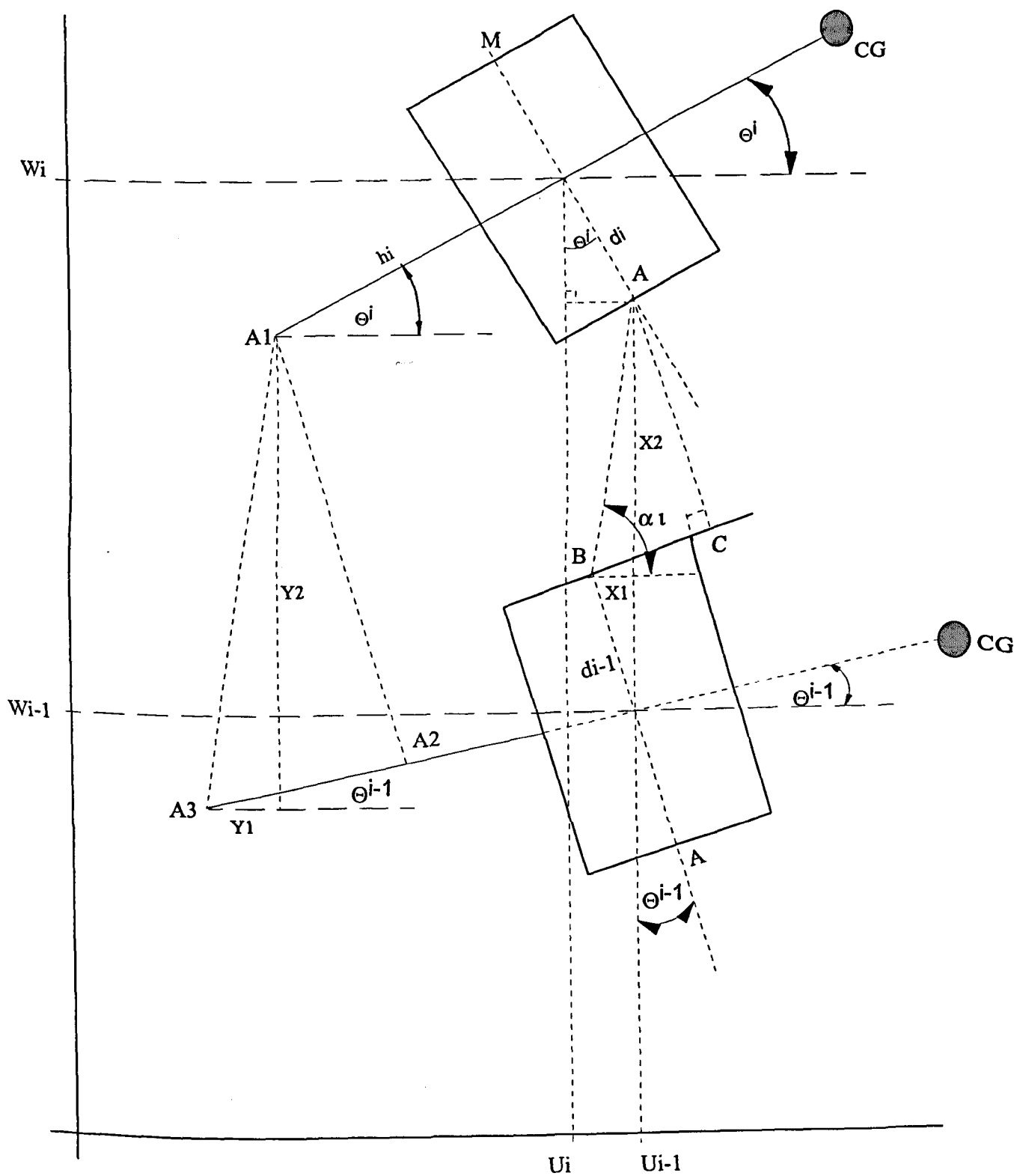


Figure 218. Configuration Of Two Successive Vertebrae

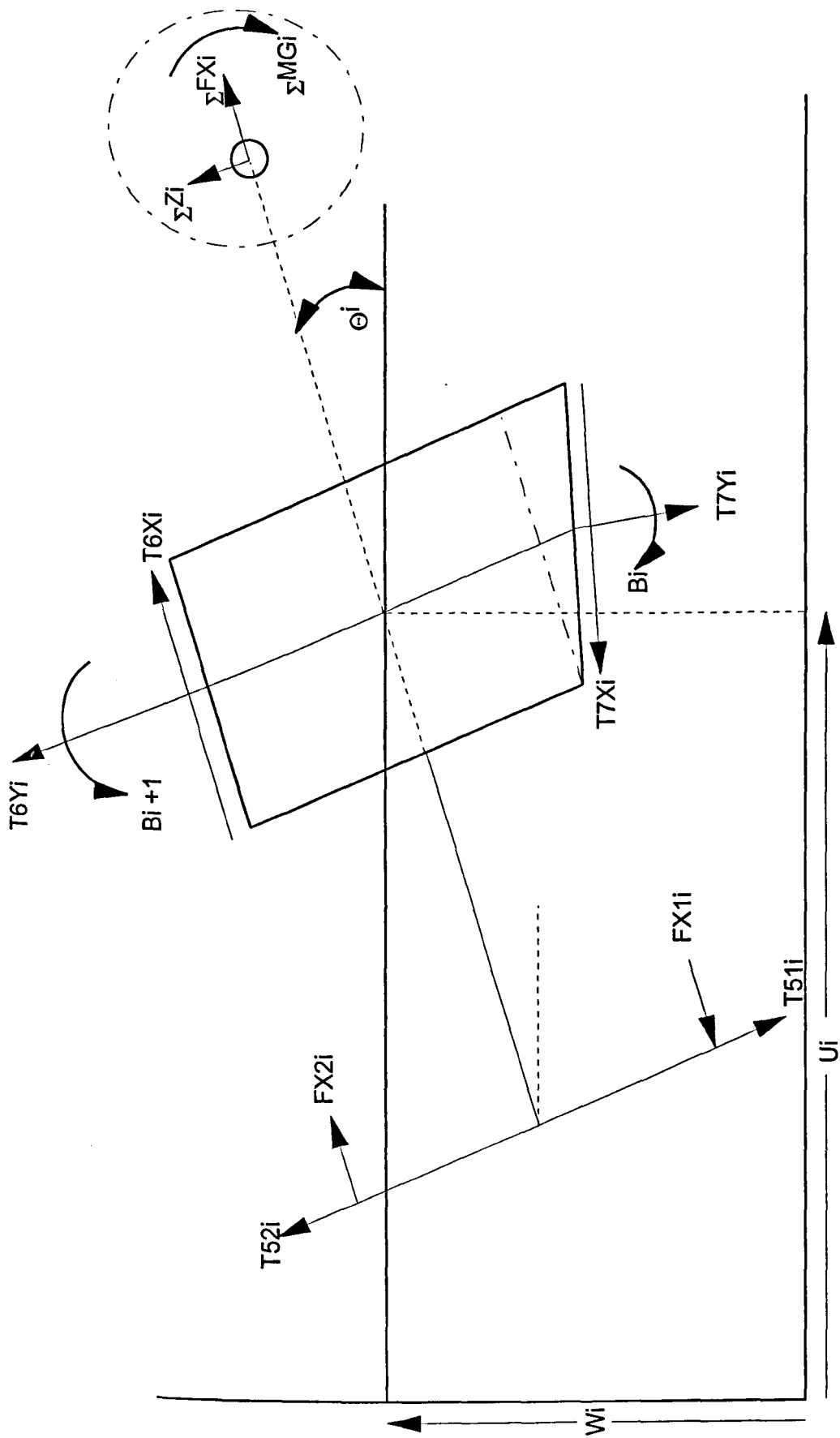


Figure 219. Free Body Diagram Of Vertebral Body

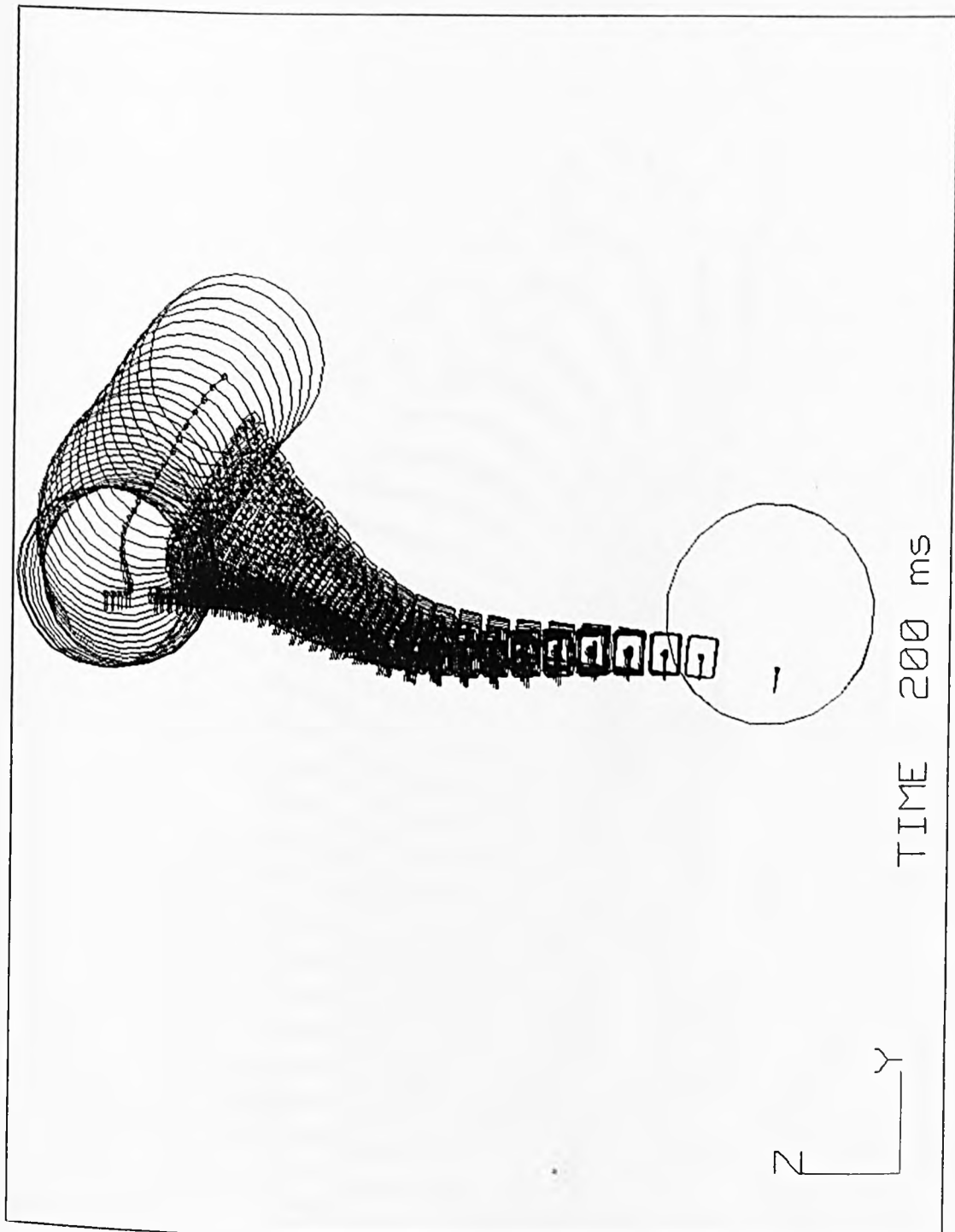


Figure 220. Spine Model with Full Harness Undergoing Ejection for a Period of 200ms

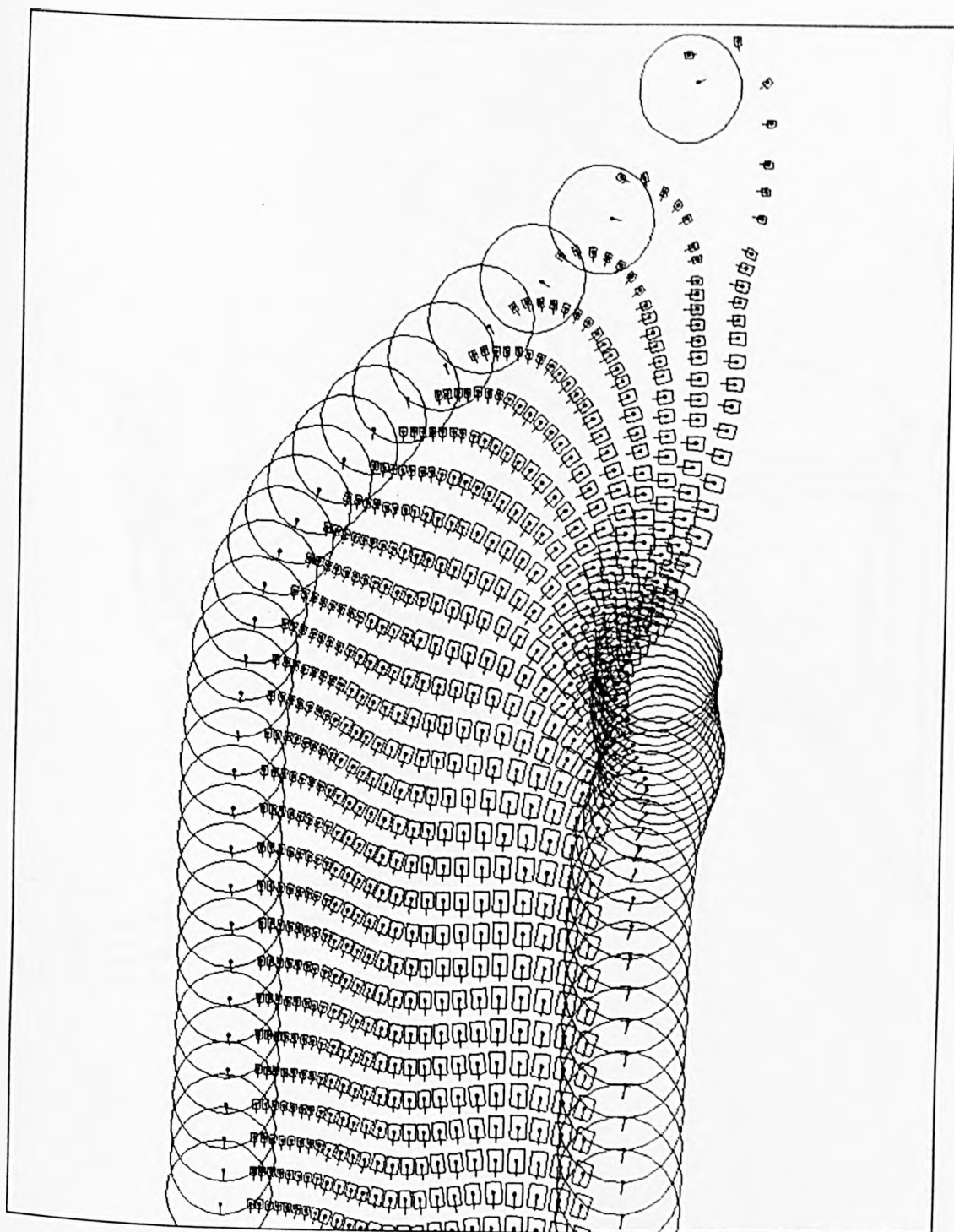


Figure 221. Spine Model with Lap Belt Only Undergoing 16G Test Pulse

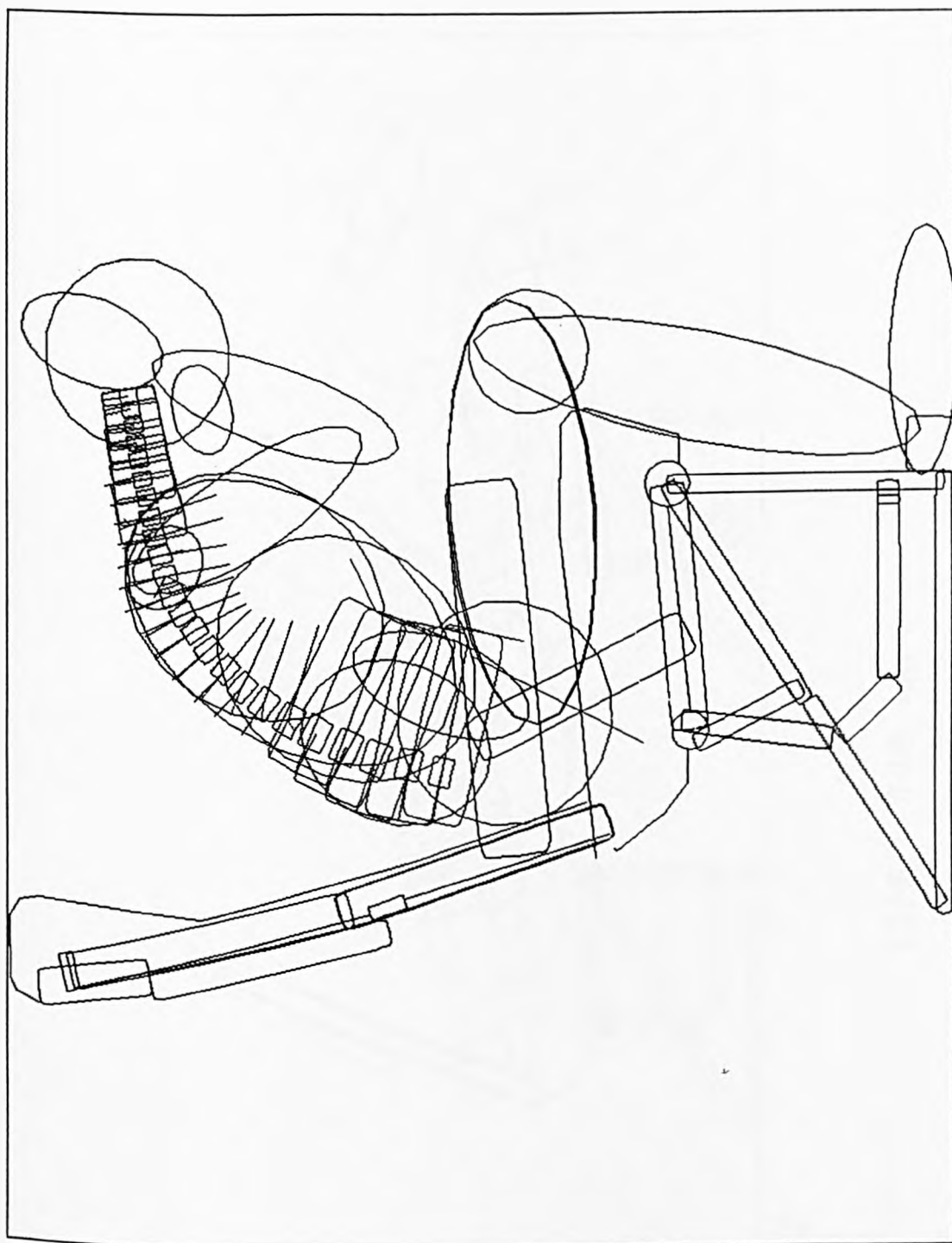


Figure 222. Dataset for Spine Modelling

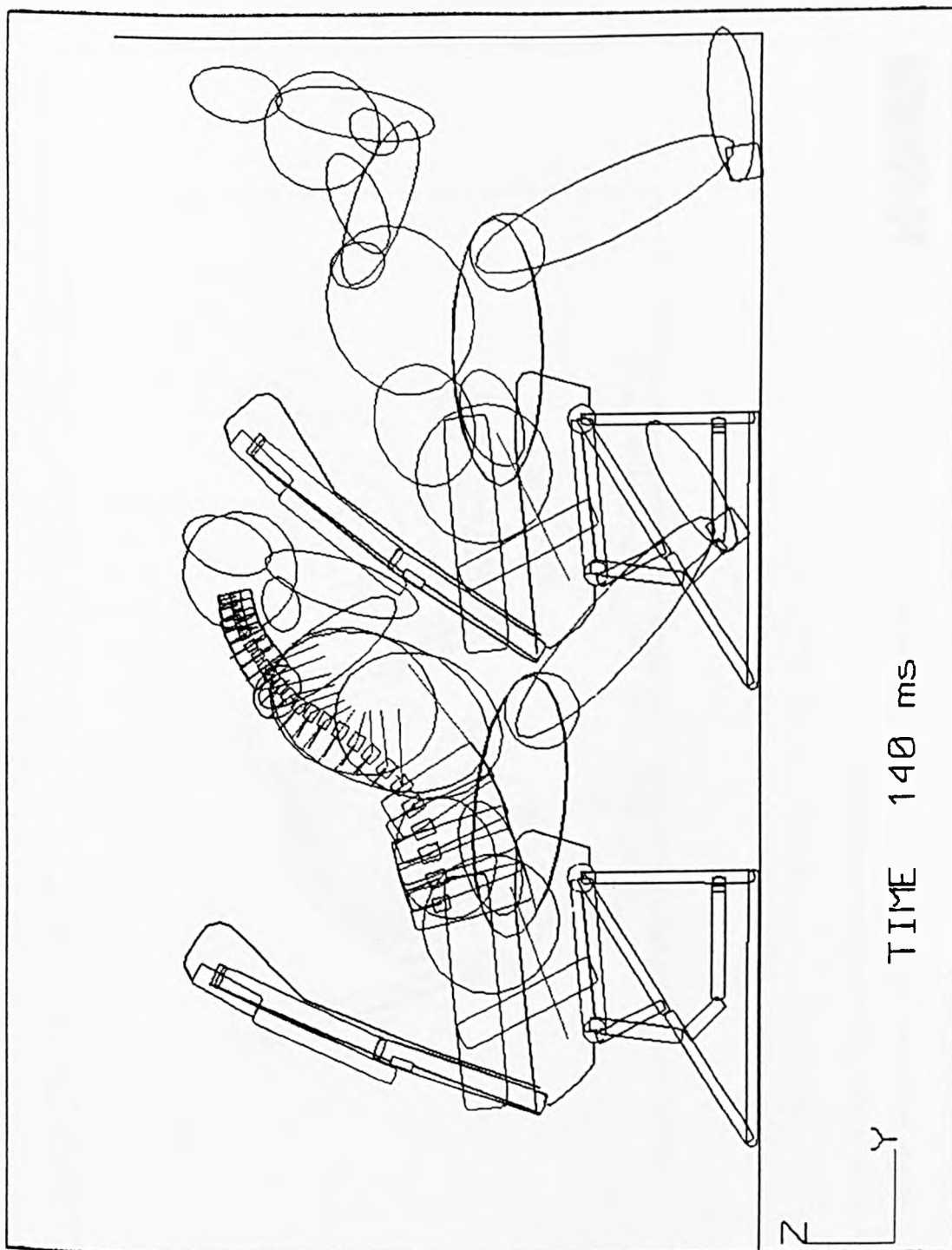


Figure 223. Spine Model Kinematics with Legs Forward at 140ms

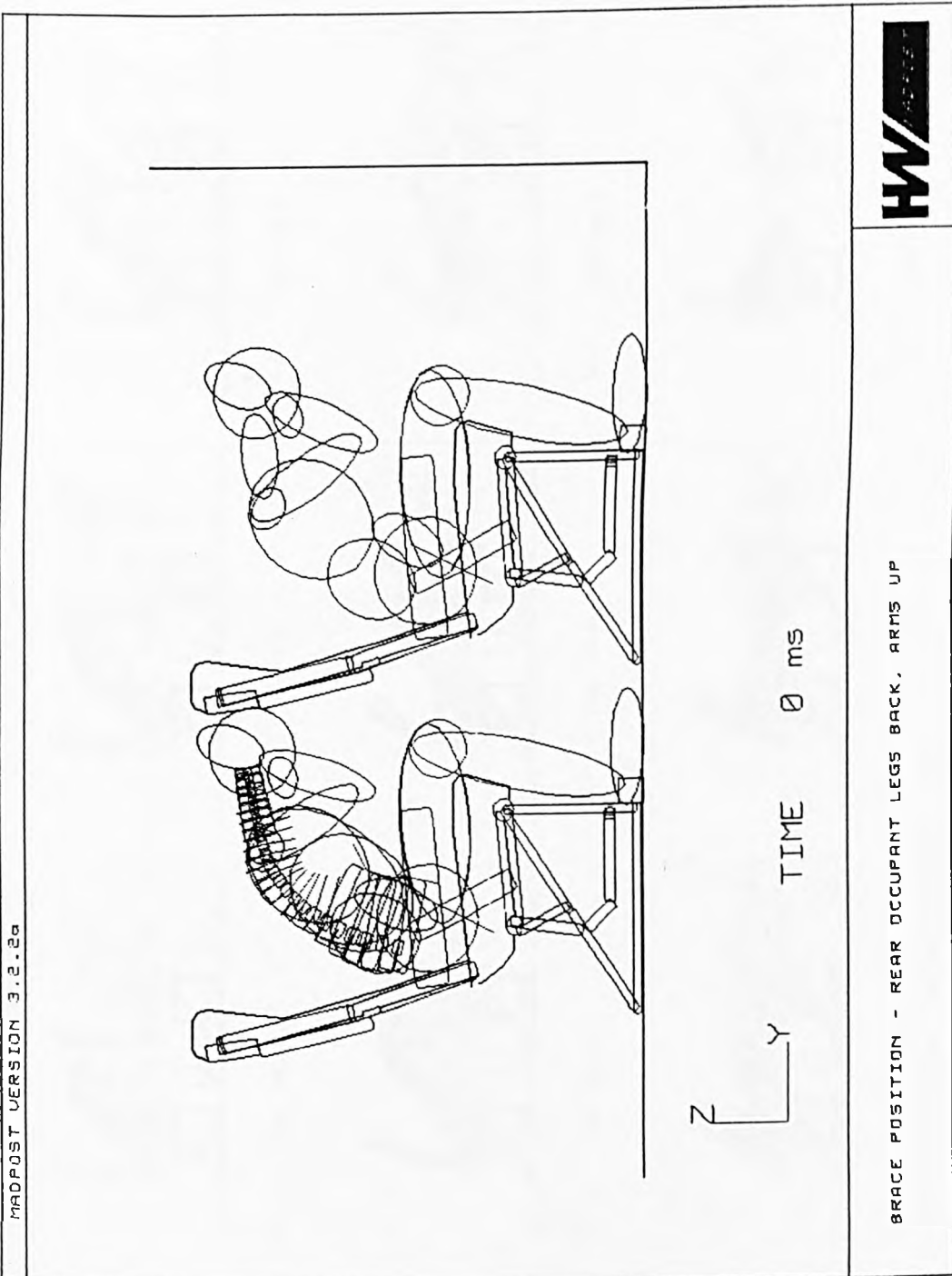


Figure 224. Brace Position - Rear Occupant Legs Back, Arms Up at 0ms

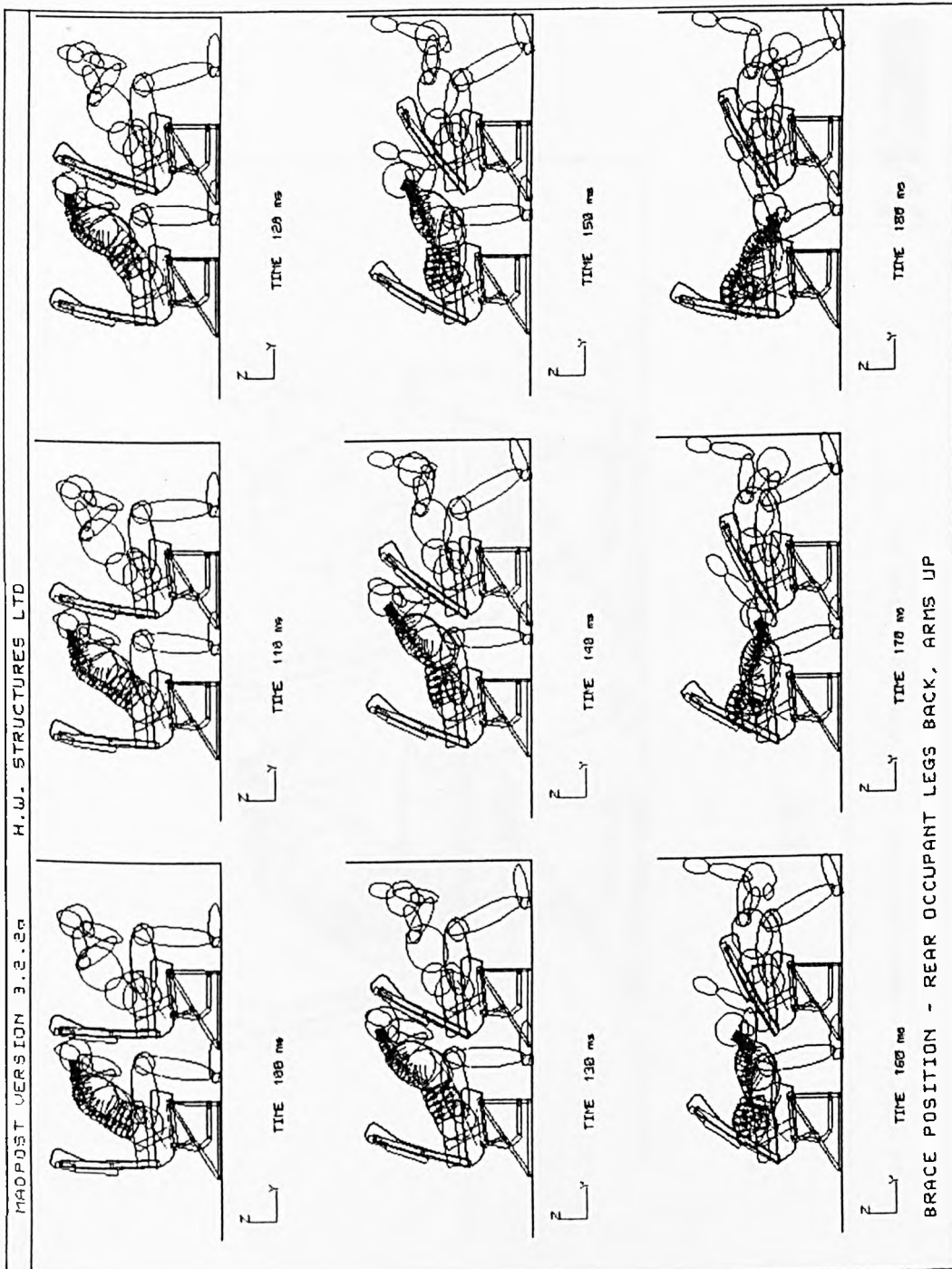


Figure 225. Brace Position Simulation - Rear Occupant Legs Back, Arms Up At 100ms To 180ms

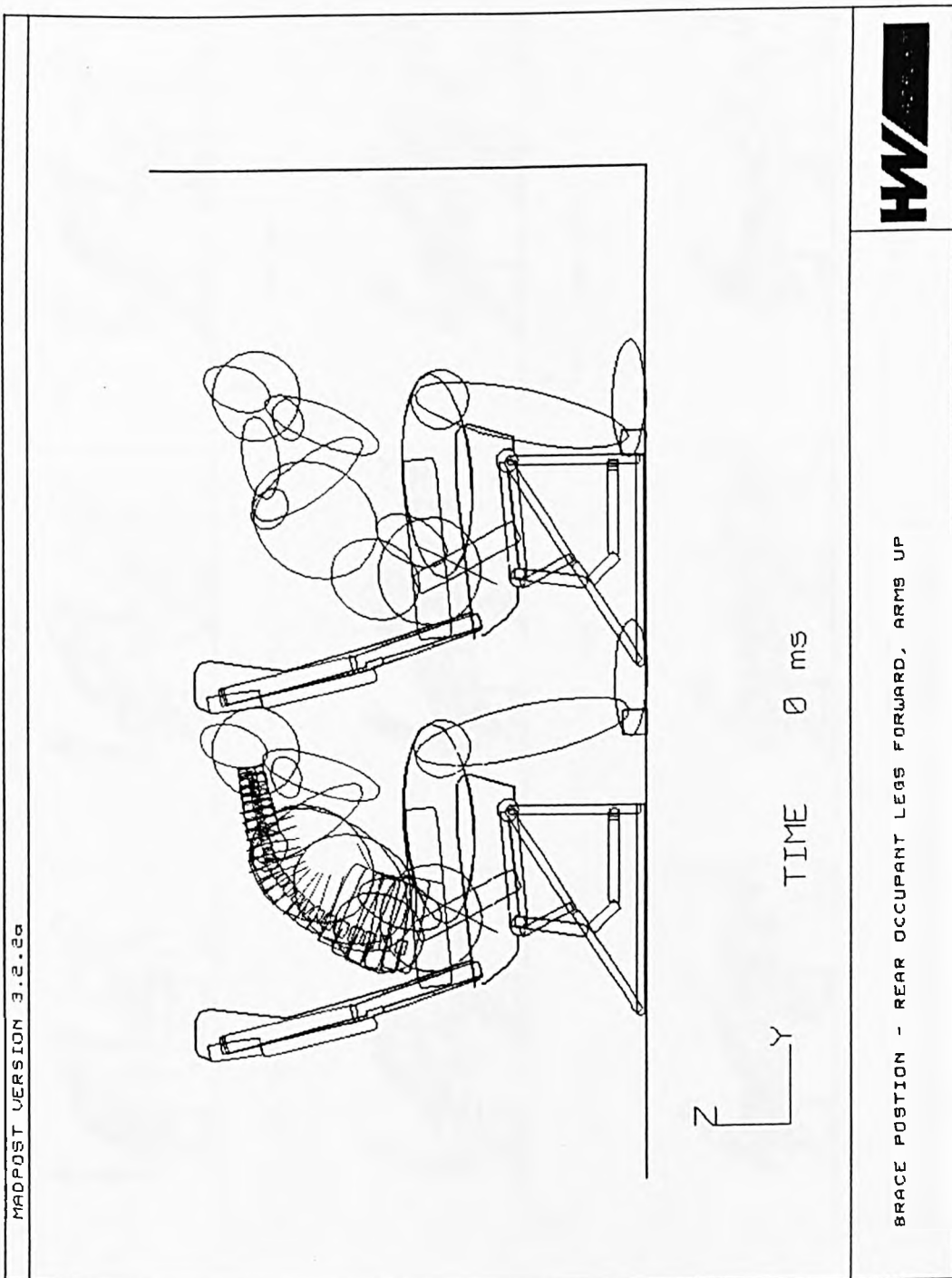
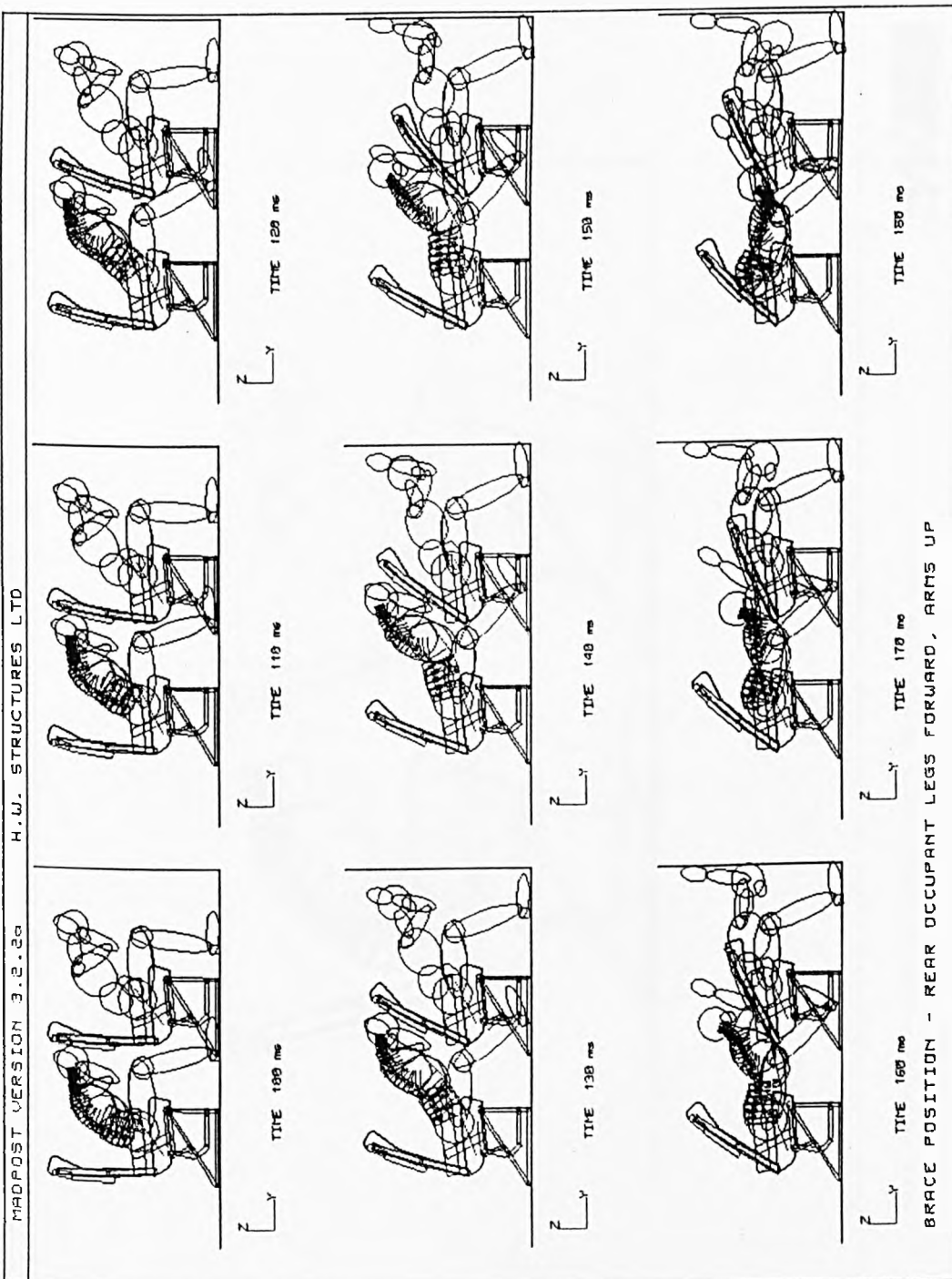


Figure 226. Brace Position - Rear Occupant Legs Forward, Arms Up At 0ms



**Figure 227. Brace Position Simulation - Rear Occupant Legs Forward, Arms Up
At 100ms to 180ms**

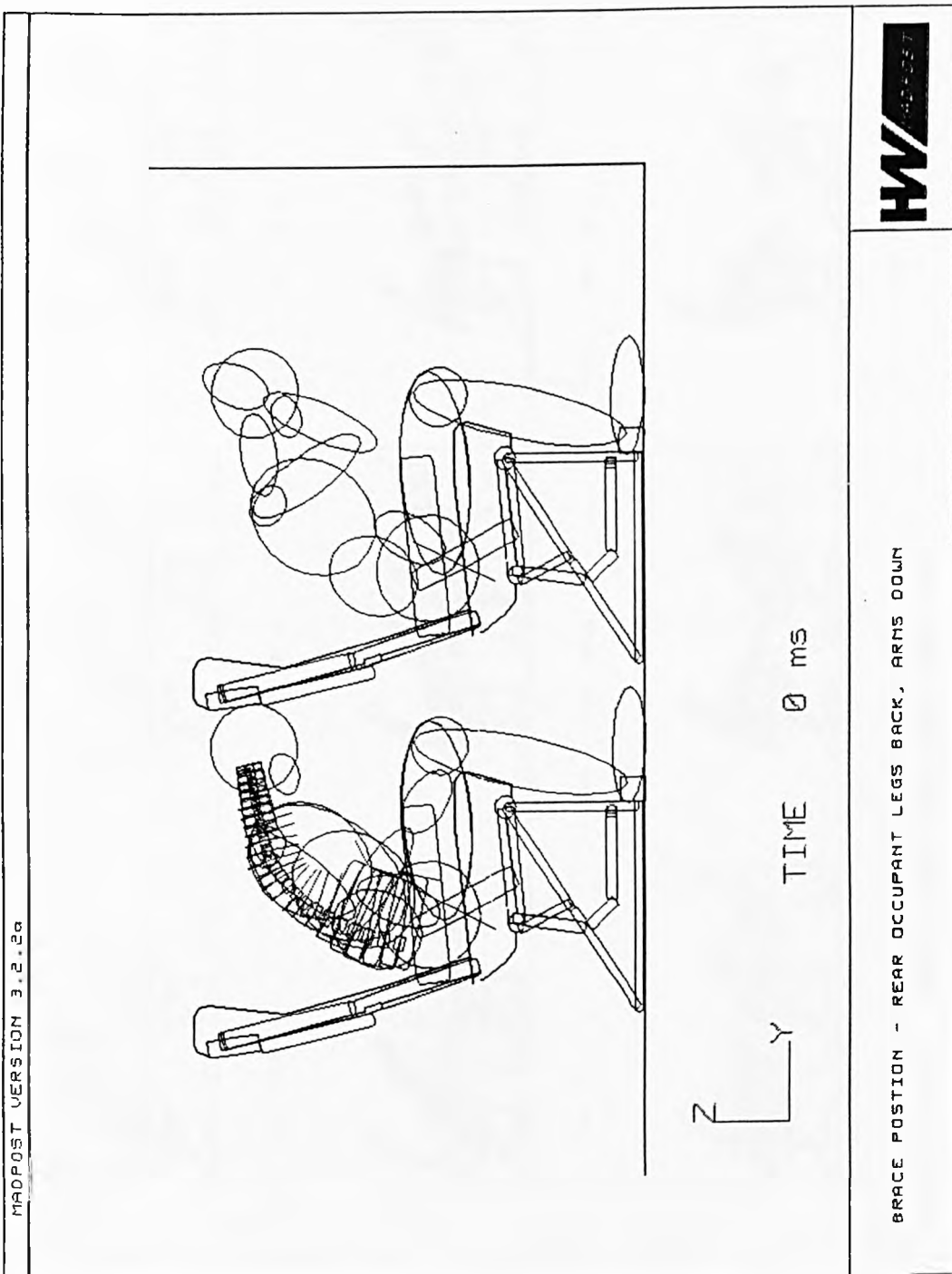
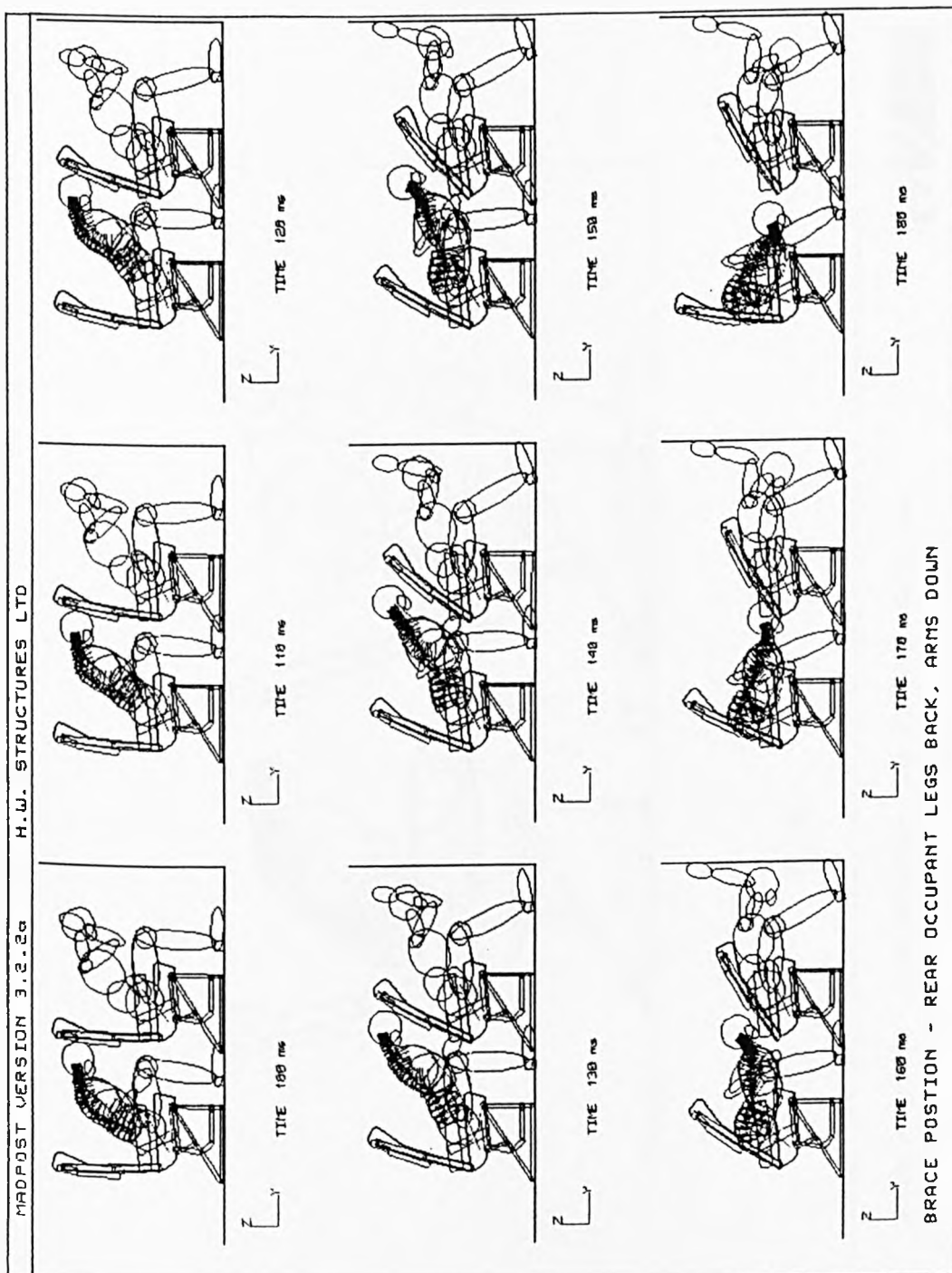


Figure 228. Brace Position - Rear Occupant Legs Back, Arms Down At 0ms



**Figure 229. Brace Position Simulation - Rear Occupant Legs Back, Arms Down
At 100ms To 180ms**

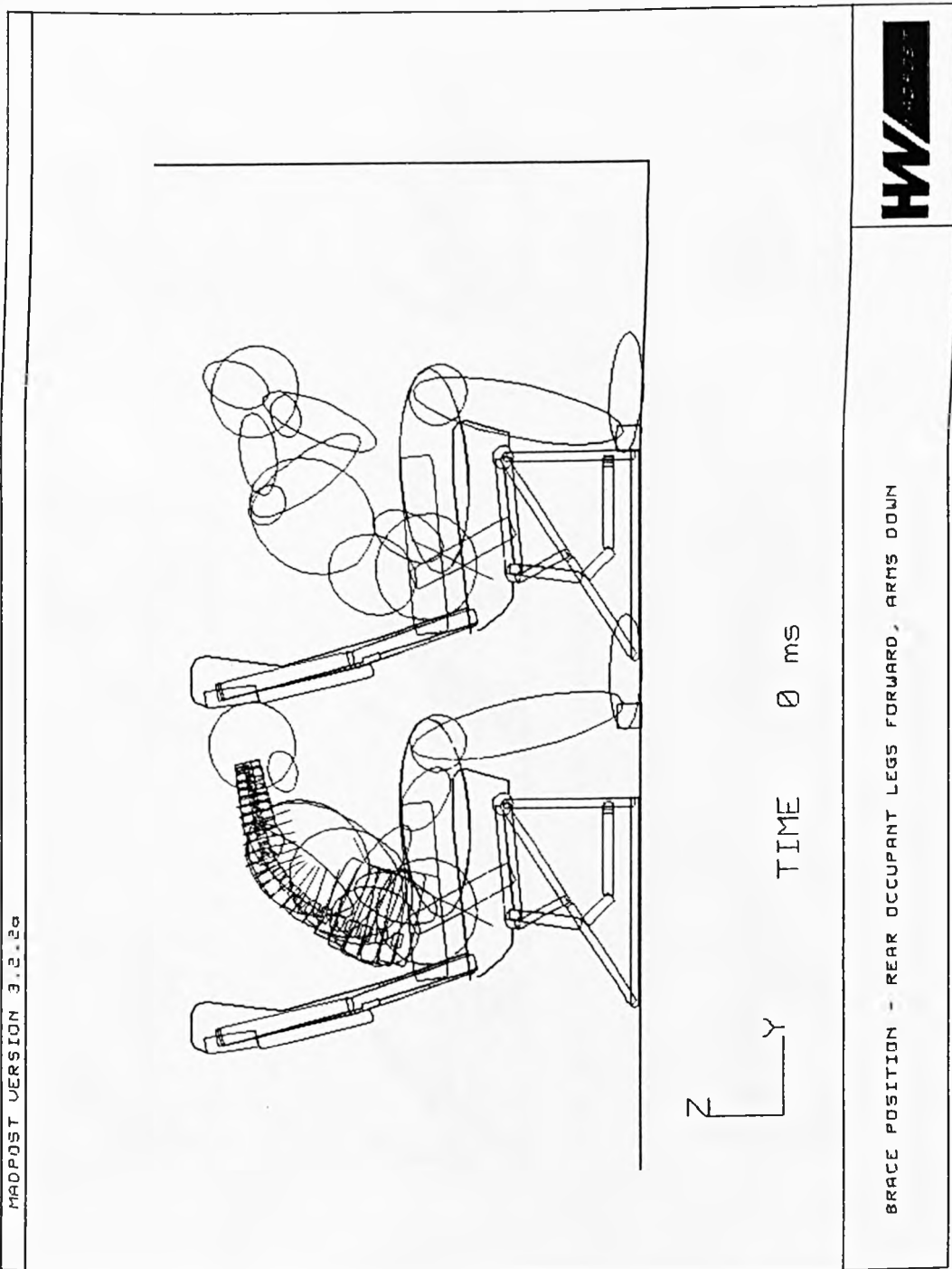


Figure 230. Brace Position - Rear Occupant Legs Forward, Arms Down At 0ms

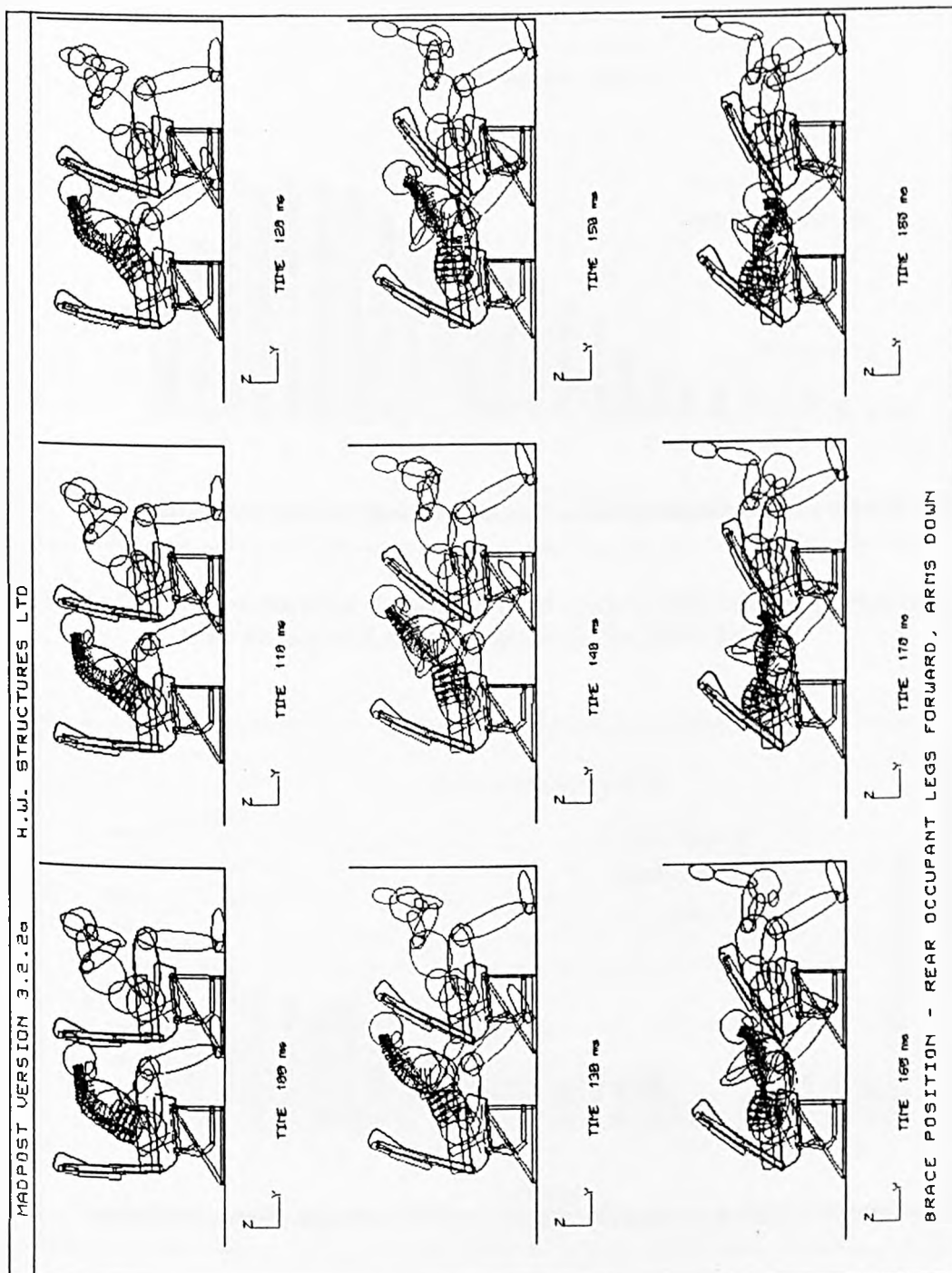


Figure 231. Brace Position Simulation - Rear Occupant Legs Forward, Arms Down At 100ms To 180ms

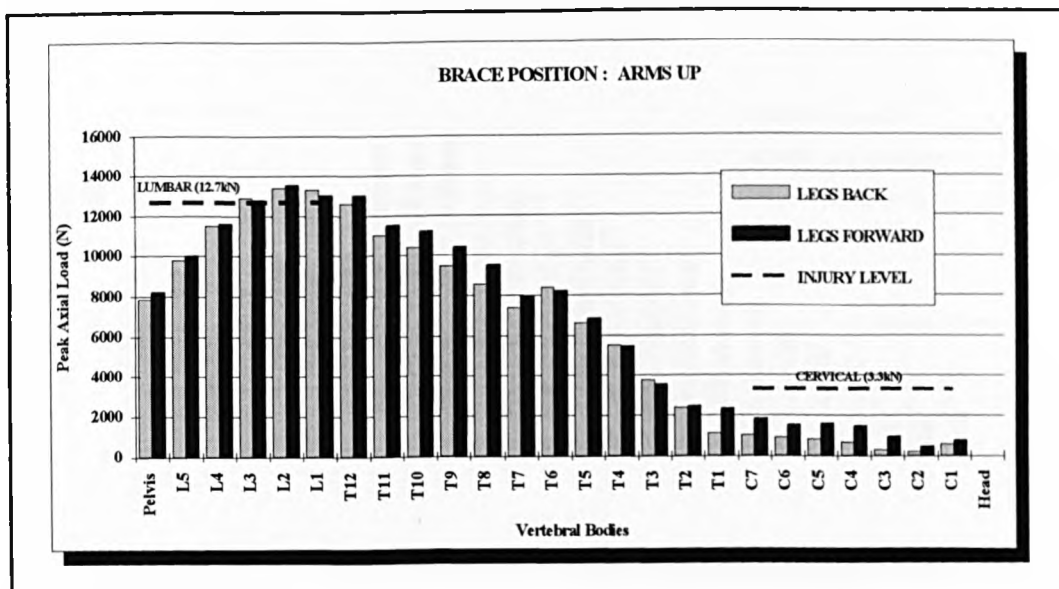


Figure 232. Brace Position - Comparison of Peak Axial Loads in Vertebrae for Legs Back and Legs Forward with the Arms Up

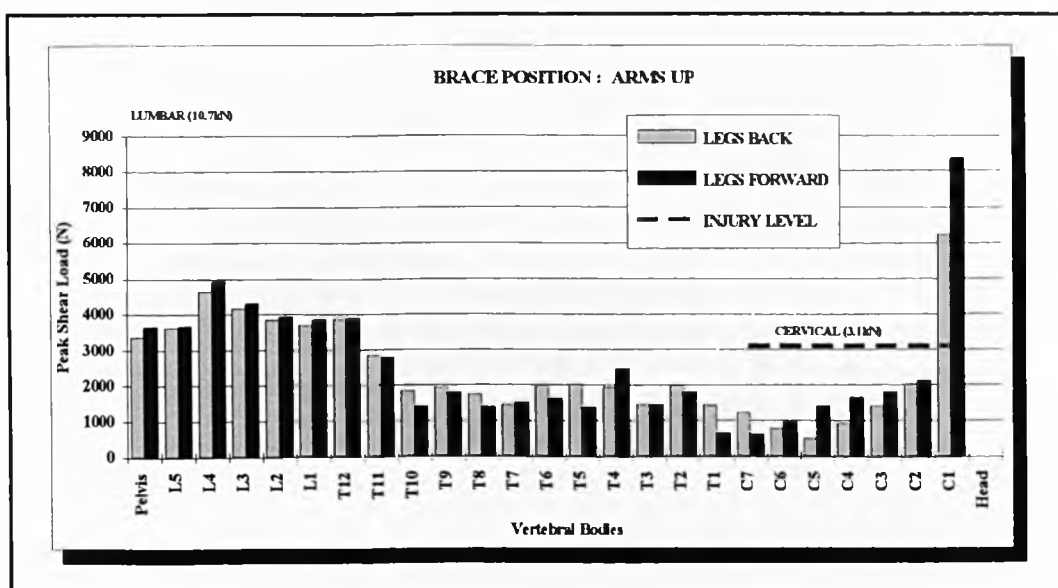


Figure 233. Brace Position - Comparison of Peak Shear Loads in Vertebrae for Legs Back and Legs Forward with the Arms Up

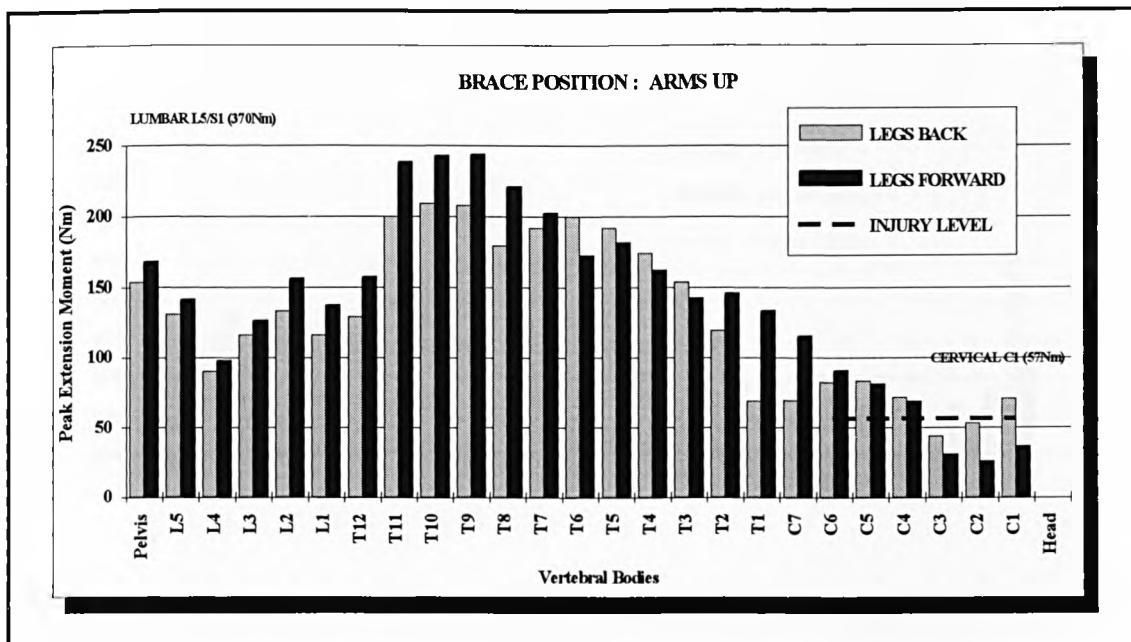


Figure 234. Brace Position - Comparison of Peak Extension Moments in Vertebrae for Legs Back and Legs Forward with the Arms Up

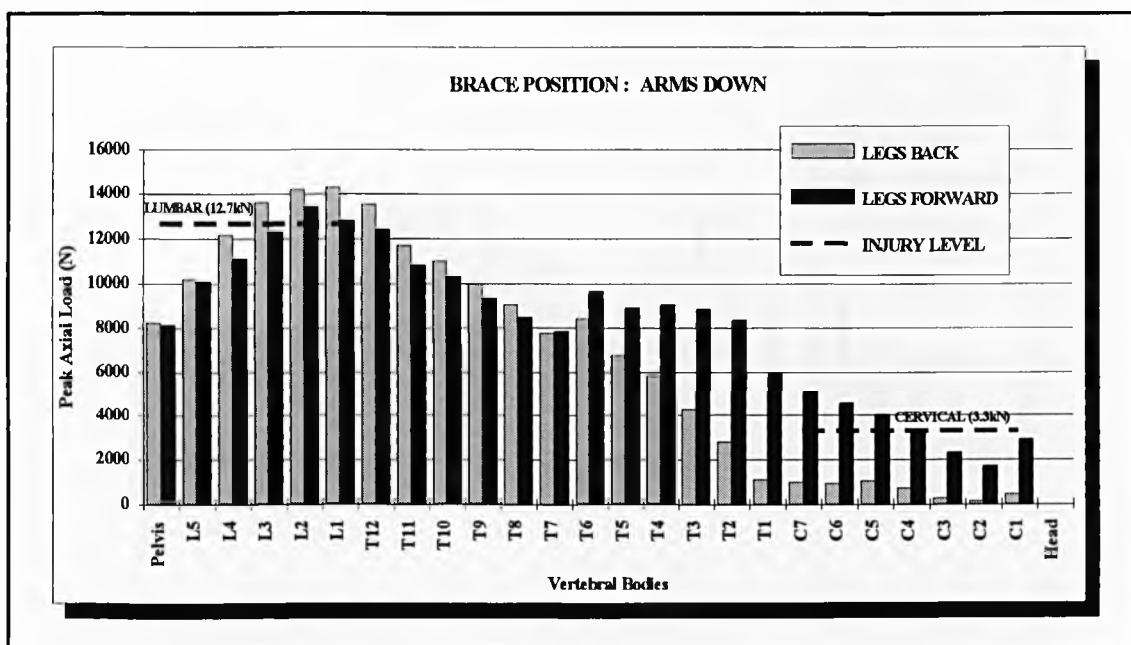


Figure 235. Brace Position - Comparison of Peak Axial Loads in Vertebrae for Legs Back and Legs Forward with the Arms Down

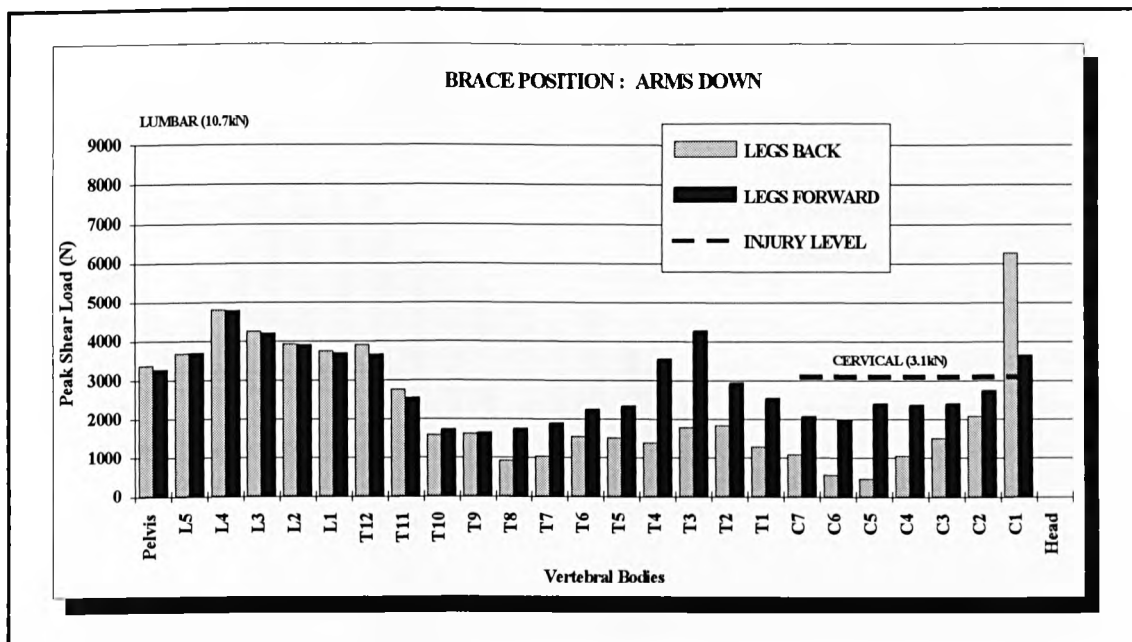


Figure 236. Brace Position - Comparison of Peak Shear Loads in Vertebrae for Legs Back and Legs Forward with the Arms Down

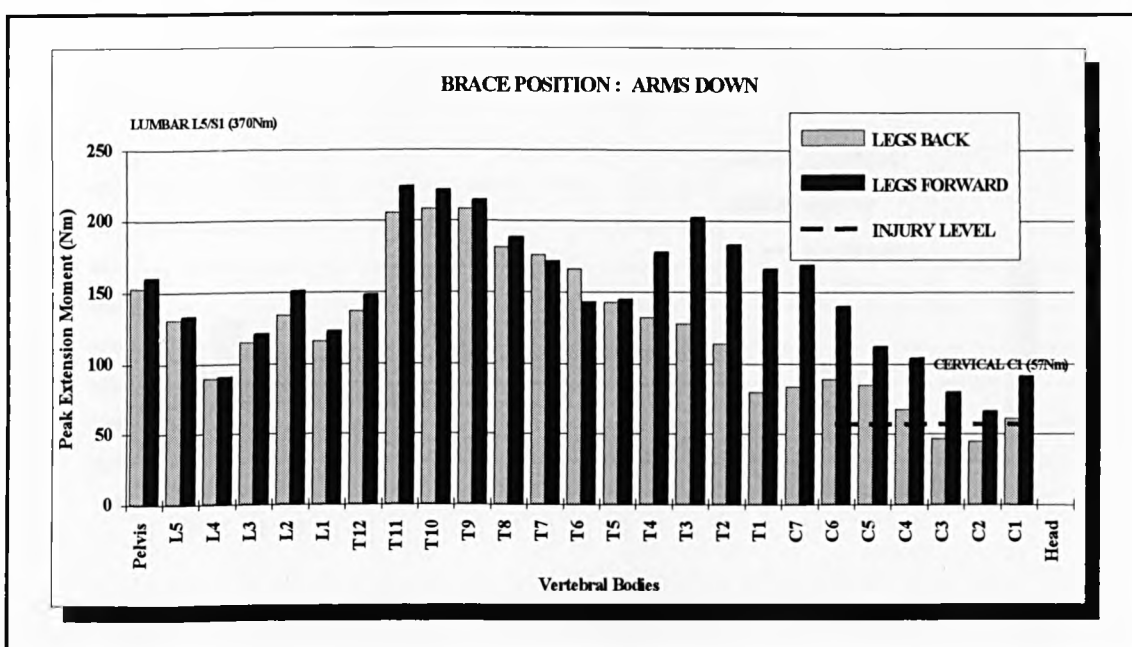


Figure 237. Brace Position - Comparison of Peak Extension Moments in Vertebrae for Legs Back and Legs Forward with the Arms Down

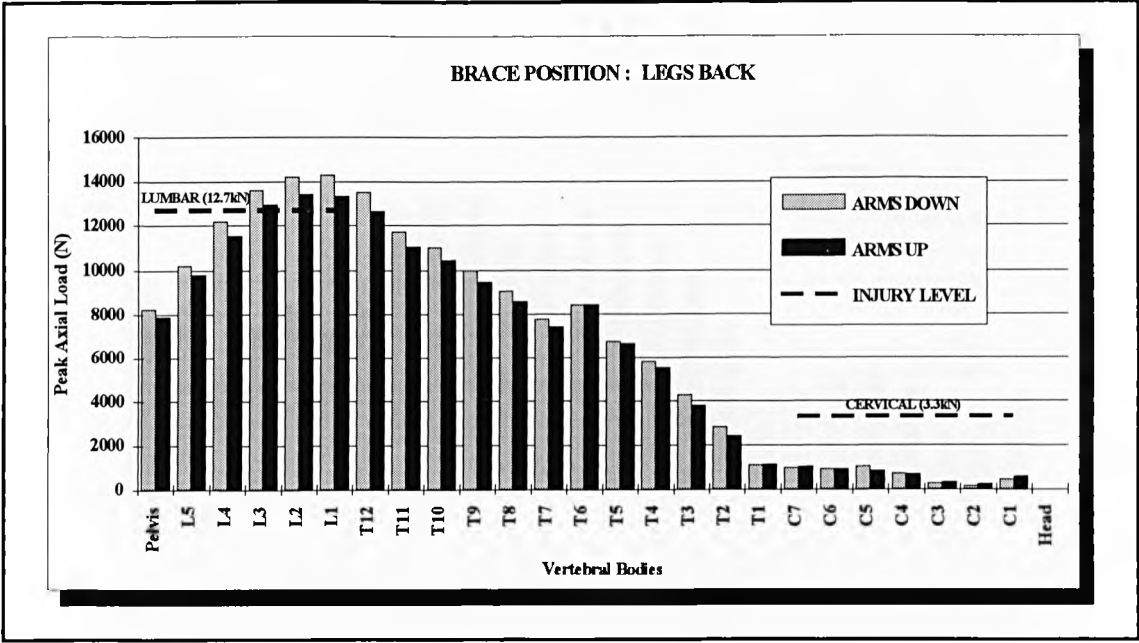


Figure 238. Brace Position - Comparison of Peak Axial Loads in Vertebrae for Arms Down and Arms Up with the Legs Back

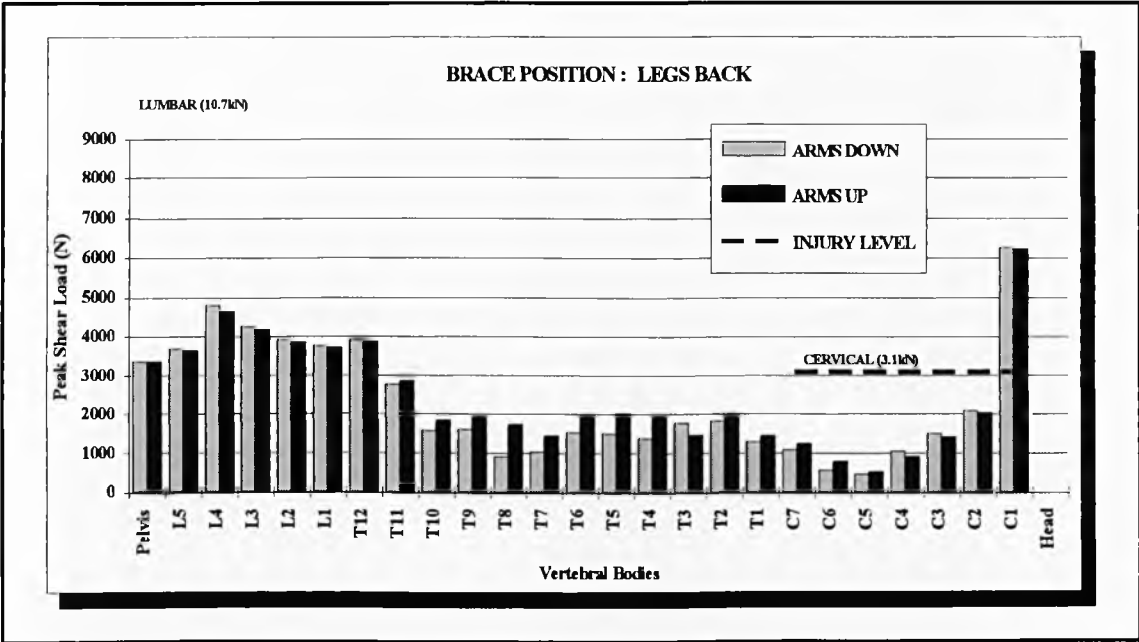


Figure 239. Brace Position - Comparison of Peak Shear Loads in Vertebrae for Arms Down and Arms Up with the Legs Back

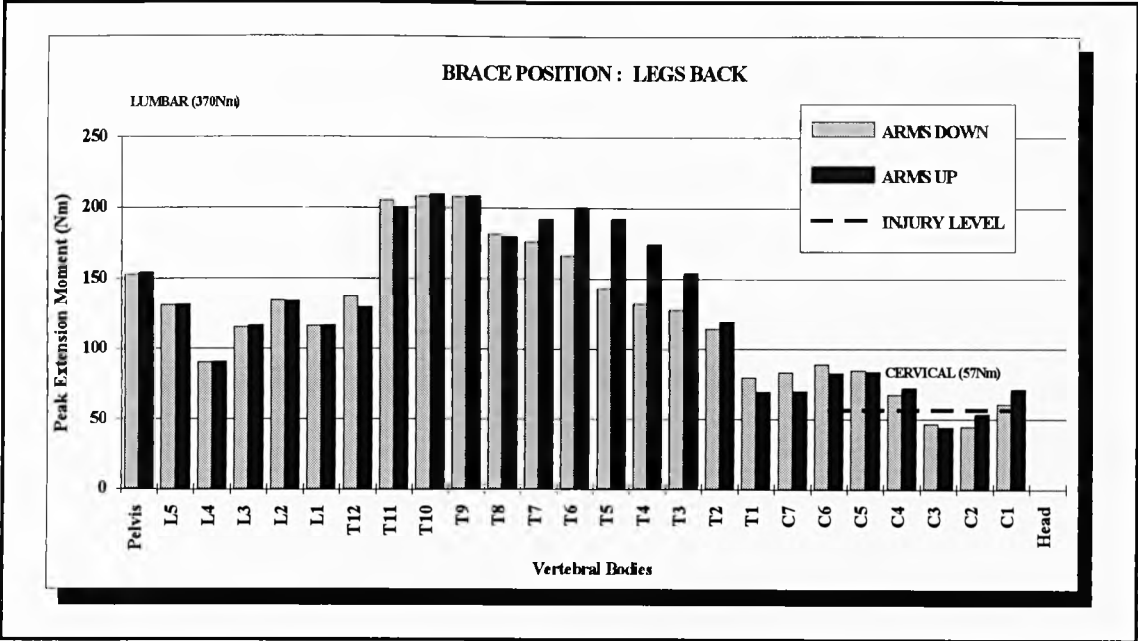


Figure 240. Brace Position - Comparison of Peak Extension Moments in Vertebrae for Arms Down and Arms Up with the Legs Back

APPENDICES

APPENDIX 1

DRAWINGS SUPPLIED BY THE AIR ACCIDENT INVESTIGATION BRANCH

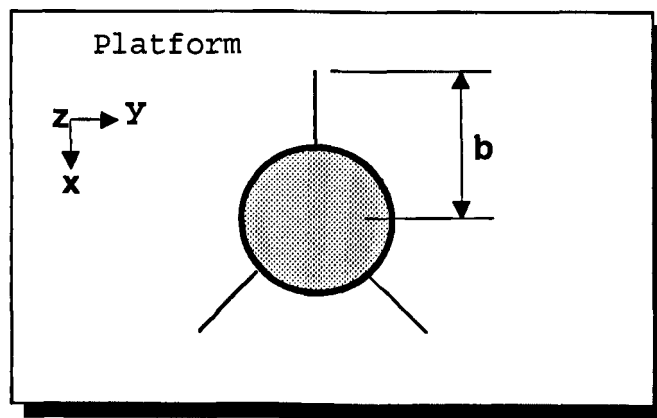
DRAWING NUMBER	DRAWING DATE	DESCRIPTION
66-18-251	3 October 1988	British Midland B737-400 156 Seat Layout
-----	28 June 1988	Boeing 737 Maintenance Training Manual
-----	January 1989	Aircraft Crash on M1 At Kegworth Plan and Cross Section
65 - 73740	28 June 1986	Centreline Diagram Body Structure Model 737 - 400
840432 18	January 1988	Aircraft Seat - Instl Boeing 737 - 400 T/C 4001

APPENDIX 2

SEAT MASS MOMENTS OF INERTIA

The moments of inertia of the seat were obtained by test using the trifilar method.

SYSTEM:



Platform radius $b = 0.887\text{m}$

Wire Length $z = 5.512\text{m}$

Mass of rig = 8.883kg

Formulae:

$$N = (b/2 * 3.142 k) \sqrt{g/z}$$

$$I = mk^2$$

For Platform :-

50 cycles at:- (66.33, 67, 66.67secs) Average = 66.67s.

$$50/66.67 = (0.887/2 \times 3.142 k) \sqrt{9.81/5.512}$$

$$k = 0.251\text{m}$$

$$I = \underline{0.559\text{kgm}^2}$$

Platform and Seatback:-

$$50 \text{ cycles at:- } (64, 64\text{secs})$$

$$50/64 = 0.188/k$$

$$k = 0.241\text{m}$$

$$I = \underline{0.705\text{kgm}^2}$$

$$I_{\text{seatback}} = \underline{0.146\text{kgm}^2}$$

$$K_{\text{seatback}} = \underline{0.212\text{m}}$$

Platform and Seat Base (including Frame):-

$$50 \text{ cycles at:- } (63, 63\text{secs})$$

$$50/63 = 0.188/k$$

$$k = 0.237\text{m}$$

$$I = 10.343 \times 0.237^2$$

$$I = \underline{0.581\text{kgm}^2}$$

$$I_{\text{base}} = \underline{0.022\text{kgm}^2}$$

$$K = \sqrt{0.022/1.47}$$

$$K = \underline{0.122\text{m}}$$

APPENDIX 3

TEST DATA AND PHOTOGRAPHS

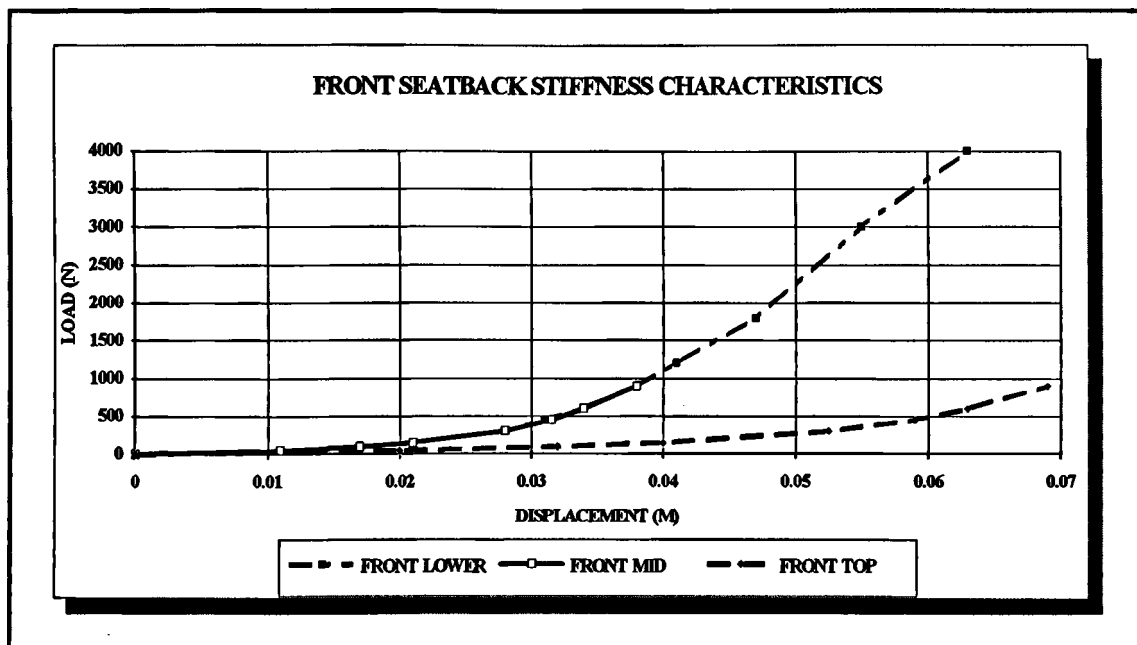


Figure A3.1. Front Seatback Stiffness - Lower, Mid and Top Load versus Displacement

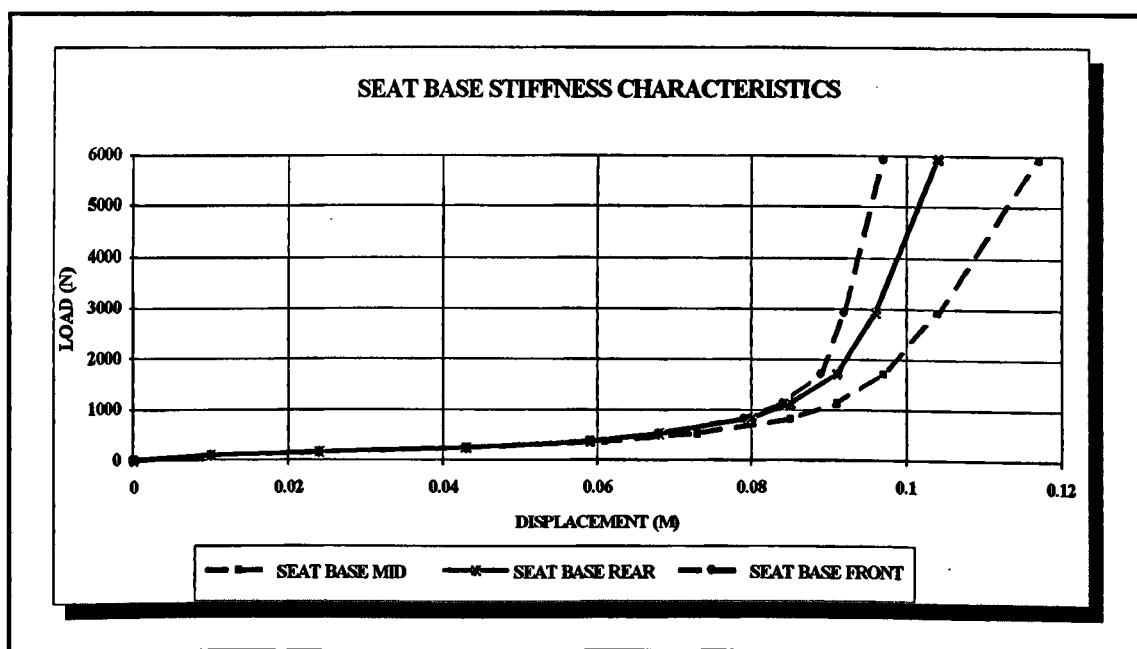


Figure A3.2. Seat Base Stiffness - Rear, Mid and Front Load versus Displacement

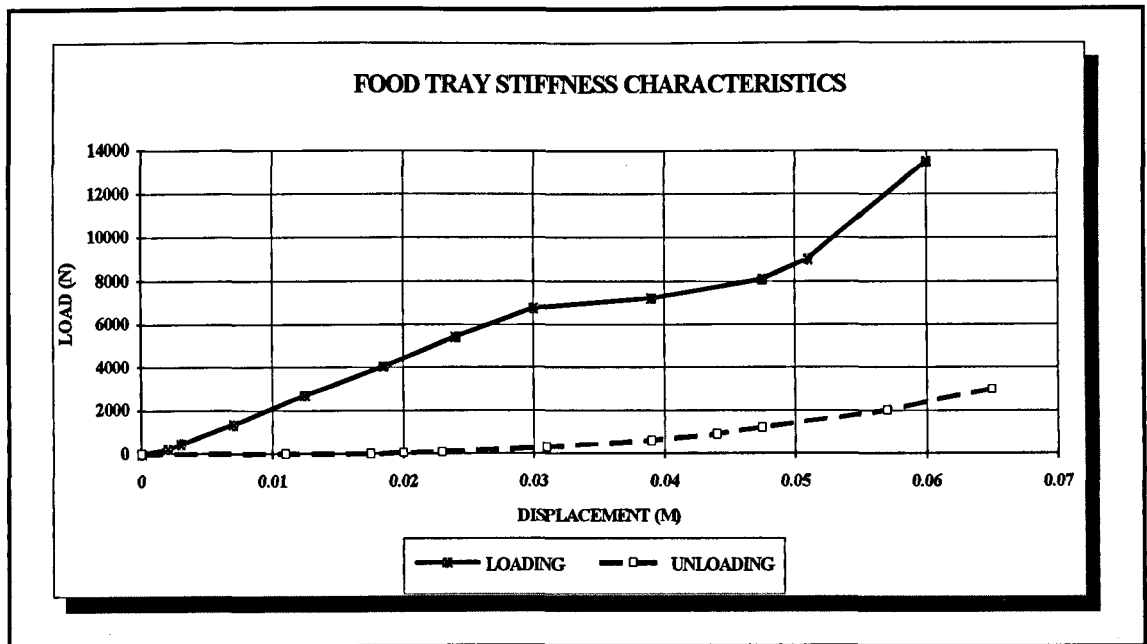


Figure A3.3. Food Tray Stiffness - Load versus Displacement

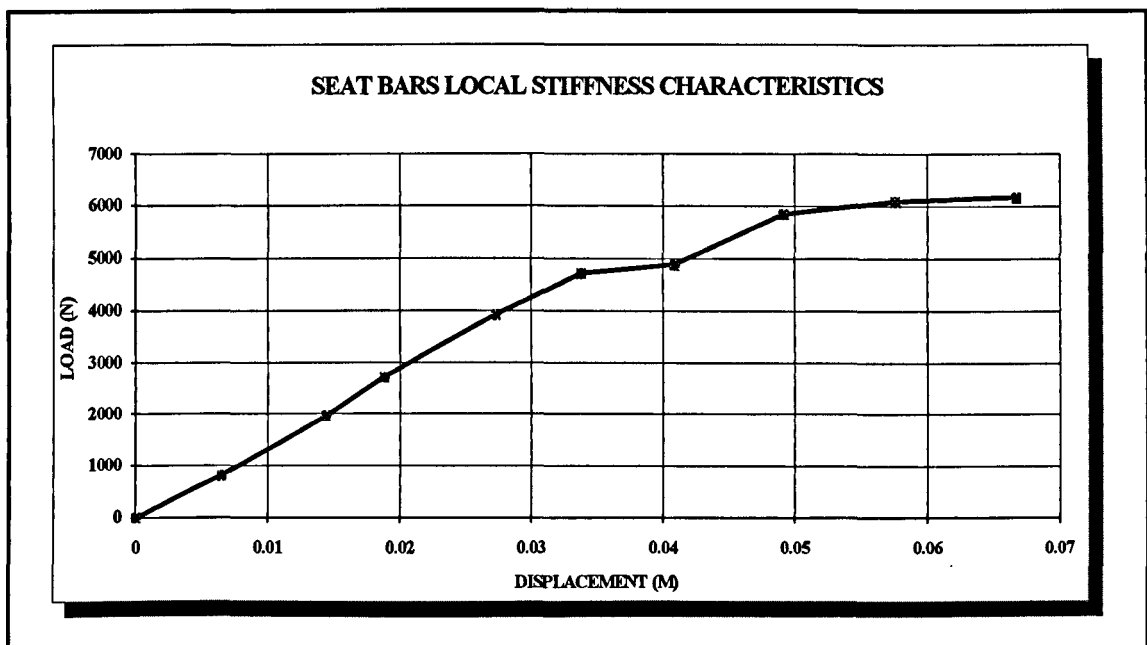


Figure A3.4. Seat Bars Local Stiffness - Load versus Displacement

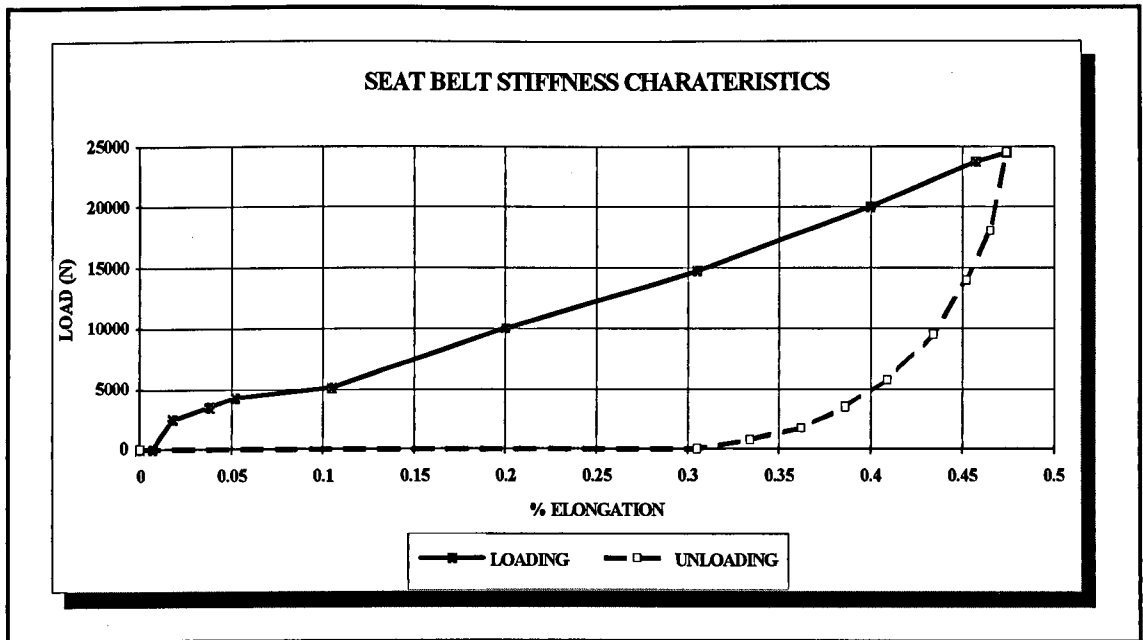


Figure A3.5. Seat Belt Stiffness - Load versus Percentage Strain

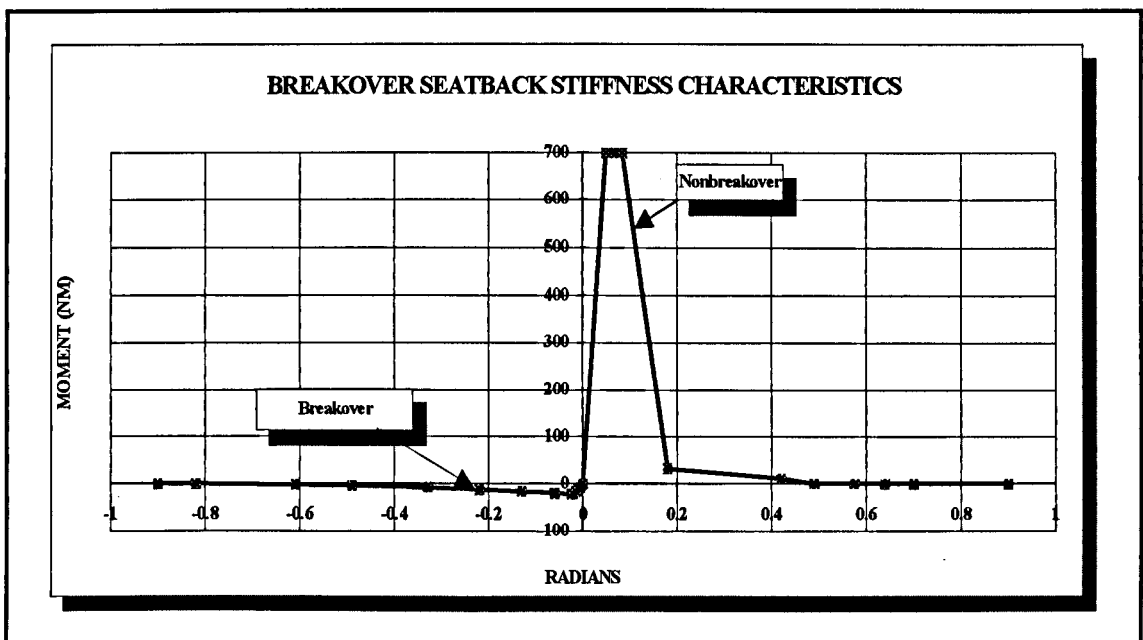


Figure A3.6. Breakover Seatback Stiffness - Bending Moment versus Rotation

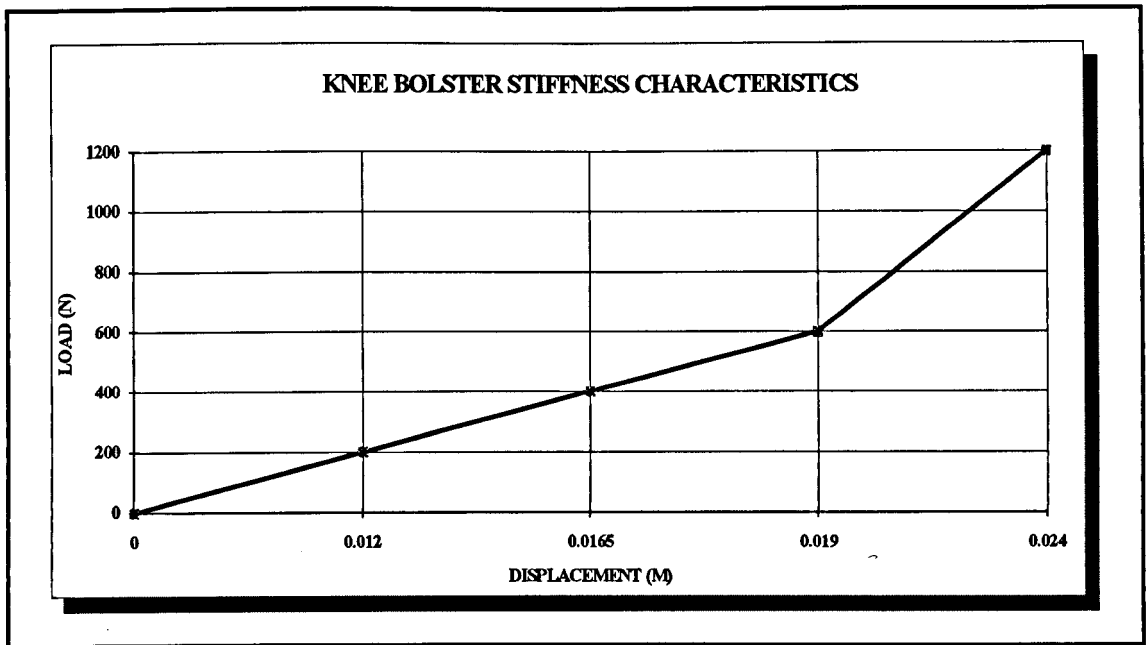


Figure A3.7. Knee Bolster Stiffness - Load versus Displacement

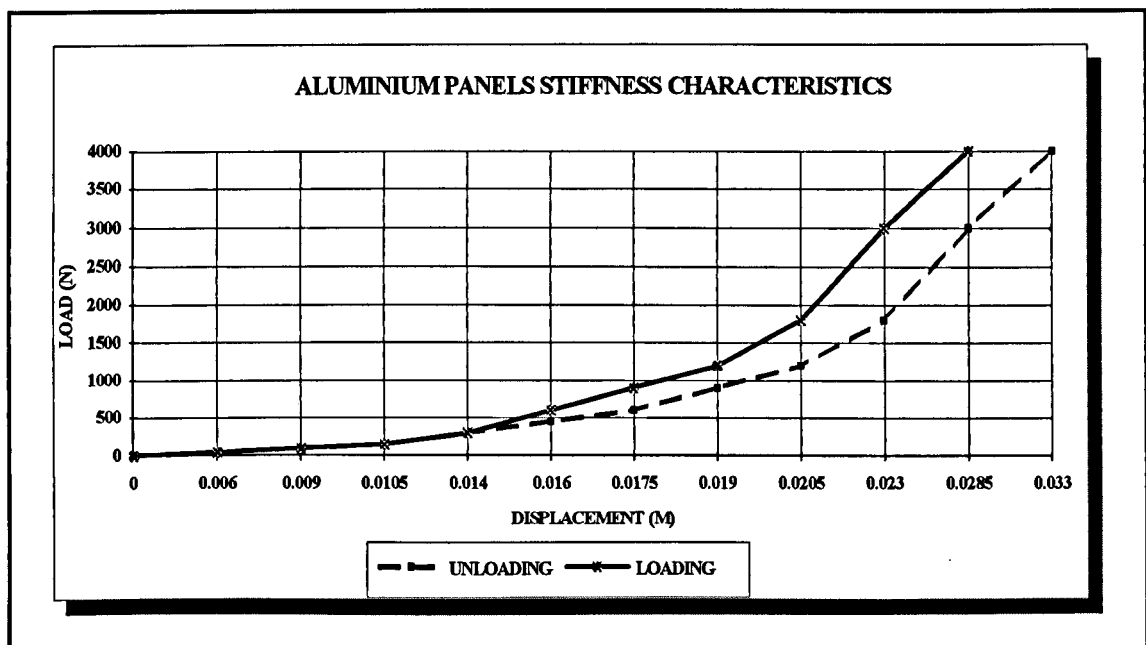


Figure A3.8. Aluminium Panels Stiffness - Load versus Displacement

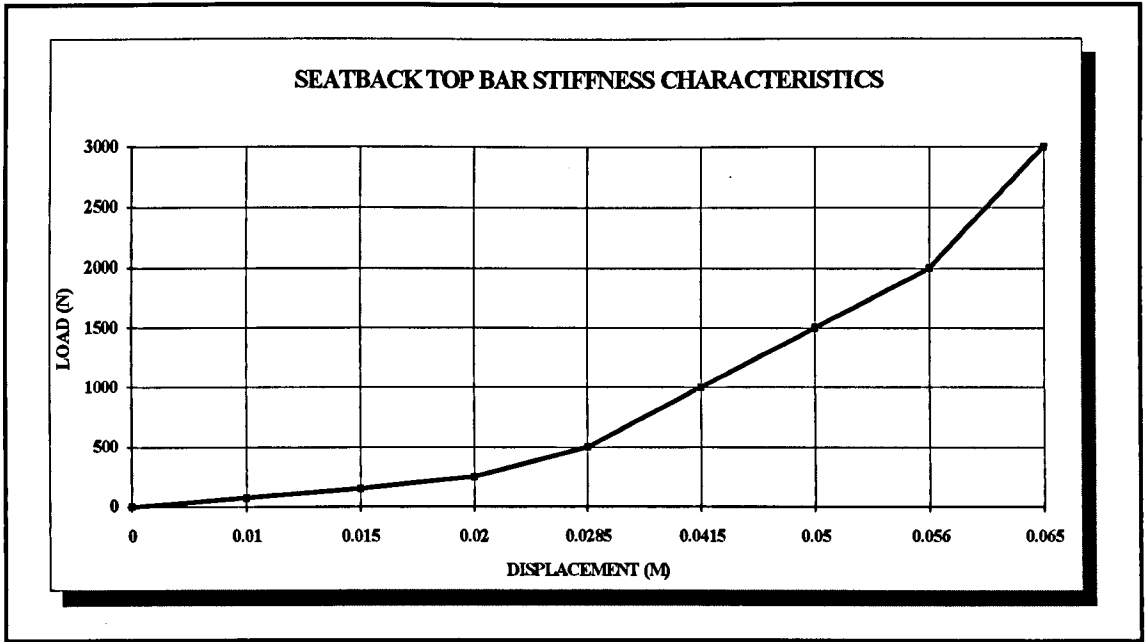


Figure A3.9. Seatback Top Bar Stiffness - Load versus Displacement

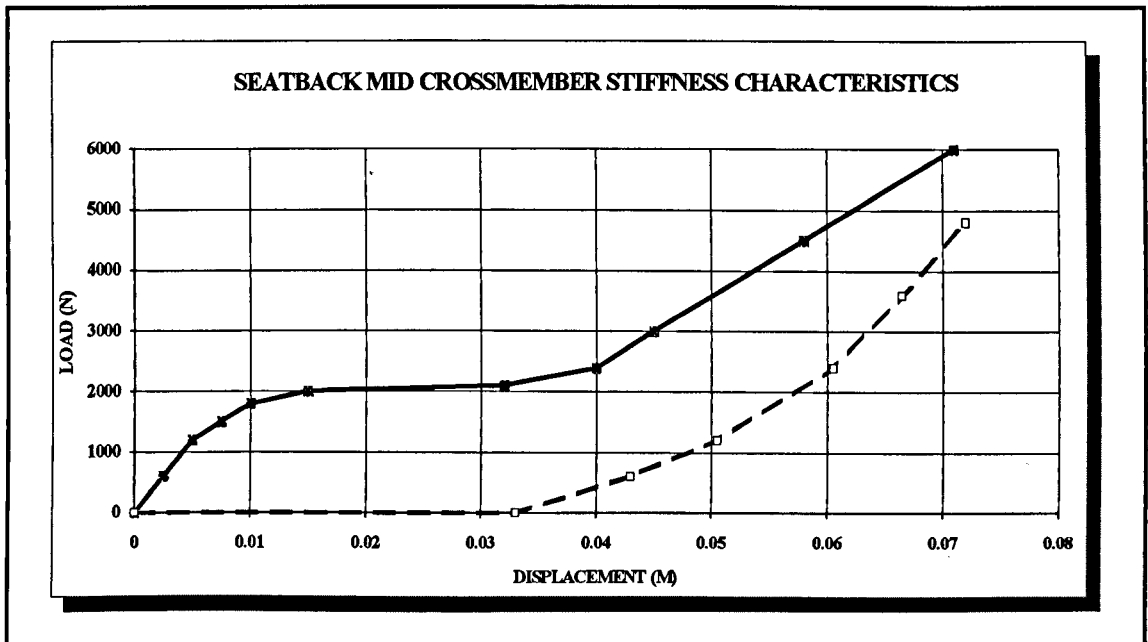


Figure A3.10. Seatback Mid Crossmember Stiffness - Load versus Displacement

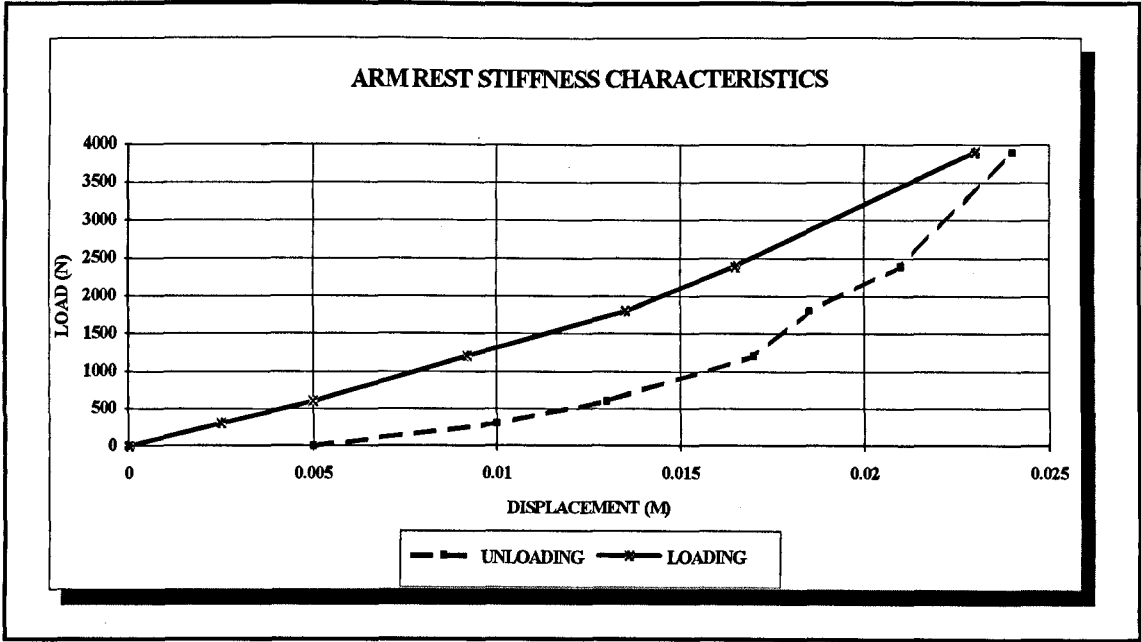


Figure A3.11. Arm Rest Stiffness - Load versus Displacement

SCHEMATIC DIAGRAM OF SUPPORT FOR ALUMINIUM ALLOY SPAR

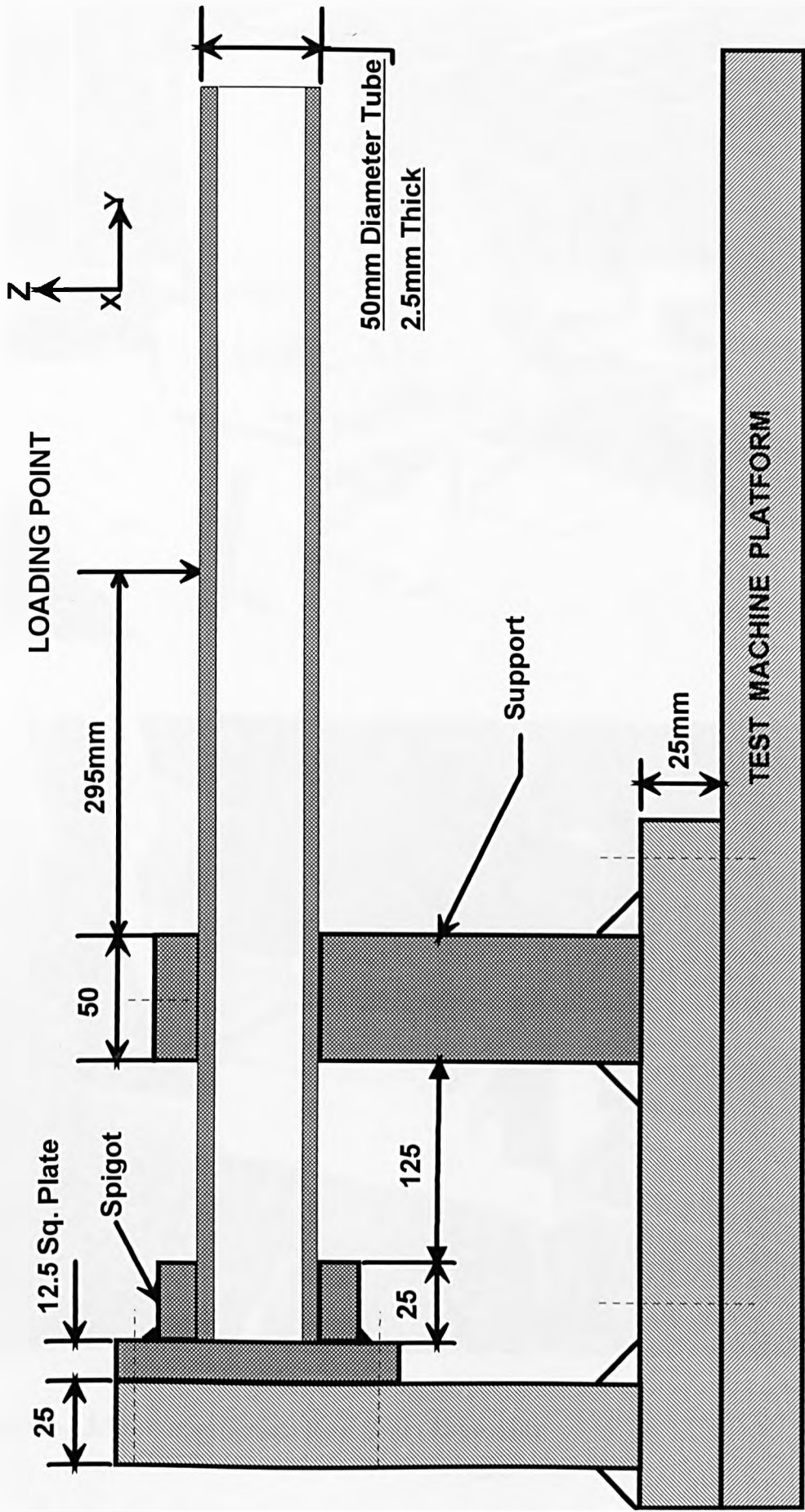


Figure A3.12 Support Jig.

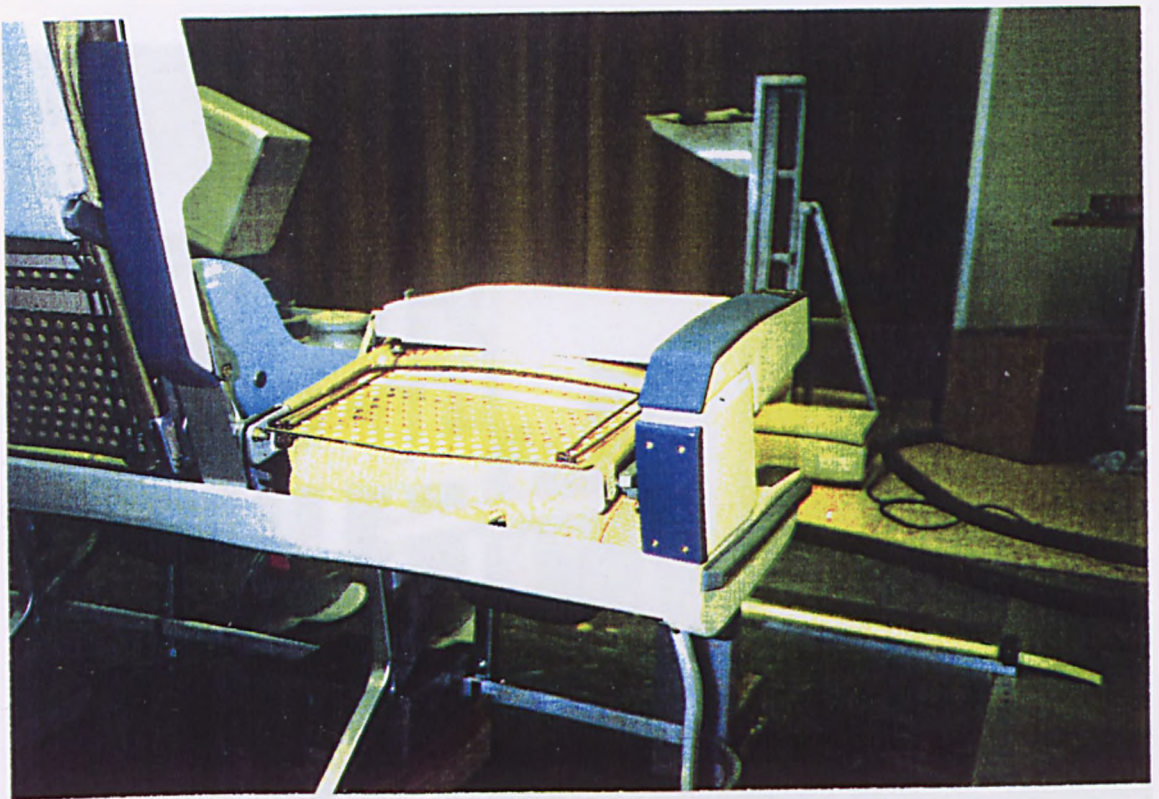
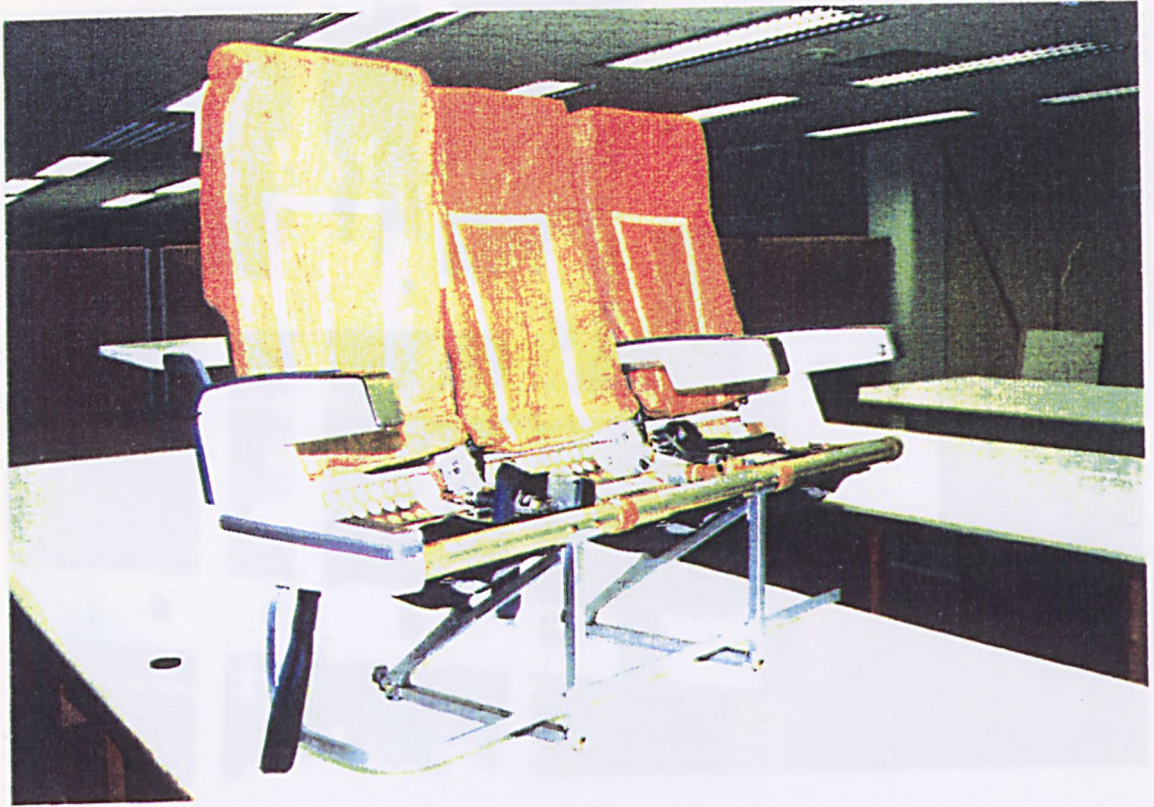


Figure A3.13 Weber Triple Row Seat (Type 424)

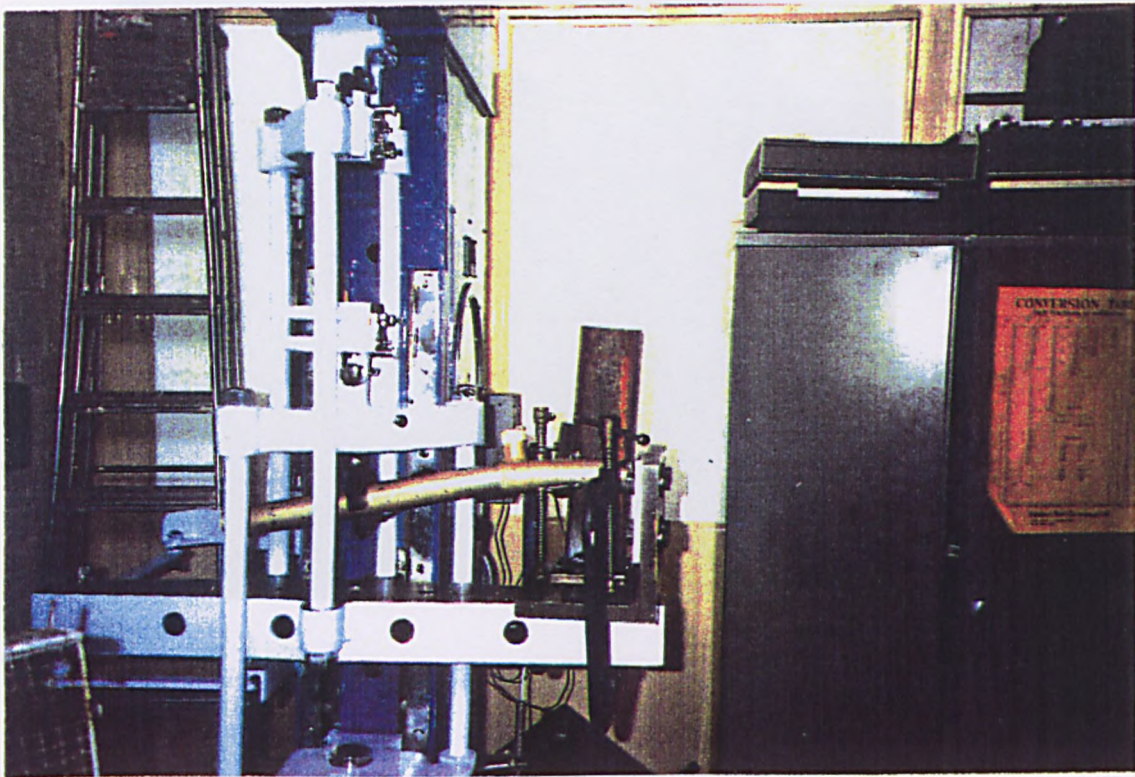
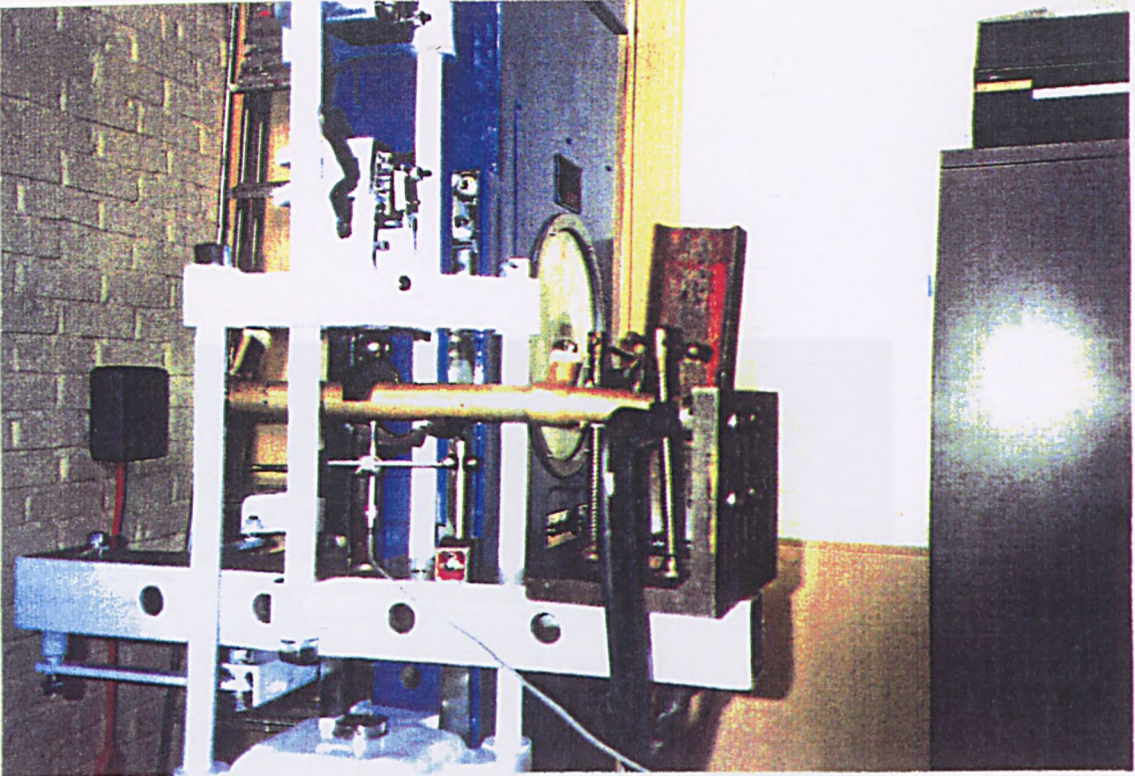


Figure A3.14 Front Seat Bar Load Deflection Test



Figure A3.15 Seat Profile And 'H' Point Measurement

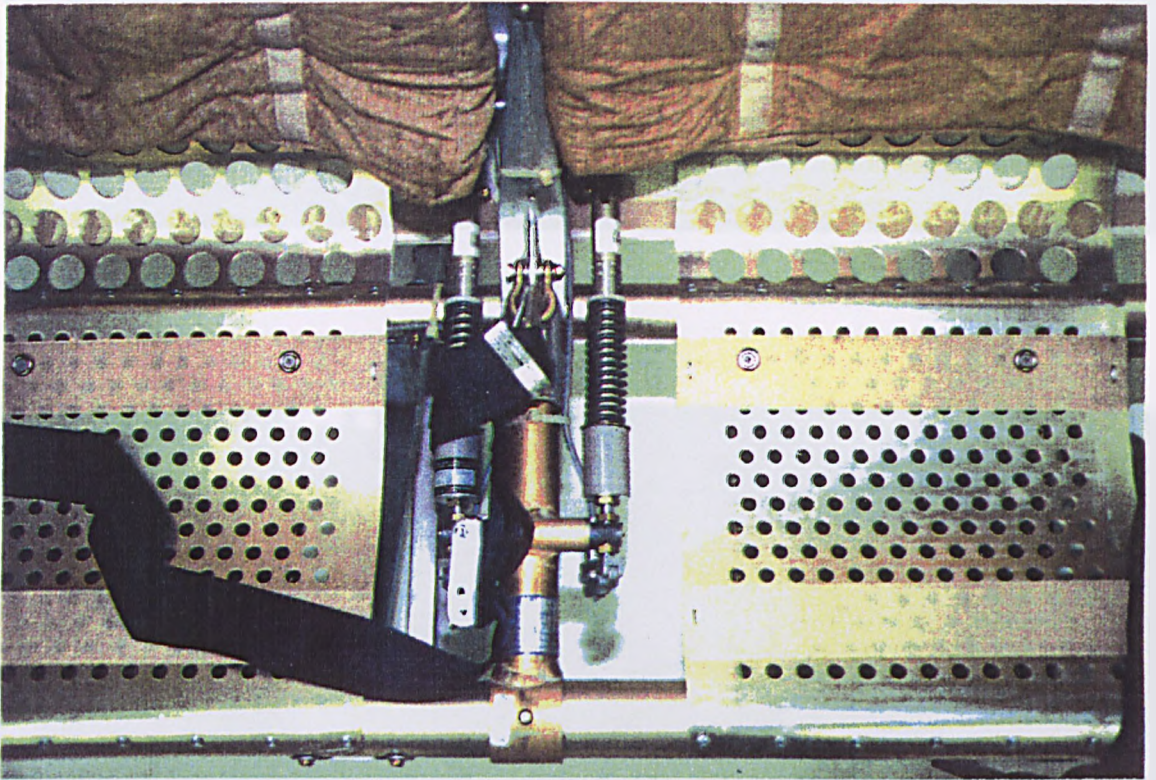


Figure A3.16 Seat Base Construction And Seat Belt Anchorages

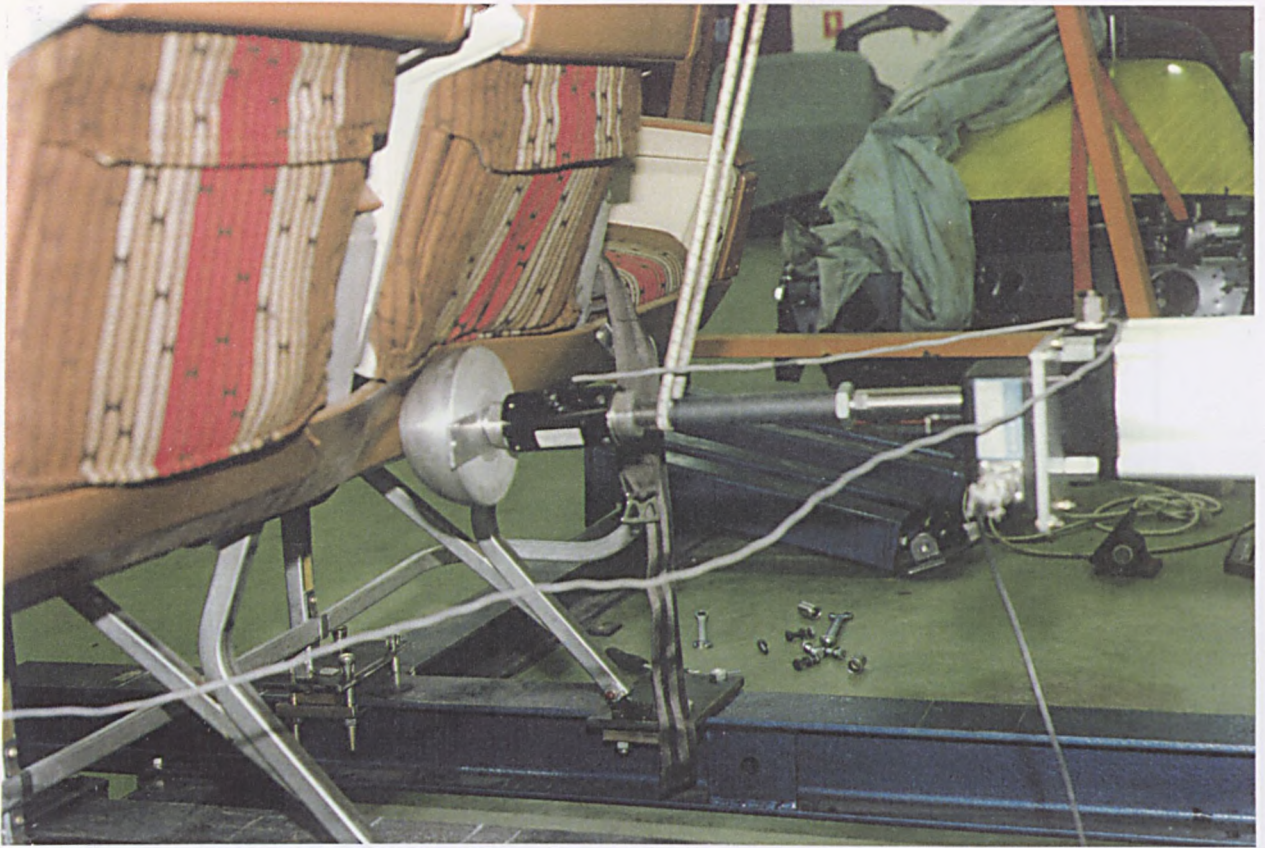


Figure A3.17 Knee Panel Contact Stiffness Test

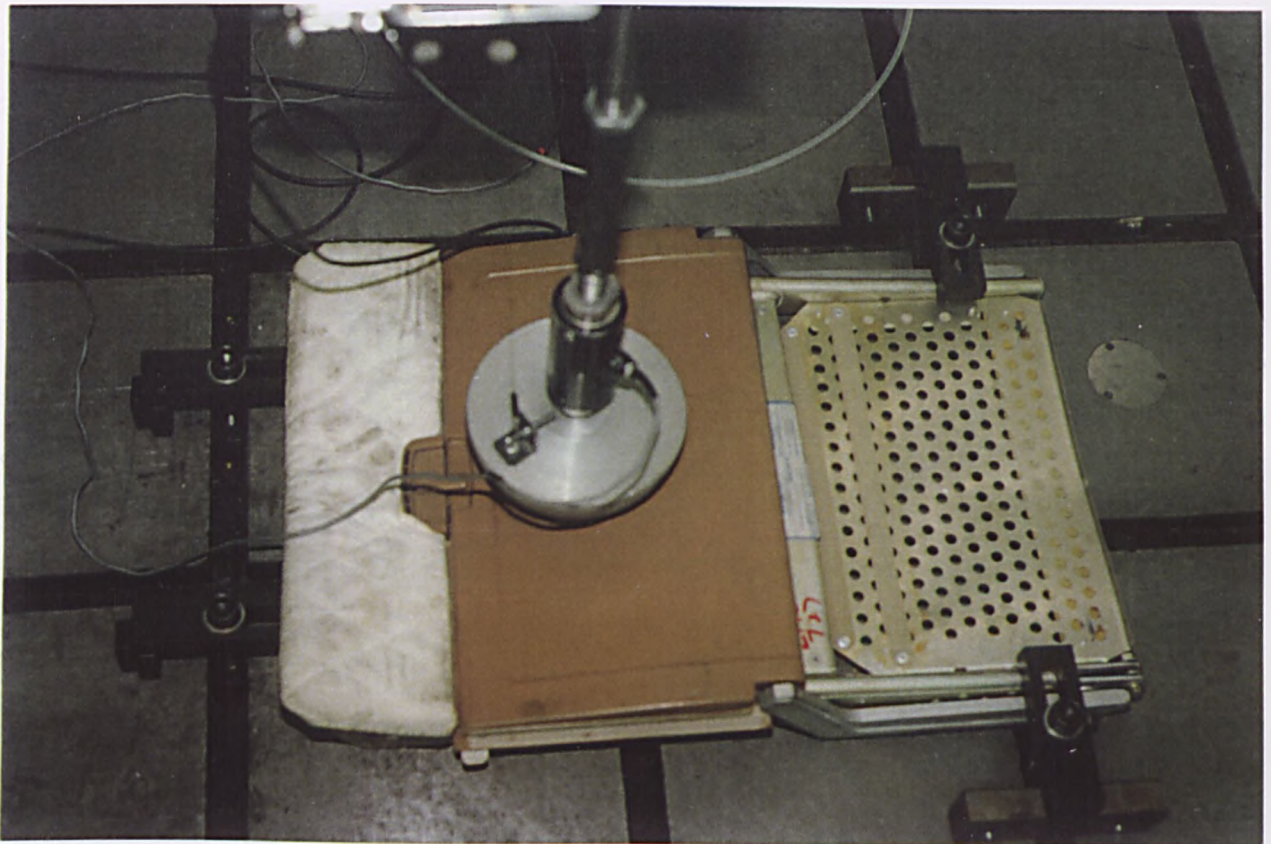


Figure A3.18 Food Tray Stiffness Test

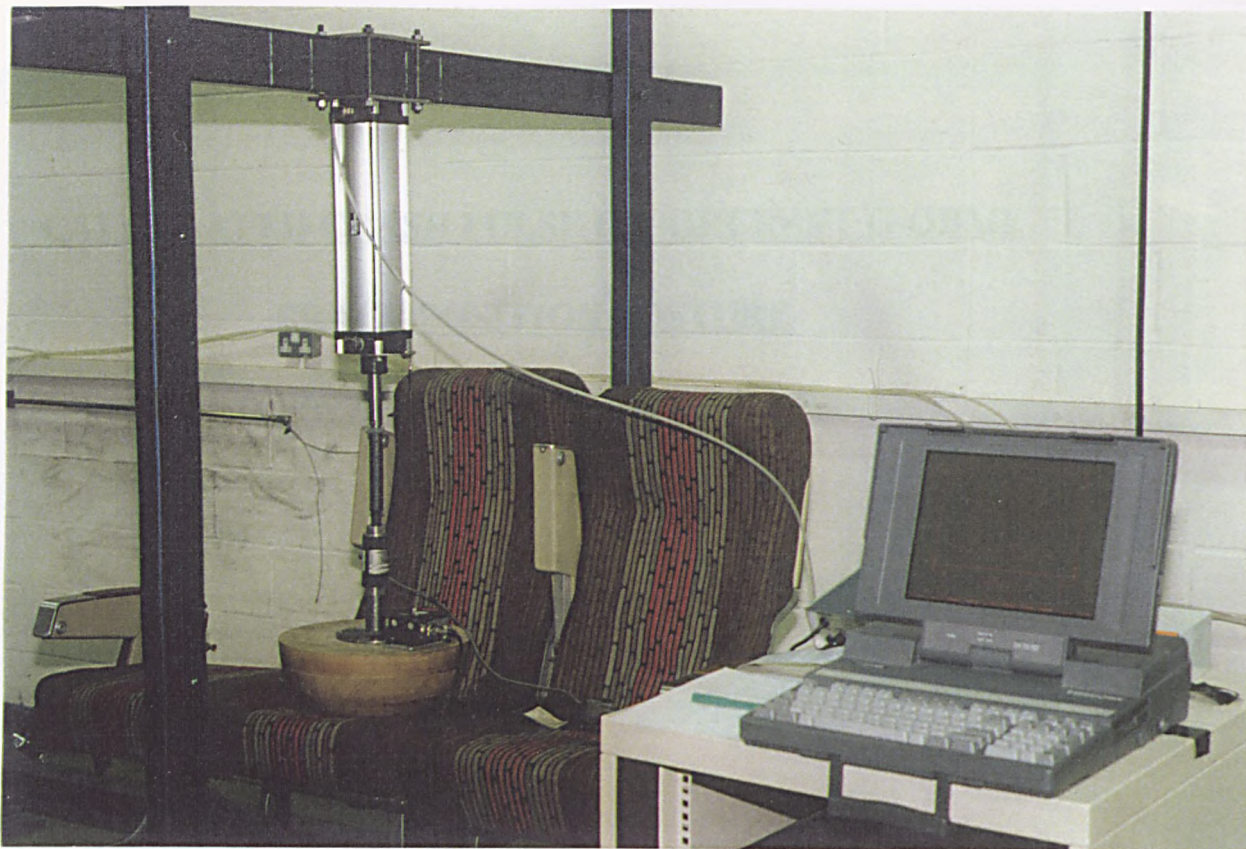


Figure A3.19 Seat Base Stiffness Test



Figure A3.20 Seat Back Stiffness Test

APPENDIX 4

CALCULATED CRASH PULSE OF AIRCRAFT G-OBME

BRACE POSITION POSTURE

LOWER EXTREMITIES LOADS

CRASH PULSE OF AIRCRAFT G-OBME AT CENTRE SECTION

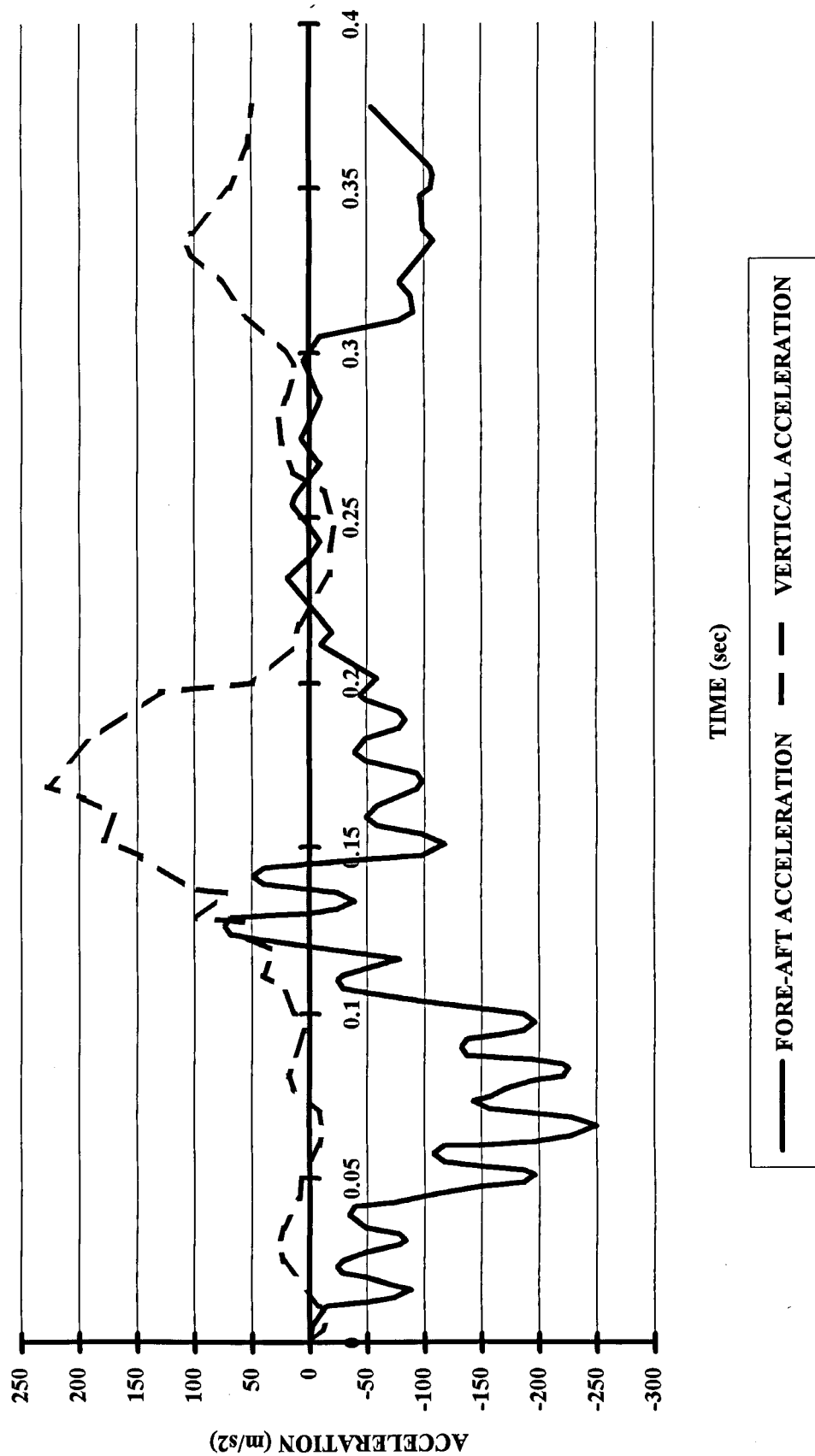


Figure A4.1. Calculated Crash Pulse of Aircraft G-OBME



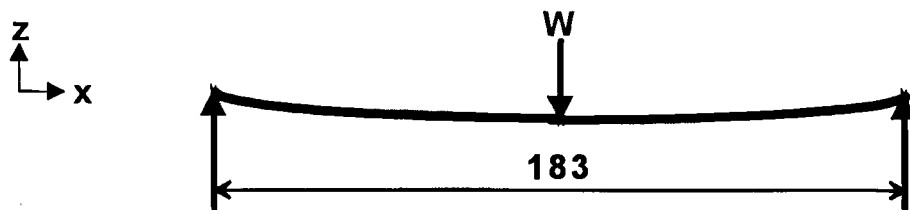
Figure A4.2. Brace Positions In Aircraft G-OBMF

FEMUR AND TIBIA BENDING LOAD CALCULATIONS

The calculations of the maximum sustainable forces by the femurs and tibias are made with reference to the work which was carried out by GW Nyquist of Wayne State University entitled Injury Tolerance Characteristics of the Adult Human Lower Extremities under Static and Dynamic Loading. SAE 861925.

Femur Static Normal Loading - No Age Group Specified.

Span used = 183mm.



Bending Moment $M = WL/4$

- (i) For a male, the average maximum bending moment $M_m = 233 \text{ Nm}$.
(Sample of 4).

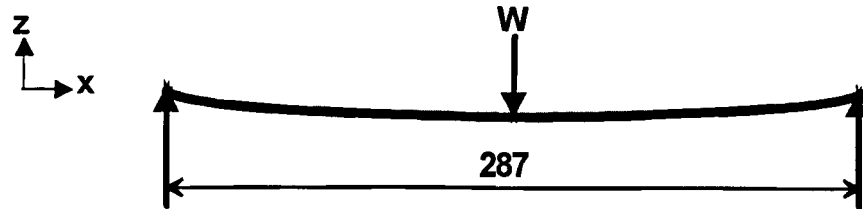
$$W_m = \frac{233 \times 4}{0.183} = \underline{5092\text{N}}$$

- (ii) For a female, the average maximum bending moment $M_f = 182 \text{ Nm}$.
(Sample of 5).

$$W_f = \frac{182 \times 4}{0.183} = \underline{3978\text{N}}$$

Tibia Static Normal Loading - No Age Group Specified.

Span used = 287mm.



Bending Moment $M = WL/4$

(i) For Age Group (20 - 39 years), the bending moment $M_i = 208 \text{ Nm}$.

$$W_m = \frac{208 \times 4}{0.287} = \underline{2898 \text{ N}}$$

(ii) For Age Group (40 - 39 years), the bending moment $M_{ii} = 180 \text{ Nm}$.

$$W_f = \frac{180 \times 4}{0.287} = \underline{2508 \text{ N}}$$

(iii) For Age Group (70 - 89 years), the bending moment $M_{iii} = 164 \text{ Nm}$.

$$W_{iii} = \frac{164 \times 4}{0.287} = \underline{2286 \text{ N}}$$

APPENDIX 5

ACCELERATION PULSE COMPARISONS

COMPARISON OF THE KEGWORTH, NACA AND 14G TEST PULSES

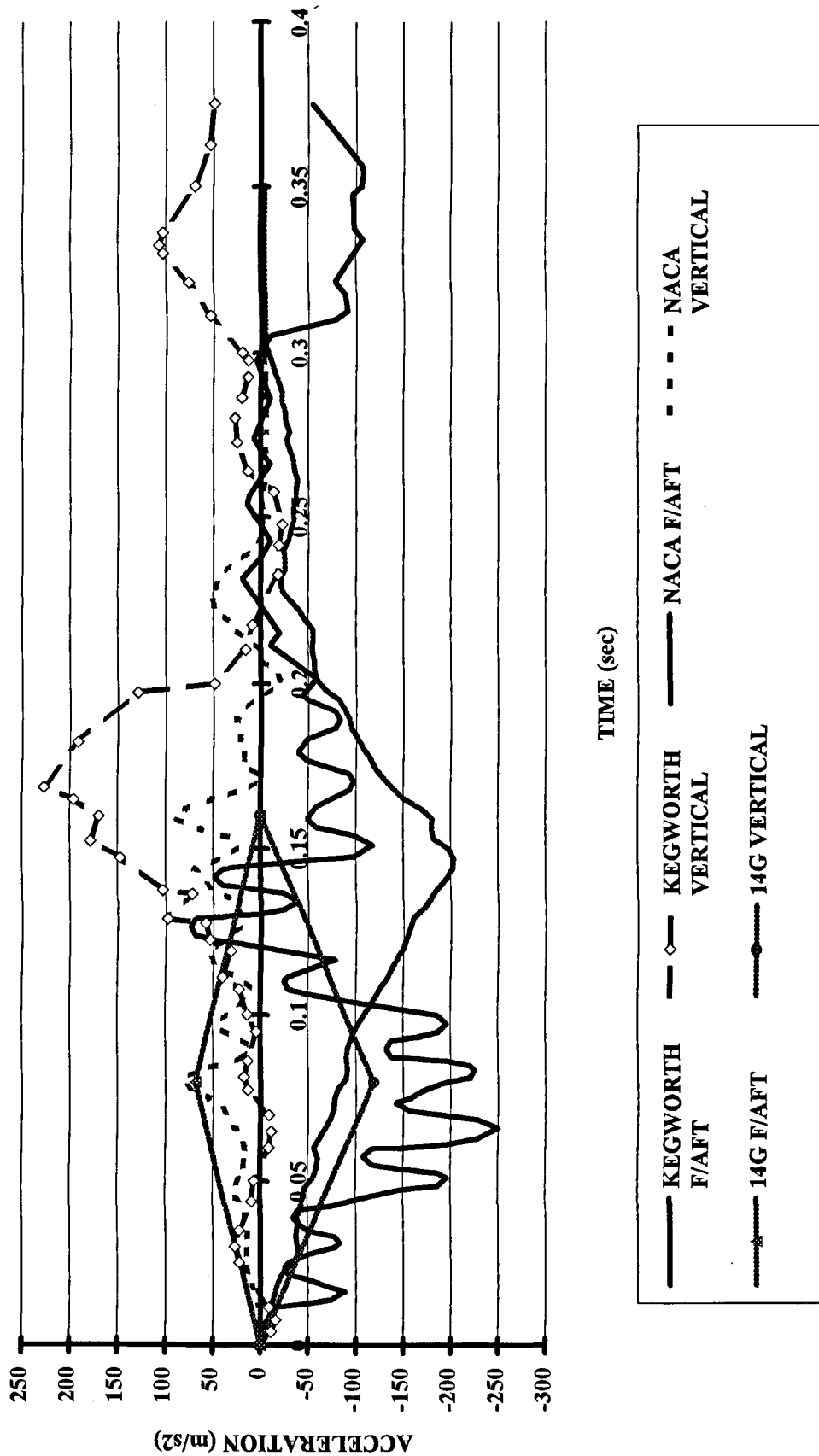
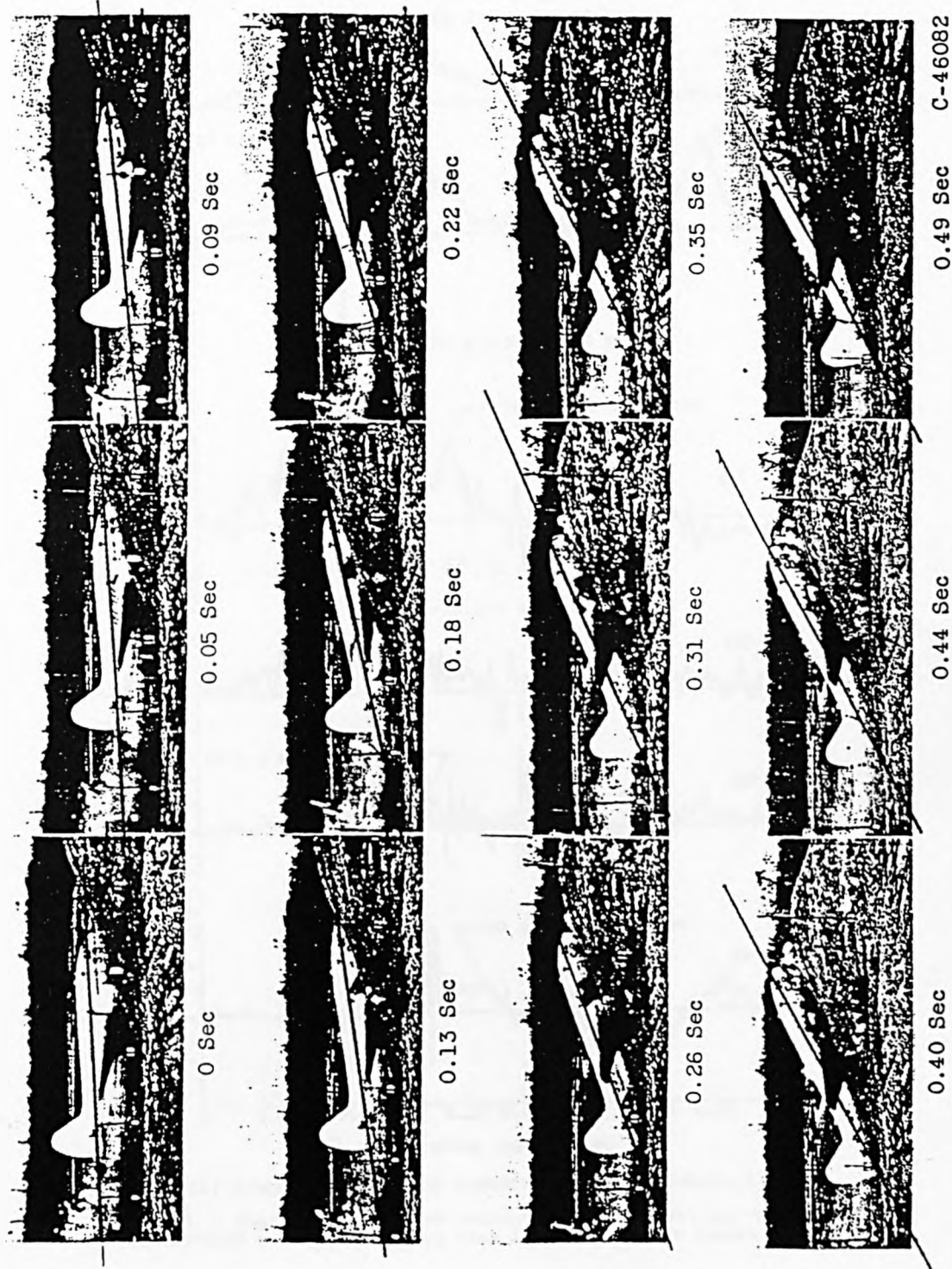
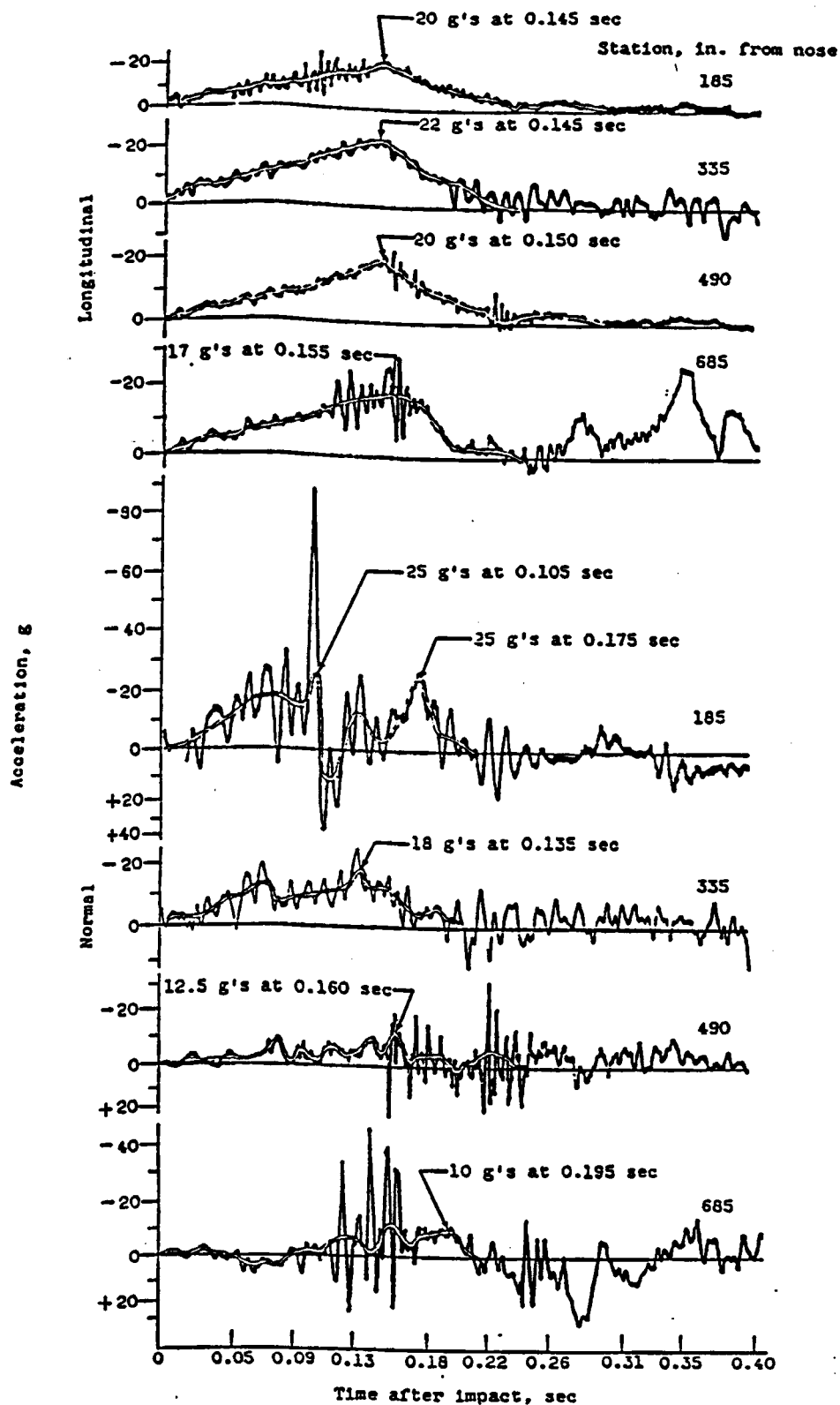


Figure A5.1 Comparison of the Kegworth, NACA and 14G Test Pulses



(c) Angle of impact, 29°; impact speed, 97 mph.

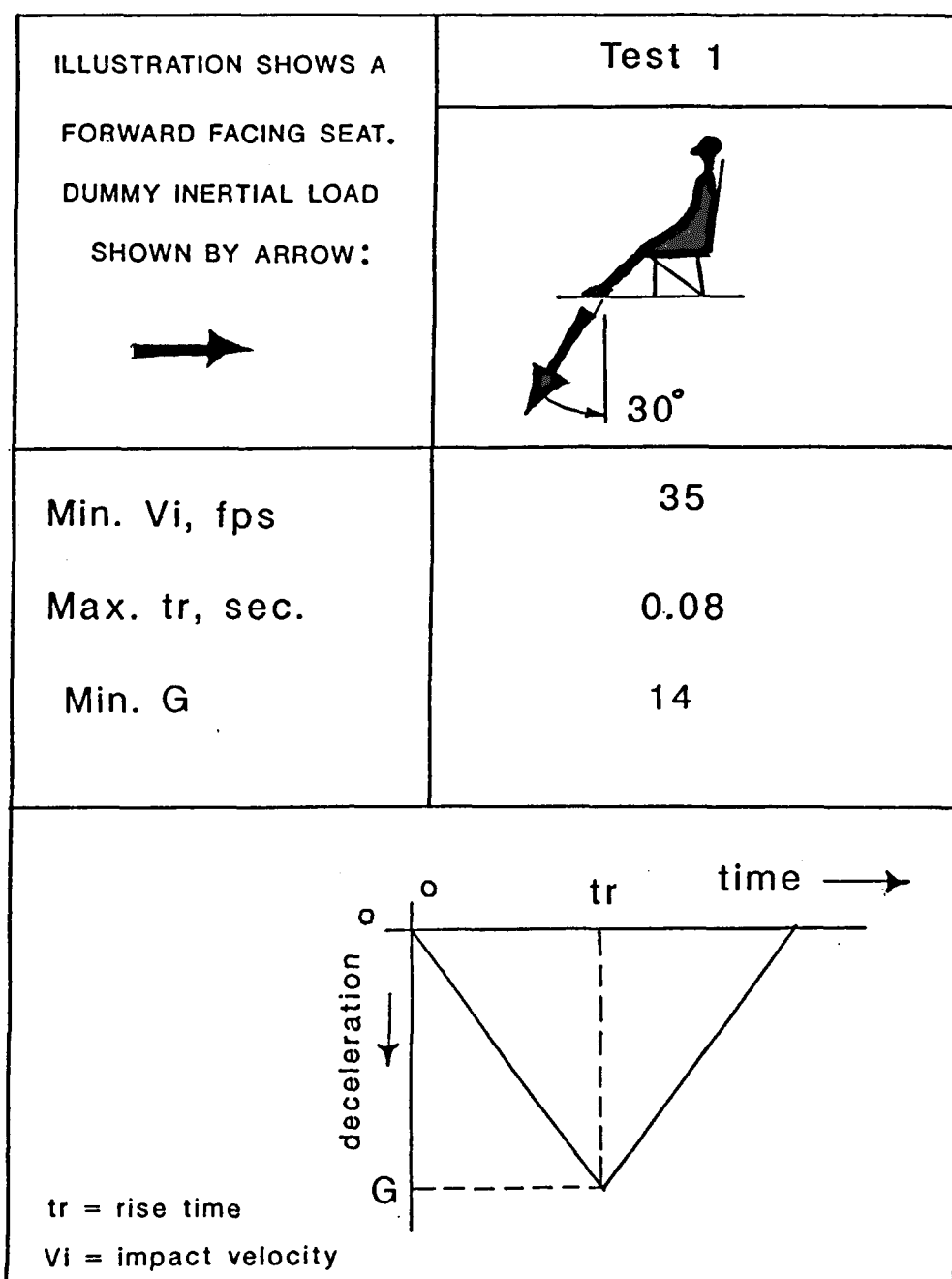
Figure A5.2. Variation in Impact Angle of NACA Pulse



(c) Concluded. Angle of impact, 29° ; impact speed, 97 mph.

Figure 3. - Concluded. Sequence pictures and accelerations of crashes of pressurized transports. (Zero time is fuselage nose impact with ground.)

Figure A5.3. Acceleration Measurements at Various Locations Aboard the NACA Aircraft (Station 490 was chosen for the simulation)



SEAT/RESTRAINT SYSTEM DYNAMIC TEST

Figure A5.4. 14 G Test Pulse (Aerospace Standard 8049)

APPENDIX 6

NACA ACCELERATION PULSE COMPONENTS

NACA, KEGWORTH AND 16G PULSE COMPARISONS

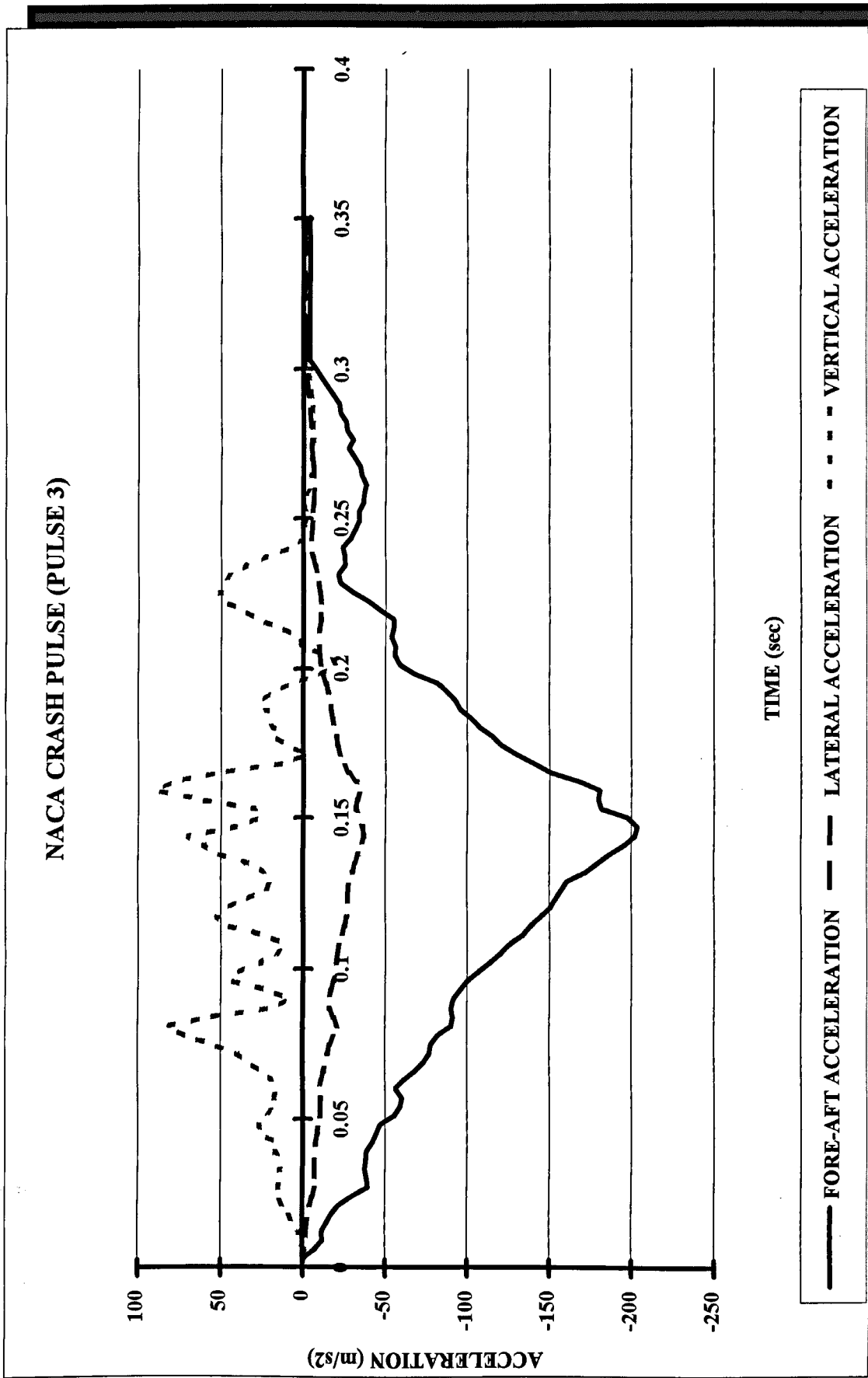


Figure A6.1. NACA Impact Acceleration Time History

COMPARISON OF THE KEGWORTH, NACA AND 16G FORE-AFT PULSES

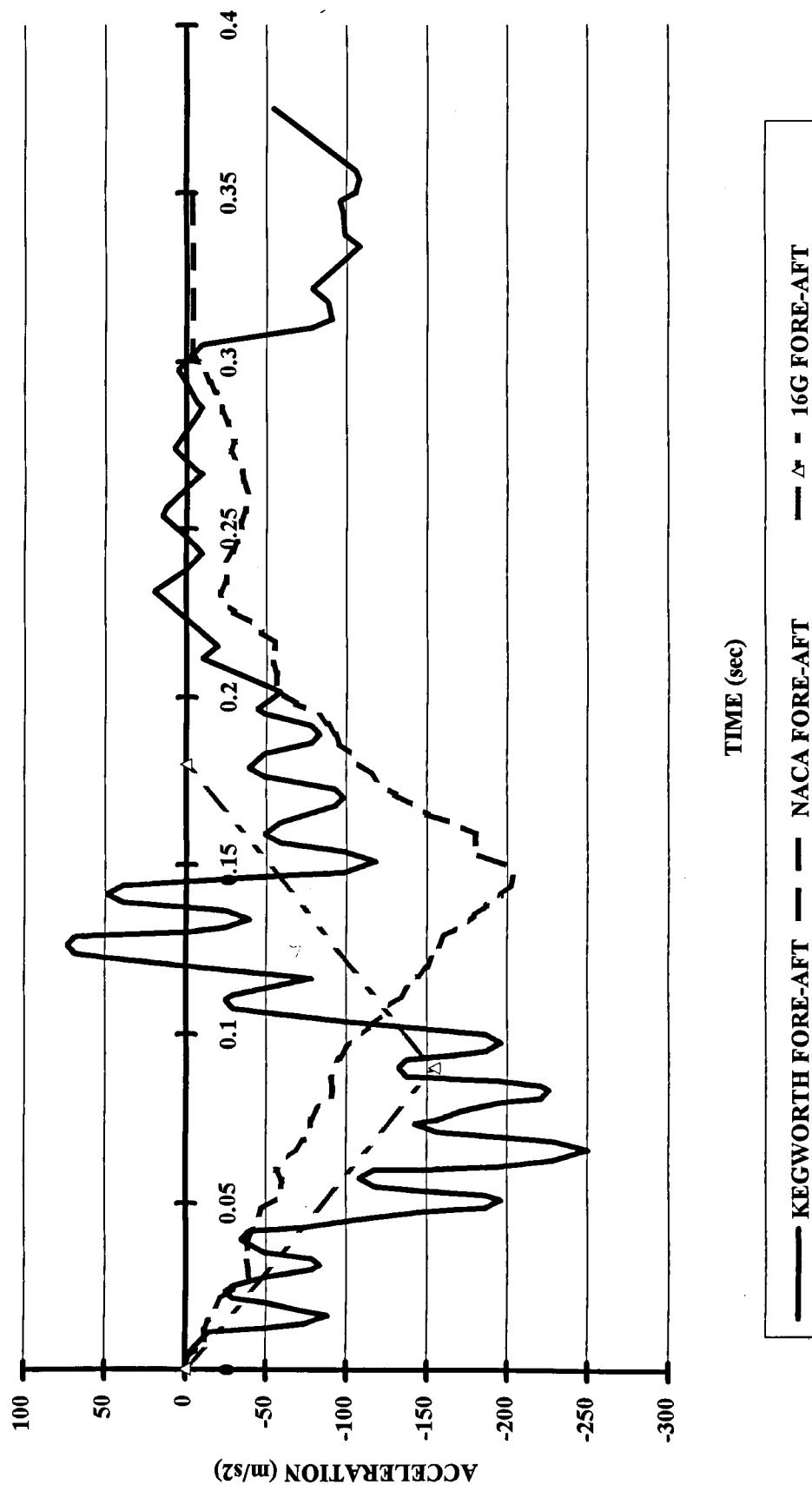


Figure A6.2. Comparison of NACA, Kegworth and 16G Pulse Fore-Aft Accelerations

COMPARISON OF THE NACA AND 16G LATERAL PULSES

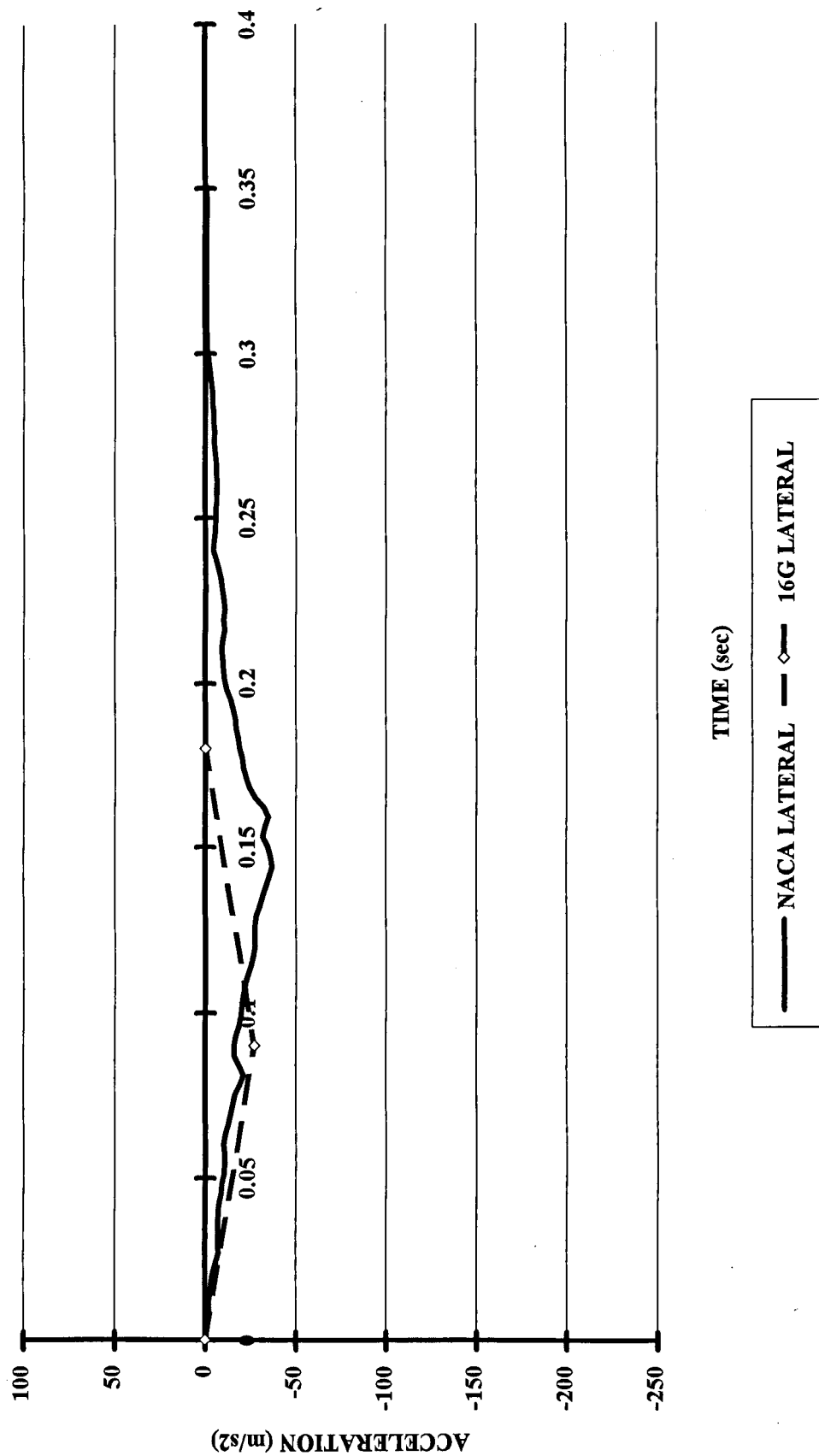


Figure A6.3. Comparison of NACA and 16G Pulse Lateral Accelerations

APPENDIX 7

SEAT BELT STIFFNESS CHARACTERISTICS

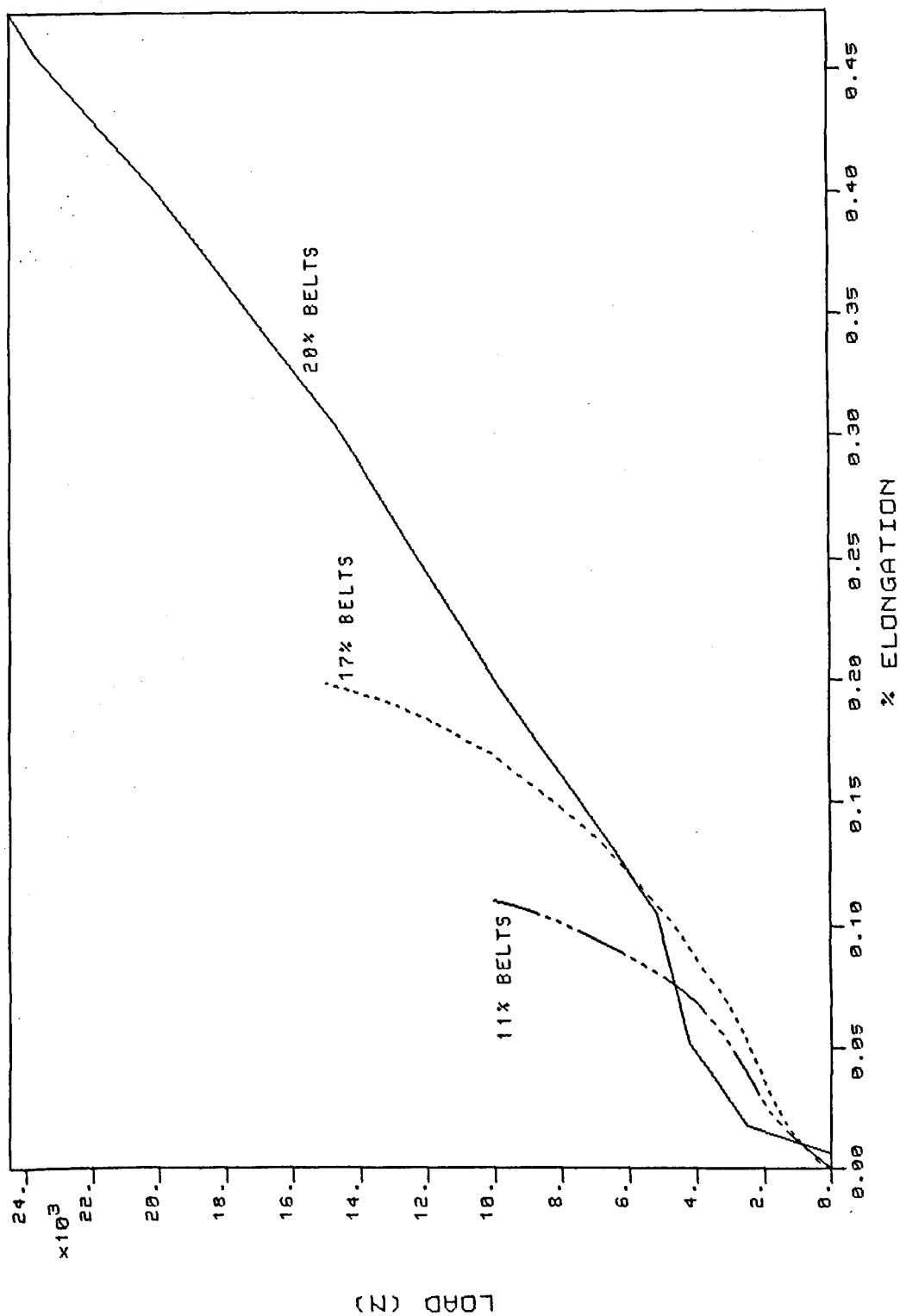
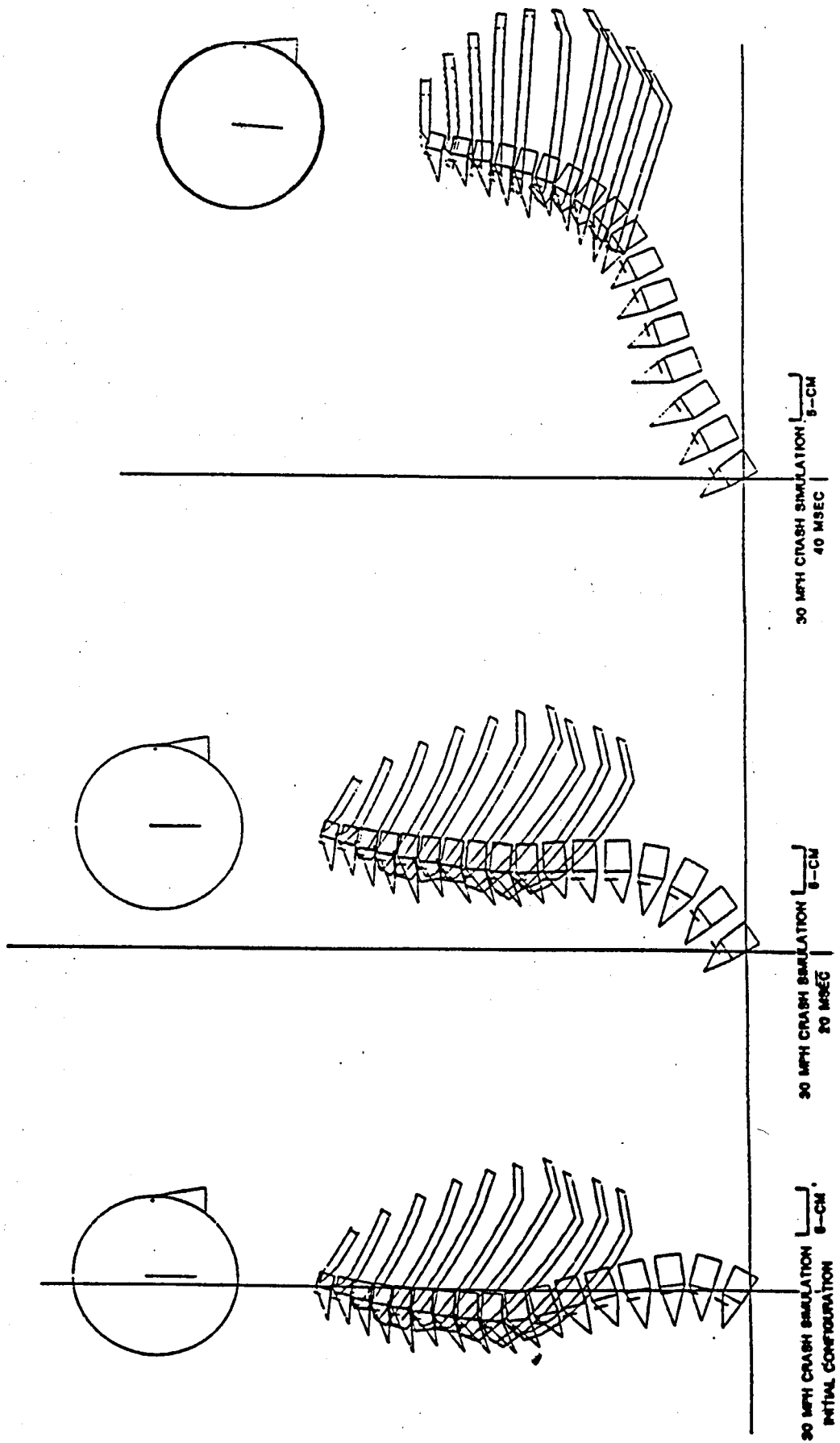


Figure A7.1. Seat Belt Stiffness Characteristics - Load versus Percentage Elongation

APPENDIX 8

WPAFB FINITE ELEMENT MODEL OF THE SPINE



Frontal impact deformed configurations.

Figure A8.1. WPAFB Finite Element Model of the Spine